U.S. DEPARTMENT OF COMMERCE
National Technical Information Service

PB-293 120

The Development of Mathematical Models for the Prediction of Anthropogenic Visibility Impairment
Volume II: Appendices

Systems Applications, Inc., San Rafael, CA

Prepared for

Environmental Protection Agency, Research Triangle Park, NC

Sep 78

TECHNICAL REPORT DATA

(Please read Instructions on the reverse before completing)

1. REPORT NO. EPA-450/3-78-110b

2.

3. RECIPIENT'S ACCESSION NO. PB293120

4. TITLE AND SUBTITLE
THE DEVELOPMENT OF MATHEMATICAL MODELS FOR THE PREDICTION OF ANTHROPOGENIC VISIBILITY IMPAIRMENT
VOLUME 2

5. REPORT DATE November 1978

6. PERFORMING ORGANIZATION CODE

7. AUTHOR(S)
D. A. Latimer, R. W. Bergstrom, S. R. Hayes, M. K. Liu, J. H. Seinfeld, G. Z. Whitten, M. A. Wojcik, M. J. Hillyer

8. PERFORMING ORGANIZATION REPORT NO. EF78-68B

9. PERFORMING ORGANIZATION NAME AND ADDRESS
Systems Applications, Incorporated
950 Northgate Drive
San Rafael, California 94903

10. PROGRAM ELEMENT NO.

11. CONTRACT/GRANT NO. EPA 68-01-3947 and 68-02-2593

12. SPONSORING AGENCY NAME AND ADDRESS
U.S. Environmental Protection Agency
Waterside Mall
401 M Street, S.W.
Washington, D.C. 20460

13. TYPE OF REPORT AND PERIOD COVERED Final Report: 10/77 to 9/78

14. SPONSORING AGENCY CODE EPA-OPE/OAQPS

15. SUPPLEMENTARY NOTES

16. ABSTRACT

This report describes a nine-month study to recommend and develop models that predict the contribution of man-made air pollution to visibility impairment in federal Class I areas. Two models were developed. A near-source plume model based on a Gaussian formulation was designed to compute the impact of a plume on visual range and atmospheric coloration. A regional model was designed to calculate pollutant concentrations and visibility impairment resulting from emissions from multiple sources within a region with a spatial scale of 1000 km and a temporal scale of several days. The objective of this effort was to develop models that are useful predictive tools for making policy and regulatory decisions, for evaluating the impacts of proposed new sources, and for determining the amount of emissions reduction required from existing sources, as mandated by the Clean Air Act Amendments of 1977. Volume I of this report contains the main text; Volume II contains the appendices; Volume III presents case studies of power plant plume visual impact for a variety of emission, meteorological, and ambient background scenarios.

17. KEY WORDS AND DOCUMENT ANALYSIS

a. DESCRIPTORS	b. IDENTIFIERS/OPEN ENDED TERMS	c. COSATI Field/Group
Air quality modeling Visual range Atmospheric discoloration Power plants		

18. DISTRIBUTION STATEMENT RELEASE TO PUBLIC

19. SECURITY CLASS *(This Report)* UNCLASSIFIED

20. SECURITY CLASS *(This page)* UNCLASSIFIED

21. NO. OF PAGES 519

22. PRICE PC A22/MF A01

PB 293120

United States
Environmental Protection
Agency

Office of Air Quality
Planning and Standards
Research Triangle Park NC 27711

EPA-450/3-78-110b
September 1978

Air

EPA

The Development of Mathematical Models for the Prediction of Anthropogenic Visibility Impairment

Volume II: Appendices

REPRODUCED BY
NATIONAL TECHNICAL
INFORMATION SERVICE
U. S. DEPARTMENT OF COMMERCE
SPRINGFIELD, VA. 22161

519

EPA-450/3/78-110b

Volume II: Appendices

THE DEVELOPMENT OF MATHEMATICAL MODELS FOR THE PREDICTION OF ANTHROPOGENIC VISIBILITY IMPAIRMENT

by

Douglas A. Latimer, Robert W. Bergstrom, Stanley R. Hayes
Mei-Kao Liu, John H. Seinfeld, Gary Z. Whitten
Michael A. Wojcik, Martin J. Hillyer

Systems Application, Incorporated
San Rafael, California 94903

Contract 68-01-3947

EPA Project Officers: John Butler, David Shaver, James Dicke

Prepared for

U. S. ENVIRONMENTAL PROTECTION AGENCY

Office of Planning and Evaluation
401 M Street, SW
Washington, DC 20460

Office of Air Noise and Radiation
Office of Air Quality Planning and Standards
Research Triangle Park, NC 27711

September 1978

1a

DISCLAIMER

This report has been reviewed by the Office of Air Quality Planning and Standards and the Office of Planning and Evaluation, U.S. Environmental Protection Agency and approved for publication. Approval does not signify that the contents necessarily reflect the views and policies of the U.S. Environmental Protection Agency, nor does mention of trade names or commercial products constitute endorsement or recommendation for use.

CONTENTS

DISCLAIMER ii

LIST OF ILLUSTRATIONS v

LIST OF TABLES xxiii

APPENDIX A: ANALYSIS OF VISUAL RANGE IN THE NORTHERN GREAT PLAINS AND THE SOUTHWEST 1

1. Objectives and Scope of the Study 2
2. Availability of Data on the Northern Great Plains 4
3. Selection of the Southwest for Data Analysis 8
4. The Data Analysis 17
5. The Frequency Distribution of Visual Range in the West 22
6. Yearly Trends in Visual Range 29
7. Effect of Relative Humidity 53
8. Effect of Cloud Cover 74
9. Effect of Barometric Pressure 93
10. Effect of Ventilation 93
11. Effect of Wind Speed 112
12. Seasonal Variations 149
13. Diurnal Variations 149
14. Variation With Wind Direction 186

APPENDIX B: ATMOSPHERIC OPTICS CALCULATION 213

1. Methods of Calculating Scattering and Extinction Coefficients 214
2. Methods for Calculating and Displaying Visual Degradation and Discoloration 227

APPENDIX C: THE CHEMISTRY OF SULFATE FORMATION 244

1. Homogeneous Oxidation of SO_2 249
2. Heterogeneous Oxidation of SO_2 252
3. Sulfate Formation in Remote Areas 258

APPENDIX D: DESCRIPTION OF THE PLUME VISIBILITY MODEL 263

1. Computational Procedure (Logic Flow) 264
2. Program Structure 268
3. Program Use 269

APPENDIX E: PLUME MODEL SAMPLE OUTPUT 273

Example 1: Output for a Plume from a Hypothetical 3000 Mwe Coal-Fired Power Plant 275
Example 2: Output for a Plume from a Copper Smelter 304

APPENDIX F: DESCRIPTION OF THE NORTHERN GREAT PLAINS REGIONAL MODEL 323

1. The Mixing Layer Model 326
2. The Surface Layer Model 333

APPENDIX G: APPLICATION OF THE REGIONAL MODEL TO THE PREDICTION OF VISIBILITY IMPAIRMENT IN THE NORTHERN GREAT PLAINS . . . 338

1. Application of the Regional-Scale Model. 339
2. Analysis of the Modeling Results 352

REFERENCES APPEAR AT THE END OF VOLUME I

ILLUSTRATIONS

A-1 Logic Flow and Elements of the Visual Range Data Analysis . . 5

A-2 Map of the Western United States Showing the Locations of Large Point Sources, Mandatory Federal Class I Areas, and NWS Stations Where Visibility Observations Are Made 10

A-3 AQCRs in the West Whose Emissions of TSP, SO_2, NO_x, or Hydrocarbons Exceeded 300,000 Tons in 1973 12

A-4 Distribution of Pollution Emissions Within a 1400 km Radius of a Location in South Central Utah Weighted by the Reciprocal of the Distance 15

A-5 Effect of Precipitation on Visual Range at Winslow, Arizona, 1967-1976 21

A-6 Frequency Distributions of Visual Range at 13 Western U.S. Locations on Days Without Precipitation or Fog in 1976 23

A-7 Frequency Distributions of Extinction Coefficients Based on Visual Range Observations at 13 Western U.S. Locations on Days Without Precipitation or Fog in 1976 25

A-8 Frequency Distributions of Extinction Coefficients Based on Photographic Photometry in the Petrified Forest, Arizona, in 1973 and 1974 26

A-9 Frequency Distribution of Extinction Coefficients Based on Visibility Observations at 8 National Park Service Sites in the Southwest in 1976 28

A-10 Percentage of Daylight Observations for Which Visual Range Exceeded an Indicated Value, as a Function of Year, in Denver, Colorado, 1948-1976 30

A-11 Percentage of Daylight Observations for Which Visual Range Exceeded an Indicated Value, as a Function of Year, in Las Vegas, Nevada, 1951-1976 31

A-12 Percentage of Daylight Observations for Which Visual Range Exceeded an Indicated Value, as a Function of Year, in Phoenix, Arizona, 1948-1976 32

A-13 Percentage of Daylight Observations for Which Visual Range Exceeded an Indicated Value, as a Function of Year, in Salt Lake City, Utah, 1948-1976 33

A-14 Percentage of Daylight Observations for Which Visual Range Exceeded an Indicated Value, as a Function of Year, in Tucson, Arizona, 1949-1976 34

A-15 Percentage of Daylight Observations for Which Visual Range Exceeded an Indicated Value, as a Function of Year, in Alamogordo, New Mexico, 1955-1970 35

A-16 Percentage of Daylight Observations for Which Visual Range Exceeded an Indicated Value, as a Function of Year, in Billings, Montana, 1948-1976 36

A-17 Percentage of Daylight Observations for Which Visual Range Exceeded an Indicated Value, as a Function of Year, in Colorado Springs, Colorado, 1948-1976 37

A-18 Percentage of Daylight Observations for Which Visual Range Exceeded an Indicated Value, as a Function of Year, in Cheyenne, Wyoming, 1948-1976 38

A-19 Percentage of Daylight Observations for Which Visual Range Exceeded an Indicated Value as a Function of Year, in Ely, Nevada, 1953-1976 39

A-20 Percentage of Daylight Observations for Which Visual Range Exceeded an Indicated Value, as a Function of Year, in Farmington, New Mexico, 1949-1976 40

A-21 Percentage of Daylight Observations for Which Visual Range Exceeded an Indicated Value, as a Function of Year, in Ft. Huachuca, Arizona, 1954-1971 41

A-22 Percentage of Daylight Observations for Which Visual Range Exceeded an Indicated Value, as a Function of Year, in Grand Junction, Colorado, 1948-1976 42

A-23 Percentage of Daylight Observations for Which Visual Range Exceeded an Indicated Value, as a Function of Year, in Great Falls, Montana, 1948-1976 43

A-24 Percentage of Daylight Observations for Which Visual Range Exceeded an Indicated Value, as a Function of Year, in Prescott, Arizona, 1948-1976 44

A-25 Percentage of Daylight Observations for Which Visual Range Exceeded an Indicated Value, as a Function of Year, in Pueblo, Colorado, 1954-1976 45

A-26 Percentage of Daylight Observations for Which Visual Range Exceeded an Indicated Value, as a Function of Year, at Rock Springs, Wyoming, 1948-1976 46

A-27 Percentage of Daylight Observations for Which Visual Range Exceeded an Indicated Value, as a Function of Year, in Winslow, Arizona, 1948-1976 47

A-28 Yearly Trends in SO_2 Emissions from Copper Smelters in Arizona 50

A-29 Yearly Trends in U.S. Copper Production 51

A-30 Effect of Relative Humidity on b_{scat} of a Laboratory Sulfate Aerosol 53

A-31 Percentage of Daylight Observations for Which Visual Range Exceeded 97 km, as a Function of Relative Humidity, at Denver, Colorado 54

A-32 Percentage of Daylight Observations for Which Visual Range Exceeded 48 km, as a Function of Relative Humidity, at Las Vegas, Nevada 55

A-33 Percentage of Daylight Observations for Which Visual Range Exceeded 64 km, as a Function of Relative Humidity, at Phoenix, Arizona 56

A-34 Percentage of Daylight Observations for Which Visual Range Exceeded 64 km, as a Function of Relative Humidity, at Salt Lake City, Utah 57

A-35 Percentage of Daylight Observations for Which Visual Range Exceeded 97 km, as a Function of Relative Humidity, at Tucson, Arizona 58

A-36 Percentage of Daylight Observations for Which Visual Range Exceeded 64 km, as a Function of Relative Humidity, at Alamogordo, New Mexico 59

A-37 Percentage of Daylight Observations for Which Visual Range Exceeded 97 km, as a Function of Relative Humidity, at Billings, Montana 60

A-38 Percentage of Daylight Observations for Which Visual Range Exceeded 145 km, as a Function of Relative Humidity, at Cheyenne, Wyoming 61

A-39 Percentage of Daylight Observations for Which Visual Range Exceeded 105 km, as a Function of Relative Humidity, at Colorado Springs, Colorado 62

A-40 Percentage of Daylight Observations for Which Visual Range Exceeded 72 km, as a Function of Relative Humidity, at Ely, Nevada 63

A-41 Percentage of Daylight Observations for Which Visual Range Exceeded 121 km, as a Function of Relative Humidity, at Farmington, New Mexico 64

A-42 Percentage of Daylight Observations for Which Visual Range Exceeded 89 km, as a Function of Relative Humidity, at Ft. Huachuca, Arizona 65

A-43 Percentage of Daylight Observations for Which Visual Range Exceeded 113 km, as a Function of Relative Humidity, at Grand Junction, Colorado 66

A-44 Percentage of Daylight Observations for Which Visual Range Exceeded 97 km, as a Function of Relative Humidity, at Great Falls, Montana 67

A-45 Percentage of Daylight Observations for Which Visual Range Exceeded 105 km, as a Function of Relative Humidity, at Prescott, Arizona 68

A-46 Percentage of Daylight Observations for Which Visual Range Exceeded 113 km, as a Function of Relative Humidity, at Pueblo, Colorado 69

A-47 Percentage of Daylight Observations for Which Visual Range Exceeded 64 km, as a Function of Relative Humidity, at Rock Springs, Wyoming 70

A-48 Percentage of Daylight Observations for Which Visual Range Exceeded 97 km, as a Function of Relative Humidity, at Winslow, Arizona 71

A-49 Percentage of Daylight Observations for Which Visual Range Exceeded 97 km, as a Function of Cloud Cover, at Denver, Colorado 75

A-50 Percentage of Daylight Observations for Which Visual Range Exceeded 48 km, as a Function of Cloud Cover at Las Vegas, Nevada 76

A-51 Percentage of Daylight Observations for Which Visual Range Exceeded 64 km, as a Function of Cloud Cover, at Phoenix, Arizona 77

A-52 Percentage of Daylight Observations for Which Visual Range Exceeded 64 km, as a Function of Cloud Cover, at Salt Lake City, Utah 78

A-53 Percentage of Daylight Observations for Which Visual Range Exceeded an Indicated Value, as a Function of Cloud Cover, at Tucson, Arizona 79

A-54 Percentage of Daylight Observations for Which Visual Range Exceeded 64 km, as a Function of Cloud Cover, at Alamogordo, New Mexico 80

A-55 Percentage of Daylight Observations for Which Visual Range Exceeded 97 km, as a Function of Cloud Cover, at Billings, Montana 81

A-56 Percentage of Daylight Observations for Which Visual Range Exceeded 145 km, as a Function of Cloud Cover, at Cheyenne, Wyoming 82

A-57 Percentage of Daylight Observations for Which Visual Range Exceeded 105 km, as a Function of Cloud Cover, at Colorado Springs, Colorado 83

A-58 Percentage of Daylight Observations for Which Visual Range Exceeded 72 km, as a Function of Cloud Cover, at Ely, Nevada 84

A-59 Percentage of Daylight Observations for Which Visual Range Exceeded 121 km, as a Function of Cloud Cover, at Farmington, New Mexico 85

A-60 Percentage of Daylight Observations for Which Visual Range Exceeded 64 km, as a Function of Cloud Cover, at Ft. Huachuca, Arizona 86

A-61 Percentage of Daylight Observations for Which Visual Range Exceeded 97 km, as a Function of Cloud Cover, at Grand Junction, Colorado 87

A-62 Percentage of Daylight Observations for Which Visual Range Exceeded 97 km, as a Function of Cloud Cover, at Great Falls, Montana 88

A-63 Percentage of Daylight Observations for Which Visual Range Exceeded 105 km, as a Function of Cloud Cover, at Prescott, Arizona 89

A-64 Percentage of Daylight Observations for Which Visual Range Exceeded 97 km, as a Function of Cloud Cover, at Pueblo, Colorado 90

A-65 Percentage of Daylight Observations for Which Visual Range Exceeded 64 km, as a Function of Cloud Cover, at Rock Springs, Wyoming 91

A-66 Percentage of Daylight Observations for Which Visual Range Exceeded 97 km, as a Function of Cloud Cover, at Winslow, Arizona 92

A-67 Percentage of Daylight Observations for Which Visual Range Exceeded 97 km, as a Function of Barometric Pressure, at Denver, Colorado 94

A-68 Percentage of Daylight Observations for Which Visual Range Exceeded an Indicated Value, as a Function of Barometric Pressure, at Las Vegas, Nevada 95

A-69 Percentage of Daylight Observations for Which Visual Range Exceeded 64 km, as a Function of Barometric Pressure, at Phoenix, Arizona 96

A-70 Percentage of Daylight Observations for Which Visual Range Exceeded 64 km, as a Function of Barometric Pressure, at Salt Lake City, Utah 97

A-71 Percentage of Daylight Observations for Which Visual Range Exceeded 64 km, as a Function of Barometric Pressure, at Tucson, Arizona 98

A-72 Percentage of Daylight Observations for Which Visual Range Exceeded 64 km, as a Function of Barometric Pressure, at Alamogordo, New Mexico 99

A-73 Percentage of Daylight Observations for Which Visual Range Exceeded 97 km, as a Function of Barometric Pressure, at Billings, Montana 100

A-74 Percentage of Daylight Observations for Which Visual Range Exceeded an Indicated Value, as a Function of Barometric Pressure, at Cheyenne, Wyoming 101

A-75 Percentage of Daylight Observations for Which Visual Range Exceeded 105 km, as a Function of Barometric Pressure, at Colorado Springs, Colorado 102

A-76 Percentage of Daylight Observations for Which Visual Range Exceeded 72 km, as a Function of Barometric Pressure, at Ely, Nevada 103

A-77 Percentage of Daylight Observations for Which Visual Range Exceeded 121 km, as a Function of Barometric Pressure, at Farmington, New Mexico 104

A-78 Percentage of Daylight Observations for Which Visual Range Exceeded 64 km, as a Function of Barometric Pressure, at Ft. Huachuca, Arizona 105

A-79 Percentage of Daylight Observations for Which Visual Range Exceeded 97 km, as a Function of Barometric Pressure, at Grand Junction, Colorado 106

A-80 Percentage of Daylight Observations for Which Visual Range Exceeded 97 km, as a Function of Barometric Pressure, at Great Falls, Montana 107

A-81 Percentage of Daylight Observations for Which Visual Range Exceeded 105 km, as a Function of Barometric Pressure, at Prescott, Arizona 108

A-82 Percentage of Daylight Observations for Which Visual Range Exceeded 97 km, as a Function of Barometric Pressure, at Pueblo, Colorado 109

A-83 Percentage of Daylight Observations for Which Visual Range Exceeded 64 km, as a Function of Barometric Pressure, at Rock Springs, Wyoming 110

A-84 Percentage of Daylight Observations for Which Visual Range Exceeded 97 km, as a Function of Barometric Pressure, at Winslow, Arizona 111

A-85 Percentage of Daylight Observations for Which Visual Range Exceeded 97 km, as a Function of Ventilation at Denver, Colorado 113

A-86 Percentage of Daylight Observations for Which Visual Range Exceeded an Indicated Value, as Function of Ventilation, at Las Vegas, Nevada, 1960-1964 114

A-87 Percentage of Daylight Observations for Which Visual Range Exceeded an Indicated Value, as a Function of Ventilation, at Phoenix, Arizona, 1960-1964 115

A-88 Percentage of Daylight Observations for Which Visual Range Exceeded an Indicated Value, as a Function of Ventilation, at Salt Lake City, Utah, 1960-1964 116

A-89 Percentage of Daylight Observations for Which Visual Range Exceeded an Indicated Value, as a Function of Ventilation, at Tucson, Arizona, 1960-1964 117

A-90 Percentage of Daylight Observations for Which Visual Range Exceeded 113 km, as a Function of Ventilation, at Alamogordo, New Mexico, 1960-1964 118

A-91 Percentage of Daylight Observations for Which Visual Range Exceeded an Indicated Value, as a Function of Ventilation, at Billings, Montana, 1960-1964 119

A-92 Percentage of Daylight Observations for Which Visual Range Exceeded an Indicated Value, as a Function of Ventilation, at Cheyenne, Wyoming, 1960-1964 120

A-93 Percentage of Daylight Observations for Which Visual Range Exceeded an Indicated Value, as a Function of Ventilation, at Colorado Springs, Colorado, 1960-1964 121

A-94 Percentage of Daylight Observations for Which Visual Range Exceeded 72 km, as a Function of Ventilation, at Ely, Nevada, 1960-1964 122

A-95 Percentage of Daylight Observations for Which Visual Range Exceeded an Indicated Value, as a Function of Ventilation, at Farmington, New Mexico, 1960-1964 123

A-96 Percentage of Daylight Observations for Which Visual Range Exceeded 64 km, as a Function of Ventilation, at Ft. Huachuca Arizona, 1960-1964 124

A-97 Percentage of Daylight Observations for Which Visual Range Exceeded an Indicated Value, as a Function of Ventilation, at Grand Junction, Colorado, 1960-1964 125

A-98 Percentage of Daylight Observations for Which Visual Range Exceeded 97 km, as a Function of Ventilation, at Great Falls, Montana, 1960-1964 126

A-99 Percentage of Daylight Observations for Which Visual Range Exceeded an Indicated Value, as a Function of Ventilation, at Prescott, Arizona, 1960-1964 127

A-100 Percentage of Daylight Observations for Which Visual Range Exceeded an Indicated Value, as a Function of Ventilation, at Pueblo, Colorado, 1960-1964 128

A-101 Percentage of Daylight Observations for Which Visual Range Exceeded 64 km, as a Function of Ventilation, at Rock Springs, Wyoming, 1960-1964 129

A-102 Percentage of Daylight Observations for Which Visual Range Exceeded 97 km, as a Function of Ventilation, at Winslow, Arizona, 1960-1964 130

A-103 Percentage of Daylight Observations for Which Visual Range Exceeded 97 km, as a Function of Surface Wind Speed, at Denver, Colorado 131

A-104 Percentage of Daylight Observations for Which Visual Range Exceeded 105 km, as a Function of Surface Wind Speed, at Las Vegas, Nevada 132

A-105 Percentage of Daylight Observations for Which Visual Range Exceeded 64 km, as a Function of Surface Wind Speed, at Phoenix, Arizona 133

A-106 Percentage of Daylight Observations for Which Visual Range Exceeded 64 km, as a Function of Surface Wind Speed, at Salt Lake City, Utah 134

A-107 Percentage of Daylight Observations for Which Visual Range Exceeded 97 km, as a Function of Surface Wind Speed, at Tucson, Arizona 135

A-108 Percentage of Daylight Observations for Which Visual Range Exceeded 64 km, as a Function of Surface Wind Speed, as Alamogordo, New Mexico 136

A-109 Percentage of Daylight Observations for Which Visual Range Exceeded 97 km, as a Function of Surface Wind Speed, at Billings, Montana 137

A-110 Percentage of Daylight Observations for Which Visual Range Exceeded 97 km, as a Function of Surface Wind Speed, at Cheyenne, Wyoming 138

A-111 Percentage of Daylight Observations for Which Visual Range Exceeded 105 km, as a Function of Surface Wind Speed, at Colorado Springs, Colorado 139

A-112 Percentage of Daylight Observations for Which Visual Range Exceeded 72 km, as a Function of Surface Wind Speed, at Ely, Nevada 140

A-113 Percentage of Daylight Observations for Which Visual Range Exceeded 121 km, as a Function of Surface Wind Speed, at Farmington, New Mexico 141

A-114 Percentage of Daylight Observations for Which Visual Range Exceeded 97 km, as a Function of Surface Wind Speed, at Ft. Huachuca, Arizona 142

A-115 Percentage of Daylight Observations for Which Visual Range Exceeded 113 km, as a Function of Surface Wind Speed, at Grand Junction, Colorado 143

A-116 Percentage of Daylight Observations for Which Visual Range Exceeded 97 km, as a Function of Surface Wind Speed, at Great Falls, Montana 144

A-117 Percentage of Daylight Observations for Which Visual Range Exceeded 105 km, as a Function of Surface Wind Speed, at Prescott, Arizona 145

A-118 Percentage of Daylight Observations for Which Visual Range Exceeded 97 km, as a Function of Surface Wind Speed, at Pueblo, Colorado 146

A-119 Percentage of Daylight Observations for Which Visual Range Exceeded 64 km, as a Function of Surface Wind Speed, at Rock Springs, Wyoming 147

A-120 Percentage of Daylight Observations for Which Visual Range Exceeded 97 km, as a Function of Surface Wind Speed, at Winslow, Arizona 148

A-121 Seasonal Variation in Visual Range at Denver, Colorado, 1948-1976 150

A-122 Seasonal Variation in Visual Range at Las Vegas, Nevada, 1948-1976 151

A-123 Seasonal Variation in Visual Range at Phoenix, Arizona, 1948-1976 152

A-124 Seasonal Variation in Visual Range at Salt Lake City, Utah, 1948-1976 153

A-125 Seasonal Variation in Visual Range at Tucson, Arizona, 1948-1976 154

A-126 Seasonal Variation in Visual Range at Alamogordo, New Mexico, 1948-1976 155

A-127 Seasonal Variation in Visual Range at Billings, Montana, 1948-1976 156

A-128 Seasonal Variation in Visual Range at Cheyenne, Wyoming, 1948-1976 157

A-129 Seasonal Variation in Visual Range at Colorado Springs, Colorado, 1948-1976 158

A-130 Seasonal Variation in Visual Range at Ely, Nevada, 1953-1976 159

A-131 Seasonal Variation in Visual Range at Farmington, New Mexico, 1948-1976 160

A-132 Seasonal Variation in Visual Range at Ft. Huachuca, Arizona, 1957-1971 161

A-133 Seasonal Variation in Visual Range at Grand Junction, Colorado, 1948-1976 162

A-134 Seasonal Variation in Visual Range at Great Falls, Montana, 1948-1976 163

A-135 Seasonal Variation in Visual Range at Prescott, Arizona, 1948-1976 164

A-136 Seasonal Variation in Visual Range at Pueblo, Colorado, 1954-1976 165

A-137 Seasonal Variation in Visual Range at Rock Springs, Wyoming, 1948-1976 166

A-138 Seasonal Variation in Visual Range at Winslow, Arizona, 1948-1976 167

A-139 Variation in Visual Range as a Function of Time of Day at Denver, Colorado, 1948-1976 168

A-140 Variation in Visual Range as a Function of Time of Day at Las Vegas, Nevada, 1948-1976 169

A-141 Variation in Visual Range as a Function of Time of Day at Phoenix, Arizona, 1948-1976 170

A-142 Variation in Visual Range as a Function of Time of Day at Salt Lake City, Utah, 1948-1976 171

A-143 Variation in Visual Range as a Function of Time of Day at Tucson, Arizona, 1948-1976 172

A-144 Variation in Visual Range as a Function of Time of Day at Alamogordo, New Mexico, 1948-1970 173

A-145 Variation in Visual Range as a Function of Time of Day at Billings, Montana, 1948-1976 174

A-146 Variation in Visual Range as a Function of Time of Day at Cheyenne, Wyoming, 1948-1976 175

A-147 Variation in Visual Range as a Function of Time of Day at Colorado Springs, Colorado, 1948-1976 176

A-148 Variation in Visual Range as a Function of Time of Day at Ely, Nevada, 1953-1976 177

A-149 Variation in Visual Range as a Function of Time of Day at Farmington, New Mexico, 1949-1976 178

A-150 Variation in Visual Range as a Function of Time of Day at Ft. Huachuca, Arizona, 1954-1971 179

A-151 Variation of Visual Range as a Function of Time of Day at Grand Junction, Colorado, 1948-1976 180

A-152 Variation in Visual Range as a Function of Time of Day at Great Falls, Montana, 1948-1976 181

A-153 Variation in Visual Range as a Function of Time of Day at Prescott, Arizona, 1948-1976 182

A-154 Variation in Visual Range as a Function of Time of Day at Pueblo, Colorado, 1954-1976 183

A-155 Variation of Visual Range as a Function of Time of Day at Rock Springs, Wyoming, 1948-1976 184

A-156 Variation of Visual Range as a Function of Time of Day at Winslow, Arizona, 1948-1976 185

A-157 Percentage of Daylight Observations for Which Visual Range Exceeded 97 km, as a Function of Wind Direction, at Denver, Colorado, 1948-1976 187

A-158 Percentage of Daylight Observations for Which Visual Range Exceeded an Indicated Value, as a Function of Wind Direction, at Las Vegas, Nevada, 1948-1976 188

A-159 Percentage of Daylight Observations for Which Visual Range Exceeded an Indicated Value, as a Function of Wind Direction, at Phoenix, Arizona, 1948-1976 189

A-160 Percentage of Daylight Observations for Which Visual Range Exceeded 64 km, as a Function of Wind Direction at Salt Lake City, Utah, 1948-1976 190

A-161 Percentage of Daylight Observations for Which Visual Range Exceeded an Indicated Value as a Function of Wind Direction, at Tucson, Arizona, 1948-1976 191

A-162 Percentage of Daylight Observations for Which Visual Range Exceeded 113 km as a Function of Wind Direction, at Alamogordo, New Mexico, 1957-1970 192

A-163 Percentage of Daylight Observations for Which Visual Range Exceeded 97 km, as a Function of Wind Direction, at Billings, Montana, 1948-1976 193

A-164 Percentage of Observations for Which Visual Range Exceeded 145 km, as a Function of Wind Direction, at Cheyenne, Wyoming, 1948-1976 194

A-165 Percentage of Daylight Observations for Which Visual Range Exceeded 145 km, as a Function of Wind Direction, at Colorado Springs, Colorado, 1948-1976 195

A-166 Percentage of Daylight Observations for Which Visual Range Exceeded 72 km, as a Function of Wind Direction, at Ely, Nevada, 1948-1976 196

A-167 Percentage of Daylight Observations for Which Visual Range Exceeded an Indicated Value, as a Function of Wind Direction, at Farmington, New Mexico, 1949-1976 197

A-168 Percentage of Daylight Observations for Which Visual Range Exceeded an Indicated Value, as a Function of Wind Direction, at Ft. Huachuca, Arizona, 1957-1970 198

A-169 Percentage of Daylight Observations for Which Visual Range Exceeded an Indicated Value, as a Function of Wind Direction, at Grand Junction, Colorado, 1948-1976 199

A-170 Percentage of Daylight Observations for Which Visual Range Exceeded 97 km, as a Function of Wind Direction, at Great Falls, Montana, 1948-1976 200

A-171 Percentage of Daylight Observations for Which Visual Range Exceeded an Indicated Value, as a Function of Wind Direction, at Prescott, Arizona, 1948-1976 201

A-172 Percentage of Daylight Observations for Which Visual Range Exceeded 113 km, as a Function of Wind Direction, at Pueblo, Colorado, 1954-1976 202

A-173 Percentage of Daylight Observations for Which Visual Range Exceeded 64 km, as a Function of Wind Direction, at Rock Springs, Wyoming, 1948-1976 203

A-174 Percentage of Daylight Observations for Which Visual Range Exceeded 97 km, as a Function of Wind Direction, at Winslow Arizona, 1948-1976 204

A-175 Percentage of Daylight Observations with RH < 60 Percent for Which Visual Range Exceeded 105 km, as a Function of Wind Direction, at Prescott, Arizona, 1948-1976 210

A-176 Percentage of Daylight Observations with RH < 60 Percent for Which Visual Range Exceeded 97 km, as a Function of Wind Direction, at Winslow, Arizona, 1948-1976 211

A-177 Percentage of Daylight Observations with RH < 60 Percent for Which Visual Range Exceeded 121 km, as a Function of Wind Direction, at Farmington, New Mexico, 1948-1976 212

B-1 Extinction and Absorption per Unit Mass as a Function of Particle Radius for Four Different Refractive Indices at a Solar Wavelength of 0.55 μm 221

B-2 Scattering-to-Mass Ratios for Various Size Distributions 222

B-3 The Scattering Distribution Function for the Accumulation Mode, r_{og} = 0.1 μm, σ = 2.0 μm at Two Different Wavelengths . . 224

B-4 Ratio of Light Scattering to Mass as a Function of Relative Humidity 226

B-5 Diagram of the Physical Situation 229

B-6 Diagram of the Two Atmospheric Layers 233

B-7 Coordinate System and Angles 235

D-1 Flowchart of the Computer Code Calculations and Program Structure for the Plume Visibility Model 266

F-1 Schematic of the Regional Model Configuration 325

F-2 850-mb Weather Map for 1700 MST 30 January 1976 331

F-3 Bicubic Spline Fit of Geopotential Height (in Meters) 332

F-4 Meridional Wind (m/s) Generated by a Bicubic Spline Fit of Geopotential Height 332

F-5 Zonal Wind (m/s) Generated by a Bicubic Spline Fit of Geopotential Height 332

F-6 Computed Horizontal Eddy Diffusivities (10^4 m^2/s) 332

F-7 Schematic Illustration of the Surface Layer 334

G-1 Relative Locations of the Hypothetical Copper Smelters 344

G-2 SO_2 Concentrations Predicted by the Regional Air Pollution Model for the Winter Case. 347

G-3 850 Millibar Weather Map for 500 MST on 10 July 1975 349

G-4 Photodissociation Rate Constant Temporal Variation 351

G-5 Hypothetical Copper Smelter Isopleths for 1700-2000 MST on 4 April 1976 Assuming 0.5 Percent per Hour Sulfate Formation. 353

G-6 Hypothetical Copper Smelter Isopleths for 200-500 MST on 5 April 1976 Assuming 0.5 Percent per Hour Sulfate Formation. 356

G-7 Hypothetical Copper Smelter Isopleths for 1100-1400 MST on 5 April 1976 Assuming 0.5 Percent per Hour Sulfate Formation. 359

G-8 Hypothetical Copper Smelter Isopleths for 2000-2300 MST on 5 April 1976 Assuming 0.5 Percent per Hour Sulfate Formation. 362

G-9 Hypothetical Copper Smelter Isopleths for 500-800 MST on 6 April 1976 Assuming 0.5 Percent per Hour Sulfate Formation. 365

G-10 Hypothetical Copper Smelter Isopleths for 1400-1700 MST on 6 April 1976 Assuming 0.5 Percent per Hour Sulfate Formation. 368

G-11 Hypothetical Copper Smelter Isopleths for 1700-2000 MST on 9 July 1975 Assuming 0.5 Percent per Hour Sulfate Formation. 372

G-12 Hypothetical Copper Smelter Isopleths for 200-500 MST on 10 July 1975 Assuming 0.5 Percent per Hour Sulfate Formation. 375

G-13 Hypothetical Copper Smelter Isopleths for 1100-1400 MST on 10 July 1975 Assuming 0.5 Percent per Hour Sulfate Formation 378

G-14 Hypothetical Copper Smelter Isopleths for 2000-2300 MST on 10 July 1975 Assuming 0.5 Percent per Hour Sulfate Formation 381

G-15 Hypothetical Copper Smelter Isopleths for 500-800 MST on 10 July 1975 Assuming 0.5 Percent per Hour Sulfate Formation 384

G-16 Hypothetical Copper Smelter Isopleths for 1400-1700 MST on 10 July 1975 Assuming 0.5 Percent per Hour Sulfate Formation 387

G-17 Hypothetical Copper Smelter Isopleths for 1700-2000 MST on 27 January 1976 Assuming 0.5 Percent per Hour Sulfate Formation 390

G-18 Hypothetical Copper Smelter Isopleths for 200-500 MST on 28 January 1976 Assuming 0.5 Percent per Hour Sulfate Formation 393

G-19 Hypothetical Copper Smelter Isopleths for 1100-1400 MST on 28 January 1975 Assuming 0.5 Percent per Hour Sulfate Formation 396

G-20 Hypothetical Copper Smelter Isopleths for 2000-2300 MST on 28 January 1976 Assuming 0.5 Percent per Hour Sulfate Formation 399

G-21 Hypothetical Copper Smelter Isopleths for 500-800 MST on 29 January 1976 Assuming 0.5 Percent per Hour Sulfate Formation 402

G-22 Hypothetical Copper Smelter Isopleths for 1400-1700 MST on 29 January 1976 Assuming 0.5 Percent per Hour Sulfate Formation 405

G-23 Hypothetical Copper Smelter Isopleths for 1700-2000 MST on 4 April 1976 Assuming 1 Percent per Hour Sulfate Formation 409

G-24 Hypothetical Copper Smelter Isopleths for 200-500 MST on 5 April 1976 Assuming 1 Percent per Hour Sulfate Formation 412

G-25 Hypothetical Copper Smelter Isopleths for 1100-1400 MST on 5 April 1976 Assuming 1 Percent per Hour Sulfate Formation 415

G-26 Hypothetical Copper Smelter Isopleths for 2000-2300 MST on 5 April 1976 Assuming 1 Percent per Hour Sulfate Formation 418

G-27 Hypothetical Copper Smelter Isopleths for 500-800 MST on 6 April 1976 Assuming 1 Percent per Hour Sulfate Formation 421

G-28 Hypothetical Copper Smelter Isopleths for 1400-1700 MST on 6 April 1976 Assuming 1 Percent per Hour Sulfate Formation 424

G-29 Hypothetical Copper Smelter Isopleths for 1700-2000 MST on 4 April 1976 Assuming 0.3 Percent per Hour Sulfate Formation 427

G-30 Hypothetical Copper Smelter Isopleths for 200-500 MST on 5 April 1976 Assuming 0.3 Percent per Hour Sulfate Formation 430

G-31 Hypothetical Copper Smelter Isopleths for 1100-1400 MST on 5 April 1976 Assuming 0.3 Percent per Hour Sulfate Formation 433

G-32 Hypothetical Copper Smelter Isopleths for 2000-2300 MST on 5 April 1976 Assuming 0.3 Percent per Hour Sulfate Formation 436

G-33 Hypothetical Copper Smelter Isopleths for 500-800 MST on 6 April 1976 Assuming 0.3 Percent per Hour Sulfate Formation 439

G-34 Hypothetical Copper Smelter Isopleths for 1400-1700 MST on 6 April 1976 Assuming 0.3 Percent per Hour Sulfate Formation 442

G-35 1975 Northern Great Plains Isopleths for 1700-2000 MST on 4 April 1976 Assuming 0.5 Percent per Hour Sulfate Formation 445

G-36 1975 Northern Great Plains Isopleths for 200-500 MST on 5 April 1976 Assuming 0.5 Percent per Hour Sulfate Formation 449

G-37 1975 Northern Great Plains Isopleths for 1100-1400 MST on 5 April 1976 Assuming 0.5 Percent per Hour Sulfate Formation 453

G-38 1975 Northern Great Plains Isopleths for 2000-2300 MST on 5 April 1976 Assuming 0.5 Percent per Hour Sulfate Formation 457

G-39 1975 Northern Great Plains Isopleths for 500-800 MST on 6 April 1976 Assuming 0.5 Percent per Hour Sulfate Formation 461

G-40 1975 Northern Great Plains Isopleths for 1400-1700 MST on 6 April 1976 Assuming 0.5 Percent per Hour Sulfate Formation 465

G-41 1986 Northern Great Plains Isopleths for 1700-2000 MST on 4 April 1976 Assuming 0.5 Percent per Hour Sulfate Formation 470

G-42 1986 Northern Great Plains Isopleths for 200-500 MST on 5 April 1976 Assuming 0.5 Percent per Hour Sulfate Formation 474

G-43 1986 Northern Great Plains Isopleths for 1100-1400 MST on 5 April 1976 Assuming 0.5 Percent per Hour Sulfate Formation 478

G-44 1986 Northern Great Plains Isopleths for 2000-2300 MST on 5 April 1976 Assuming 0.5 Percent per Hour Sulfate Formation 482

G-45 1986 Northern Great Plains Isopleths for 500-800 MST on 6 April 1976 Assuming 0.5 Percent per Hour Sulfate Formation 486

G-46 1986 Northern Great Plains Isopleths for 1400-1700 MST on 6 April 1976 Assuming 0.5 Percent per Hour Sulfate Formation 490

TABLES

A-1 Distance to the Farthest Visual Range Markers at NWS Stations in the Northern Great Plains 7

A-2 Pollutant Emissions in the Western States 13

A-3 Coal-Fired Power Plants in the Southwest 18

A-4 Summary of Data Sorting 20

A-5 Components of Average Light Scattering at the Grand Canyon in 1974 27

B-1 Estimates of Extinction Coefficients per Unit Mass 217

B-2 Equations and Limitations for the Regional Model 243

B-3 Equations and Limitations for the Plume Model 243

C-1 Observed Sulfur Dioxide Oxidation Rates 248

C-2 Estimated Contributions to Atmospheric SO_2 Oxidation Rate by Homogeneous Chemical Reactions 251

C-3 Rate Constants k_s for the Liquid-Phase Oxidation of SO_2 by O_2 253

C-4 Liquid-Phase Oxidation of SO_2 by O_3 255

C-5 Metal-Ion Catalyzed Liquid-Phase Oxidation of SO_2 256

D-1 Data Requirements for the Plume Visibility Computer Program 270

F-1 Deposition Velocity ($V_g = F/\overline{c}$, in cm/s) for Sulfur Dioxide . . 337

G-1 Point Sources in the Northern Great Plains in 1976 That Emitted More Than 10,000 Tons of SO_x per Year 341

G-2 Point Sources in the Northern Great Plains in 1986 That Emitted More Than 10,000 Tons of SO_x per Year 342

G-3 Emissions Parameters for the Hypothetical Copper Smelters . . . 343

G-4 The Five Regional Visibility Model Simulations 352

APPENDIX A

ANALYSIS OF VISUAL RANGE IN THE NORTHERN GREAT PLAINS AND THE SOUTHWEST

APPENDIX A

ANALYSIS OF VISUAL RANGE IN THE NORTHERN GREAT PLAINS AND THE SOUTHWEST

Appendix A describes the data analysis objectives, progress, and results. After describing the context of this part of the study, we then discuss the availability of data, the selection of a region for data analysis, and the results.

1. OBJECTIVES AND SCOPE OF THE STUDY

In support of the development of models for the prediction of anthropogenic visibility impairment, we studied visual range data available for various locations in the western United States. The data analysis task has three objectives:

- To determine the magnitude, temporal and spatial variations, and causes of visibility impairment in the western United States.
- To identify the meteorological and geographical conditions associated with visibility impairment.
- To select a region and time period suitable for modeling, model validation, or both.

Specific questions that the study and analysis of data addressed include:

- Under what meteorological conditions is visibility impairment greatest?
- Under what meteorological conditions is visibility impairment caused by anthropogenic air pollution greatest?
- Is visibility most impaired by anthropogenic pollution on days with poor ventilation?

- > Does visibility impairment result from air pollutants transported from other areas?
- > How far is air pollution transported?
- > Does visibility depend on factors such as wind speed, mixing depth, relative humidity, and cloud cover?
- > Are there significant monthly or seasonal variations in visibility degradation?
- > Does visibility change significantly from year to year and if it does, can visibility changes be correlated with historical variations in emissions?
- > Can spatial and temporal variations in visibility be explained by variations in air pollutant concentrations caused by changing meteorological conditions?
- > Can it be determined whether local or distant sources and whether natural or anthropogenic sources cause visibility impairment?
- > How can the contribution of a given source to visibility degradation be determined?

Seven primary types of data were analyzed to meet these objectives and to answer these questions:

- > National Weather Service (NWS) three-hour surface meteorological data, including visibility, for the available recorded period of 1948 through 1976 (TDF-14 data tape).
- > Holzworth mixing depth and upper-air wind analysis for the period 1960 through 1964--twice daily values of mixing depth and average wind speed in the mixed layer.
- > Surface and constant pressure (upper-air) synoptic weather maps.
- > Magnitude and distribution of air pollution emissions [National Emissions Data System (NEDS)].

> Air quality data, in particular the concentrations of total suspended particulates, sulfate, nitrate, nitrogen dioxide, nitric oxide, and ozone (SAROAD system).
> U.S. Geological Survey topographic maps.
> Special studies of visibility and power plant plume impact [National Park Service, National Oceanic and Atmospheric Administration (NOAA), Martin-Marietta, Dames & Moore].

Figure A-1 shows the logic flow and the elements of the data analysis task. We obtained the aerometric data, created chronological data files and sorted the data available from 18 NWS stations in the West for the period 1948 through 1976. To determine the spatial variations of visibility, we have mapped visual range on selected days in 1976; other maps show the locations of major point pollution sources in the western United States. Finally, we interpreted the results of the data analysis in terms of answers to the questions listed above and also in terms of other, more specific questions that need to be answered. Because no measurements are currently made of atmospheric discoloration, this aspect of visibility impairment has not been studied. Only reductions in visual range have been studied. In subsequent sections of Appendix A the term "visibility" is used synonymously for "visual range."

2. AVAILABILITY OF DATA ON THE NORTHERN GREAT PLAINS

The Northern Great Plains region offers specific advantages as a modeling region:

> It is flat and hence does not have the complicated flow conditions that occur in complex terrain.
> SAI has already developed a regional air quality model for the Northern Great Plains that could be modified to predict regional visibility.

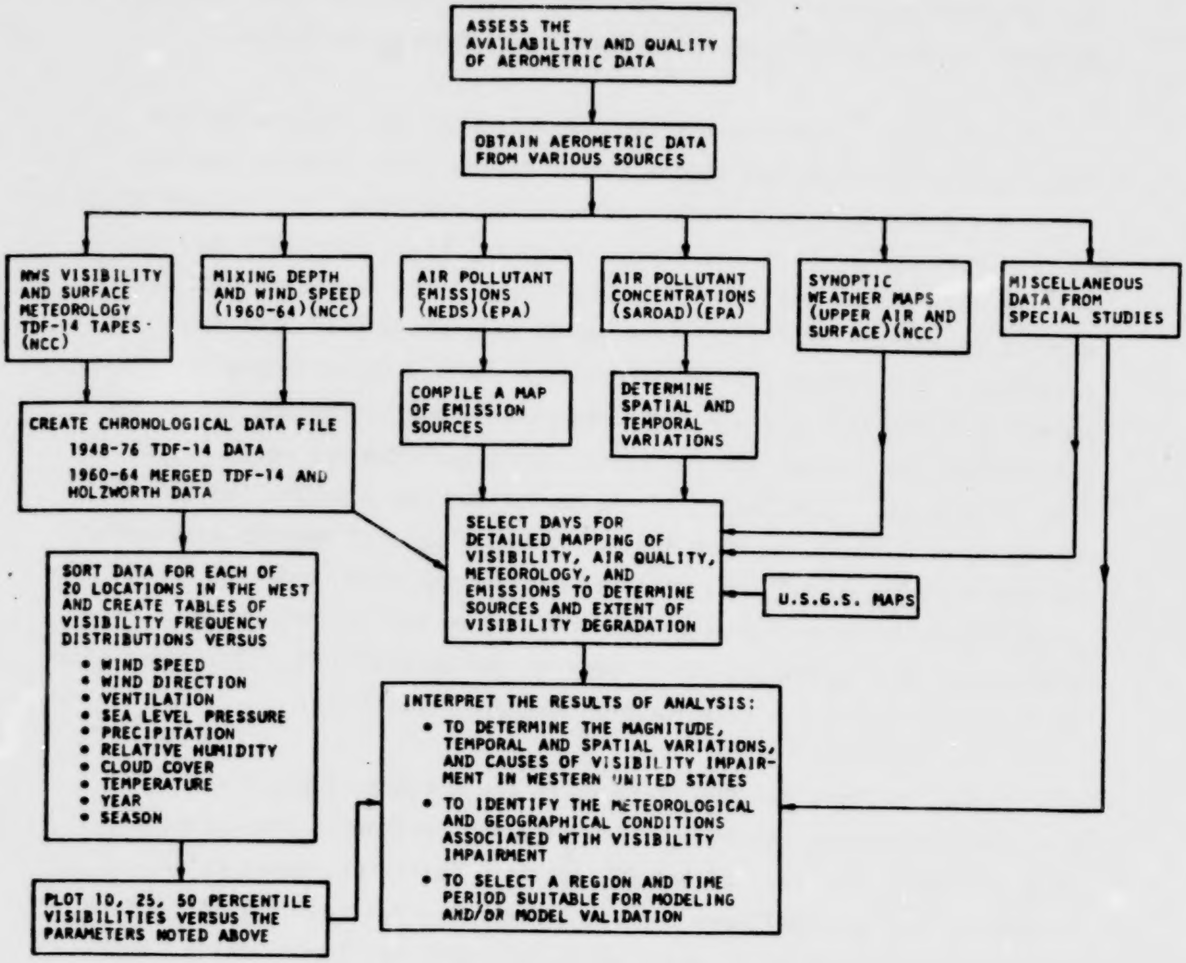
ASSESS THE AVAILABILITY AND QUALITY OF AEROMETRIC DATA
OBTAIN AEROMETRIC DATA FROM VARIOUS SOURCES
NWS VISIBILITY AND SURFACE METEOROLOGY TDF-14 TAPES (NCC)
MIXING DEPTH AND WIND SPEED (1960-64)(NCC)
AIR POLLUTANT EMISSIONS (NEDS)(EPA)
AIR POLLUTANT CONCENTRATIONS (SAROAD)(EPA)
SYNOPTIC WEATHER MAPS (UPPER AIR AND SURFACE)(NCC)
MISCELLANEOUS DATA FROM SPECIAL STUDIES
CREATE CHRONOLOGICAL DATA FILE
1948-76 TDF-14 DATA
1960-64 MERGED TDF-14 AND HOLZWORTH DATA
COMPILE A MAP OF EMISSION SOURCES
DETERMINE SPATIAL AND TEMPORAL VARIATIONS
SELECT DAYS FOR DETAILED MAPPING OF VISIBILITY, AIR QUALITY, METEOROLOGY, AND EMISSIONS TO DETERMINE SOURCES AND EXTENT OF VISIBILITY DEGRADATION
U.S.G.S. MAPS
SORT DATA FOR EACH OF 20 LOCATIONS IN THE WEST AND CREATE TABLES OF VISIBILITY FREQUENCY DISTRIBUTIONS VERSUS
• WIND SPEED
• WIND DIRECTION
• VENTILATION
• SEA LEVEL PRESSURE
• PRECIPITATION
• RELATIVE HUMIDITY
• CLOUD COVER
• TEMPERATURE
• YEAR
• SEASON
INTERPRET THE RESULTS OF ANALYSIS:
• TO DETERMINE THE MAGNITUDE, TEMPORAL AND SPATIAL VARIATIONS, AND CAUSES OF VISIBILITY IMPAIRMENT IN WESTERN UNITED STATES
• TO IDENTIFY THE METEOROLOGICAL AND GEOGRAPHICAL CONDITIONS ASSOCIATED WTIH VISIBILITY IMPAIRMENT
• TO SELECT A REGION AND TIME PERIOD SUITABLE FOR MODELING AND/OR MODEL VALIDATION
PLOT 10, 25, 50 PERCENTILE VISIBILITIES VERSUS THE PARAMETERS NOTED ABOVE

FIGURE A-1. LOGIC FLOW AND ELEMENTS OF THE VISUAL RANGE DATA ANALYSIS

> Pollutant emissions in the area are expected to increase in the future as coal resources are utilized.

Our data analysis was initially directed toward characterizing the current regional visibility (visual range) in the Northern Great Plains.

We began by conducting a telephone survey of NWS stations in the Northern Great Plains that report visual range. Such stations measure visual range by observing distant markers and reporting the distance to the farthest marker (e.g., building, TV tower, hill, mountain) that is visible at the time the observation is made. It is essential that several markers be used so that visibility can be determined with some degree of precision. For example, if an observation station had only one visibility marker at 5 km, the observer could report only whether or not the marker was visible; if it was, the visibility could nevertheless be 5, 10, 50, 100, or more km. Conversely, if the marker was not visible, the visibility could be 1, 2, 4, or even 4.9 km. Even if several markers were used and the farthest marker were observed most of the time, only the worst visibilities could be characterized well and no information could be provided about the visibility during most of the observations. This last situation appears to be the case for the Northern Great Plains.

Table A-1 lists the NWS stations in the Northern Great Plains that provided information regarding visibility observations. The visibility data available from four of the NWS stations (Billings, Great Falls, Cheyenne, Rock Springs) were ordered through the National Climatic Center. At most of the stations in the flat terrain areas of North Dakota, South Dakota, and Nebraska, the farthest visibility markers are located 40 km or less from the station. Generally, the meteorologists at these stations reported that they saw the farthest marker more than 90 percent of the time and that natural causes (e.g., precipitation, fog, windblown sand, and snow) accounted for virtually all of the reduction in visibility.

TABLE A-1. DISTANCE TO THE FARTHEST VISUAL RANGE MARKERS AT NWS STATIONS IN THE NORTHERN GREAT PLAINS

Station Location	Distance to Farthest Markers (km)
Montana	
Billings*	97
Great Falls*	121
Helena	64
North Dakota	
Bismarck	20
Fargo	32
Grand Forks	16
Williston	40
South Dakota	
Aberdeen	56
Huron	48
Rapid City	56
Sioux Falls	18
Nebraska	
Chadron	24
Grand Island	31
Lincoln	32
Norfolk	7
North Platte	12
Omaha	24
Scottsbluff	40
Valentine	19
Wyoming	
Casper	97
Cheyenne*	145
Lander	113
Rawling	97
Rock Springs*	177
Sheridan	48

---

* NWS data ordered.

Visibility markers more than 56 km from the station are almost always terrain features, such as mountains, ridges, and buttes. The distant visibility markers in Billings and Great Falls, Montana, are the mountains in northwestern Montana; the distant markers in Cheyenne and Rock Springs are the mountain peaks of the Rockies in Wyoming. In flat terrain, the distant markers are generally television towers or buildings within about 55 km. Thus, in flat terrain, where pollutant transport and diffusion are easiest to predict, available visibility data do not fully characterize the magnitude and variations in visibility. In complex terrain areas, where pollutant transport and diffusion is complicated by drainage flows and terrain-channeled winds, visibility is better characterized by NWS data. Thus, the availability of NWS data that is useful in characterizing the full range of visibility was one reason for selecting the Southwest rather than the Northern Great Plains as the study region to investigate the causes of visibility degradation and the meteorological conditions that influence regional visibility.

3. SELECTION OF THE SOUTHWEST FOR DATA ANALYSIS

The Southwest has several unique characteristics that make it a valuable region to study:

> It has several NWS stations at which long range visibility observations are made.

> Additional visibility data are available from the National Park Service, NOAA, and from monitoring programs conducted for industrial developments.

> Copper smelters there emit large quantities of SO_2. Coal-fired power plants there emit large quantities of fly ash, sulfur dioxide, and nitrogen oxides.

> It is in the prevailing downwind direction from a major urban region (southern California), and it contains several large urban areas (e.g., Las Vegas, Phoenix, and Tucson) in an otherwise nonurban region.

- It contains a large number of national parks, national forests, wilderness areas, and other Class I areas that have been tentatively designated by the Department of the Interior as areas where visibility is important and should be protected.
- Major energy developments are planned for the area.

Figure A-2 is a map of the western United States showing the locations of NWS stations that have produced visibility data acceptable for the study of meteorological and anthropogenic visibility impairment. These data have been obtained from the National Climatic Center. As noted above, the visibility data available in many locations in the Northern Great Plains are of limited value because the most distant visibility markers are less than 56 km away. However, all of the 20 NWS stations shown in Figure A-2 use visibility markers farther than 64 km, thus making the data of much greater value in characterizing the frequency distribution of visibility. As Figure A-2 indicates, the region including Arizona, New Mexico, Utah, Colorado, the southern portion of Wyoming, and the eastern portion of Nevada is relatively well covered by available visibility data. Because the NWS visibility observations are made at three-hour intervals and because data are available for the period of January 1948 through December 1976, excellent documentation of the temporal as well as the spatial distribution of visibility in the Southwest is available.

The NWS visibility data are supplemented by additional visibility observations made since January 1976 by the National Park Service at 12 locations in southern Utah, northern Arizona, and southwestern Colorado. Each visibility observation is a measurement not only of the local atmosphere, but of the atmosphere between the observer and the farthest visible marker as well. Because visibility in the Southwest is commonly greater than 100 km, the visibility observation stations in the region form a comprehensive network for measuring the aerosol concentration (scattering coefficient) of the atmosphere of the Southwest.

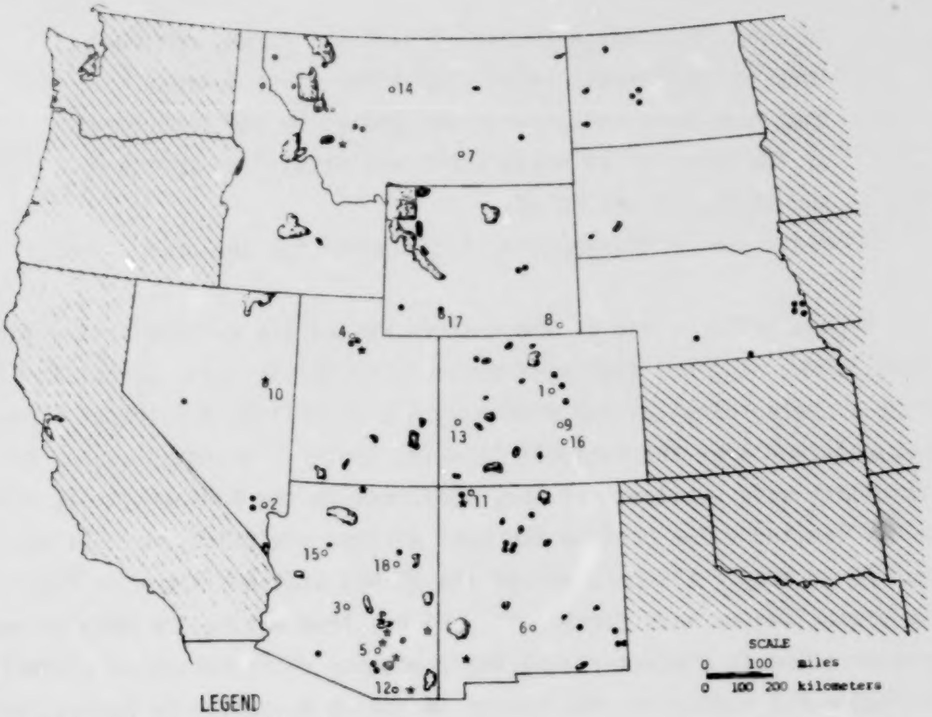

LEGEND

▭ MANDATORY FEDERAL CLASS I AREAS WHERE VISIBILITY IS IMPORTANT.

▨ STATES NOT INCLUDED IN REGIONAL STUDY.

○ NWS STATIONS WHERE VISIBILITY OBSERVATIONS ARE TAKEN.

● POINT SOURCES EMITTING MORE THAN 20 TONS PER DAY OF SO_x OR NO_x OR 10 TONS PER DAY OF PARTICULATE MATTER.

★ POINT SOURCES EMITTING MORE THAN 200 TONS PER DAY OF SO_x.

NWS WEATHER STATIONS

URBAN LOCATIONS

1. DENVER, CO
2. LAS VEGAS, NV
3. PHOENIX, AZ
4. SALT LAKE CITY, UT
5. TUCSON, AZ

NONURBAN LOCATIONS

6. ALAMOGORDO, NM
7. BILLINGS, MT
8. CHEYENNE, WY
9. COLORADO SPRINGS, CO
10. ELY, NV
11. FARMINGTON, NM
12. FT. HUACHUCA, AZ
13. GRAND JUNCTION, CO
14. GREAT FALLS, MT
15. PRESCOTT, AZ
16. PUEBLO, CO
17. ROCK SPRINGS, WY
18. WINSLOW, AZ

FIGURE A-2. MAP OF THE WESTERN UNITED STATES SHOWING THE LOCATIONS OF LARGE POINT SOURCES, MANDATORY FEDERAL CLASS I AREAS, AND NWS STATIONS WHERE VISIBILITY OBSERVATIONS ARE MADE

The Southwest is also of interest because of the nature and spatial and temporal distribution of pollutant emissions. One unique feature is that although most of the region is unpopulated and does not contain anthropogenic sources of air pollutants, large quantities of pollutants are emitted from relatively small areas within the region. Figure A-3 shows only four air quality control regions (AQCRs) in the western United States having emissions of particulate matter, sulfur dioxide, nitrogen oxides, or hydrocarbons in excess of 300,000 tons in 1973. The San Francisco Bay Area emitted 420,000 tons of hydrocarbons and 284,000 tons of nitrogen oxides; metropolitan Los Angeles emitted 1,065,000 tons of hydrocarbons, 646,000 tons of nitrogen oxides, and 257,000 tons of sulfur dioxide; copper smelters in southeastern Arizona and southwestern New Mexico emitted 2,191,000 tons of sulfur dioxide; and the Amarillo, Texas, area emitted 369,000 tons of hydrocarbons. The copper smelters in southeastern Arizona and southwestern New Mexico contributed 44 percent of the SO_2 emissions of the entire western United States and 81 percent of the SO_2 emissions of a four-state region of Arizona, New Mexico, Utah, and Colorado in 1973.

Table A-2 lists the pollutant emissions in the western United States in 1973 by state and pollutant category (EPA, 1976a). Emissions from California and Arizona dominate those of other states. Identification of the causes of visibility degradation in the Southwest is simplified by the existence of relatively small, localized areas that contain sources of large pollutant emissions. Figure A-4 shows the directional distribution of emissions within a 1400 km radius of a location in south central Utah, weighted by the reciprocal of the distance. It is clear from the figure that SO_2 emissions sources (copper smelters) are principally to the south-southeast of this location and that few other pollutants are emitted from that direction. Similarly, from the west-southwest a large source (metropolitan Los Angeles) emits hydrocarbons and nitrogen oxides. To the east of this location (in Oklahoma and Texas) are large emitters of hydrocarbons and nitrogen oxides. Emissions from the Salt Lake City area cause the small peak to the north-northwest of this location.

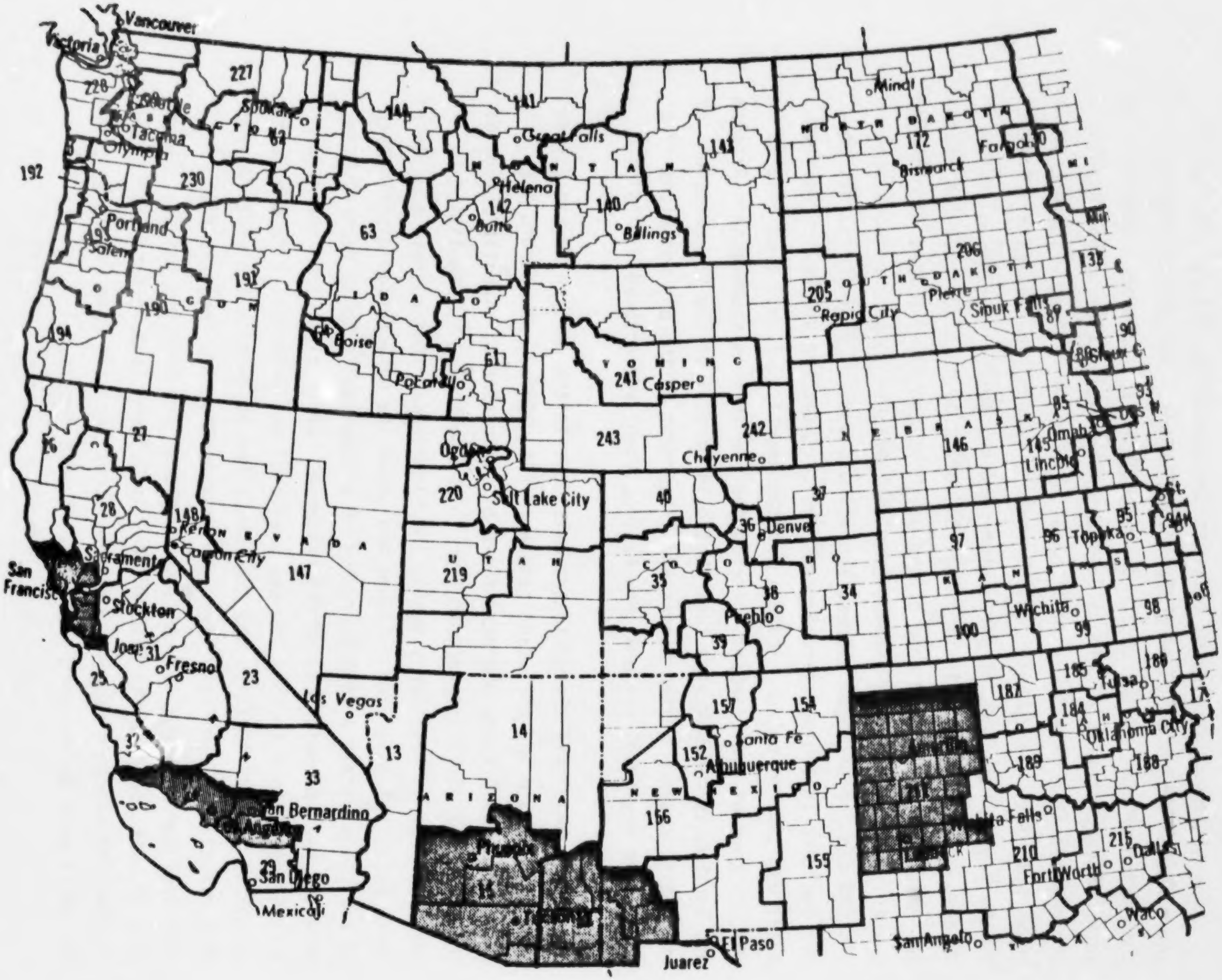
Vancouver
Victoria
Seattle
Tacoma
Olympia
Portland
Salem
Spokane
Boise
Pocatello
Helena
Butte
Great Falls
Billings
Casper
Cheyenne
Minot
Bismarck
Fargo
Pierre
Rapid City
Sioux Falls
Omaha
Lincoln
Topeka
Wichita
Tulsa
Oklahoma City
Wichita Falls
Fort Worth
Dallas
Waco
San Angelo
El Paso
Juarez
Denver
Pueblo
Santa Fe
Albuquerque
Ogden
Salt Lake City
Reno
Carson City
Las Vegas
Sacramento
San Francisco
Stockton
Fresno
San Bernardino
Los Angeles
San Diego
Mexicali
227
228
230
192
191
190
194
62
63
141
142
143
144
140
61
241
242
243
172
130
205
206
139
90
85
93
145
146
95
96
97
98
99
100
185
184
186
187
188
189
210
215
36
37
38
39
40
34
35
157
154
152
156
155
220
219
147
148
14
13
33
29
23
31
32
25
28
27
26

FIGURE A-3. AQCRs IN THE WEST WHOSE EMISSIONS OF TSP, SO_2, NO_x OR HYDROCARBONS EXCEEDED 300,000 TONS IN 1973

TABLE A-2. POLLUTANT EMISSIONS IN THE WESTERN STATES

(10^3 tons per year)

(a) Ranking of Western States by Particulate Emissions

Rank	State	1973 Emissions
1	California	535
2	Nebraska	301
3	Colorado	232
4	Kansas	214
5	Washington	184
6	Oregon	148
7	Montana	134
8	New Mexico	132
9	Arizona	123
10	Nevada	119
11	Wyoming	87
12	North Dakota	85
13	Utah	81
14	Idaho	75
15	South Dakota	60

(b) Ranking of Western States by SO_x Emissions

Rank	State	1973 Emissions
1	Arizona	2052
2	California	540
3	New Mexico	426
4	Washington	350
5	Nevada	342
6	Utah	183
7	Montana	132
8	Kansas	97
9	North Dakota	80
10	Wyoming	70
11	Idaho	56
12	Nebraska	55
13	Colorado	48
14	Oregon	42
15	South Dakota	15

TABLE A-2 (Concluded)

(c) Ranking of Western States by NO_x Emissions

Rank	State	1973 Emissions
1	California	1371
2	Washington	349
3	Kansas	303
4	New Mexico	220
5	Oregon	198
6	Colorado	185
7	Nebraska	174
8	Arizona	169
9	Nevada	141
10	Montana	113
11	Utah	108
12	Wyoming	102
13	North Dakota	98
14	Idaho	78
15	South Dakota	53

(d) Ranking of Western States by Hydrocarbon Emissions

Rank	State	1973 Emissions
1	California	2115
2	Nebraska	379
3	Washington	337
4	Kansas	337
5	Oregon	290
6	Arizona	242
7	Colorado	225
8	Montana	198
9	New Mexico	143
10	Idaho	119
11	Utah	103
12	South Dakota	85
13	North Dakota	72
14	Wyoming	68
15	Nevada	53

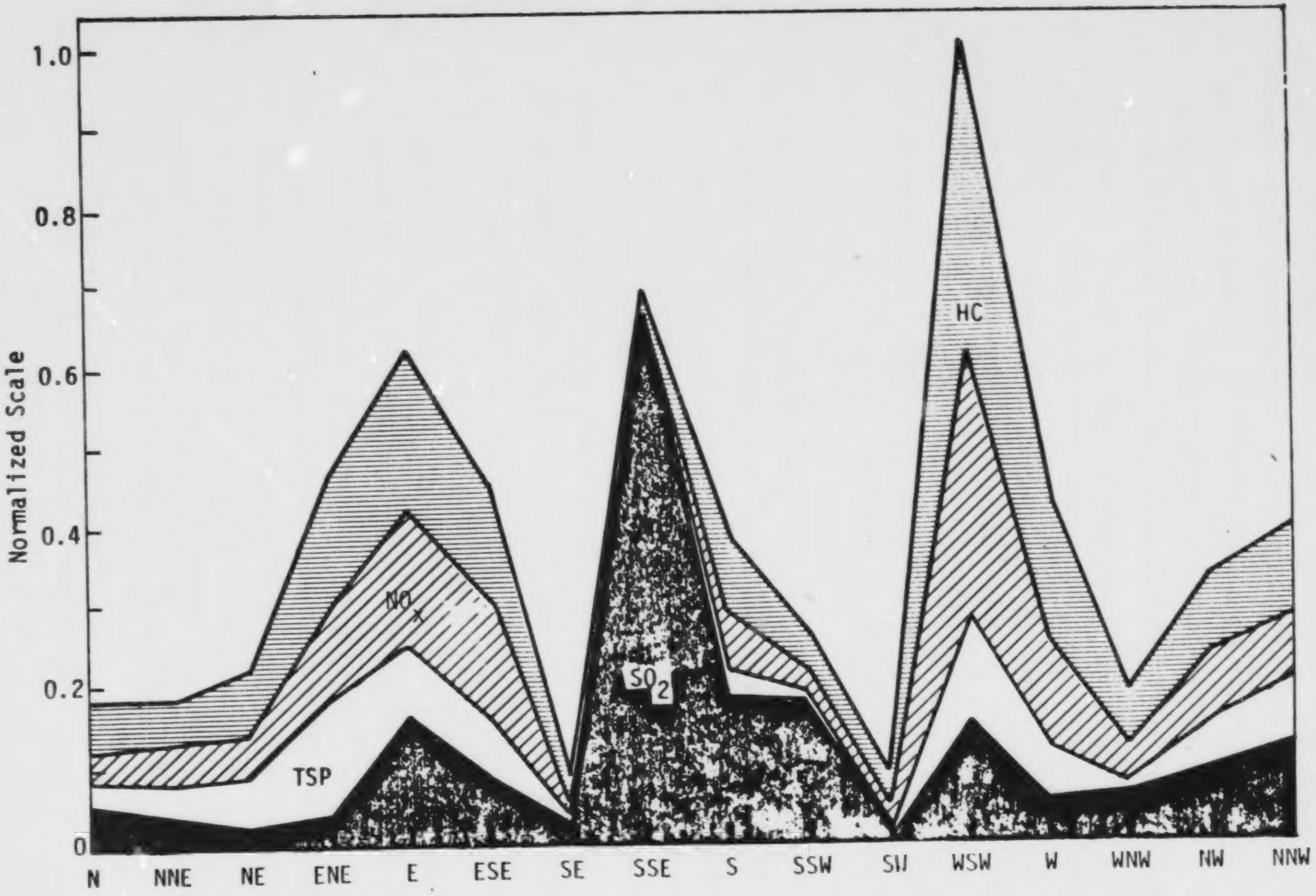

Source: Based on data from EPA (1976a).

FIGURE A-4. DISTRIBUTION OF POLLUTION EMISSIONS WITHIN A 1400 km RADIUS OF A LOCATION IN SOUTH CENTRAL UTAH WEIGHTED BY THE RECIPROCAL OF THE DISTANCE

It is clear from this figure that the pollutant concentration in an air parcel in the Southwest is expected to be a strong function of the trajectory of the air parcel. If the parcel is transported from polluted areas, such as Los Angeles* or Tucson-Phoenix, it is reasonable to expect higher pollutant concentrations (and scattering coefficients) than those for an air parcel transported over the clean, undeveloped areas of the Southwest. As a corollary, if air is stagnant over pollution sources, a buildup of pollutant concentrations can be expected; however, if air is stagnant over clean, nonurban areas, the air can be expected to remain clean (or become cleaner as pollutants are removed from the air by natural processes). As is pointed out below, the concentrated and localized distribution of pollutant emissions sources should be helpful in determining the causes of visibility reduction in the West.

Temporal as well as spatial variations in emissions are noteworthy in the West. For example, emissions of hydrocarbons, nitrogen oxides, and sulfur dioxide have been reduced significantly over the last few years in Los Angeles County (LACAPCD, 1971). Sulfur dioxide emissions from copper smelters in Arizona were reduced by a factor of 2 in the period 1972 through 1976. If visibility in remote areas of the Southwest is affected by anthropogenic sources of air pollution, then variations in visibility can be expected to result from changes in such emissions.

The Southwest is also of interest because of the large coal-fired power plants currently in operation, undergoing construction, or being planned for the region. Since the beginning of its operation in the 1960s, the Four Corners power plant near Farmington, New Mexico, has become a symbol of human impact on visibility in the Southwest because of the plant's high particulate emissions rate. Newer power plants (e.g., the Navajo plant) have benefited from better particulate control technology that reduce particulate emissions to the point where plumes are almost clear; however, modern coal-fired plants emit larger quantities of sulfur dioxide and nitrogen oxides, which have the potential for causing visual impacts. Table A-3 lists the coal-fired power plants in the Southwest currently in operation (indicated by an asterisk) and those being planned. Although the coal-fired power plants emit sulfur dioxide, current copper smelter SO_2 emissions are considerably larger than current power plant SO_2 emissions.

---

*There are severe topographical restrictions on the transport of pollutants out of the Los Angeles basin. Hence, although we do not mean to imply that there is significant evidence for transport from this area, we do not rule out the possibility of transport.

4. THE DATA ANALYSIS

This section reviews the preliminary analysis of the visibility data for the period 1948 through 1976 from eight NWS stations in the Southwest. The data were gathered from the following stations:

Station	Period
Ft. Huachuca, AZ	10/54 - 07/71
Alamogordo, NM	01/49 - 12/70
Denver, CO	01/48 - 12/76
Grand Junction, CO	01/48 - 12/76
Farmington, NM	01/49 - 12/76
Ely, NV	01/55 - 12/76
Tucson, AZ	10/48 - 12/76
Las Vegas, NV	12/48 - 12/76
Phoenix, AZ	01/48 - 12/76
Prescott, AZ	01/48 - 12/76
Winslow, AZ	01/48 - 12/76
Rock Springs, WY	01/48 - 12/76
Wendover, UT	03/50 - 12/76
Billings, MT	01/48 - 12/76
Cheyenne, WY	01/48 - 12/76
Dugway, UT	12/49 - 12/70
Salt Lake City, UT	01/48 - 12/76
Great Falls, MT	01/48 - 12/76
Colorado Springs, CO	07/48 - 12/76
Pueblo, CO	07/54 - 12/76

TABLE A-3. COAL-FIRED POWER PLANTS IN THE SOUTHWEST

State	Name of Power Plant	Location	Capacity (MW)
Arizona	Cholla*	Joseph City	620
	Coronado	St. Johns	1050
	Navajo*	Page	2409
	Springerville	Springerville	312
Colorado	Arapaho*	Denver	250
	Cherokee*	Denver	801
	Commanche*	Pueblo	700
	Drake*	Colorado Springs	288
	Hayden*	Hayden	430
	Valmont*	Boulder	282
	Craig	Craig	1520
	--	Rangely	250
	Pawnee	Ft. Morgan	1000
	Southeastern	--	1000
	R. D. Nixon	Fountain	400
	Rawhide	Wellington	200
Nevada	Harry Allen	Las Vegas	2000
	Mohave*	Bullhead City	1582
	Reid Gardner*	Moapa	500
New Mexico	Four Corners*	Farmington	2175
	San Juan*	Waterflow	1588
Utah	Carbon*	Castle Gate	166
	Emery	Castledale	830
	Gadsby*	Salt Lake City	246
	Garfield	Escalante	2000
	Huntington Canyon*	Huntington	860
	Intermountain Power Project	Factory Butte	3000
	Nephi	Nephi	500
	Warner Valley	St. George	500
Wyoming	Naughton*	Kemmerer	710†
	Jim Bridger*	Rock Springs	2000
	Dave Johnston*	Glenrock	750
	Laramie River	Wheatland	1500

---

* Power plant currently in operation.

† An additional capacity of 830 MW is planned.

The visual range and the following meteorological data from these stations were recorded at three-hour intervals:

- Wind direction
- Wind speed
- Temperature
- Relative humidity
- Atmospheric pressure (corrected to sea level)
- Total sky cover
- Ceiling height
- Occurrence of precipitation, fog, or smoke

In addition to the 29-year record of surface meteorological data, we obtained five years of upper air data used by Holzworth (1972) in his mixing depth study of the United States. From these data, the following parameters were obtained for the five-year period 1960 through 1964:

- Average wind speed in the mixed layer
- Mixing depth
- Ventilation.

Thus we have a large visibility and meteorological data base with which to determine the dependence of visibility on various meteorologocal conditions. Table A-4 summarizes the sorting of the data from the 18 NWS stations in the West.

Of the meteorological conditions that cause or contribute to a reduction in visual range, precipitation is clearly one natural cause having a significant impact. Figure A-5 illustrates that at Winslow, Arizona, which is representative of other locations in the Southwest, precipitation significantly reduces visibility. Visibility during periods of precipitation is greater than 40 km less than 20 percent of the time, whereas visibility during periods without precipitation is greater than 40 km more than 80 percent of the time. At Winslow, Arizona, precipitation was reported to occur only 2.2 percent of the daylight hours; thus precipitation has a small effect on the overall frequency distribution of visual range there.

TABLE A-4. SUMMARY OF DATA SORTING

Time Period	Independent Variable
Yearly	Year
1960-1964	Mixing height
	Mixing layer wind speed
	Ventilation
1948-1956	Precipitation
1957-1966	Surface wind speed
1967-1976	Surface wind direction
	Atmospheric pressure
	Relative humidity
	Total sky cover
	Season
	Time of day

Fog is another natural cause of reduced visibility. At Winslow, fog occurs 0.3 percent of the time and always reduces visibility to less than 10 km.

In subsequent data sortings, only the days without precipitation or fog were used to calculate the frequency distribution of visual range as a function of various parameters, thus eliminating the variability that might occur by comparing "wet" years with "dry" years. However, since the percentage of total daytime observations with precipitation is small (2 percent) in the West, the frequency distributions would not have been changed much by including them with the "no precipitation or fog" values.

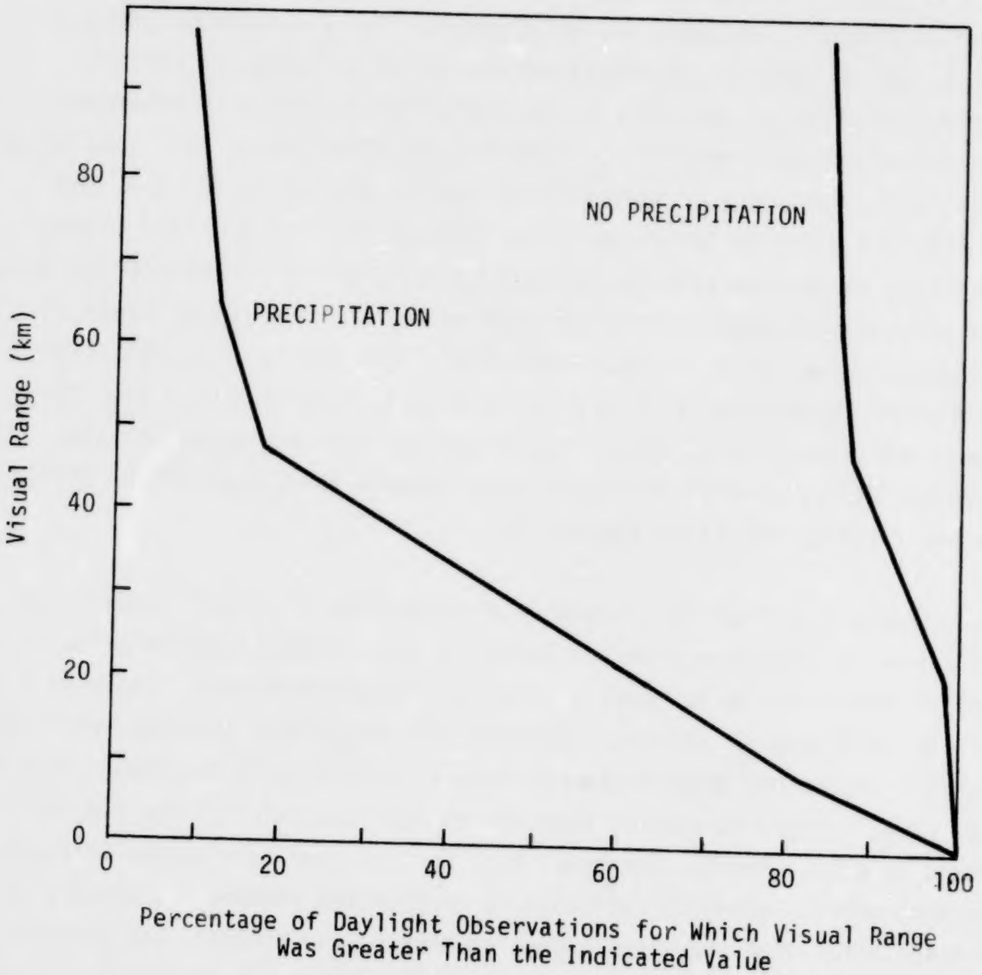

FIGURE A-5. EFFECT OF PRECIPITATION ON VISUAL RANGE AT WINSLOW, ARIZONA, 1967-1976

5. THE FREQUENCY DISTRIBUTION OF VISUAL RANGE IN THE WEST

Because of the nature of the NWS visual range observations, the data must be carefully analyzed and interpreted. The visual range "measurements" can be taken by observing whether or not a series of distant markers is visible, and therefore the data can be used only to answer questions such as: What is the frequency of visual range less than 64 km? What is the frequency of visual range greater than 64 km but less than 97 km? How often is the visual range greater than 121 km? The record of visual range observations can best be analyzed and interpreted by using the cumulative frequency of occurrence of visual range greater than an indicated value (or extinction coefficient less than a given value) as an indicator. A location with high visibility is suggested by a high frequency of occurrence of visual ranges greater than an indicated value. The frequency of occurrence of visual range between two ranges can be obtained by subtracting cumulative frequencies.

Figure A-6 shows the frequency distributions of visual range in 13 locations in the western United States on days without precipitation or fog in 1976 based on National Weather Service observations. The data points (indicated by circles) represent the cumulative frequency with which markers at the indicated distances were visible at each location. Note that the visual range was greater than 120 km more than half of the time at Grand Junction, Pueblo, Cheyenne, Rock Springs, and Farmington. Although distant markers were not available to confirm the finding, it appears by extrapolation that the visual range at Winslow and Prescott was greater than 120 km more than half of the time. The median (50 percentile) visual ranges in the urban areas of the West (Salt Lake City, Phoenix, Denver, Tucson, and Las Vegas) were considerably less than the nonurban visual ranges. The highest visual ranges were observed in Grand Junction, Colorado, where the most distant visibility marker at 145 km (90 miles) was visible more than 51 percent of the time.

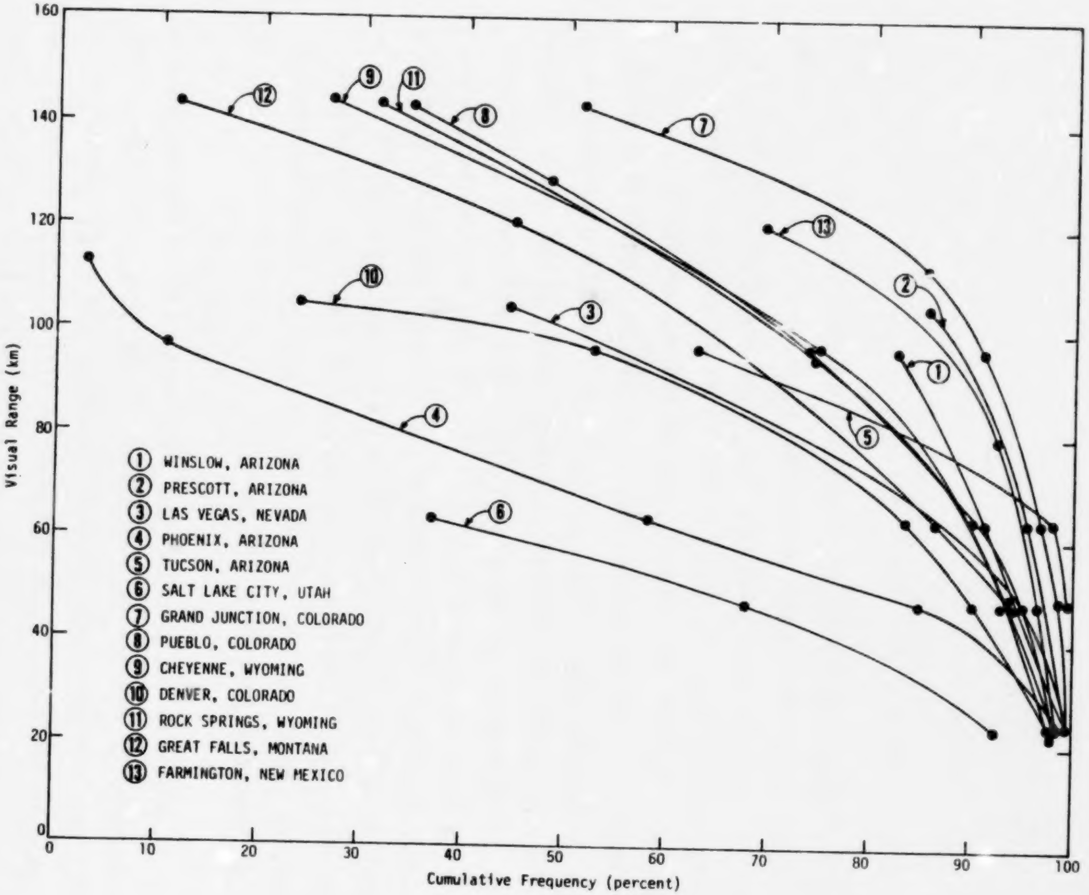

FIGURE A-6. FREQUENCY DISTRIBUTIONS OF VISUAL RANGE AT 13 WESTERN U.S. LOCATIONS ON DAYS WITHOUT PRECIPITATION OR FOG IN 1976

A better understanding of the causes of visibility impairment and the frequency distribution of visual range can be obtained by plotting the cumulative frequency of the extinction coefficient calculated from the visual range by using the Koschmieder relationship:

$$r_v = \frac{3.912}{b_{ext}} \quad ,$$

$$b_{ext} = b_R + b_{sp} + b_{abs} \quad .$$

Figure A-7 shows the frequency distributions for 13 western locations. The upper bound on visual range (and the lower bound on extinction coefficient) is suggested more strongly in Figure A-7 than in Figure A-6. The extinction coefficients at nonurban NWS sites in the West appear to be approaching $0.2 \times 10^{-4}\ m^{-1}$ (a visual range of 196 km, or 122 mi) as an asymptote. This value of the extinction coefficient is more than twice the Rayleigh scattering coefficient (at 0.55 μm). If the atmosphere were completely free of particles, the visual range would be 390 km or greater depending on the elevation of the site (atmospheric pressure). Further evidence that a lower bound of $0.2 \times 10^{-4}\ m^{-1}$ for the extinction coefficient is representative is indicated by the data collected by Roberts et al. (1975) in the Petrified Forest of Arizona (see Figure A-8). A median extinction coefficient between roughly $0.3 \times 10^{-4}\ m^{-1}$ (a visual range of 130 km) and $0.4 \times 10^{-4}\ m^{-1}$ (a visual range of 98 km) appears to be typical of nonurban locations in the West.

It is instructive to consider the contribution of different atmospheric components to the median extinction coefficient. Consider, for example, the measured pollutant concentrations at the Grand Canyon in 1974, as shown in Table A-5. We computed scattering coefficients per unit mass of sulfate, nitrate, and coarse mode particulate (TSP - $[SO_4^=]$ - $[NO_3^-]$) using the "clean continental background" particle size distributions reported by Whitby and Sverdrup (1978), and we multiplied these coefficients by the measured pollutant concentrations to estimate the median

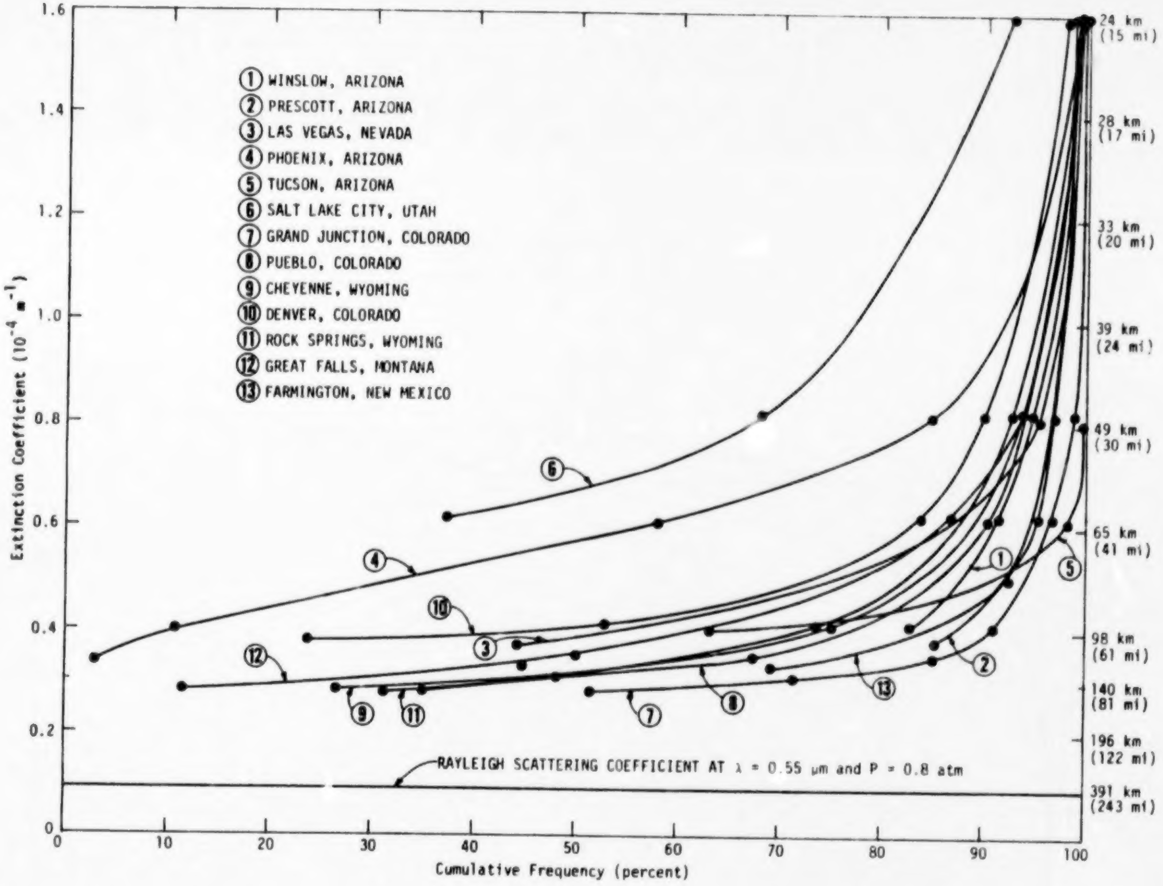

FIGURE A-7. FREQUENCY DISTRIBUTIONS OF EXTINCTION COEFFICIENTS BASED ON VISUAL RANGE OBSERVATIONS AT 13 WESTERN U.S. LOCATIONS ON DAYS WITHOUT PRECIPITATION OR FOG IN 1976

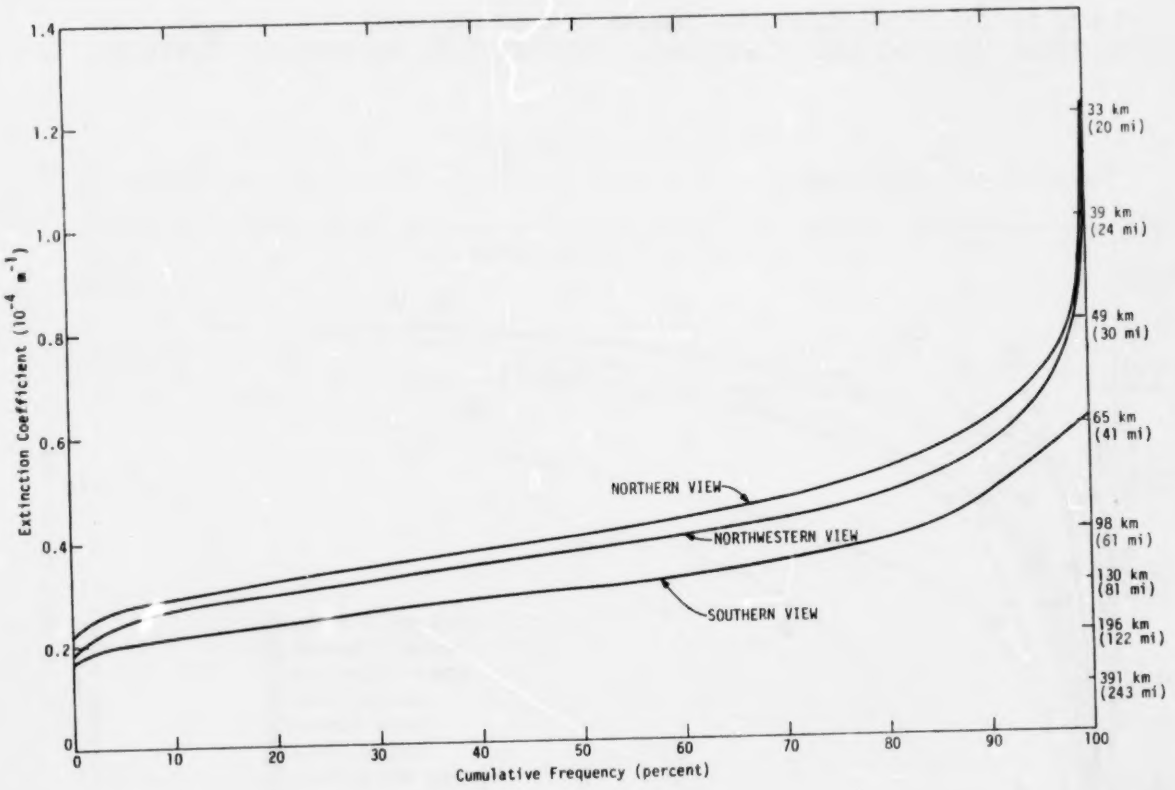

FIGURE A-8. FREQUENCY DISTRIBUTIONS OF EXTINCTION COEFFICIENTS BASED ON PHOTOGRAPHIC PHOTOMETRY IN THE PETRIFIED FOREST, ARIZONA, IN 1973 AND 1974 extinction coefficient for the Grand Canyon. We obtained a mediam extinction coefficient of $0.26 \times 10^{-4}\ m^{-1}$, which corresponds to a visual range of 150 km. The median sulfate concentration of 1.9 $\mu g/m^3$ accounts for 41 percent of the total extinction, nitrate for 9 percent, and coarse mode particles for 19 percent. The rest of the extinction is due to the molecules of air (Rayleigh scattering) at an elevation of 7000 ft msl (2100 msl).

TABLE A-5. COMPONENTS OF AVERAGE LIGHT SCATTERING AT THE GRAND CANYON IN 1974

Component	Concentration ($\mu g/m^3$)	b_{scat}/Mass ($10^{-4}\ m^{-1}/\mu g/m^3$)	b_{scat} ($10^{-4}\ m^{-1}$)	Percentage of Total
Pure air	--	--	0.080	31%
Sulfate	1.9	0.056	0.106	41
Nitrate	0.4	0.056	0.022	9
Coarse mode	16	0.003	0.048	19
Total			0.256	100%

It is also instructive to compute the extinction coefficient for 1 November 1974 in the Grand Canyon when measured pollutant concentrations were lowest for that year ($[SO_4^=] = 0.3\ \mu g/m^3$; $[NO_3^-] = 0.1\ \mu g/m^3$; TSP = 5 $\mu g/m^3$). On that day the computed extinction coefficient was $0.12 \times 10^4\ m^{-1}$, which corresponds to a visual range of more than 330 km (200 mi).

Figure A-9 shows the frequency distributions of extinction coefficients calculated from visual range observations at 8 National Park Service (NPS) sites in the Southwest in 1976. Because the most distant markers at these sites are visible more than 60 percent of the time, it is difficult to extrapolate to the cleanest conditions; however, the shapes of the NPS curves suggest that the air in national parks in the Southwest is cleaner

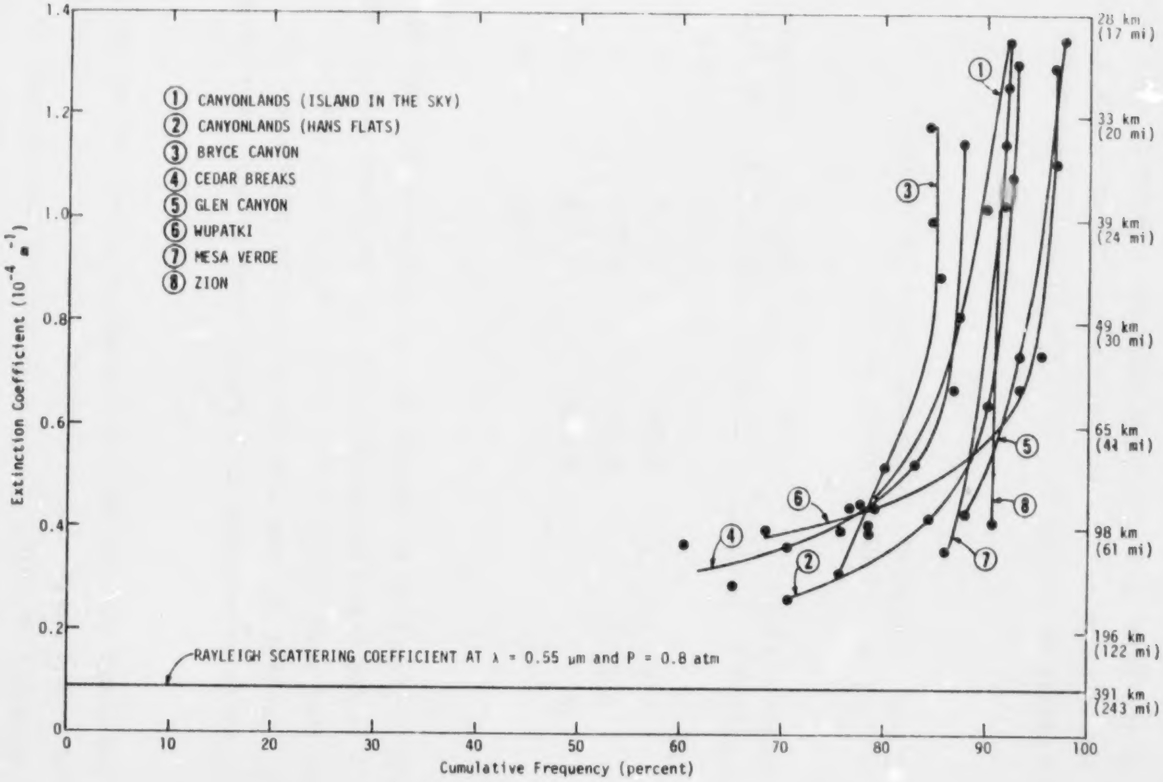

FIGURE A-9. FREQUENCY DISTRIBUTION OF EXTINCTION COEFFICIENTS BASED ON VISUAL RANGE OBSERVATIONS AT 8 NATIONAL PARK SERVICE SITES IN THE SOUTHWEST IN 1976 than that of the nonurban NWS sites. The calculated extinction coefficient for the clean day at the Grand Canyon noted above also suggests this conclusion. Indeed, Charlson (1978) reported b_{sp} measurements in Bryce Canyon on the order of 0.02×10^{-4} m^{-1} (giving a total extinction coefficient, including Rayleigh scattering, of 0.1×10^{-4} m^{-1}).

A word of caution is advisable here. The visibility of distant markers is essentially an indication of the pollutant concentration (aerosol) integrated along the given sight path. Visual range estimates based on point measurements (pollutant concentrations, nephelometry) may therefore give different results from spatially integrated measurements (observations of distant markers, telephotometry, photographic photometry) if the ground-level ambient conditions at a given location are different from those for the spatial average. Such differences could easily result from greater coarse particulates near ground level, decreased or increased relative humidity near ground level as a result of different lapse rates, and decreased aerosol concentrations due to surface deposition. Also, if there are significant inhomogeneities in the atmosphere aerosol because of the presence of plumes, a point measurement will not be representative of the spatial average.

Figures A-7, A-8, and A-9 suggest that most of the time in nonurban areas in the West extinction coefficients are extremely low, a condition characteristic of clean, background continental air with background sulfate concentrations of 1 to 2 $\mu g/m^3$. At times, however, extinction coefficients can be considerably higher. Higher extinction coefficients and reduced visual range at nonurban areas appear to result primarily from the hygroscopic growth of aerosol particles at relative humidities approaching 100 percent. This topic is discussed further in Section 7.

6. YEARLY TRENDS IN VISUAL RANGE

Figures A-10 through A-27 show the yearly trends in visual range at the 18 NWS sites in the West during the period from 1948 through 1976.

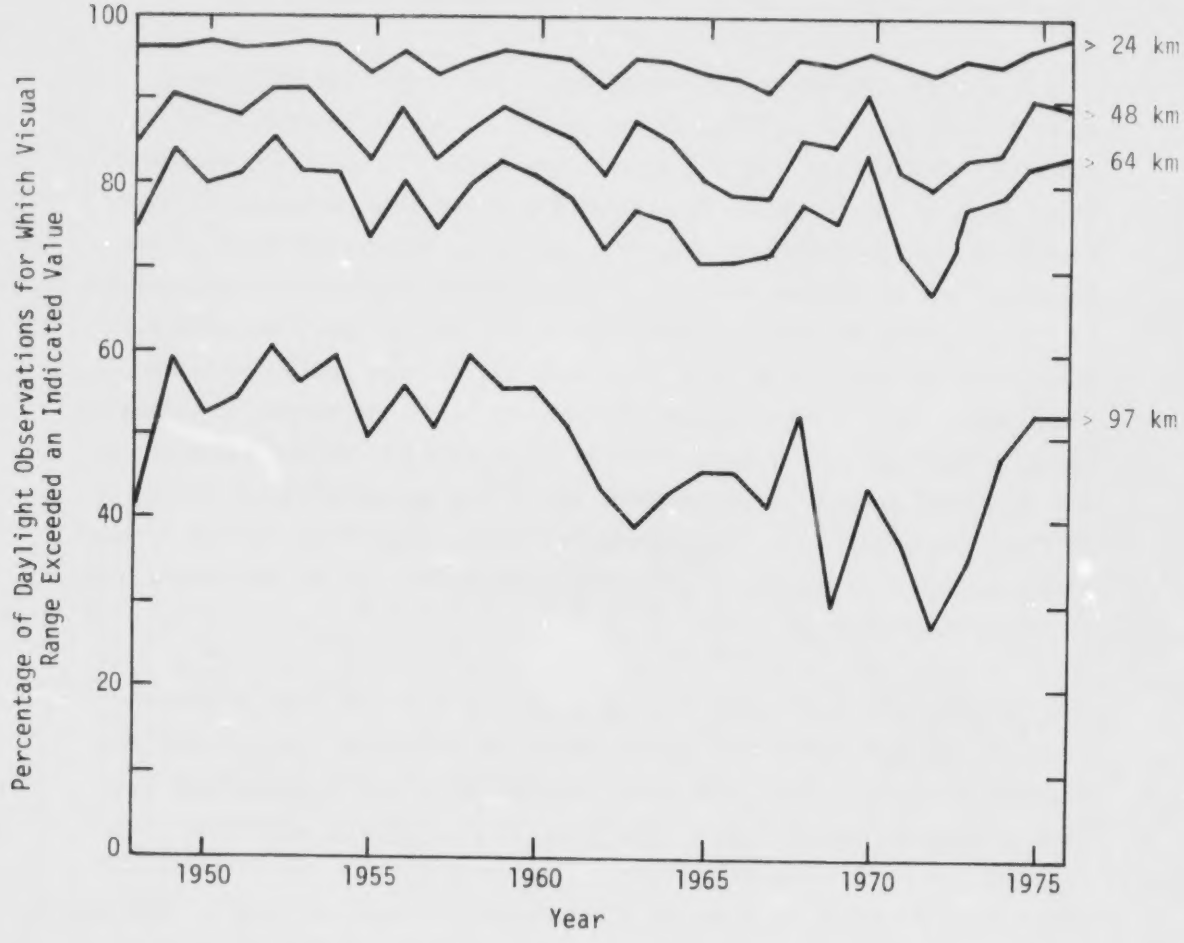

FIGURE A-10. PERCENTAGE OF DAYLIGHT OBSERVATIONS FOR WHICH VISUAL RANGE EXCEEDED AN INDICATED VALUE, AS A FUNCTION OF YEAR, IN DENVER, COLORADO, 1948-1976

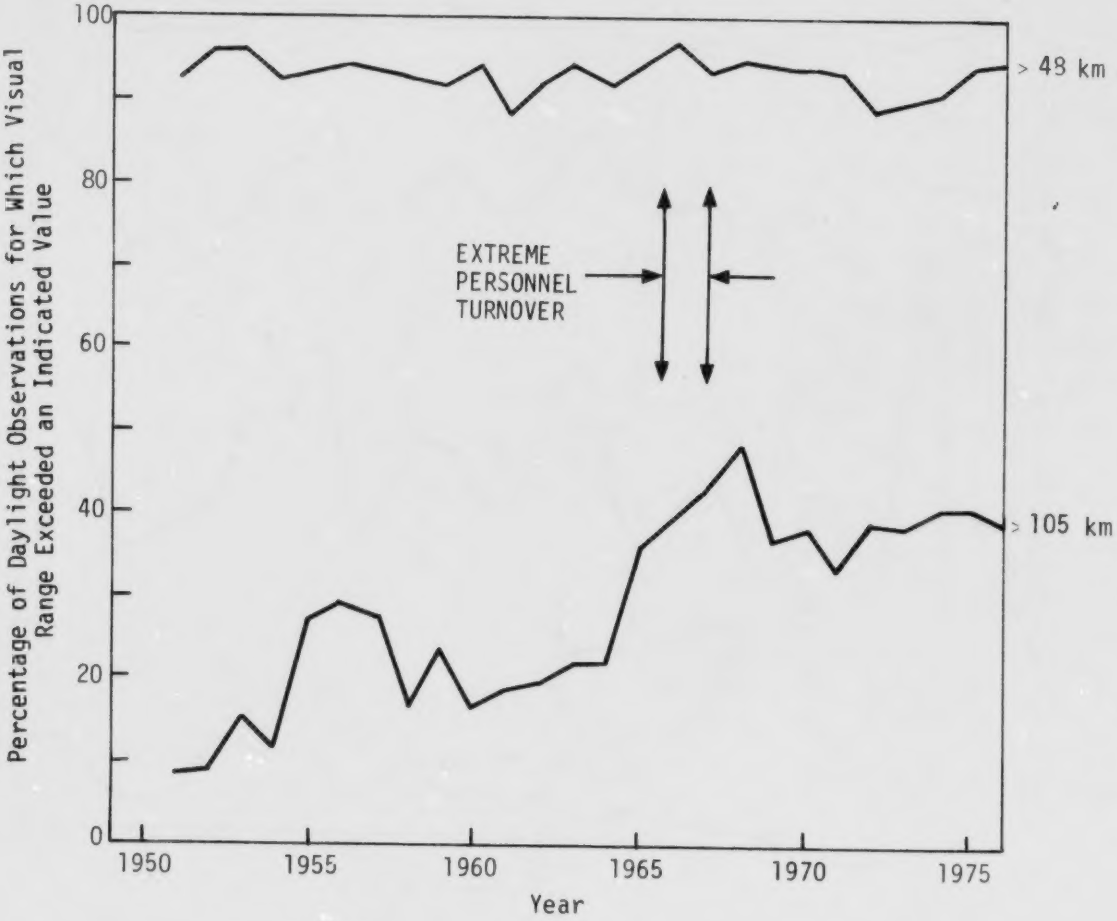

FIGURE A-11. PERCENTAGE OF DAYLIGHT OBSERVATIONS FOR WHICH VISUAL RANGE EXCEEDED AN INDICATED VALUE, AS A FUNCTION OF YEAR, IN LAS VEGAS, NEVADA, 1951-1976

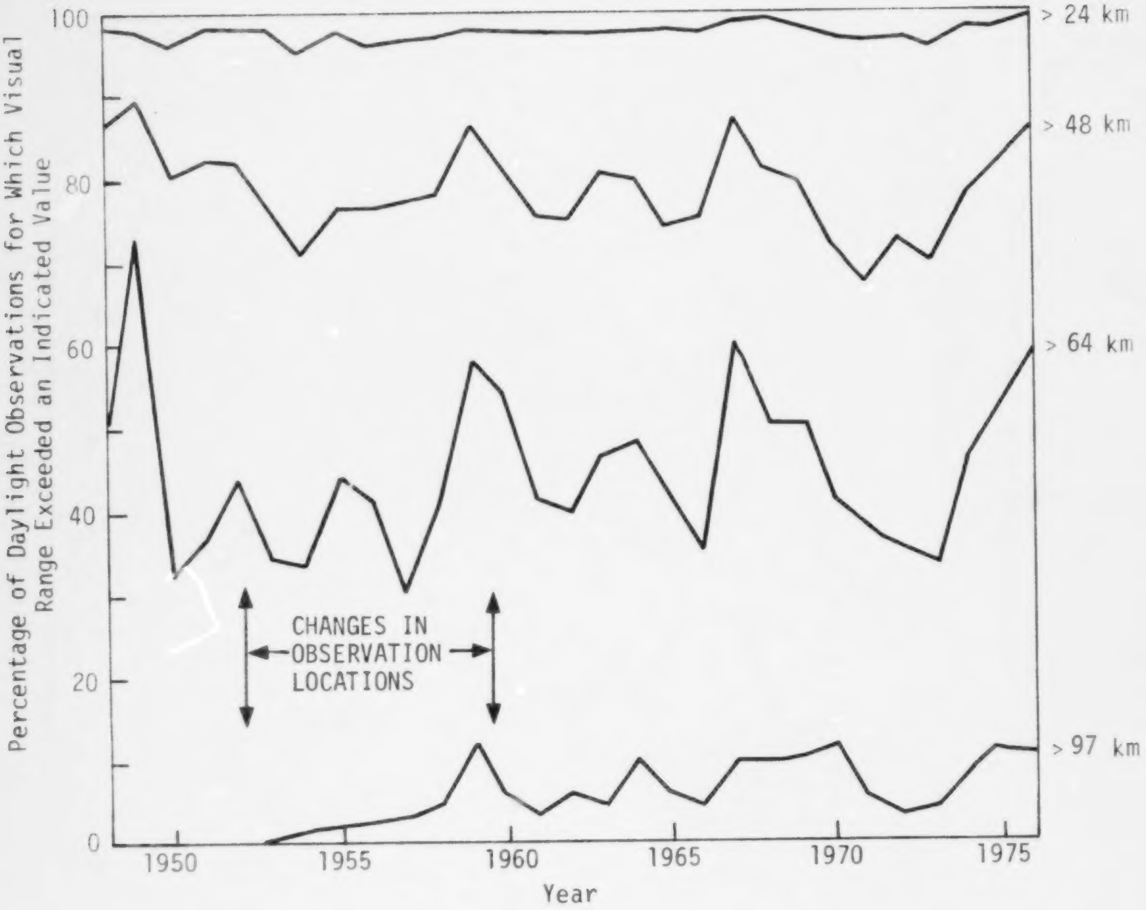

FIGURES A-12. PERCENTAGE OF DAYLIGHT OBSERVATIONS FOR WHICH VISUAL RANGE EXCEEDED AN INDICATED VALUE, AS A FUNCTION OF YEAR, IN PHOENIX, ARIZONA, 1948-1976

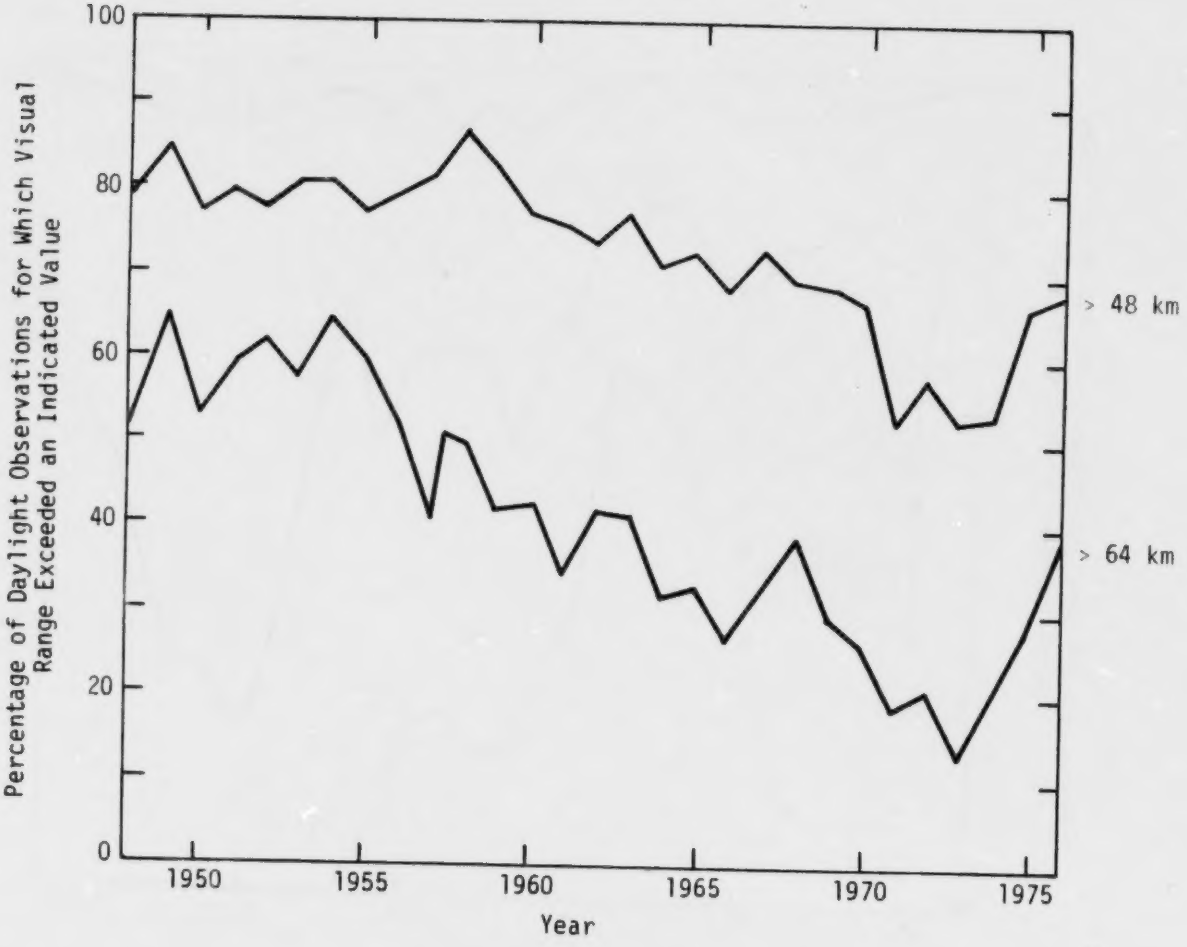

FIGURE A-13. PERCENTAGE OF DAYLIGHT OBSERVATIONS FOR WHICH VISUAL RANGE EXCEEDED AN INDICATED VALUE, AS A FUNCTION OF YEAR, IN SALT LAKE CITY, UTAH, 1948-1976

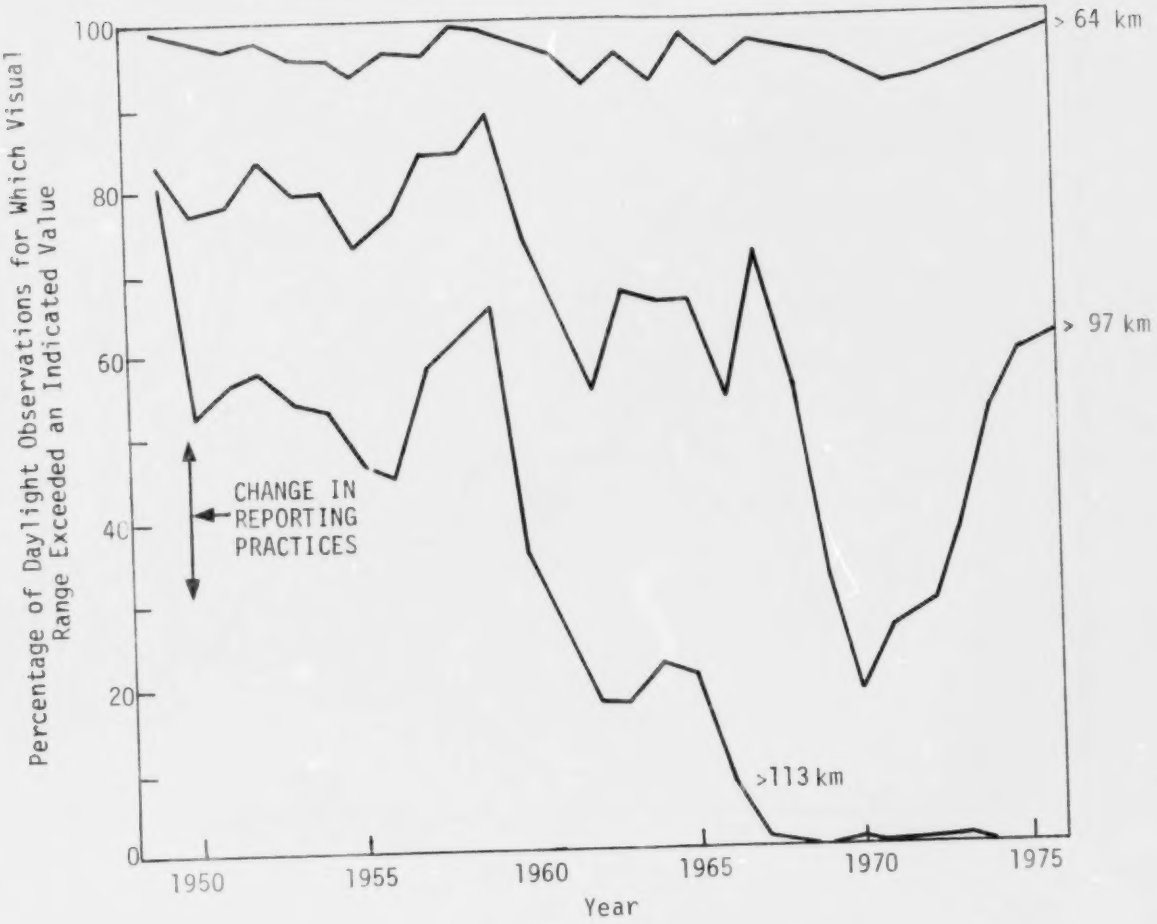

FIGURE A-14. PERCENTAGE OF DAYLIGHT OBSERVATIONS FOR WHICH VISUAL RANGE EXCEEDED AN INDICATED VALUE, AS A FUNCTION OF YEAR, IN TUCSON, ARIZONA, 1949-1976

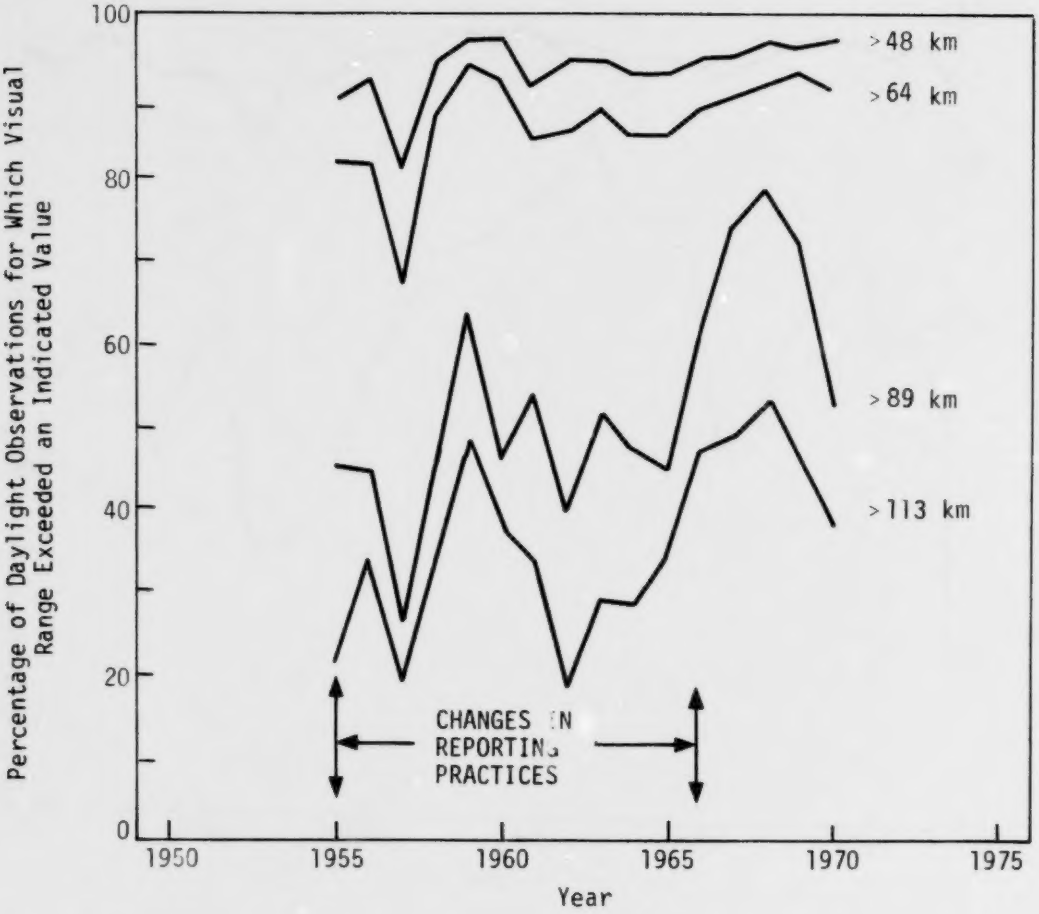

FIGURE A-15. PERCENTAGE OF DAYLIGHT OBSERVATIONS FOR WHICH VISUAL RANGE EXCEEDED AN INDICATED VALUE, AS A FUNCTION OF YEAR, IN ALAMOGORDO, NEW MEXICO, 1955-1970

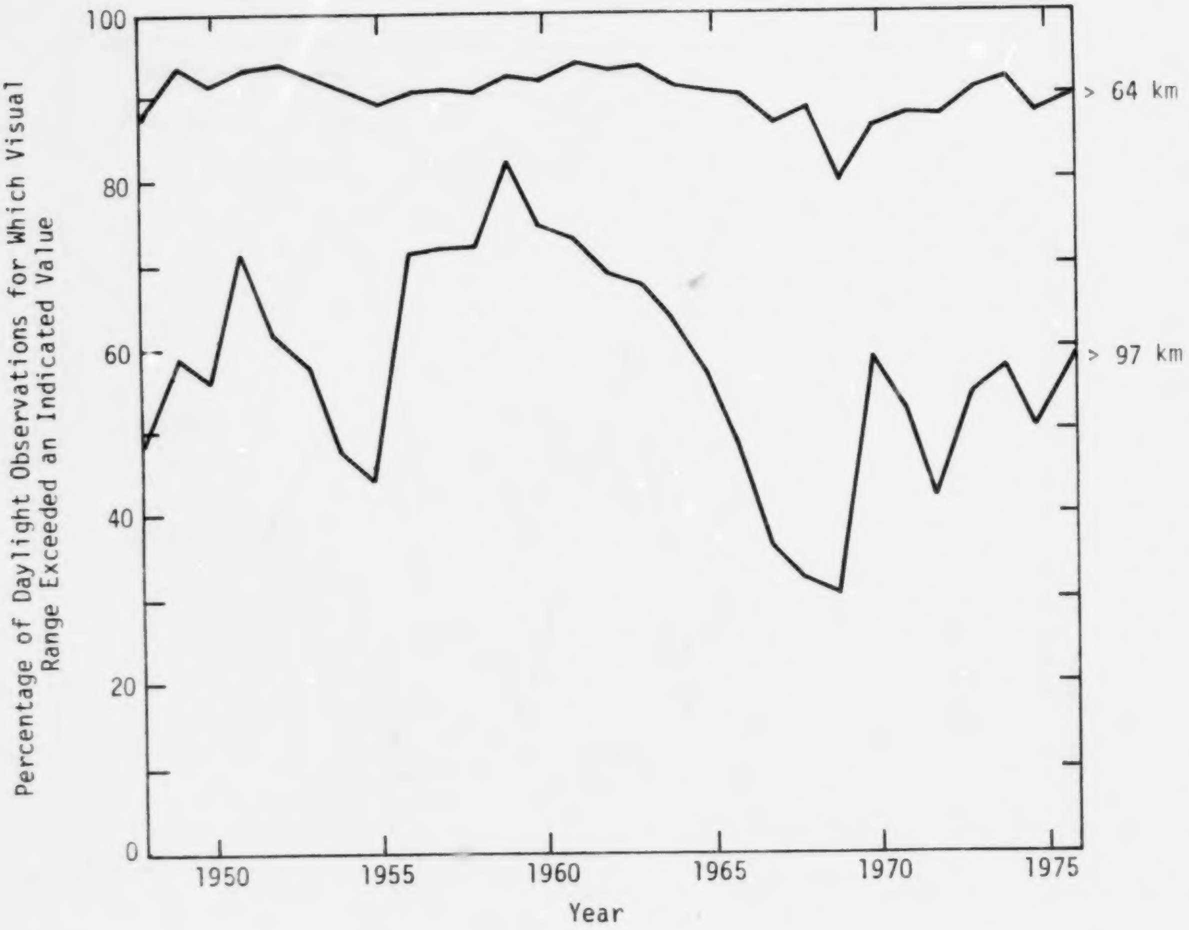

FIGURE A-16. PERCENTAGE OF DAYLIGHT OBSERVATIONS FOR WHICH VISUAL RANGE EXCEEDED AN INDICATED VALUE, AS A FUNCTION OF YEAR, IN BILLINGS, MONTANA, 1948-1976

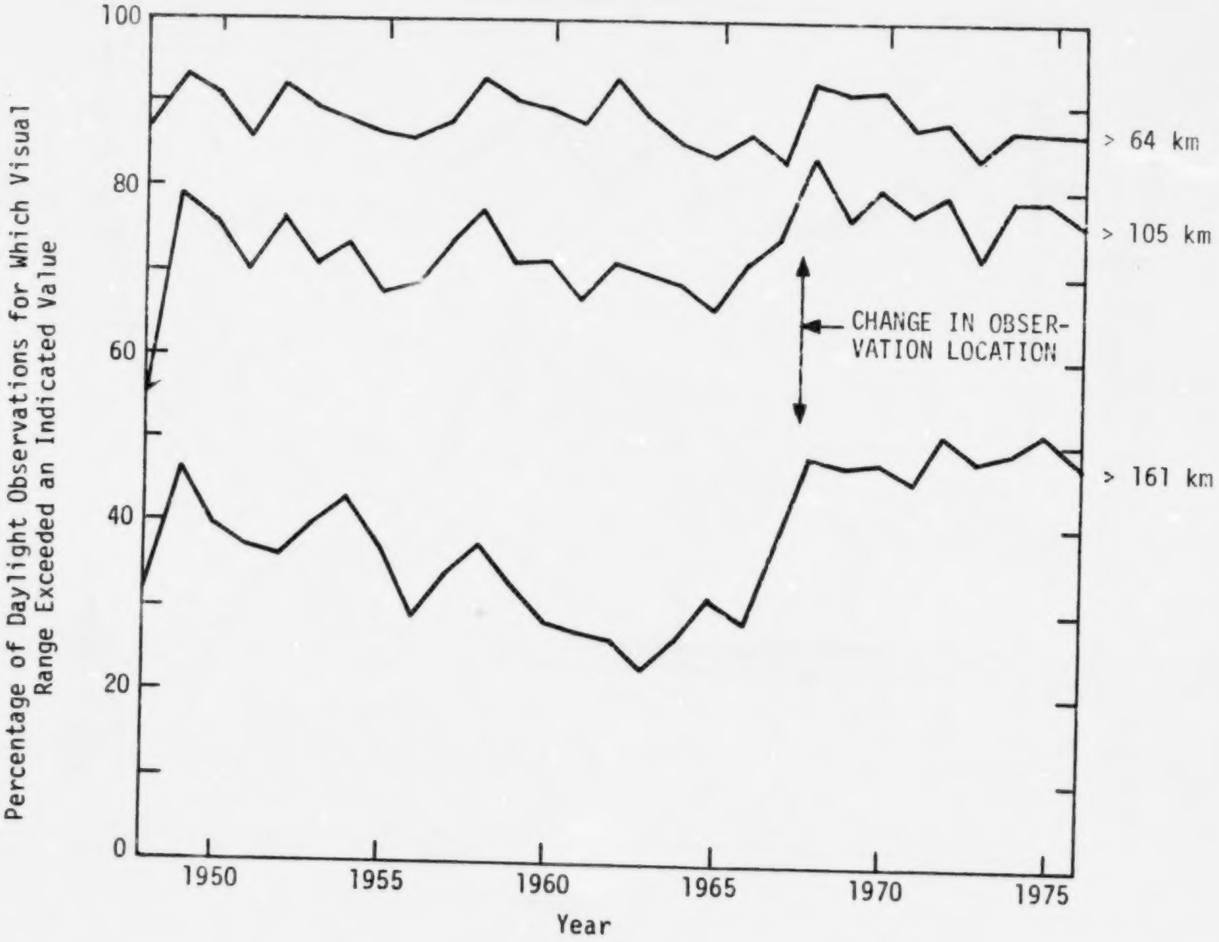

FIGURE A-17. PERCENTAGE OF DAYLIGHT OBSERVATIONS FOR WHICH VISUAL RANGE EXCEEDED AN INDICATED VALUE, AS A FUNCTION OF YEAR, IN COLORADO SPRINGS, COLORADO, 1948-1976

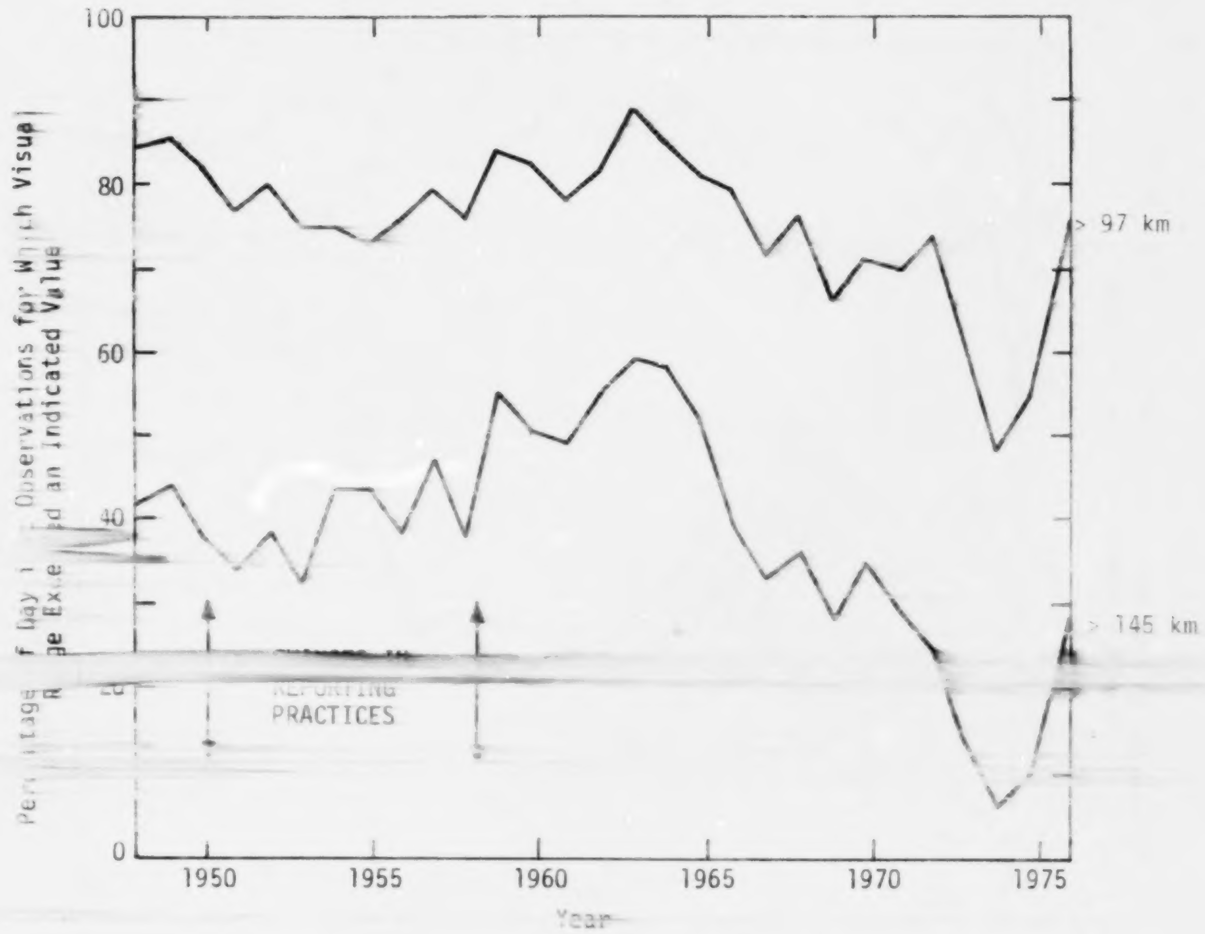

FIGURE A-18. PERCENTAGE OF DAYLIGHT OBSERVATIONS FOR WHICH VISUAL RANGE EXCEEDED AN INDICATED VALUE, AS A FUNCTION OF YEAR, IN CHEYENNE, WYOMING, 1948-1976

Reproduced from best available copy.

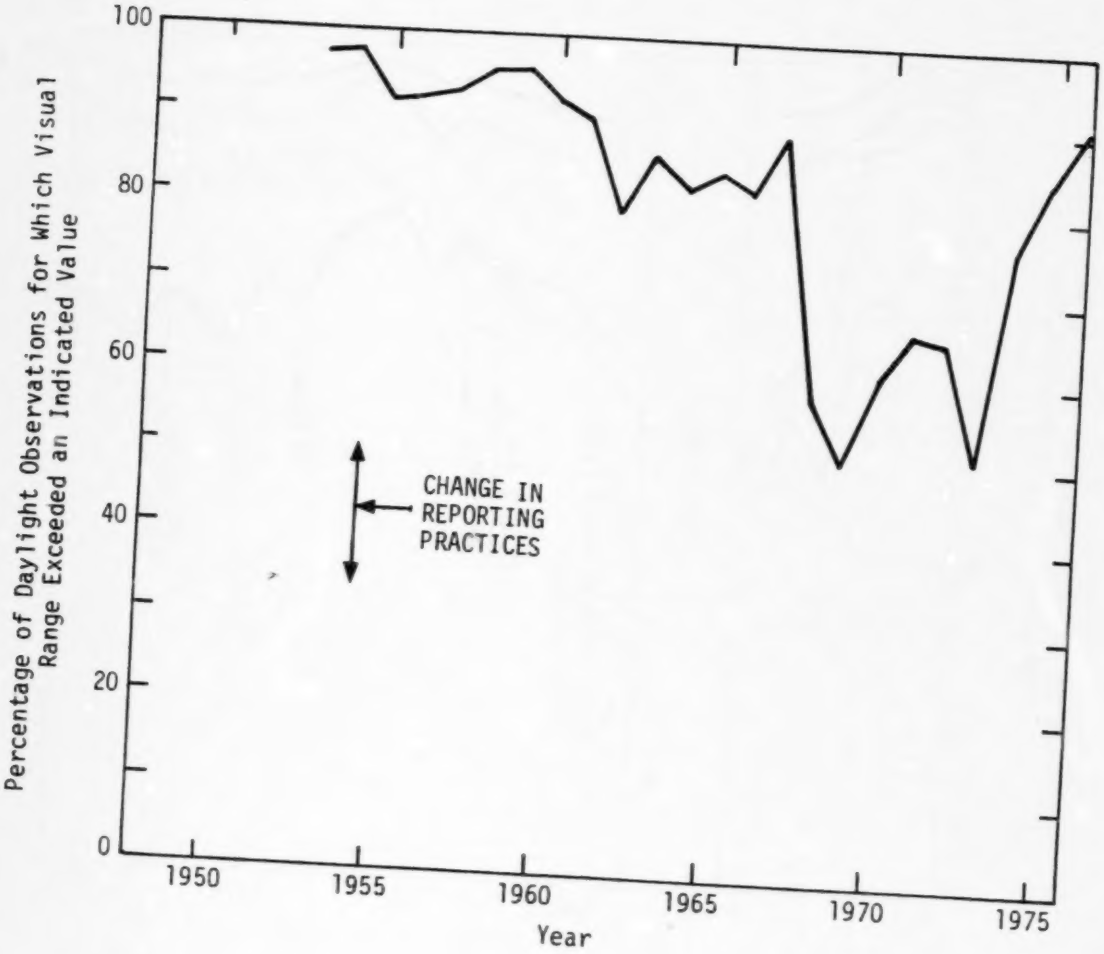

FIGURE A-19. PERCENTAGE OF DAYLIGHT OBSERVATIONS FOR WHICH VISUAL RANGE EXCEEDED AN INDICATED VALUE AS A FUNCTION OF YEAR, IN ELY, NEVADA, 1953-1976

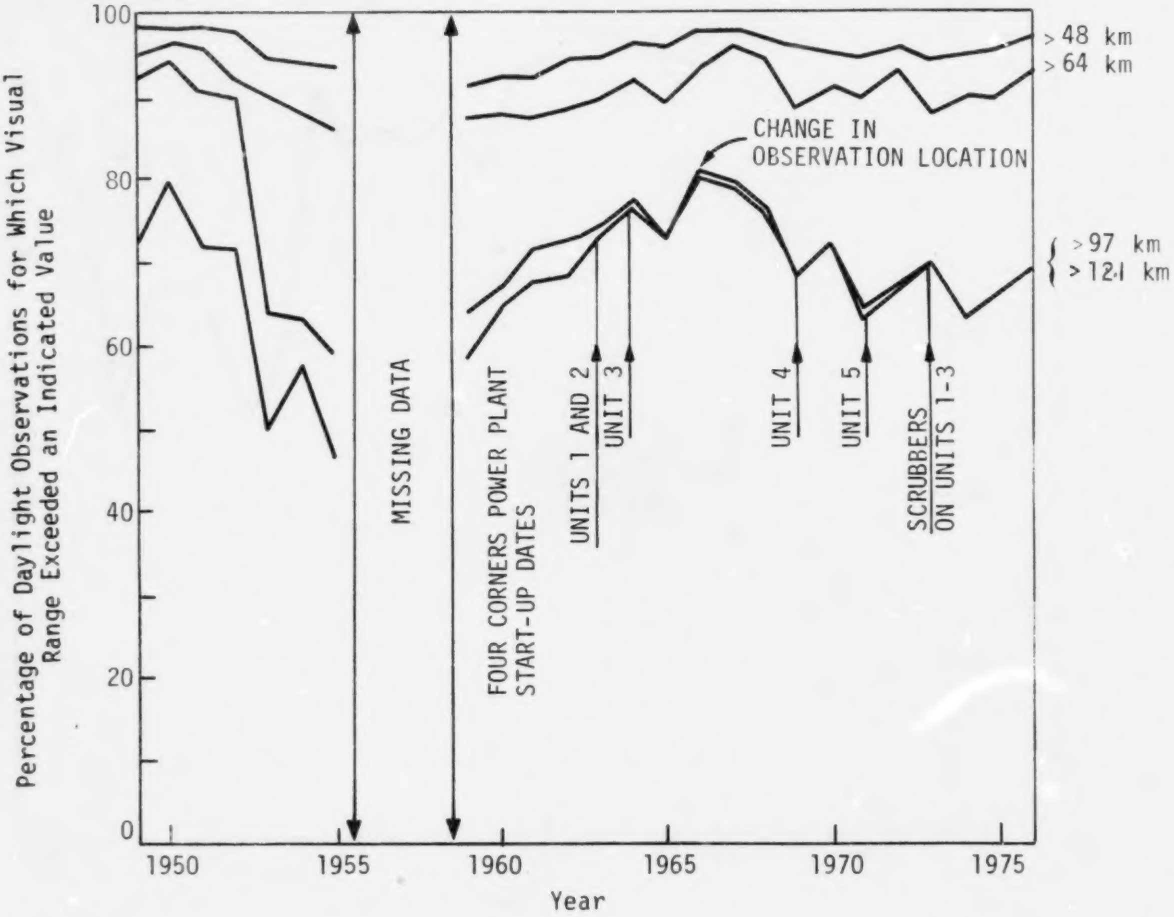

FIGURE A-20. PERCENTAGE OF DAYLIGHT OBSERVATIONS FOR WHICH VISUAL RANGE EXCEEDED AN INDICATED VALUE, AS A FUNCTION OF YEAR, IN FARMINGTON, NEW MEXICO, 1949-1976

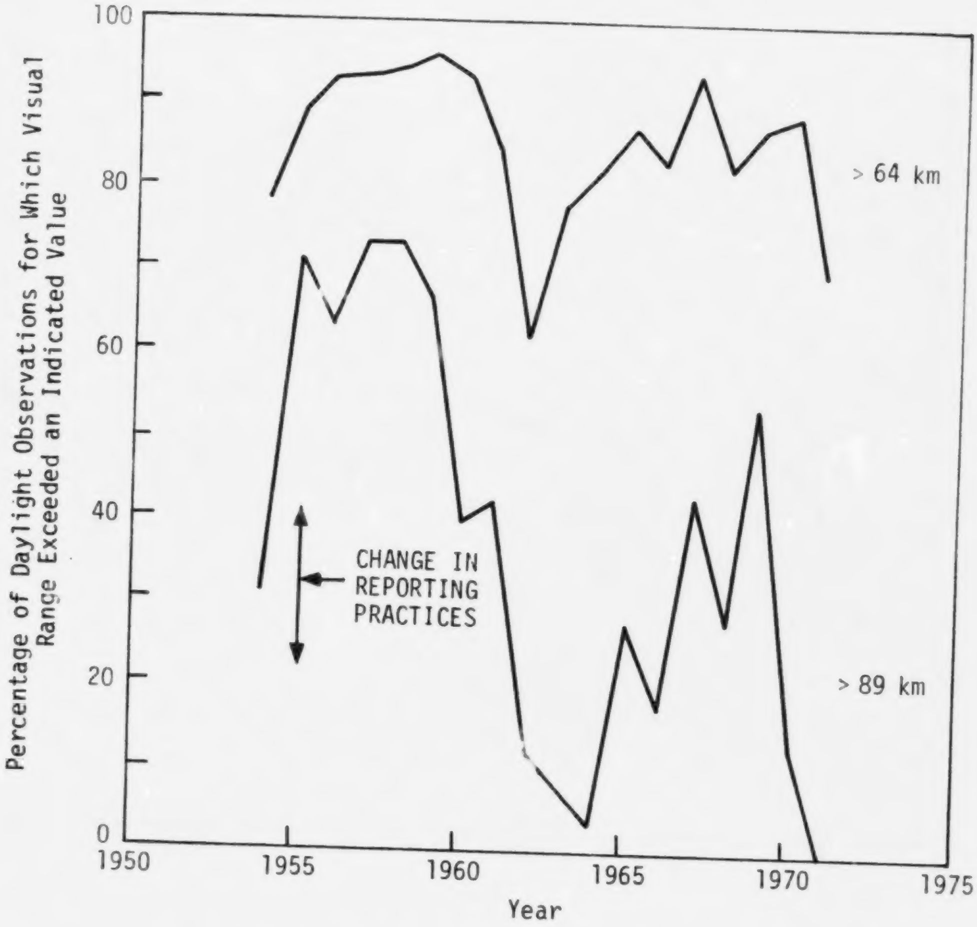

FIGURE A-21. PERCENTAGE OF DAYLIGHT OBSERVATIONS FOR WHICH VISUAL RANGE EXCEEDED AN INDICATED VALUE, AS A FUNCTION OF YEAR, IN FT. HUACHUCA, ARIZONA, 1954-1971

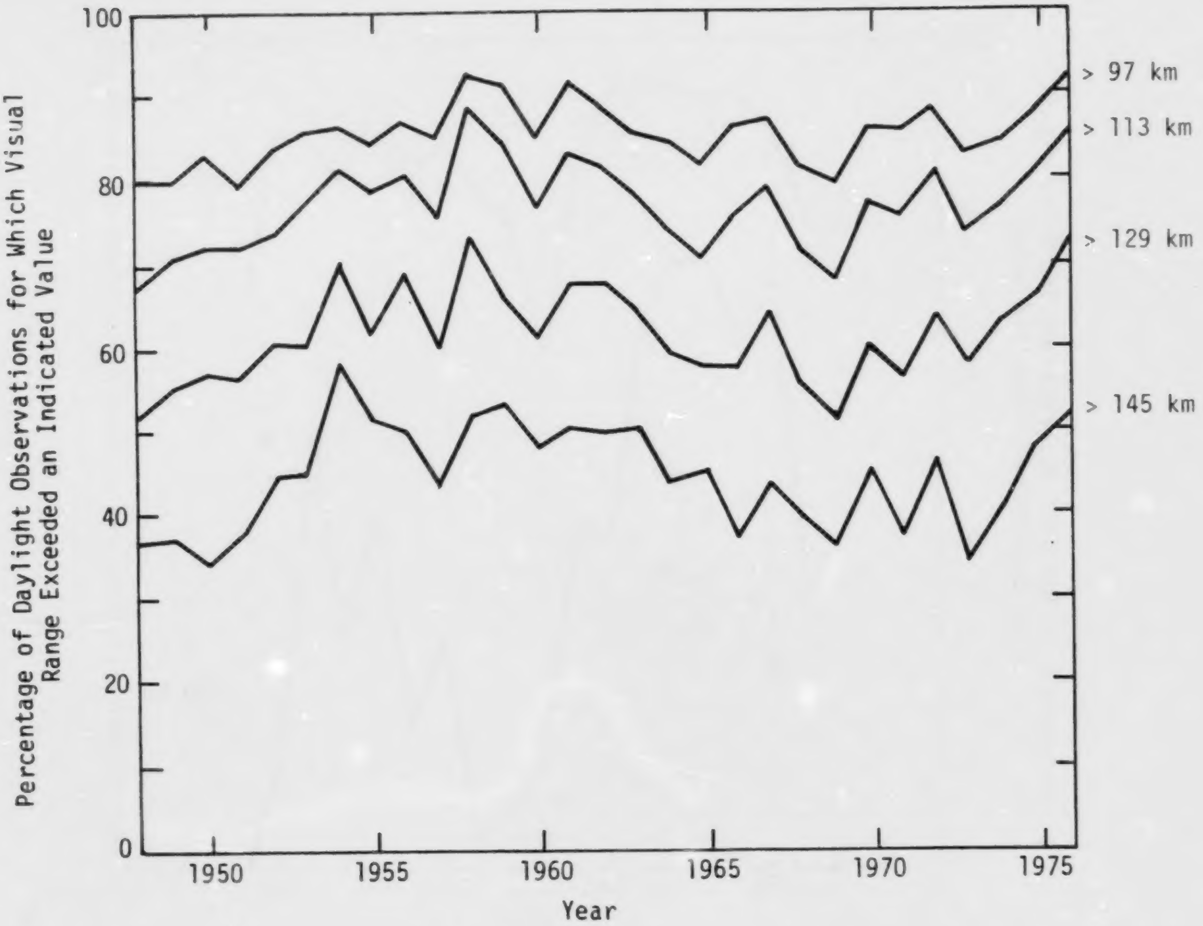

FIGURE A-22. PERCENTAGE OF DAYLIGHT OBSERVATIONS FOR WHICH VISUAL RANGE EXCEEDED AN INDICATED VALUE, AS A FUNCTION OF YEAR, AT GRAND JUNCTION, COLORADO, 1948-1976

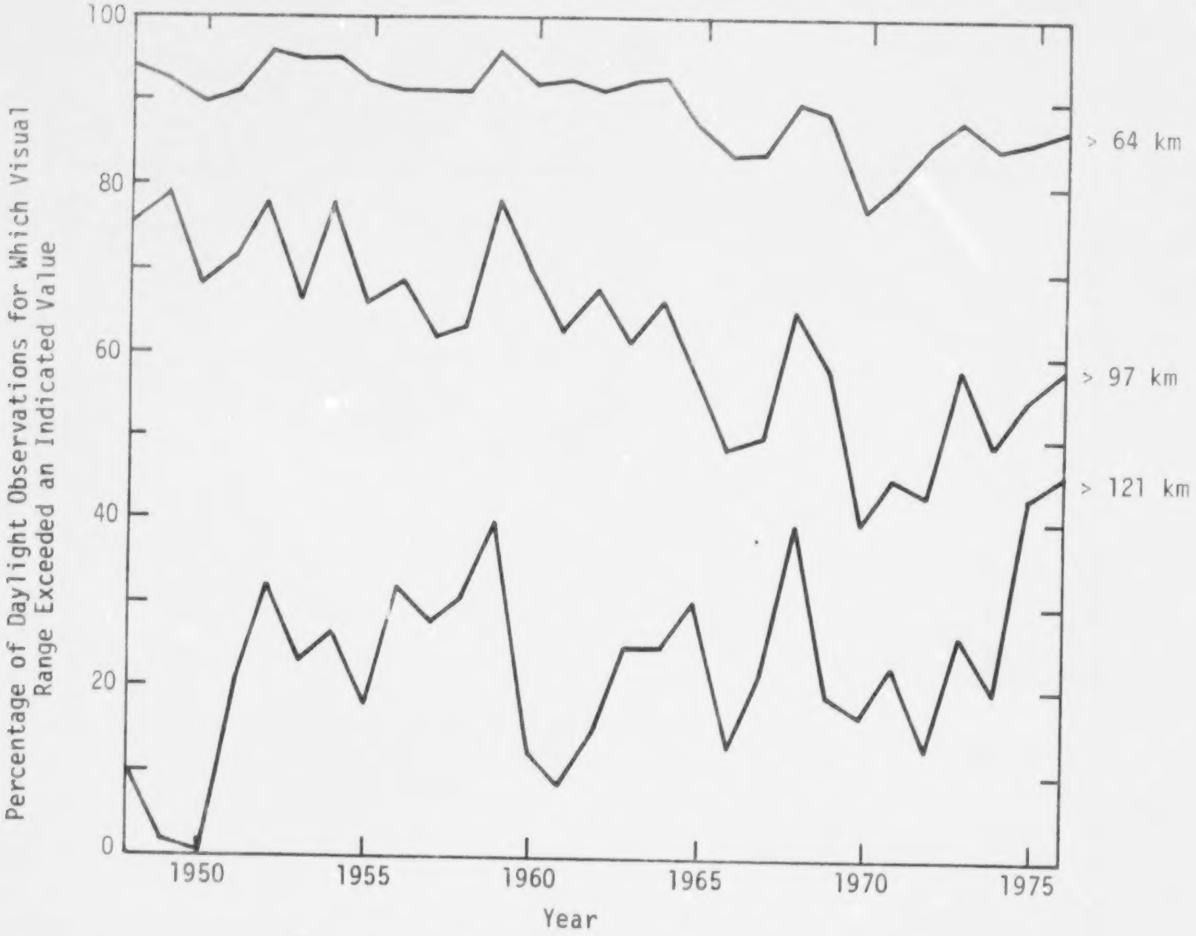

FIGURE A-23. PERCENTAGE OF DAYLIGHT OBSERVATIONS FOR WHICH VISUAL RANGE EXCEEDED AN INDICATED VALUE, AS A FUNCTION OF YEAR, IN GREAT FALLS, MONTANA, 1948-1976

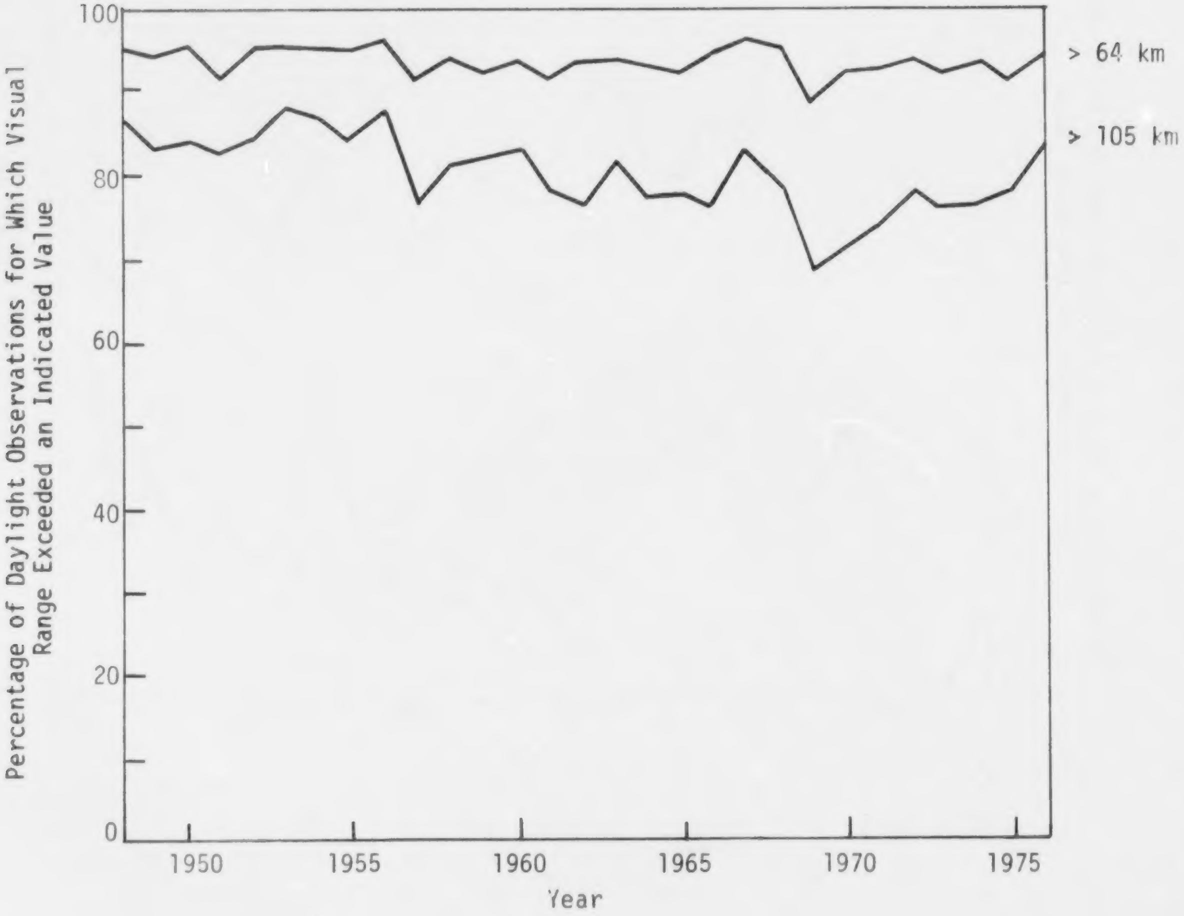

FIGURE A-24. PERCENTAGE OF DAYLIGHT OBSERVATIONS FOR WHICH VISUAL RANGE EXCEEDED AN INDICATED VALUE, AS A FUNCTION OF YEAR, IN PRESCOTT, ARIZONA, 1948-1976

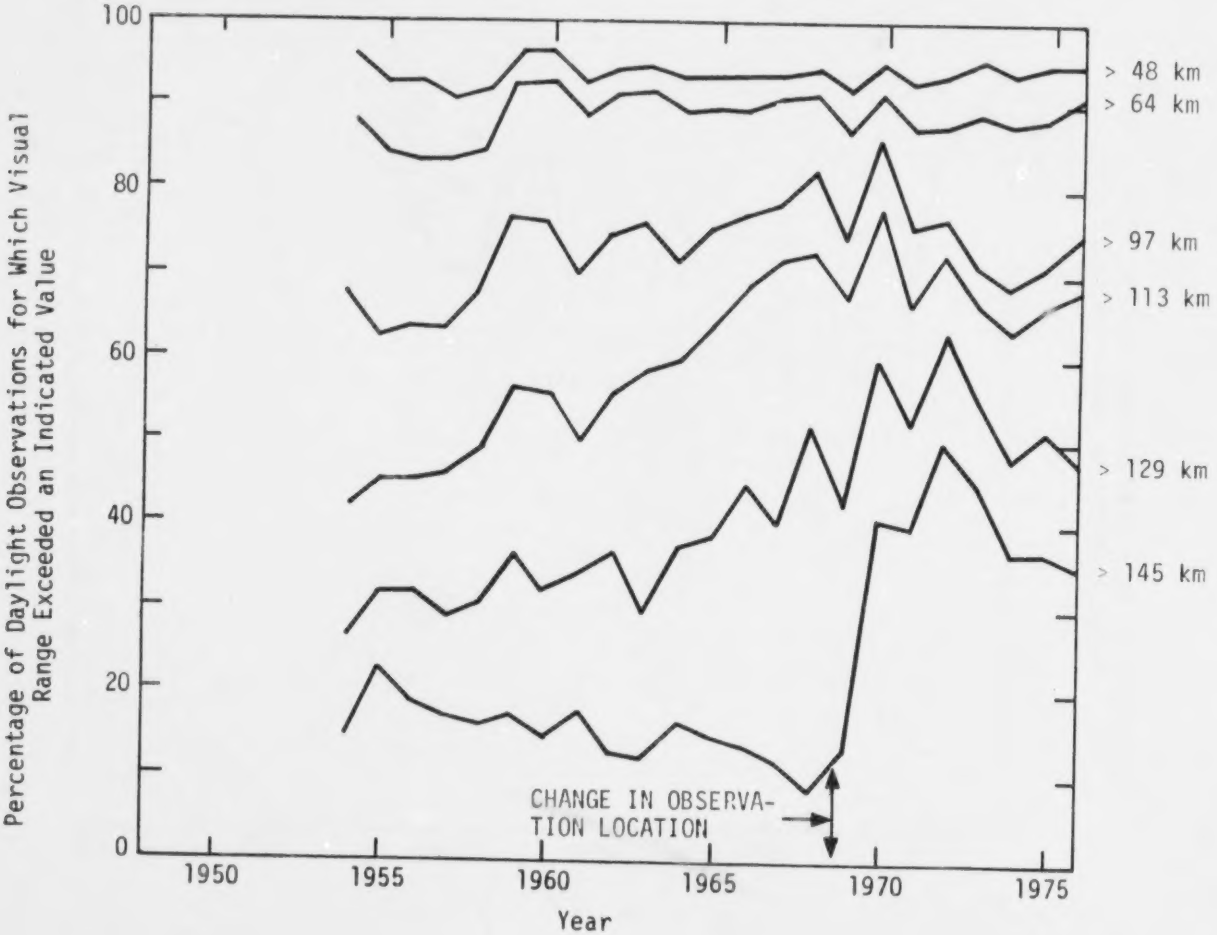

FIGURE A-25. PERCENTAGE OF DAYLIGHT OBSERVATIONS FOR WHICH VISUAL RANGE EXCEEDED AN INDICATED VALUE, AS A FUNCTION OF YEAR, IN PUEBLO, COLORADO, 1954-1976

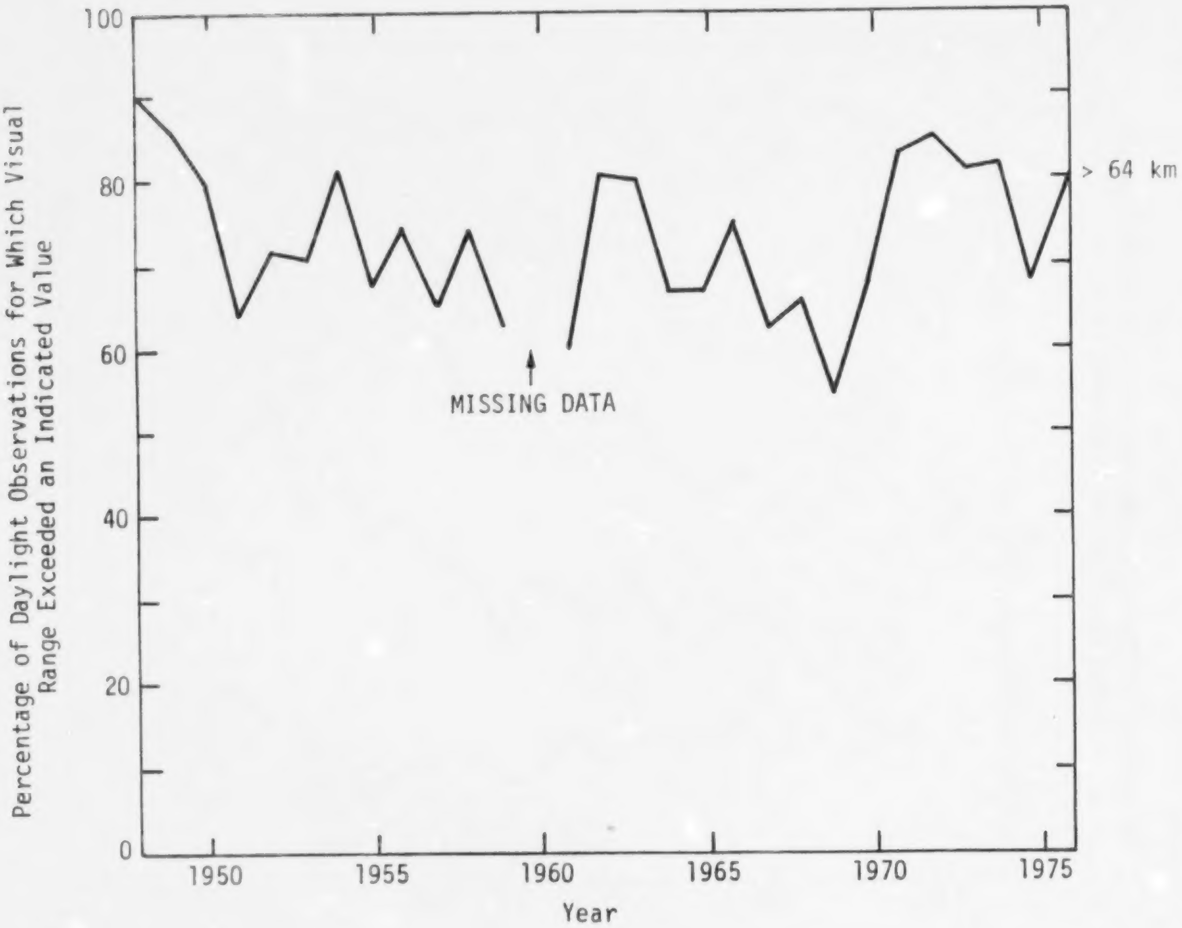

FIGURE A-26. PERCENTAGE OF DAYLIGHT OBSERVATIONS FOR WHICH VISUAL RANGE EXCEEDED AN INDICATED VALUE, AS A FUNCTION OF YEAR, AT ROCK SPRINGS, WYOMING, 1948-1976

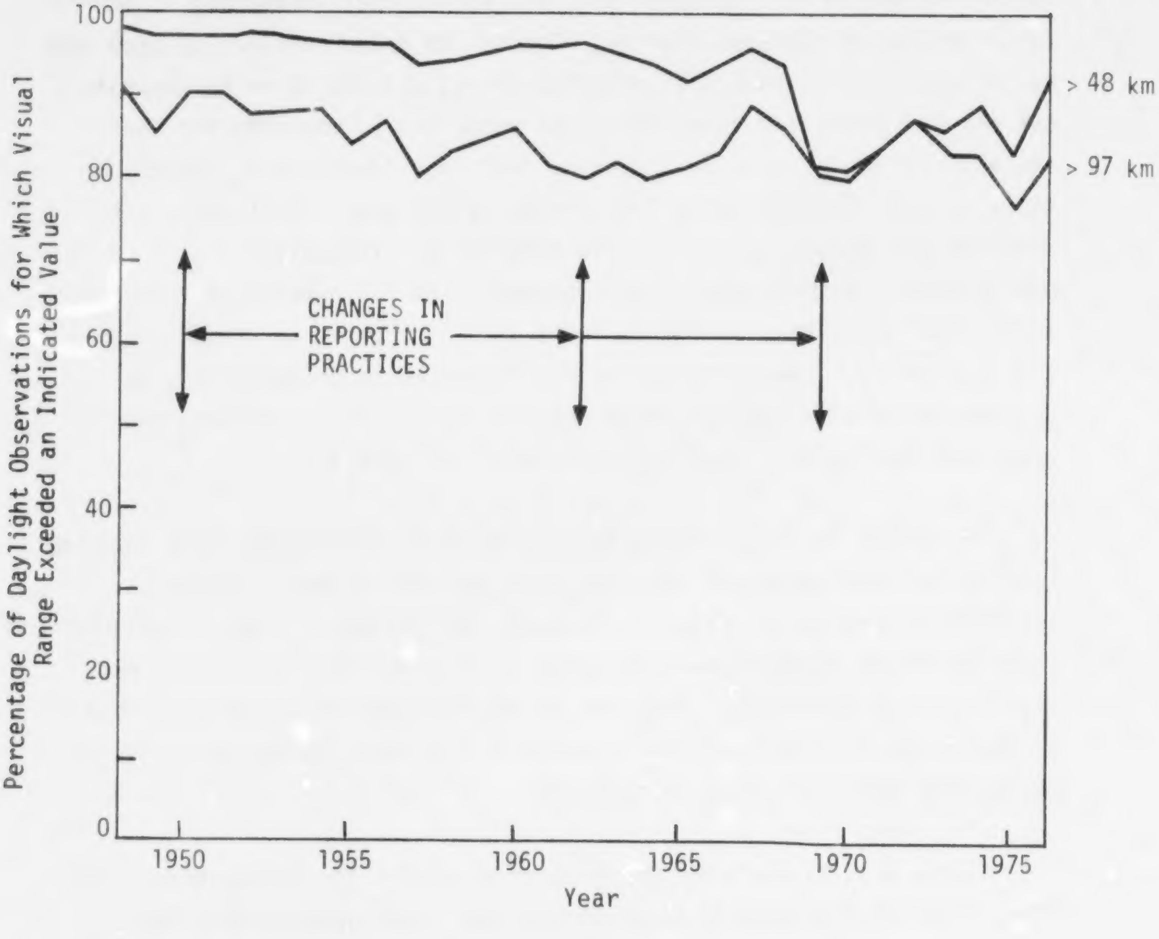

FIGURE A-27. PERCENTAGE OF DAYLIGHT OBSERVATIONS FOR WHICH VISUAL RANGE EXCEEDED AN INDICATED VALUE, AS A FUNCTION OF YEAR, IN WINSLOW, ARIZONA, 1948-1976

These figures are similar to those obtained by Trijonis and Yuan (1977) with the following exceptions. First, our data base extends through 1976, whereas that of Trijonis and Yuan extends only through 1972. As noted later, some significant upward trends in visual range occurred during the period 1972 through 1976, suggesting that visibility is improving as pollution controls improve. Second, as noted earlier, we used days in our analysis on which precipitation or fog did not occur to separate out these obvious influences on visual range and to minimize the variability that would occur by comparing "wet" and "dry" years. Third, we chose to plot the cumulative frequencies rather than visual range percentiles for two reasons: (1) Interpolation or extrapolation of data is not necessary to plot cumulative frequency, and (2) cumulative frequencies are in most cases more sensitive indicators of changes in visual range than percentiles. Recognizing these differences in presentation, we checked our results against those obtained by Trijonis and Yuan, and we concluded that we are correctly describing the same data.

The trends in visual range for the urban sites (Figures A-10 through A-14) offer some important insights into the anthropogenic causes of visibility impairment. Figure A-10 shows that in Denver the gradual downward trend in visual range changed abruptly in 1972 and that visibility has improved since that year. This recent upward trend in visual range may be the result of the control of automobile and point source emissions during the last five years in that city.

Figure A-11 illustrates the history of visibility in Las Vegas. It shows that the frequency with which a visual range greater than 105 km is reported has increased over the years, indicating improving visibility. However, a telephone interview with the meteorologist in charge at the NWS station in Las Vegas revealed that observers in the past frequently did not bother to report whether the most distant visibility marker was visible because they felt that for aviation purposes no one needed to know whether visibility was that good! Thus, these visibility data should be treated with caution.

One can, however, cursorily test whether a given visibility marker was consistently observed and reported by checking the frequency with which other visibility markers were observed. For example, as shown in Figure A-12, the frequency with which 40 km visibility is reported at Las Vegas has not changed significantly since 1951 even though reported visibilities of over 100 km have increased. This discrepancy could be interpreted as improper data collection (as appears to be the case here), or the frequency of occurrence of visibilities less than 40 km could have remained the same while the frequency of occurrence of visibilities greater than 100 km increased.

The recent dramatic upward trends in visual range in Phoenix, Salt Lake City, and Tucson, as shown in Figures A-12 through A-14, may be the result of decreased automobile emissions and the significant reduction in SO_2 emissions from copper smelters in Arizona in recent years, as shown in Figure A-28 (Arizona Department of Health Services, 1977). Also, the significant increases in visual range in Phoenix and Tucson during the years 1949, 1959, and 1967 to 1968 appear to be the result of reductions in SO_2 emissions during copper strikes and periods of reduced copper production (see Figure A-29).

The yearly visual range trends at nonurban sites are shown in Figures A-16 through A-27. The visual range at Cheyenne, Wyoming, decreased dramatically from 1963 to 1974 and increased in 1975 and 1976. The visual range in Ely, Nevada, which is near a copper smelter, has varied significantly during the last decade; however, the significant increase in visual range during the last four years may have resulted from the installation of a tall stack and the control of SO_2 emissions.

Figure A-20 shows the history of visibility in Farmington, New Mexico, which is about 20 to 30 km northeast of the Four Corners coal-fired power plant. The most significant decrease in visibility occurred during the early 1950s, before the power plant was built, but it is not clear what caused this decrease. Visibility improved until about 1967 and

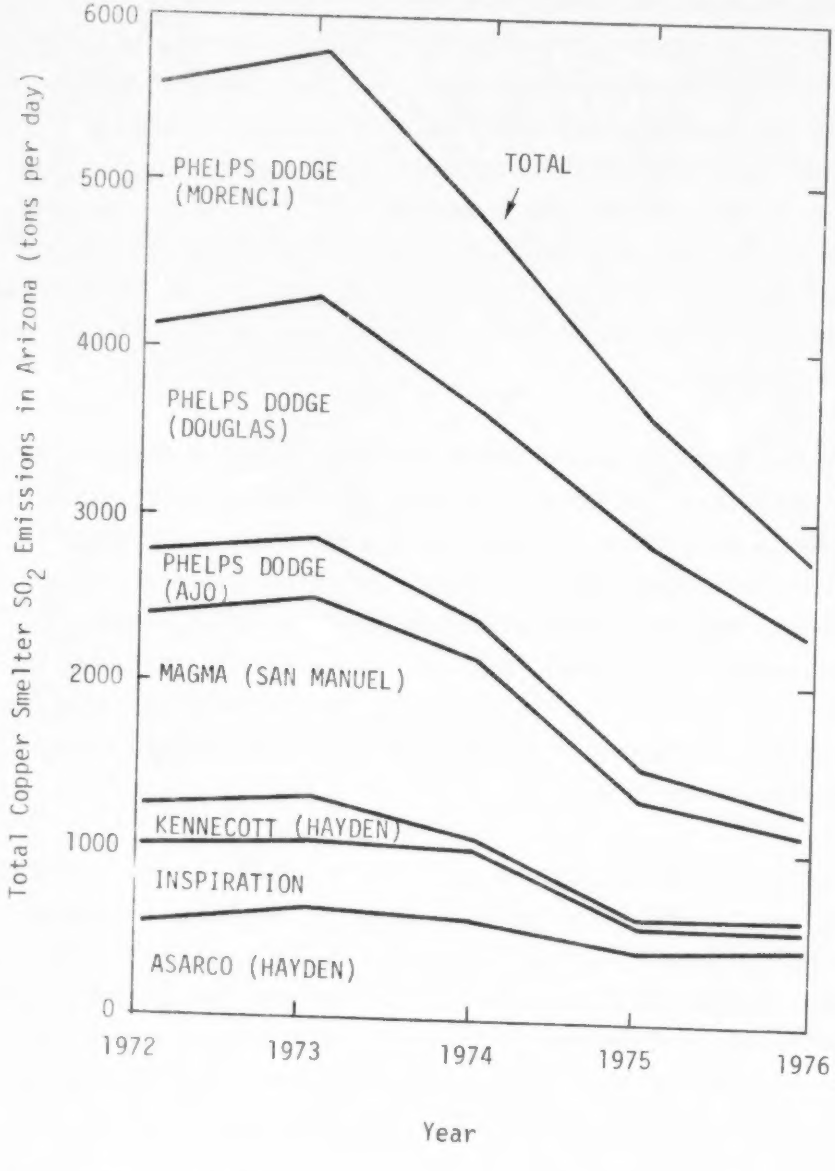

FIGURE A-28. YEARLY TRENDS IN SO_2 EMISSIONS FROM COPPER SMELTERS IN ARIZONA

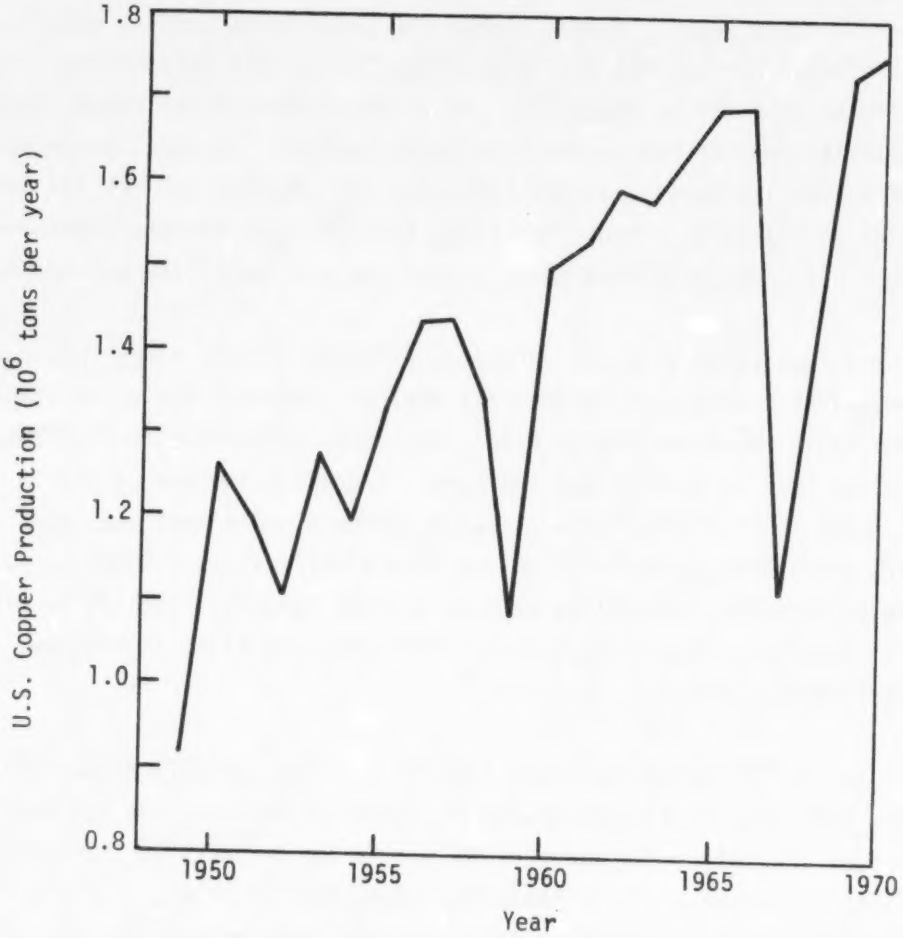

FIGURE A-29. YEARLY TRENDS IN U.S. COPPER PRODUCTION then decreased from 1967 to 1973; it has apparently been improving since 1973. The years in which the coal-fired boilers at Four Corners began operation are shown in Figure A-20. The start-up of Units 1, 2, and 3 had no noticeable effect on visibility in 1963 and 1964; indeed, visibility improved in these years. However, when the large units (Nos. 4 and 5) began operation during 1969 and 1971, respectively, the frequency of visibilities over 121 km decreased. It is not clear whether these changes in visibility were caused by the Four Corners plant. In fact, the most distant visibility markers at the Farmington NWS station are the San Juan Mountains to the north. Thus, the plume from the Four Corners plant would intersect the Farmington observer's sight path only when flow was southerly.

The visual range at Grand Junction, Colorado (Figure A-22), has improved significantly during the last decade. Although the visual range in Great Falls, Montana (Figure A-23), decreased significantly from 1948 to 1970, since 1970 visibility has improved. A gradual downward trend in visual range in Prescott, Arizona, was observed between 1948 and 1969; however, since 1969 visibility has improved significantly. Conversely, in Pueblo, Colorado, visibility appears to have improved until 1970, after which it declined. There has been a slight downward trend in Winslow, Arizona (Figure A-27).

Of the 16 NWS locations where long-term visibility data appear to be accurate (the data at Alamogordo and Ft. Huachuca were erratic and did not extend over the entire 29-year period) during the period 1948 through 1970, visibility decreased at seven locations, remained relatively constant (though with year-to-year variations) at eight, and improved at one. Since 1970, visibility has improved at twelve locations, remained relatively constant at three, and decreased at one. Thus, the data suggest that pollution control during the 1970s has reversed the downward trend in visibility that was observed in many western locations in the 1950s and 1960s.

7. EFFECT OF RELATIVE HUMIDITY

Relative humidity was found to be the meteorological parameter having the greatest effect on visual range in the western United States. In most of the 18 locations studied, the frequency of good visual range decreased significantly with increasing relative humidity. The effect was expected because the hygroscopic growth of aerosol particles such as sulfate (see Figure A-30) has been known and well documented for many years.

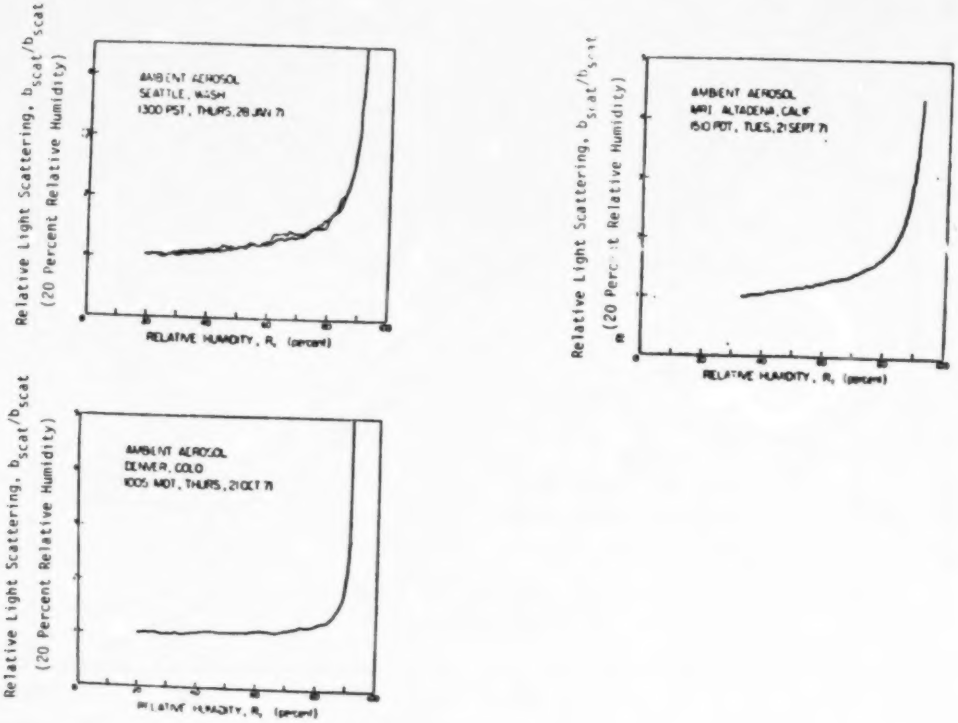

Source: Covert, Charlson, and Ahlquist (1972).

FIGURE A-30. EFFECT OF RELATIVE HUMIDITY ON b_{scat} OF AMBIENT AEROSOL

Figures A-31 through A-48 show the effect of relative humidity on visual range at each of the 18 NWS locations. Visual range data were sorted into 10 relative humidity groups (0 to 10, 10 to 20, ..., 90 to 100 percent) and grouped by decades (1948 through 1956, 1957 through 1966,

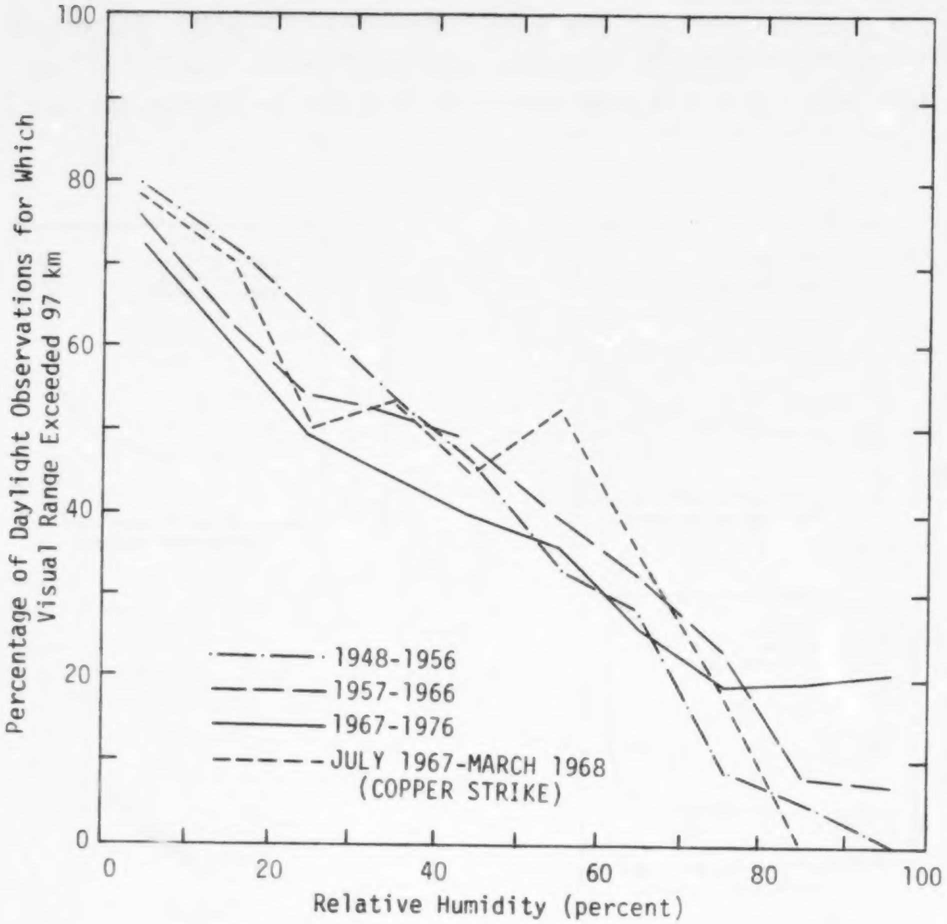

FIGURE A-31. PERCENTAGE OF DAYLIGHT OBSERVATIONS FOR WHICH VISUAL RANGE EXCEEDED 97 km, AS A FUNCTION OF RELATIVE HUMIDITY, AT DENVER, COLORADO

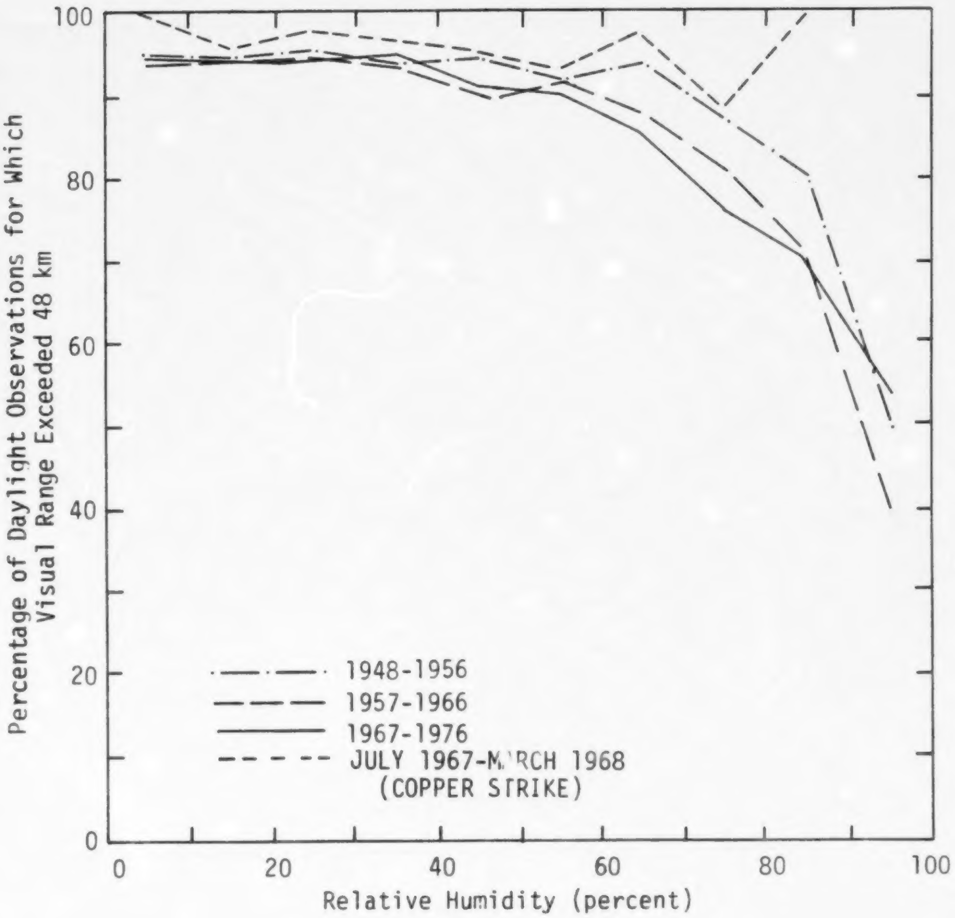

FIGURE A-32. PERCENTAGE OF DAYLIGHT OBSERVATIONS FOR WHICH VISUAL RANGE EXCEEDED 48 km, AS A FUNCTION OF RELATIVE HUMIDITY, AT LAS VEGAS, NEVADA

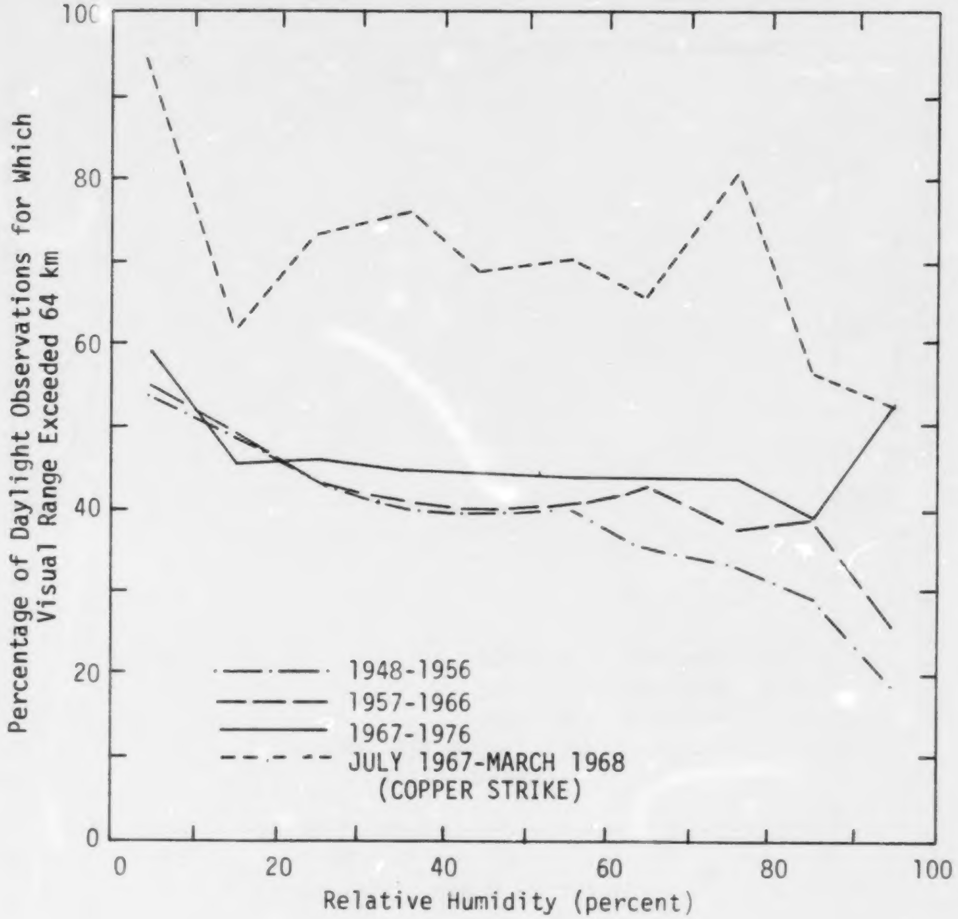

FIGURE A-33. PERCENTAGE OF DAYLIGHT OBSERVATIONS FOR WHICH VISUAL RANGE EXCEEDED 64 km, AS A FUNCTION OF RELATIVE HUMIDITY, AT PHOENIX, ARIZONA

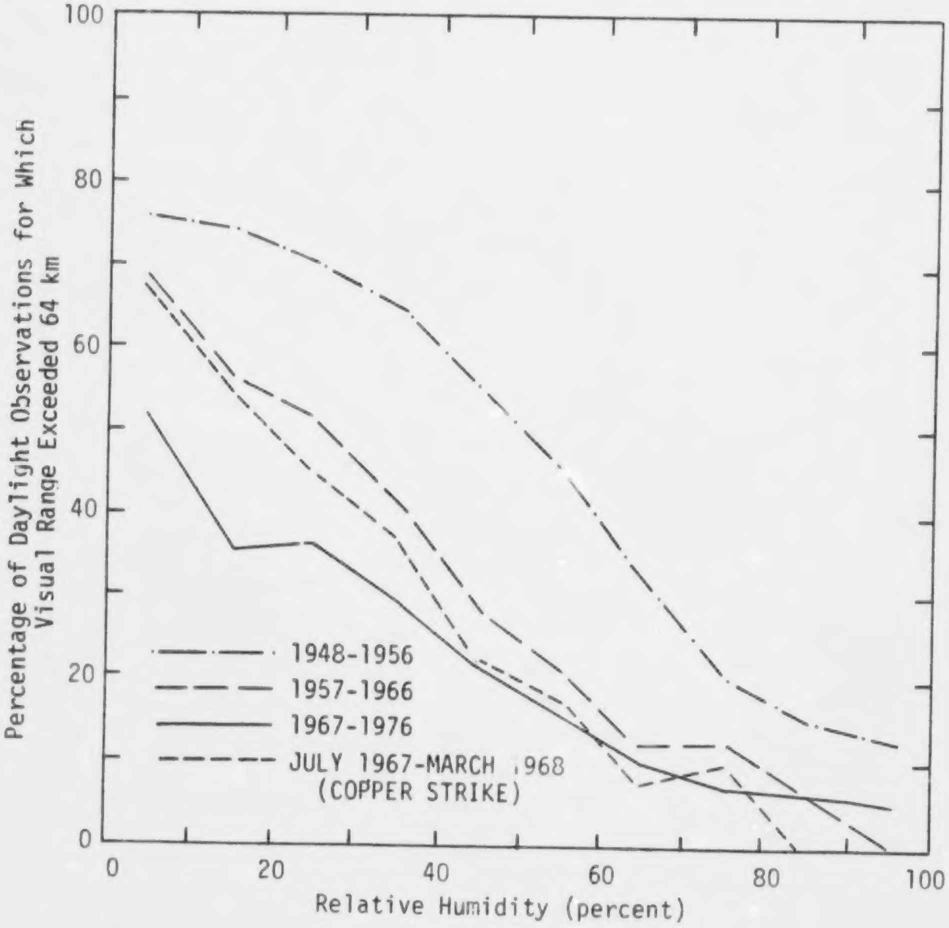

FIGURE A-34. PERCENTAGE OF DAYLIGHT OBSERVATIONS FOR WHICH VISUAL RANGE EXCEEDED 64 km, AS A FUNCTION OF RELATIVE HUMIDITY, AT SALT LAKE CITY, UTAH

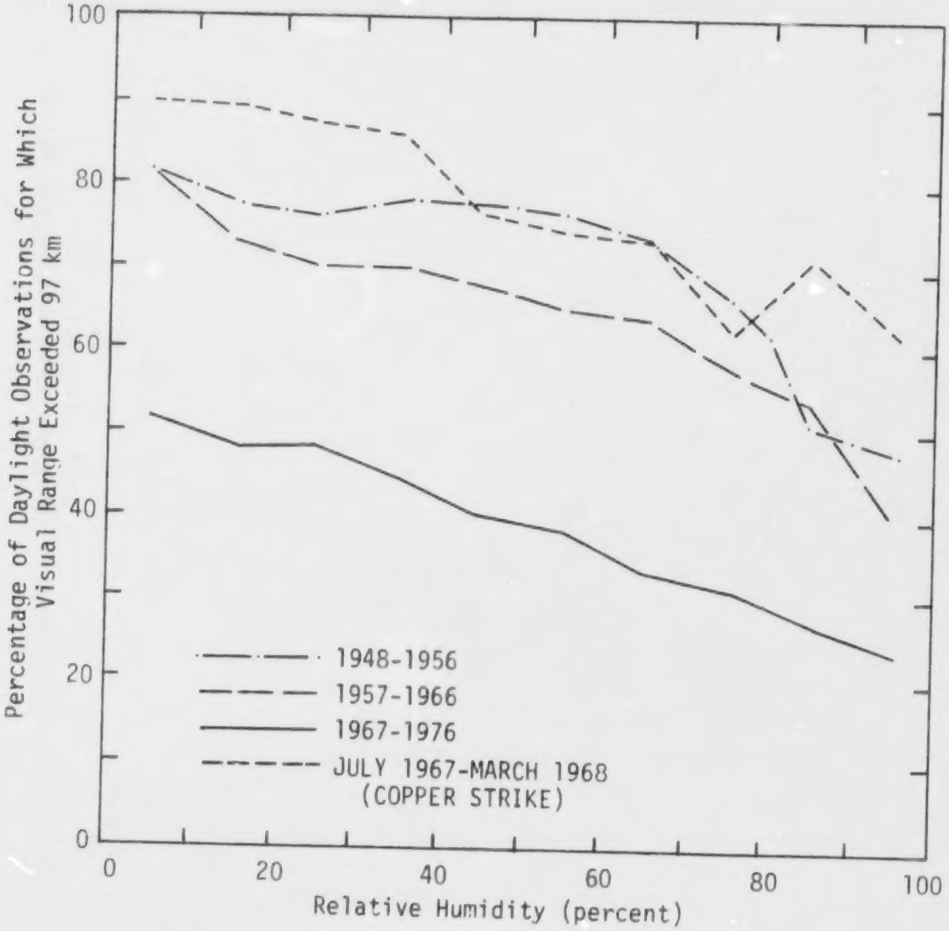

FIGURE A-35. PERCENTAGE OF DAYLIGHT OBSERVATIONS FOR WHICH VISUAL RANGE EXCEEDED 97 km, AS A FUNCTION OF RELATIVE HUMIDITY, AT TUCSON, ARIZONA

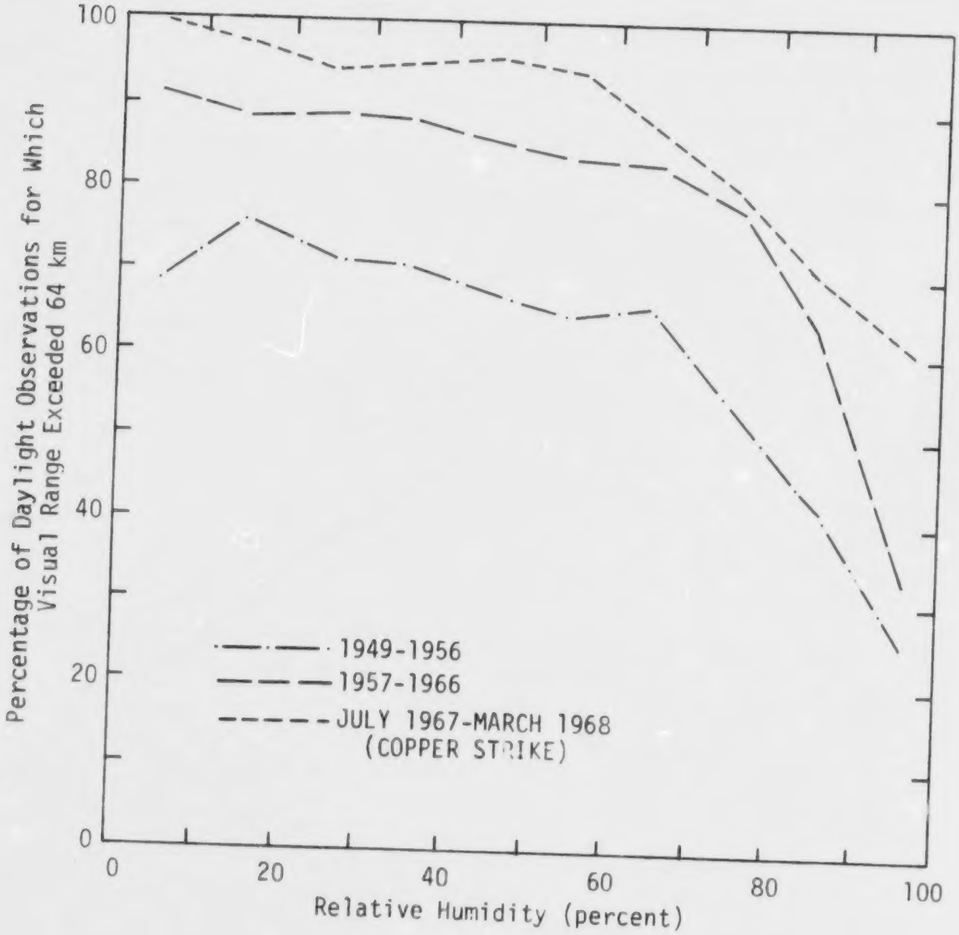

FIGURE A-36. PERCENTAGE OF DAYLIGHT OBSERVATIONS FOR WHICH VISUAL RANGE EXCEEDED 64 km, AS A FUNCTION OF RELATIVE HUMIDITY, AT ALAMOGORDO, NEW MEXICO

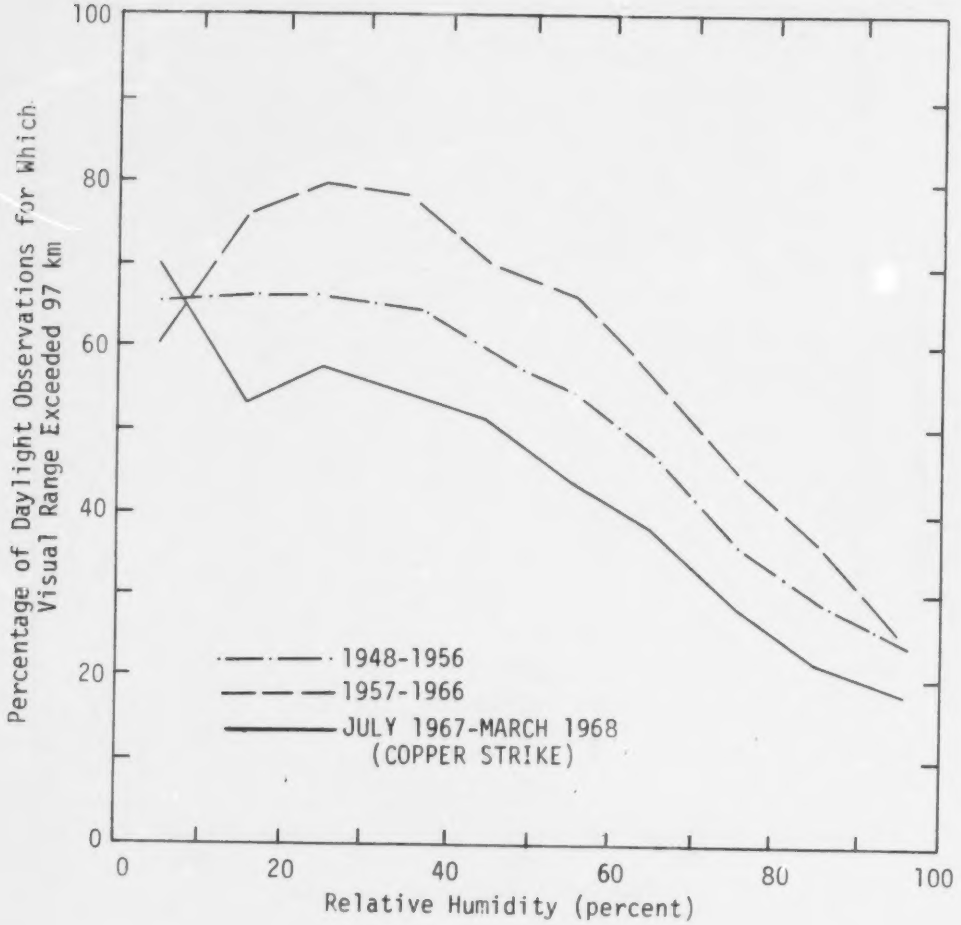

FIGURE A-37. PERCENTAGE OF DAYLIGHT OBSERVATIONS FOR WHICH VISUAL RANGE EXCEEDED 97 km, AS A FUNCTION OF RELATIVE HUMIDITY, AT BILLINGS, MONTANA

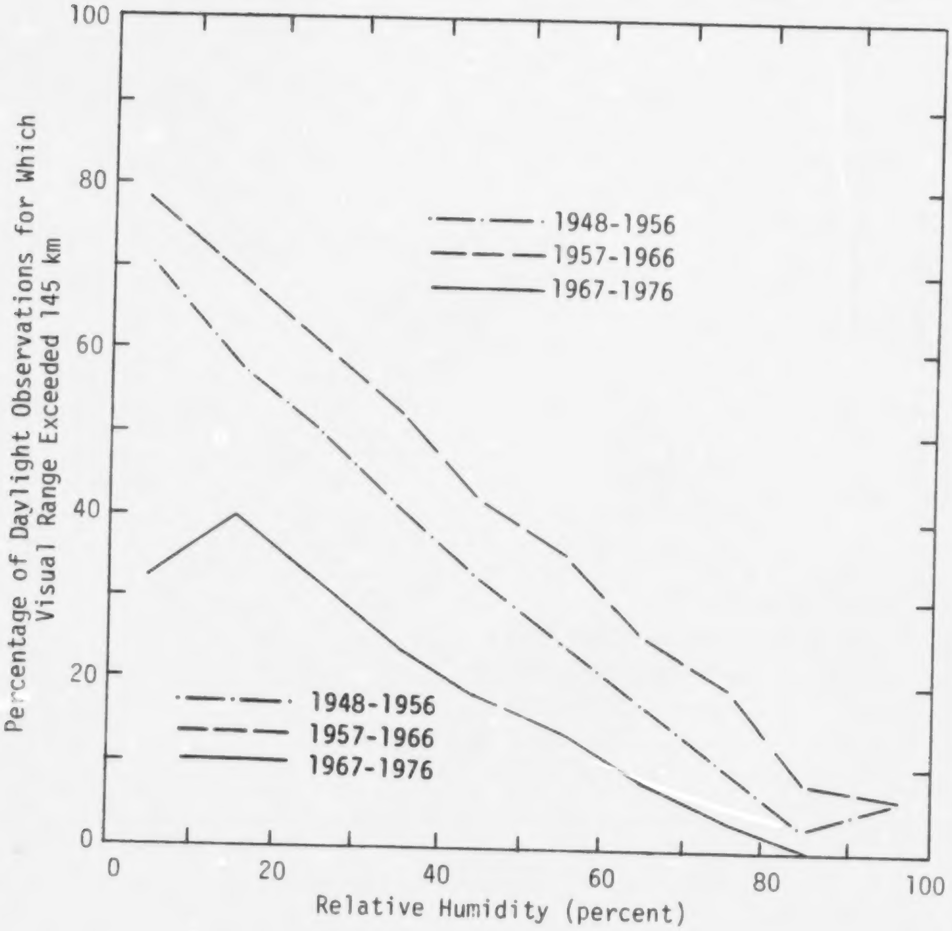

FIGURE 38. PERCENTAGE OF DAYLIGHT OBSERVATIONS FOR WHICH VISUAL RANGE EXCEEDED 145 km, AS A FUNCTION OF RELATIVE HUMIDITY, AT CHEYENNE, WYOMING

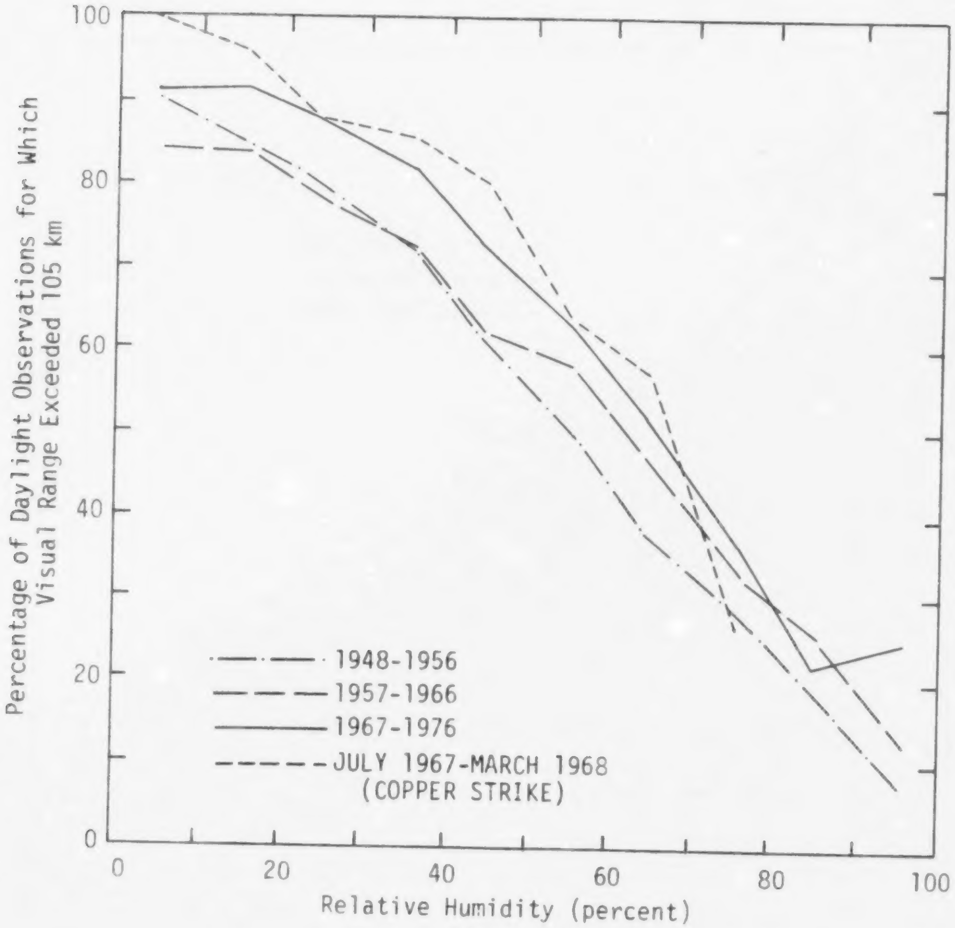

FIGURE A-39. PERCENTAGE OF DAYLIGHT OBSERVATIONS FOR WHICH VISUAL RANGE EXCEEDED 105 km, AS A FUNCTION OF RELATIVE HUMIDITY, AT COLORADO SPRINGS, COLORADO

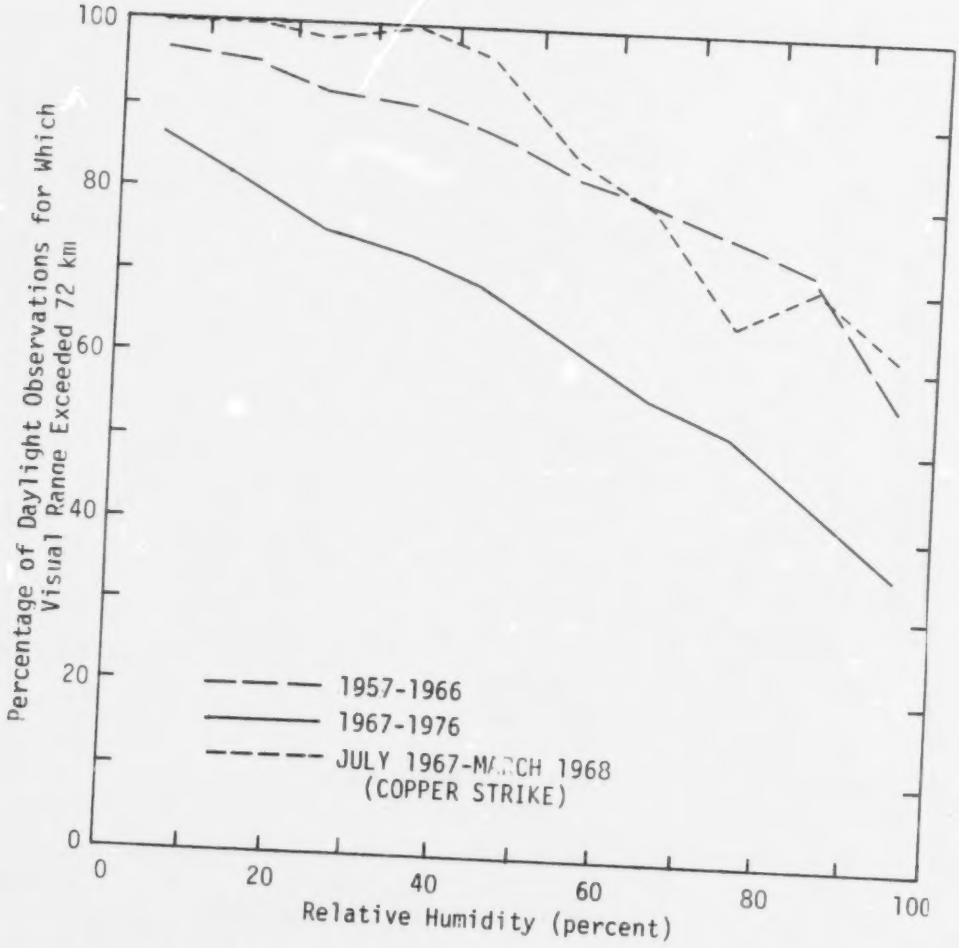

FIGURE A-40. PERCENTAGE OF DAYLIGHT OBSERVATIONS FOR WHICH VISUAL RANGE EXCEEDED 72 km, AS A FUNCTION OF RELATIVE HUMIDITY, AT ELY, NEVADA

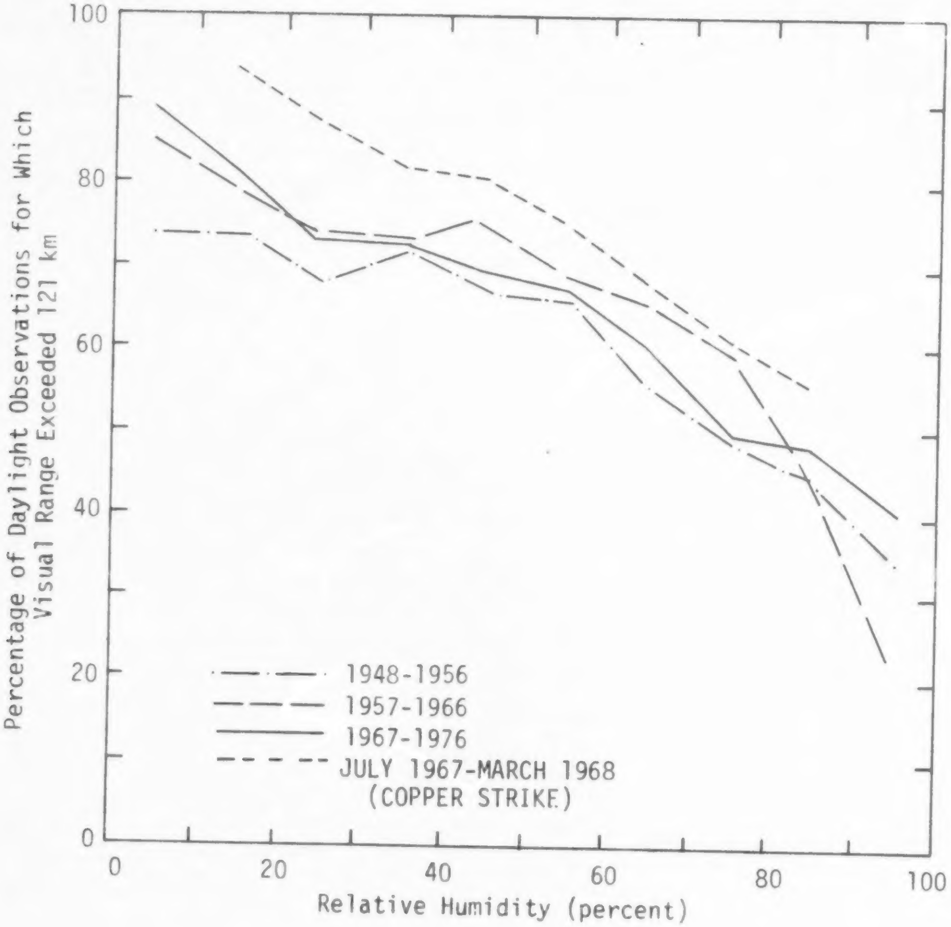

FIGURE A-41. PERCENTAGE OF DAYLIGHT OBSERVATIONS FOR WHICH VISUAL RANGE EXCEEDED 121 km, AS A FUNCTION OF RELATIVE HUMIDITY, AT FARMINGTON, NEW MEXICO

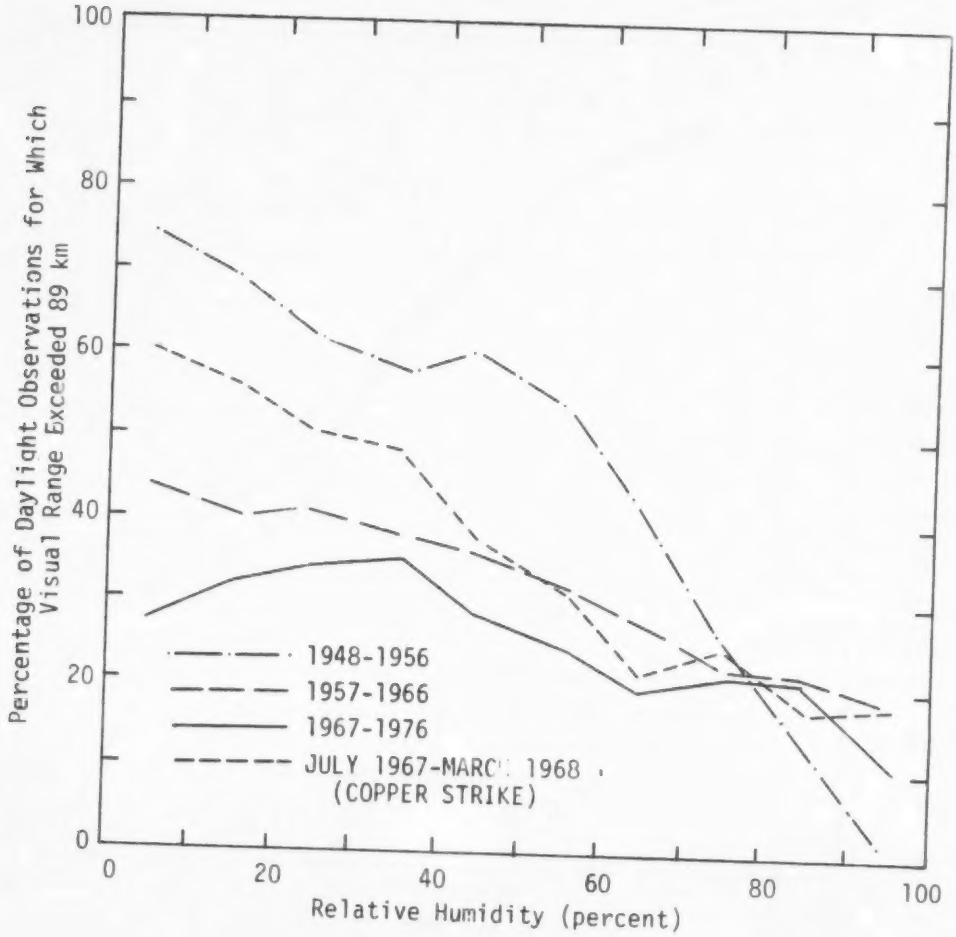

FIGURE A-42. PERCENTAGE OF DAYLIGHT OBSERVATIONS FOR WHICH VISUAL RANGE EXCEEDED 89 km, AS A FUNCTION OF RELATIVE HUMIDITY, AT FT. HUACHUCA, ARIZONA

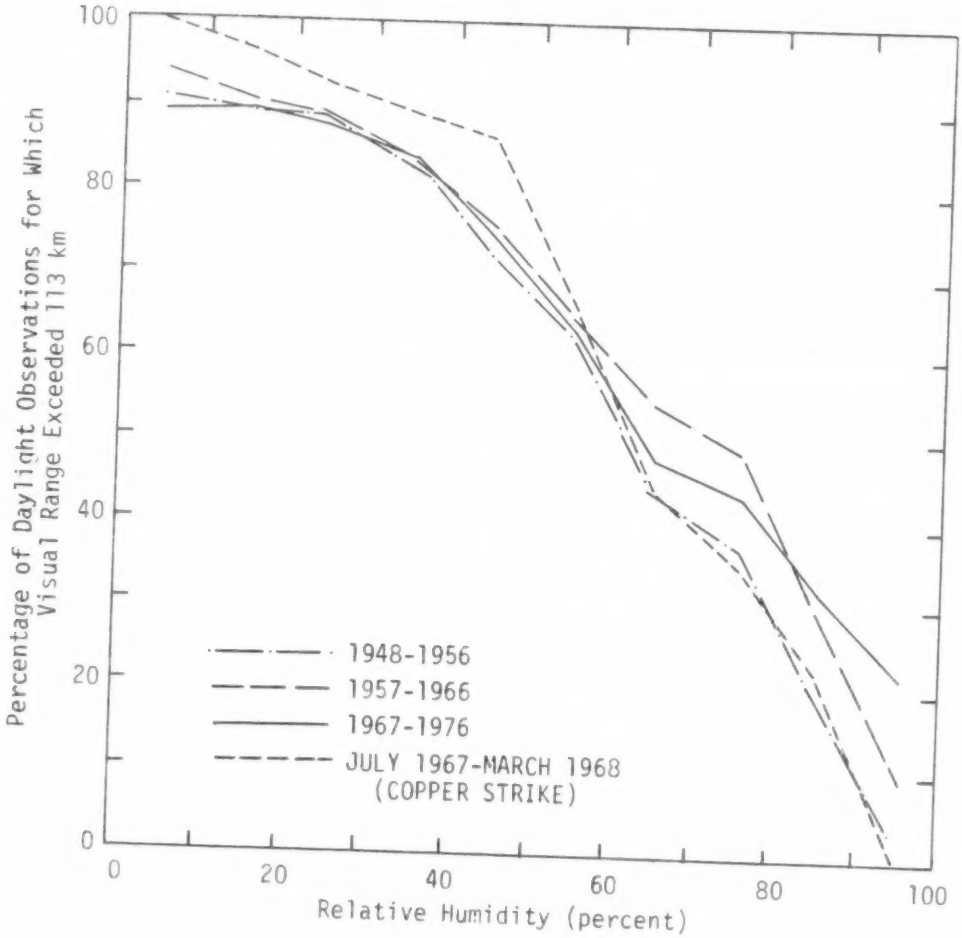

FIGURE A-43. PERCENTAGE OF DAYLIGHT OBSERVATIONS FOR WHICH VISUAL RANGE EXCEEDED 113 km, AS A FUNCTION OF RELATIVE HUMIDITY, AT GRAND JUNCTION, COLORADO

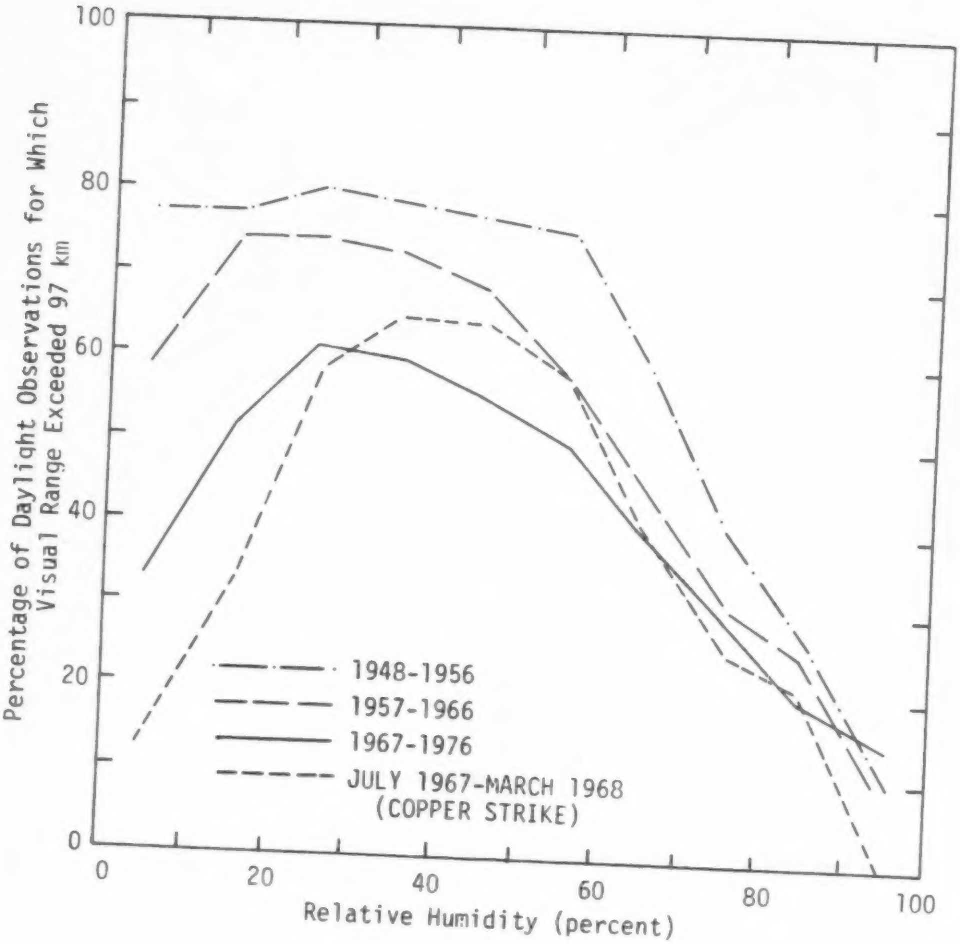

FIGURE A-44. PERCENTAGE OF DAYLIGHT OBSERVATIONS FOR WHICH VISUAL RANGE EXCEEDED 97 km, AS A FUNCTION OF RELATIVE HUMIDITY, AT GREAT FALLS, MONTANA

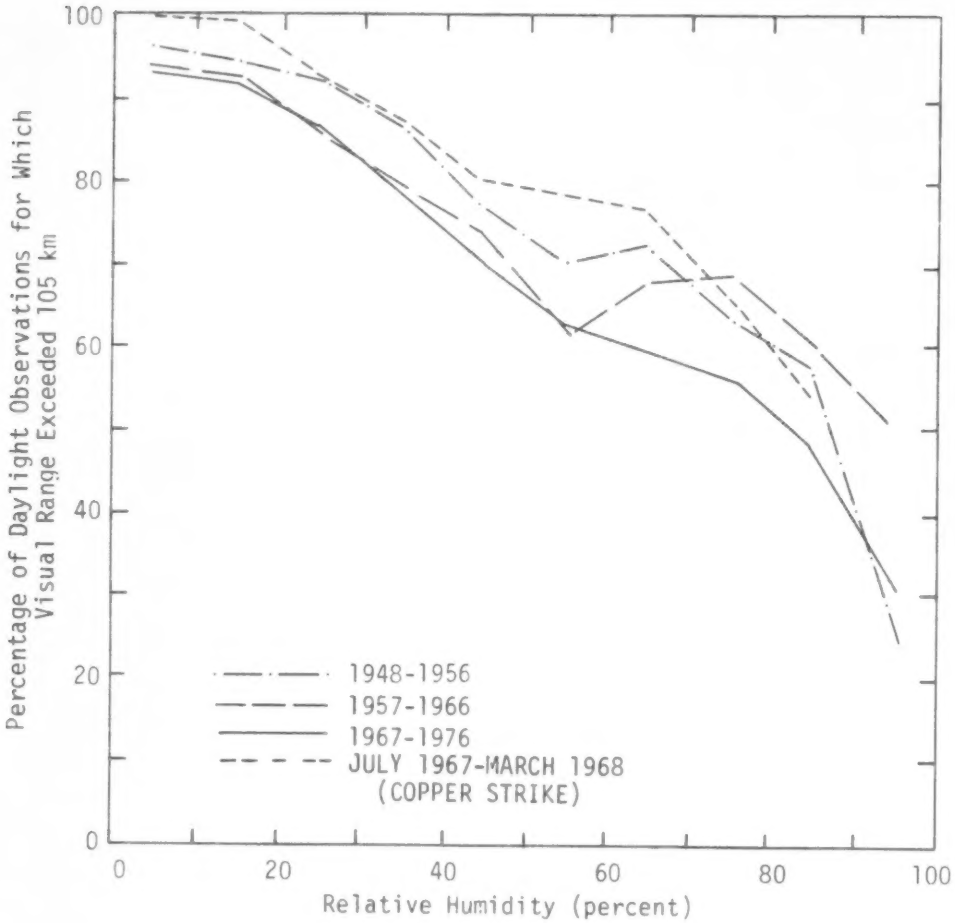

FIGURE A-45. PERCENTAGE OF DAYLIGHT OBSERVATIONS FOR WHICH VISUAL RANGE EXCEEDED 105 km, AS A FUNCTION OF RELATIVE HUMIDITY, AT PRESCOTT, ARIZONA

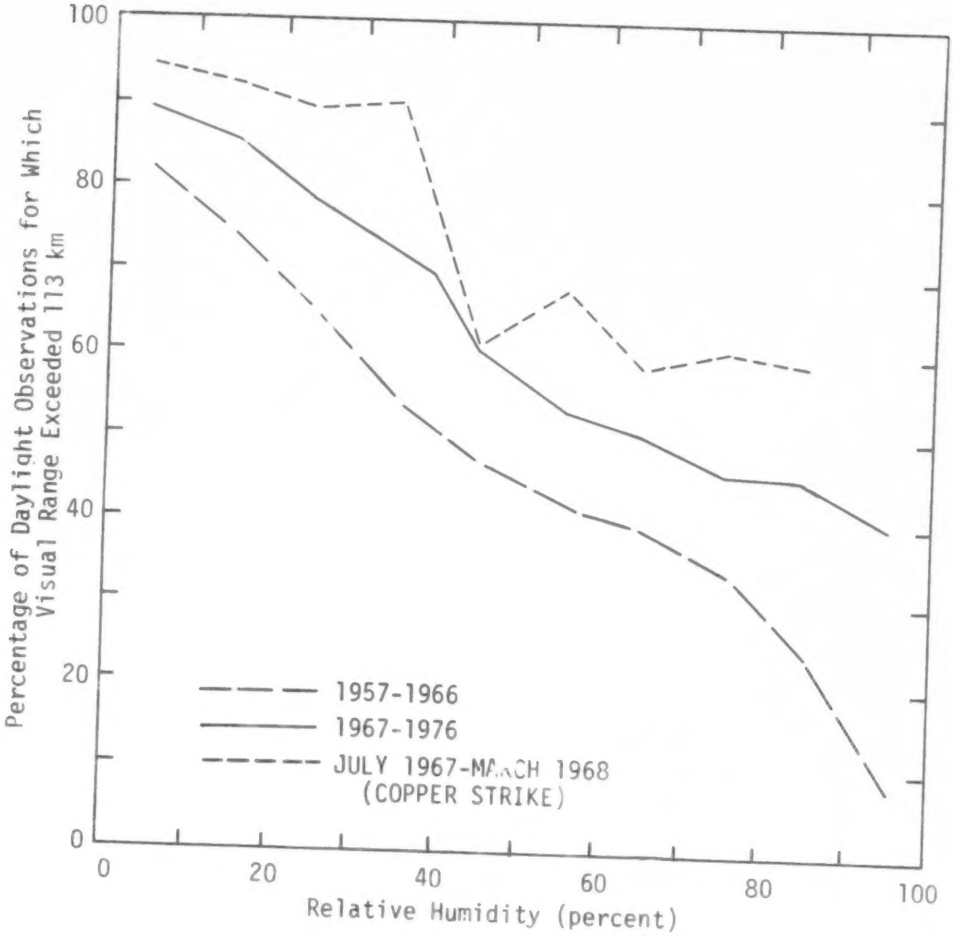

FIGURE A-46. PERCENTAGE OF DAYLIGHT OBSERVATIONS FOR WHICH VISUAL RANGE EXCEEDED 113 km, AS A FUNCTION OF RELATIVE HUMIDITY, AT PUEBLO, COLORADO

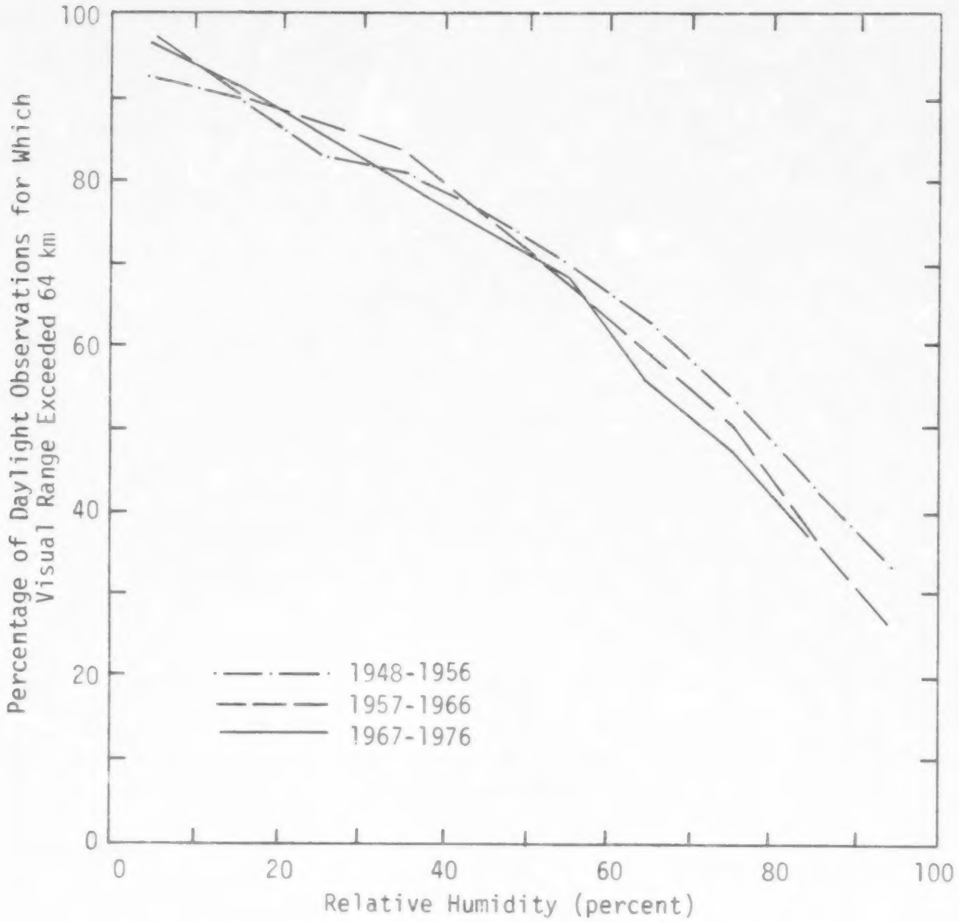

FIGURE A-47. PERCENTAGE OF DAYLIGHT OBSERVATIONS FOR WHICH VISUAL RANGE EXCEEDED 64 km, AS A FUNCTION OF RELATIVE HUMIDITY, AT ROCK SPRINGS, WYOMING

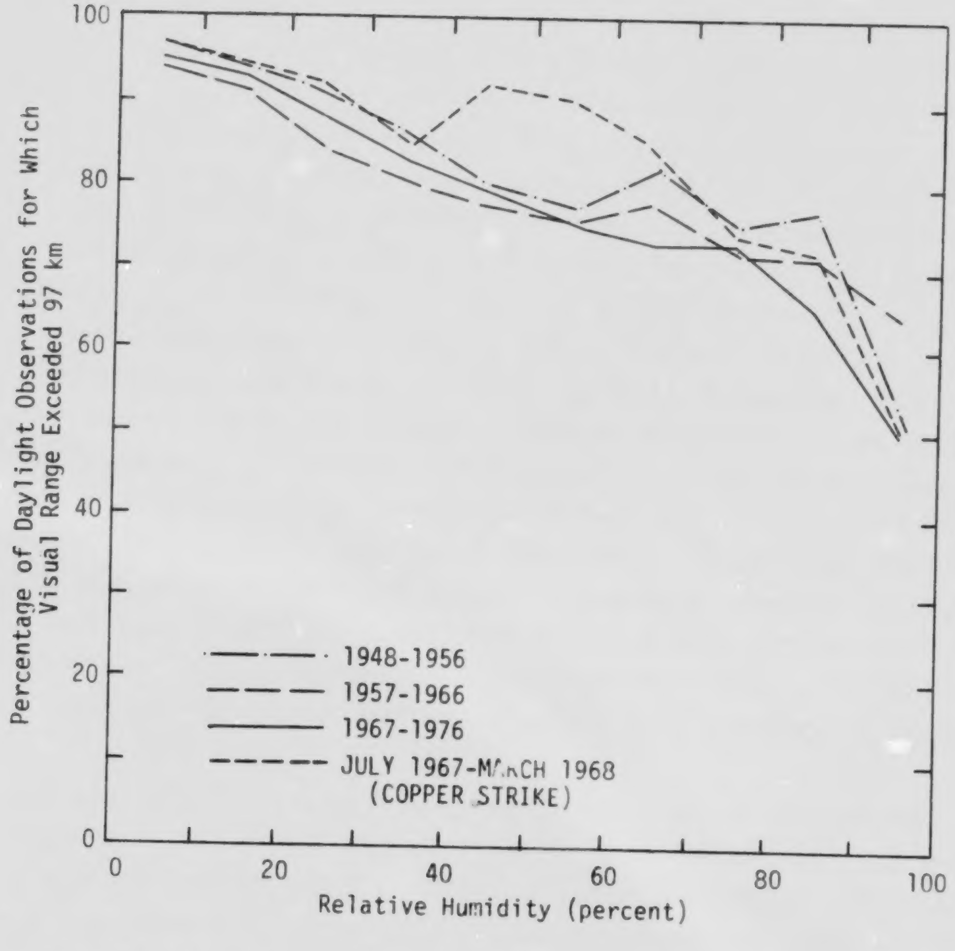

FIGURE A-48. PERCENTAGE OF DAYLIGHT OBSERVATIONS FOR WHICH VISUAL RANGE EXCEEDED 97 km, AS A FUNCTION OF RELATIVE HUMIDITY, AT WINSLOW, ARIZONA

1967 through 1976). For selected locations data for the period of a copper strike (July 1967 to March 1968) were displayed on a separate curve. As these figures indicate, relative humidity has a strong effect on visual range, yet the relative humidity dependence varies significantly from location to location, suggesting that the composition of the aerosol is a function of location. For example, in most locations, the frequency of good visibility decreases monotonically with increasing relative humidity. However, in Billings and Great Falls, Montana, visibility increases with increasing relative humidity in the range 0 to 30 percent. The reason for this relationship is not clear; perhaps the increase is the result of more wind-blown dust at very low humidities. The dependence on relative humidity in Las Vegas is different from that of other locations: A very sharp reduction in visual range occurs at relative humidities above 70 percent, suggesting the presence of an aerosol consisting of a deliquescent salt such as ammonium sulfate. Phoenix differs considerably from other locations in that visual range is almost independent of relative humidity, a condition that could be explained if the aerosol were constituted of hydrophobic organics. However, the dramatic increase in visibility in Phoenix during the copper strike suggests that a large fraction of the aerosol there is sulfate. Significant improvements in visual range resulted from the cutback in SO_2 emissions from the copper smelters during 1967 and 1968.

In addition to the dramatic improvements in visibility at the locations near the smelters (e.g., Phoenix, Tucson, Ely, and Ft. Huachuca), significant improvements were observed at locations distant from the smelters (e.g., Las Vegas, Alamogordo, Farmington, Grand Junction, Prescott, Pueblo, and Winslow). Our tentative conclusion is that visual range is impaired at locations more than 400 km away from the emission sources, which is consistent with the regional modeling results and with the observed low sulfate formation rates in clean, dry environments. The effects of SO_x emissions from copper smelters on visual range are discussed further in subsequent sections of this appendix.

It is clear from both a fundamental and phenomenological view that relative humidity has a strong effect on the mass of the liquid water associated with the accumulation mode of aerosol sulfate and nitrate and hence on the scattering coefficient and the visual range. Indeed, the strong dependence of scattering coefficient on relative humidity suggests a possible explanation for the hyperbolic shape of the scattering coefficient cumulative frequency curves shown in Figure A-7. Note that the frequency distribution curve is flat until the cumulative frequency approaches 100 percent, and then the extinction coefficient increases dramatically. The hyperbolic shape of the cumulative frequency curve suggests a mathematical relationship similar to the relationship of scattering coefficient to relative humidity (RH) for a fixed mass concentration of pollutant (i.e., sulfate). Several investigators (e.g., Trijonis and Yuan, 1977) found through multivariate analysis that the relative humidity dependence of b_{sp} can be described as follows:

$$\frac{b_{sp-SO_4^=}}{[SO_4^=]} = \frac{K_1}{1 - RH} \quad ,$$

where K_1 for Salt Lake City, for example, was found to be $0.024 \times 10^{-4} m^{-1}/\mu g/m^3$. A similar expression holds for nitrates.

We found that at the 18 NWS sites studied relative humidity is related to its cumulative frequency as follows:

$$1 - RH = (1 - x)^n \quad ,$$

where $n = 0.45 \pm 0.10$.

If we assume that the sulfate concentration at a given location is independent of the relative humidity at a given time (which is a reasonable assumption, particularly for locations distant from major SO_2 emission sources) and that the concentration of coarse mode particulate matter is also independent of relative humidity, we can combine the above two expressions with an expression for total extinction:

$$
\begin{aligned}
b_{ext} &= b_R + b_{sp\text{-}coarse} + b_{sp\text{-}accumulation} \\
&= \left[0.1 + (0.003)(\bar{x}_{coarse}) + \frac{(0.024)\left(\bar{x}_{SO_4^=} + \bar{x}_{NO_3^-}\right)}{(1 - x)^{0.45}} \right] \left[10^{-4}\ m^{-1} \right] \quad .
\end{aligned}
$$

If we substitute into this formula the values that were used earlier in the 1974 Grand Canyon example for the median concentrations of coarse mode, sulfate, and nitrate aerosol mass of 16, 1.9, and 0.4 $\mu g/m^3$, we obtain the following expression for b_{ext} as a function of cumulative frequency:

$$
b_{ext}(x) = \left[0.148 + \frac{0.053}{(1 - x)^{0.45}} \right] \left[10^{-4}\ m^{-1} \right] \quad .
$$

Using this formula, we predicted a lower bound b_{ext} of approximately $0.2 \times 10^{-4}\ m^{-1}$. This discussion suggests an approach to fitting the frequency distributions of extinction coefficient with an equation of the form:

$$
b_{ext}(x) = K_1 + \frac{K_2}{(1 - x)^{K_3}} \quad .
$$

8. EFFECT OF CLOUD COVER

The effect of cloud cover on visual range is summarized in Figures A-49 through A-66. Although visual range decreased slightly with increasing cloud cover, the dependence is not as dramatic as it is with relative humidity. One would expect that cloud cover and relative humidity are interrelated, so that the dependence on cloud cover results from the dependence on realtive humidity.

If sulfate formation were entrained in clouds, then a stronger dependence of visual range on cloud cover might occur. However, at

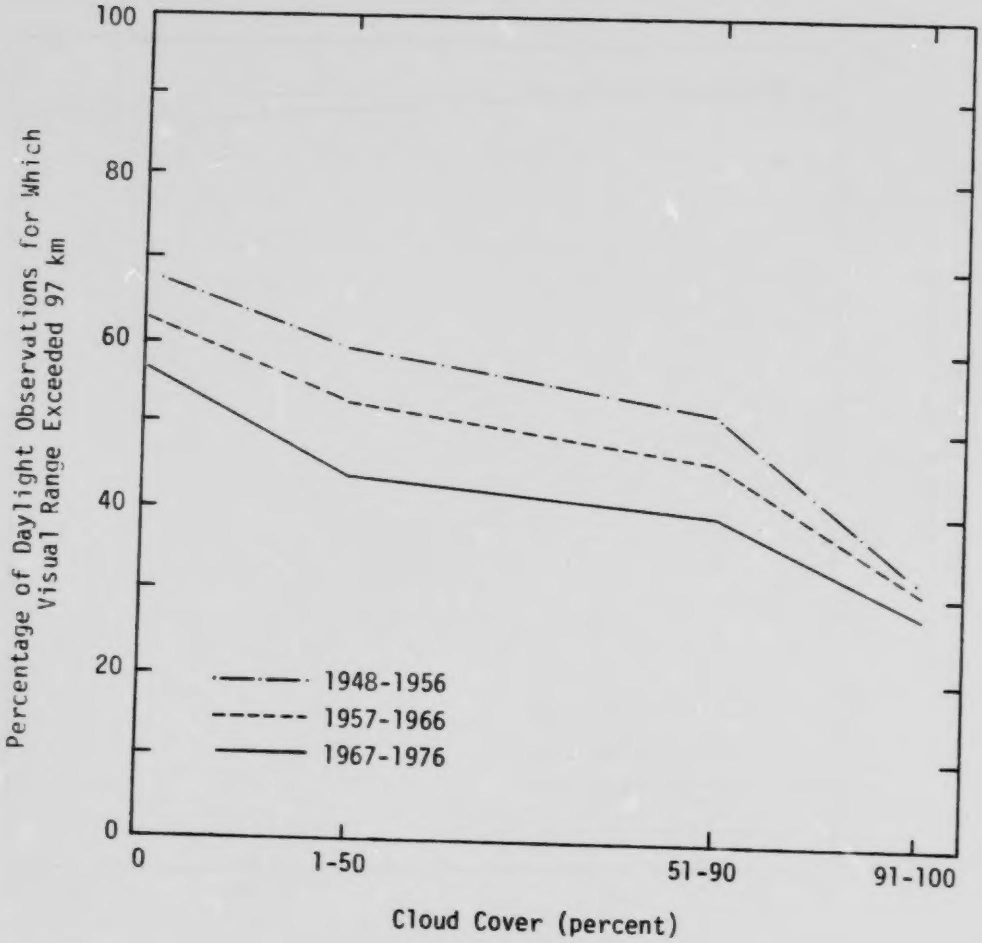

FIGURE A-49. PERCENTAGE OF DAYLIGHT OBSERVATIONS FOR WHICH VISUAL RANGE EXCEEDED 97 km, AS A FUNCTION OF CLOUD COVER, AT DENVER, COLORADO

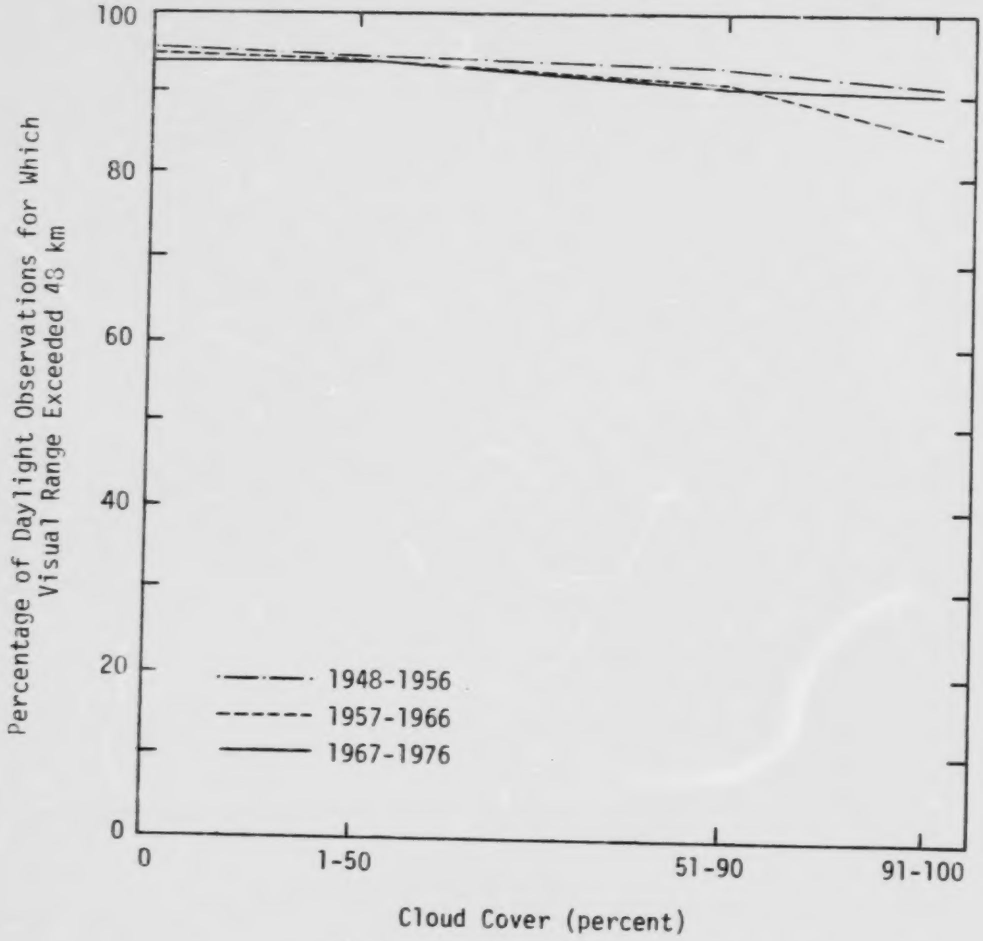

FIGURE 50. PERCENTAGE OF DAYLIGHT OBSERVATIONS FOR WHICH VISUAL RANGE EXCEEDED 48 km, AS A FUNCTION OF CLOUD COVER, AT LAS VEGAS, NEVADA

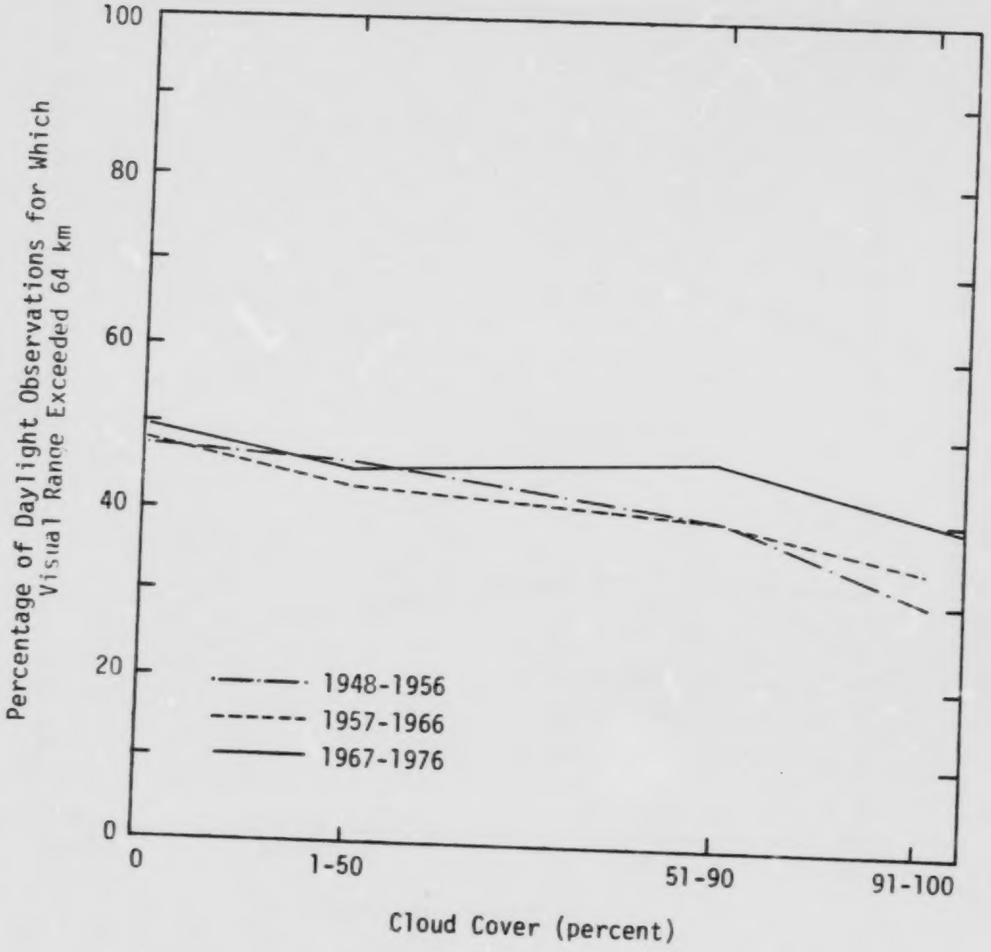

FIGURE A-51. PERCENTAGE OF DAYLIGHT OBSERVATIONS FOR WHICH VISUAL RANGE EXCEEDED 64 km, AS A FUNCTION OF CLOUD COVER, AT PHOENIX, ARIZONA

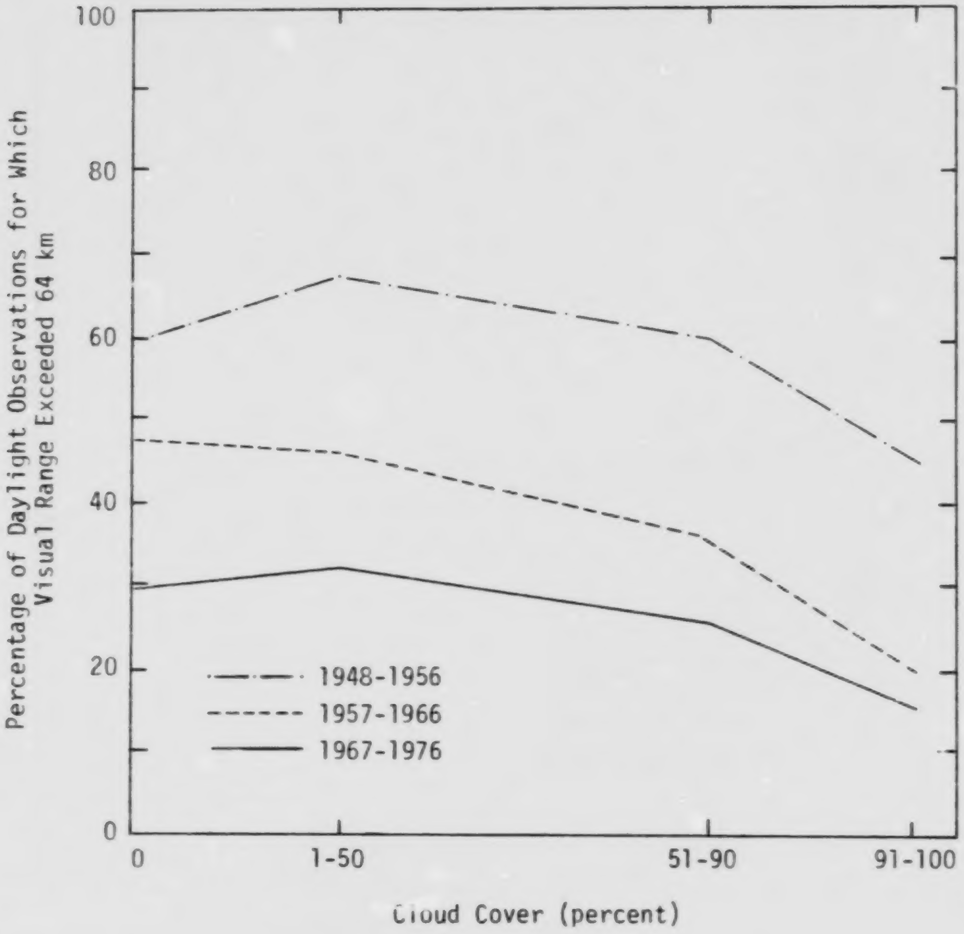

FIGURE A-52. PERCENTAGE OF DAYLIGHT OBSERVATIONS FOR WHICH VISUAL RANGE EXCEEDED 64 km, AS A FUNCTION OF CLOUD COVER, AT SALT LAKE CITY, UTAH

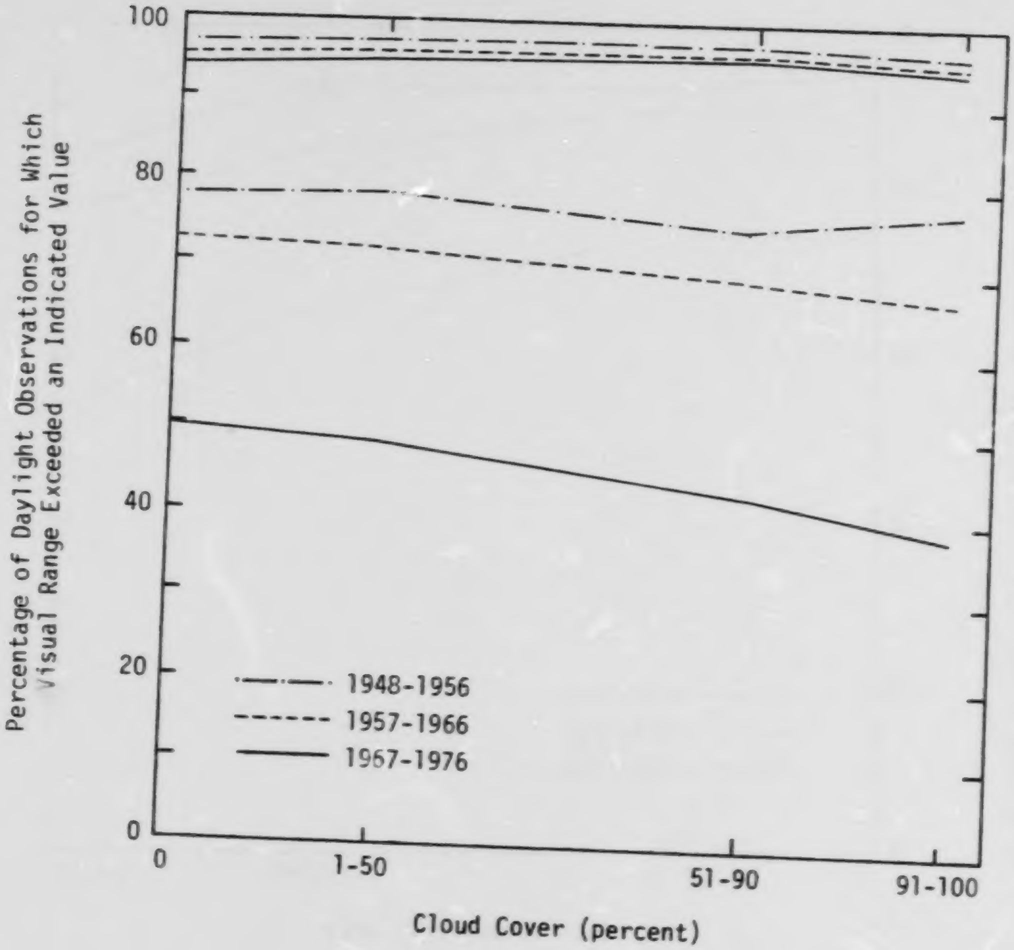

FIGURE A-53. PERCENTAGE OF DAYLIGHT OBSERVATIONS FOR WHICH VISUAL RANGE EXCEEDED AN INDICATED VALUE, AS A FUNCTION OF CLOUD COVER, AT TUCSON, ARIZONA

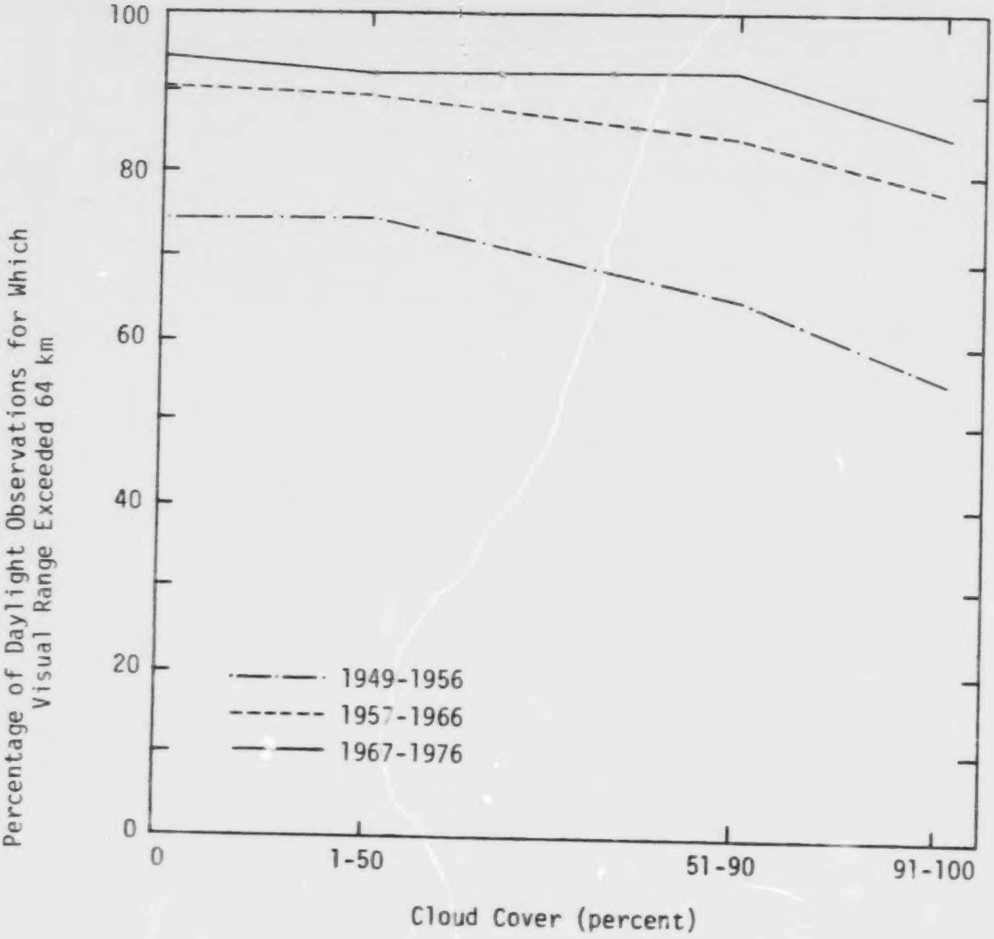

FIGURE A-54. PERCENTAGE OF DAYLIGHT OBSERVATIONS FOR WHICH VISUAL RANGE EXCEEDED 64 km, AS A FUNCTION OF CLOUD COVER, AT ALAMOGORDO, NEW MEXICO

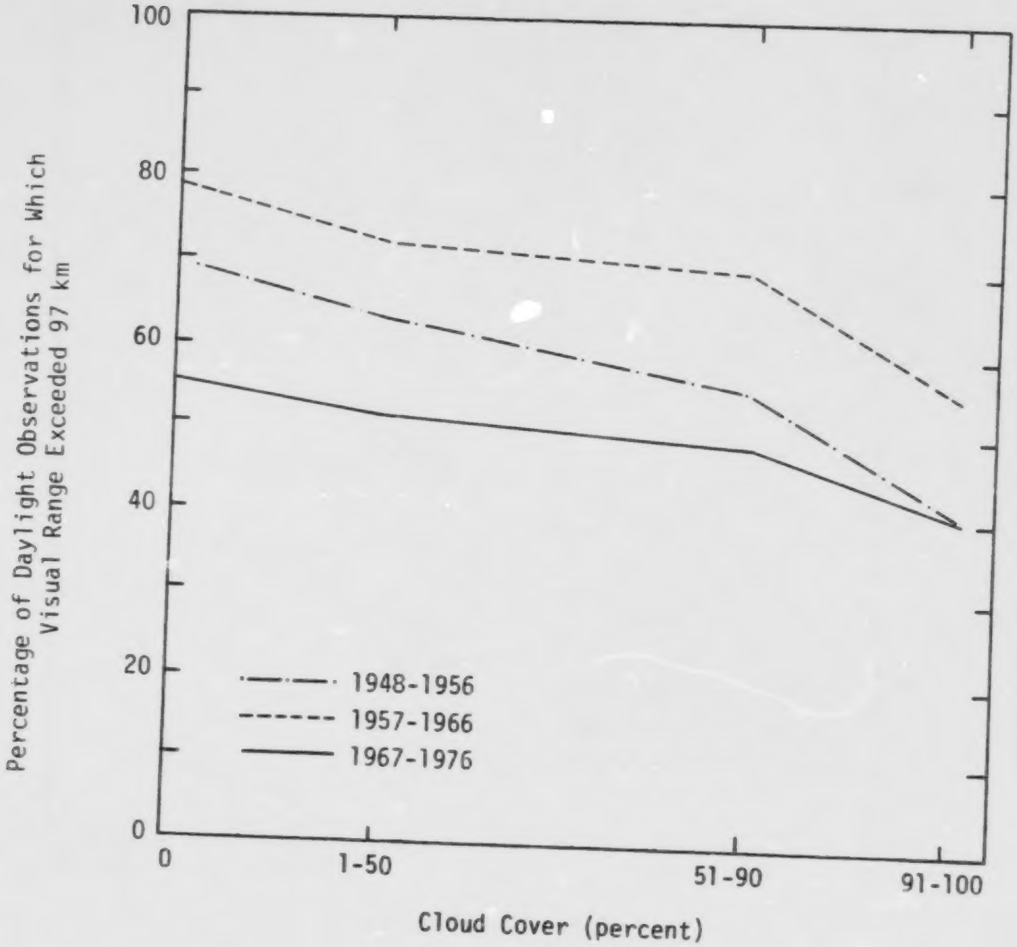

FIGURE A-55. PERCENTAGE OF DAYLIGHT OBSERVATIONS FOR WHICH VISUAL RANGE EXCEEDED 97 km, AS A FUNCTION OF CLOUD COVER, AT BILLINGS, MONTANA

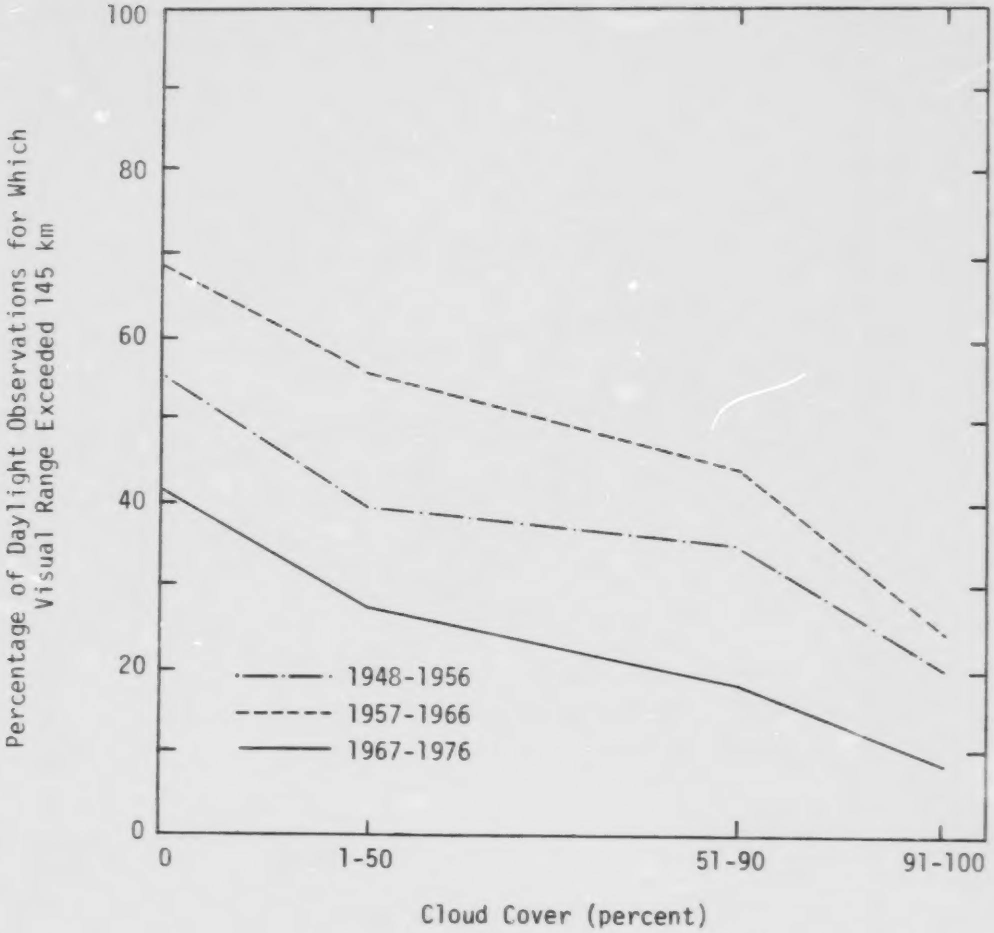

FIGURE A-56. PERCENTAGE OF DAYLIGHT OBSERVATIONS FOR WHICH VISUAL RANGE EXCEEDED 145 km, AS A FUNCTION OF CLOUD COVER, AT CHEYENNE, WYOMING

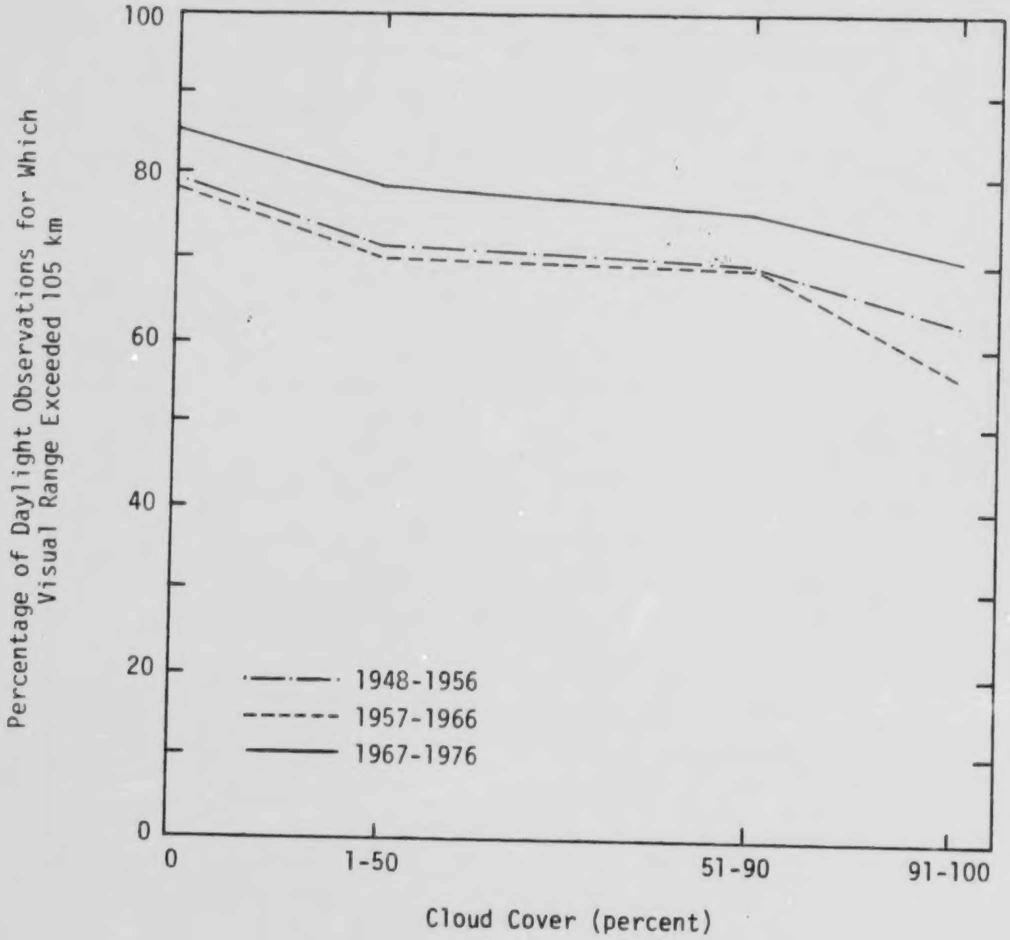

FIGURE A-57. PERCENTAGE OF DAYLIGHT OBSERVATIONS FOR WHICH VISUAL RANGE EXCEEDED 105 km, AS A FUNCTION OF CLOUD COVER, AT COLORADO SPRINGS, COLORADO

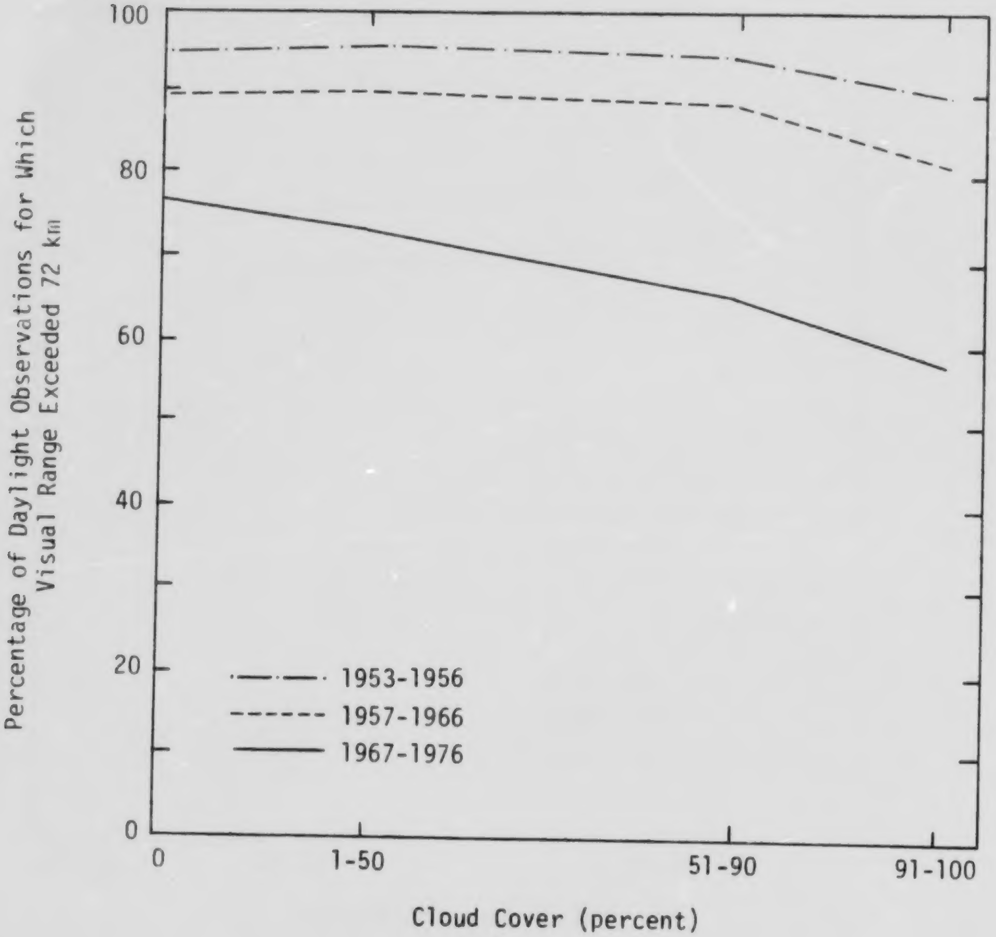

FIGURE A-58. PERCENTAGE OF DAYLIGHT OBSERVATIONS FOR WHICH VISUAL RANGE EXCEEDED 72 km, AS A FUNCTION OF CLOUD COVER, AT ELY, NEVADA

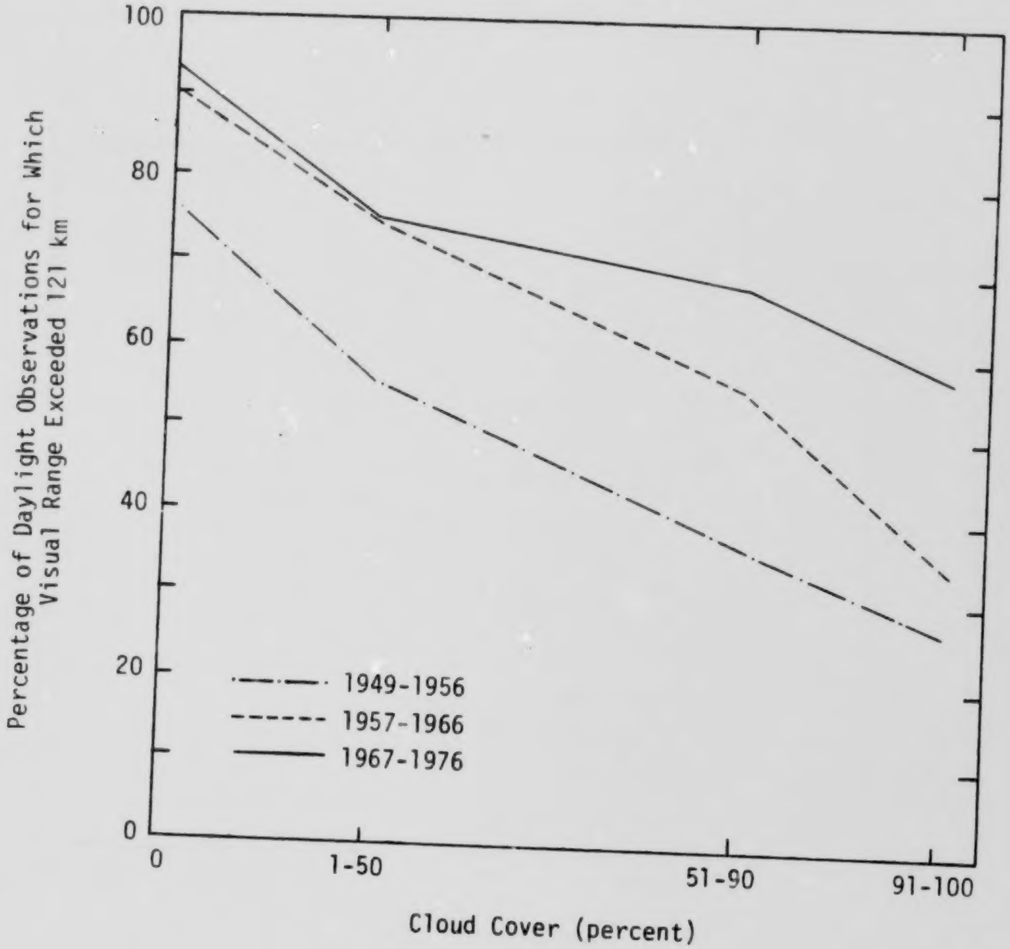

FIGURE A-59. PERCENTAGE OF DAYLIGHT OBSERVATIONS FOR WHICH VISUAL RANGE EXCEEDED 121 km, AS A FUNCTION OF CLOUD COVER, AT FARMINGTON, NEW MEXICO

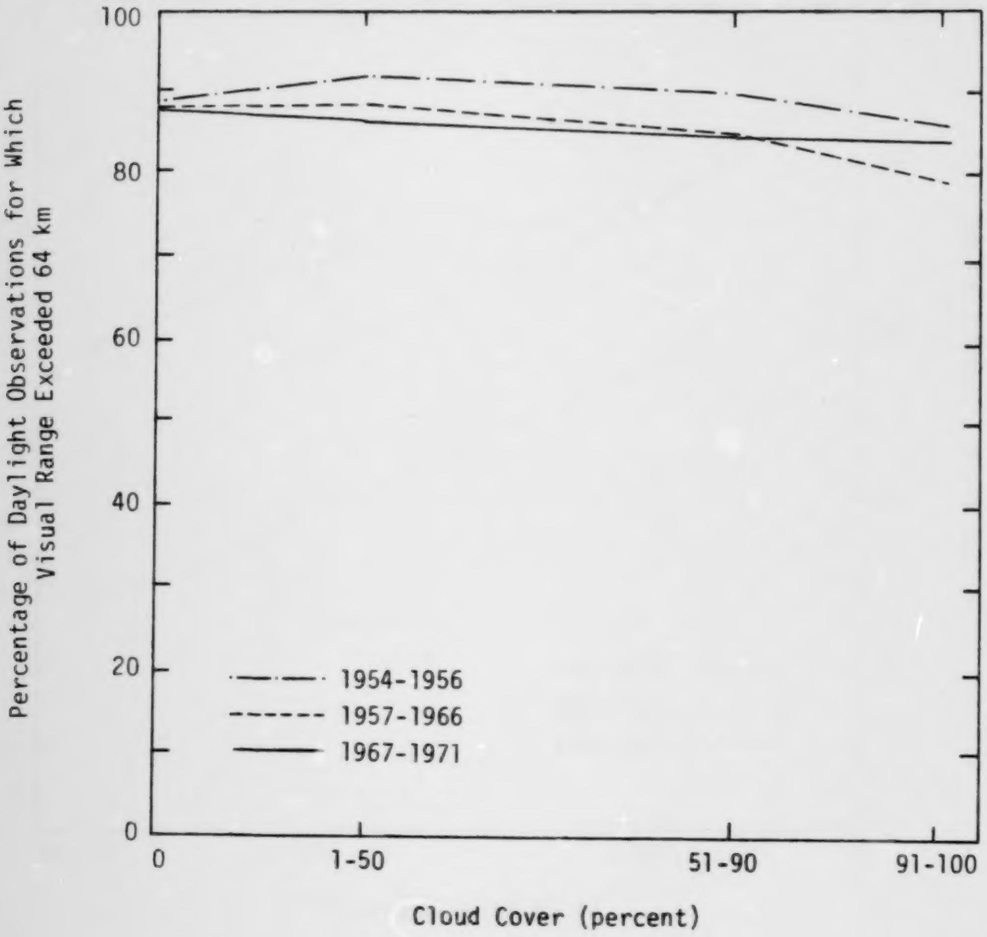

FIGURE A-60. PERCENTAGE OF DAYLIGHT OBSERVATIONS FOR WHICH VISUAL RANGE EXCEEDED 64 km, AS A FUNCTION OF CLOUD COVER, AT FT. HUACHUCA, ARIZONA

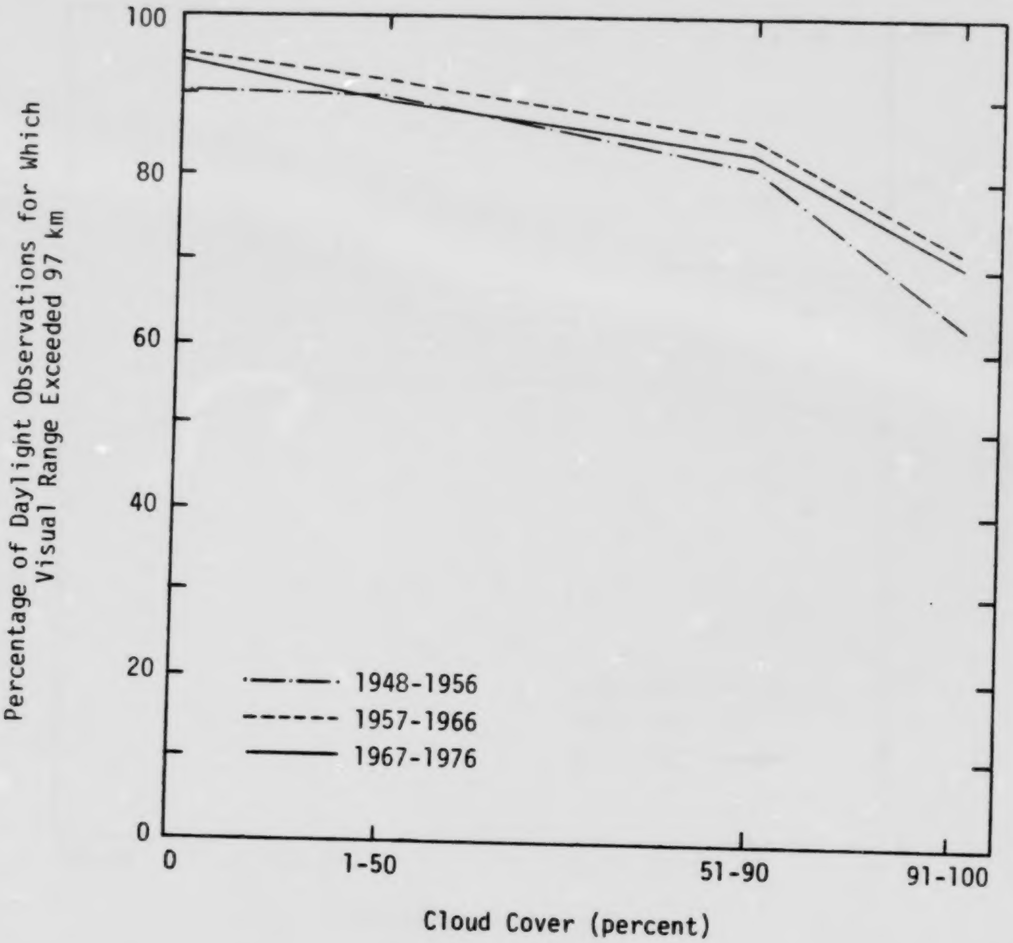

FIGURE A-61. PERCENTAGE OF DAYLIGHT OBSERVATIONS FOR WHICH VISUAL RANGE EXCEEDED 97 km, AS A FUNCTION OF CLOUD COVER, AT GRAND JUNCTION, COLORADO

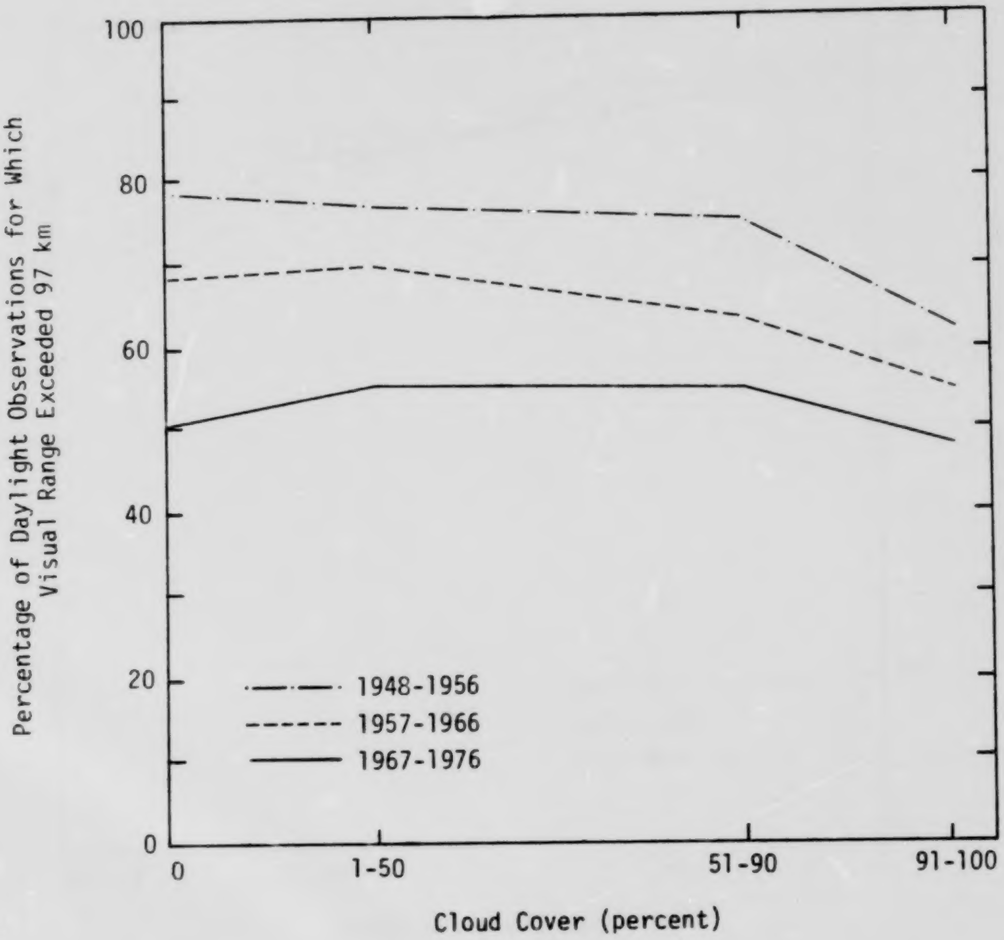

FIGURE A-62. PERCENTAGE OF DAYLIGHT OBSERVATIONS FOR WHICH VISUAL RANGE EXCEEDED 97 km, AS A FUNCTION OF CLOUD COVER, AT GREAT FALLS, MONTANA

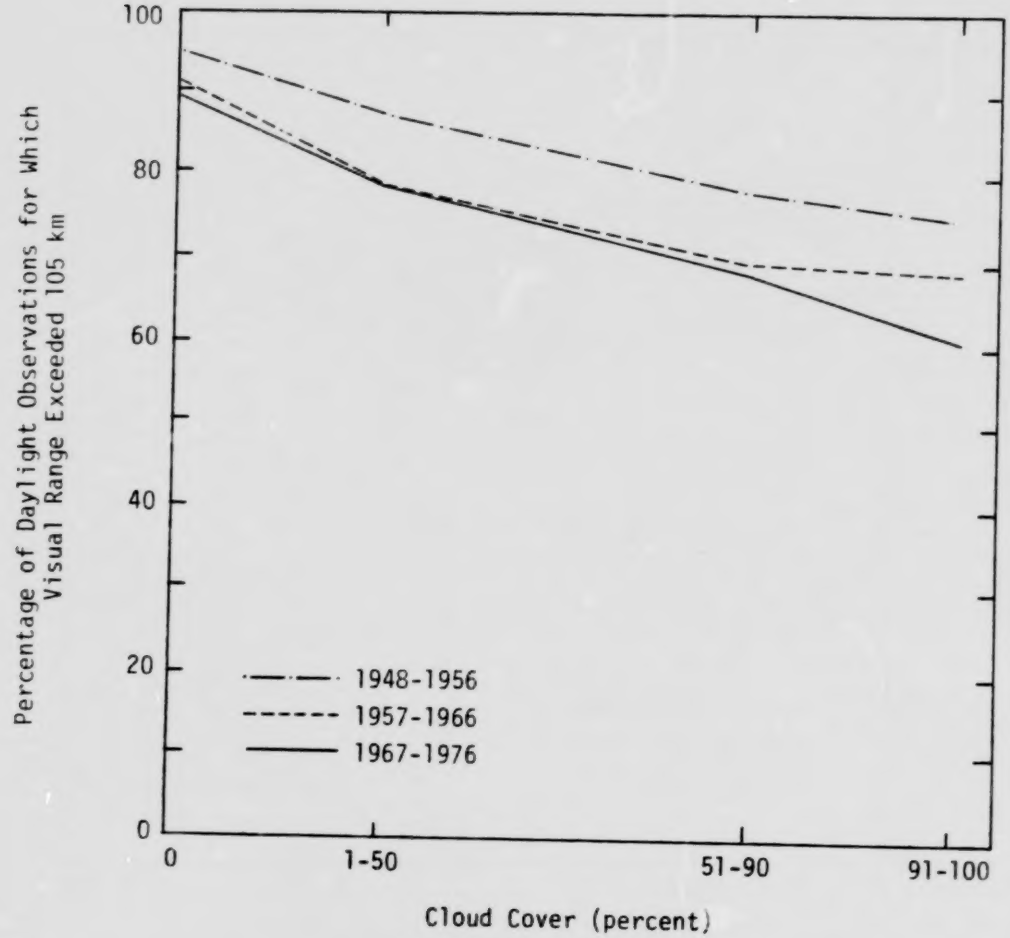

FIGURE A-63. PERCENTAGE OF DAYLIGHT OBSERVATIONS FOR WHICH VISUAL RANGE EXCEEDED 105 km, AS A FUNCTION OF CLOUD COVER, AT PRESCOTT, ARIZONA

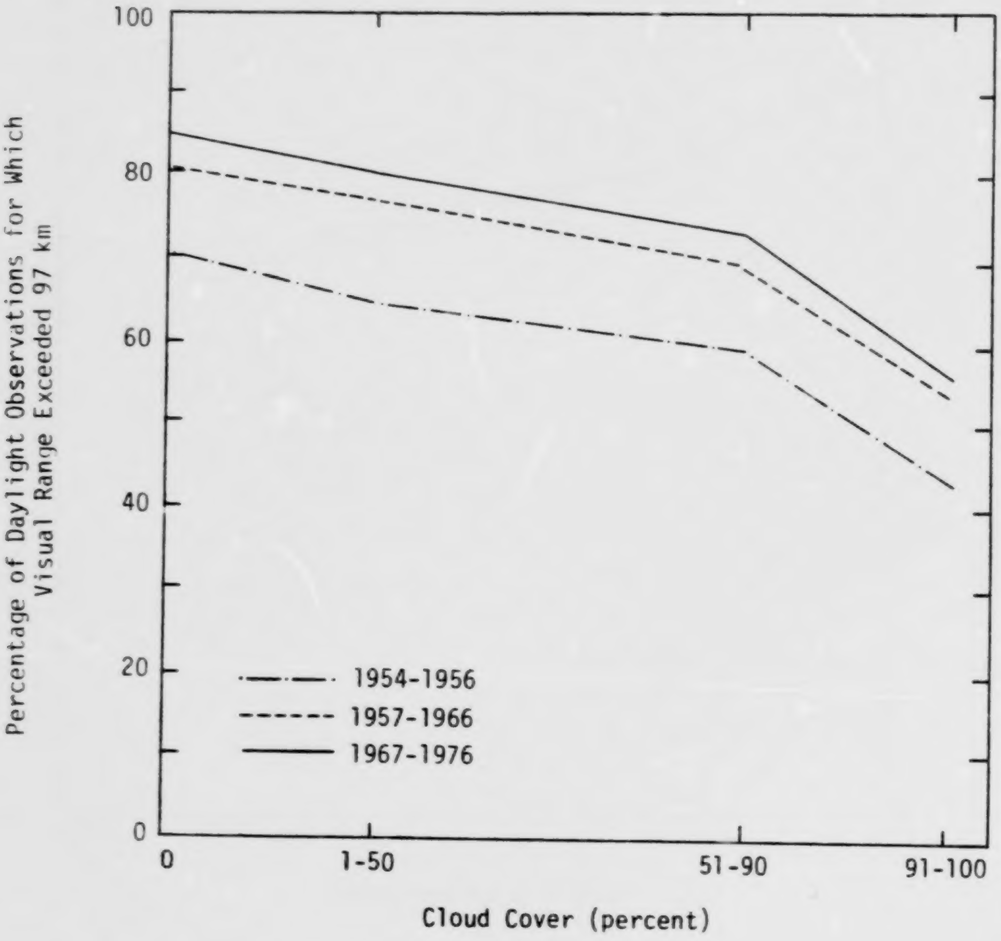

FIGURE A-64. PERCENTAGE OF DAYLIGHT OBSERVATIONS FOR WHICH VISUAL RANGE EXCEEDED 97 km, AS A FUNCTION OF CLOUD COVER, AT PUEBLO, COLORADO

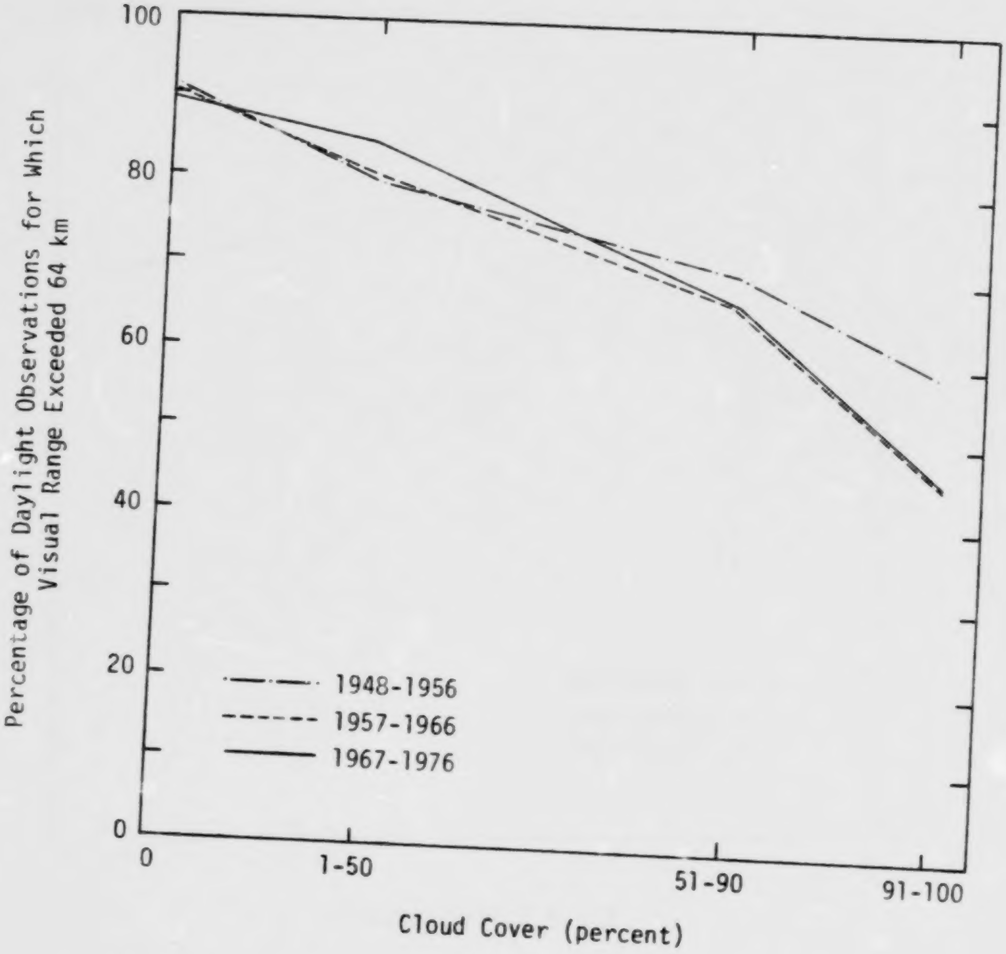

FIGURE A-65. PERCENTAGE OF DAYLIGHT OBSERVATIONS FOR WHICH VISUAL RANGE EXCEEDED 64 km, AS A FUNCTION OF CLOUD COVER, AT ROCK SPRINGS, WYOMING

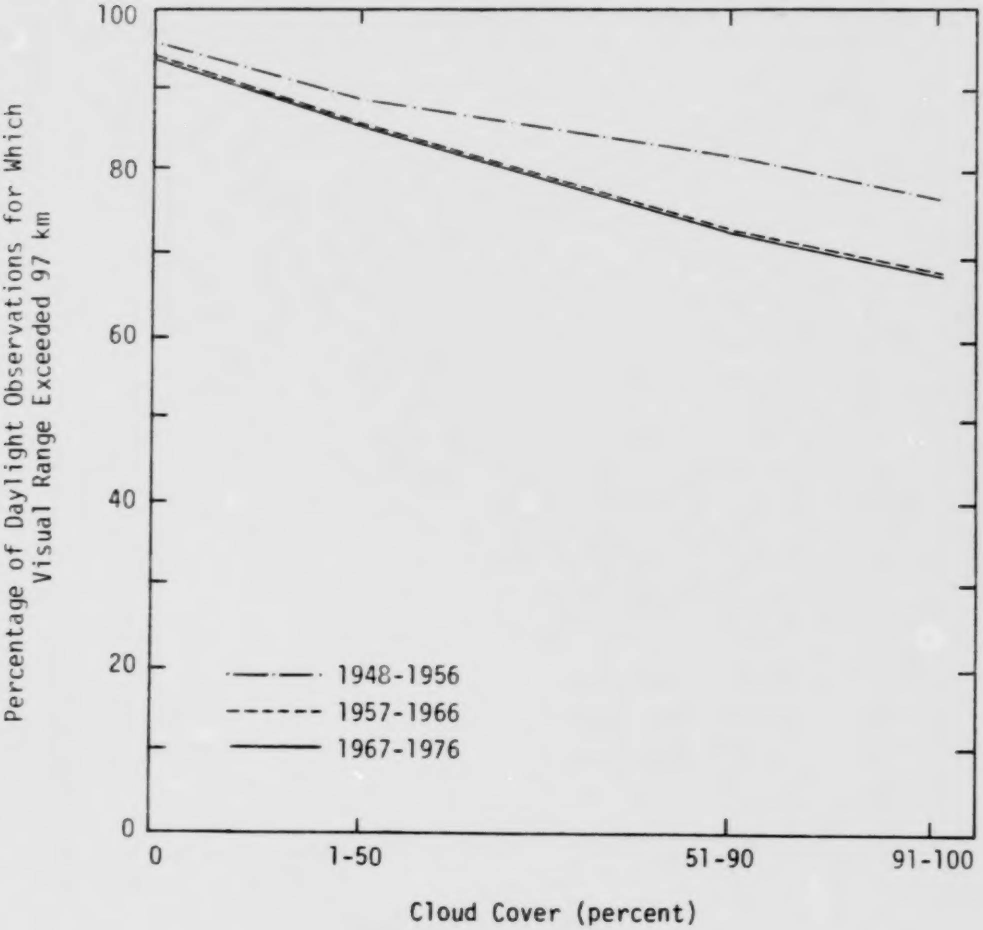

FIGURE A-66. PERCENTAGE OF DAYLIGHT OBSERVATIONS FOR WHICH VISUAL RANGE EXCEEDED 97 km, AS A FUNCTION OF CLOUD COVER, AT WINSLOW, ARIZONA

Phoenix, Salt Lake City, Tucson, and Ely, which are located near copper smelters that emit large quantities of SO_2, there is not a strong dependence on cloud cover.

Cloud cover may cause a reduction in visual range simply by obscuring the distant visibility marker, a condition that would occur if, for example, the marker were a mountain.

9. EFFECT OF BAROMETRIC PRESSURE

Figures A-67 through A-84 show the effect of barometric pressure on visual range at the 18 NWS locations. At most locations a reduction in visual range was observed at low atmospheric pressures; this effect appears to be caused by the high relative humidity and cloud cover associated with lows. Conversely, highs are associated with dry, clear skies.

However, stagnation conditions are also associated with high pressure systems, and therefore, one might expect reduced visibility during highs in an area where the pollution emission density is large. Such an effect was observed only at Salt Lake City (Figure A-70), Ely (Figure A-76), Grand Junction (Figure A-79), and Pueblo (Figure A-82). Ely and Salt Lake City are near large copper smelters; during a high, pollution may be trapped in a stagnating air mass, thus decreasing visual range. Although similar results might be expected at Denver, Las Vegas, Phoenix, and Tucson, such effects were not observed. The effect of atmospheric stagnation and ventilation was studied directly by analyzing the dependence of visual range on ventilation, which is reported in Section 10.

10. EFFECT OF VENTILATION

Ventilation, which is the product of the mixing depth and the average wind speed in the mixed layer, is a measure of the dilution capacity of the atmosphere at a given location and time. The mixing depth and wind speed data that were developed by Holzworth (1972) for several locations

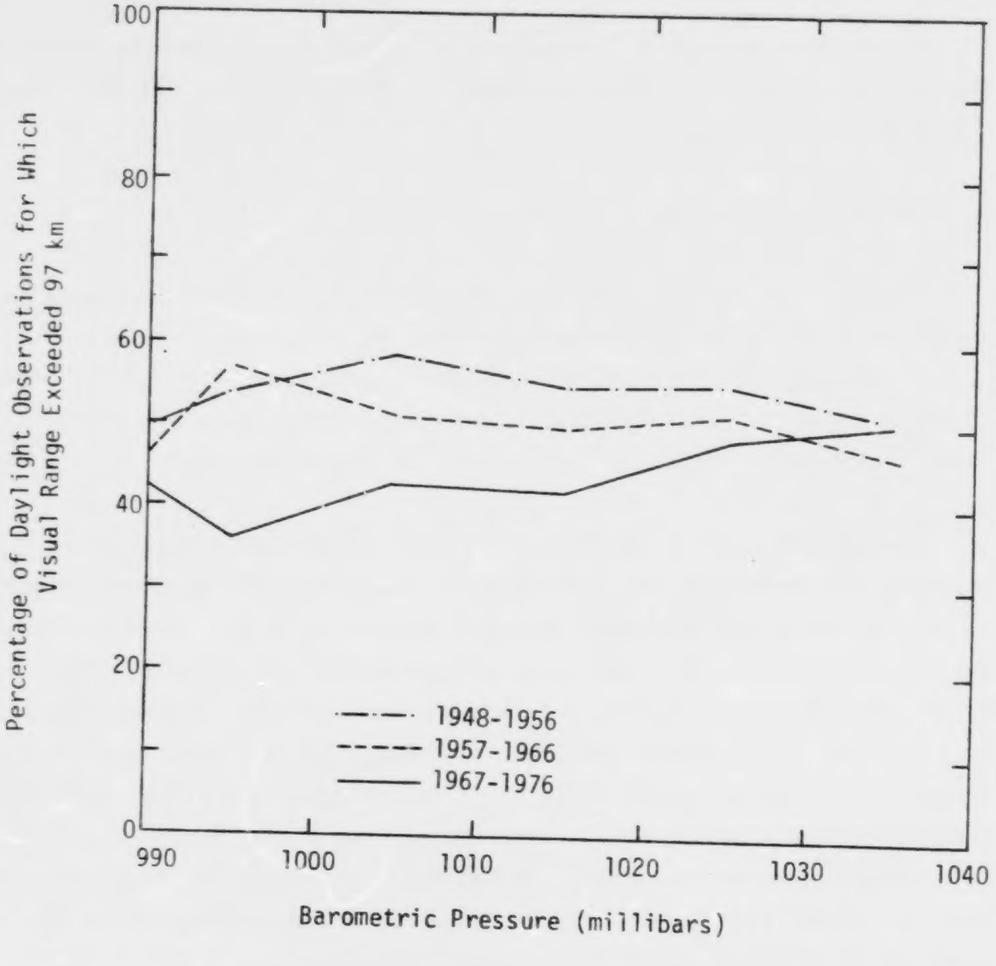

FIGURE A-67. PERCENTAGE OF DAYLIGHT OBSERVATIONS FOR WHICH VISUAL RANGE EXCEEDED 97 km, AS A FUNCTION OF BAROMETRIC PRESSURE, AT DENVER, COLORADO

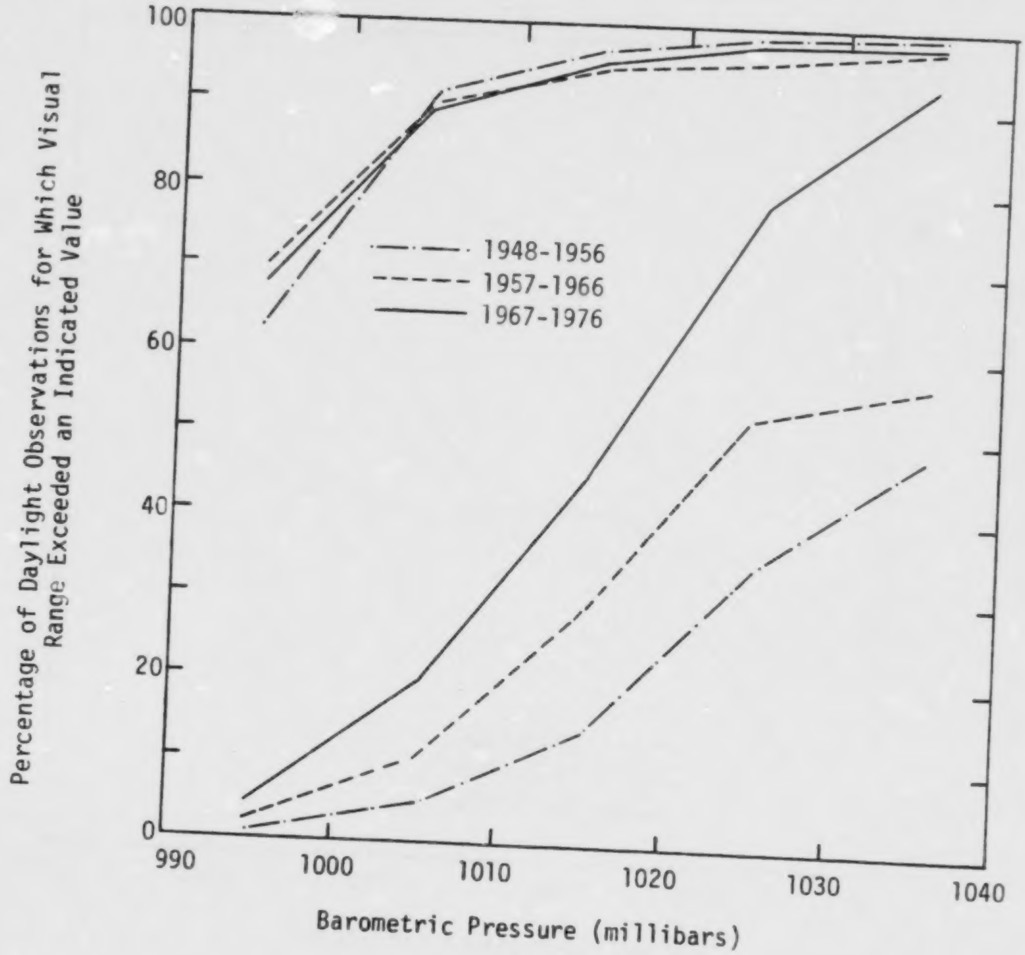

FIGURE A-68. PERCENTAGE OF DAYLIGHT OBSERVATIONS FOR WHICH VISUAL RANGE EXCEEDED INDICATED VALUE, AS A FUNCTION OF BAROMETRIC PRESSURE, AT LAS VEGAS, NEVADA

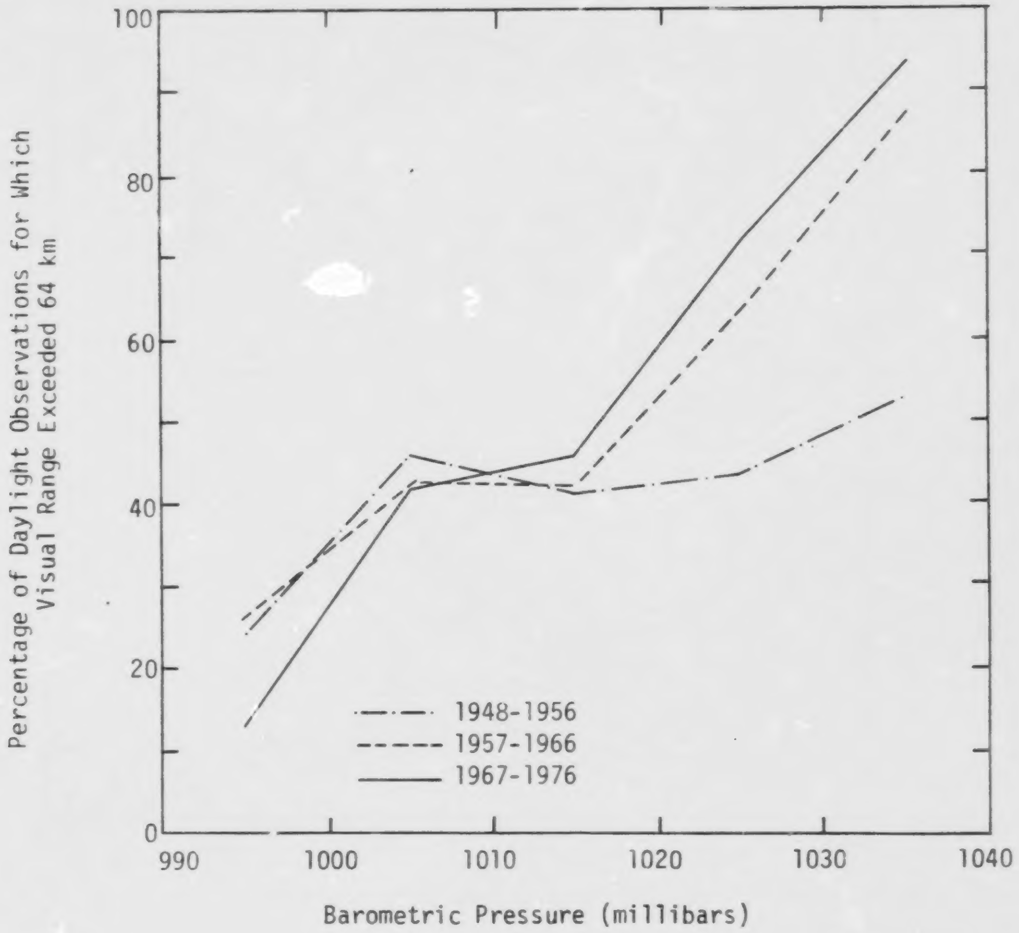

FIGURE A-69. PERCENTAGE OF DAYLIGHT OBSERVATIONS FOR WHICH VISUAL RANGE EXCEEDED 64 km, AS A FUNCTION OF BAROMETRIC PRESSURE, AT PHOENIX, ARIZONA

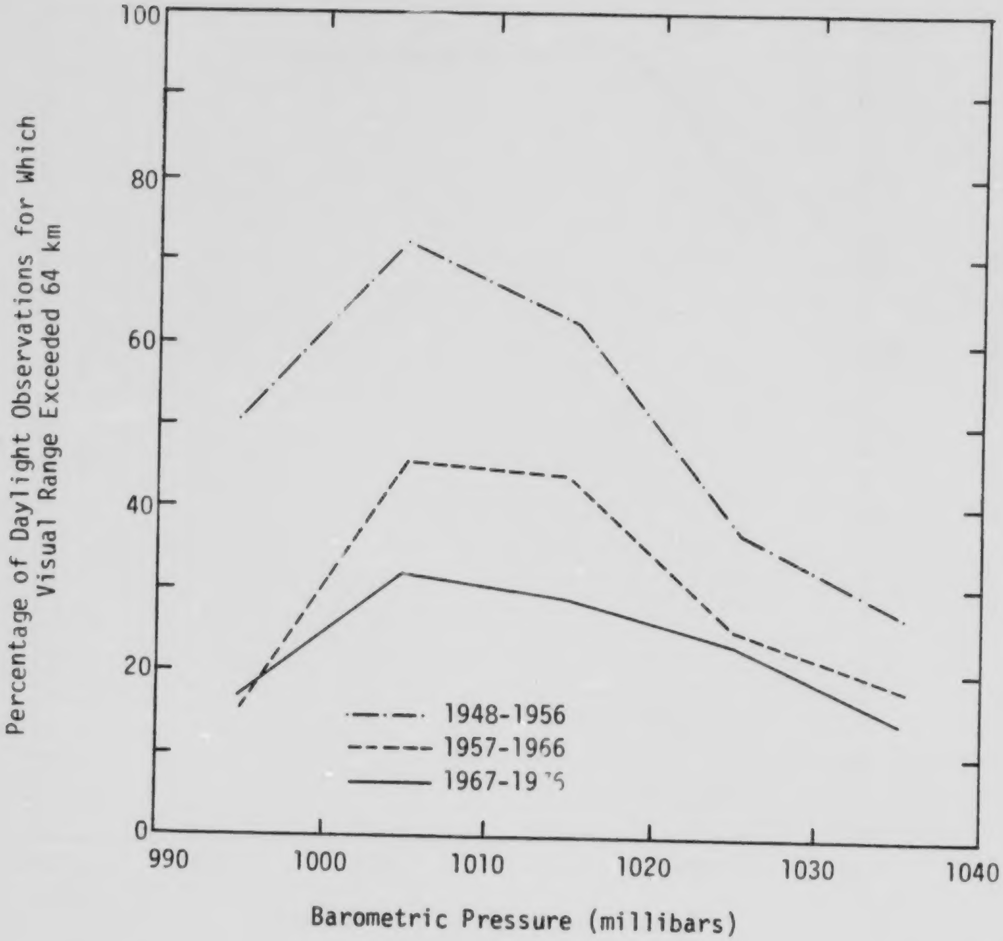

FIGURE A-70. PERCENTAGE OF DAYLIGHT OBSERVATIONS FOR WHICH VISUAL RANGE EXCEEDED 64 km, AS A FUNCTION OF BAROMETRIC PRESSURE, AT SALT LAKE CITY, UTAH

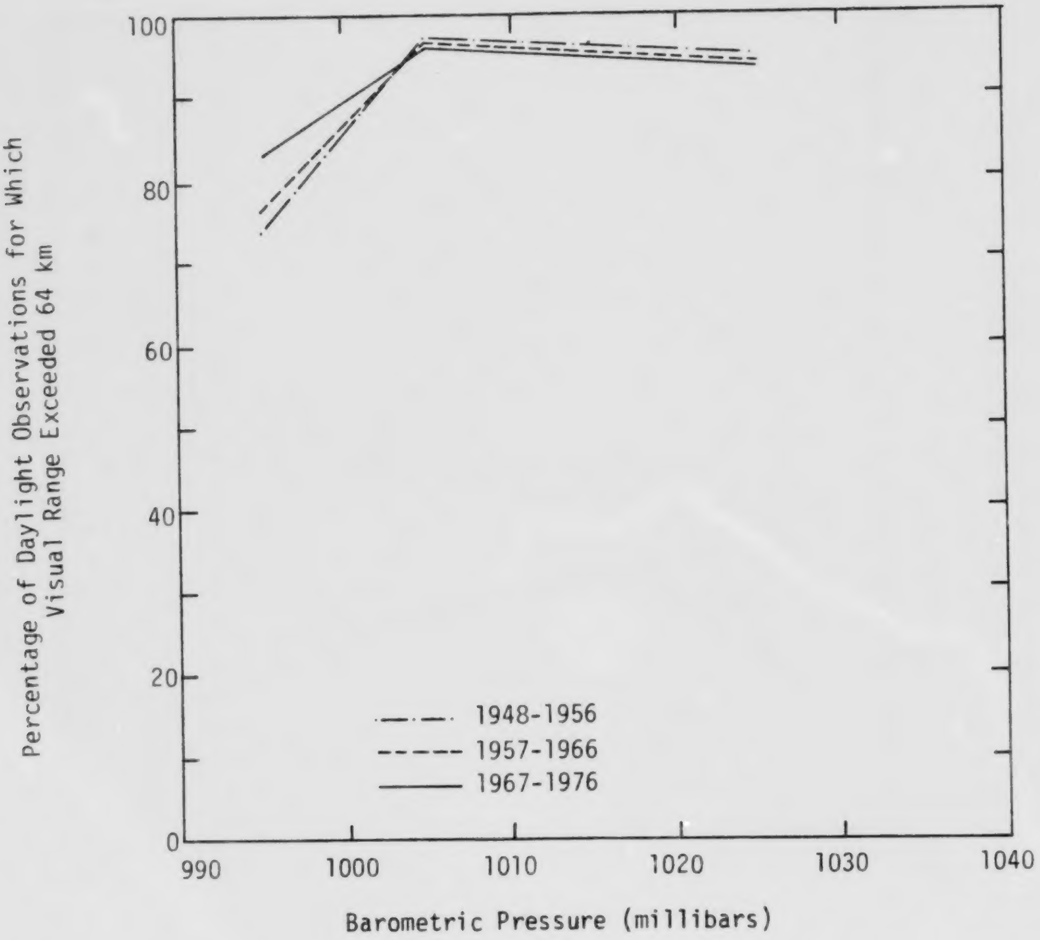

FIGURE A-71. PERCENTAGE OF DAYLIGHT OBSERVATIONS FOR WHICH VISUAL RANGE EXCEEDED 64 km, AS A FUNCTION OF BAROMETRIC PRESSURE, AT TUCSON, ARIZONA

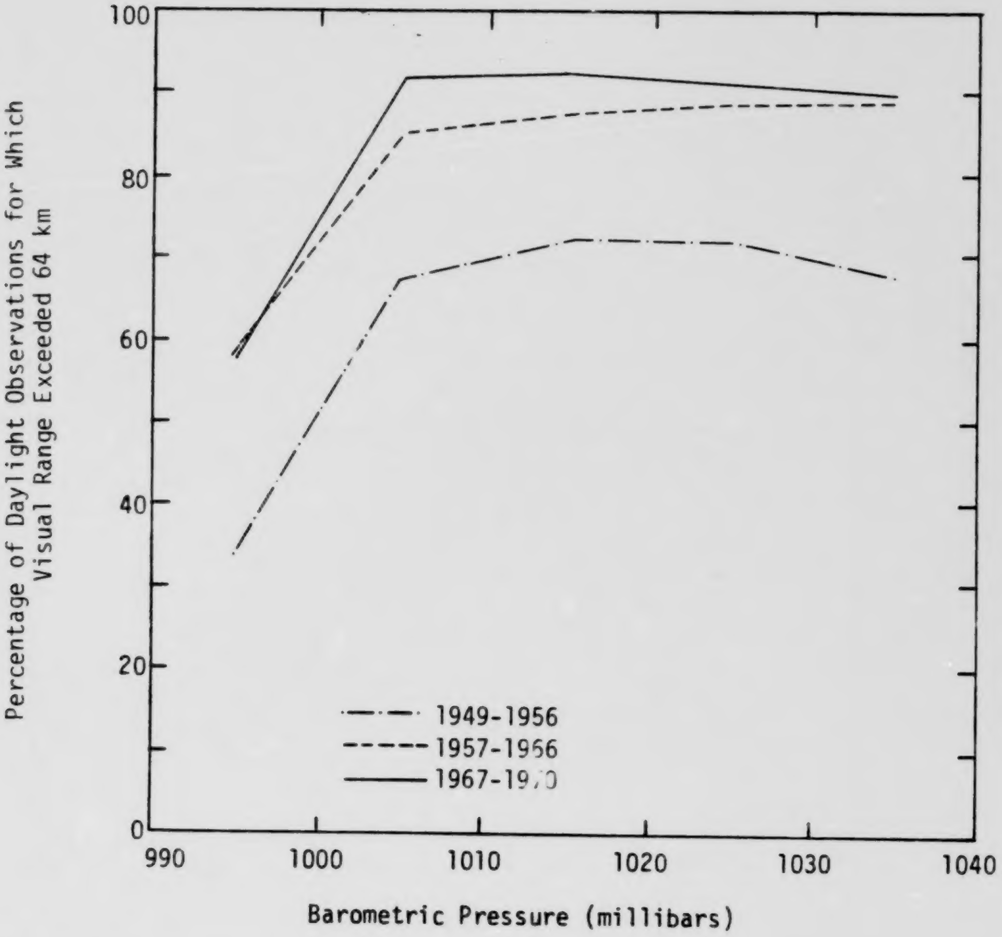

FIGURE A-72. PERCENTAGE OF DAYLIGHT OBSERVATIONS FOR WHICH VISUAL RANGE EXCEEDED 64 km, AS A FUNCTION OF BAROMETRIC PRESSURE, AT ALAMOGORDO, NEW MEXICO

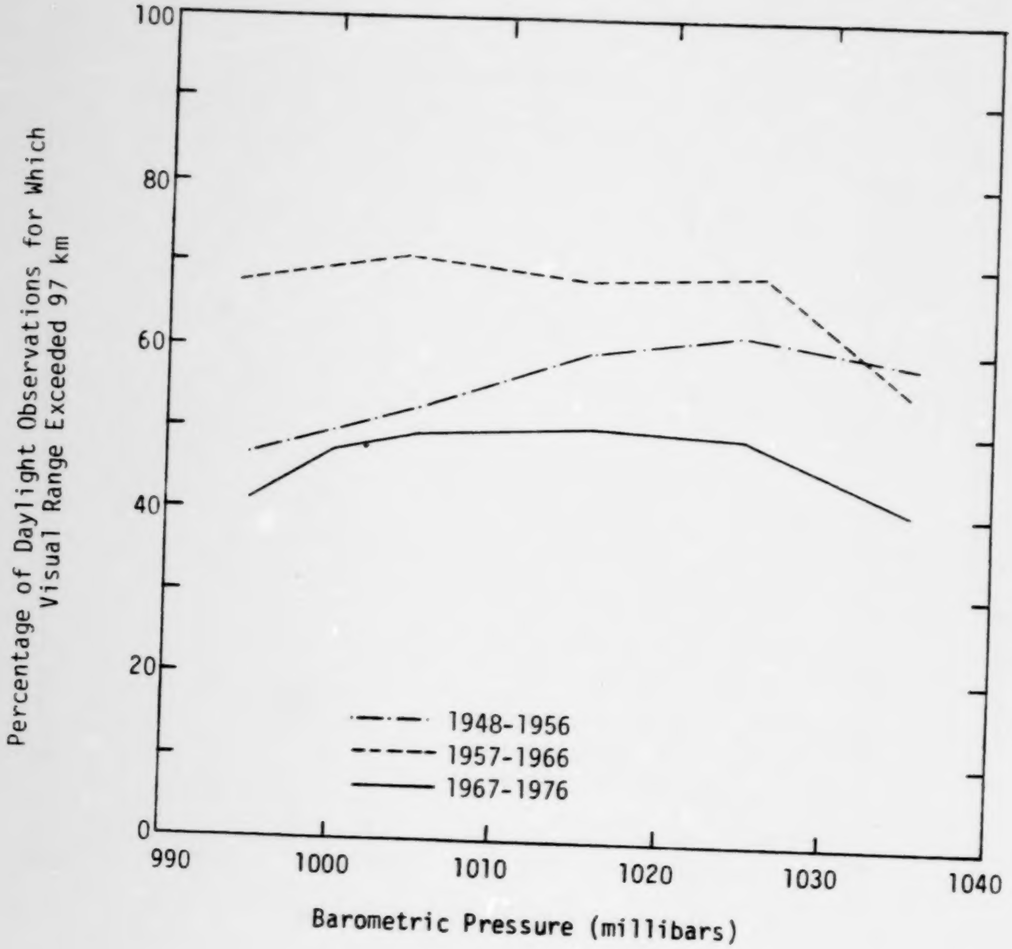

FIGURE A-73. PERCENTAGE OF DAYLIGHT OBSERVATIONS FOR WHICH VISUAL RANGE EXCEEDED 97 km, AS A FUNCTION OF BAROMETRIC PRESSURE, AT BILLINGS, MONTANA

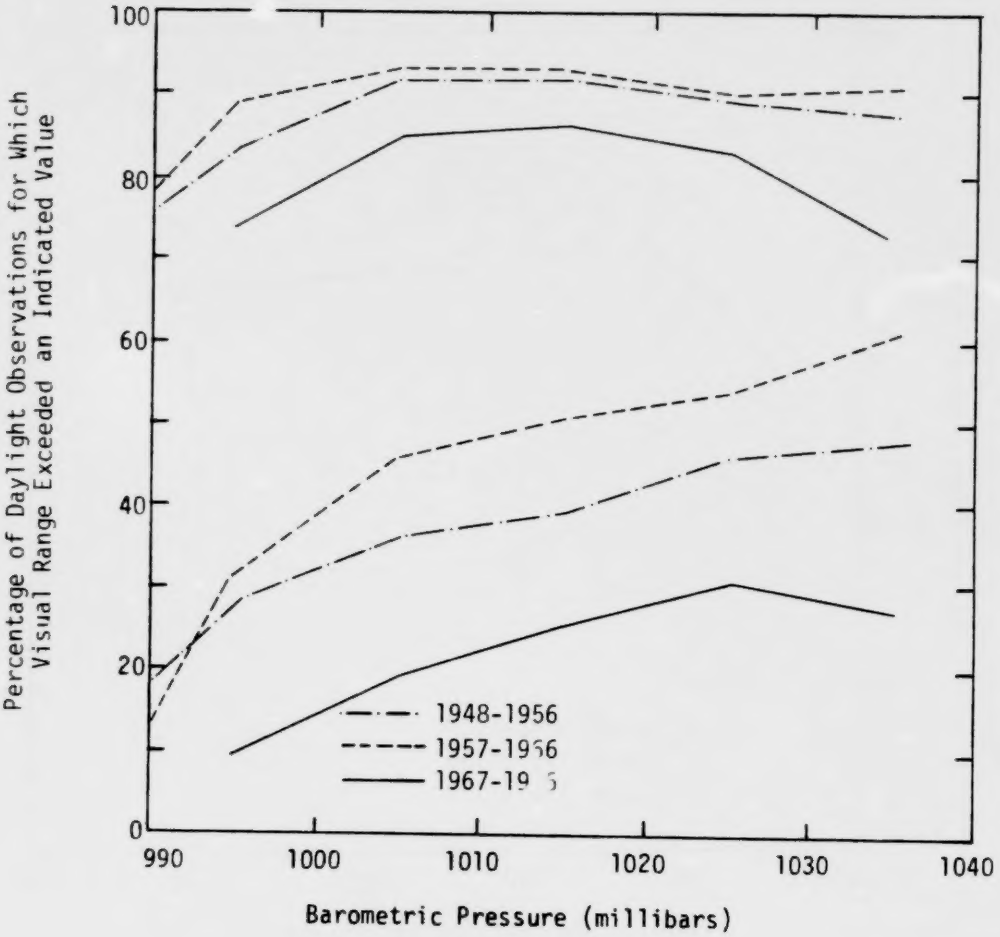

FIGURE A-74. PERCENTAGE OF DAYLIGHT OBSERVATIONS FOR WHICH VISUAL RANGE EXCEEDED AN INDICATED VALUE, AS A FUNCTION OF BAROMETRIC PRESSURE, AT CHEYENNE, WYOMING

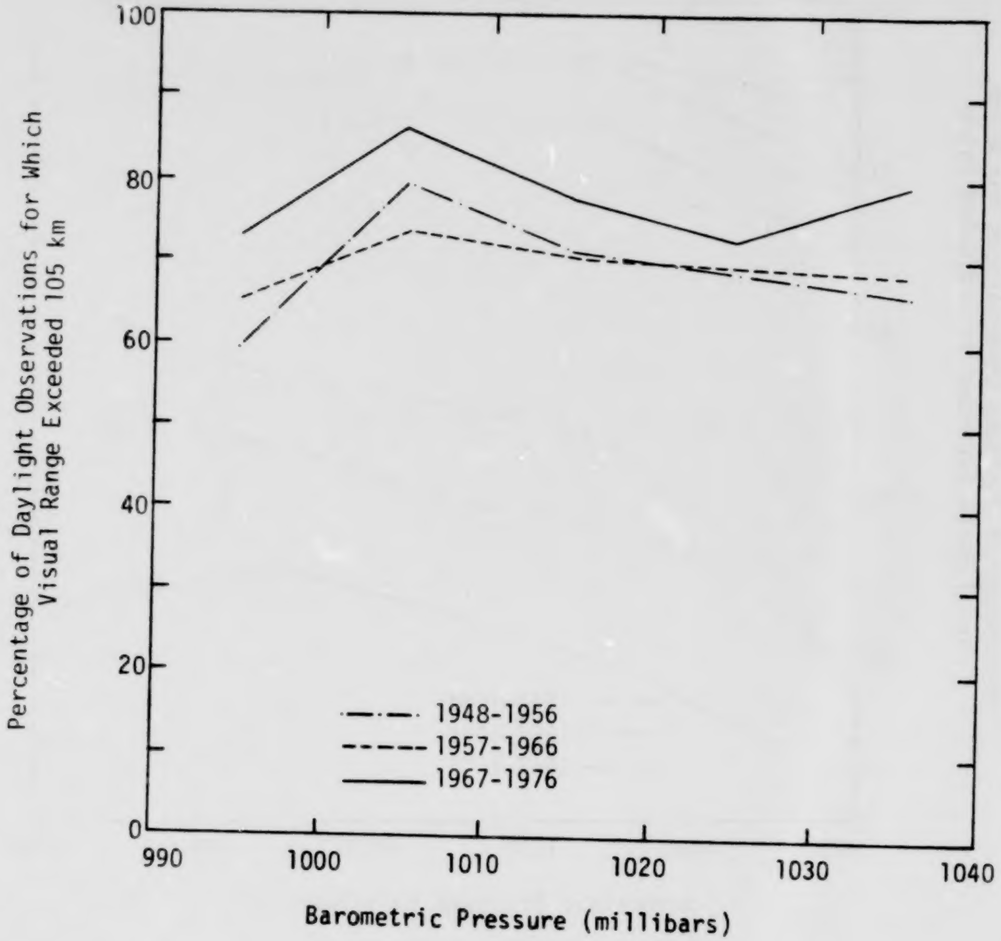

FIGURE A-75. PERCENTAGE OF DAYLIGHT OBSERVATIONS FOR WHICH VISUAL RANGE EXCEEDED 105 km, AS A FUNCTION OF BAROMETRIC PRESSURE, AT COLORADO SPRINGS, COLORADO

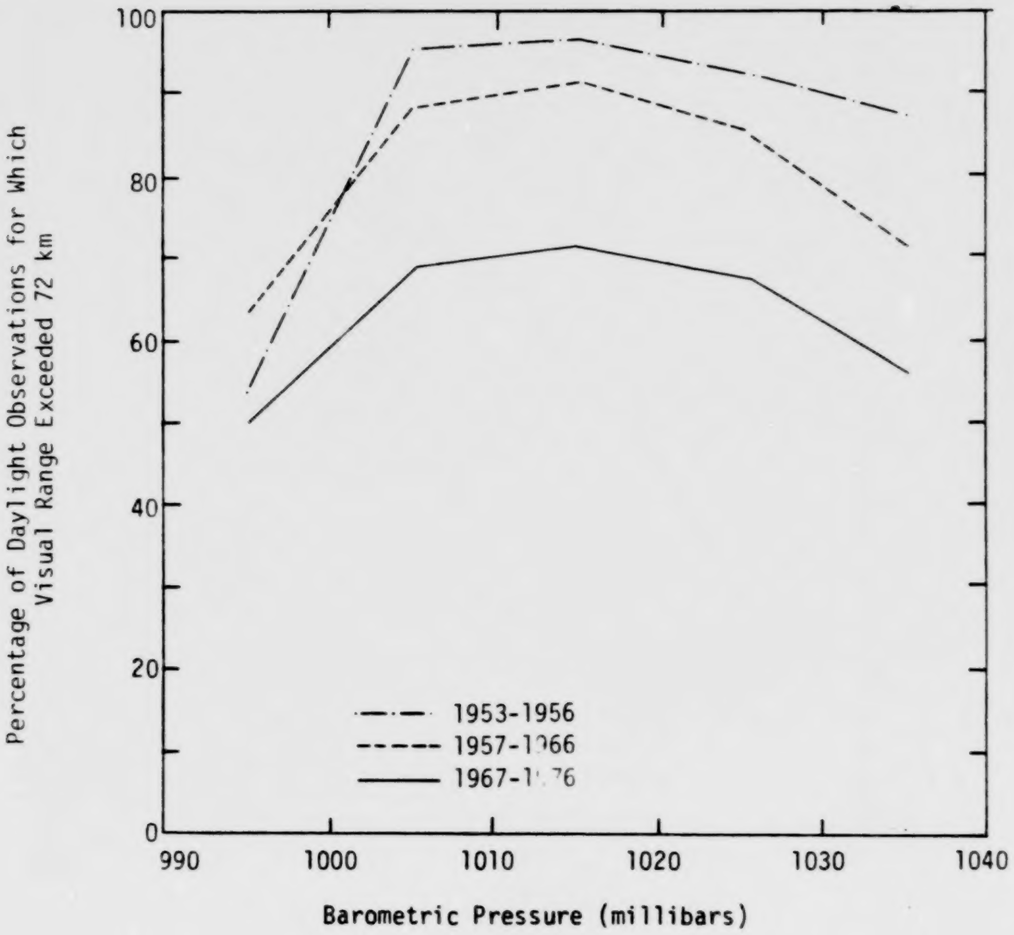

FIGURE A-76. PRECENTAGE OF DAYLIGHT OBSERVATIONS FOR WHICH VISUAL RANGE EXCEEDED 72 km, AS A FUNCTION OF BAROMETRIC PRESSURE, AT ELY, NEVADA

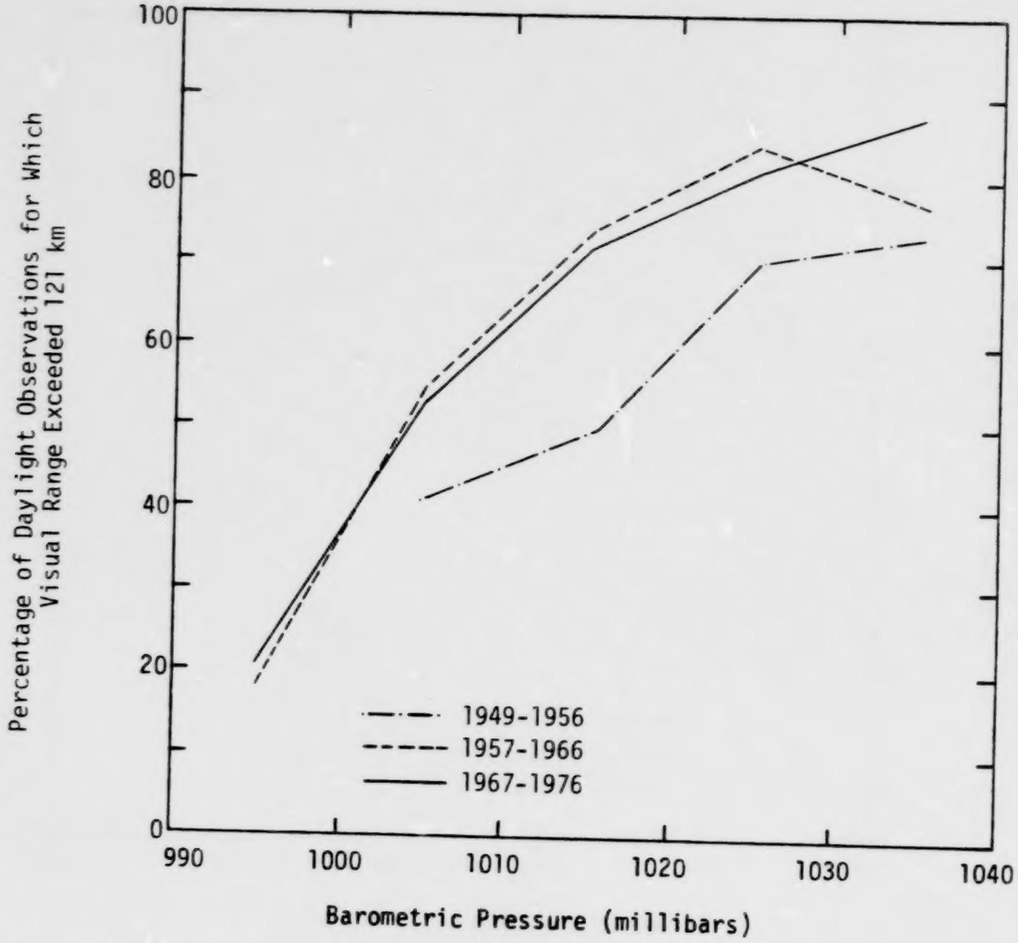

FIGURE A-77. PERCENTAGE OF DAYLIGHT OBSERVATIONS FOR WHICH VISUAL RANGE EXCEEDED 121 km, AS A FUNCTION OF BAROMETRIC PRESSURE, AT FARMINGTON, NEW MEXICO

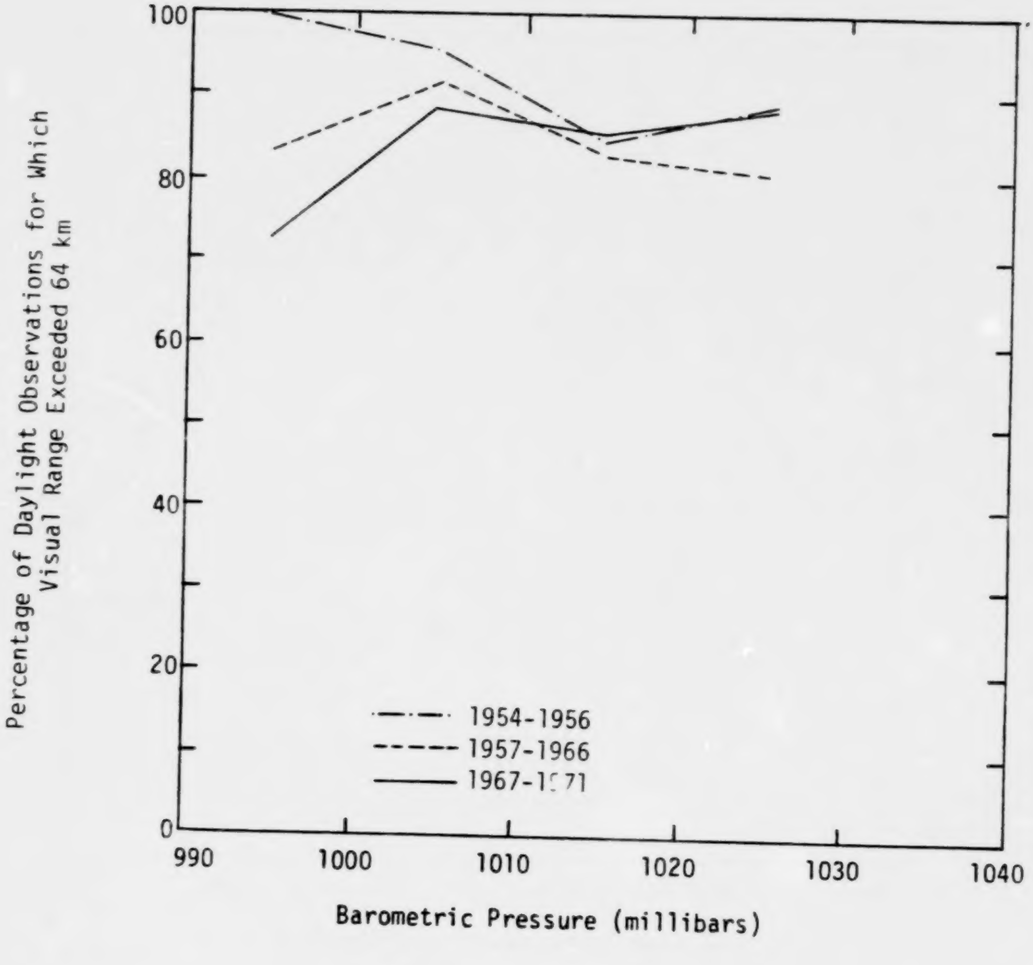

FIGURE A-78. PERCENTAGE OF DAYLIGHT OBSERVATIONS FOR WHICH VISUAL RANGE EXCEEDED 64 km, AS A FUNCTION OF BAROMETRIC PRESSURE, AT FT. HUACHUCA, ARIZONA

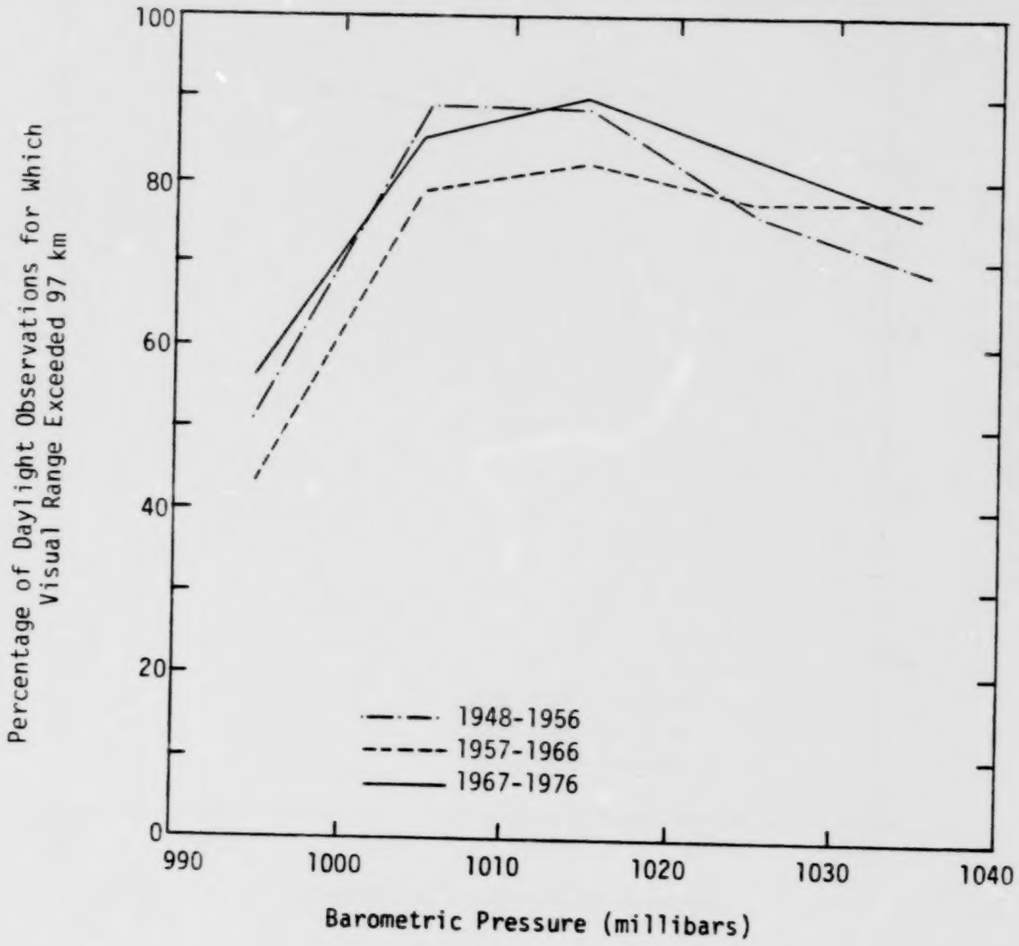

FIGURE A-79. PERCENTAGE OF DAYLIGHT OBSERVATIONS FOR WHICH VISUAL RANGE EXCEEDED 97 km, AS A FUNCTION OF BAROMETRIC PRESSURE, AT GRAND JUNCTION, COLORADO

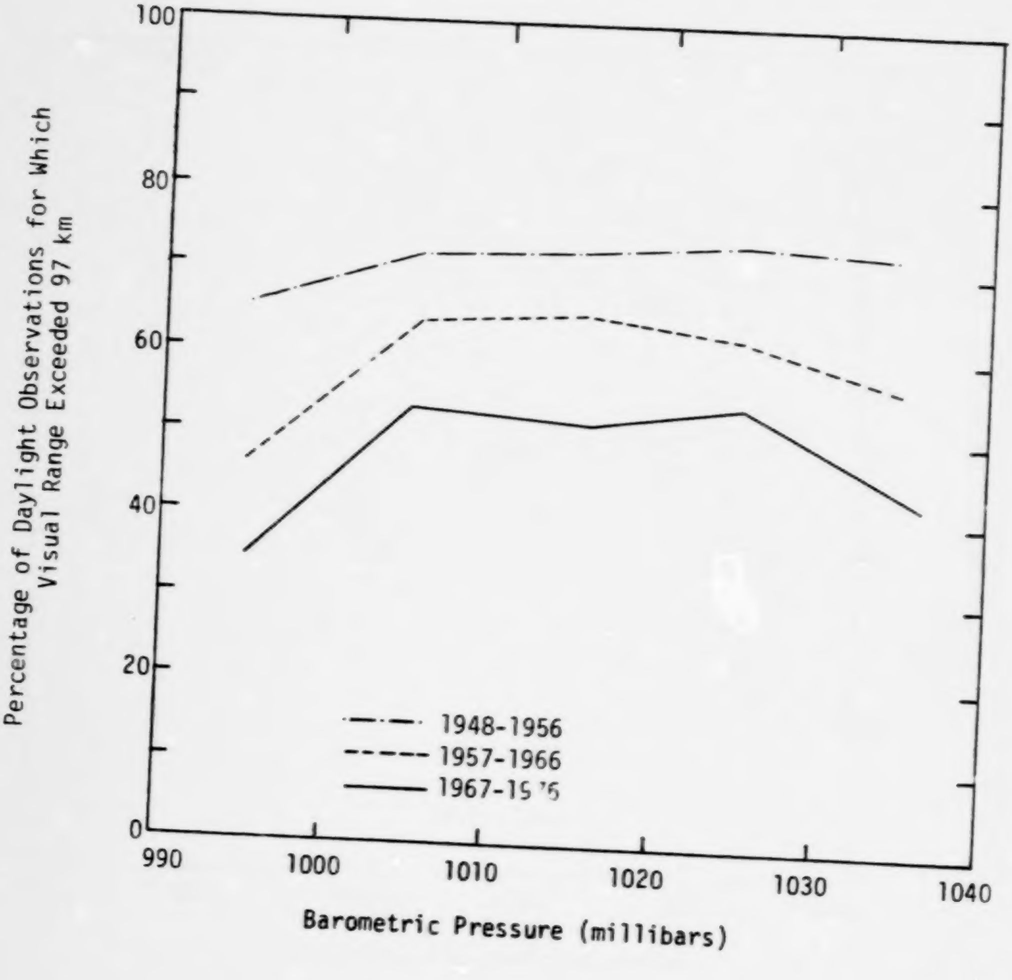

FIGURE A-80. PERCENTAGE OF DAYLIGHT OBSERVATIONS FOR WHICH VISUAL RANGE EXCEEDED 97 km, AS A FUNCTION OF BAROMETRIC PRESSURE, AT GREAT FALLS, MONTANA

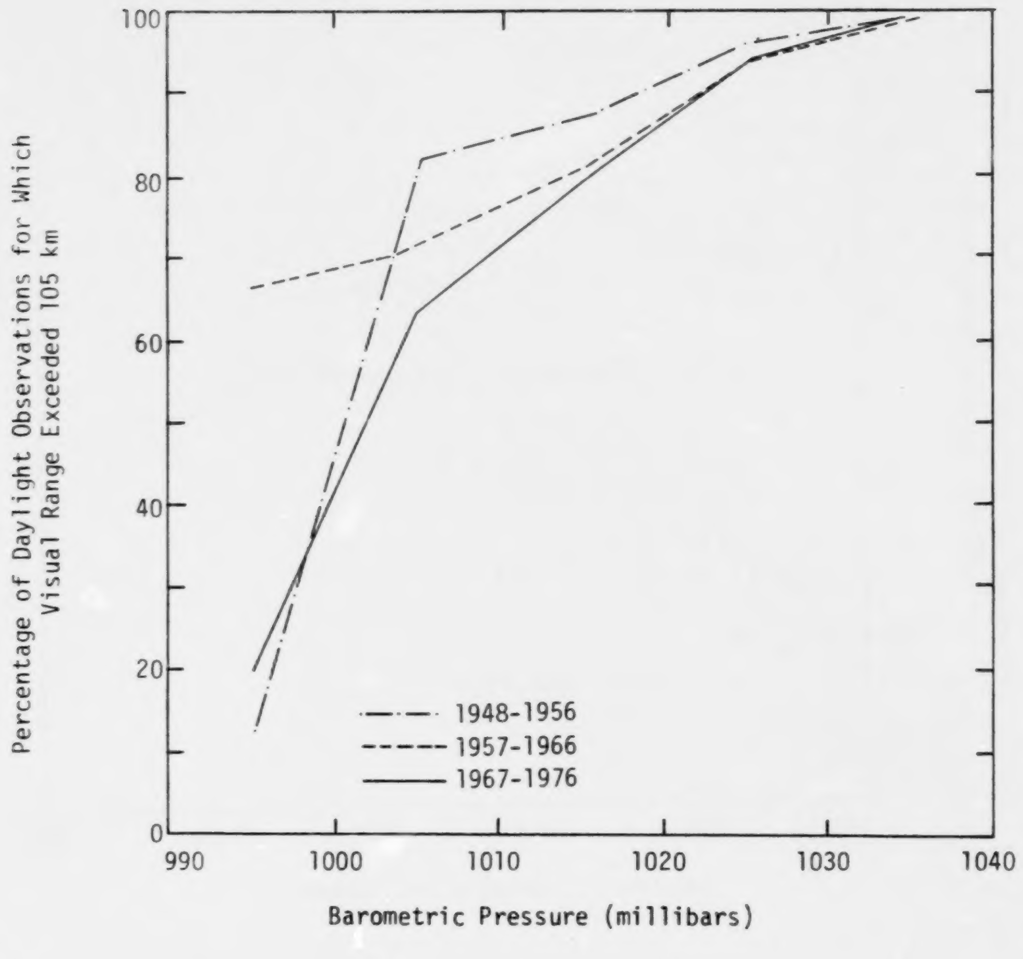

FIGURE A-81. PERCENTAGE OF DAYLIGHT OBSERVATIONS FOR WHICH VISUAL RANGE EXCEEDED 105 km, AS A FUNCTION OF BAROMETRIC PRESSURE, AT PRESCOTT, ARIZONA

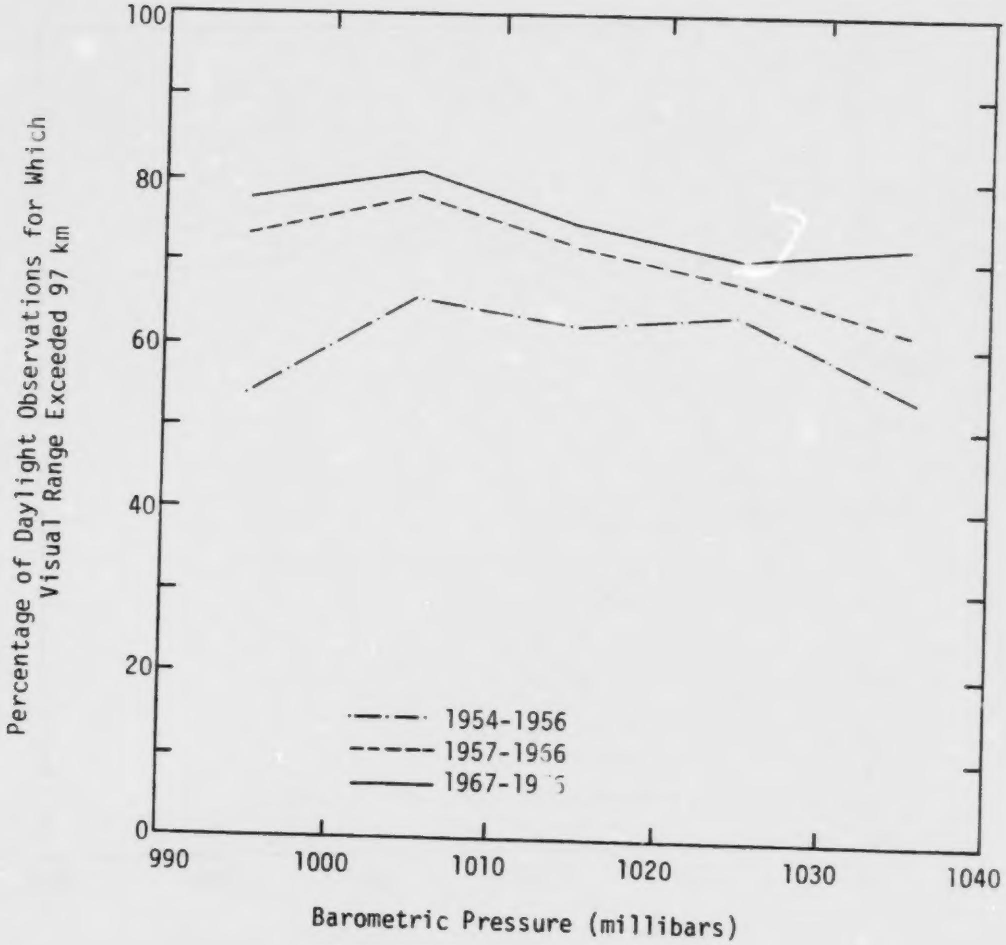

FIGURE A-82. PERCENTAGE OF DAYLIGHT OBSERVATIONS FOR WHICH VISUAL RANGE EXCEEDED 97 km, AS A FUNCTION OF BAROMETRIC PRESSURE, AT PUEBLO, COLORADO

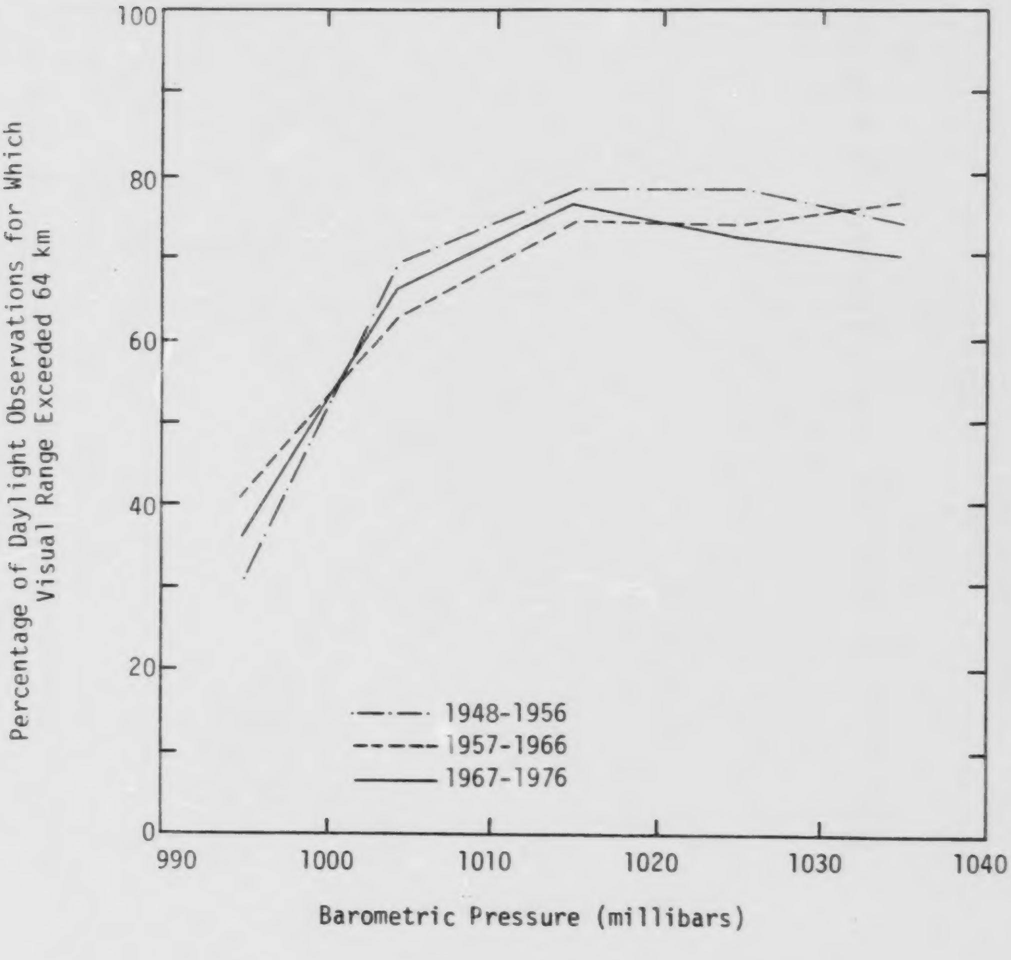

FIGURE A-83. PERCENTAGE OF DAYLIGHT OBSERVATIONS FOR WHICH VISUAL RANGE EXCEEDED 64 km, AS A FUNCTION OF BAROMETRIC PRESSURE, AT ROCK SPRINGS, WYOMING

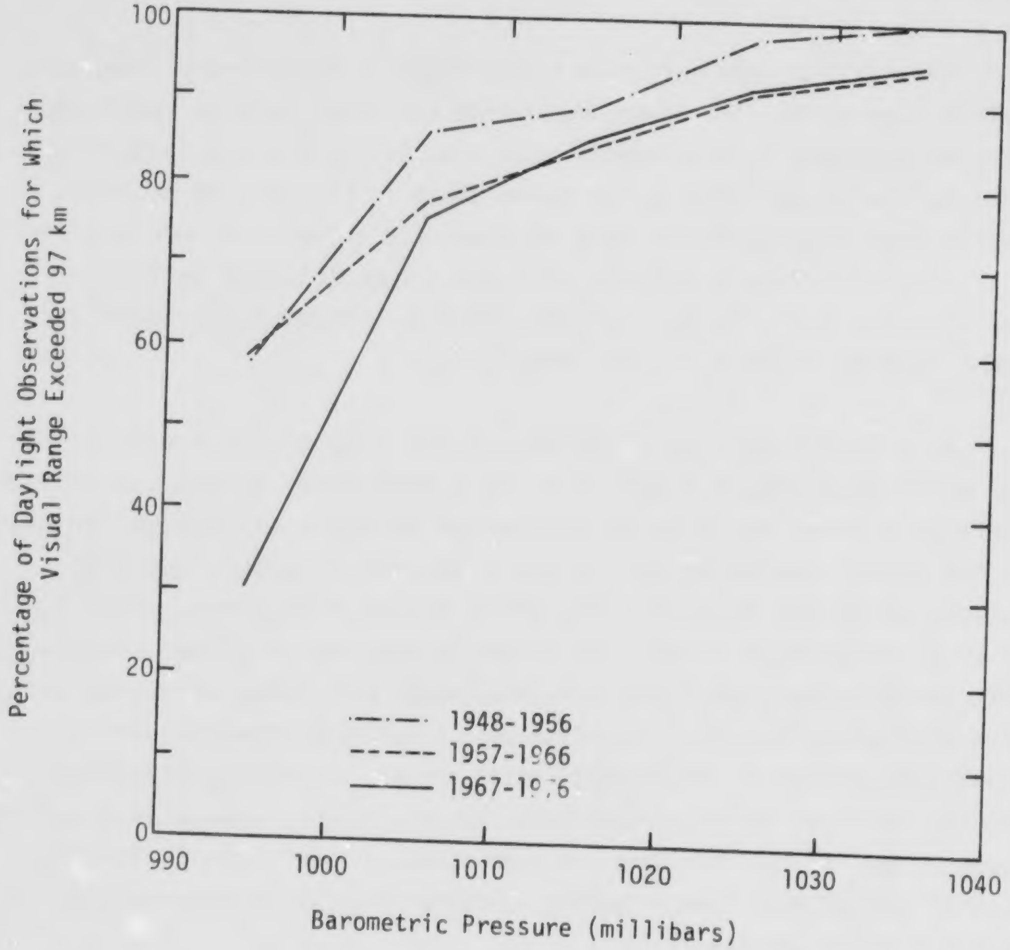

FIGURE A-84. PERCENTAGE OF DAYLIGHT OBSERVATIONS FOR WHICH VISUAL RANGE EXCEEDED 97 km, AS A FUNCTION OF BAROMETRIC PRESSURE, AT WINSLOW, ARIZONA in the United States during the period 1960 through 1964 were merged with the NWS visibility data to determine the effect of afternoon ventilation on afternoon visual range.

The effect of ventilation on visual range is summarized in Figures A-85 through A-102. The strong dependence of visual range on ventilation that was suggested by the dependence on atmospheric pressure in Salt Lake City and Ely is confirmed by the curves shown in Figures A-88 and A-94. During stagnation conditions (low ventilation), visual range was considerably reduced in these locations. The same strong effect of ventilation was also observed in Phoenix, Tucson, Billings, Cheyenne, Ft. Huachuca, Grand Junction, Great Falls, and Rock Springs.

It is significant that at Denver, visual range decreased with increasing ventilation (Figure A-85). A possible explanation is that with increased ventilation urban emissions are transported in such a way that the integral of the aerosol scattering coefficient is greater along the sight path between Denver and the distant visibility marker, Pike's Peak, which is 97 km to the south of Denver. An alternate explanation is that windblown dust concentrations are higher with the higher wind speeds associated with high ventilation values. The influences of pollutant transport and windblown dust at high values of ventilation are also possible explanations for the Las Vegas curves (Figure A-86) and the slight decrease in visual range at many of the locations for high values of ventilation. The effect of high surface wind speeds causing windblown dust was studied more directly, as discussed in Section 11.

11. EFFECT OF WIND SPEED

Figures A-103 through A-120 illustrate the effect of the surface wind speed on visual range. At many locations, most notably at Las Vegas, Phoenix, Tucson, Alamogordo, Farmington, Grand Junction, Prescott, and Winslow, a reduction in visual range occurs at high surface wind speeds.

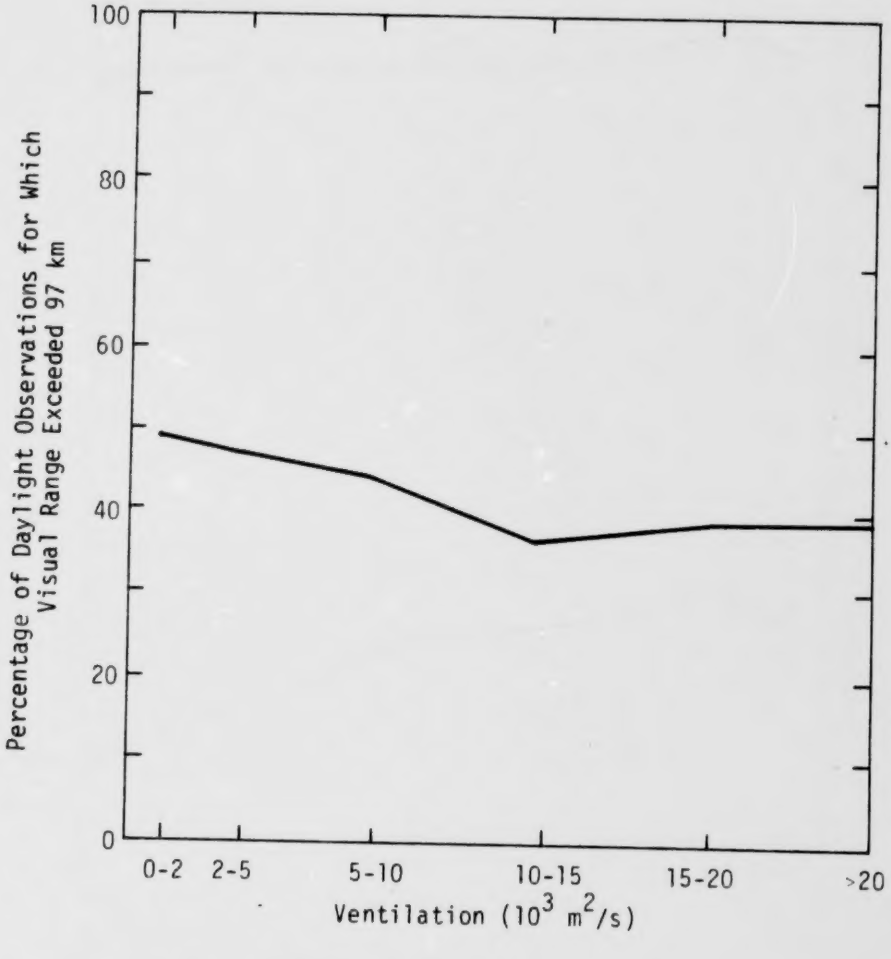

FIGURE A-85. PERCENTAGE OF DAYLIGHT OBSERVATIONS FOR WHICH VISUAL RANGE EXCEEDED 97 km, AS A FUNCTION OF VENTILATION, AT DENVER, COLORADO, 1960-1964

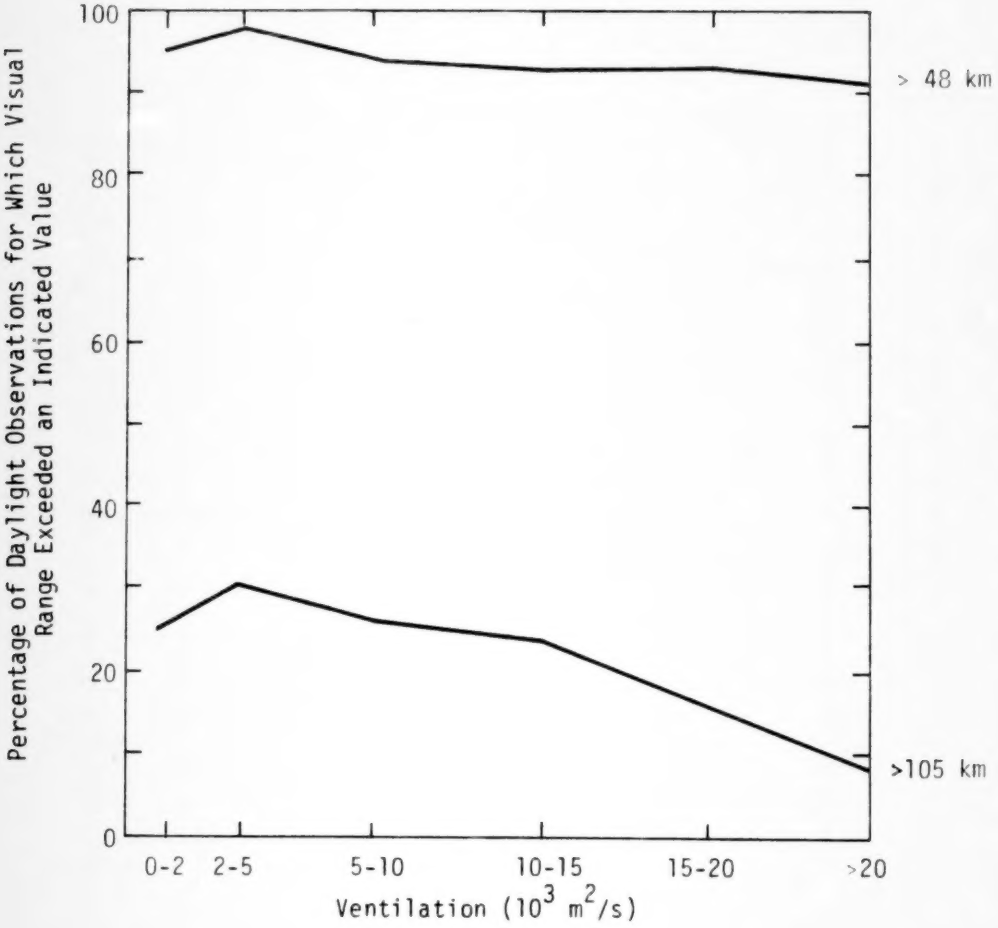

FIGURE A-86. PERCENTAGE OF DAYLIGHT OBSERVATIONS FOR WHICH VISUAL RANGE EXCEEDED AN INDICATED VALUE, AS A FUNCTION OF VENTILATION, AT LAS VEGAS, NEVADA, 1960-1964

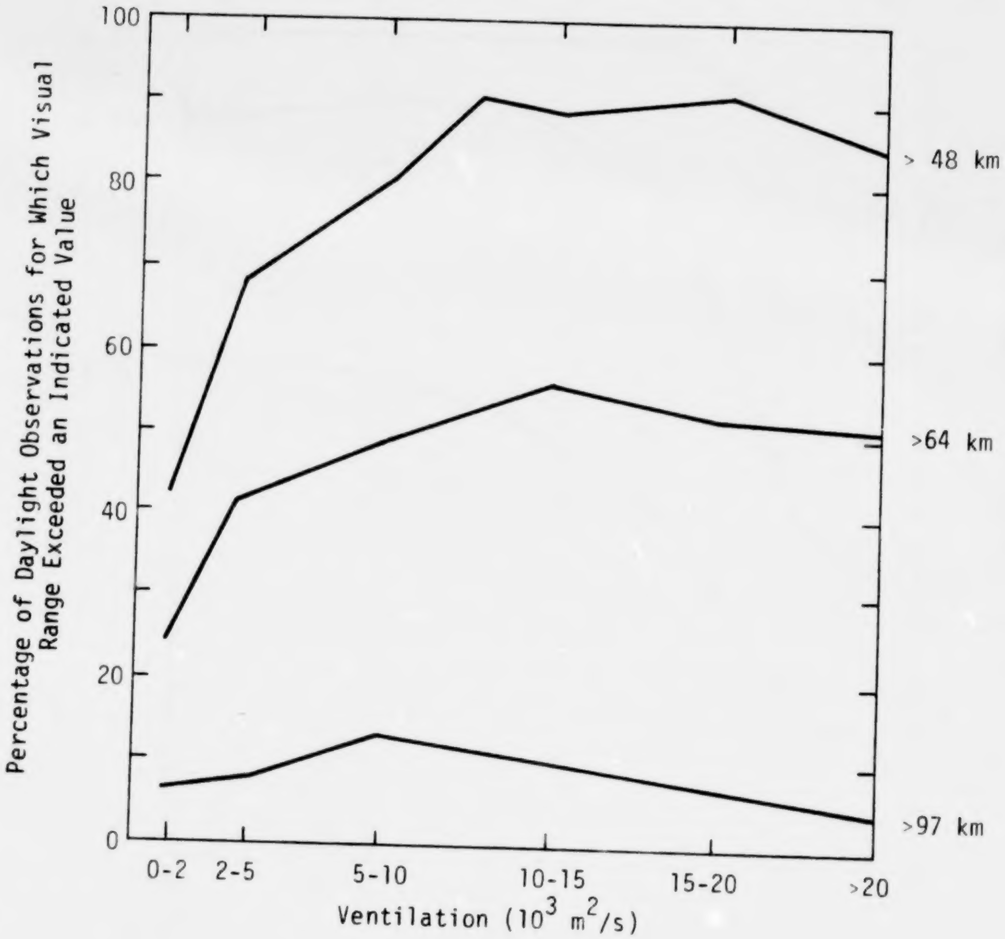

Note: Tucson upper air data were used for ventilation.

FIGURE A-87. PERCENTAGE OF DAYLIGHT OBSERVATIONS FOR WHICH VISUAL RANGE EXCEEDED AN INDICATED VALUE, AS A FUNCTION OF VENTILATION, AT PHOENIX, ARIZONA, 1960-1964

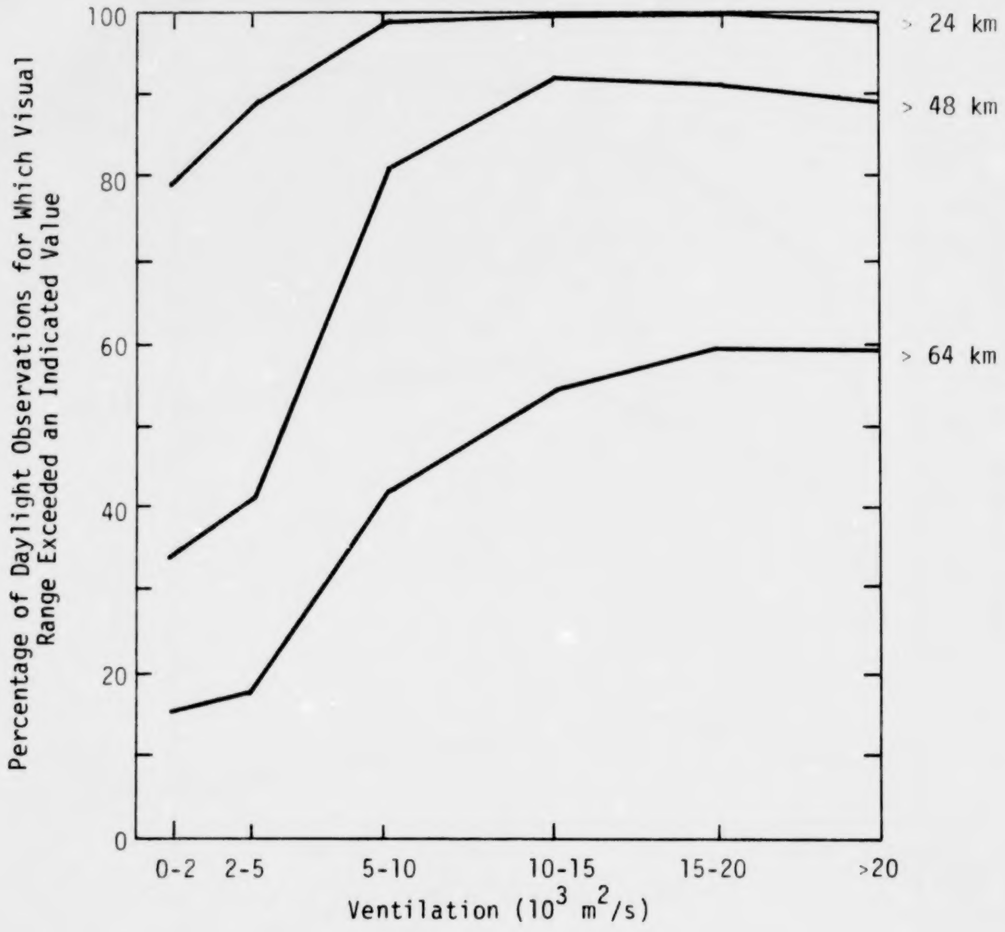

FIGURE A-88. PERCENTAGE OF DAYLIGHT OBSERVATIONS FOR WHICH VISUAL RANGE EXCEEDED AN INDICATED VALUE, AS A FUNCTION OF VENTILATION, AT SALT LAKE CITY, UTAH, 1960-1964

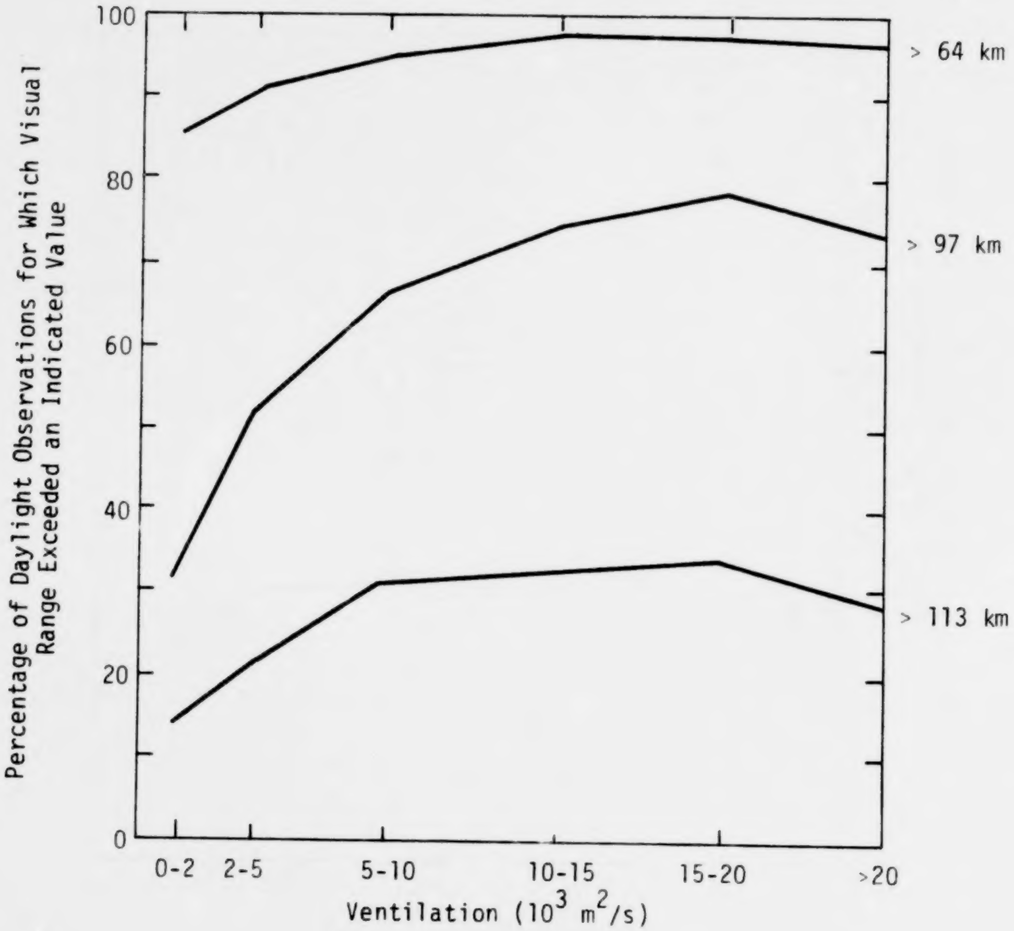

FIGURE A-89. PERCENTAGE OF DAYLIGHT OBSERVATIONS FOR WHICH VISUAL RANGE EXCEEDED AN INDICATED VALUE, AS A FUNCTION OF VENTILATION, AT TUCSON, ARIZONA 1960-1964

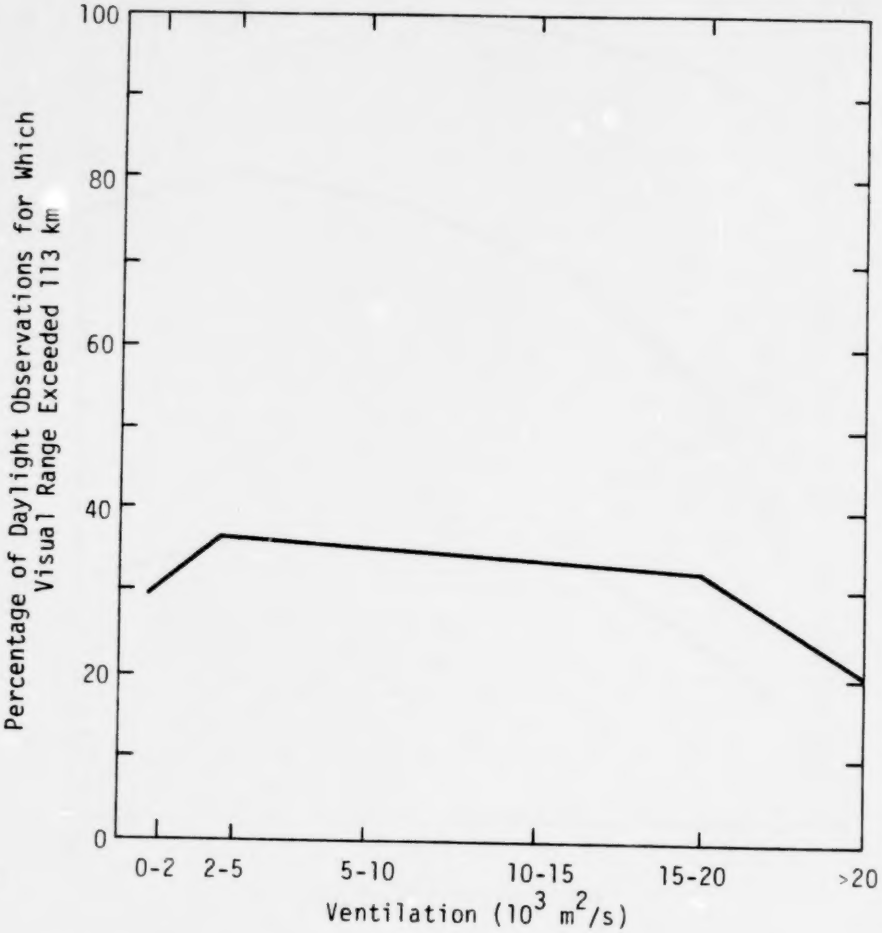

Note: El Paso upper air data were used for ventilation.

FIGURE A-90. PERCENTAGE OF DAYLIGHT OBSERVATIONS FOR WHICH VISUAL RANGE EXCEEDED 113 km, AS A FUNCTION OF VENTILATION, AT ALAMOGORDO, NEW MEXICO, 1960-1964

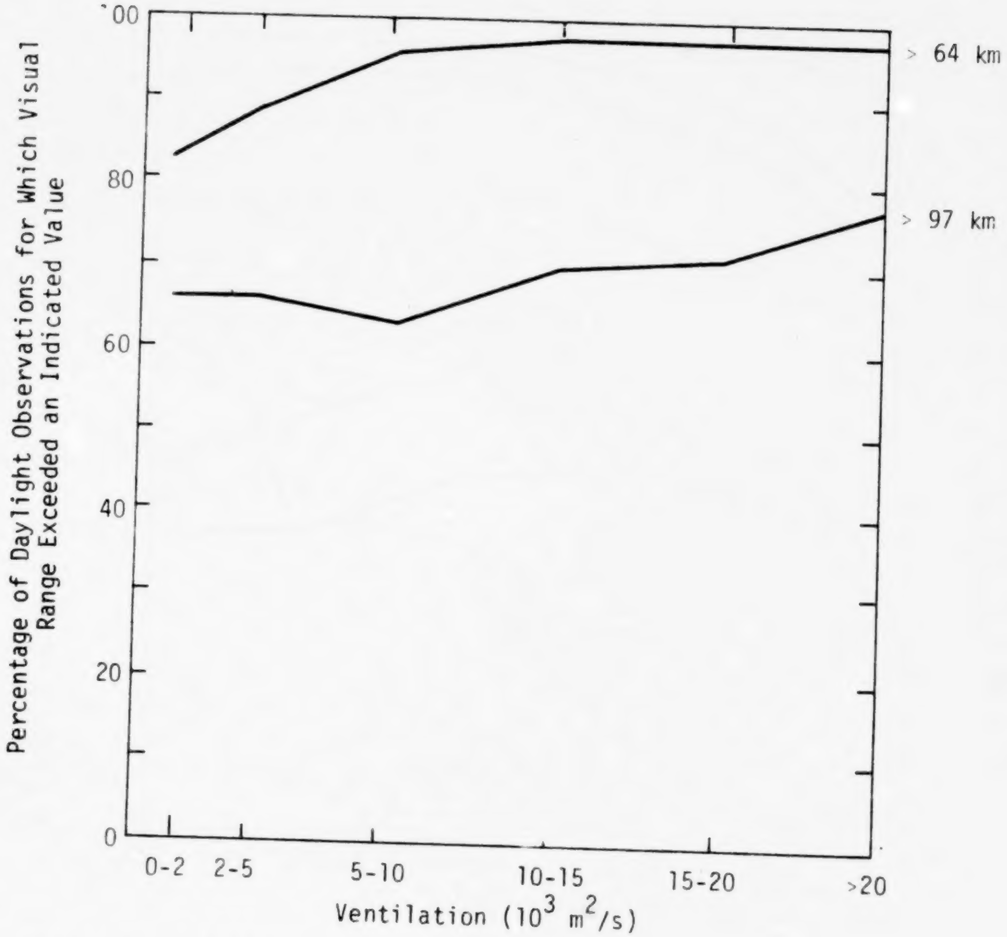

Note: Great Falls upper air data were used for ventilation.

FIGURE A-91. PERCENTAGE OF DAYLIGHT, OBSERVATIONS FOR WHICH VISUAL RANGE EXCEEDED AN INDICATED VALUE, AS A FUNCTION OF VENTILATION, AT BILLINGS, MONTANA 1960-1964

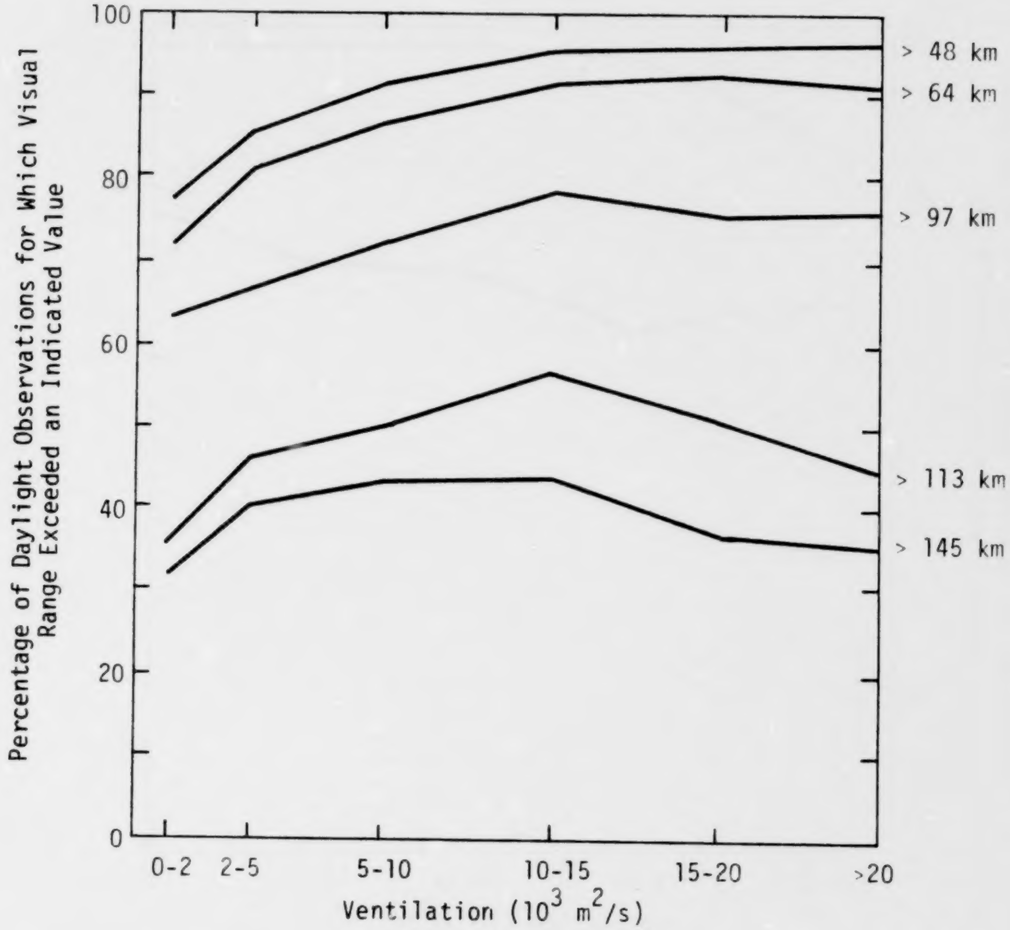

Note: Denver upper air data were used for ventilation.

FIGURE A-92. PERCENTAGE OF DAYLIGHT OBSERVATIONS FOR WHICH VISUAL RANGE EXCEEDED AN INDICATED VALUE, AS A FUNCTION OF VENTILATION, AT CHEYENNE, WYOMING, 1960-1964

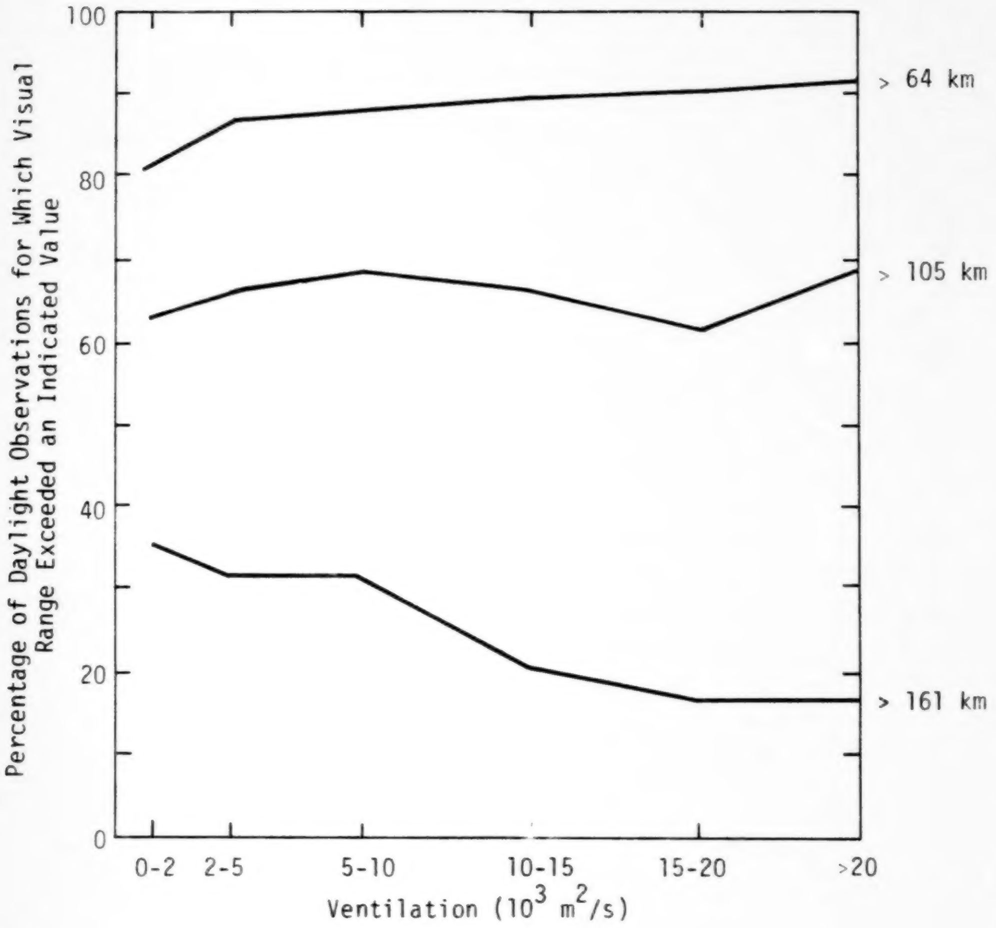

Note: Denver upper air data were used for ventilation.

FIGURE A-93. PERCENTAGE OF DAYLIGHT OBSERVATIONS FOR WHICH VISUAL RANGE EXCEEDED AN INDICATED VALUE, AS A FUNCTION OF VENTILATION, AT COLORADO SPRINGS, COLORADO, 1960-1964

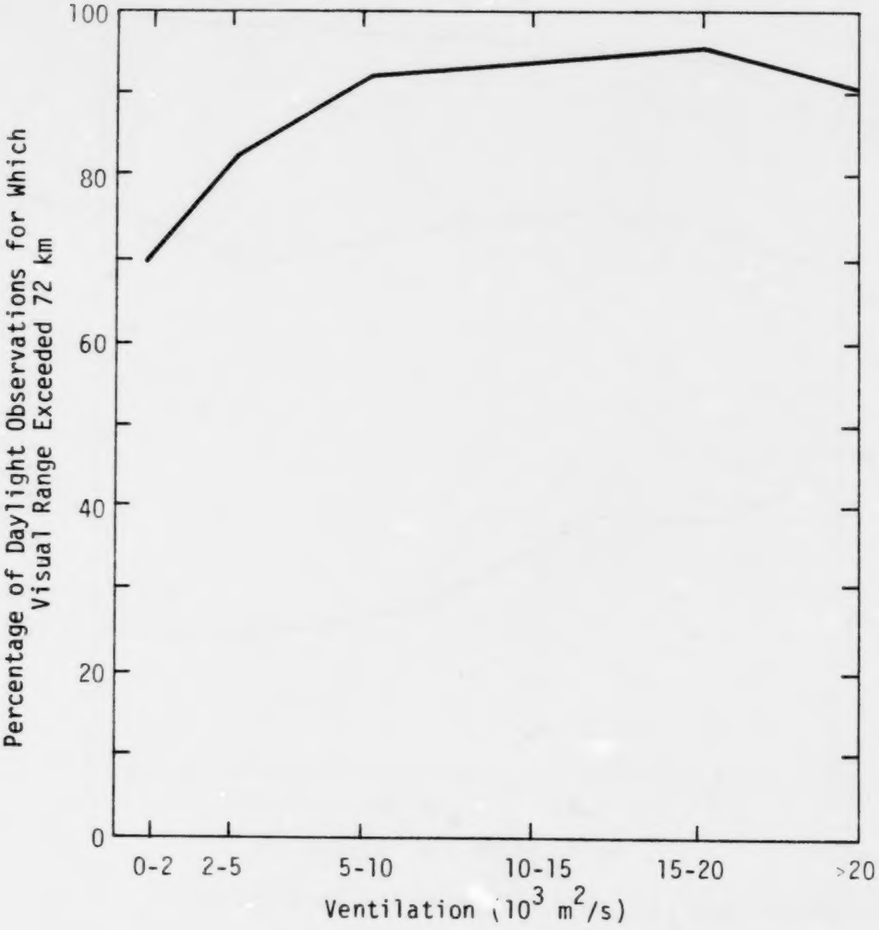

FIGURE A-94. PERCENTAGE OF DAYLIGHT OBSERVATIONS FOR WHICH VISUAL RANGE EXCEEDED 72 km, AS A FUNCTION OF VENTILATION, AT ELY, NEVADA, 1960-1964

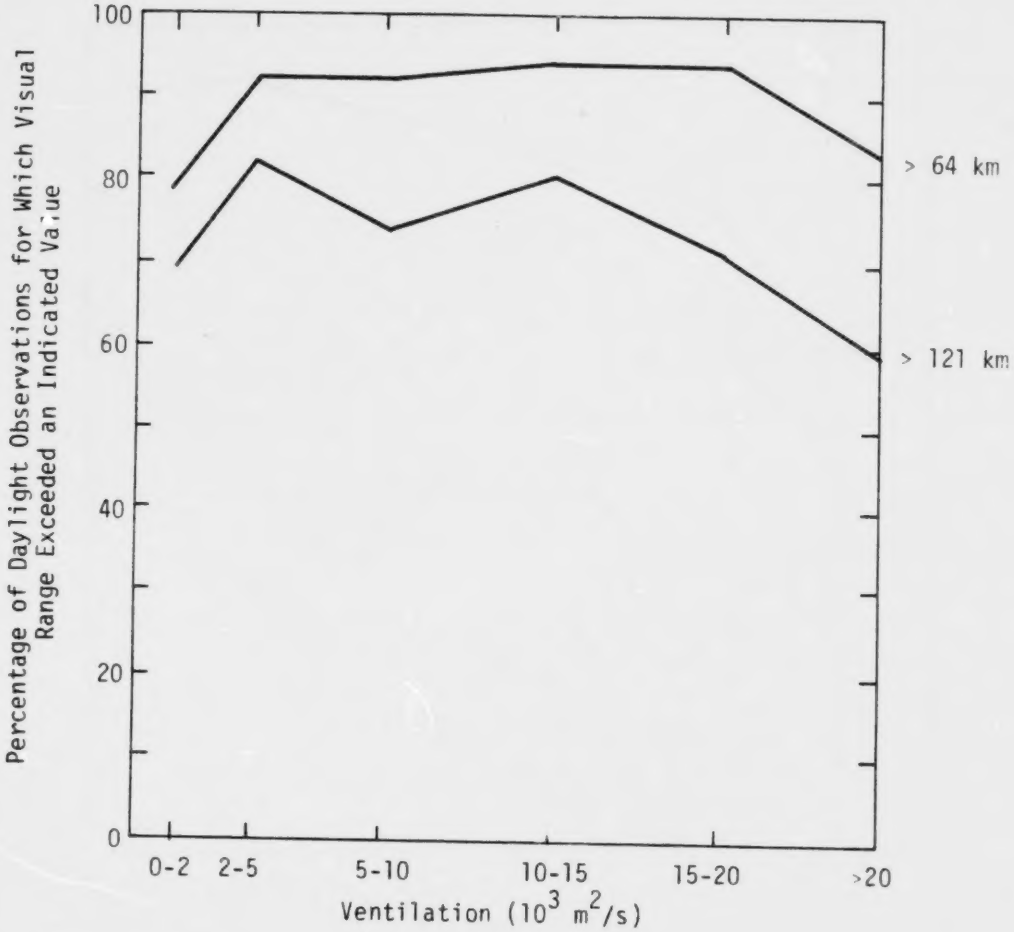

Note: Albuquerque upper air data were used for ventilation.

FIGURE A-95. PERCENTAGE OF DAYLIGHT OBSERVATIONS FOR WHICH VISUAL RANGE EXCEEDED AN INDICATED VALUE, AS FUNCTION OF VENTILATION, AT FARMINGTON, NEW MEXICO, 1960-1964

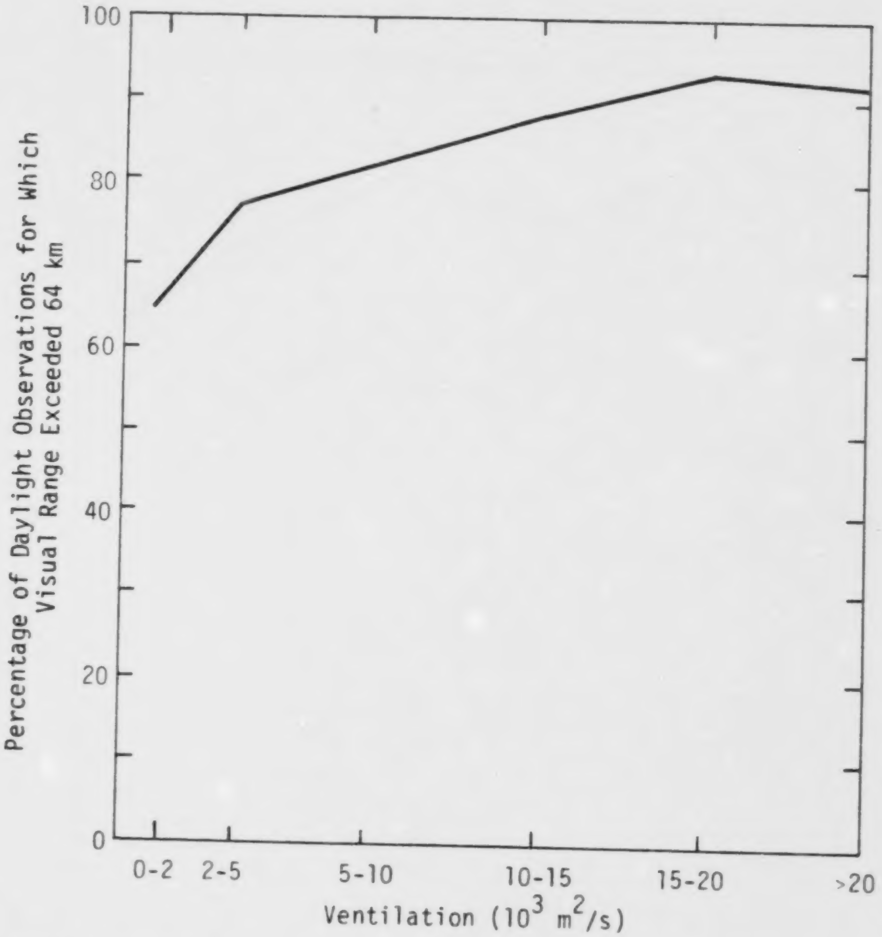

Note: Tucson upper air data were used for ventilation.

FIGURE A-96. PERCENTAGE OF DAYLIGHT OBSERVATIONS FOR WHICH VISUAL RANGE EXCEEDED 64 km, AS A FUNCTION OF VENTILATION, AT FT. HUACHUCA, ARIZONA, 1960-1964

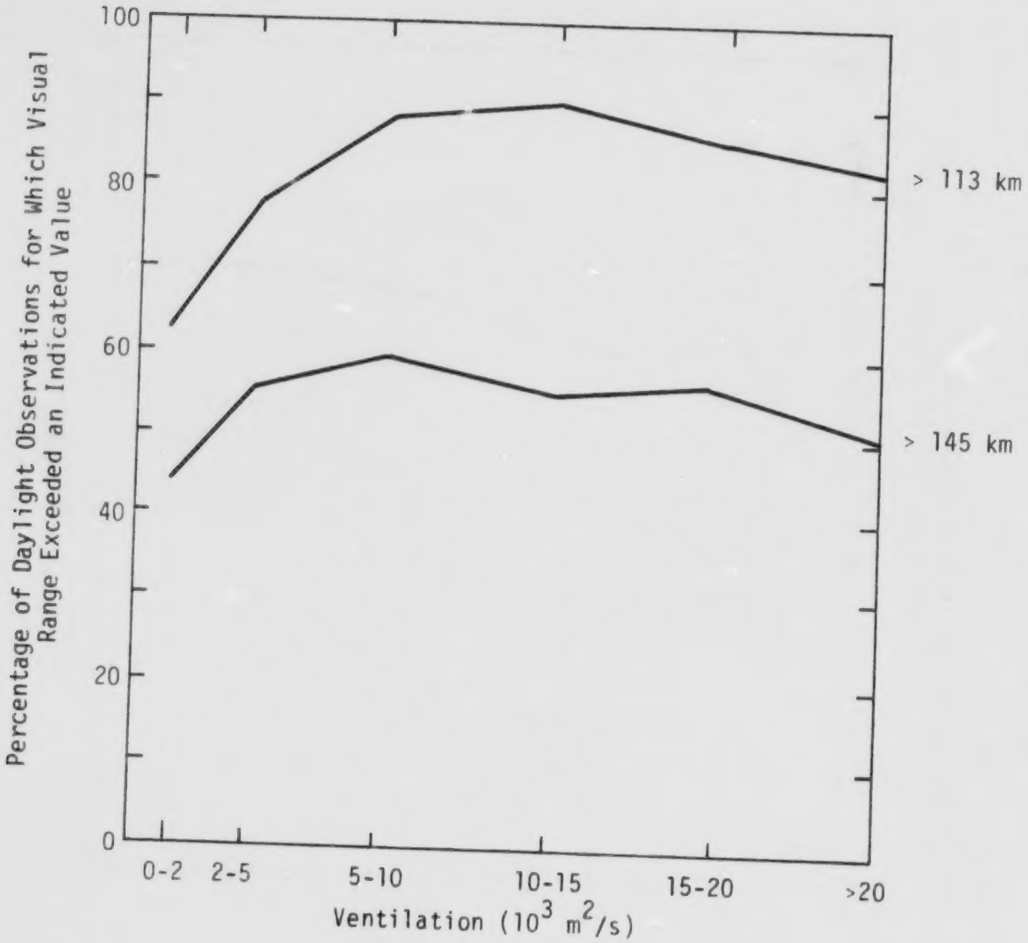

FIGURE A-97. PERCENTAGE OF DAYLIGHT OBSERVATIONS FOR WHICH VISUAL RANGE EXCEEDED AN INDICATED VALUE, AS A FUNCTION OF VENTILATION, AT GRAND JUNCTION, COLORADO, 1960-1964

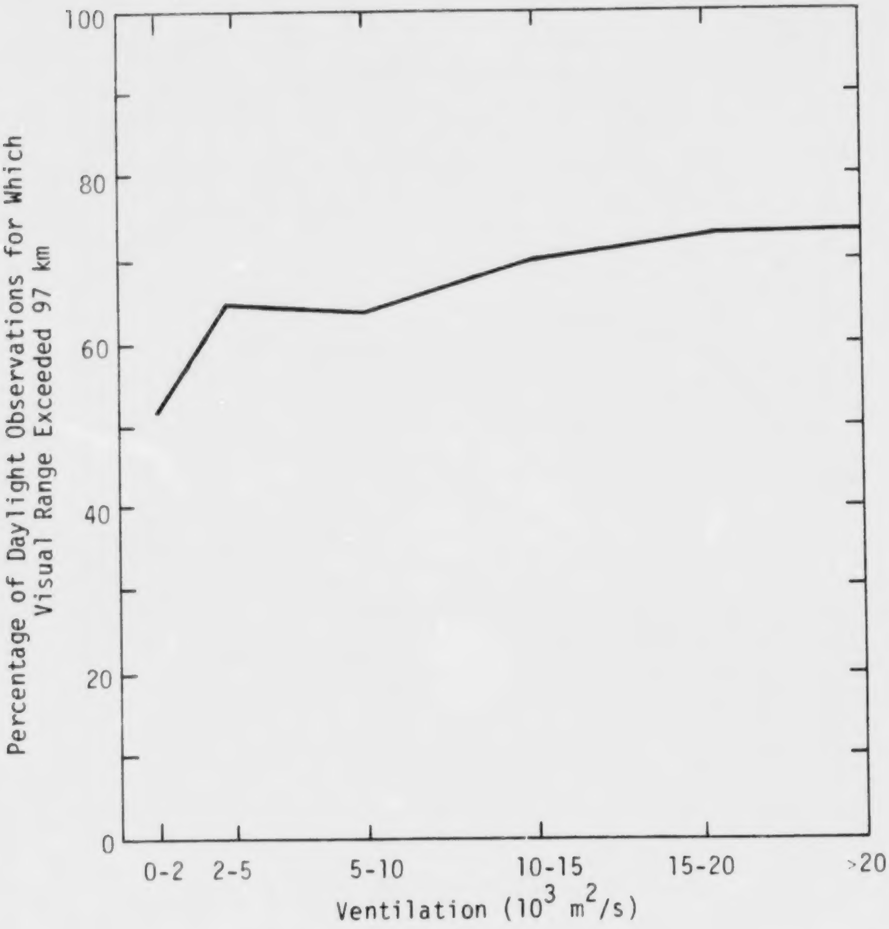

FIGURE A-98. PERCENTAGE OF DAYLIGHT OBSERVATIONS FOR WHICH VISUAL RANGE EXCEEDED 97 km, AS A FUNCTION OF VENTILATION, AT GREAT FALLS, MONTANA, 1960-1964

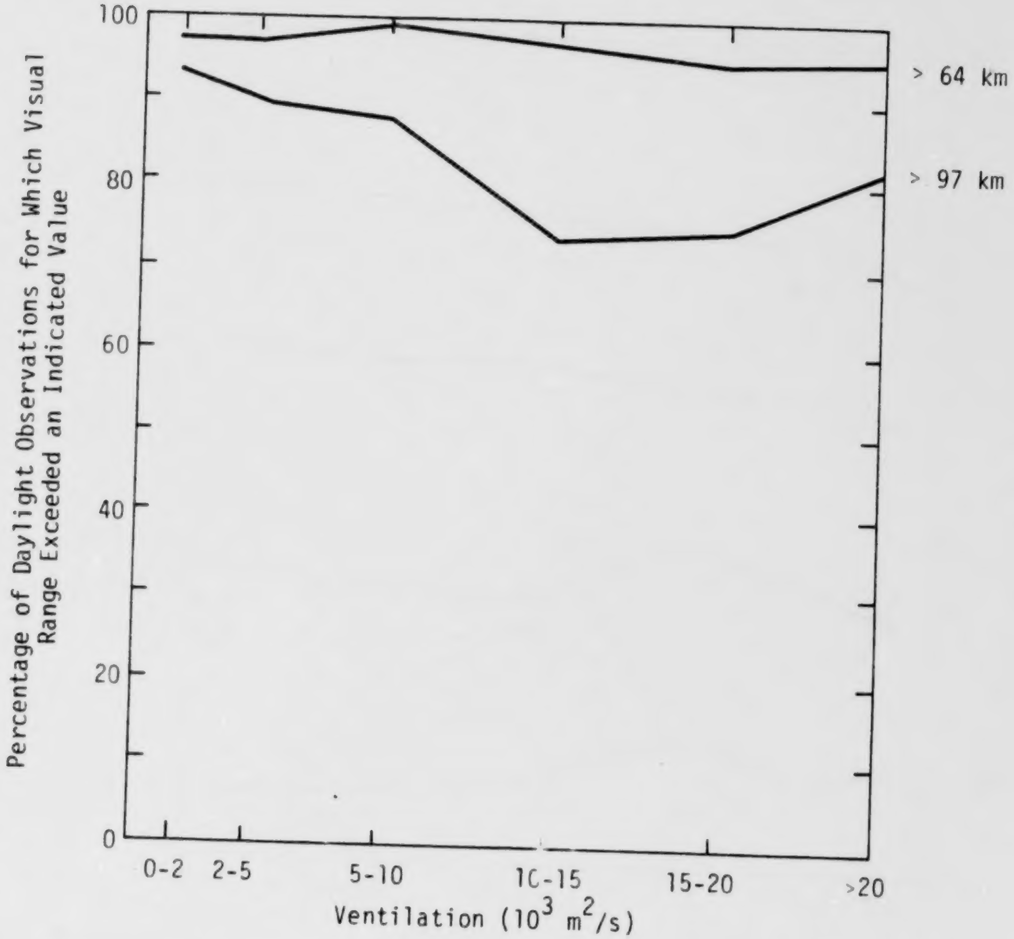

Note: Winslow upper air data were used for ventilation.

FIGURE A-99. PERCENTAGE OF DAYLIGHT OBSERVATIONS FOR WHICH VISUAL RANGE EXCEEDED AN INDICATED VALUE, AS A FUNCTION OF VENTILATION, AT PRESCOTT, ARIZONA, 1960-1964

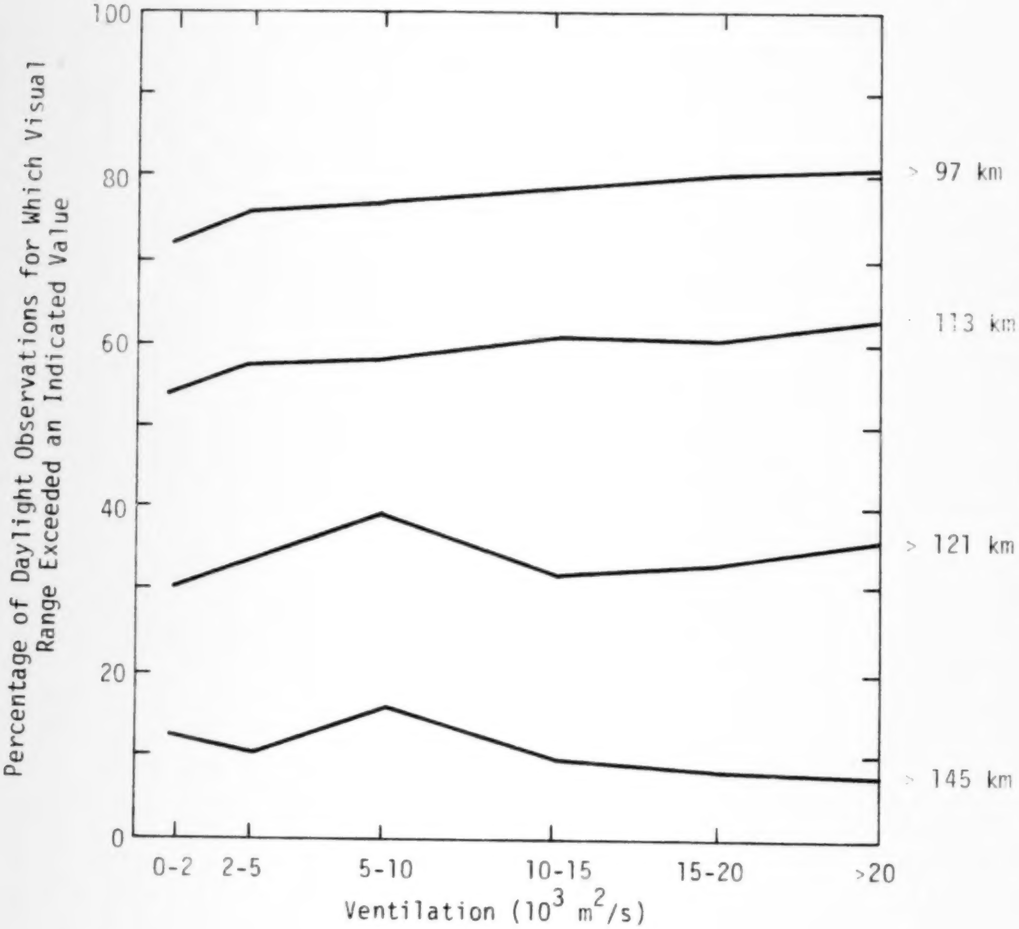

Note: Denver upper air data were used for ventilation.

FIGURE A-100. PERCENTAGE OF DAYLIGHT OBSERVATIONS FOR WHICH VISUAL RANGE EXCEEDED AN INDICATED VALUE, AS A FUNCTION OF VENTILATION, AT PUEBLO, COLORADO, 1960-1964

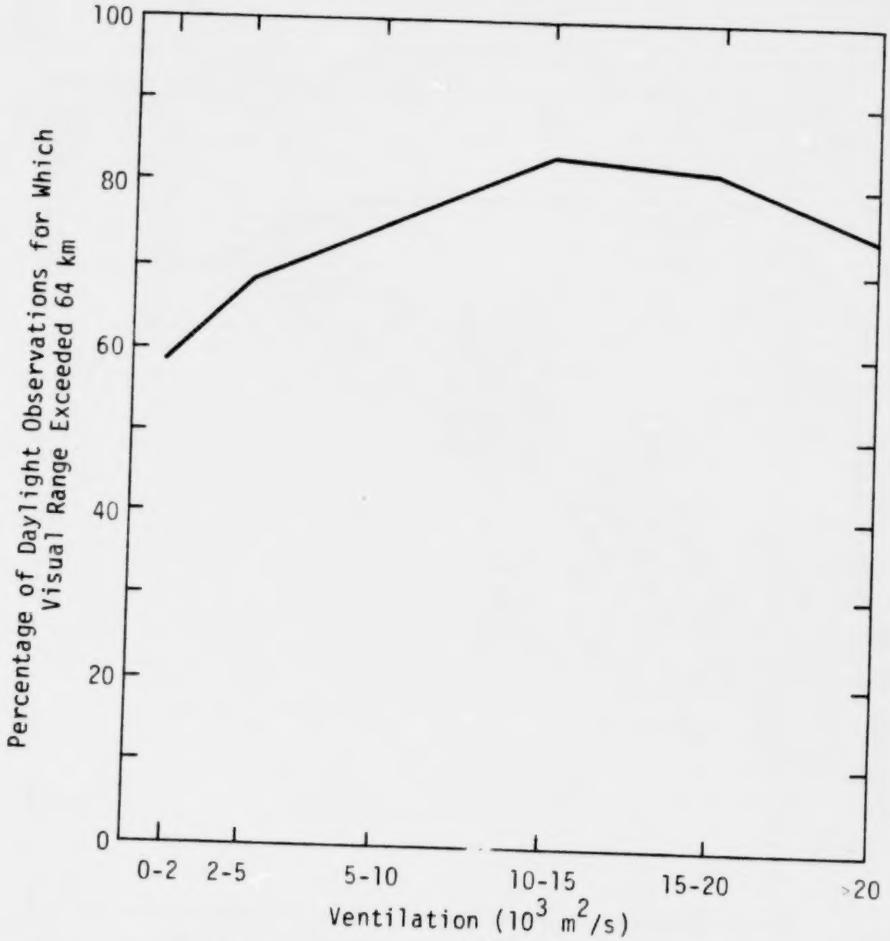

Note: Lander upper air data were used for ventilation.

FIGURE A-101. PERCENTAGE OF DAYLIGHT OBSERVATIONS FOR WHICH VISUAL RANGE EXCEEDED 64 km, AS A FUNCTION OF VENTILATION, AT ROCK SPRINGS, WYOMING, 1960-1964

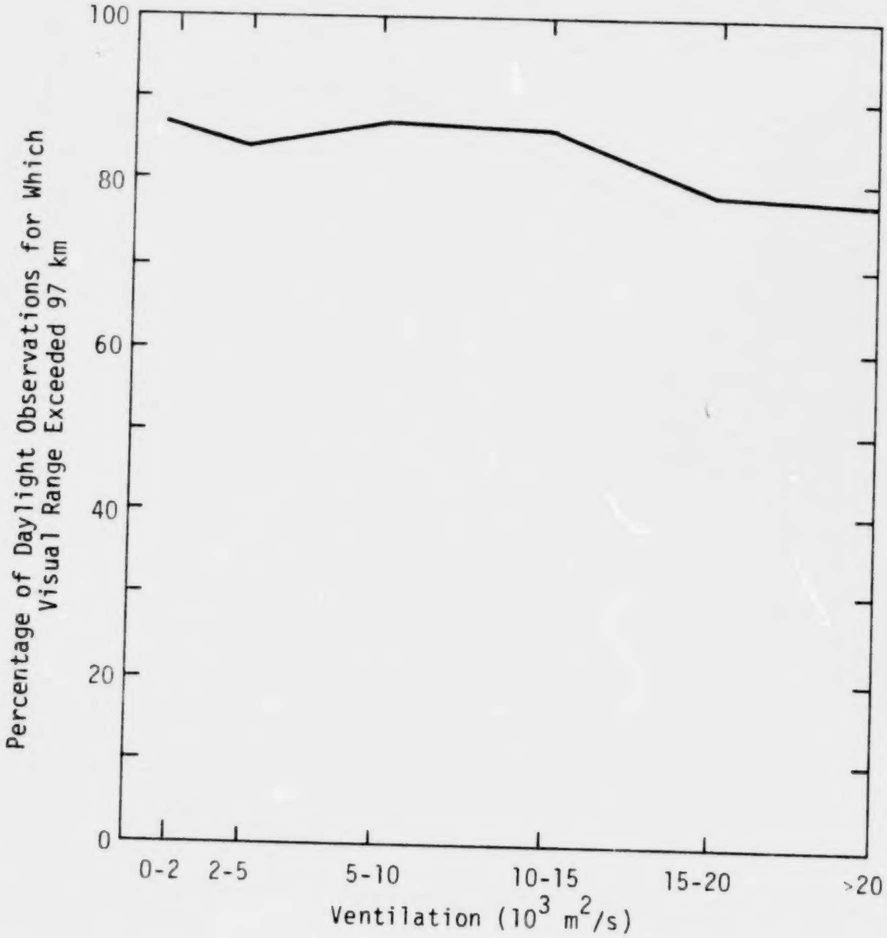

FIGURE A-102. PERCENTAGE OF DAYLIGHT OBSERVATIONS FOR WHICH VISUAL RANGE EXCEEDED 97 km, AS A FUNCTION OF VENTILATION, AT WINSLOW, ARIZONA, 1960-1964

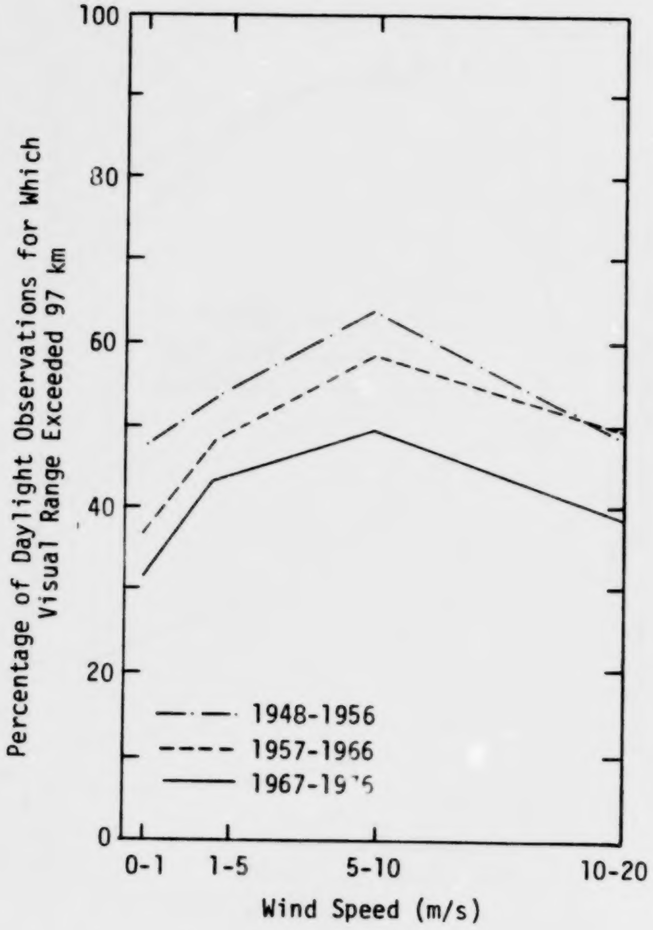

FIGURE A-103. PERCENTAGE OF DAYLIGHT OBSERVATIONS FOR WHICH VISUAL RANGE EXCEEDED 97 km, AS A FUNCTION OF SURFACE WIND SPEED, AT DENVER, COLORADO

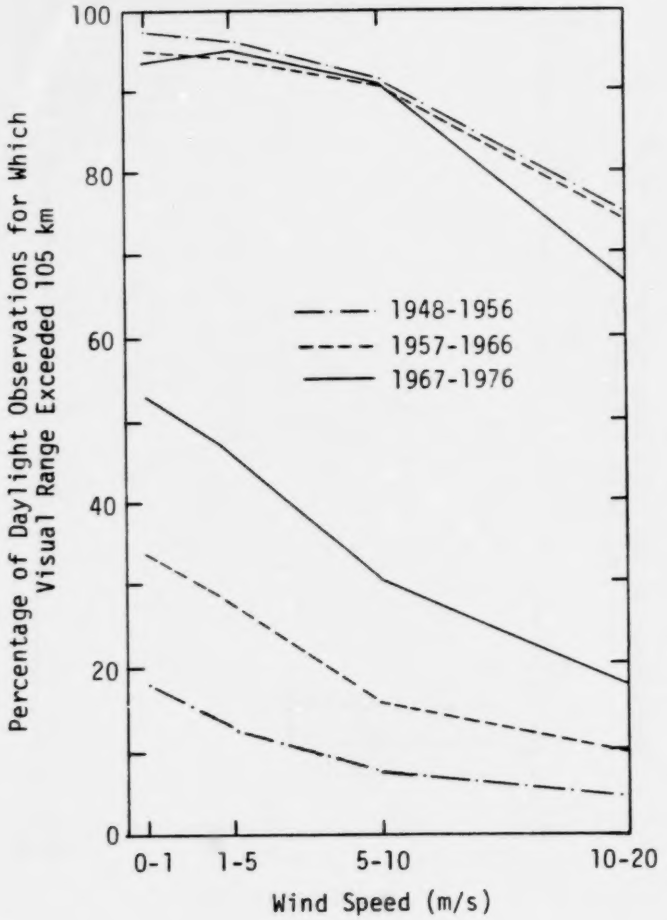

FIGURE A-104. PERCENTAGE OF DAYLIGHT OBSERVATIONS FOR WHICH VISUAL RANGE EXCEEDED 105 km, AS A FUNCTION OF SURFACE WIND SPEED, AT LAS VEGAS, NEVADA

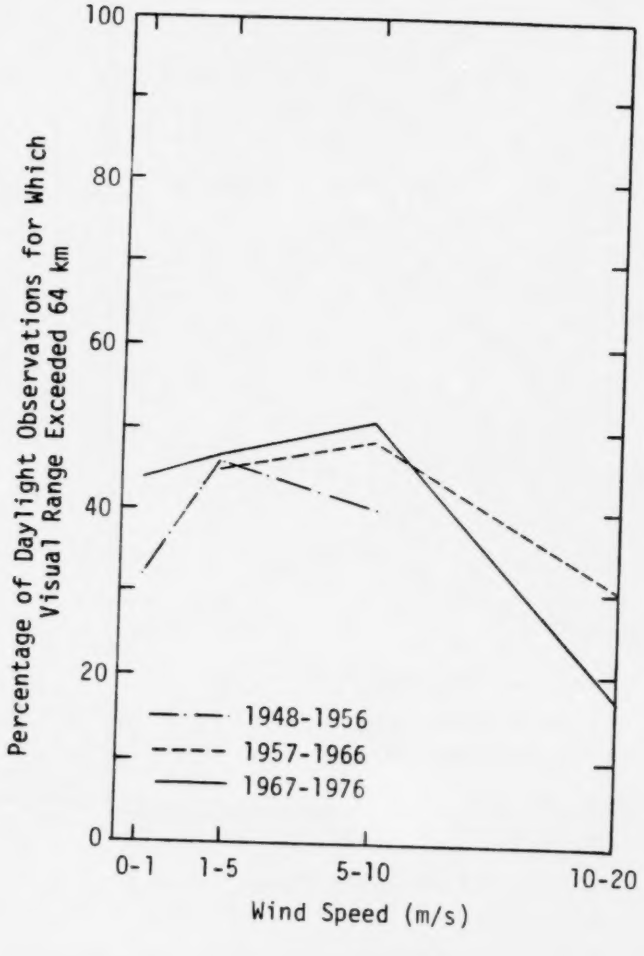

FIGURE A-105. PERCENTAGE OF DAYLIGHT OBSERVATIONS FOR WHICH VISUAL RANGE EXCEEDED 64 km, AS A FUNCTION OF SURFACE WIND SPEED, AT PHOENIX, ARIZONA

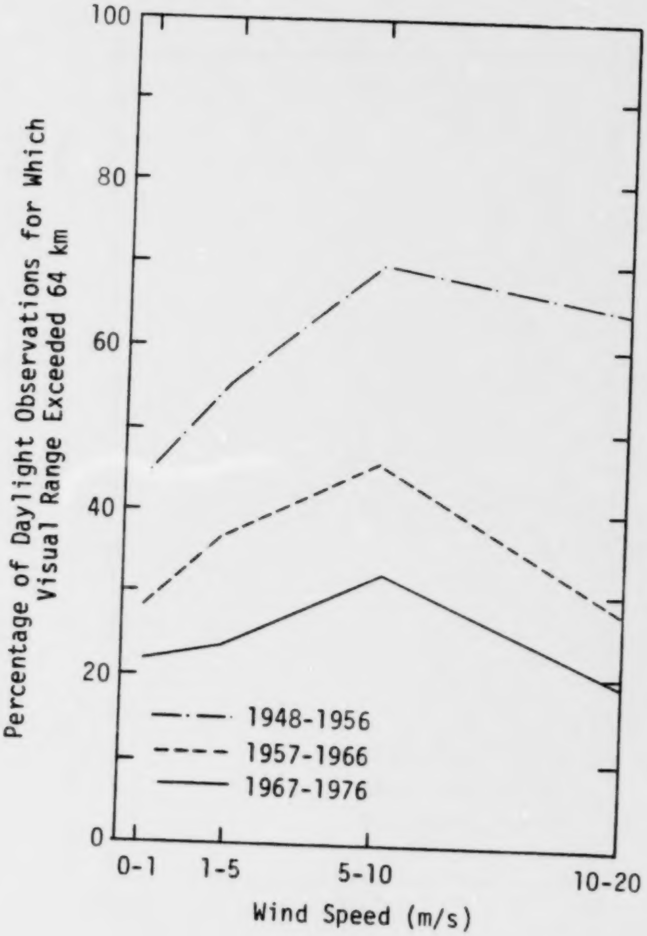

FIGURE A-106. PERCENTAGE OF DAYLIGHT OBSERVATIONS FOR WHICH VISUAL RANGE EXCEEDED 64 km, AS A FUNCTION OF SURFACE WIND SPEED, AT SALT LAKE CITY, UTAH

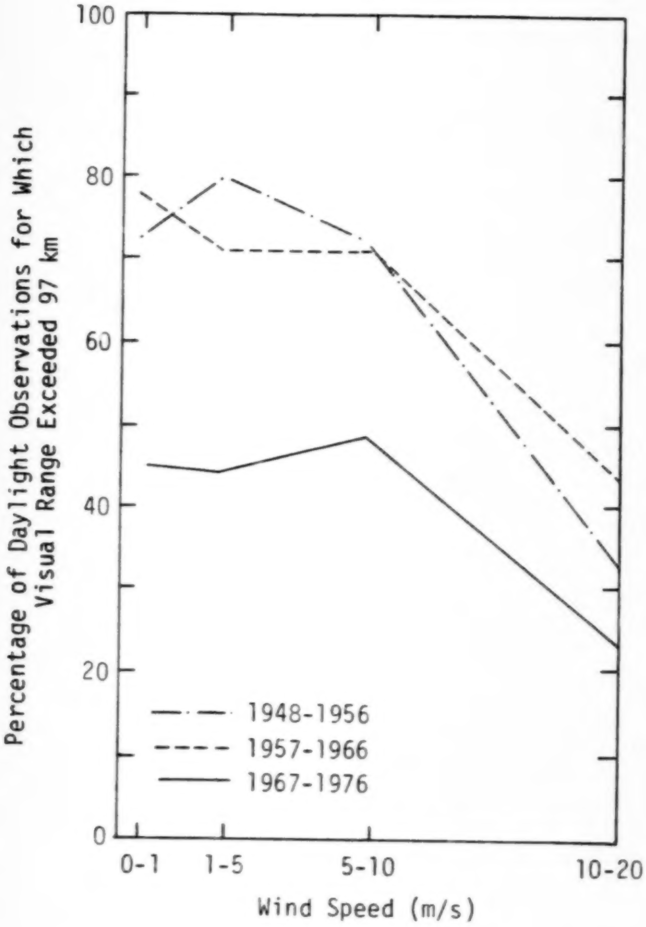

FIGURE A-107. PERCENTAGE OF DAYLIGHT OBSERVATIONS FOR WHICH VISUAL RANGE EXCEEDED 97 km, AS A FUNCTION OF SURFACE WIND SPEED, AT TUCSON, ARIZONA

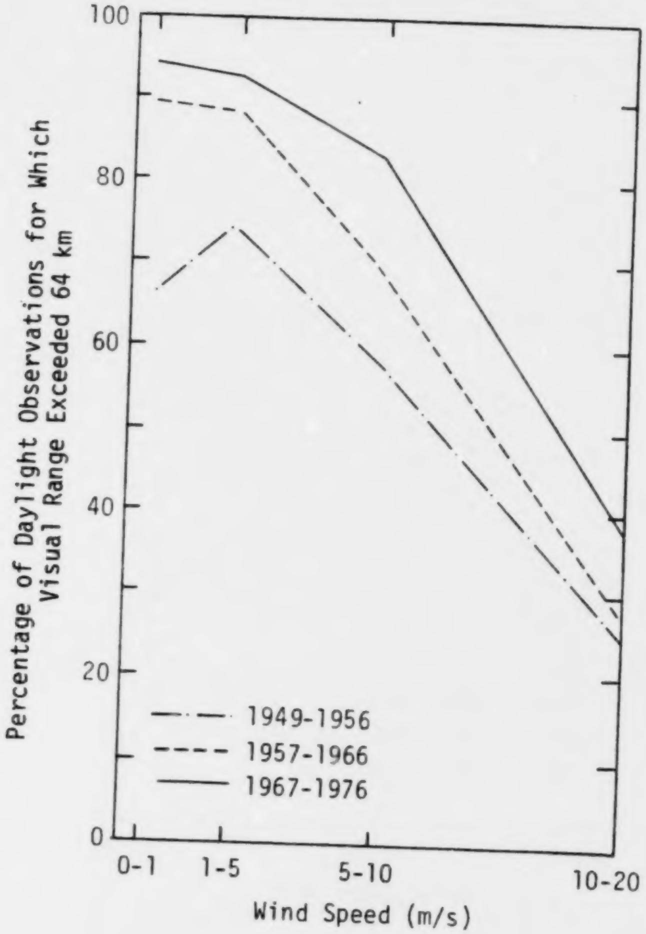

FIGURE A-108. PERCENTAGE OF DAYLIGHT OBSERVATIONS FOR WHICH VISUAL RANGE EXCEEDED 64 km, AS A FUNCTION OF SURFACE WIND SPEED, AT ALAMOGORDO, NEW MEXICO

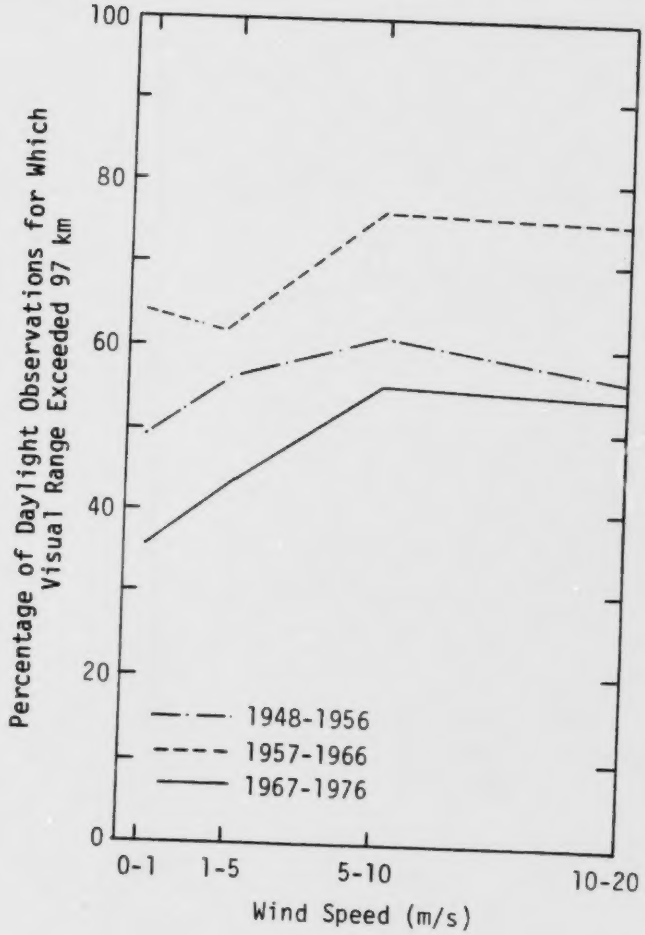

FIGURE A-109. PERCENTAGE OF DAYLIGHT OBSERVATIONS FOR WHICH VISUAL RANGE EXCEEDED 97 km, AS A FUNCTION OF SURFACE WIND SPEED, AT BILLINGS, MONTANA

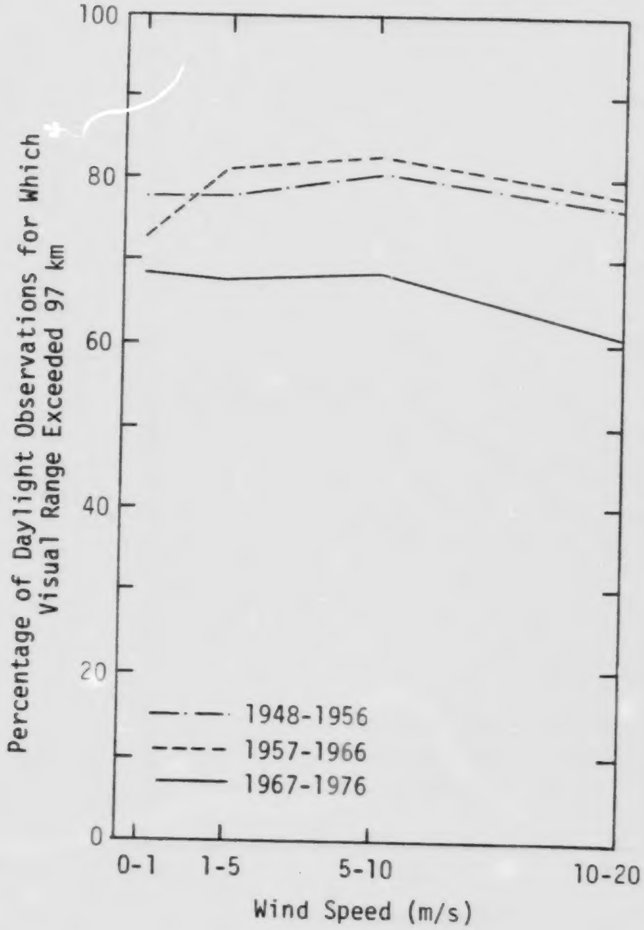

FIGURE A-110. PERCENTAGE OF DAYLIGHT OBSERVATIONS FOR WHICH VISUAL RANGE EXCEEDED 97 km, AS A FUNCTION OF SURFACE WIND SPEED, AT CHEYENNE, WYOMING

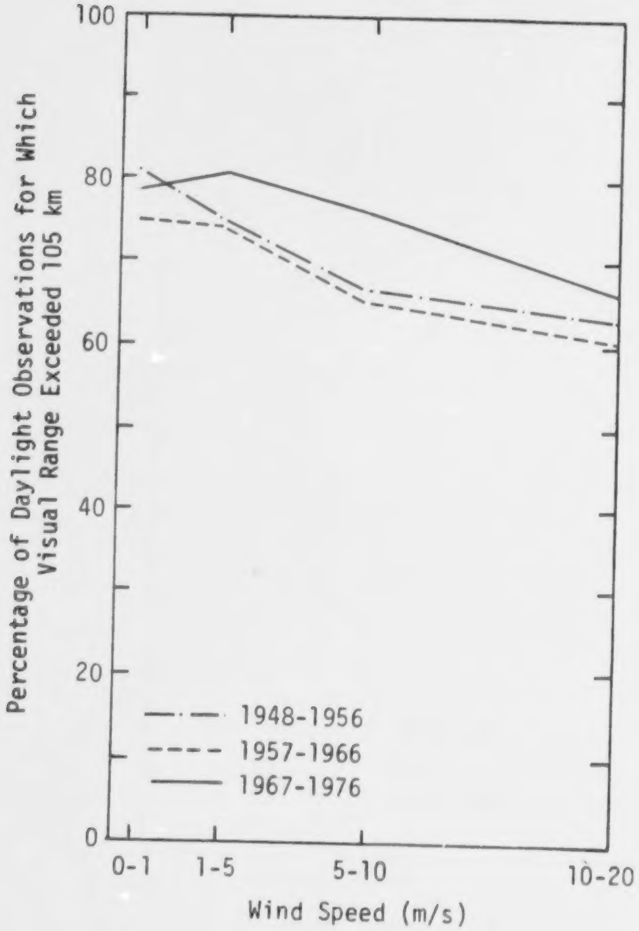

FIGURE A-111. PERCENTAGE OF DAYLIGHT OBSERVATIONS FOR WHICH VISUAL RANGE EXCEEDED 105 km, AS A FUNCTION OF SURFACE WIND SPEED, AT COLORADO SPRINGS, COLORADO

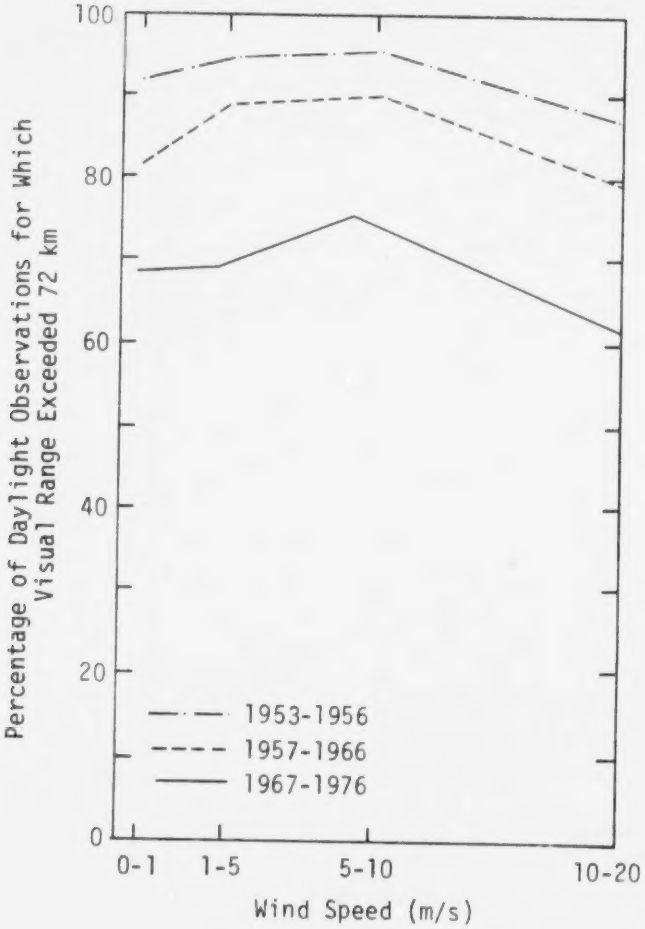

FIGURE A-112. PERCENTAGE OF DAYLIGHT OBSERVATIONS FOR WHICH VISUAL RANGE EXCEEDED 72 km, AS A FUNCTION OF SURFACE WIND SPEED, AT ELY, NEVADA

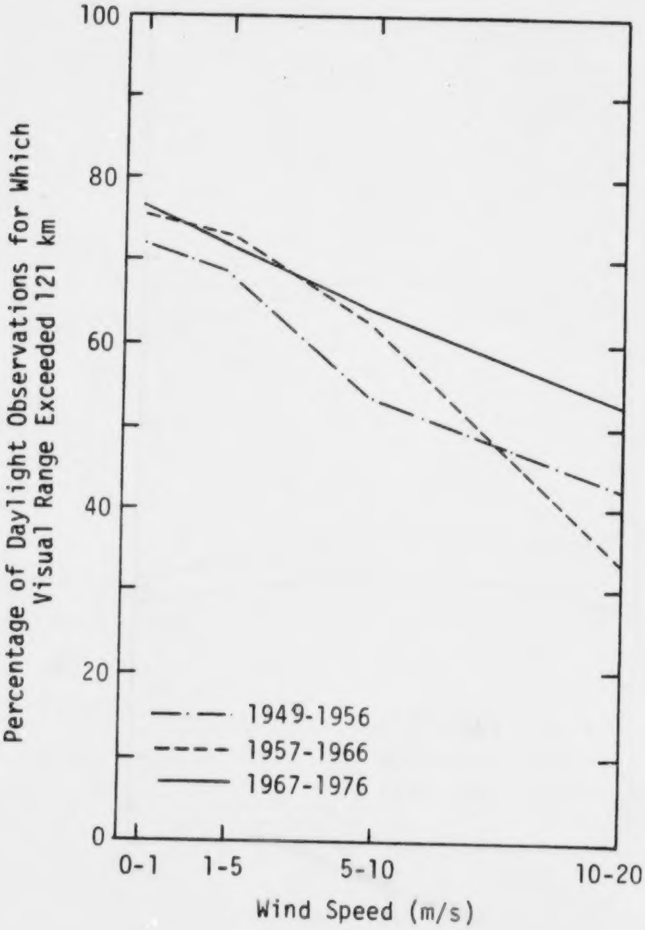

FIGURE A-113. PERCENTAGE OF DAYLIGHT OBSERVATIONS FOR WHICH VISUAL RANGE EXCEEDED 121 km, AS A FUNCTION OF SURFACE WIND SPEED, AT FARMINGTON, NEW MEXICO

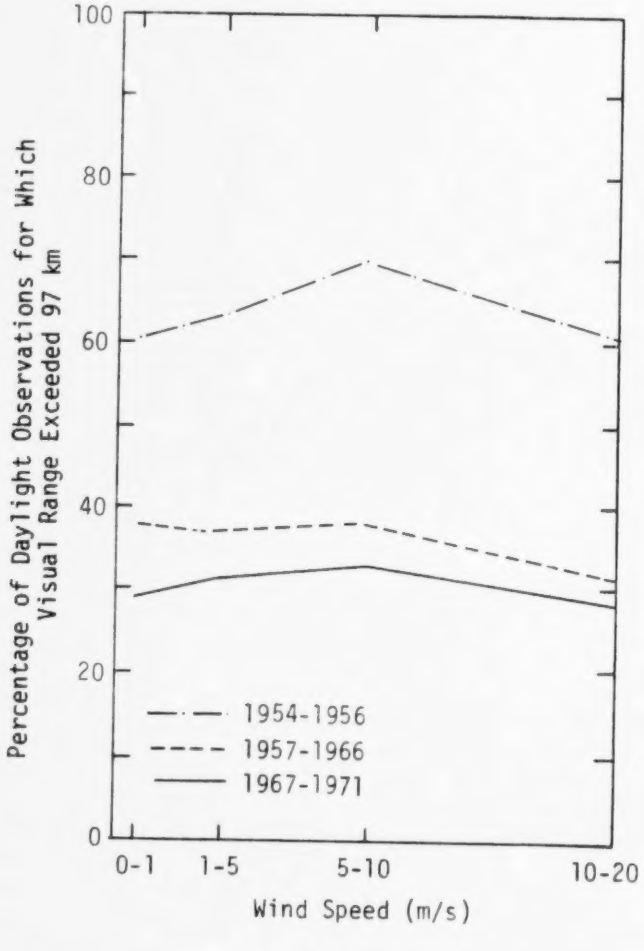

FIGURE A-114. PERCENTAGE OF DAYLIGHT OBSERVATIONS FOR WHICH VISUAL RANGE EXCEEDED 97 km, AS A FUNCTION OF SURFACE WIND SPEED, AT FT. HUACHUCA, ARIZONA

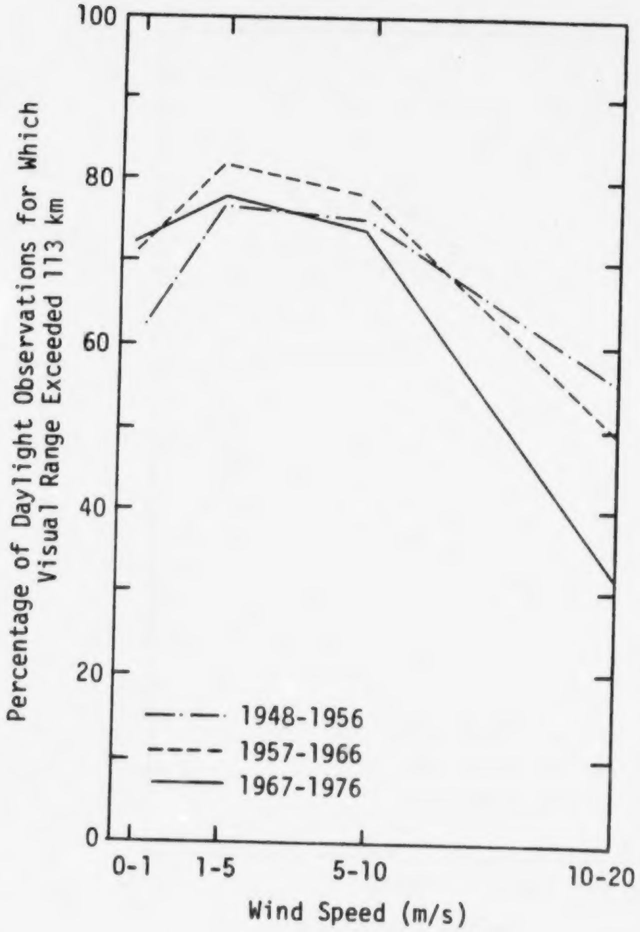

FIGURE A-115. PERCENTAGE OF DAYLIGHT OBSERVATIONS FOR WHICH VISUAL RANGE EXCEEDED 113 km, AS A FUNCTION OF SURFACE WIND SPEED, AT GRAND JUNCTION, COLORADO

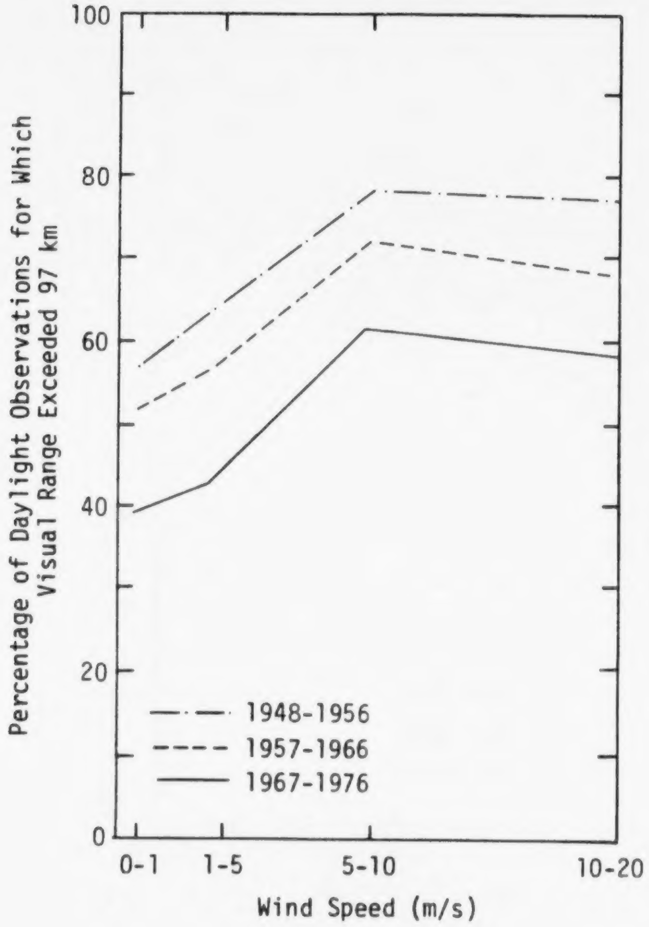

FIGURE A-116. PERCENTAGE OF DAYLIGHT OBSERVATIONS FOR WHICH VISUAL RANGE EXCEEDED 97 km, AS A FUNCTION OF SURFACE WIND SPEED, AT GREAT FALLS, MONTANA

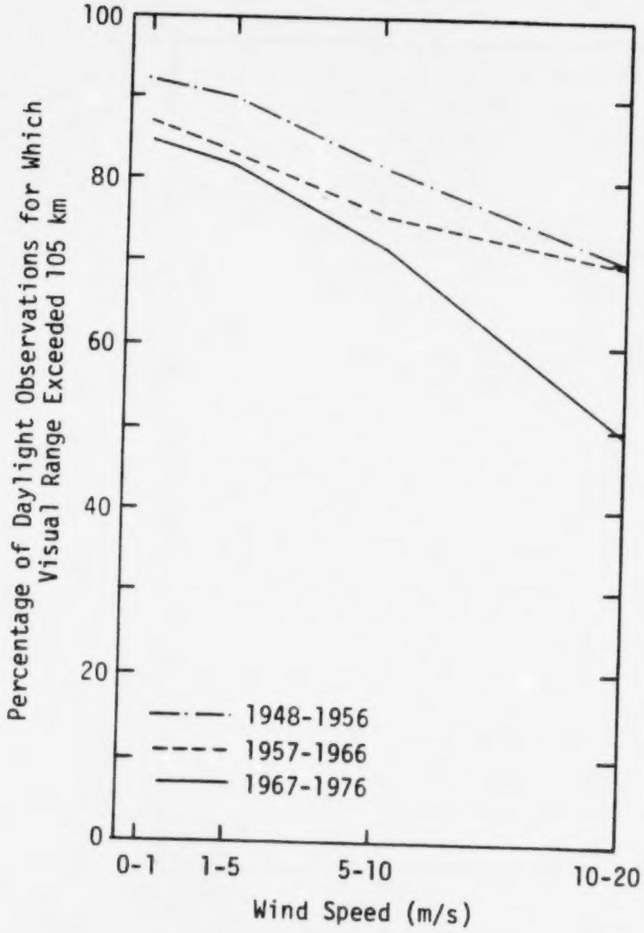

FIGURE A-117. PERCENTAGE OF DAYLIGHT OBSERVATIONS FOR WHICH VISUAL RANGE EXCEEDED 105 km, AS A FUNCTION OF SURFACE WIND SPEED, AT PRESCOTT, ARIZONA

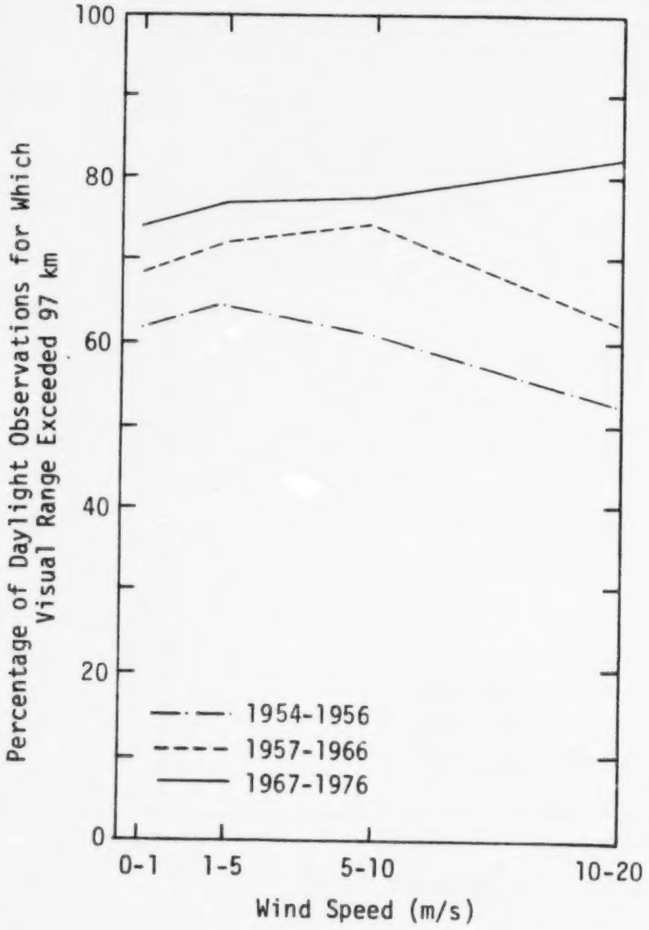

FIGURE A-118. PERCENTAGE OF DAYLIGHT OBSERVATIONS FOR WHICH VISUAL RANGE EXCEEDED 97 km, AS A FUNCTION OF SURFACE WIND SPEED, AT PUEBLO, COLORADO

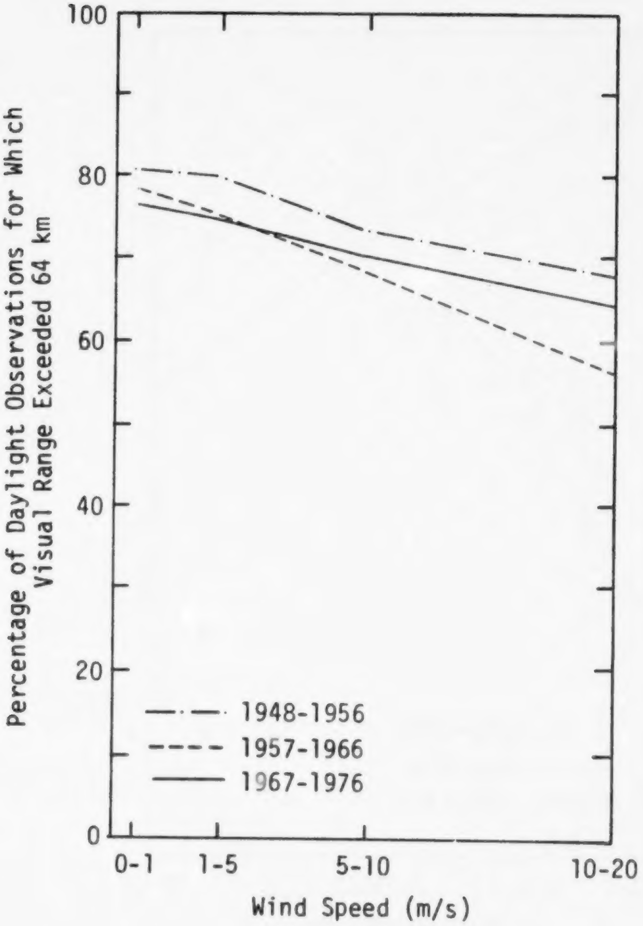

FIGURE A-119. PERCENTAGE OF DAYLIGHT OBSERVATIONS FOR WHICH VISUAL RANGE EXCEEDED 64 km, AS A FUNCTION OF SURFACE WIND SPEED, AT ROCK SPRINGS, WYOMING

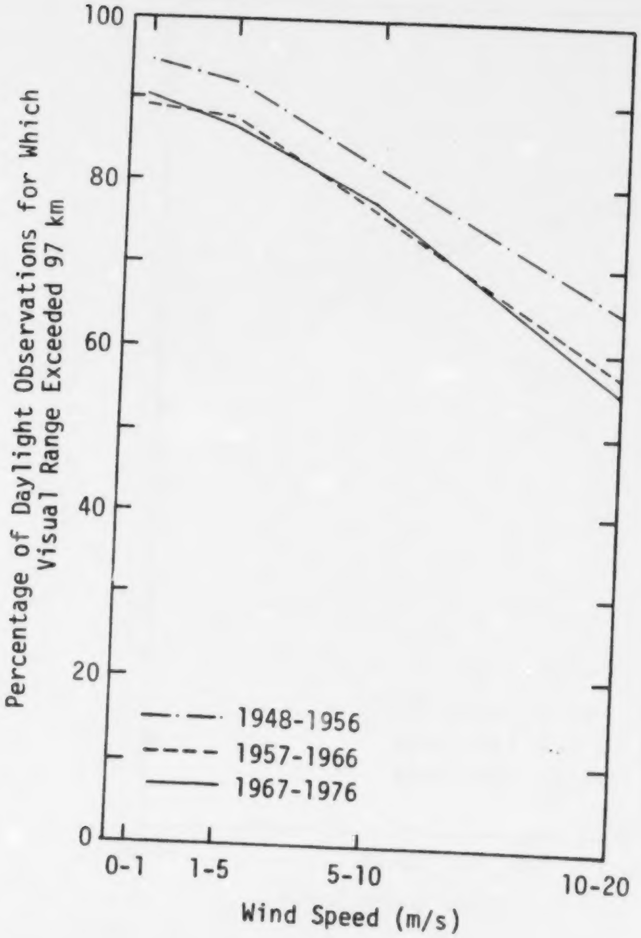

FIGURE A-120. PERCENTAGE OF DAYLIGHT OBSERVATIONS FOR WHICH VISUAL RANGE EXCEEDED 97 km, AS A FUNCTION OF SURFACE WIND SPEED, AT WINSLOW, ARIZONA

These data suggest that high concentrations of coarse particulates raised by the wind are responsible for this visibility degradation. At very high wind speeds, these reductions in visual range are called dust storms. However, at many locations, such as Denver, Phoenix, Salt Lake City, Billings, and Great Falls, visual range increases as wind speed increases from near zero to moderate values because of dilution of the pollutant emissions in these areas.

12. SEASONAL VARIATIONS

Figures A-121 through A-138 show the seasonal variations in visual range at the 18 NWS locations. No general seasonal variations occur at all stations. At some locations, such as Denver, Las Vegas, and Colorado Springs, summer visibilities are poorest. At other locations, notably Phoenix, Salt Lake City, Ely, Grand Junction, and Rock Springs, summer visibilities are best and winter visibilities are worst. At most locations, however, there are no significant seasonal variations in visual range.

Several hypotheses could be advanced to explain the differences in seasonal visibility. Because afternoon mixing depths in the West during the summer are from two to four times greater than winter mixing depths, one would expect greater dilution of natural and anthropogenic emissions in the summer and hence increased visual range. However, enhanced photochemical activity in the summer, resulting from greater insolation, could increase the amount of secondary particulate matter formed in the atmosphere. In addition, concentrations of windblown dust may be greater on dry, hot summer days.

13. DIURNAL VARIATIONS

The dependence of visual range on time of day is illustrated in Figures A-139 through A-156. Increases in visual range with changes in time from early morning (before 1000 hours), through midday (1000 to 1400 hours), and into afternoon (after 1400 hours), such as those observed

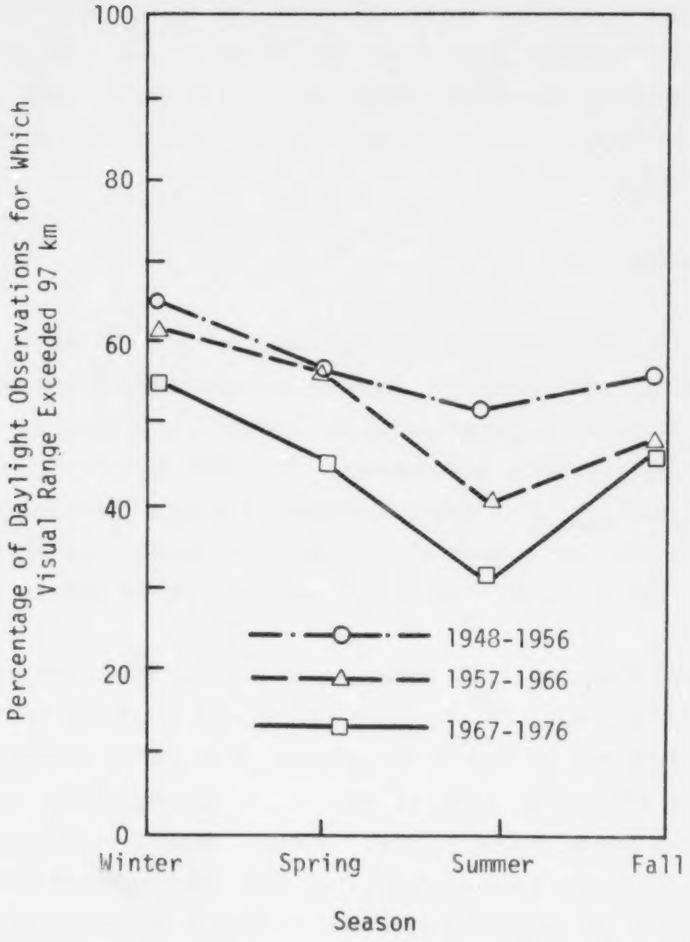

FIGURE A-121. SEASONAL VARIATION IN VISUAL RANGE AT DENVER, COLORADO, 1948-1976

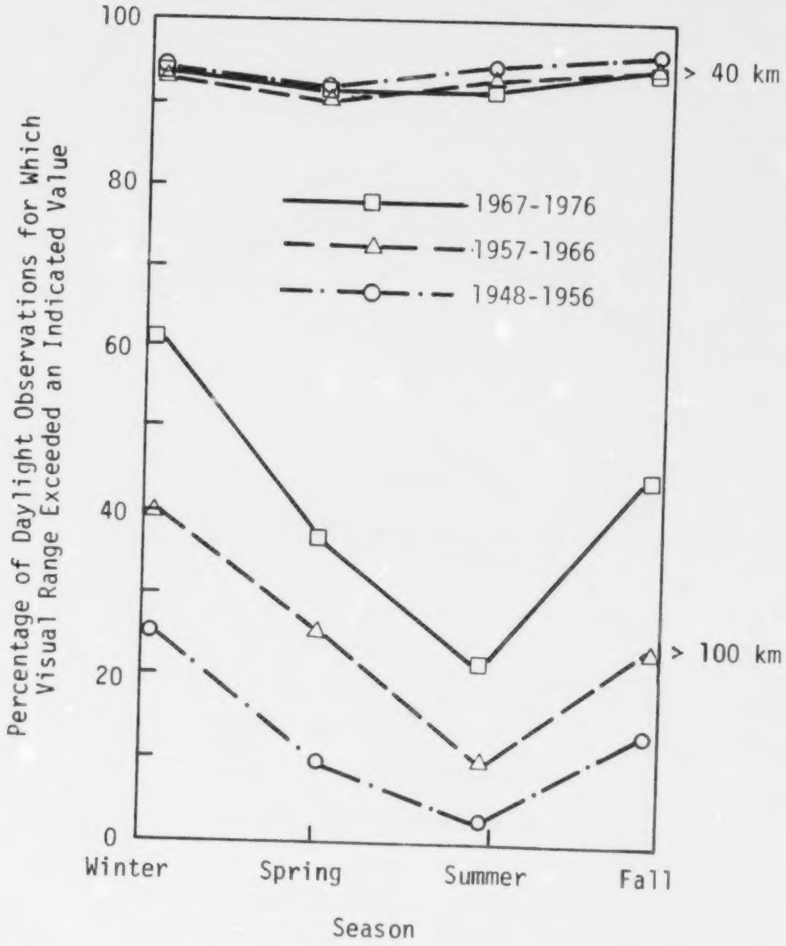

FIGURE A-122. SEASONAL VARIATION IN VISUAL RANGE AT LAS VEGAS, NEVADA, 1948-1976

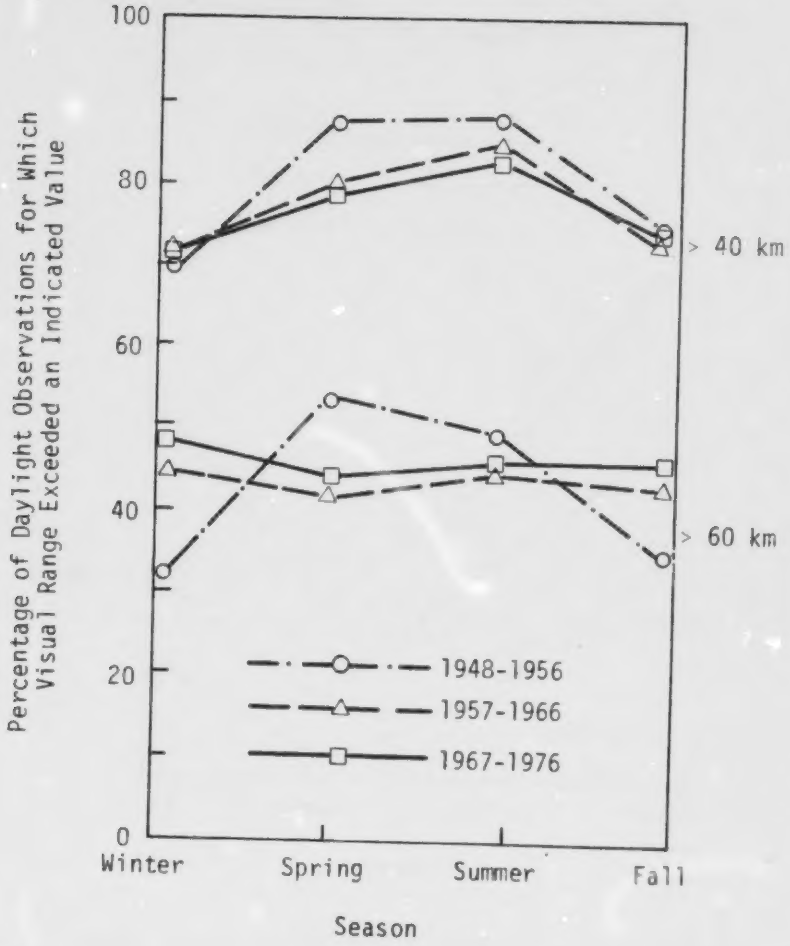

FIGURE A-123. SEASONAL VARIATION IN VISUAL RANGE AT PHOENIX, ARIZONA, 1948-1976

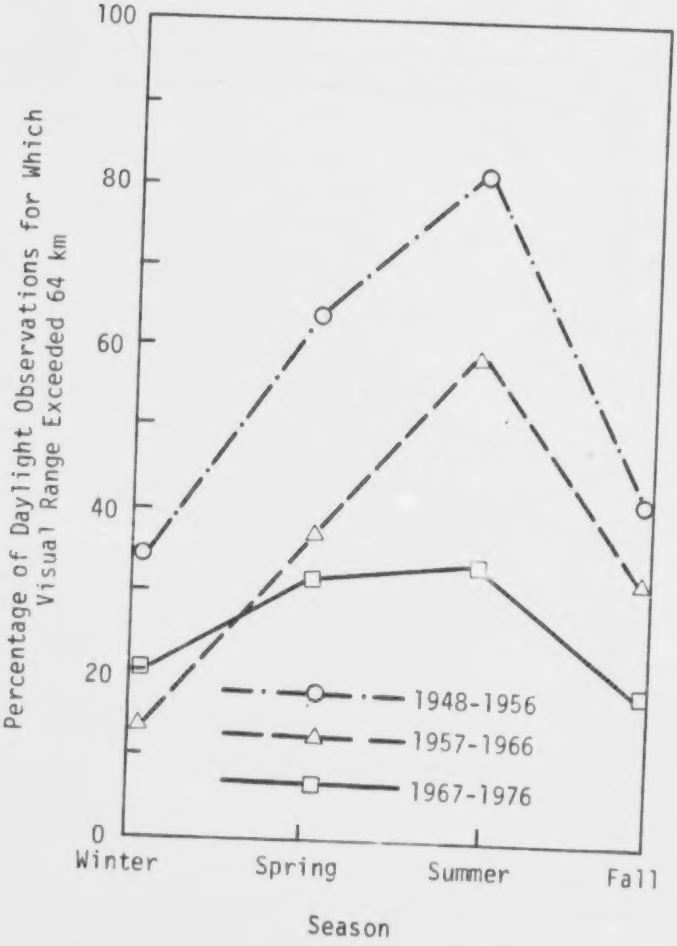

FIGURE A-124. SEASONAL VARIATION IN VISUAL RANGE AT SALT LAKE CITY, UTAH, 1948-1976

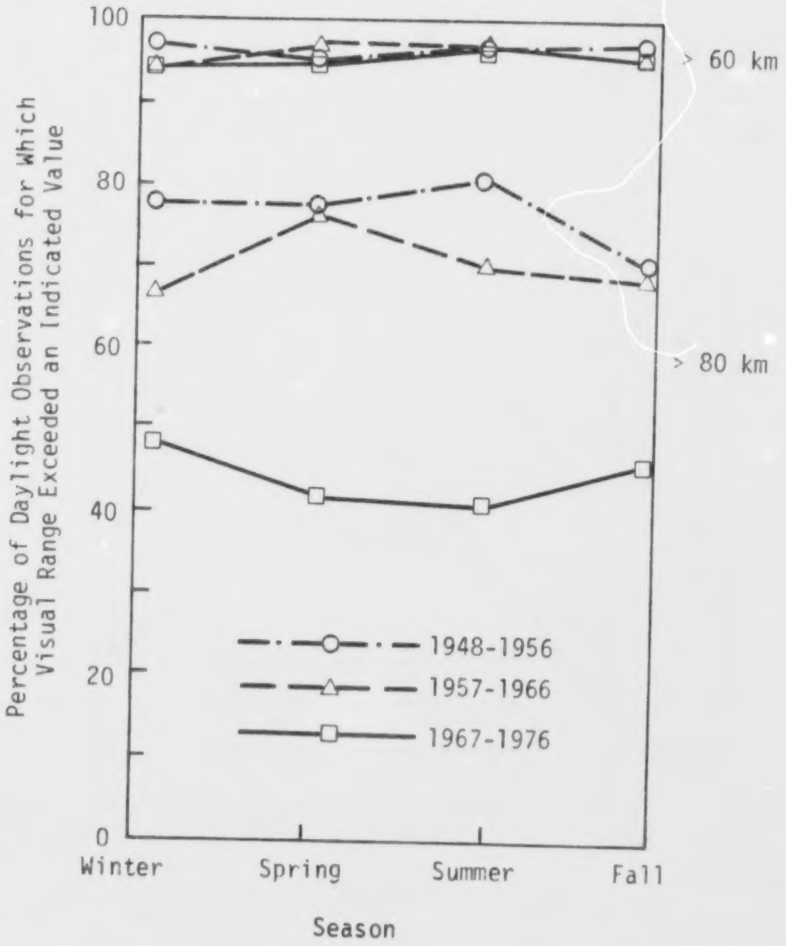

FIGURE A-125. SEASONAL VARIATION IN VISUAL RANGE AT TUCSON, ARIZONA, 1948-1976

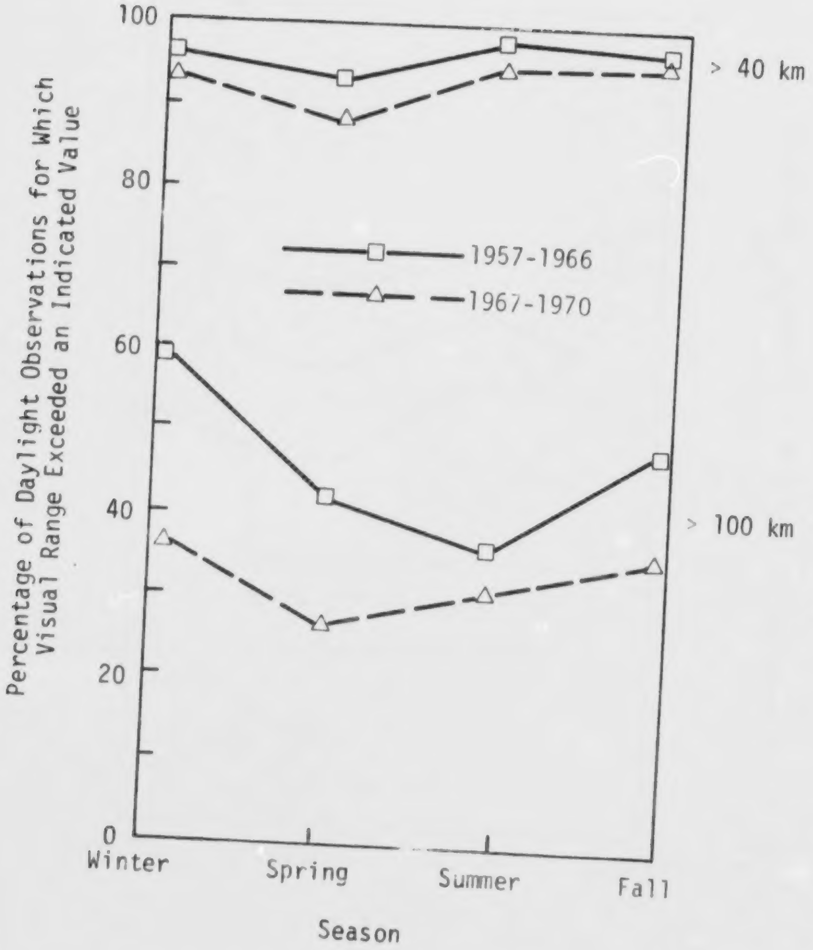

FIGURE A-126. SEASONAL VARIATION IN VISUAL RANGE AT ALAMOGORDO, NEW MEXICO, 1957-1970

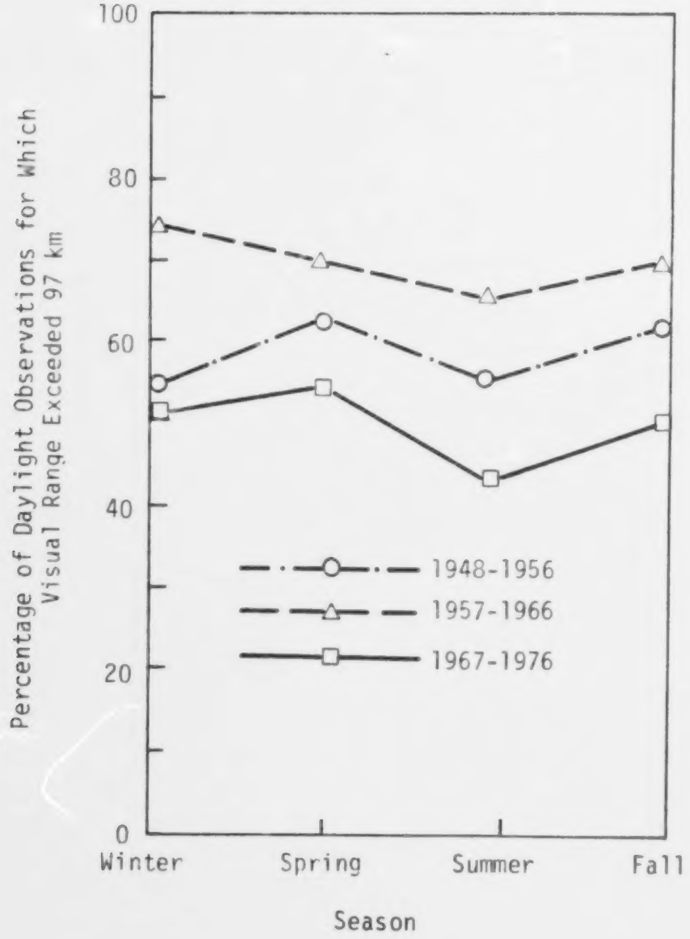

FIGURE A-127. SEASONAL VARIATION IN VISUAL RANGE AT BILLINGS, MONTANA, 1948-1976

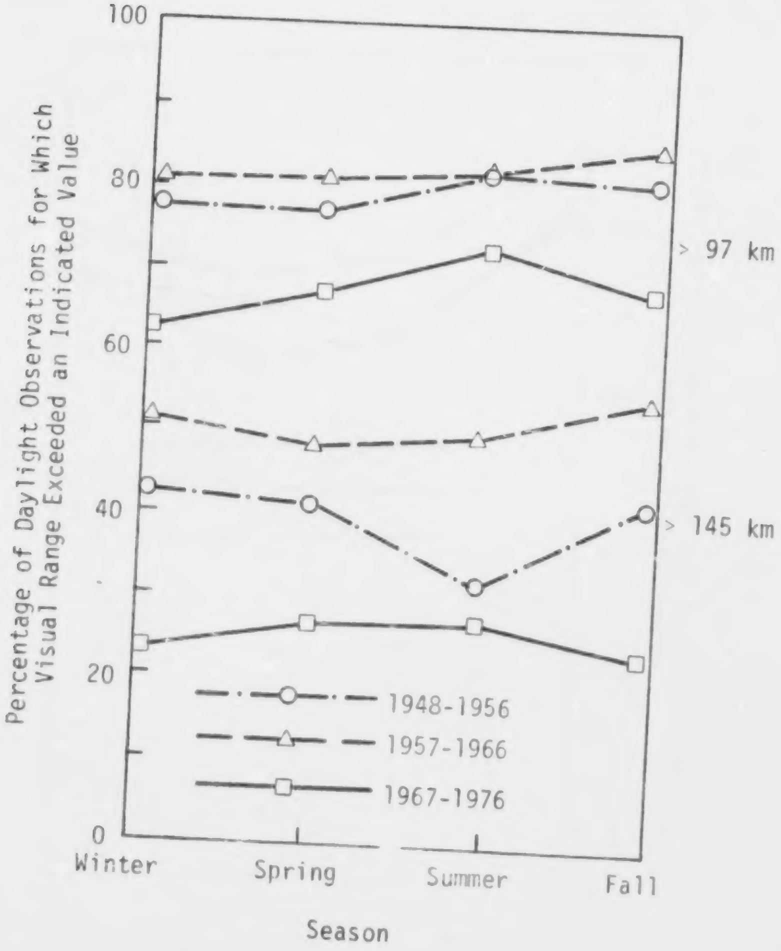

FIGURE A-128. SEASONAL VARIATION IN VISUAL RANGE AT CHEYENNE, WYOMING, 1948-1976

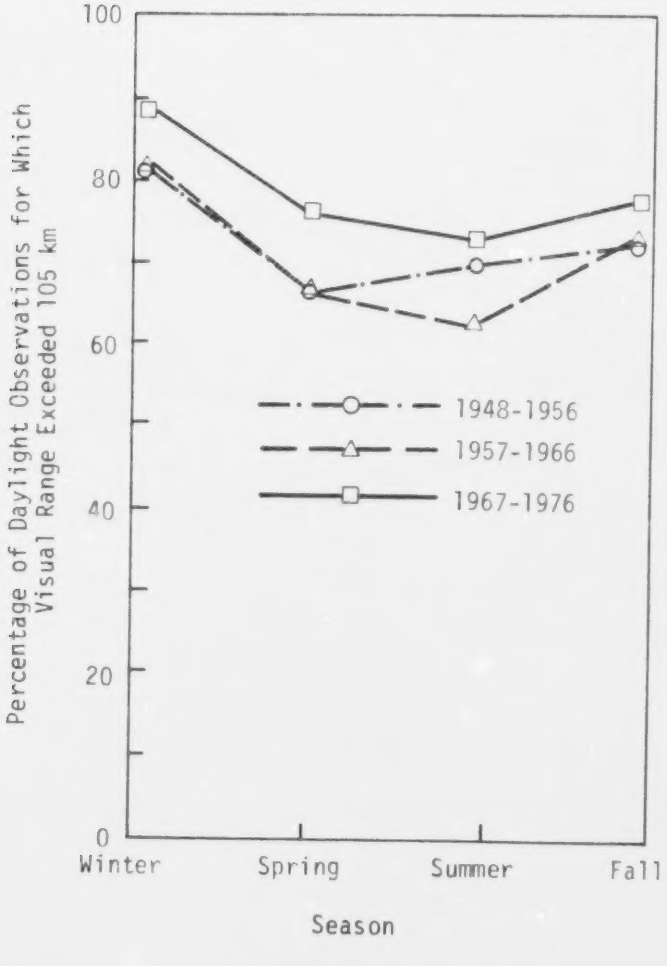

FIGURE A-129. SEASONAL VARIATION IN VISUAL RANGE AT COLORADO SPRINGS, COLORADO, 1948-1976

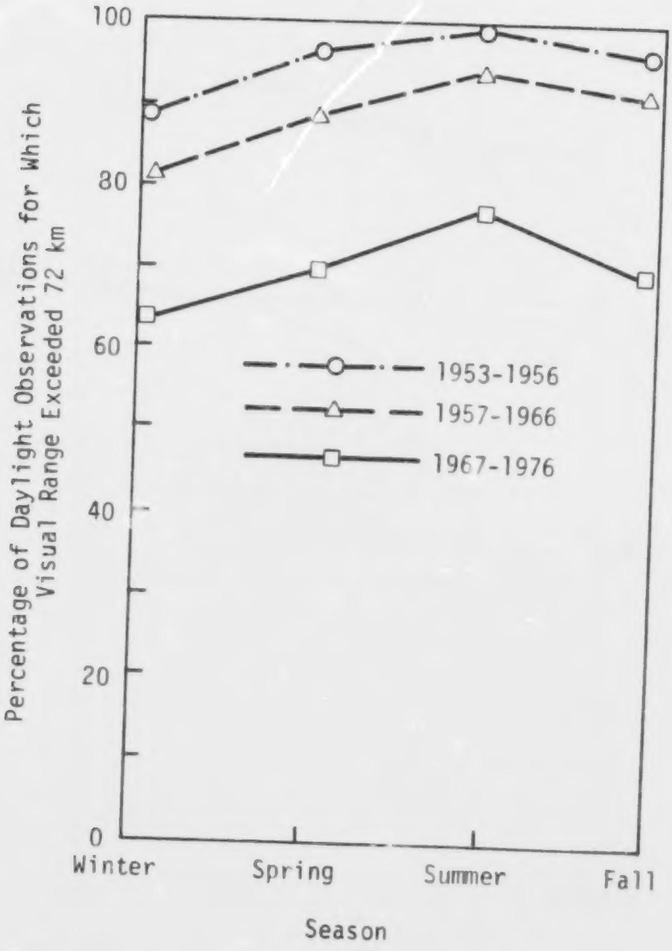

FIGURE A-130. SEASONAL VARIATION IN VISUAL RANGE AT ELY, NEVADA, 1953-1976

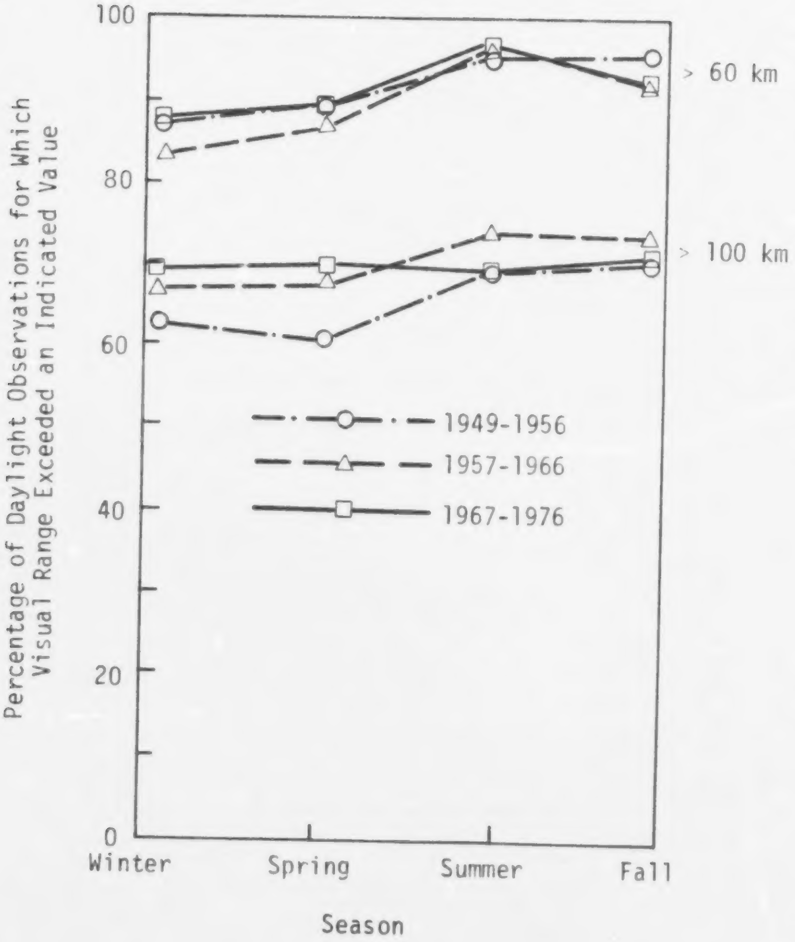

FIGURE A-131. SEASONAL VARIATION IN VISUAL RANGE AT FARMINGTON, NEW MEXICO, 1949-1976

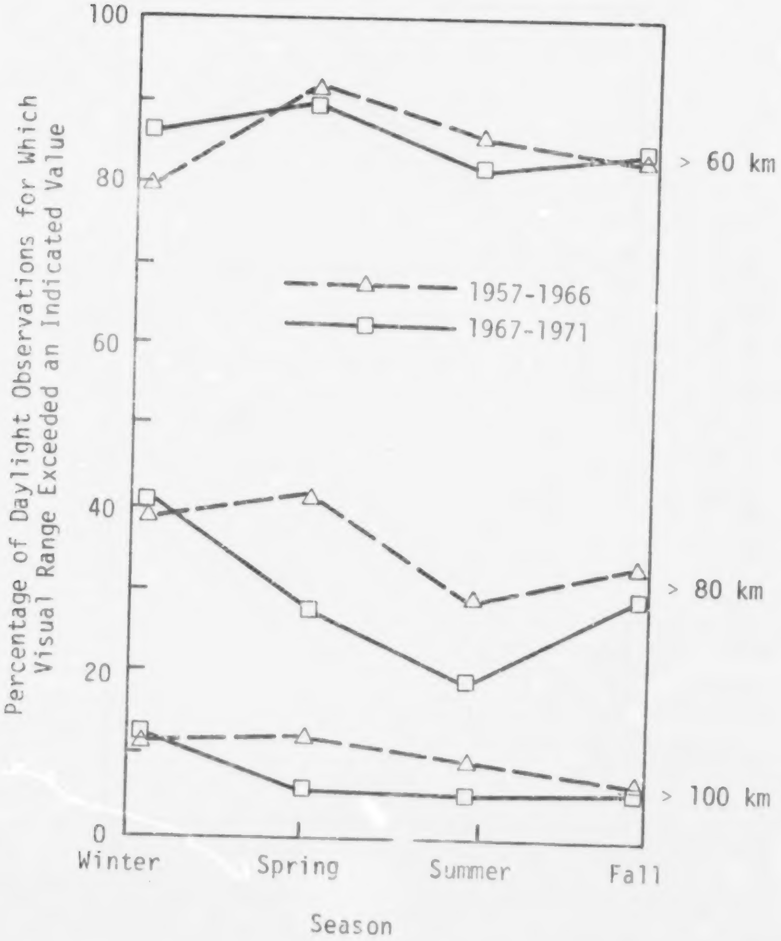

FIGURE 132. SEASONAL VARIATION IN VISUAL RANGE AT FT. HUACHUCA, ARIZONA, 1957-1971

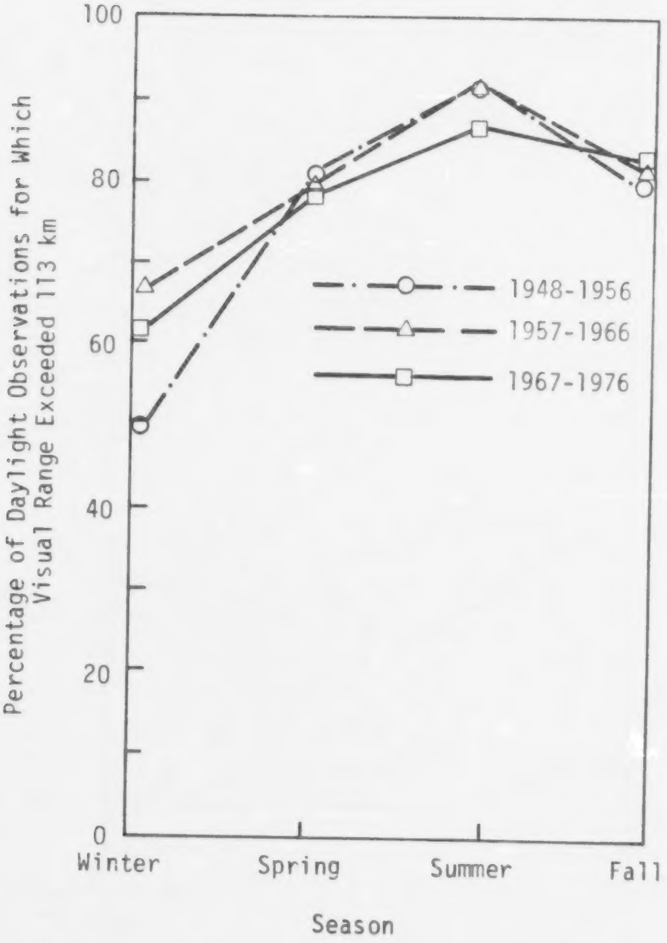

FIGURE A-133. SEASONAL VARIATION IN VISUAL RANGE AT GRAND JUNCTION, COLORADO, 1948-1976

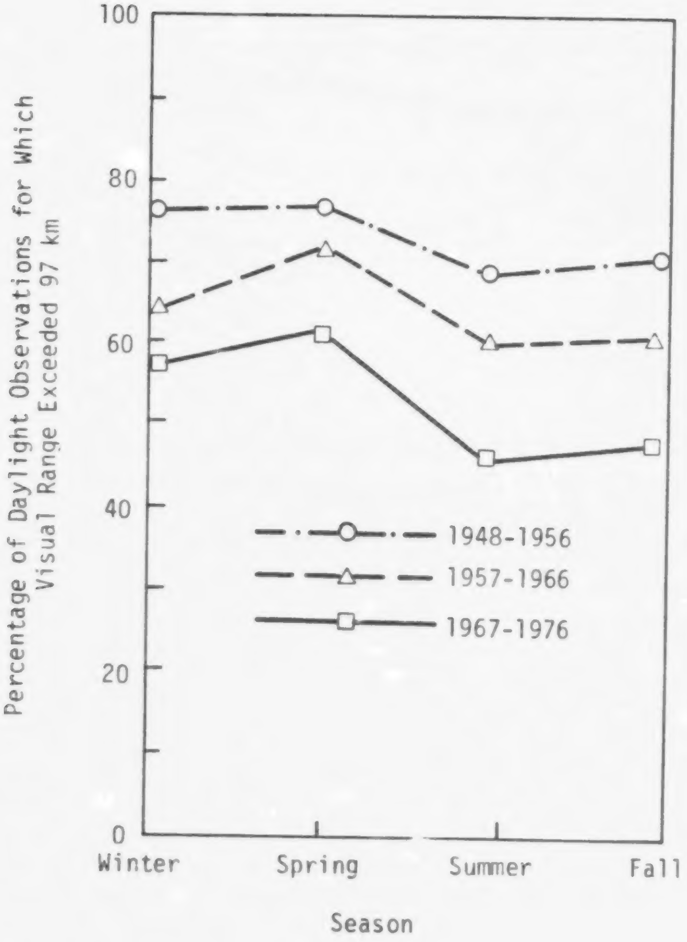

FIGURE A-134. SEASONAL VARIATION IN VISUAL RANGE AT GREAT FALLS, MONTANA, 1948-1976

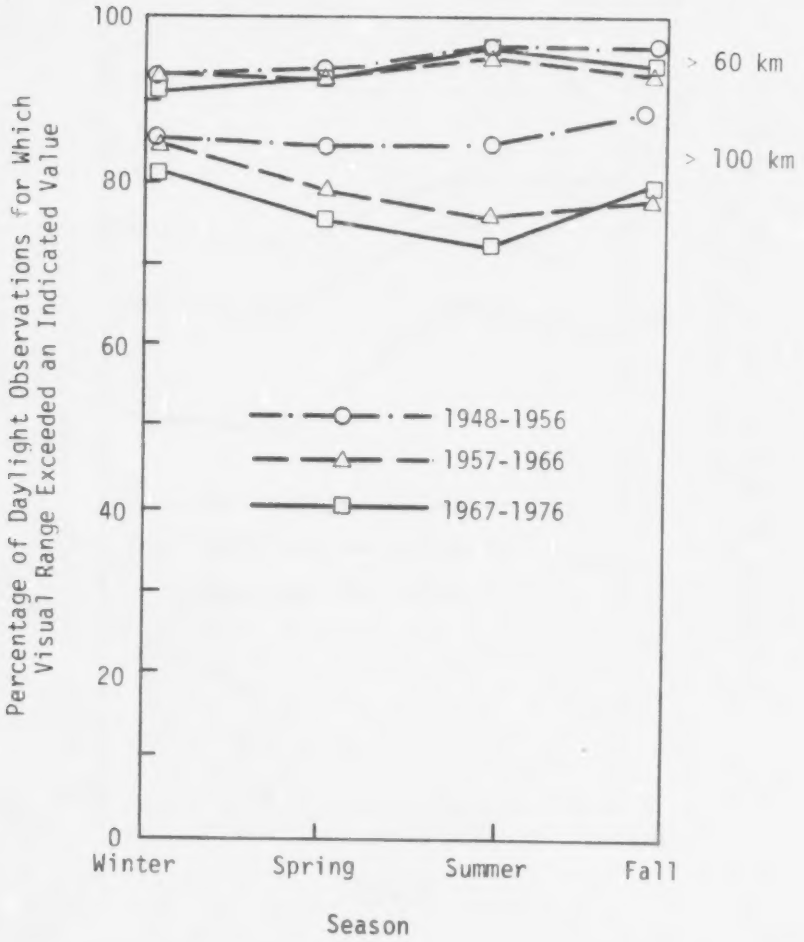

FIGURE A-135. SEASONAL VARIATION IN VISUAL RANGE AT PRESCOTT, ARIZONA, 1948-1976

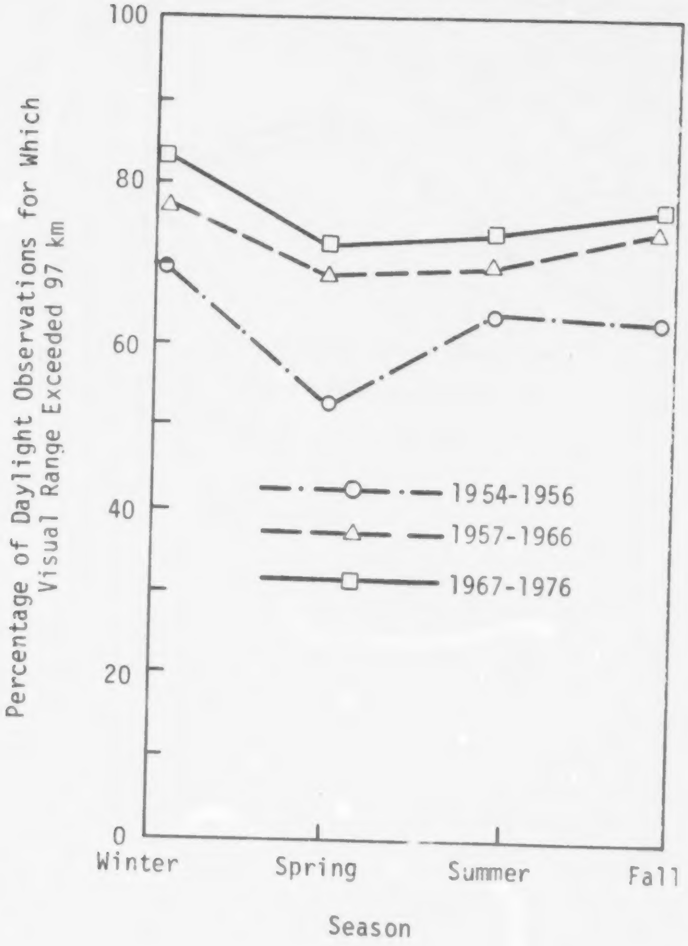

FIGURE A-136. SEASONAL VARIATION IN VISUAL RANGE AT PUEBLO, COLORADO, 1954-1976

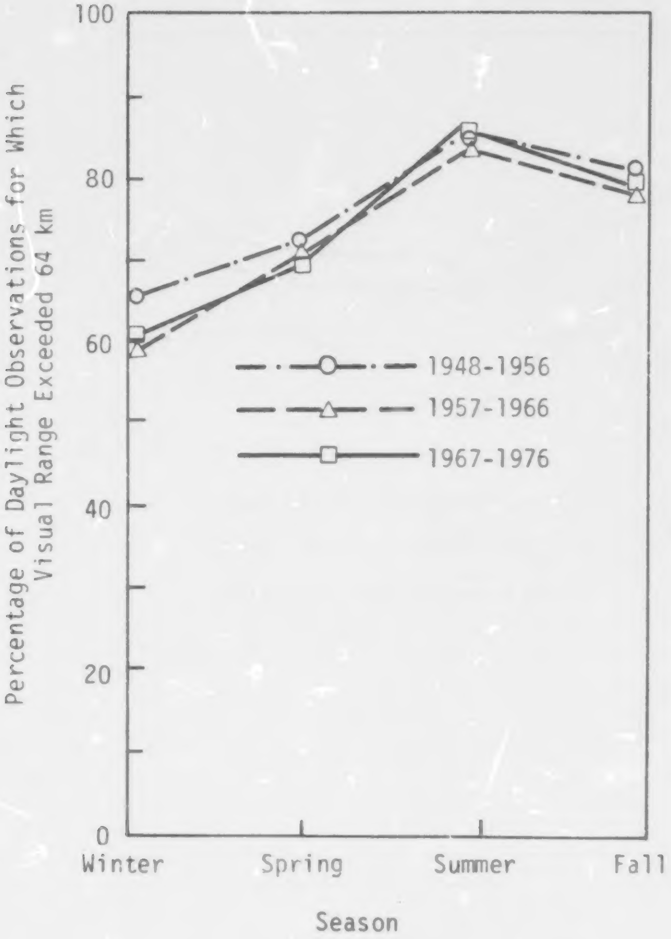

FIGURE A-137. SEASONAL VARIATION IN VISUAL RANGE AT ROCK SPRINGS, WYOMING, 1948-1976

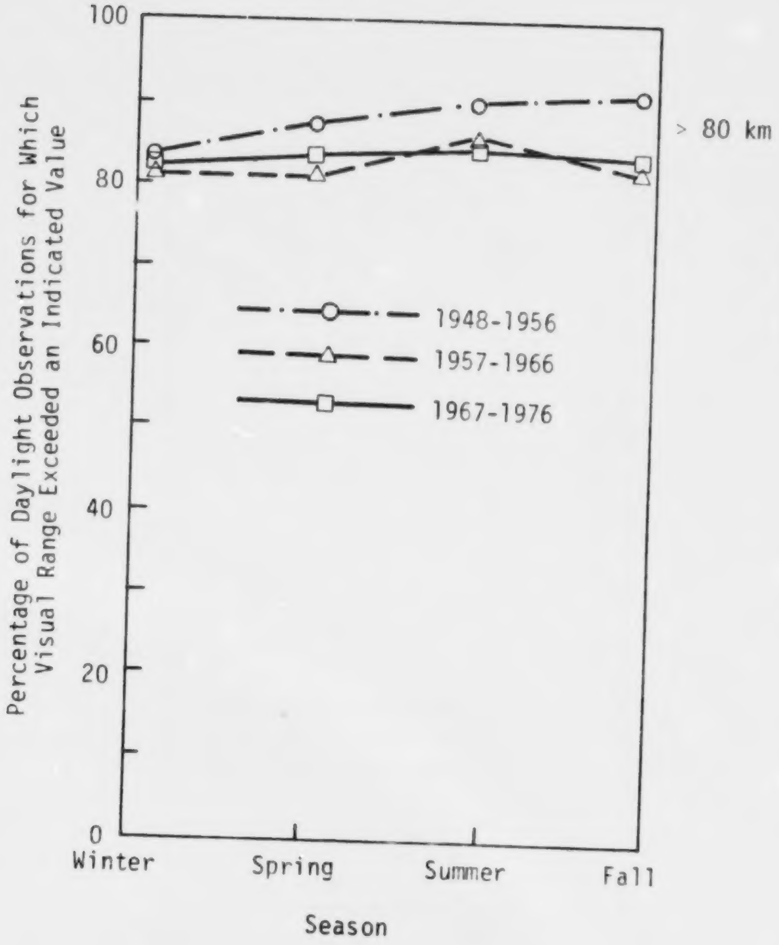

FIGURE A-138. SEASONAL VARIATION IN VISUAL RANGE AT WINSLOW, ARIZONA, 1948-1976

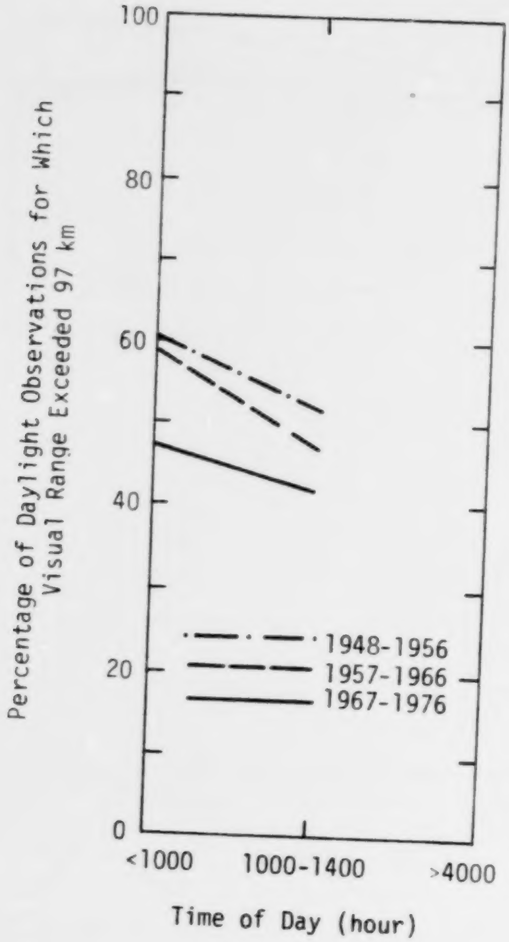

FIGURE A-139. VARIATION IN VISUAL RANGE AS A FUNCTION OF TIME OF DAY AT DENVER, COLORADO, 1948-1976

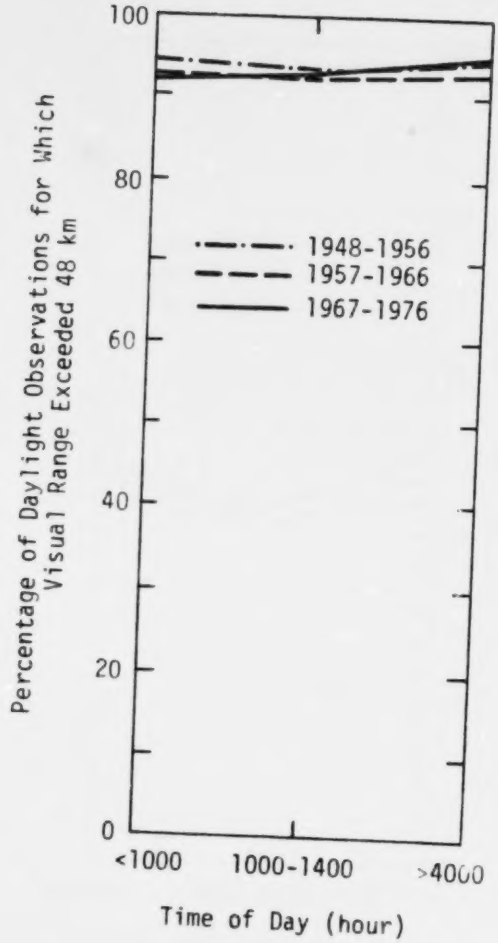

FIGURE A-140. VARIATION IN VISUAL RANGE AS A FUNCTION OF TIME OF DAY AT LAS VEGAS, NEVADA 1948-1976

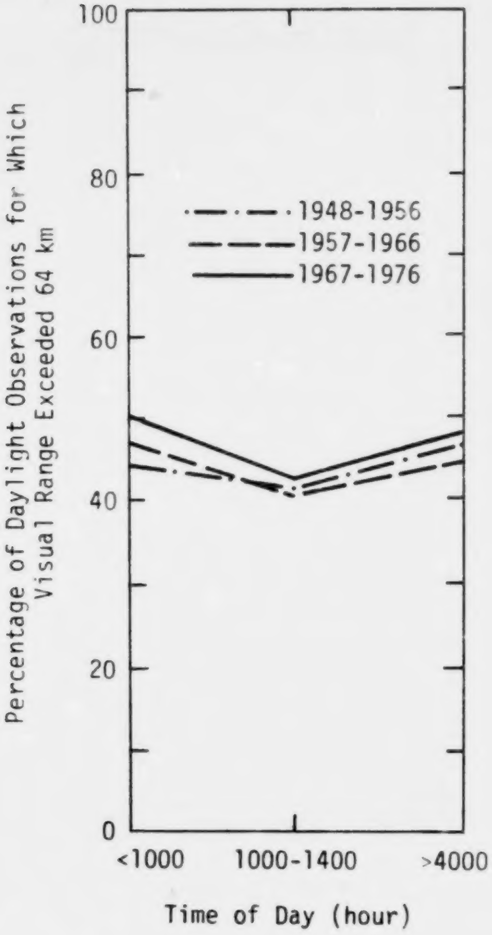

FIGURE A-141. VARIATION IN VISUAL RANGE AS A FUNCTION OF TIME OF DAY AT PHOENIX, ARIZONA, 1948-1976

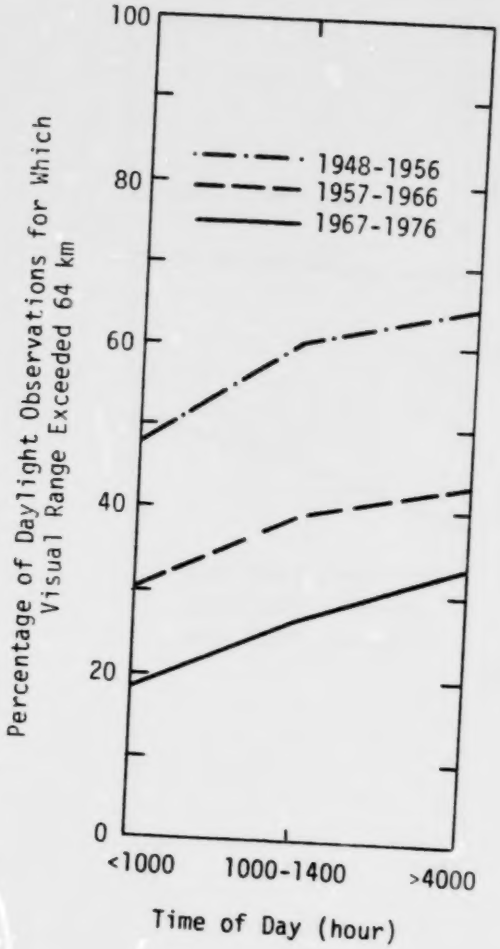

FIGURE A-142. VARIATION IN VISUAL RANGE AS A FUNCTION OF TIME OF DAY AT SALT LAKE CITY, UTAH 1948-1976

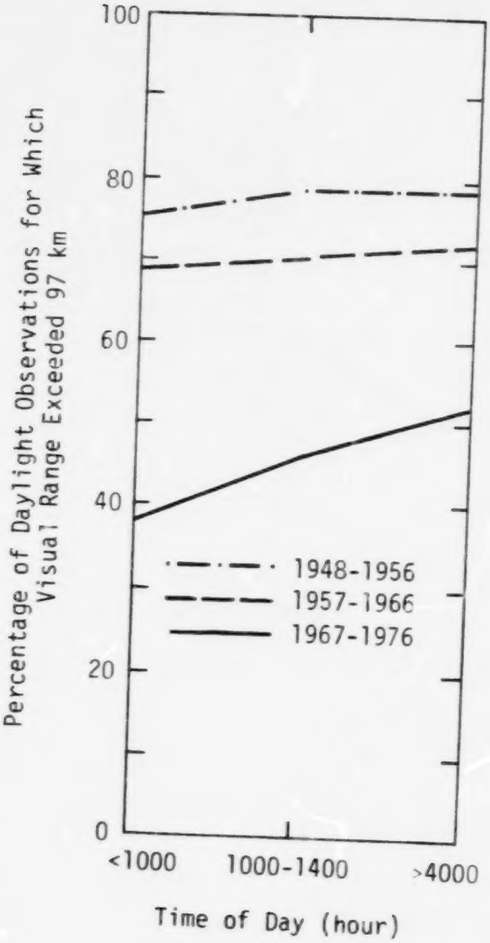

FIGURE A-143. VARIATION IN VISUAL RANGE AS A FUNCTION OF TIME OF DAY AT TUCSON, ARIZONA, 1948-1976

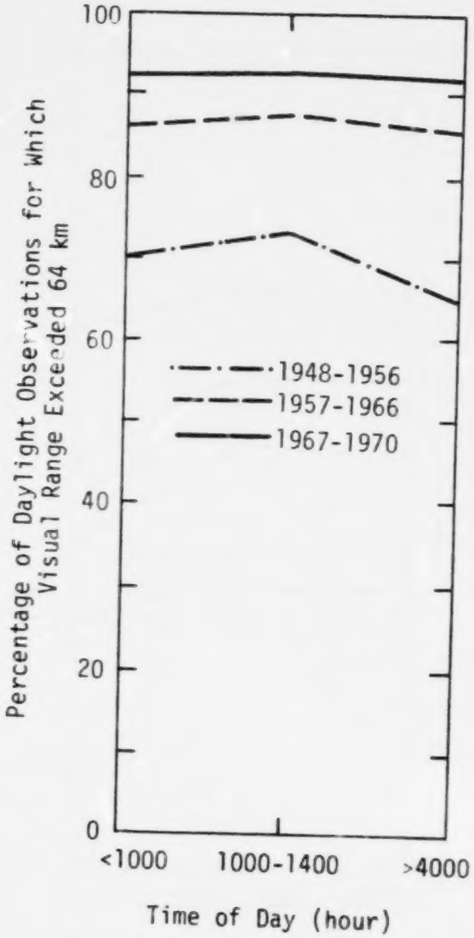

FIGURE A-144. VARIATION IN VISUAL RANGE AS A FUNCTION OF TIME OF DAY AT ALAMAGORDO, NEW MEXICO, 1948-1970

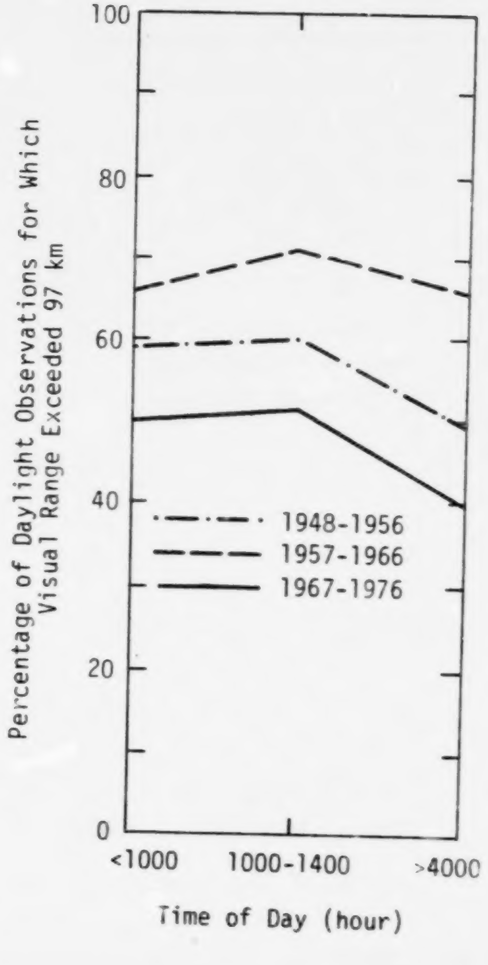

FIGURE A-145. VARIATION IN VISUAL RANGE AS A FUNCTION OF TIME OF DAY AT BILLINGS, MONTANA, 1948-1976

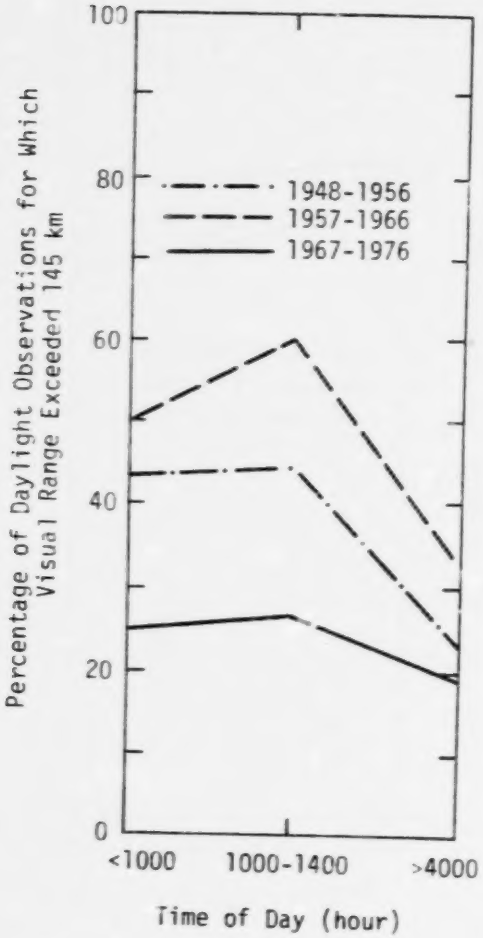

FIGURE A-146. VARIATION IN VISUAL RANGE AS A FUNCTION OF TIME OF DAY AT CHEYENNE, WYOMING, 1948-1976

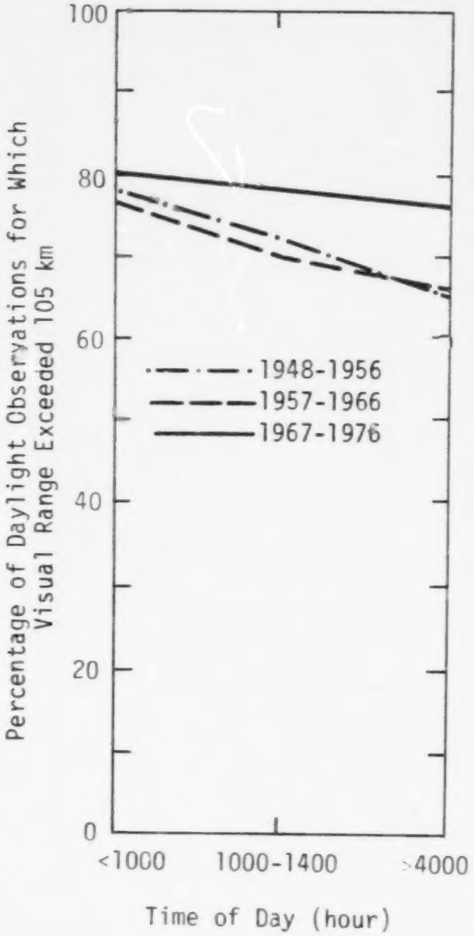

FIGURE A-147. VARIATION IN VISUAL RANGE AS A FUNCTION OF TIME OF DAY AT COLORADO SPRINGS, COLORADO 1948-1976

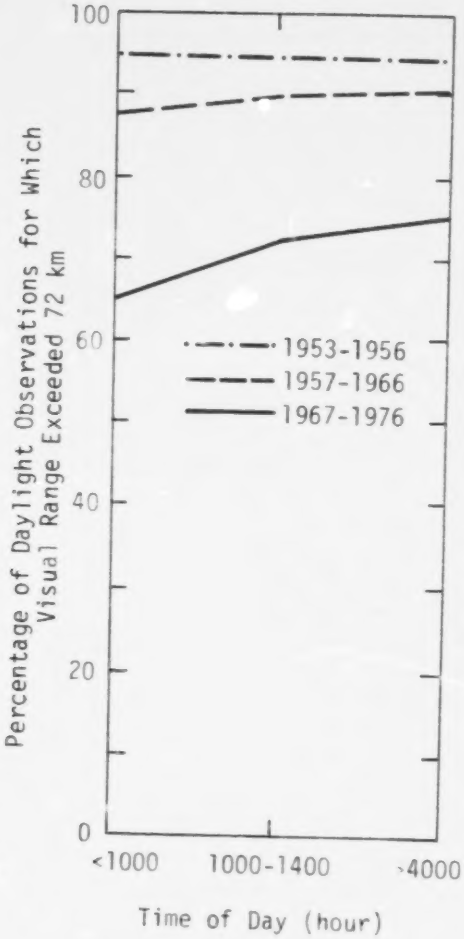

FIGURE A-148. VARIATION IN VISUAL RANGE AS A FUNCTION OF TIME OF DAY AT ELY, NEVADA, 1953-1976

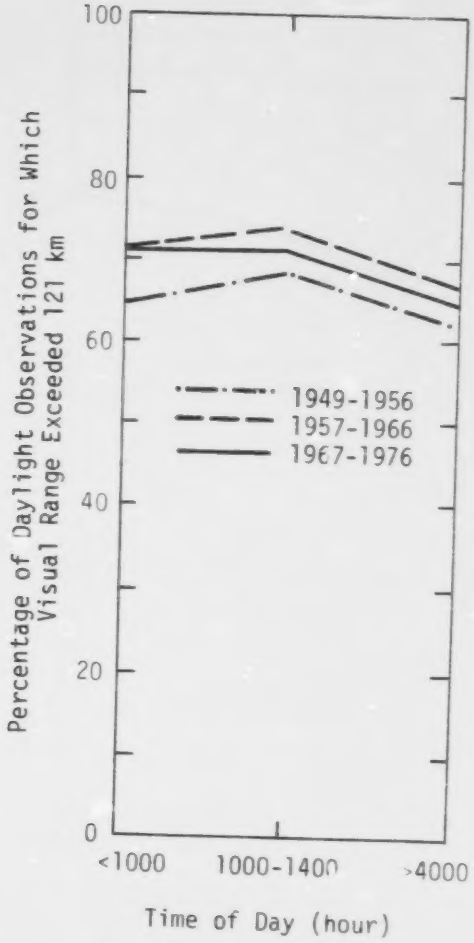

FIGURE A-149. VARIATION IN VISUAL RANGE AS A FUNCTION OF TIME OF DAY AT FARMINGTON, NEW MEXICO, 1949-1976

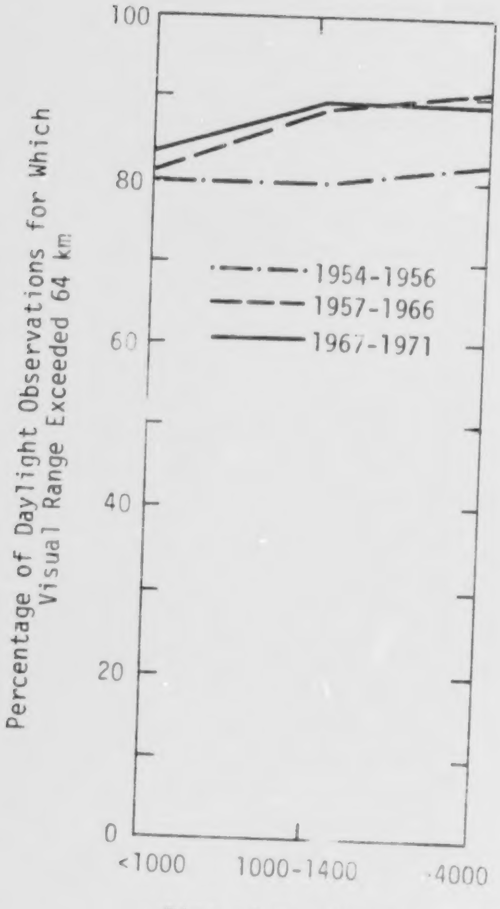

FIGURE A-150. VARIATION IN VISUAL RANGE AS A FUNCTION OF TIME OF DAY AT FT. HUACHUCA, ARIZONA, 1954-1971

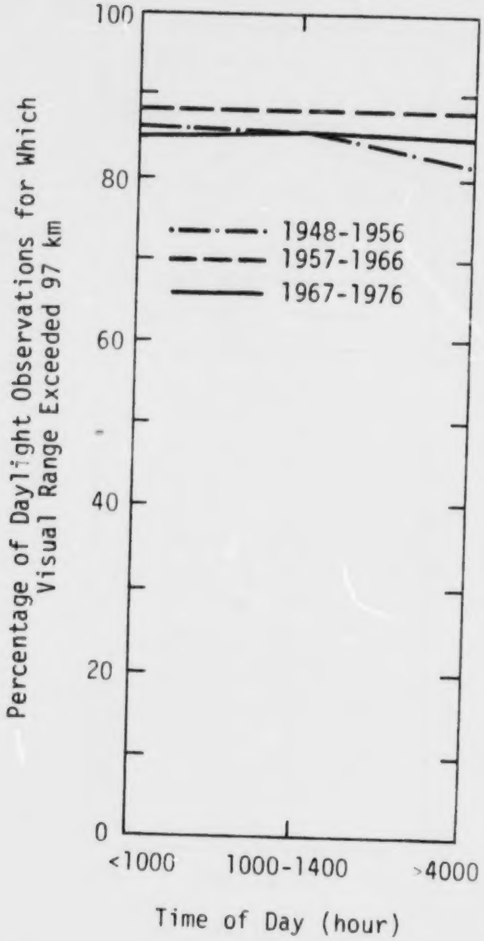

FIGURE A-151. VARIATION IN VISUAL RANGE AS A FUNCTION OF TIME OF DAY AT GRAND JUNCTION, COLORADO, 1948-1976

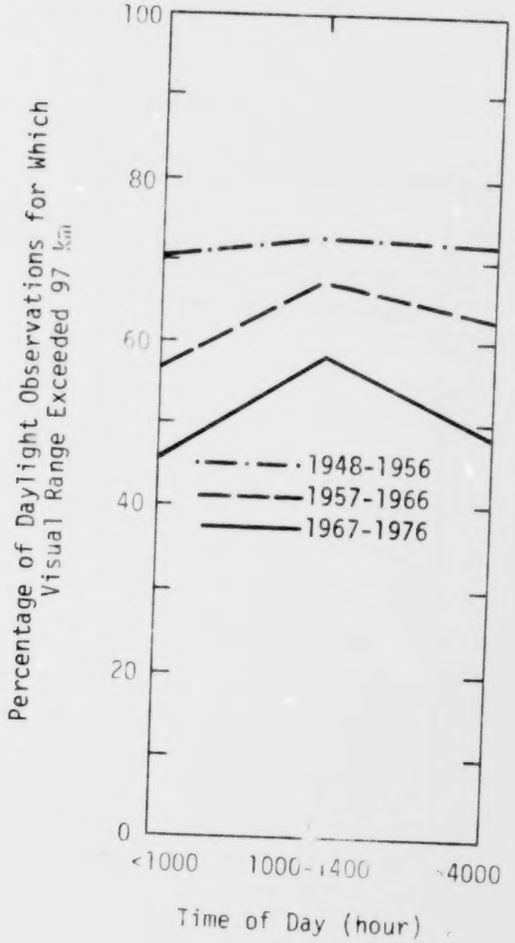

FIGURE A-152. VARIATION IN VISUAL RANGE AS A FUNCTION OF TIME OF DAY AT GREAT FALLS, MONTANA, 1948-1976

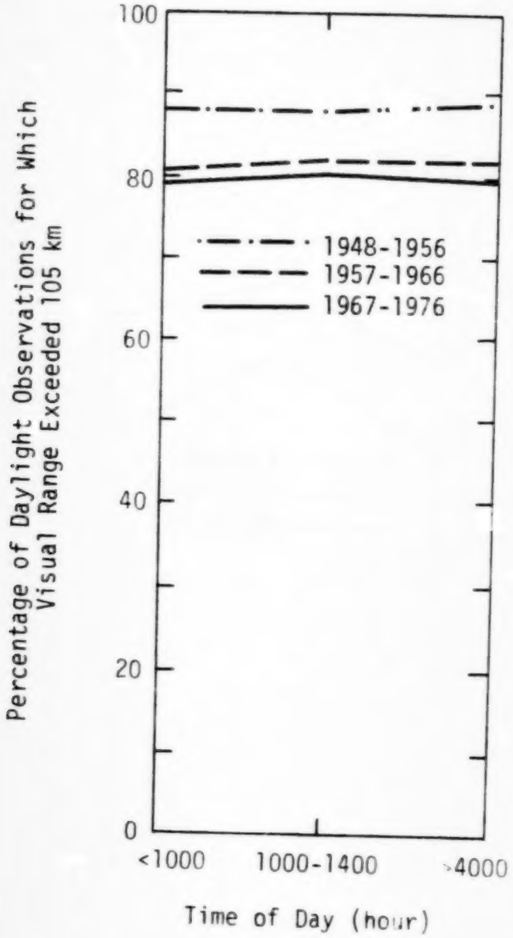

FIGURE A-153. VARIATION IN VISUAL RANGE AS A FUNCTION OF TIME OF DAY AT PRESCOTT, ARIZONA, 1948-1976

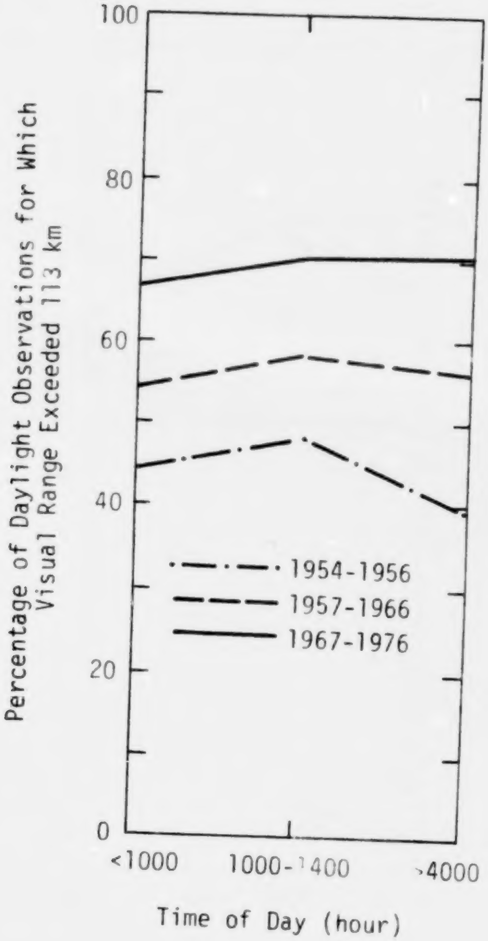

FIGURE A-154. VARIATION IN VISUAL RANGE AS A FUNCTION OF TIME OF DAY AT PUEBLO, COLORADO, 1954-1976

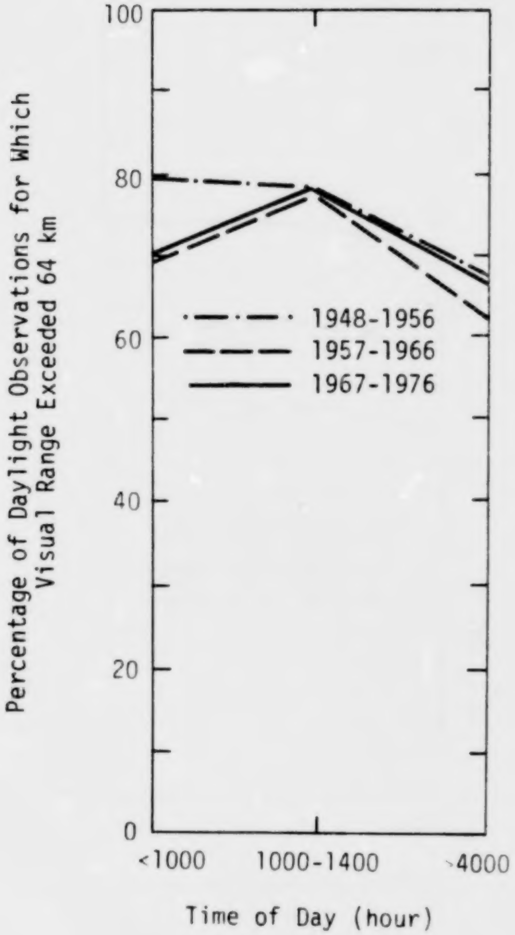

FIGURE A-155. VARIATION OF VISUAL RANGE AS A FUNCTION OF TIME OF DAY AT ROCK SPRINGS, WYOMING, 1948-1976

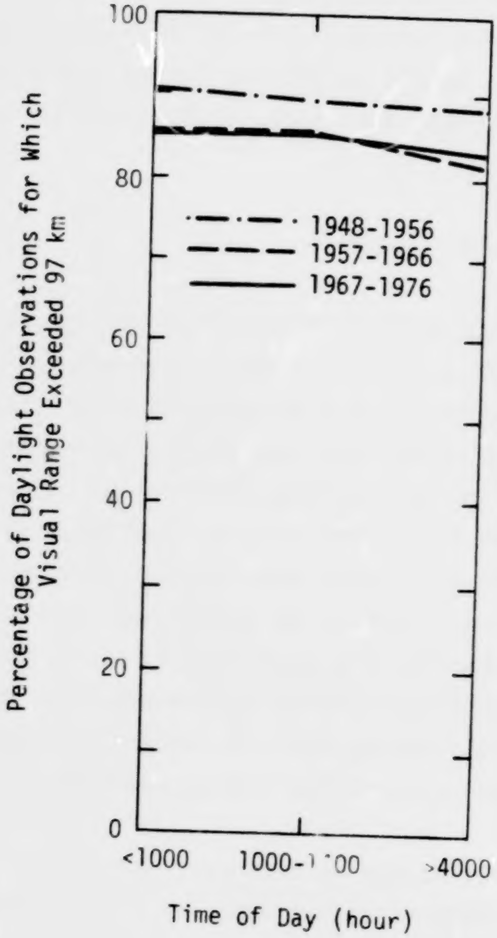

FIGURE A-156. VARIATION IN VISUAL RANGE AS A FUNCTION OF TIME OF DAY AT WINSLOW, ARIZONA, 1948-1976 at Salt Lake City and Tucson, suggest that an increasing mixing depth dilutes the aerosol concentration, thereby increasing the visual range. However, at some locations, such as Billings, Cheyenne, Farmington, Great Falls, and Rock Springs, daytime visibility reaches a peak at midday (1000 to 1100 hours). At most locations, however, diurnal variations are small.

14. VARIATION WITH WIND DIRECTION

Figures A-157 through A-174 illustrate the results of the data sorting as a function of the surface wind direction. The purpose of this analysis was to determine whether the sources of the pollutants that cause visibility impairment could be deduced from the variations in frequency distributions of visual range with wind direction at different locations. For example, a reduction in the frequency of occurrence of good visibility with southerly winds might indicate that natural or man-made pollutants emitted south of the given location are responsible for the visibility impairment. However, consideration must also be given to the wind direction dependence of other meteorological parameters that affect visual range, such as relative humidity, before definite conclusions can be drawn about the emission sources that cause visibility degradation.

There are other limitations to data sorting by wind direction. It is recognized that the wind direction at the surface, which was used in this analysis, may not always be the same as the upper-air transport winds, particularly in complex terrain. Also, spatial and temporal changes in wind direction and speed can transport an air parcel from a source to a receptor via a circuitous route. In the future, a more sophisticated (and more costly) analysis could be carried out using trajectory analysis to identify the transport of air parcels from emission sources to receptors with greater accuracy. For example, upper-air winds could be spatially and temporally interpolated to compute forward trajectories from emission sources (e.g., urban areas, copper smelters, power plants) to receptors or back trajectories from receptors. One could then determine whether

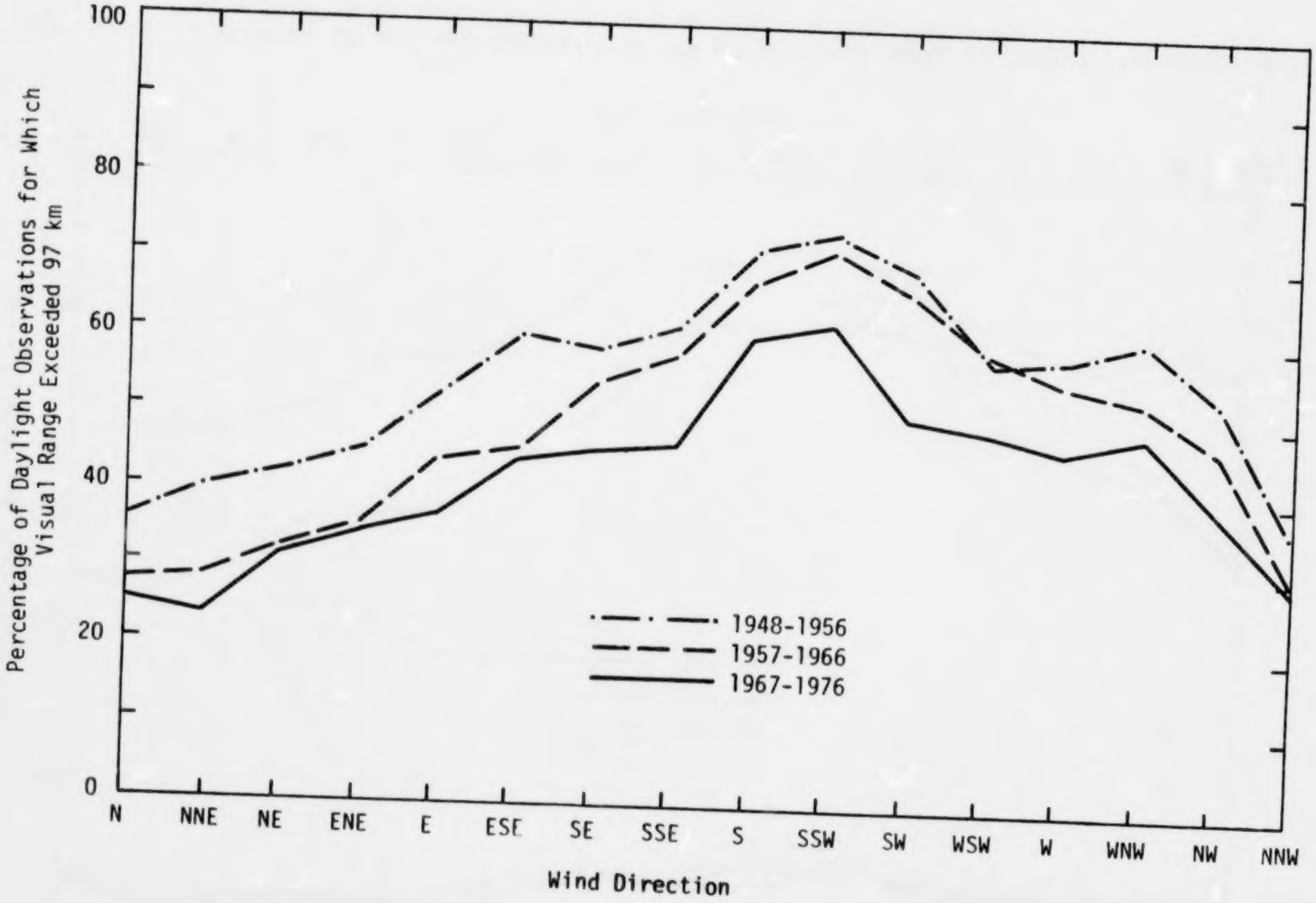

FIGURE A-157. PERCENTAGE OF DAYLIGHT OBSERVATIONS FOR WHICH VISUAL RANGE EXCEEDED 97 km, AS A FUNCTION OF WIND DIRECTION, AT DENVER, COLORADO, 1948-1976

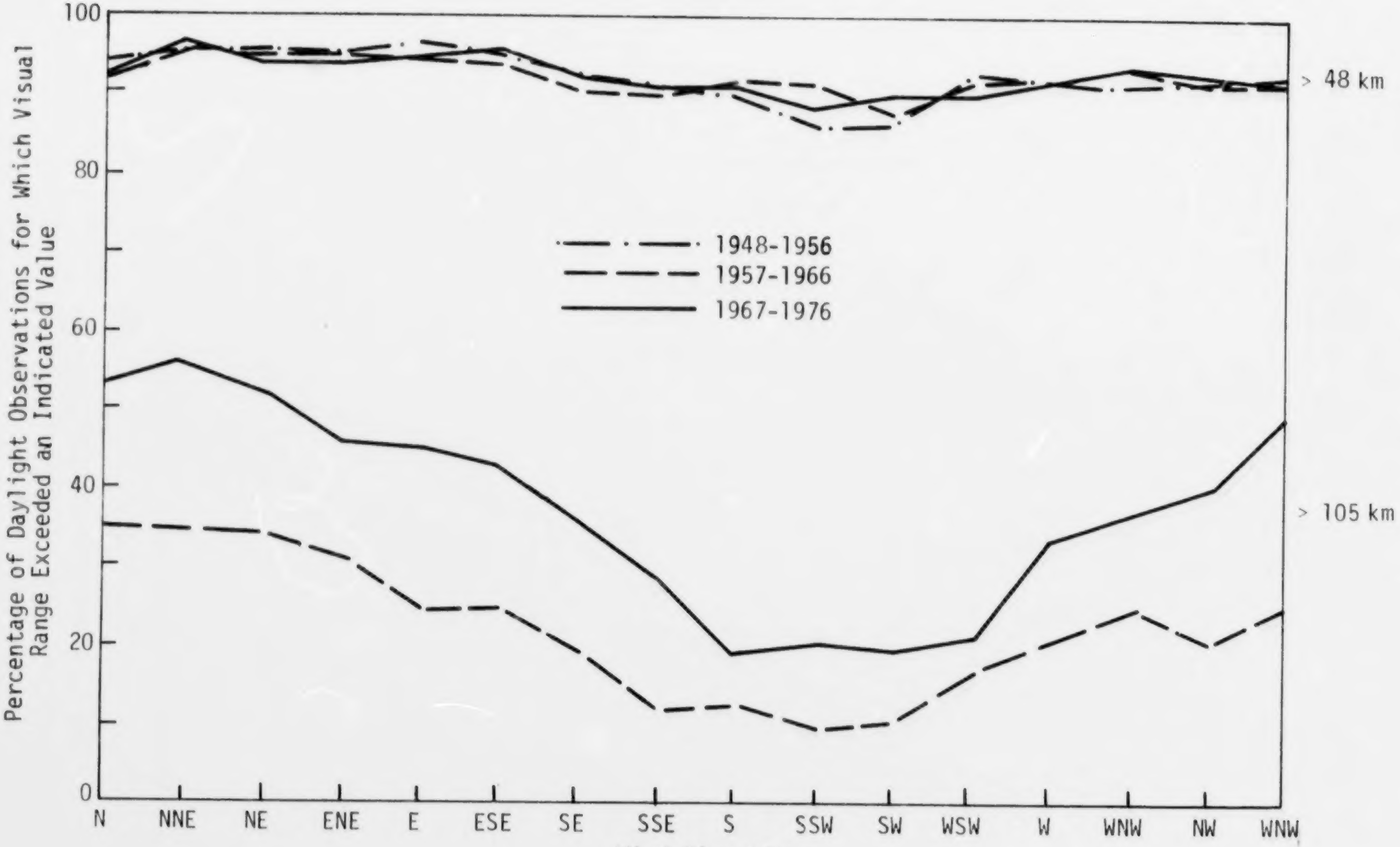

FIGURE A-158. PERCENTAGE OF DAYLIGHT OBSERVATIONS FOR WHICH VISUAL RANGE EXCEEDED AN INDICATED VALUE, AS A FUNCTION OF WIND DIRECTION, AT LAS VEGAS, NEVADA, 1948-1976

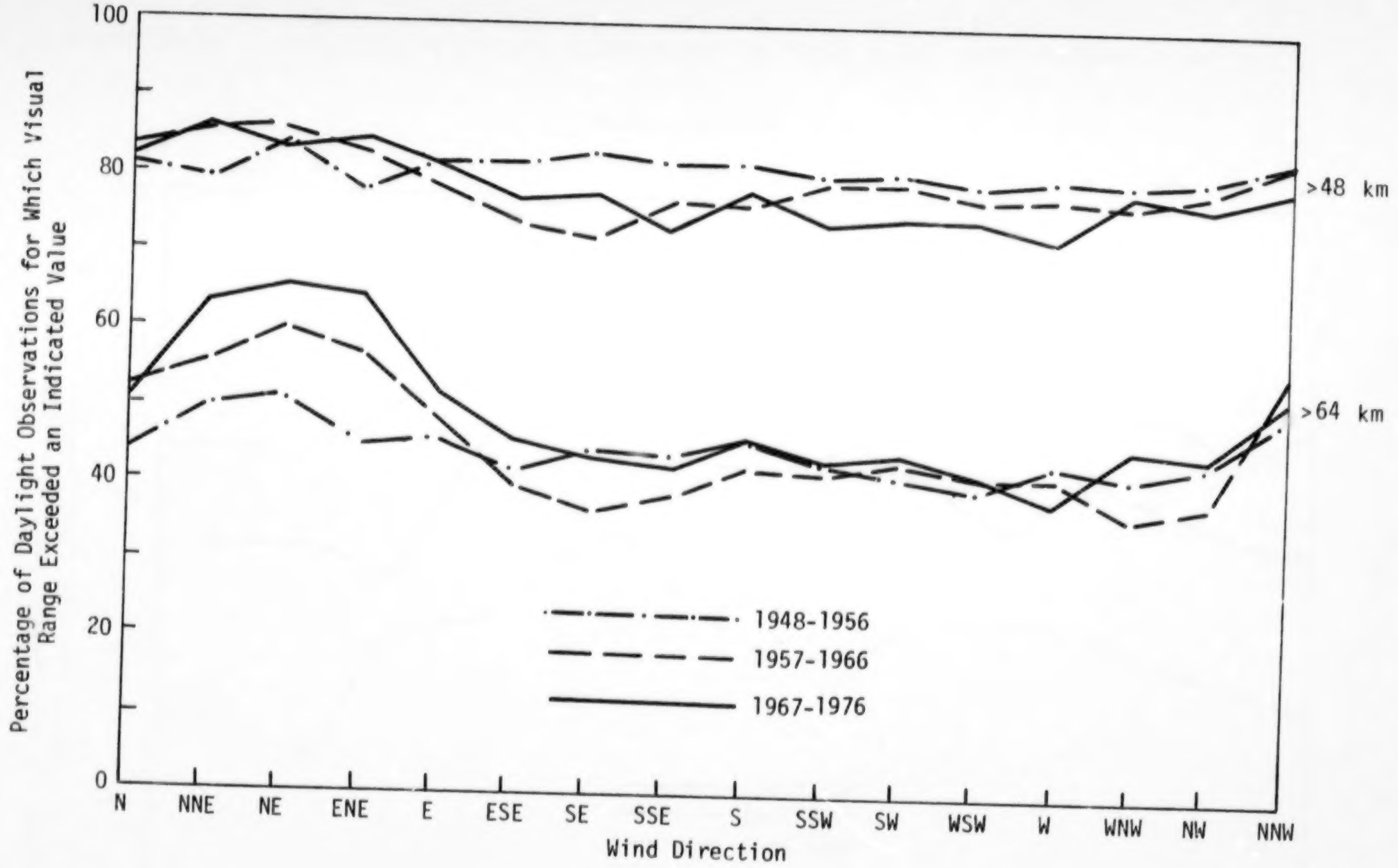

FIGURE A-159. PERCENTAGE OF DAYLIGHT OBSERVATIONS FOR WHICH VISUAL RANGE EXCEEDED AN INDICATED VALUE, AS A FUNCTION OF WIND DIRECTION, AT PHOENIX, ARIZONA, 1948-1976

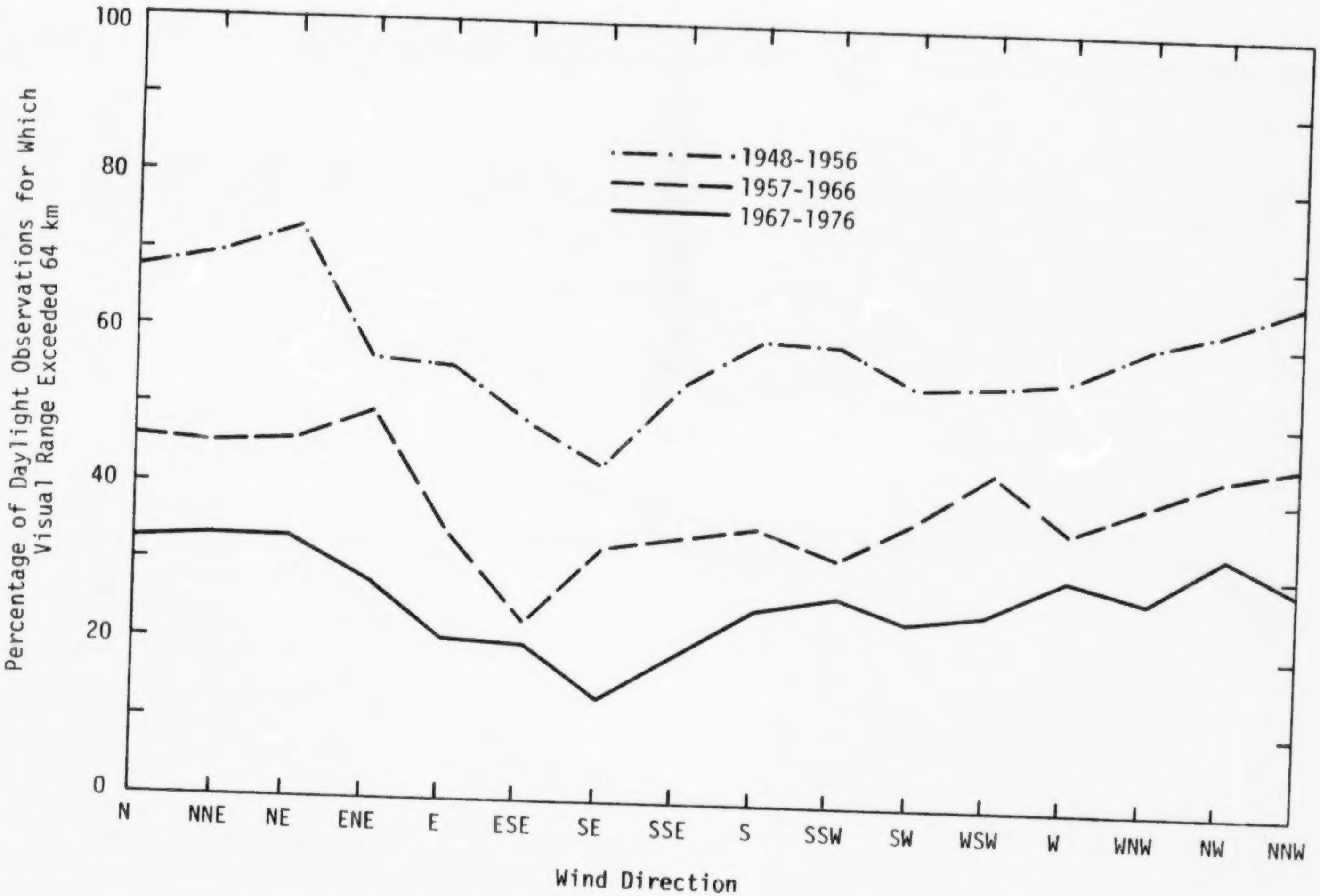

FIGURE A-160. PERCENTAGE OF DAYLIGHT OBSERVATIONS FOR WHICH VISUAL RANGE EXCEEDED 64 km, AS A FUNCTION OF WIND DIRECTION AT SALT LAKE CITY, UTAH, 1948-1976

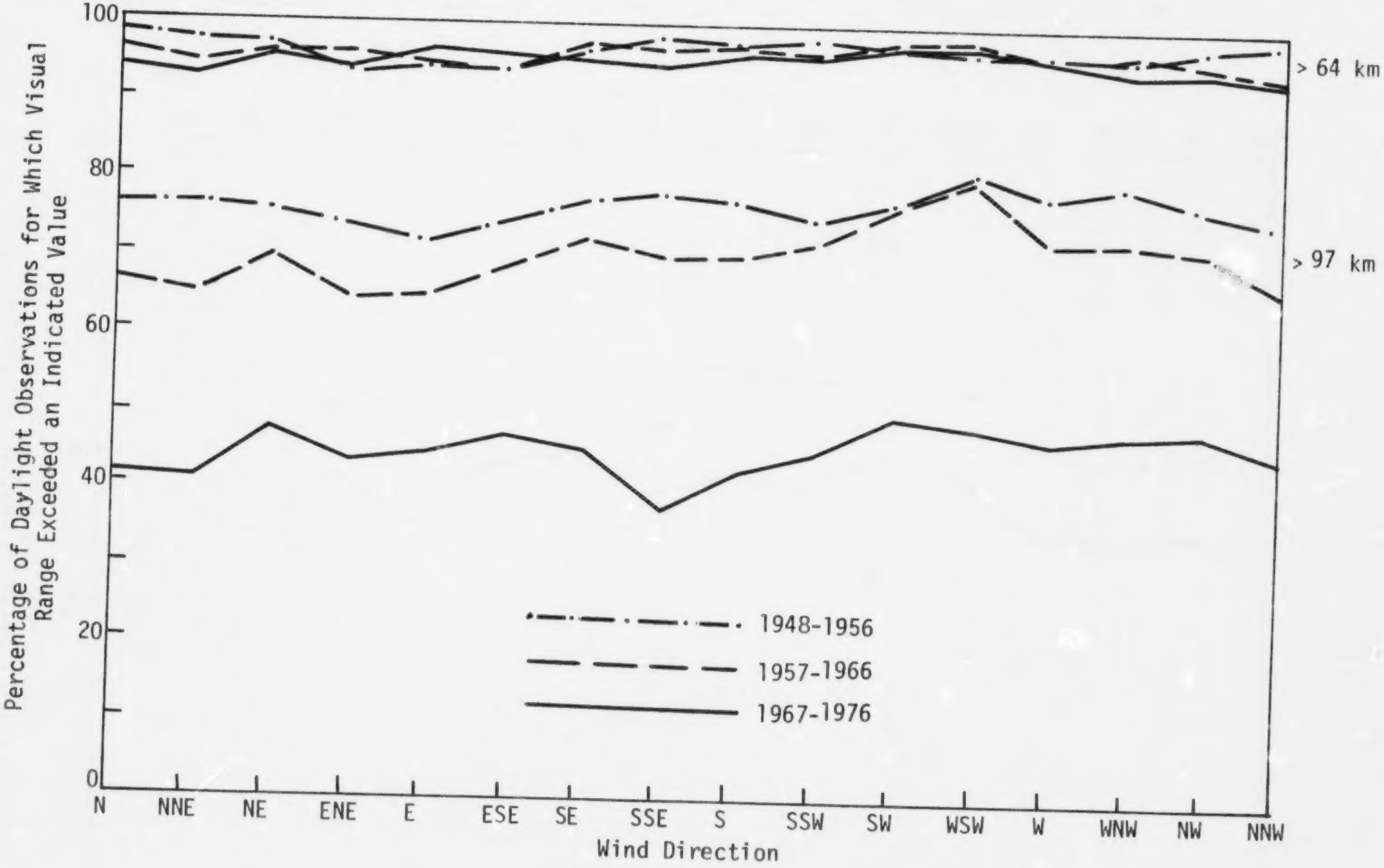

FIGURE A-161. PERCENTAGE OF DAYLIGHT OBSERVATIONS FOR WHICH VISUAL RANGE EXCEEDED AN INDICATED VALUE AS A FUNCTION OF WIND DIRECTION, AT TUCSON, ARIZONA, 1948-1976

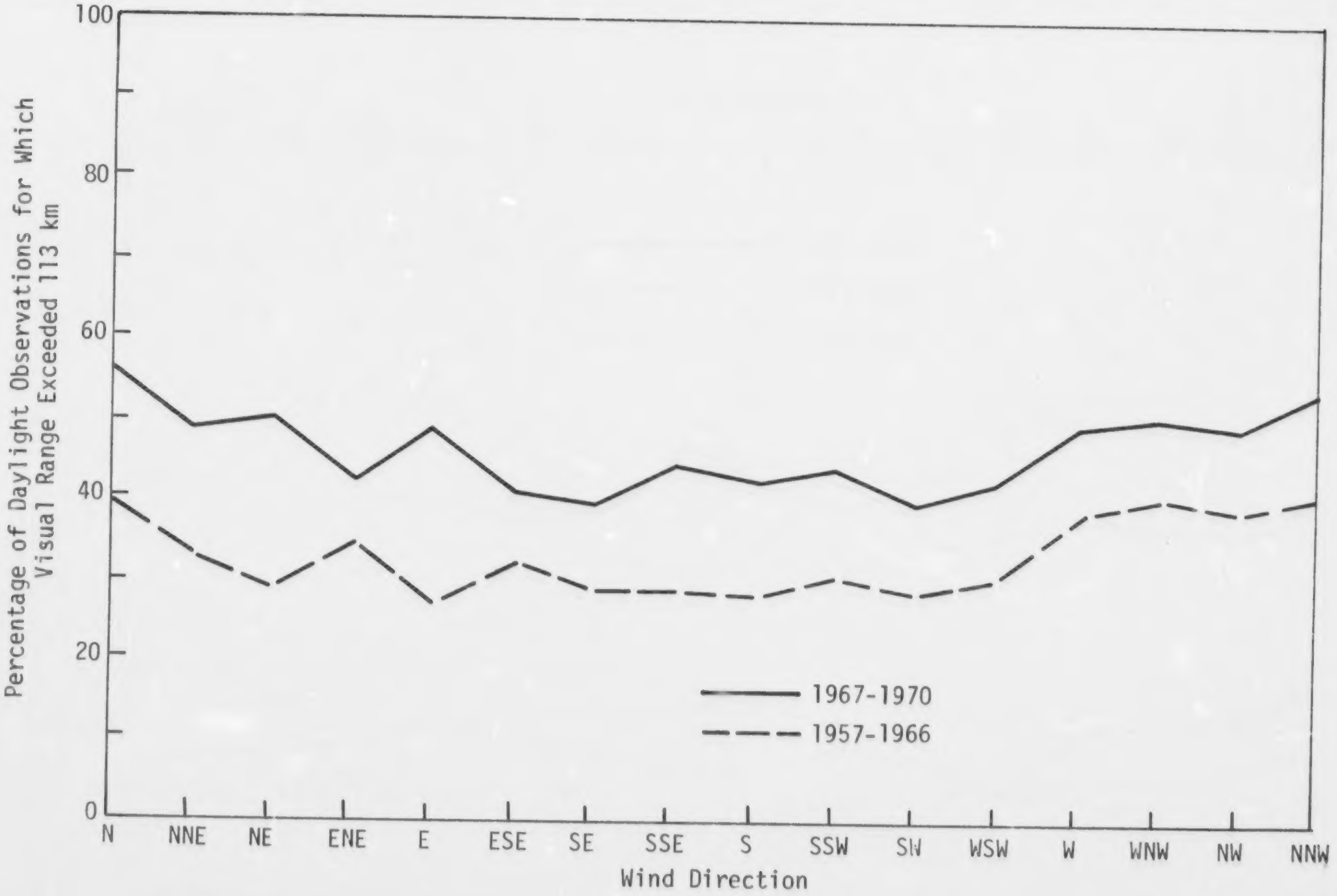

FIGURE A-162. PERCENTAGE OF DAYLIGHT OBSERVATIONS FOR WHICH VISUAL RANGE EXCEEDED 113 km AS A FUNCTION OF WIND DIRECTION, AT ALAMOGORDO, NEW MEXICO, 1957-1970

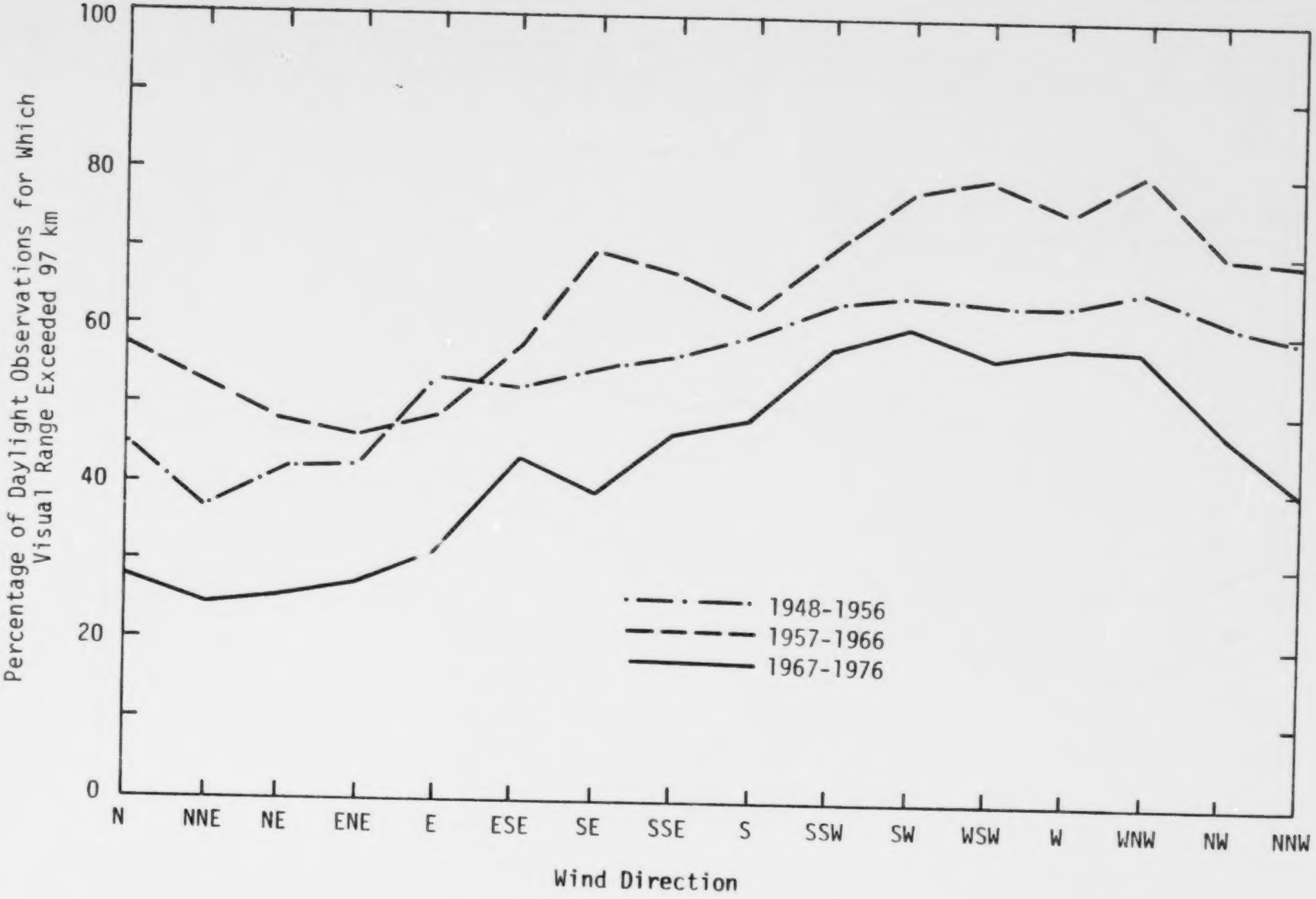

FIGURE A-163. PERCENTAGE OF DAYLIGHT OBSERVATIONS FOR WHICH VISUAL RANGE EXCEEDED 97 km, AS A FUNCTION OF WIND DIRECTION, AT BILLINGS, MONTANA, 1948-1976

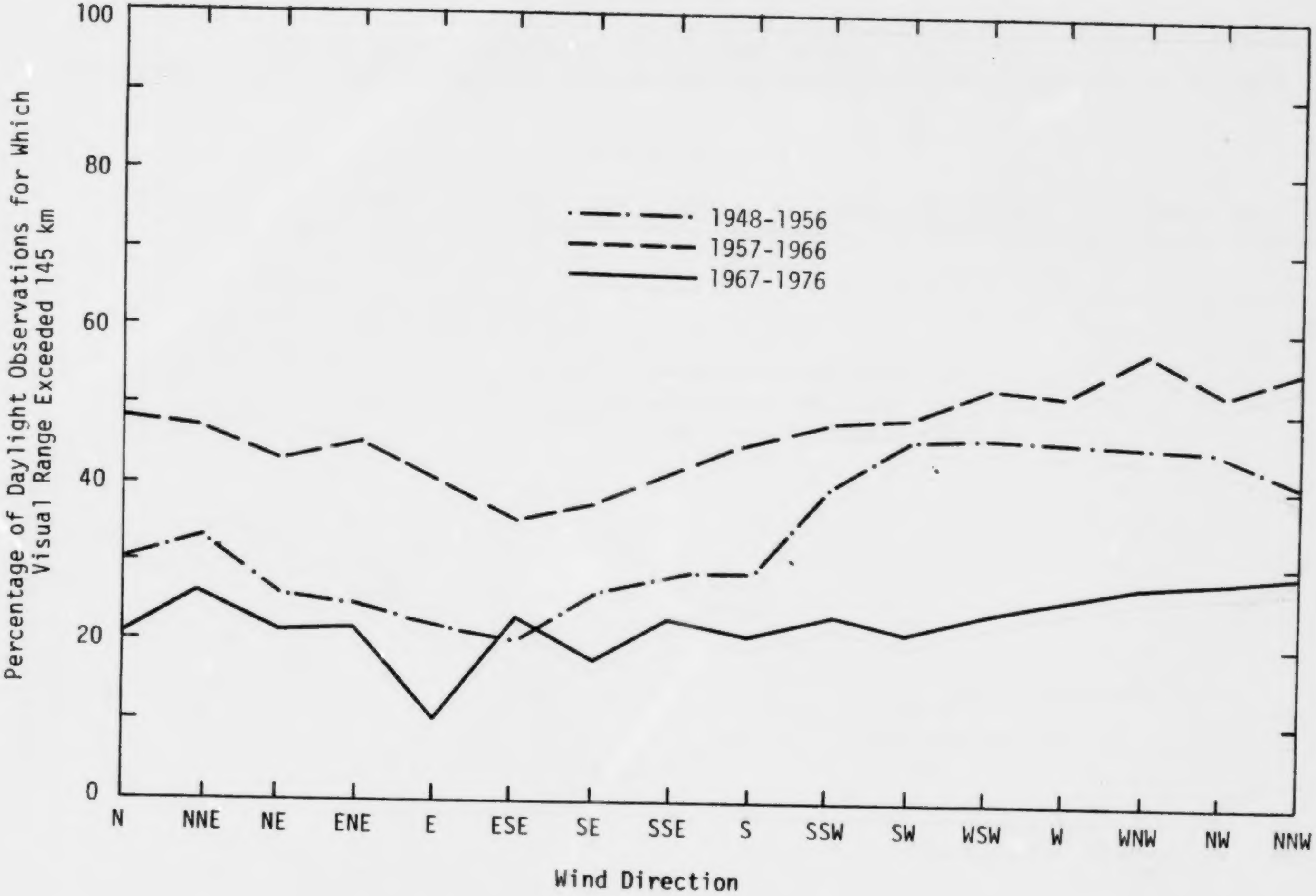

FIGURE A-164. PERCENTAGE OF OBSERVATIONS FOR WHICH VISUAL RANGE EXCEEDED 145 km, AS A FUNCTION OF WIND DIRECTION, AT CHEYENNE, WYOMING, 1948-1976

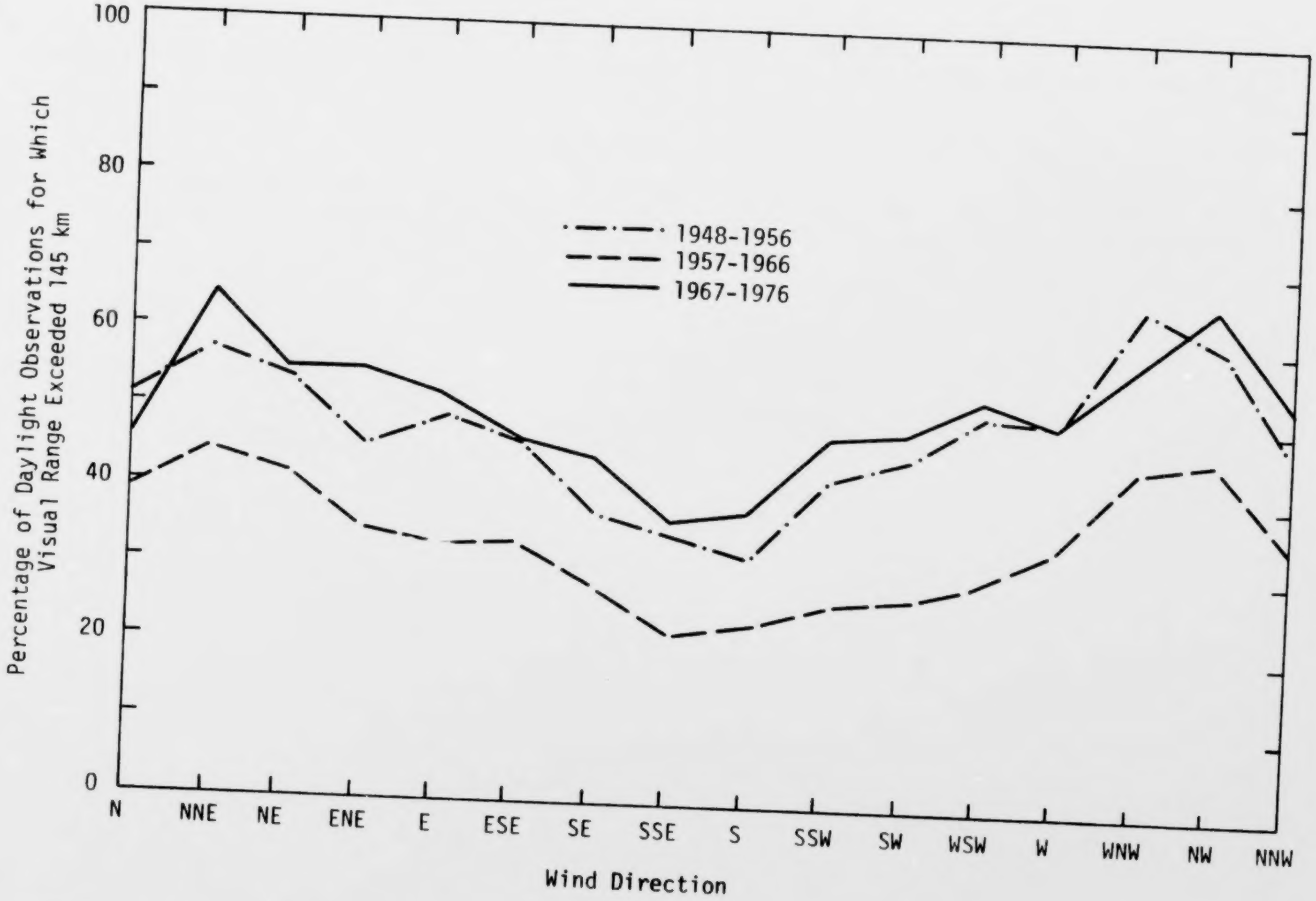

FIGURE A-165. PERCENTAGE OF DAYLIGHT OBSERVATIONS FOR WHICH VISUAL RANGE EXCEEDED 145 km, AS A FUNCTION OF WIND DIRECTION, AT COLORADO SPRINGS, COLORADO, 1948-1976

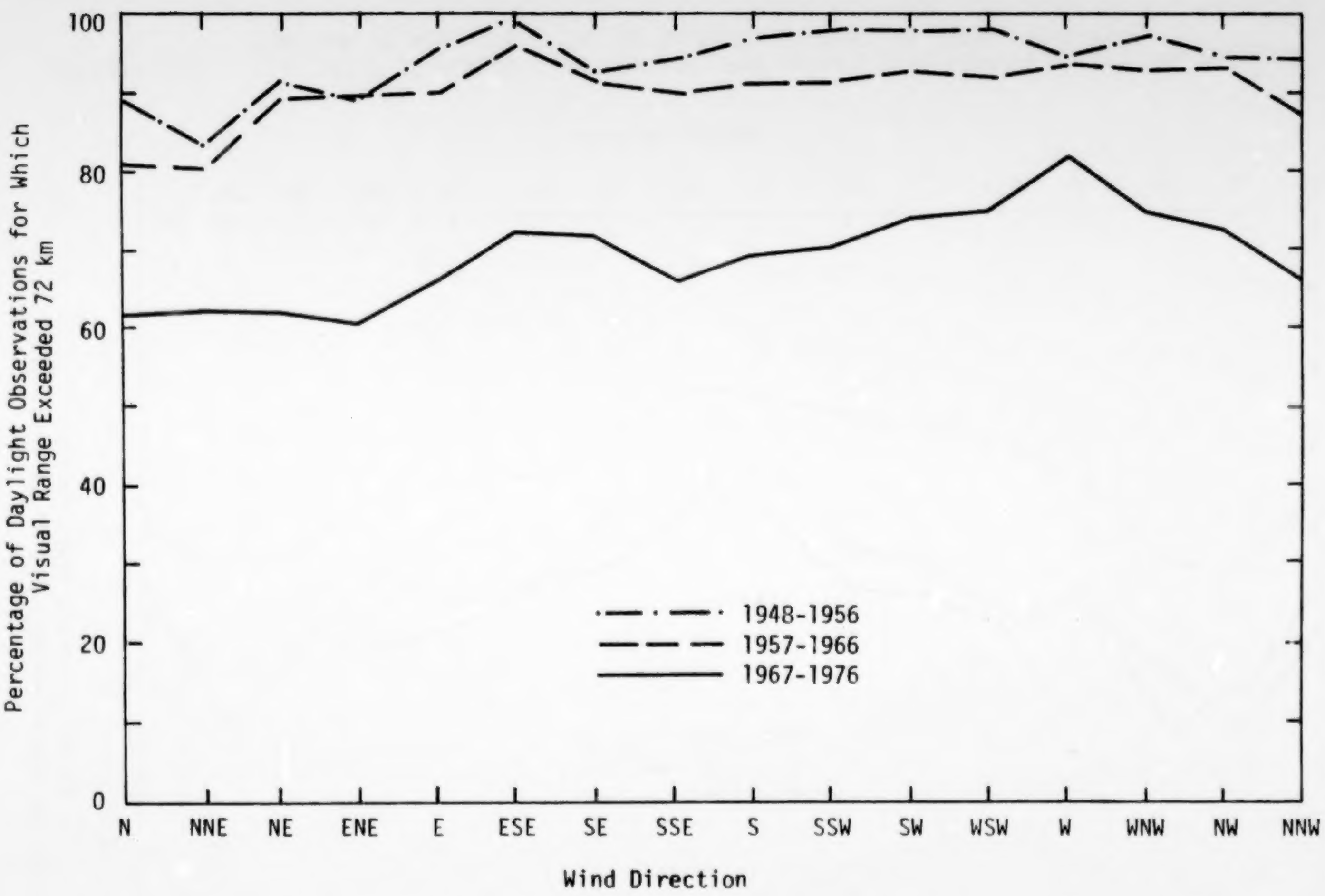

FIGURE A-166. PERCENTAGE OF DAYLIGHT OBSERVATIONS FOR WHICH VISUAL RANGE EXCEEDED 72 km, AS A FUNCTION OF WIND DIRECTION, AT ELY, NEVADA, 1948-1976

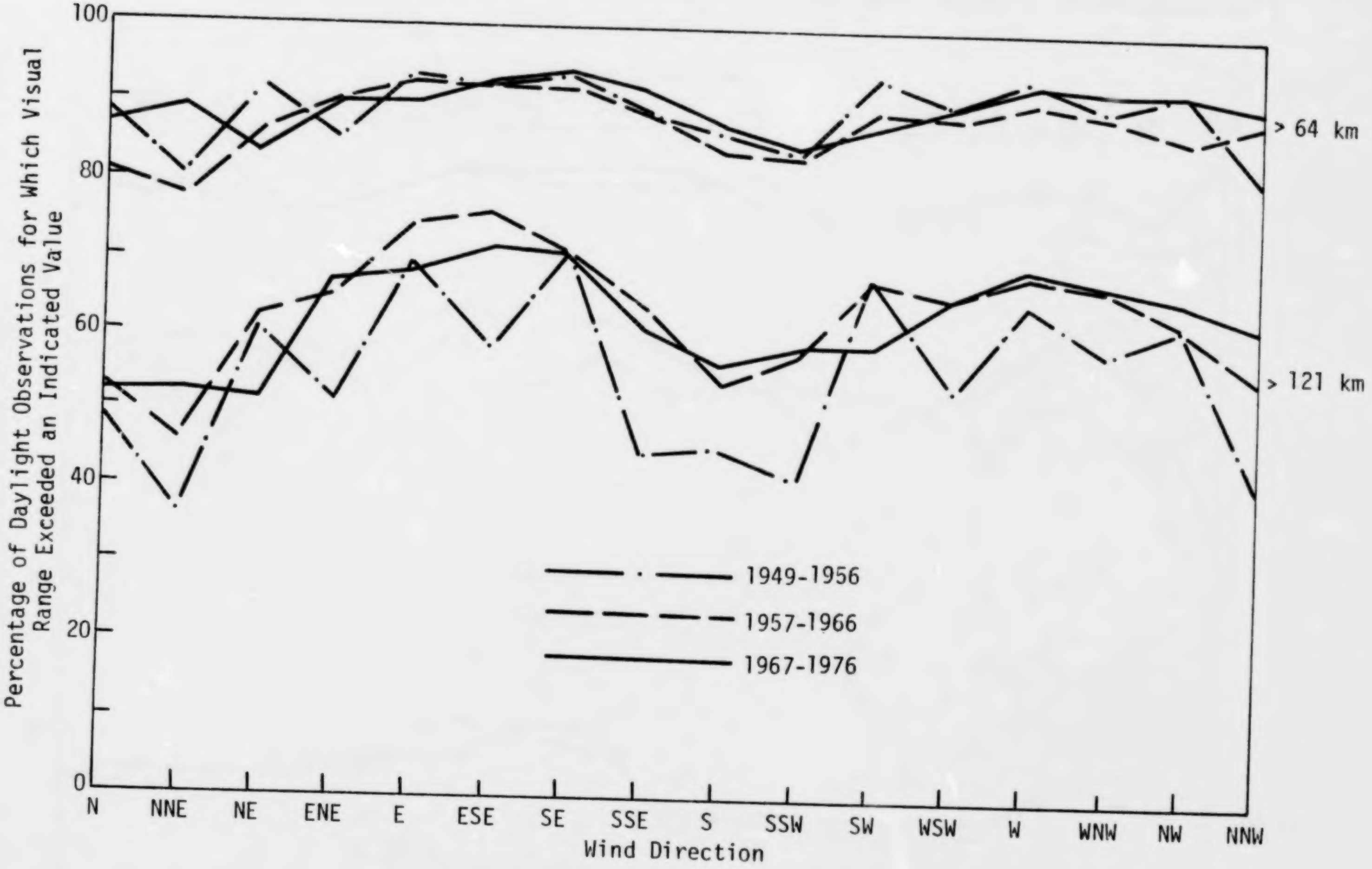

FIGURE A-167. PERCENTAGE OF DAYLIGHT OBSERVATIONS FOR WHICH VISUAL RANGE EXCEEDED AN INDICATED VALUE, AS A FUNCTION OF WIND DIRECTION, AT FARMINGTON, NEW MEXICO, 1949-1976

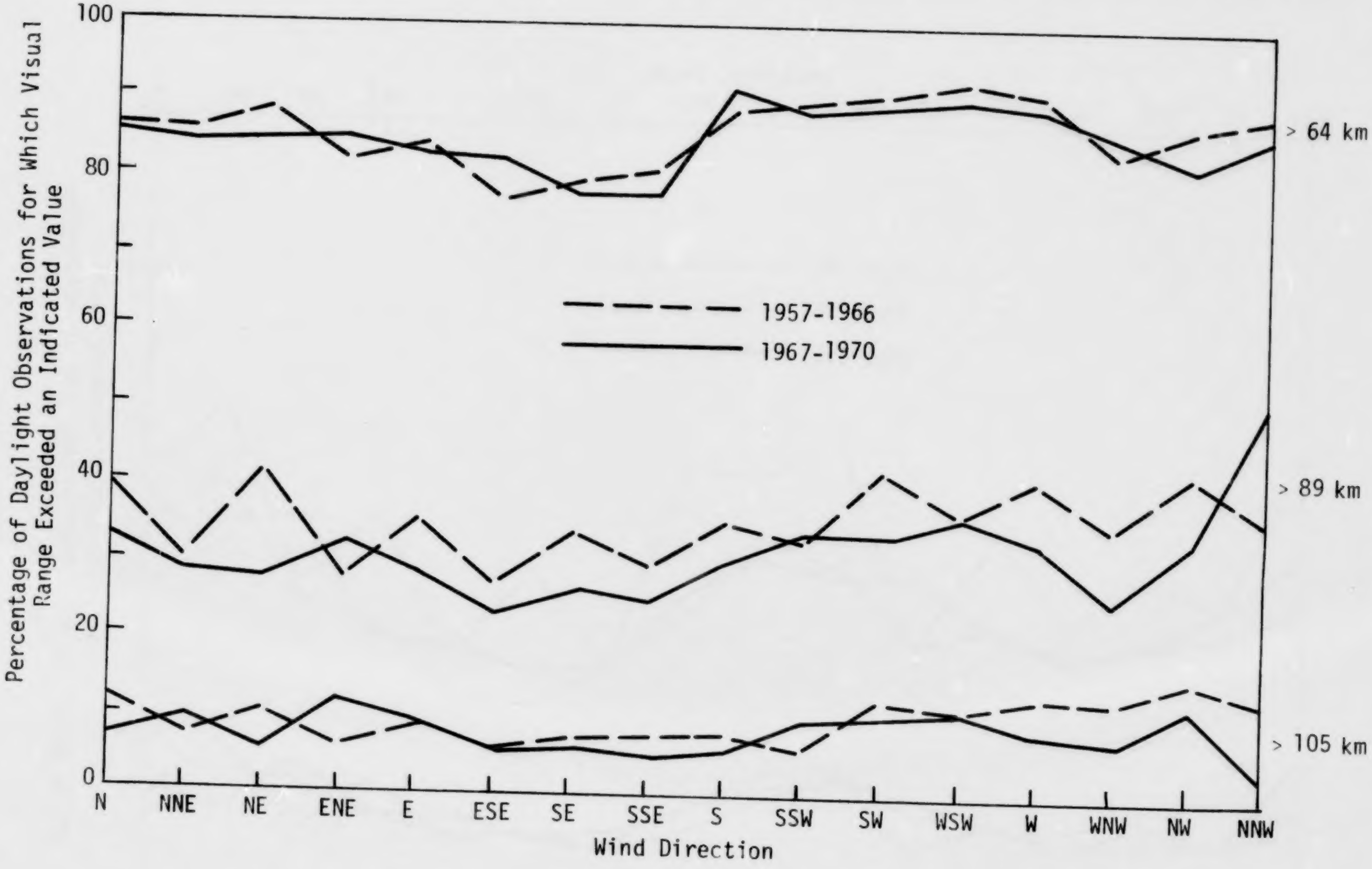

FIGURE A-168. PERCENTAGE OF DAYLIGHT OBSERVATIONS FOR WHICH VISUAL RANGE EXCEEDED AN INDICATED VALUE, AS A FUNCTION OF WIND DIRECTION, AT FT. HUACHUCA, ARIZONA, 1957-1970

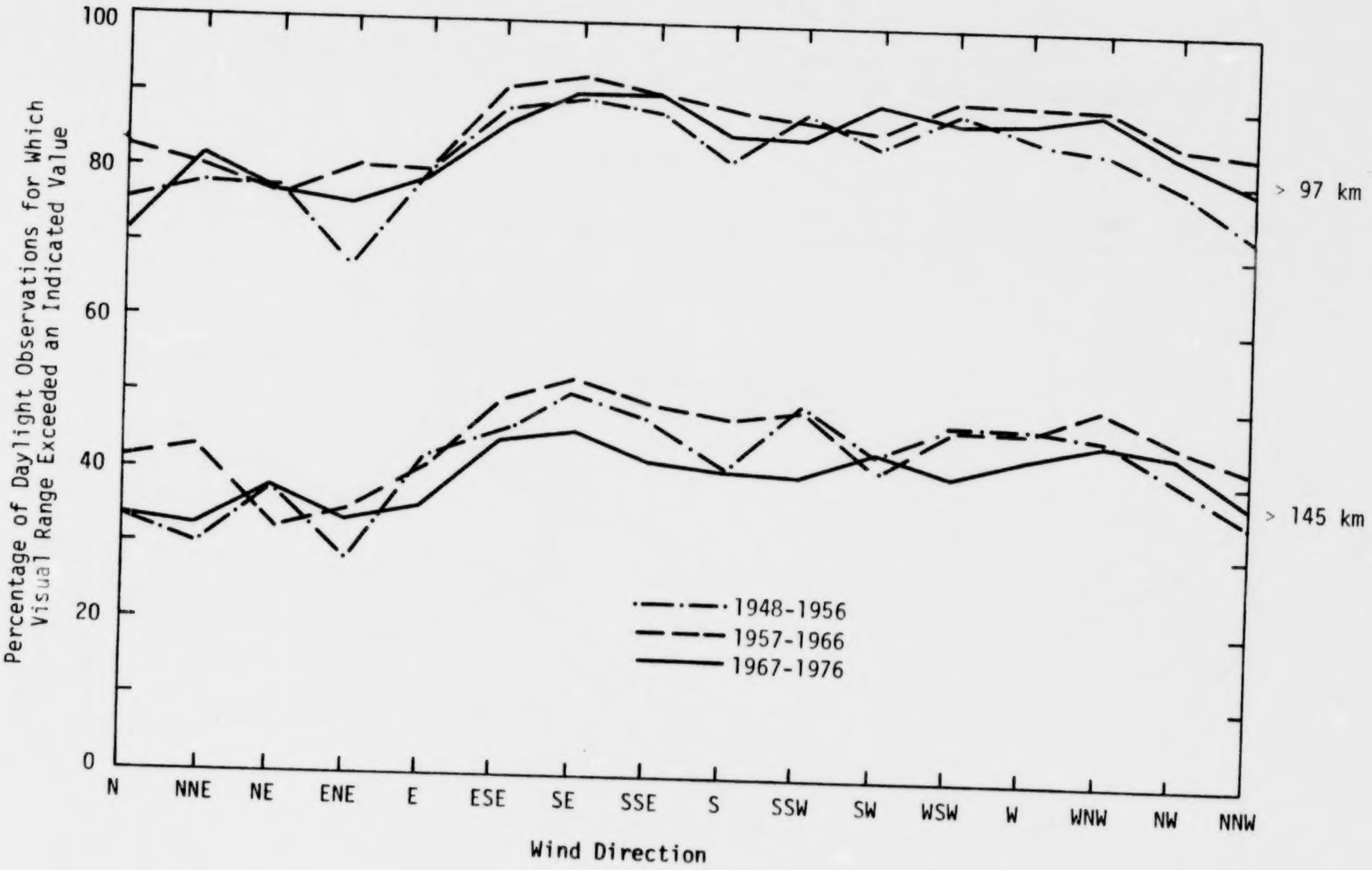

FIGURE A-169. PERCENTAGE OF DAYLIGHT OBSERVATIONS FOR WHICH VISUAL RANGE EXCEEDED AN INDICATED VALUE, AS A FUNCTION OF WIND DIRECTION, AT GRAND JUNCTION, COLORADO, 1948-1976

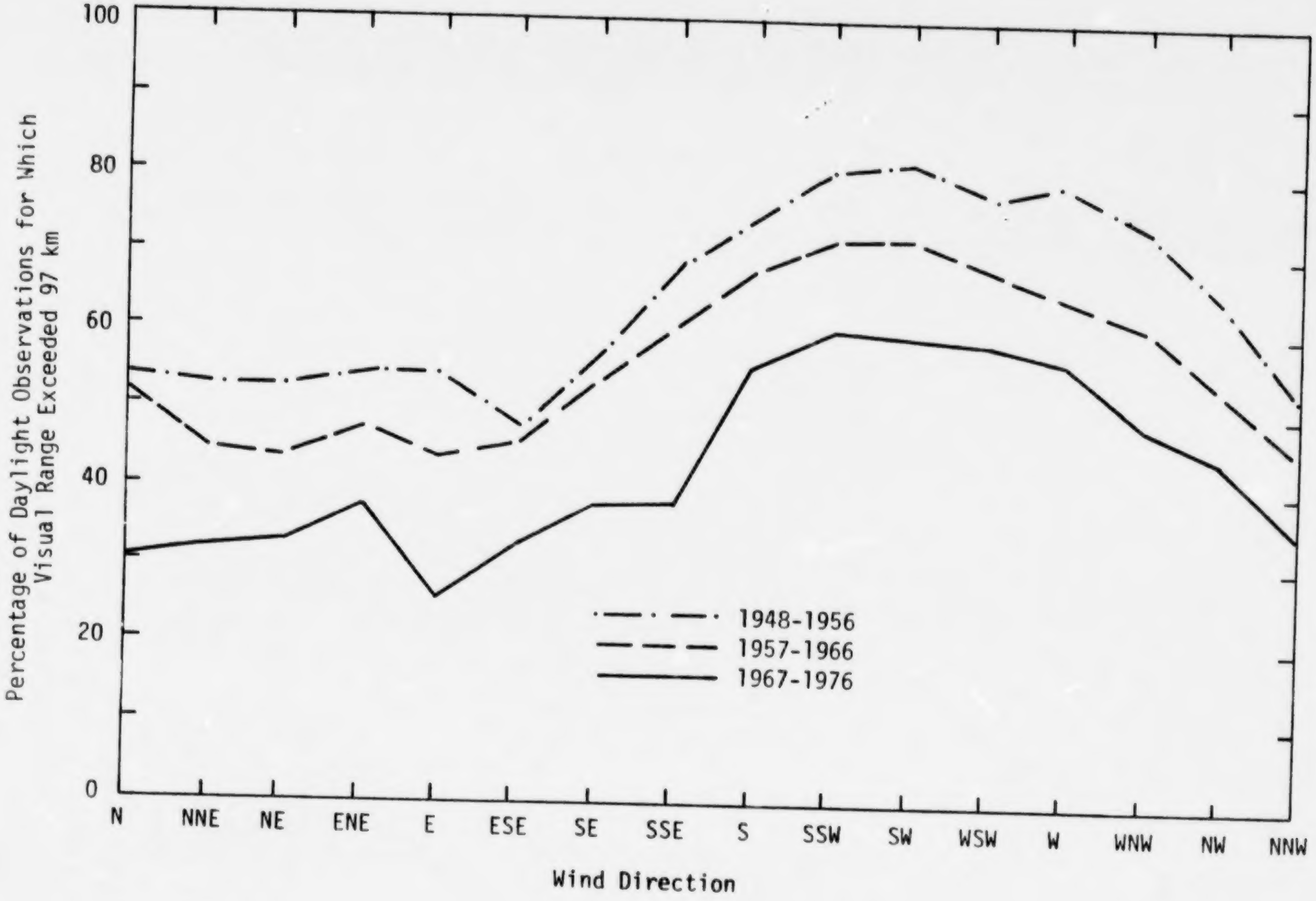

FIGURE A-170. PERCENTAGE OF DAYLIGHT OBSERVATIONS FOR WHICH VISUAL RANGE EXCEEDED 97 km, AS A FUNCTION OF WIND DIRECTION, AT GREAT FALLS, MONTANA, 1948-1976

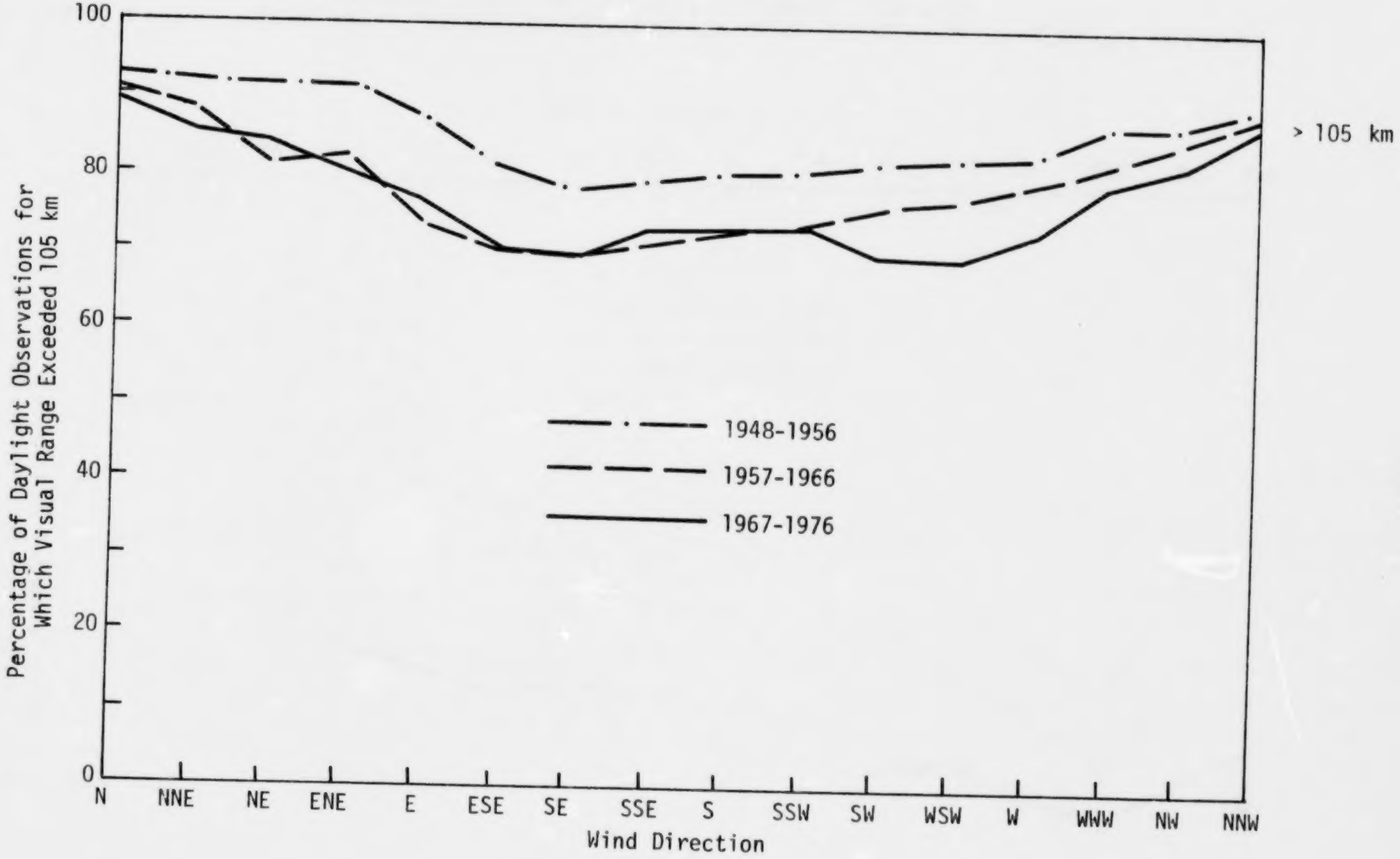

FIGURE A-171. PERCENTAGE OF DAYLIGHT OBSERVATIONS FOR WHICH VISUAL RANGE EXCEEDED AN INDICATED VALUE, AS A FUNCTION OF WIND DIRECTION, AT PRESCOTT, ARIZONA, 1948-1976

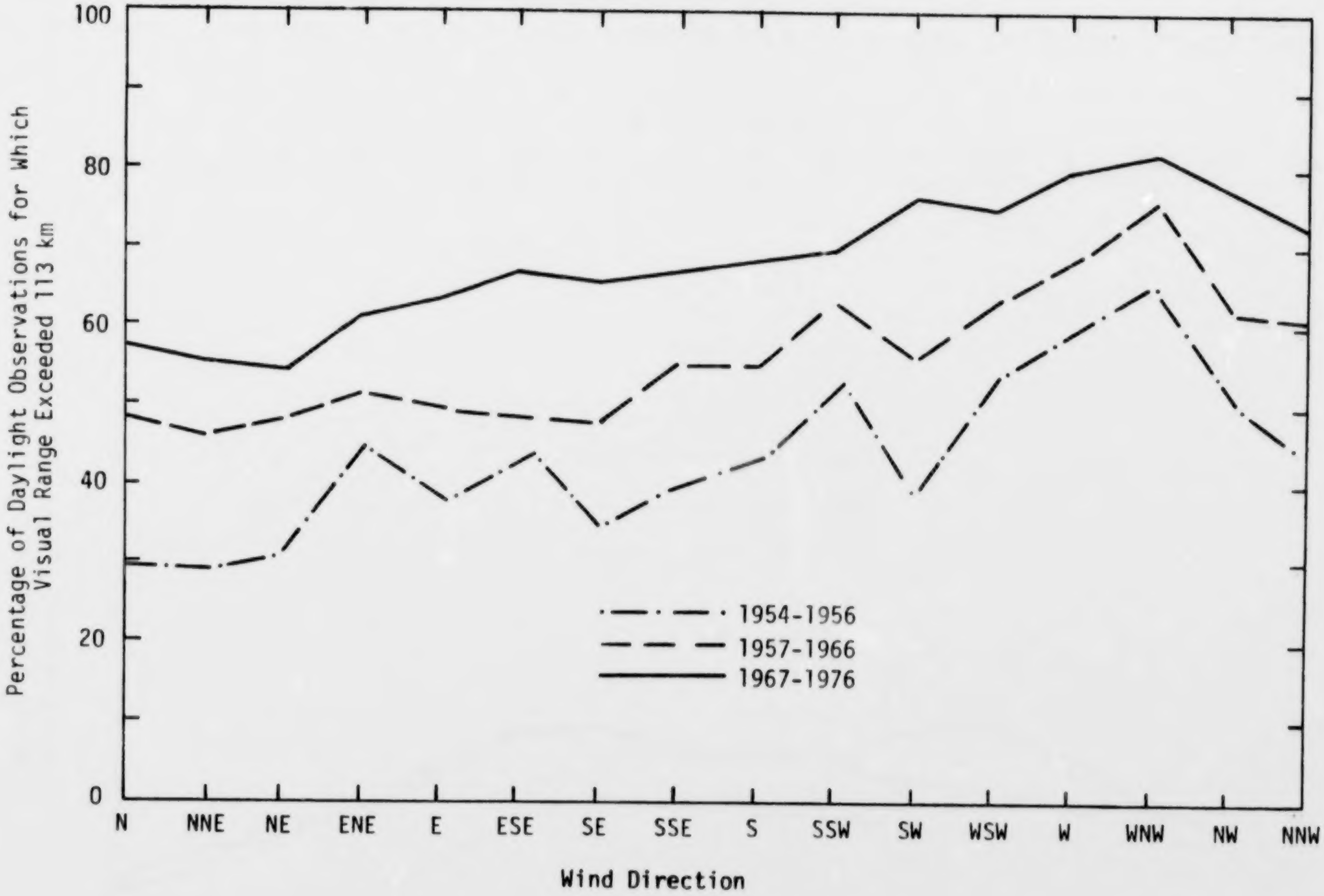

FIGURE A-172. PERCENTAGE OF DAYLIGHT OBSERVATIONS FOR WHICH VISUAL RANGE EXCEEDED 113 km, AS A FUNCTION OF WIND DIRECTION, AT PUEBLO, COLORADO, 1954-1976

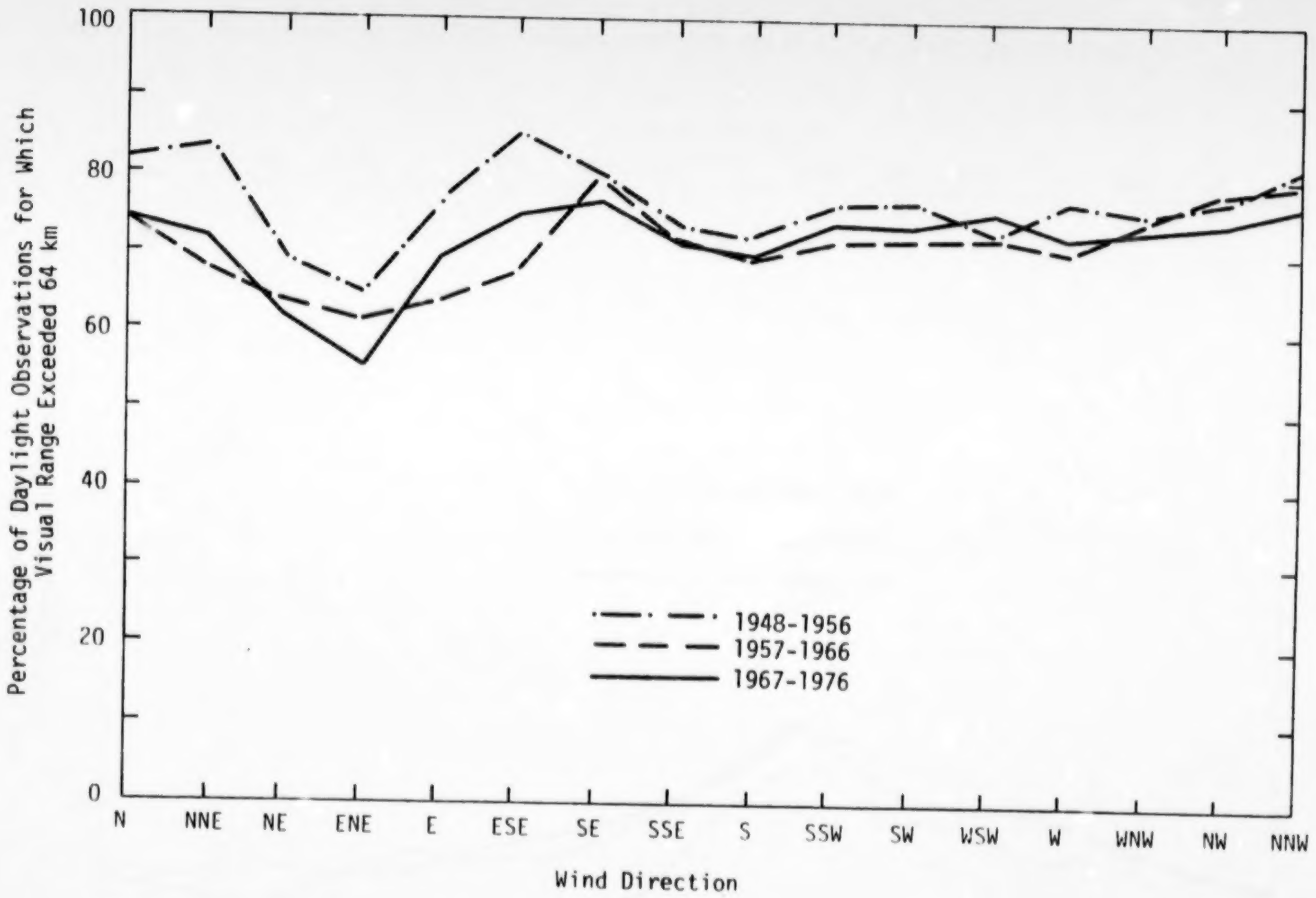

FIGURE A-173. PERCENTAGE OF DAYLIGHT OBSERVATIONS FOR WHICH VISUAL RANGE EXCEEDED 64 km, AS A FUNCTION OF WIND DIRECTION, AT ROCK SPRINGS, WYOMING, 1948-1976

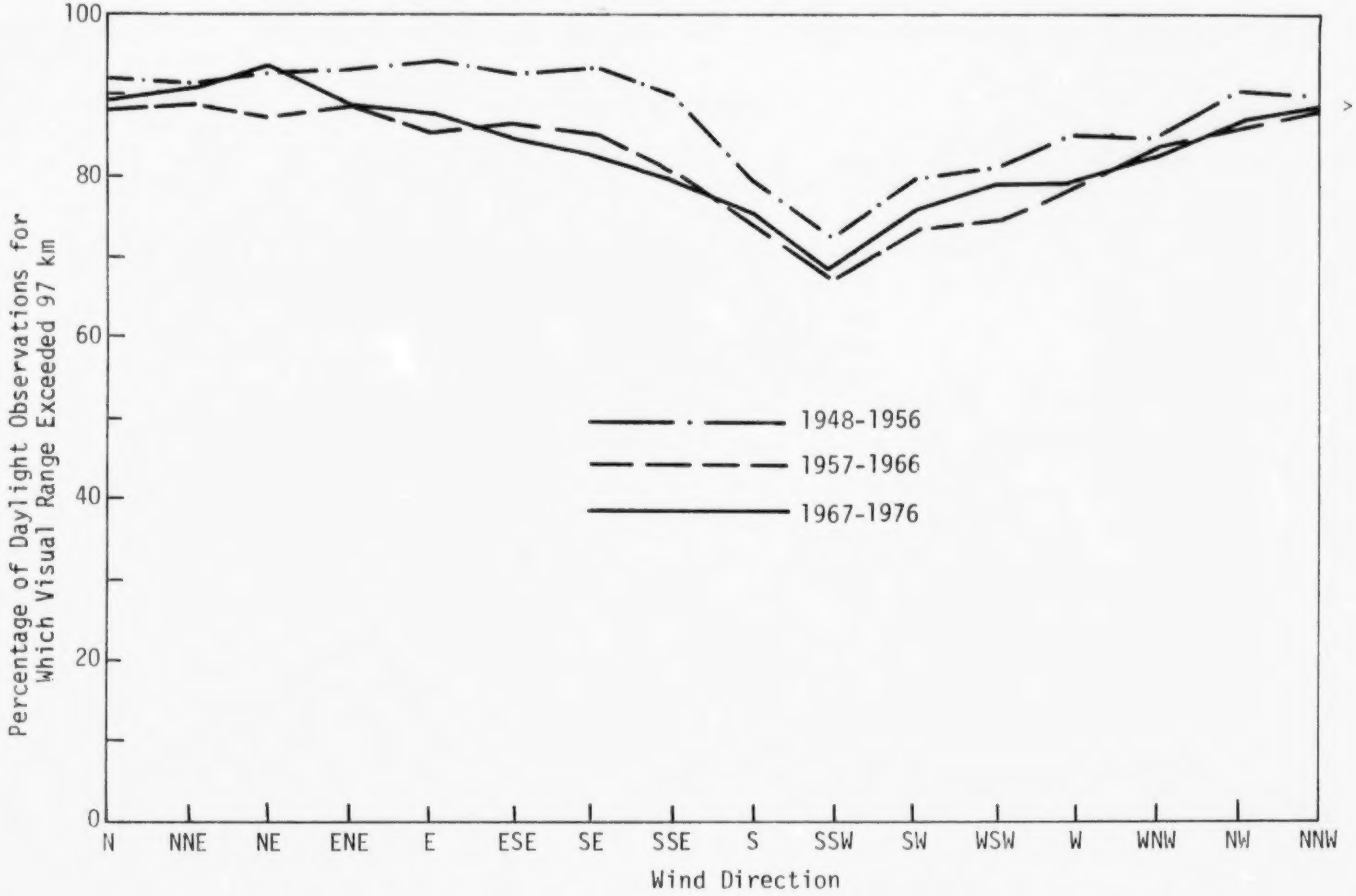

FIGURE A-174. PERCENTAGE OF DAYLIGHT OBSERVATIONS FOR WHICH VISUAL RANGE EXCEEDED 97 km AS A FUNCTION OF WIND DIRECTION, AT WINSLOW, ARIZONA, 1948-1976 the air parcels associated with reduced visual range are indeed transported from pollution sources. Of course, the trajectory analysis technique would also be limited by the accuracy of the interpolation scheme, particularly in rough terrain where channeled winds and drainage winds complicate the flow patterns.

Despite these limitations of the wind direction sorting analysis, in many instances the known spatial distribution of emission sources can explain the variations as a function of wind direction of visual range that were observed at many locations. For example, the dependence of visual range on wind direction in Denver is shown in Figure A-157. Good visibility in Denver is less frequent with northerly flow than with southerly flow. Because higher humidities are slightly more frequent with southerly flow, the wind direction dependence of relative humidity cannot account for the dependence on wind direction. Rather, the dependence appears to result from the transport of urban emissions from Denver toward the distant visibility marker, Pike's Peak, which is 97 km south of Denver. Thus, with northerly flow, aerosol from Denver is transported toward the marker, thereby intersecting a larger portion of the 97 km sight path.

A similar explanation can account for the decreased visibility in Las Vegas that occurs with southerly flow (see Figure A-158). The distant visibility marker in Las Vegas is to the northeast of the city; the entire sight path between the NWS observer and the most distant marker would be within the Las Vegas urban plume only when winds were generally southwesterly.

Figure A-159 shows that in Phoenix a visual range greater than 64 km is much more frequent with northeasterly flow than with any other wind direction. This suggests that air transported from the northeast off the Colorado Plateau is cleaner than air transported from the desert and from the copper smelters to the south.

There are no known emission sources to the east of Billings and Great Falls, Montana, that would account for the decrease in visual range with generally easterly flow that is observed at these locations (see Figures A-163 and A-170). Also, the dependence of relative humidity on wind direction does not account for the variation. However, wind speeds greater than 5 m/sec, which are correlated with increased visual range at these locations, are less frequent with easterly winds. This effect is the only apparent explanation for the dependence of visual range on wind direction in Montana.

In Colorado Springs the distant (145 km) visibility marker, Blanca Peak, is visible less frequently with southerly flow (Figure A-165). Also, good visibility occurs less frequently with winds from the north and north-northwest, perhaps as a result of air pollution transported from Denver. The reduction in visibility in air parcels transported from the south could be due to pollution emitted in the smelter complex of Arizona and New Mexico or in west Texas. The visual range in Pueblo (see Figure A-172), which is 60 km to the south of Colorado Springs, is smallest with winds from the north through northeast. There is no obvious explanation for the occurrence of reduced visibility associated with southerly flow at Colorado Springs but not at Pueblo. At both locations, however, the best visibility is associated with northwesterly winds, which transport relatively clean, dry air from the Rockies.

Figure A-171 shows the dependence of visibility in Prescott on wind direction. Visibility less than 105 km occurred more frequently when winds were from the southeast than when they were northerly. One explanation for this dependence is that southerly winds in Prescott are more often associated with high (exceeding 60 percent) relative humidity conditions. Another possible explanation is that there are fewer pollution sources to the north than to the southeast; thus, the decreased visibility associated with southeasterly flow may be caused by pollutants transported from the cities of Phoenix and Tucson or from the copper smelters in southeastern Arizona. Prescott's visual range during periods of low relative humidity (less than 60 percent) was analyzed as a function of wind direction to attempt to eliminate the effect of relative humidity; the results are reported in subsequent paragraphs.

Another interesting observation is evident in Figure A-171; a significant reduction in visibility, not observed during the earlier two decades, is associated with winds from the southwest to west directions during the last 10-year period. One possible explanation is that winds from the west and southwest carried pollution to Prescott and its farthest visibility marker, Humphreys Peak (north of Flagstaff), from a recently created or expanded emissions source. The Mohave coal-fired power plant, which is located about 200 to 300 km west of the sight path from Prescott to Humphreys Peak, is one such source. Another possibility is an urban plume from Las Vegas or some other metropolitan area.

Figure A-174 shows the dependence of visibility in Winslow on wind direction. Reduced visibility in Winslow appears to be correlated with winds from the south-southwest, indicating that pollution from the Phoenix and Tucson urban areas or from the copper smelters may be causing reduced visibility. Virtually the same dependence on wind direction can be observed for each of the three decades.

It should be noted here that Roberts et al. (1975) reported that the visual range measured in the Petrified Forest (east of Winslow) was shortest when winds were from the southwesterly 90° quadrant, which suggests, as do the Prescott and Winslow data, that emissions from southern Arizona contribute to visibility impairment in remote areas under certain transport wind conditions.

Figure A-167 illustrates a similar dependence of visibility on wind direction in Farmington, New Mexico. Reduced visibility is associated with south-southwesterly winds, suggesting again that pollution transported from southeastern Arizona may be responsible for visibility degradation. Pollution from the Four Corners power plant would be transported toward Farmington and its visibility markers to the north. But no significant change is apparent in the wind direction dependence between the last decade (when the power plant was operating) and the previous two decades (before the plant was in operation). Therefore, it appears that visibility is reduced principally by other pollution sources to the south. Although visibility also seems to be reduced when winds are from the north-northeast, the visibility degradation associated with that wind direction appears to have diminished over the past three decades and, as we point out in subsequent paragraphs, north-northeasterly winds at Farmington are very infrequent.

Substantial evidence indicates that the transport of pollution from southeastern Arizona causes visibility reduction in remote areas in the Southwest. Southeasterly winds are associated with reduced visibility in Prescott, south-southwesterly winds have the same effect in Winslow, and south-southwesterly winds degrade visibility in Farmington. These data were analyzed further to study the influence of copper smelter emissions, in particular, on visual range in remote areas.

As we have noted, the copper smelters in southeastern Arizona and southwestern New Mexico are the dominant SO_2 sources in the Southwest. Before emissions controls were implemented in 1973, the copper smelter complex emitted more than 6000 tons of SO_2 per day. The analysis of the yearly trends in visual range and the dependence of visual range on relative humidity showed a dramatic improvement in visibility, particularly in Phoenix and Tucson, during the period 1973 through 1976, when smelter emissions were reduced to half of what they were in 1973. During the copper strike from July 1967 through March 1968, there were no smelter SO_2 emissions; thus, the strike is a control period that can be used to evaluate the effect of smelter emissions on visibility.

We used the visual range observed during the copper strike for comparison with the visual range in Prescott, Winslow, and Farmington when the smelters were operating. The purpose of this analysis was to determine whether the reduction in visual range associated with certain wind directions at these locations was the result of the transport of smelter emissions.

Figures A-175 through A-177 show the results of this analysis for Prescott, Winslow, and Farmington, respectively. These graphs show the frequencies of occurrence of visual range greater than the indicated value, only for daylight observations during which relative humidity was less than 60 percent, as a function of the surface wind direction. The purpose of eliminating high relative humidity cases was to minimize any influence from the dependence of relative humidity on wind direction.

When the frequencies of good visibility during the copper strike (1967 to 1968) are compared with those during the decade 1967 to 1976, dramatic improvements in visual range are noticeable, particularly for wind directions that would cause the transport of smelter SO_2 emissions directly to the given location (i.e., the southeasterly quadrant for Prescott, the southerly quadrant for Winslow, and the southwesterly quadrant for Farmington). These improvements in visibility were tested for statistical significance by comparing the strike period observations with the remainder of the observations in the decade 1967 to 1976. In Figures A-175 through A-177, the points indicated with closed circles are the wind directions for which significant improvements in visibility were observed during the copper strike period (at the 95 percent confidence level; that is, such differences could have resulted from chance variations with less than 5 percent probability). The most significant increases in visual range during the strike occurred at Farmington, New Mexico, situated more than 400 km to the north and northeast of the smelters in Arizona and New Mexico, rather than at Prescott and Winslow, which are about 250 km north of the smelters. One explanation for the increased visual range at the more distant locations is that if sulfate is formed slowly in the dry desert environment, a greater amount of sulfate would have formed in the time required for an air parcel to be transported 400 km (22 hours with a 5 m/s wind).

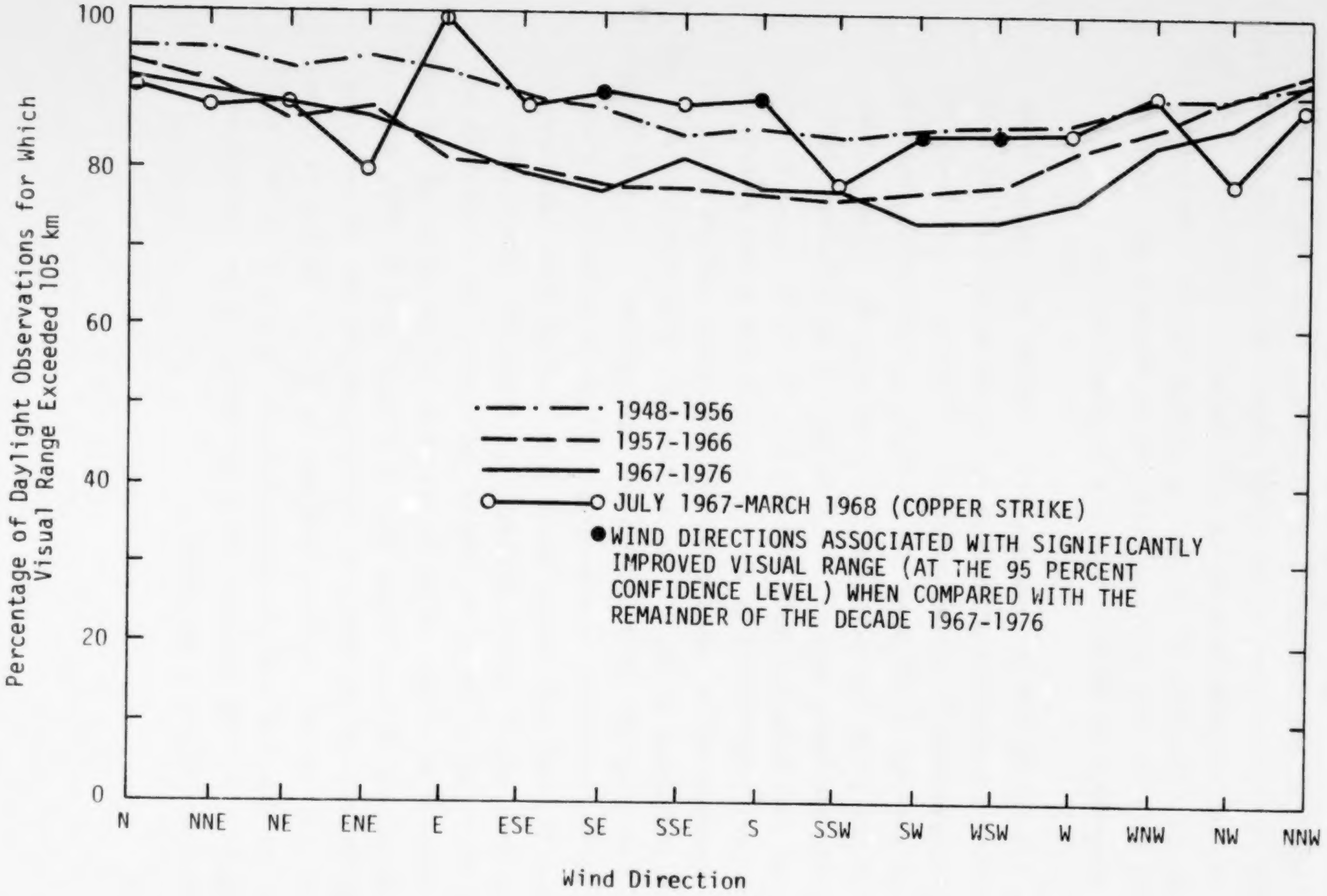

FIGURE A-175. PERCENTAGE OF DAYLIGHT OBSERVATIONS WITH RH < 60 PERCENT FOR WHICH VISUAL RANGE EXCEEDED 105 km, AS A FUNCTION OF WIND DIRECTION, AT PRESCOTT, ARIZONA, 1948-1976

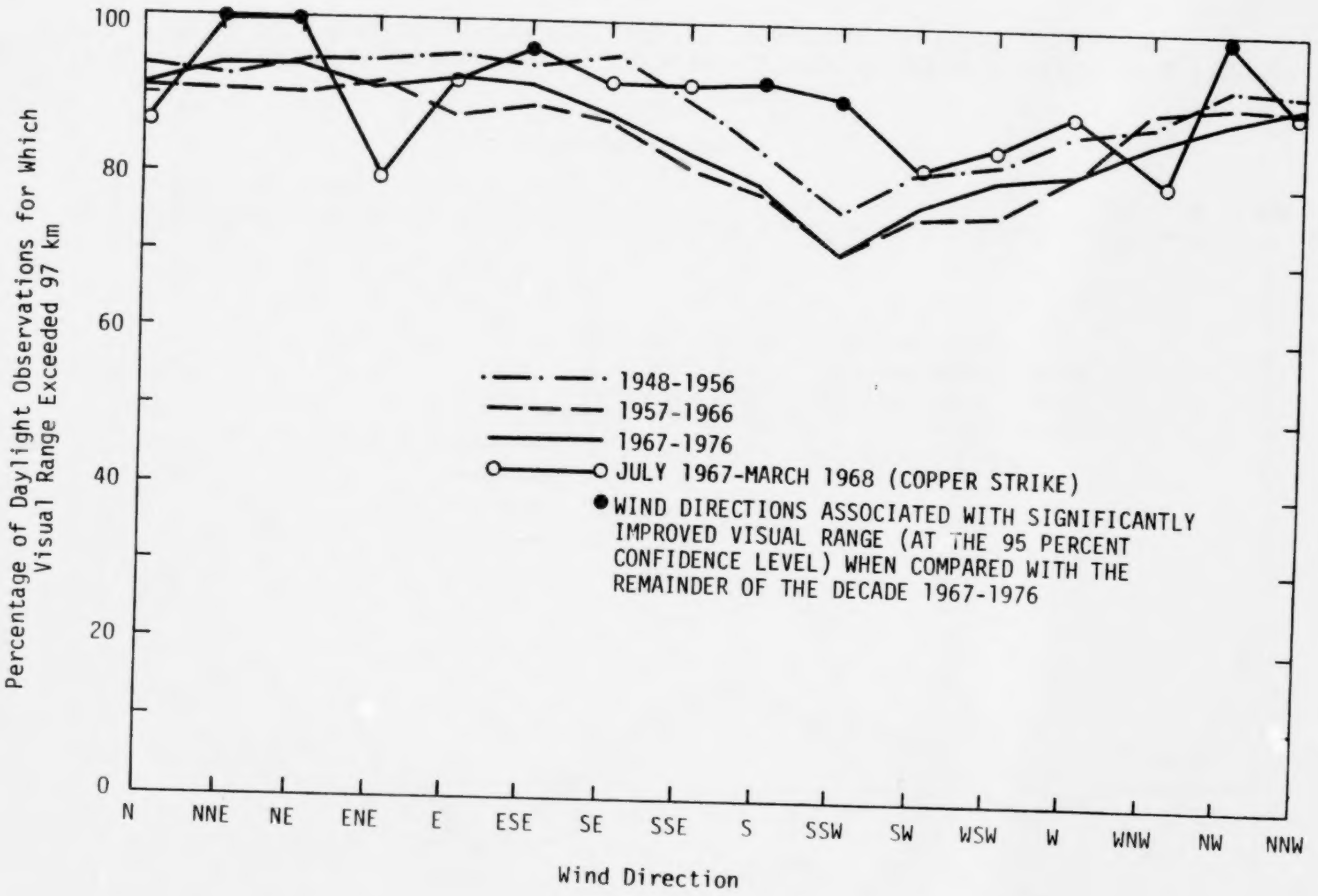

FIGURE A-176. PERCENTAGE OF DAYLIGHT OBSERVATIONS WITH RH < 60 PERCENT FOR WHICH VISUAL RANGE EXCEEDED 97 km, AS A FUNCTION OF WIND DIRECTION, AT WINSLOW, ARIZONA, 1948-1976

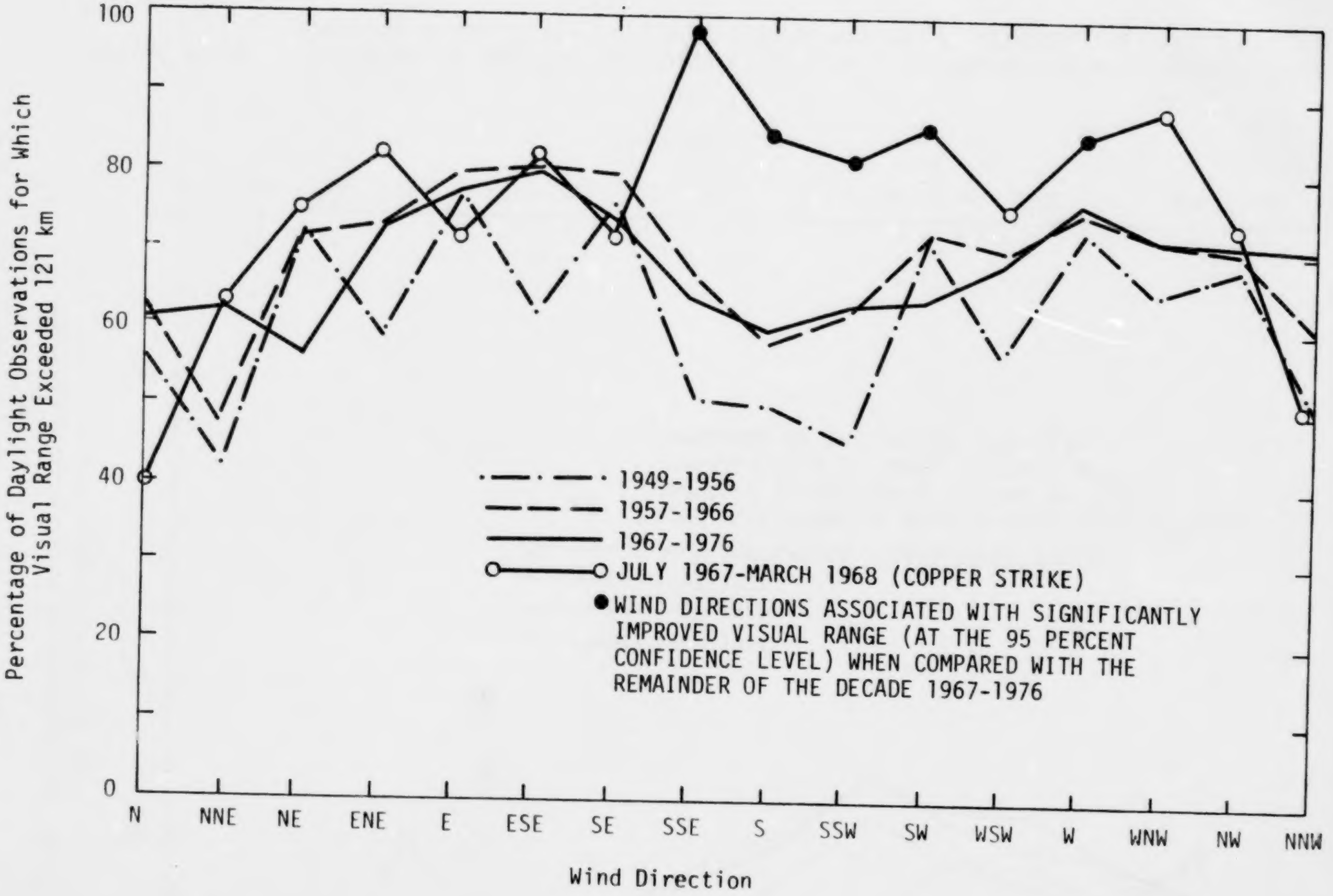

FIGURE A-177. PERCENTAGE OF DAYLIGHT OBSERVATIONS WITH RH < 60 PERCENT FOR WHICH VISUAL RANGE EXCEEDED 121 km, AS A FUNCTION OF WIND DIRECTION, AT FARMINGTON, NEW MEXICO, 1949-1976

APPENDIX B
ATMOSPHERIC OPTICS CALCULATION

APPENDIX B
ATMOSPHERIC OPTICS CALCULATION

Appendix B discusses the connection between prescription of the pollutant concentration from the dispersion and chemistry components of the models and determination and display of visibility degradation. This relationship involves two processes:

- Calculation of the scattering and extinction properties of the aerosol.
- Calculation of radiative transfer and display of the visual impact.

We describe our treatment of these processes in some detail to make clear the assumptions and simplifications behind them.

1. METHODS OF CALCULATING SCATTERING AND EXTINCTION COEFFICIENTS

This section discusses the various possibilities for determining the scattering and absorption properties of air pollutants. Because the process is straightforward for gases (NO_2), we concentrate on particulates. First, we review the empirical relationships that have been developed through correlation techniques among visual range, scattering coefficient, and aerosol mass (more importantly, sulfate mass). Then we discuss the ways in which the scattering and absorption properties of aerosols can be computed given certain information about their size and composition. We show how some calculations of scattering properties compare with the empirically determined values. Finally, we discuss the way in which the coefficients are calculated in the visibility models.

a. Empirical Correlations Among Visual Range, Scattering Coefficient, and Aerosol Mass

1) Visual Range and Scattering Coefficient

Middleton (1952) presented Koschmieder's result that for a uniform medium the visual range (how far one can see a black object against the background sky) is linearly related to the scattering coefficient of the atmospheric aerosol. Samuels, Twiss, and Wong (1973) found that in three California cities the correlation between visual range and scattering coefficient measured at a point was very good ($r \sim 0.8$). In that study the location of the scattering coefficient measuring device and the observer who determined the visual range were not the same, indicating that the spatial inhomogeneities in the cities were not large enough to invalidate the use of a point measurement of the scattering coefficient to compute a spatially integrated quantity (visual range). Several studies (Cass, 1976; Trijonis and Yuan, 1977) used visual range data to compute an effective scattering coefficient based on the Koschmieder relationship.

2) Scattering Coefficient and Mass

Several studies have attempted to correlate observed scattering coefficients (or observed visual range and computed scattering coefficients) with total aerosol mass (Charlson, Ahlquist, and Horvath, 1968; Noll, Mueller, and Imada, 1968; Ettinger and Royer, 1972; Hidy et al., 1975; White and Roberts, 1975; Samuels, Twiss, and Wong, 1973; Grosjean and Friedlander, 1975; Cass, 1976). Initially, Charlson, Ahlquist, and Horvath reported a high correlation ($r = 0.81$); however, more recent measurements have shown a lower correlation (Cass found $r = 0.4$). Samuels, Twiss, and Wong, White and Roberts, and Cass all stated that the total aerosol mass was a poor indicator of the scattering coefficient. Their findings indicate that the size distribution of the aerosols is not the same at all times. As we show later, the scattering-to-mass ratio is dependent on particle size. Thus, if the aerosol is composed of two components, one that has a large scattering-to-mass ratio and another that has a small ratio, the two could combine in such a way that variations in the scattering coefficient would not show up in the amount of aerosol mass.

An analysis of the dynamics of the aerosol size distribution [see, for example, Friedlander (1977)] for typical primary distributions would indicate that in general one can expect secondary aerosols (those formed by gas-to-particle conversion) to scatter more light than an equivalent mass of the sum of primary size distributions, simply because more of their mass accumulates in a size range where light scattering is very efficient. It makes sense, therefore, to attempt a multivariate analysis to correlate various components of the aerosol (specifically, the principal secondary components and the remaining aerosol) with the light scattering.

3) Scattering Coefficient and Sulfate Mass

During the ACHEX study in Los Angeles, it was possible to correlate the observed scattering to the various components of the submicron particles. White and Roberts (1975) reported a high correlation of scattering coefficients with sulfate and nitrate mass. Cass (1976) also reported such a correlation using visibility measurements in Los Angeles. Finally, Trijonis and Yuan (1977) reported correlations in the Southwest. Table B-1, taken from Trijonis and Yuan (1978), summarizes sulfate extinction per mass coefficient at various locations. Similar tables were presented by Charlson (1978, private communication) and Trijonis and Yuan (1977). We have modified the entries for the nonlinear regression coefficients so that both regressions are of the form:

$$b_{scat} = a + b_1 \frac{\text{TSP - Sulfate - Nitrate}}{\left(1 - \frac{RH}{100}\right)} + b_2 \frac{\text{Sulfate}}{\left(1 - \frac{RH}{100}\right)} + b_3 \frac{\text{Nitrate}}{\left(1 - \frac{RH}{100}\right)} \quad .$$

The similarity of the Los Angeles results and the results of the Southwest visibility study are striking at low relative humidities.

TABLE B-1. ESTIMATES OF EXTINCTION COEFFICIENTS PER UNIT MASS

Source	Location	Extinction Coefficients $[(10^4 m^{-1}/(\mu g/m^3)]$		
		Sulfates	Nitrates	Remainder of TSP
Regression models (Trijonis and Yuan, 1978)	Chicago	0.04	(0.00)	(0.000)
		0.03*	(0.00*)	(0.000*)
	Newark	(0.02)	(0.00)	0.026
		0.06*	(0.00*)	0.014*
	Cleveland	0.08	(0.00)	(0.000)
		0.07*	(0.00*)	(0.000*)
	Lexington	0.06	(0.00)	(0.000)
		0.06*	(0.04*)	0.019*
	Charlotte	0.11	(0.00)	(0.001)
		0.11*	(0.00*)	(0.000*)
	Columbus	0.12	0.09	(0.000)
		0.13*	(0.06*)	(0.001*)
Regression models (Trijonis and Yuan, 1977)	Salt Lake City	0.04	0.13	0.004
		0.04*	0.10*	0.004*
	Phoenix (county data)	0.04	0.05	(0.000)
	Phoenix (NASN data)	0.03	0.03	(0.000)
Duststorms (Hagen and Woodruff, 1973)	Great Plains	NC	NC	0.001
Regression model (White and Roberts, 1975)	Los Angeles	0.07	0.05	0.015
Regression model (Cass, 1976)	Los Angeles	0.16	(0.00)	0.008
		0.09*	0.05*	(0.004*)
Calculations for a model aerosol of $(NH_4)_2SO_4$ at 70% RH (Waggoner et al., 1976)		0.05-0.10	NC	NC
Regression model (Waggoner et al., 1975)	Southern Sweden	0.05	NC	NC

( ) = not significant at the 95 percent confidence level.
NC = not calculated.
*Based on nonlinear RH regression model, with insertion of average RH.

Source: Trijonis and Yuan (1978).

Although unresolved issues such as the accuracy of the nitrate measurement still exist, it is apparent that the so-called secondary aerosol contributes significantly to the scattering coefficient. Although these empirical correlations relate the aerosol scattering coefficient to the sulfate mass, there are no such correlations for the scattering distribution functions. Also, the wavelength dependence of the scattering coefficient has not been as extensively studied, and the data show relatively wide variations. Thus, to predict coloration effects, one must calculate the scattering and absorption properties based on measured aerosol size distributions.

b. Scattering and Absorption Calculations for Aerosols

For a sphere of uniform refractive index, it is possible to obtain a closed-form solution to Maxwell's equations. This solution, the so-called Mie equations, enables calculation of the scattering and absorption of light at a particular wavelength for a particle given its size and refractive index. Computer programs for this computation exist and are readily available (Dave, 1970; Hansen and Travis, 1974). For these calculations, we used the IBM computer program DAMIE, written by J. V. Dave (Dave, 1970).

The problem with using these calculations for particle scattering in the atmosphere is that most of the particles are not spheres, and they are of mixed composition. This concern over the applicability of these calculations to particles in the real atmosphere has prompted much discussion, the salient points of which are:

- The Mie equations are essentially the only way of computing the effect of particle size and index of refraction on scattering and absorption.
- Regardless of the degree of nonspherocity and mixed composition, the particles can be considered to have an effective radius and an effective index of refraction. These effective values are determined by comparing calculations with observed scattering and absorption (Bergstrom and Peterson, 1977).

To describe a particle's interaction with light, one must know its scattering coefficient, absorption coefficient, and scattering distribution. The scattering coefficient, b_{scat}, is a measure of the particle's ability to intercept light and to redirect it. The absorption coefficient, b_{abs}, is a measure of the particle's ability to absorb light. The description of the probability of the redirection of the scattered light into a particular angle Θ is called the scattering distribution function (or phase function).

The scattering coefficient for a single particle is defined as:

$$b_{scat} = \pi r^2 Q_{scat}(\lambda, r, \tilde{n}) \quad , \qquad \text{(B-1)}$$

where

r = the radius of the particle,
Q_{scat} = the scattering efficiency factor computed from the Mie equations,
λ = the wavelength,
$\tilde{n}$ = the index of refraction.

The absorption coefficient is similarly defined as:

$$b_{abs} = \pi r^2 Q_{abs}(\lambda, r, \tilde{n}) \quad , \qquad \text{(B-2)}$$

where Q_{abs} is the absorption efficiency factor. The sum of the scattering and absorption coefficients is called the extinction coefficient, b_{ext}.

When there are many particles of different sizes in a particular volume element, the total scattering and extinction coefficient is simply the integral over size:

$$\begin{aligned} b_{ext} &= \int_0^\infty \pi r^2 (Q_{scat} + Q_{abs}) n(r)\, dr \\ &= \int_0^\infty Q_{ext} s(r)\, dr \quad , \qquad \text{(B-3)} \end{aligned}$$

where $n(r)$ is the number distribution (number of particles per radius interval) and $s(r)$ is the surface area distribution equal to $\pi r^2 n(r)$. The scattering distribution function $p(\Theta)$ is written:

$$p(\Theta) = \frac{\lambda^2}{b_{scat}} \int_0^r \frac{1}{2} \left[i_{\parallel}(\Theta) + i_{\perp}(\Theta) \right] n(r) \ dr \quad , \qquad \text{(B-4)}$$

where $i_{\parallel}$ and $i_{\perp}$ are the intensity of parallel and perpendicularly polarized scattering radiation, respectively (computed from the Mie equations).

The scattering and extinction coefficients are usually expressed per unit mass (aerosol density, $\mu g/m^3$). The quantity for a single particle is then:

$$\frac{b_{ext}}{M} = \frac{Q_{ext}(2\pi r/\lambda, \tilde{n})}{\left(\frac{4}{3}\right)\rho r} \quad , \qquad \text{(B-5)}$$

and for many particles,

$$\frac{b_{ext}}{M} = \frac{\int_0^\infty \pi r^2 Q_{ext} n(r) \ dr}{\left(\frac{4}{3}\right)\rho \int_0^\infty \pi r^3 n(r) \ dr} = \frac{\int_0^\infty Q_{ext} \ S(r) \ dr}{\rho V_T} \quad . \qquad \text{(B-6)}$$

The curve of Eq. (B-5) for $\lambda = 0.55$ μm and various indices of refraction is shown in Figure B-1 from Bergstrom (1973). As shown in this figure, the function approaches zero as $r \rightarrow 0$ (for nonabsorbing particles) and also as $r \rightarrow \infty$. The scattering-to-mass ratio goes through a maximum, indicating that on a per-mass basis particles with radius ∿0.3 μm are much more effective light scatters than are larger or smaller particles.

For large particles ($2\pi r/\lambda > 3$), $Q_{ext} \rightarrow 2$ and the function becomes $(3/2)(1/\rho r)$, so that a particle at 10 μm is approximately 10 times less

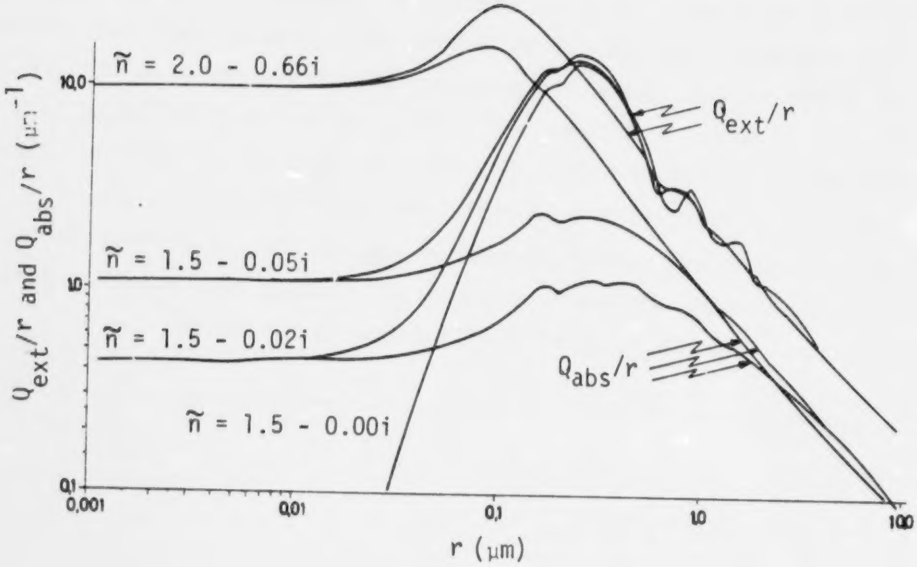

Source: Bergstrom (1973).

FIGURE B-1. EXTINCTION AND ABSORPTION PER UNIT MASS AS A FUNCTION OF PARTICLE RADIUS FOR FOUR DIFFERENT REFRACTIVE INDICES AT A SOLAR WAVELENGTH OF 0.55 μm effective in scattering per unit mass than a particle of 1 μm. Therefore, if a small percentage of the total mass is in the range of maximum effectiveness, it will dominate the light scattering. This fact explains why sulfates and other secondary aerosols that contribute only a small part of the total mass dominate the light scattering. Figure B-2 shows for an aerosol with a lognormal size distribution the scattering per unit mass (for a particle density of unity) as a function of the aerosol mass median radius (r_{og}) for various geometric standard deviations for a refractive index of 1.5 - 0i and $\lambda = 0.5$ μm. To convert to the units of Table B-1, divide the values in Figure B-2 by the particle density. Figure B-2 shows that significant changes in the aerosol size distribution ($0.1\ \mu m < r_{og} < 1\ \mu m$) result in only relatively small changes in the scattering-to-mass ratio, which helps explain why the various empirical studies have achieved good correlations and why the range of coefficients is not large.

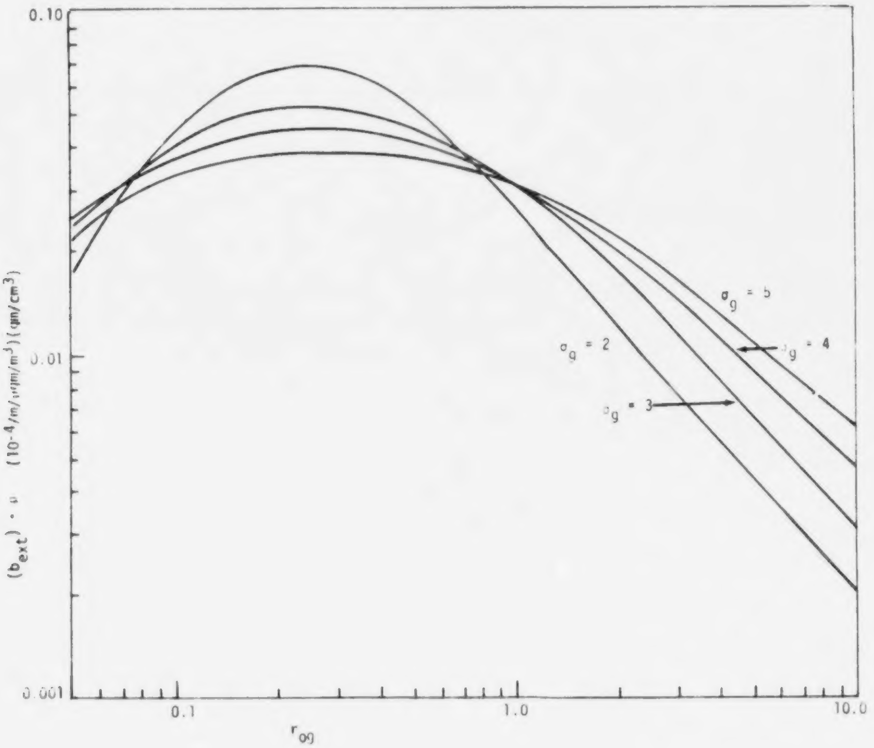

FIGURE B-2. SCATTERING-TO-MASS RATIOS FOR VARIOUS SIZE DISTRIBUTIONS

Calculating the coloration effects of the aerosol (discussed in Chapter III) requires knowledge of the wavelength dependence of the extinction coefficient and the scattering distribution function. This information is obtained by evaluating these quantities from the Mie equations for the wavelengths in the solar spectrum. The extinction coefficient is often parameterized by:

$$b_{ext} \propto \lambda^{-c} \quad ,$$

where c is either 1 or 2, depending on the aerosol size distribution. For the background aerosol, c is about 2 for the accumulation mode and closer to 0 for the coarse mode.

The dependence of the scattering function on wavelength has been shown to result in a coloration effect by Husar and White (1976). Accumulation mode particles scatter more blue light than red light in the forward direction and more red light than blue light in the backscattered direction. This effect is shown in Figure B-3, which also illustrates the angular dependence of the scattering distribution function.

The calculations can be extended to include the effects of relative humidity. Since, as shown in Figure B-2, the scattering per unit mass is not a strong function of the aerosol mass median radius for $0.1 < r < 1.0$ μm, we can approximate the scattering of a particle growing hygroscopically with relative humidity as the product of the scattering-to-mass ratio for the dry sulfate aerosol and the mass of sulfate and water, i.e.,

$$b_{scat} = \left(\frac{b_{scat}}{M}\right)_{Sulfate} \cdot \left(Mass_{Sulfate} + Mass_{Water}\right) \quad .$$

Then, following Winkler (1973), we can write the mass of water in terms of relative humidity (RH), and the expression becomes:

$$b_{scat} = \left(\frac{b_{scat}}{M}\right)_{Sulfate} \cdot Mass_{Sulfate} \left\{1 + \left[\frac{C^{*}F(RH)}{1 - RH}\right] \frac{\rho_w}{\rho_s}\right\} \quad , \qquad \text{(B-7)}$$

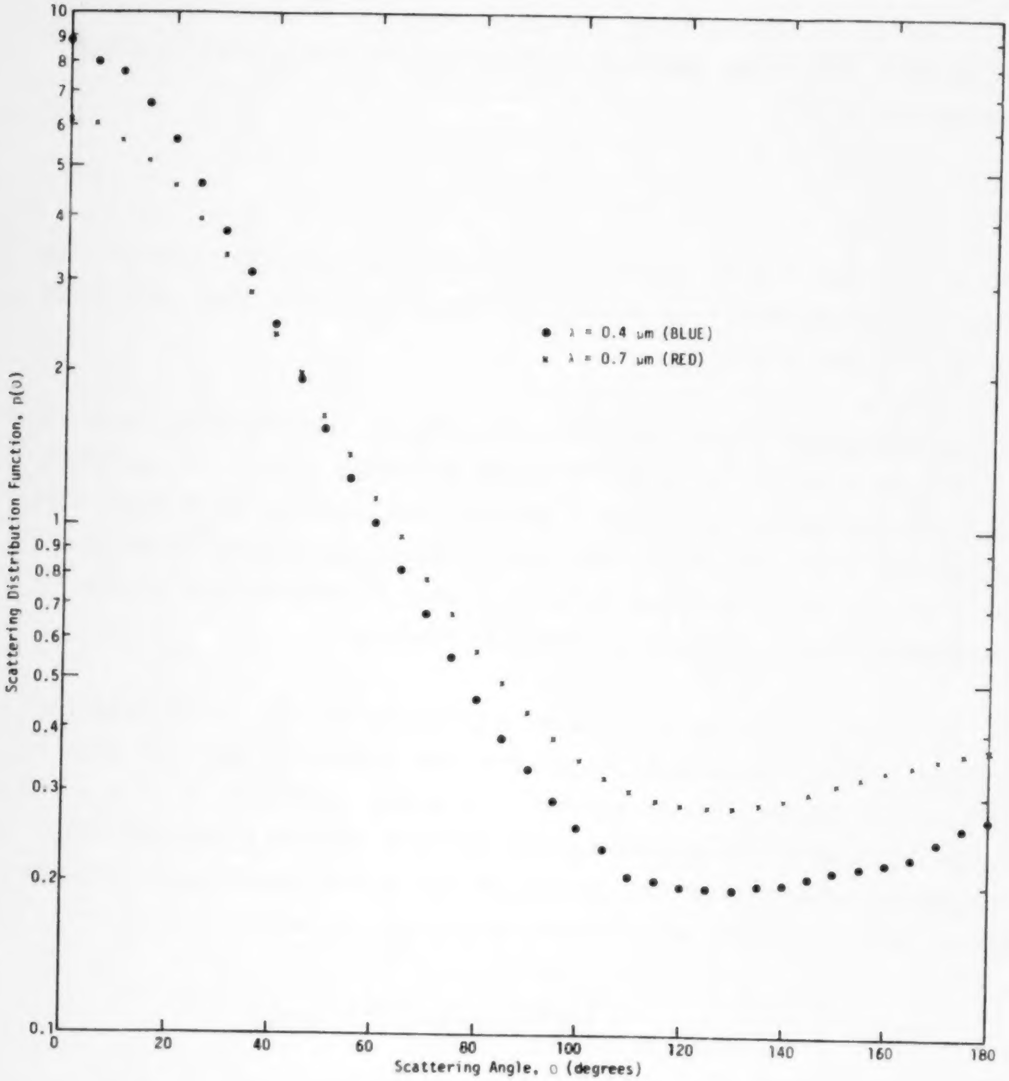

FIGURE B-3. THE SCATTERING DISTRIBUTION FUNCTION FOR THE ACCUMULATION MODE, r_{og} = 0.1 μm, σ = 2.0 μm AT TWO DIFFERENT WAVELENGTHS where C*F(RH) are tabulated values. This expression accounts for the increase in scattering due to the growth of the particle by relative humidity.

c. Comparison of Observed and Predicted Scattering-to-Mass Ratios

The range of the coefficient of the scattering-to-mass ratio, in units of $10^{-4}/\text{m} \cdot 1/(\mu\text{g/m}^3)$, is from 0.03 to 0.1 depending on the correlation technique and the investigation. Figure B-2 shows that for a particle density of 1.8 g/cm^3 (ammonium sulfate), the maximum particle scattering-to-mass ratio is about 0.037 in the same units.* This raises some questions about the observed values. It seems most likely that the higher values (mostly from Los Angeles data) can be explained by the presence of sulfate found in water droplets. Two analyses (Cass, 1976; Trijonis and Yuan, 1977) attempted to account for the water effects through nonlinear regression analysis of the form:

$$b_{scat} = \frac{C}{(1 - RH)} \cdot M_{Sulfate} \quad .$$

This form is similar to Eq. (B-7), which we derived from Winkler's results. We compared the dependence of the scattering-to-mass ratio on relative humidity determined by Trijonis and Yuan with our calculations using Eq. (B-7) and the following assumptions:

- Aerosol with a lognormal size distribution and a mass median diameter of 0.2 μm and a geometric standard deviation equal to 2.0.
- Index of refraction equal to 1.5 - 0i.
- Density equal to 1.8 g/cm^3.
- Light of 0.5 μm wavelength.

Figure B-4 shows the striking agreement between our calculations and the dependence of scattering-to-mass ratio on relative humidity observed by Trijonis and Yuan in the Southwest.

---

* If we use an accumulation mode $b_{scat}/V = 0.06 \times 10^{-4}/(\mu\text{m}^3/\text{cm}^3)$ we obtain $b_{scat}/(\mu\text{g/m}^3\ SO_4^=)$ ranging from 0.034 to $0.046 \times 10^{-4}\ \text{m}^{-1}/\mu\text{g/m}^3$ depending on whether the sulfate is H_2SO_4 or $(NH_4)_2SO_4$.

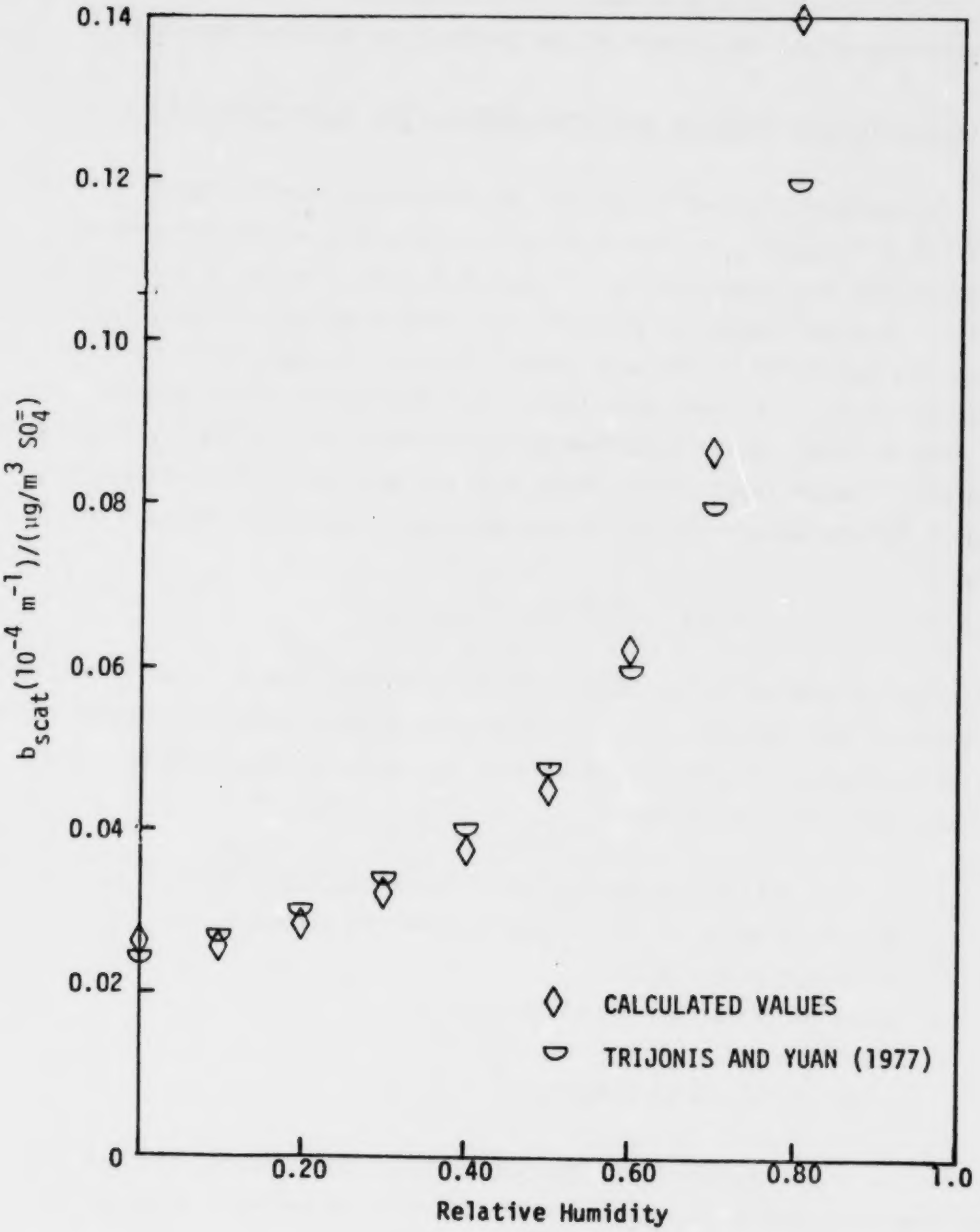

FIGURE B-4. RATIO OF LIGHT SCATTERING TO MASS AS A FUNCTION OF RELATIVE HUMIDITY

The results shown in Figure B-4 are encouraging because they imply that, for a first approximation, the dynamics of aerosol growth need not be considered and that accumulation mode size distributions suffice in calculating the visual impact of sulfate aerosol particles. Size distribution information is still required, however, for the primary particles. The size of the particles has an effect on the coloration of all but very large particles. Size also affects the scattering phase functions. Small particles are much more isotropic (equal probability of scattering to all angles) than large particles. Large particles scatter mostly in the forward direction and have highly irregular backward scattering distributions (see Hansen and Travis, 1974).

d. Procedure for Calculating the Extinction Coefficients and Scattering Distribution in the Visibility Model

For the given size distributions of the particles, the extinction coefficients and scattering distribution functions are calculated from the Mie equations. The index of refraction is assumed to be 1.5 - 0i for all particles, and the calculations are made for wavelengths between 0.37 and 0.75 μm. The effect of relative humidity on the accumulation mode particles is included as described.

The current procedure assumes that the sulfate particle size does not change with distance from the source, but the effect of particle growth with distance could be easily included by recomputing the extinction coefficient and scattering distribution function for time-dependent size distributions.

2. METHODS FOR CALCULATING AND DISPLAYING VISUAL DEGRADATION AND DISCOLORATION

As previously pointed out, visibility impairment means a change in a given observer's visual perception of the terrain or atmospheric features. The cause of the change can be subtle--for example, a general haziness (the regional problem)--or dramatic--for example, a large plume of smoke (the plume problem).

Visibility has historically been associated with the term "visual range," which is the distance at which a black object can be seen against the background sky. The reason for this association is that many people (e.g., military or airport personnel) have been interested in detecting an object and that visual range is easy to calculate and relatively easy to determine. But visual range does not indicate, for example, whether a plume of smoke is visible to an observer. Thus, the question of visual degradation and discoloration goes well beyond the concept of visual range.

Jerskey and Burton (1977) recently reviewed visibility measurement programs and currently available visibility models. The influence of aerosols and NO_2 on the coloration of haze has been debated by Hodkinson (1966), Charlson and Ahlquist (1969), Horvath (1971), Waggoner and Charlson (1971), Waggoner, Charlson, and Ahlquist (1972), Horvath (1972), Husar and White (1976), and Megaw (1977). Both aerosols and NO_2 can produce discoloration, and the relative importance of each depends on the situation.

Some work has been reported on the problem of relating plume opacity, Ringlemann number, and mass concentration (Conner and Hodkinson, 1972; Pilat and Ensor, 1971; Halow and Zeek, 1973; Weir et al., 1975, 1976). Also, recent studies have investigated the transmission, visual range, and coloration effects of plumes (Ensor, Sparks, and Pilat, 1973; Williams and Cudney, 1976; Jarmen and DeTurville, 1969; Latimer and Samuelsen, 1977).

In Section 2 we dicuss the ways in which visual effect (changes in light intensity and coloration) can be calculated. We begin with basic equations to show that the methods used in the calculations apply the same principle once or several times. We then present the techniques used in the visibility models.

a. Intensity, Contrast, and Visual Range

In the daytime, the ability to see an object that is not self-illuminating is determined by the contrast in intensity between the object and its background at the point of observation. This contrast is defined simply as:

$$C \equiv \frac{I_b - I_{obj}}{I_b}$$

where I_b is the intensity [Energy/(Time · Area · Solid Angle)] of radiation (often called radiance, luminance, or brightness) from the background and I_{obj} is that in the direction of the object. The physical situation represented by this equation is depicted in Figure B-5. For a given object and set of atmospheric conditions, the contrast is a function of the location of the observer, $\vec{s}$; the direction of the observation, Ω; and the solar angle, Ω_s. The contrast must also be defined for a particular wavelength interval (e.g., 0.55 μm). The visual range, r_v, is the distance at which an object can no longer be distinguished from the background. This indistinguishability occurs when the contrast is reduced to some minimum value (usually 0.02).

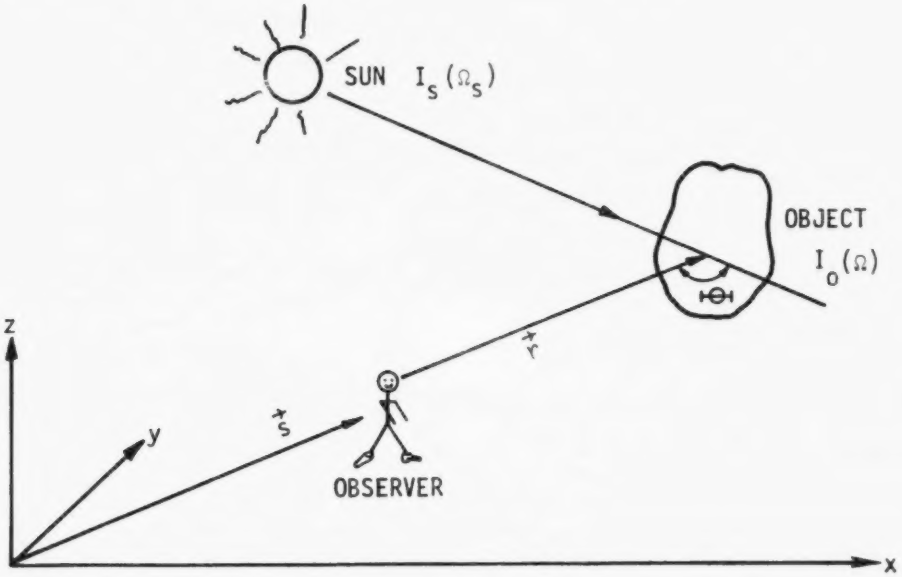

FIGURE B-5. DIAGRAM OF THE PHYSICAL SITUATION

1) The General Expression for the Radiant Intensity and the Contrast

The background intensity at a particular wavelength looking up from the surface can be written as:

$$I_b(\Omega,s) = I_\infty(\Omega)e^{-\tau_\infty} + \int_0^{\tau_\infty} \frac{\omega(\tau)}{4\pi} \int_{\Omega'=4\pi} I(\Omega',\tau')\, p(\Omega'\to\Omega,\tau')\, d\Omega'\, e^{-\tau'}\, d\tau' \quad , \qquad \text{(B-8)}$$

where

τ = the optical depth ($\tau \equiv \int_0^r b_{ext}\, dr$, where b_{ext} is the extinction coefficient),

ω = the albedo for single scattering ($\omega \equiv b_{scat}/b_{ext}$, where b_{scat} is the scattering coefficient),

$p(\Omega' \to \Omega)$ = the scattering distribution function for the angle $\Omega' \to \Omega$,

I_∞ = the downward-directed intensity at the edge of the atmosphere.

Equation (B-8) is valid for the usual continuum, no refraction, random polarization assumptions.

The intensity seen by an observer in direction Ω of an object at a distance R is:

$$I_{obj}(\Omega,s) = I_o(\Omega)e^{-\tau_R} + \int_0^{\tau_R} \frac{\omega(\tau')}{4\pi} \int_{\Omega'=4\pi} I(\Omega',\tau')\, p(\Omega'\to\Omega,\tau')\, d\Omega'\, e^{-\tau'}\, d\tau' \quad , \qquad \text{(B-9)}$$

where $I_0(\Omega)$ is the intensity leaving the object. The general expression for contrast is then simply:

$$C(\Omega,s) = 1 - \frac{I_{obj}(\Omega)e^{-\tau_R} + G(\tau_R)}{I_\infty(\Omega)e^{-\tau_\infty} + G(\tau_\infty)} \quad , \qquad \text{(B-10)}$$

where

$$G(\tau) = \int_0^\tau \frac{\omega(\tau')}{4\pi} \int_{\Omega'=4\pi} I(\Omega',\tau')\ p(\Omega'\to\Omega,\tau')\ d\Omega'\ e^{-\tau'}\ d\tau' \quad .$$

To evaluate Eq. (B-10), one must know the intensities $I(\Omega',\tau')$, $I_0(\Omega)$, and $I_\infty(\Omega)$ and the radiative properties of the atmosphere. Usually some simplifications are introduced to determine these quantities.

2) Radiation Field Approximations

The first assumption is that the radiation field is plane parallel; hence:

$$I(\Omega,s) \cong I(\Omega,z) \quad . \qquad \text{(B-11)}$$

This assumption is valid if local inhomogeneities do not affect the radiation field and if the curvature of the earth is ignored.

In the visible spectrum, the intensity can be divided into the direct solar radiation, I_s^{dir}, and diffuse (scattered) solar radiation, I_s^{dif}. Then,

$$\begin{aligned} I_s(\Omega,z) &= I_s^{dir}(z)\delta(\Omega_s,\Omega) + I_s^{dif}(\Omega,z) \\ &= F_s e^{-\tau_z/\mu_s}\delta(\Omega_s,\Omega) + I_s^{dif}(\Omega,z) \quad , \end{aligned} \qquad \text{(B-12)}$$

where $\tau_z \equiv \int_\infty^z b_{ext}\, dz$, μ_s is the cosine of the solar zenith angle, and F_s is the solar flux normal to ray. Then,

$$I_b = I_\infty(\Omega)e^{-\tau_\infty} + F_s \int_0^{\tau_\infty} \frac{\omega(\tau')}{4\pi} e^{-\tau_z/\mu_s}\, p(\Omega_s \to \Omega, \tau')\, e^{-\tau'}\, d\tau$$

$$+ \int_0^{\tau_\infty} \frac{\omega(\tau')}{4\pi} \int_{\Omega'=4\pi} I_s^{dif}(\Omega', \tau')\, p(\Omega' \to \Omega)\, d\Omega'\, e^{-\tau'}\, d\tau' \quad . \tag{B-13}$$

If I^{dif} is isotropic so that $I_s^{dif}(\Omega, z) = I_s^{dif}(z)$, then,

$$I_b = I_\infty(\Omega)e^{-\tau_\infty} + F_s \int_0^{\tau_\infty} \frac{\omega(\tau')}{4\pi} e^{-\tau_z/\mu_s}\, p(\Omega_s \to \Omega, \tau')\, e^{-\tau'}\, d\tau'$$

$$+ \int_0^{\tau_\infty} \omega(\tau')\, I^{dif}(z)\, e^{-\tau'}\, d\tau' \quad , \tag{B-14}$$

with similar expressions for I_{obj}.

The next assumption concerns the radiative properties of the background atmosphere. To evaluate the integrals in Eq. (B-14), one must prescribe the dependence of p, ω, and I^{dif} along the optical path τ. The normal assumption is to represent the inhomogeneous atmosphere by a series of homogeneous layers.

We chose to divide the atmosphere into two layers (see Figure B-6)--an upper layer and a planetary boundary layer--because this structure has been shown to be a reasonable approximation (Bergstrom and Viskanta, 1974). The two layers are assumed to be homogeneous in the optical depth τ, not the vertical coordinate z, and thus we can still account for the vertical variation in the scattering and extinction coefficients.

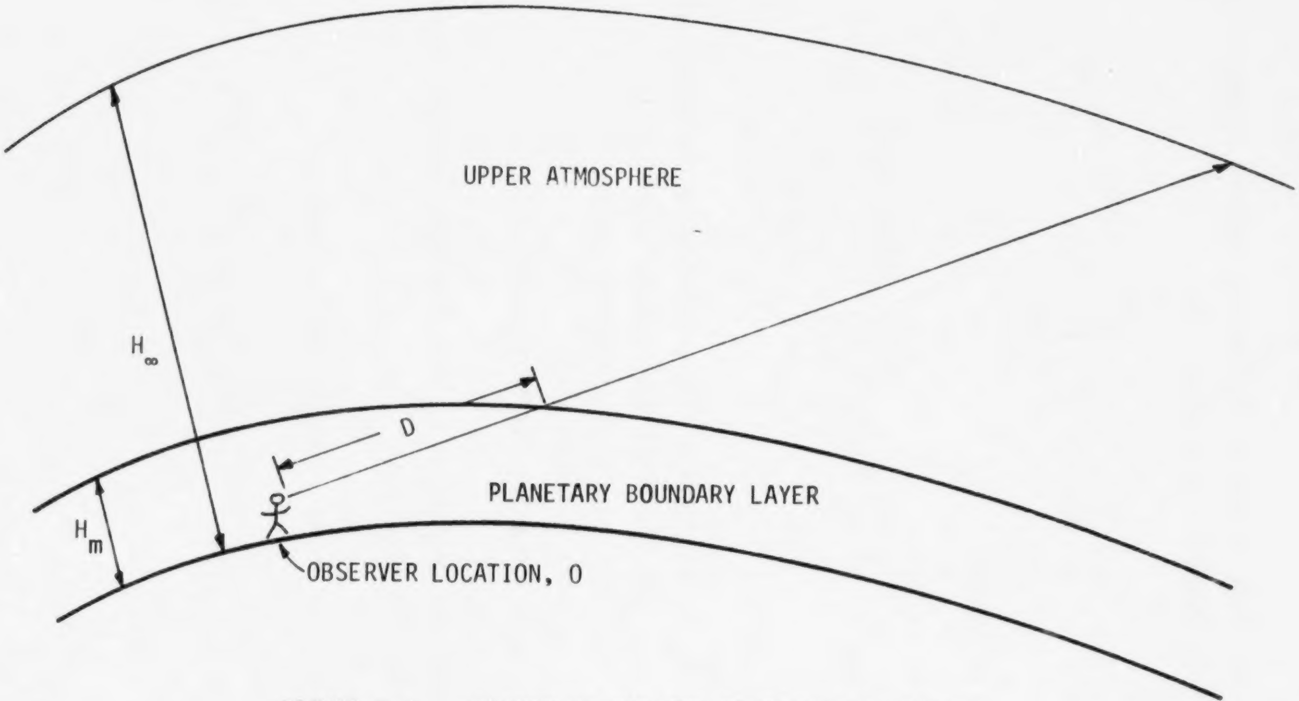
UPPER ATMOSPHERE
H_∞
D
PLANETARY BOUNDARY LAYER
H_m
OBSERVER LOCATION, O

FIGURE B-6. DIAGRAM OF THE TWO ATMOSPHERIC LAYERS

We can now write an expression for the radiant intensity impinging on the planetary boundary layer as:

$$I_{sky}(\phi,\mu) = \frac{\overline{\omega}_{0\infty}}{4\pi} \overline{p}_{D\infty}(\Omega_s \rightarrow \Omega) F_s \int_{\tau_{0D}}^{\tau_{0\infty}} e^{-\tau_z/\mu_s} e^{-\tau'} d\tau' \; , \; ,$$

which we approximate as

$$I_{sky}(\phi,\mu) \cong \frac{\overline{\omega}_{D\infty}}{4\pi} \overline{p}_{D\infty}(\Theta_s) F_s \left[1 - e^{-(\tau_{0\infty}-\tau_{0D})}\right] \quad , \qquad \text{(B-15)}$$

where

$\overline{\omega}_{D\infty}$, $\overline{p}_{D\infty}$ = the average albedo and scattering distribution in the upper atmosphere, respectively,
μ = the cosine of the zenith angle,
ϕ = the azmuthal angle,
Θ_s = the solar scattering angle.

Figure B-7 shows the definition of the zenith and azimuth angles and also the solar scattering angle, Θ_s.

Then Eq. (B-14) becomes for the horizon sky:

$$I_b(\mu,\phi) = I_{sky}(\mu,\phi) e^{-\tau_{0D}} + \frac{\overline{\omega}_{0D}}{4\pi} \overline{p}_{0D}(\Theta_s) F_s \int_0^{\tau_{0D}} e^{-\tau_z/\mu_s} e^{-\tau'} d\tau'$$

$$+ \int_0^{\tau_{0\infty}} \omega I^{dif}(z) e^{-\tau'} d\tau' \quad . \qquad \text{(B-16)}$$

Then, defining the averages for the planetary boundary layer,

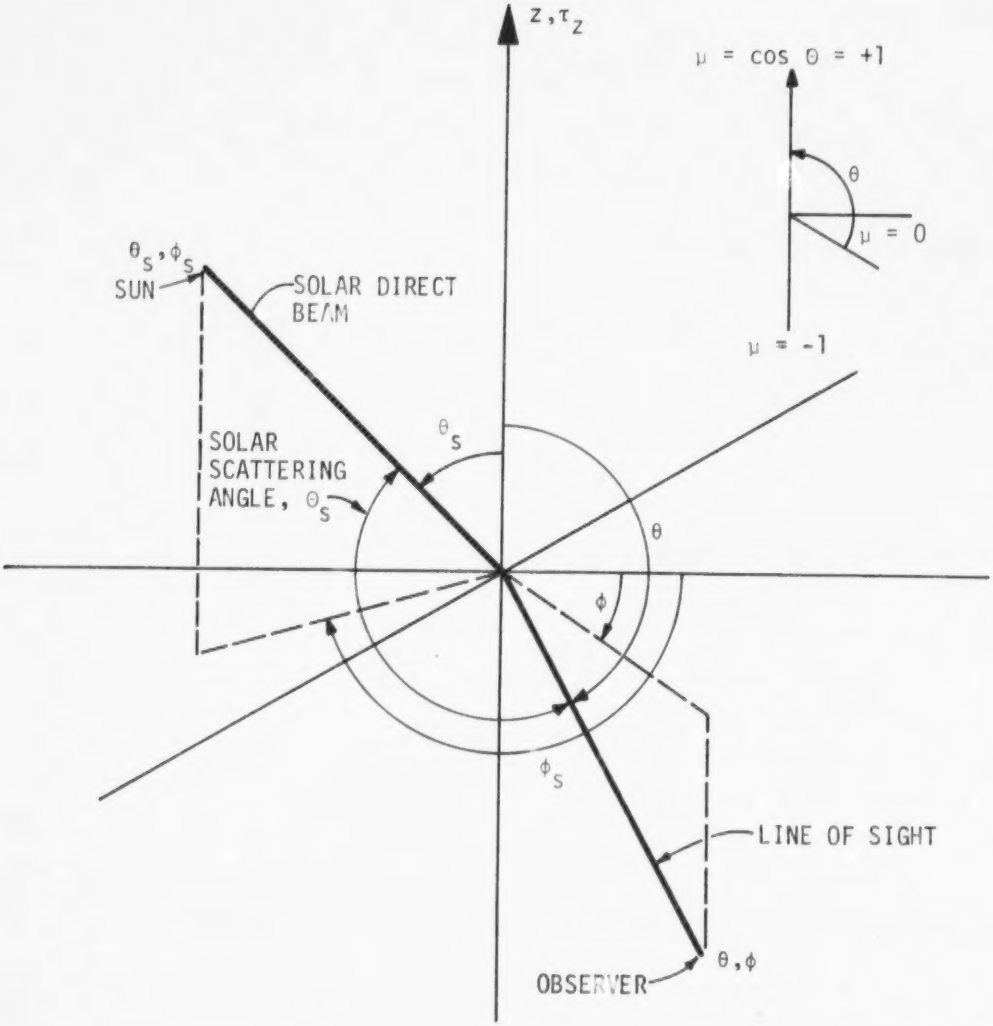
Z, τ_Z
$\mu = \cos\Theta = +1$
θ
$\mu = 0$
$\mu = -1$
θ_s, ϕ_s
SUN
SOLAR DIRECT BEAM
θ_s
SOLAR SCATTERING ANGLE, Θ_s
θ
ϕ
ϕ_s
LINE OF SIGHT
θ, ϕ
OBSERVER

FIGURE B-7. COORDINATE SYSTEM AND ANGLES

$$F_{s,av} \equiv \frac{F_s \displaystyle\int_0^{\tau_{OD}} e^{-\tau_z/\mu_s}}{1 - e^{-\tau_{OD}}} \quad ,$$

and

$$I_{av}^{dif} \equiv \frac{\displaystyle\int_0^{\tau_{0\infty}} \omega\, I^{dif}(z) e^{-\tau'}\, d\tau'}{\bar{\omega}_{OD}\left(1 - e^{-\tau_{0\infty}}\right)} \quad ,$$

so that Eq. (B-16) becomes:

$$I_b(\mu,\phi) = I_{sky}(\mu,\phi)e^{-\tau_{OD}} + \frac{\bar{\omega}_{OD}}{4\pi}\,\bar{P}_{OD}(\Theta_s)F_{s,av}\left(1 - e^{-\tau_{OD}}\right)$$

$$+ \bar{\omega}_{OD}\, I_{av}^{dif}\left(1 - e^{-\tau_{0\infty}}\right) \quad , \qquad \text{(B-17)}$$

and the intensity in the direction of an object is:

$$I_{obj} = I_o(\mu,\phi)e^{-\tau_R} + \frac{\bar{\omega}_{OD}}{4\pi}\,\bar{P}_{OD}(\Theta_s)F_{s,av}\left(1 - e^{-\tau_R}\right)$$

$$+ \bar{\omega}_{OD} I_{av}^{dif}\left(1 - e^{-\tau_R}\right) \quad . \qquad \text{(B-18)}$$

For a nonhorizontal path, the plane parallel assumption gives:

$$\tau_{OD} = \tau_{z,0m}/\mu \quad .$$

For a horizontal path, s, the plane parallel assumption is not valid. However, for an exponential vertical profile,

$$b_{ext}(z) = b_{ext,0}e^{-z/H}$$

and

$$\tau_{0\infty} = \int_0^\infty b_{ext,0}\, e^{-z/H}\, ds$$

and ds = R dz/s, where R is the radius of the earth. Then,

$$\tau_{0\infty} = \frac{b_{ext,0}}{2}\sqrt{2\pi RH} \quad ,$$

and

$$\tau_{0D} = b_{ext,0}\, \mathrm{ERF}\left(\frac{D}{2RH}\right) \quad , \qquad \text{(B-19)}$$

so that the optical depths for a horizontal path can be evaluated.

The last assumption that must be made concerns the average fluxes. The solar average was taken as the average between the solar direct flux at the surface and at H_m.

$$F_{s,av} = \frac{F^{dir}(0) + F^{dir}(H_m)}{2} \quad . \qquad \text{(B-20)}$$

Calculating the diffuse intensity average was more complicated. Initially, we assumed that the atmosphere was vertically thin and that the diffuse intensity need not be considered, which is generally the case in clean atmospheres ($I^{dif} \sim 0.1\ I^{dir}$).

We found, however, that the effects of pollution are more noticeable during sunrise and sunset than at midday. At sunrise and sunset, the solar beam path through the atmosphere is long, and the amount of diffuse light is large. Thus, it was necessary to provide an approximation of the diffuse light.

In our notation, the diffuse light represents those photons that have been scattered more than once (i.e., multiple scattering). Prediction of multiple scattering in atmospheres has a long history (see, for example, Hansen and Travis, 1974). Although computer programs exist to calculate these effects, none of the codes is analytic for the intensity, and all require a relatively large amount of computer time. Thus, we decided to proceed with a relatively simple approximation, which, after testing, could be modified if necessary.

The approximation was to equate the flux at the top of the atmosphere and the bottom, i.e., to assume no absorption. Thus,

$$F_\infty - F^{dif}{\uparrow}(\tau_\infty) = F_\infty e^{-\tau_{0\infty}/\mu_s} + F^{dif}{\downarrow}(0) + F_{reflect} \quad .$$

Then, if we assume that equal amounts of diffuse flux emerge from the top and bottom,

$$F^{dif}{\uparrow}(\tau_\infty) \cong F^{dif}{\downarrow}(0) \quad ,$$

and one can solve for the diffuse flux at the surface:

$$F^{dif}\,(0) = \frac{F_\infty\left[1 - e^{-\tau_{0\infty}/\mu_s}\,(1 - r)\right]}{(2 - r)} \quad ,$$

where r is the reflectivity of the surface. One can form an equivalent isotropic intensity $\bar{I}$ as:

$$\bar{I} \equiv \frac{F^{dif}{\downarrow}(0)}{\pi}$$

$$= \frac{\mu_s F_s}{(2 - r)\pi}\left[1 - e^{-\tau_{0\infty}/\mu_s}\,(1 - r)\right] \quad , \qquad \text{(B-21)}$$

where $F_\infty = \mu_s F_s$. The average diffuse intensity was assumed to be equal to this "equivalent isotropic intensity," and an average surface reflection of 0.3 was used. The treatment of the diffuse light is extremely heuristic, and it is intended to provide only an estimate until better models are developed. The evaluation of the model requires feedback between observations and predictions so that improvements can be made.

The expression for the background sky becomes:

$$I_b(\mu,\phi) = I_{sky}(\mu,\phi)e^{-\tau_{OD}} + \frac{\bar{\omega}_{OD}}{4\pi}\,\bar{P}_{OD}(\Theta_s)F_{s,av}\left(1 - e^{-\tau_{OD}}\right)$$

$$+ \bar{\omega}_{OD}\,\frac{\mu_s F_s}{(2 - r)\pi}\left[1 - e^{-\tau_{0\infty}/\mu_s}\,(1 - r)\right]\left(1 - e^{-\tau_{0\infty}}\right) \quad , \qquad \text{(B-22)}$$

and for the intensity in the direction of an object,

$$I_{obj}(\mu,\phi) = I_o(\mu,\phi)e^{-\tau_R} + \bar{\omega}_{OD}\,\bar{P}_{OD}(\Theta_s)F_{s,av}\left(1 - e^{-\tau_R}\right)$$

$$+ \bar{\omega}_{OD}\,\frac{\mu_s F_s}{(2 - r)\pi}\left[1 - e^{-\tau_{0\infty}/\mu_s}\,(1 - r)\right]\left(1 - e^{-\tau_R}\right) \quad . \qquad \text{(B-23)}$$

3) Specific Procedure for Evaluating the Intensities and the Limitations in the Regional and Plume Models

The procedure for evaluating the intensities in the regional model is to add the radiative properties of the sulfate and NO_2 due to anthropogenic sources to the background atmospheric properties. Then the intensity of the background sky at the surface can be evaluated from Eq. (B-21) and the intensity of an object from Eq. (B-22). The contrast can be evaluated from the definition as:

$$C \equiv \frac{I_b - I_{obj}}{I_b} \quad .$$

For an optically thick path through the planetary boundary layer,

$$\tau_{OD} >> 1 \quad ,$$

and the contrast of a black object is:

$$C_{\text{black}} = e^{-\tau_R} \quad .$$

If a detectibility criterion of 0.02 is chosen, the optical depth corresponding to that minimum detectibility criterion is $\tau_R = 3.912$. Now,

$$\tau_R \equiv \int_0^{r_v} b_{\text{ext}}(r)\, dr \quad ,$$

and for a homogeneous atmosphere $\tau_R = b_{\text{ext}} r_v$. Then, one can solve for r_v:

$$r_v = \frac{3.912}{b_{\text{ext}}} \quad . \tag{B-24}$$

This is the Koschmieder expression for the visual range.

For a vertically inhomogeneous atmosphere, one can approximate Eq. (B-24) as:

$$r_v \cong \frac{3.912}{b_{\text{ext},0}} \tag{B-25}$$

where $b_{\text{ext},0}$ is the surface extinction coefficient. Equation (B-24) then gives an estimate of the distance at which a black object will have an 0.02 contrast with the horizon sky. Initial calculations at 0.55 μm wavelength show that the actual contrast at the distance computed from Eq. (B-24) is within 20 percent of 0.02. Thus, we have used Eq. (B-24) in evaluating the visual range in the regional model.

To evaluate the intensities in the plume model, we must describe the intensity incident on the plume. From Eq. (B-21),

$$I_{ip}(\mu,\phi) = I_{sky}(\mu,\phi)e^{-\tau_{RD}} + \frac{\overline{\omega}_{OD}}{4\pi}\,\overline{p}_{OD}(\Theta_s)F_{s,av}\left(1 - e^{-\tau_{RD}}\right)$$

$$\overline{\omega}_{OD}\; I_{av}^{dif}\left(1 - e^{-\tau_{R\infty}}\right) \quad , \qquad \text{(B-26)}$$

where R is now the distance from the plume to the observer. The intensity leaving the plume is:

$$I_{\ell p}(\mu,\phi) = I_{ip}(\mu,\phi)e^{-\tau_p} + \frac{\overline{\omega}_p}{4\pi}\,\overline{p}_p(\Theta_s)F_{s,av}\left(1 - e^{-\tau_p}\right)$$

$$+\;\overline{\omega}_p\; I_{av}^{dif}\left(1 - e^{-\tau_p}\right) \quad , \qquad \text{(B-27)}$$

where $\overline{\omega}_p$ and $\overline{p}_p$ are the mean quantities in the plume and τ_p is the optical depth of the plume. For a Gaussian plume, the optical depth is (Latimer and Samuelsen, 1975):

$$\tau_p = b_{ext,max}(2\pi)^{1/2}\,\sigma_y\left\{\exp\left[-\frac{1}{2}\left(\frac{H_p + z}{\sigma_z}\right)^2\right] + \exp\left[-\frac{1}{2}\left(\frac{H_p - z}{\sigma_z}\right)^2\right]\right\} \qquad \text{(B-28a)}$$

in the horizontal cross-wind direction *y*, and

$$\tau_p = b_{ext,max}(2\pi)^{1/2}\,\sigma_z\,\exp\left[-\frac{1}{2}\left(\frac{y}{\sigma_z}\right)^2\right] \qquad \text{(B-28b)}$$

in the vertical direction z. In these equations, H_p is the plume height, σ_z and σ_y are the standard deviations, and $b_{ext,max}$ is the centerline extinction coefficient. The plume albedo is:

$$\overline{\omega}_p = 1 - \frac{\tau_{NO_2}}{\tau_{SO_4} + \tau_{NO_2} + \tau_{prim}} \quad . \qquad \text{(B-28c)}$$

Note that Eq. (B-27) ignores the effect of the plume on $F_{s,av}$ (shadowing) and is thus valid only for optically thin plumes.

The intensity at the observer's location is [from Eq. (B-23)]:

$$I_{op} = I_{\ell p}(\mu,\phi)e^{-\tau_R} + \bar{\omega}_{OD}\,\bar{P}_{OD}(\Theta_s)F_{s,av}\left(1 - e^{-\tau_R}\right)$$

$$+ \bar{\omega}_{OD}\, I_{av}^{dif}\left(1 - e^{-\tau_R}\right) \quad . \qquad \text{(B-29)}$$

The contrast of the plume is then:

$$C_p = \frac{I_{op} - I_b}{I_b} \quad ,$$

where I_b is calculated from Eq. (B-22) as usual and I_{op} is calculated from Eqs. (B-26), (B-27), and (B-28).

The intensity of an object behind the plume incident on the plume is

$$I_{io} = I_o e^{-\tau_{p,obj}} + \frac{\bar{\omega}_{OD}}{4\pi}\,\bar{p}_{OD}(\Theta_s)F_{s,av}\left(1 - e^{-\tau_{p,obj}}\right)$$

$$+ \bar{\omega}_{OD}\, I_{av}^{dif}\left(1 - e^{-\tau_{p,obj}}\right) \quad . \qquad \text{(B-30)}$$

where $\tau_{p,obj}$ is the optical depth of the atmosphere between the plume and the object. Then Eqs. (B-27) and (B-29) are evaluated to compute the intensity at the observer's location, where I_{ip} is replaced by I_{io} in Eq. (B-27).

The contrast of an object is again:

$$C_o = \frac{I_{obj} - I_b}{I_b} \quad ,$$

except that now I_{obj} is evaluated from Eqs. (B-30), (B-27), and (B-29), in that order.

Tables B-2 and B-3 present the equations and limitations for the regional model and plume model, respectively.

TABLE B-2. EQUATIONS AND LIMITATIONS FOR THE REGIONAL MODEL

Quantity Predicted	Equation Used	Approximations and Comments
Background sky	(B-22)	Two plane parallel layers Average solar flux Average diffuse intensity
Object	(B-23)	Average solar flux Average diffuse intensity
Contrast	Definition	
Koschmieder visual range	(B-25)	Implies homogeneous optically thick boundary layer

TABLE B-3. EQUATIONS AND LIMITATIONS FOR THE PLUME MODEL

Quantity Predicted	Equation Used	Approximations and Comments
Background sky	(B-22)	Two plane parallel layers Average solar flux Average diffuse intensity
Optical depth of plume	(B-28)	Assumes Gaussian plume
Intensity of background sky through plume	(B-26). (B-27), (B-29)	Average solar flux Average diffuse intensity Implies optically thin plume
Intensity of object through plume	(B-30), (B-27), (B-29)	Average solar flux Average diffuse intensity Implies optically thin plume
Contrast	Definition	

APPENDIX C

THE CHEMISTRY OF SULFATE FORMATION

APPENDIX C
THE CHEMISTRY OF SULFATE FORMATION

Sulfur oxides in the atmosphere can most conveniently be considered as occurring in three forms: sulfur dioxide (SO_2), sulfuric acid (H_2SO_4), and inorganic sulfates. Sulfur dioxide is the anhydrous form of the weak acid, sulfurous acid (H_2SO_3). The salts of this acid are sulfites and bisulfites. Sulfuric acid is the hydrated form of sulfur trioxide (SO_3), which is derived from the oxidation of sulfur dioxide. Sulfur trioxide is intensely hygroscopic and is immediately converted into sulfuric acid in the atmosphere. Inorganic sulfates are presumably derived from either the reaction of sulfuric acid with cations or the oxidation of sulfites. There is little information available concerning the formation and occurrence of organic sulfates in the atmosphere.

The oxidation of SO_2 to sulfate is an important atmospheric phenomenon. It is now recognized that both homogeneous (gas-phase) and heterogeneous (particulate-phase) processes contribute to SO_2 oxidation in the atmosphere. Possible routes that have been identified are:

> Homogeneous--Oxidation of SO_2 to H_2SO_4 by free radicals present in the polluted urban (particularly photochemical) atmosphere.

> Heterogeneous
  - Liquid-phase oxidation of SO_2 by O_2
  - Liquid-phase oxidation of SO_2 by O_3
  - Metal-ion-catalyzed liquid-phase oxidation of SO_2
  - Catalytic oxidation of SO_2 on particle surfaces.

Sulfur dioxide oxidation rates measured in the laboratory or inferred from atmospheric data vary remarkably. These rates are frequently expressed in percentage per hour. Assume that we have a curve of SO_2 concentration,

$[SO_2]$, as a function of time, t. At any time t, the fractional rate of disappearance of SO_2 is given by :

$$- \frac{1}{[SO_2]} \frac{d[SO_2]}{dt} \quad ,$$

and the oxidation rate in percent per hour is simply:

$$- \frac{1}{[SO_2]} \frac{d[SO_2]}{dt} \times 100 \quad .$$

An average oxidation rate is a constant, equal to 100k. The characteristic time of the conversion in the first-order case is readily obtained from the integrated form:

$$\frac{[SO_2]}{[SO_2]_o} = e^{-kt}$$

as $\tau = k^{-1}$. Thus, the characteristic time of the oxidation process can be obtained from the rate, expressed in percent per hour, as $\tau = 100/(\%/hr)$. (Note that after one characteristic time the concentration has decayed to 1/e of its initial value.) The characteristic times of SO_2 oxidation vary from a few minutes to several days. Sulfur dioxide in pure air is slowly oxidized in the presence of sunlight to sulfuric acid at a rate of about 0.1 percent per hour (Gerhard and Johnstone, 1955). Although current information characterizing the chemical processes by which SO_2 is oxidized in polluted urban air is inadequate, we do know that the conversion is much more rapid than in pure air. This accelerated conversion is due to the presence of other air contaminants that generally facilitate the oxidation of SO_2. As noted above, two processes appear to be involved: homogeneous oxidation by components (e.g., free radicals) present in photochemical smog and heterogeneous oxidation predominantly by certain types of aerosols.

Homogeneous (photochemical) oxidation of SO_2 is believed to result from reaction of SO_2 with a variety of free radicals present in photochemical air pollution. Rates of oxidation of SO_2 in Los Angeles have been estimated to range as high as 13 percent per hour, though these rates cannot necessarily be attributed exclusively to photochemical oxidation.

Heterogeneous oxidation of SO_2 occurs in aerosols in which SO_2 has been absorbed. Such oxidation may occur through the action of dissolved oxygen or ozone, or it may take place catalytically in the presence of metallic compounds, such as manganese, iron, vanadium, aluminum, lead, and copper. Prediction of the rate of SO_2 oxidation in a particle has proved to be quite difficult, for diffusion of gaseous SO_2 to the particle, transfer of SO_2 across the gas-particle interface, and diffusion and reaction of SO_2 within the particle must all be considered. Relative humidity is a significant factor in heterogeneous SO_2 oxidation because the process takes place, in general, in water droplets. Further, since an acidic pH generally decreases the rate of SO_2 oxidation, the formation of sulfuric acid in an aerosol would tend to be self-limiting unless the acidity is diluted by additional water vapor. In this respect, alkaline metal compounds, such as iron oxide and ammonia, also enhance the oxidation rate by decreasing droplet acidity through their buffering capacity. Extrapolated rates of oxidation through heterogeneous processes in urban air range upwards of 20 percent per hour.

Meteorology has a substantial effect on the atmospheric oxidation of SO_2. Increased humidity accelerates the heterogeneous oxidation of SO_2, whereas cloud cover can lower the rate of photochemical processes, and rain washes out sulfur oxides from the atmosphere. Temperature affects reaction rates and the solubility of gases.

Table C-1 summarizes several SO_2 oxidation rates measured in the laboratory and the atmosphere, varying from a low of 0.1 percent per hour for photooxidation of SO_2 in clean air to over 2 percent per minute measured

TABLE C-1. OBSERVED SULFUR DIOXIDE OXIDATION RATES

Experimental Conditions	Presumed Atmospheric Conditions	SO_2 Oxidation Rate	Reference
Atmospheric study of Canadian smelting area	150-4200 $\mu g/m^3$ SO_2	0.034 %/min	Katz (1950)
Sunlight; high SO_2 concentrations; no other impurities present	SO_2; sunlight; clear air	0.5 %/hr	Hall, as cited by Urone and Schroeder (1969)
Sunlamp in smog chamber; high SO_2 concentrations in pure air	SO_2; sunlight; clear air (reaction unaffected by humidity)	0.1-0.2 %/hr	Gerhard and Johnstone (1955)
Catalyst droplet exposed to high concentrations of SO_2 and metal sulfates	Natural fog containing 1 μm crystals of $MnSO_4$ in droplets; 2600 $\mu g/m^3$ SO_2	1 %/min	Johnstone and Coughanowr (1958)
Artificial fog in smog chamber; very high levels; SO_2 and metal sulfates	(Levels in smog chamber) 0.6 mg/m^3 SO_2; 2 mg/m^3 $MnSO_4$	0.01 %/min at 77% RH 2.1 %/min at 95% RH	Johnstone and Moll (1960)
Plume of coal-burning power plant	Moisture level in plume important	0.1 %/min at 70% RH 0.5 %/min at 100% RH	Gartrell, Thomas and Carpenter (1963)
NH_4 formation in water droplets exposed to NH_3 and SO_2	100 $\mu g/m^3$ SO_2; 10 $\mu g/m^3$ NH_3; cloud droplet radius of 10 μm	2.5 %/min in droplets	van der Heuvel and Mason (1963)
UV-irradiated gas mixtures; NO_x, hydrocarbons, SO_2; high levels	Noon sun	1-3 %/hr	Urone et al. (1968)
Sunlight; 200-2000 $\mu g/m^3$ SO_2; trace impurities	Assumed 300 $\mu g/m^3$ SO_2; bright sunlight for 10 hr would produce 30 $\mu g/m^3$ of sulfate	0.65 %/hr (high rate may be due to trace impurities)	Cox and Penkett (1970)
Smog chamber; light; SO_2, NO_x, olefins	SO_2, 260 $\mu g/m^3$; ozone, 100 $\mu g/m^3$; olefin, 33 $\mu g/m^3$, bright sunlight	3 %/hr for pentene; 0.4 %/hr for propene	Cox and Penkett (1971a, 1971b)
Metallic aerosol particles on Teflon beads in flow reactor; SO_2; water vapor	Natural fog (0.2 g H_2O/m^3) in industrial area; SO_2, 260 $\mu g/m^3$; $MnSO_4$, 50 $\mu g/m^3$	2 %/hr	Cheng, Corn, and Frohliger (1971)
Photochemical reactants; SO_2 in ppm concentrations	Sunlight; SO_2; 260 $\mu g/m^3$; ozone, 200 $\mu g/m^3$; olefin, 33 $\mu g/m^3$; 40% RH	3 %/hr	Cox and Penkett (1972)
Atmospheric study of Rouen (industrial city) in winter	68-242 $\mu g/m^3$ SO_2	6-25 %/hr	Benarie, Nonat, and Menard (1973)
Los Angeles air trajectories	--	1.2-13 %/hr	Roberts and Friedlander (1975)
Plume of an oil-fired power plant; airborne sampling	Catalytic oxidation by vanadium particles; distance ≤25 km	Pseudo-second-order mechanism; rate constant = 1/ppm/hr	Newman, Forrest, and Manowitz (1975)
St. Louis urban plume; airborne sampling	900-1200 m altitude 20-25 °C; 40-60% RH	10-14 %/hr	Alkezweeny and Powell (1977)
Plumes of four coal-fired power plants; airborne sampling	32-85% RH; 10-25°C; distance ≤70 km	~1 %/hr	Forrest and Newman (1977a)
Smelter plume; airborne sampling	Catalytic oxidation	Pseudo-second-order mechanism; rate constant = 0.2/ppm/hr	Forrest and Newman (1977b)

in water droplets. In the following sections, we consider the elements of both homogeneous and heterogeneous processes in an attempt to estimate the contribution of each to the atmospheric oxidation of SO_2.

1. HOMOGENEOUS OXIDATION OF SO_2

Although several homogeneous (gas-phase) reactions for the atmospheric oxidation of SO_2 are known, we review only those that have been studied.

a. Reaction of SO_2 and Atomic Oxygen

Sulfur dioxide can be converted to SO_3 through the reaction

$$SO_2 + O + M \rightarrow SO_3 + M \quad , \quad k_a = 2.8 \times 10^{-5}/\text{ppm}^2/\text{min} \quad . \qquad (C-1)$$

The source of oxygen atoms, $O(^3P)$, for Reaction (C-1) is largely from the photolysis of NO_2:

$$NO_2 + h\nu \rightarrow NO + O \quad . \qquad (C-2)$$

The primary competition for the oxygen atoms is from the ozone-forming reaction

$$O + O_2 + M \rightarrow O_3 + M \quad , \quad k_c = 2 \times 10^{-5}/\text{ppm}^2/\text{min} \quad . \qquad (C-3)$$

Oxygen atoms can be considered to be in a steady state as a result of Reactions (C-1) and (C-2) [Reaction (C-1) has a negligible effect on the concentration of oxygen atoms]:

$$[O]_{ss} = \frac{k_b[NO_2]}{k_c[O_2][M]} \quad .$$

The rate of Reaction (C-1) is estimated from:

$$\frac{d[SO_2]}{dt} = k_a[O]_{ss}[M] \quad ,$$

and thus, the characteristic time for SO_2 oxidation by Reaction (C-1) is:

$$\tau_a = \frac{k_c[O_2]}{k_a k_b[NO_2]} \quad .$$

Assuming $[NO_2] = 0.1$ ppm, $[O_2] = 2.1 \times 10^5$ ppm, and $k_b = 0.4$/min, a value typical of Los Angeles noonday intensities, we obtain $\tau_a \cong 4 \times 10^6$ min. Thus, the reaction of SO_2 with oxygen atoms is not an important SO_2 oxidizing process in the atmosphere.

b. Reaction of SO_2 and Hydroxyl Radicals

The characteristic time for the reaction

$$SO_2 + OH + M \rightarrow HOSO_2 + M \quad , \quad k_d = 9.8 \times 10^2\text{/ppm/min}^* \qquad \text{(C-4)}$$

(Atkinson, Perry, and Pitts, 1976) is:

$$\tau_d = \left\{ k_d[OH]^{-1} \right\} \quad .$$

Hydroxyl radical concentration measurements in ambient air were reported by Davis, Heaps, and McGee (1976). Peak OH concentrations in urban air were found to exceed 10^7 molecules/cm^3 ($\sim 10^{-7}$ ppm). Based on this value of [OH], we obtain $\tau_d \cong 10^4$ min. The fate of the $HOSO_2$ product is essentially unknown; it is usually assumed that it hydrates in some manner to form sulfuric acid.

c. Reaction of SO_2 and Hydroperoxyl Radicals

The characteristic time for the reaction

$$SO_2 + HO_2 \rightarrow SO_3 + OH \quad , \quad k_c = 1.3 \text{ ppm/min} \qquad \text{(C-5)}$$

(Payne, Stief, and Davis, 1973) is:

---

[*] Bimolecular rate constant at 760 torr.

$$\tau_e = \left\{ k_e[HO_2]^{-1} \right\} \quad .$$

Hydroperoxyl radical concentrations in ambient air have not been measured. Simulations of smog photochemistry yield approximate HO_2 concentrations of 10^{-4} ppm. Thus, we estimate $\tau_e \cong 0.8 \times 10^4$ min.

d. Reaction of SO_2 and Organic Free Radicals

Several reactions involving organic free radicals could possibly serve as SO_2-oxidizing steps, for example,

$$RO_2 + SO_2 \rightarrow SO_3 + RO \quad ,$$

$$RO + SO_2 + M \rightarrow ROSO_2 + M \quad .$$

Rate constants for these classes of reactions are generally not now known. Estimates for these rate constants appear in Table C-2.

TABLE C-2. ESTIMATED CONTRIBUTIONS TO ATMOSPHERIC SO_2 OXIDATION RATE BY HOMOGENEOUS CHEMICAL REACTIONS

Reaction	Rate Constant at 25°C (per ppm-min)	Contribution to SO_2 Oxidation Rate (%/hr)
$SO_2 + O + M \rightarrow SO_3 + M$	28*	1.5×10^{-3}
$SO_2 + OH + M \rightarrow HOSO_2 + M$	9.8×10^{2}*	0.6
$SO_2 + HO_2 \rightarrow SO_3 + OH$	1.3	0.75
$SO_2 + RO + M \rightarrow ROSO_2 + M$	5*	0.03[§]
$SO_2 + RO_2 \rightarrow SO_3 + RO$	1.5**	0.9[§]

---

* Pseudo-second order at 760 torr.

† Estimate (Sander and Seinfeld, 1976).

§ Assuming that $[RO_2] = 10^{-4}$ ppm and $[RO] = 10^{-6}$ ppm.

** An estimate based on the assumption that this reaction should proceed about 30 percent faster than that for $SO_2 + HO_2$ (Sander and Seinfeld, 1976).

e. Summary

Table C-2 summarizes the estimated contributions of the homogeneous reactions discussed in this section to the overall rate of SO_2 oxidation in the atmosphere. The total estimated SO_2 oxidation rate from these processes in a smoggy atmosphere is 2.3 percent per hour, a value comparable to those inferred from ambient measurements of SO_2-to-sulfate conversion rates.

2. HETEROGENEOUS OXIDATION OF SO_2

As noted above, the heterogeneous oxidation of SO_2 can take place through the following mechanisms:

- Liquid-phase oxidation of SO_2 by O_2
- Liquid-phase oxidation of SO_2 by O_3
- Metal-ion-catalyzed liquid-phase oxidation of SO_2
- Catalytic oxidation of SO_2 on particle surfaces.

In this section, we briefly review studies that have led to SO_2 oxidation rates for these mechanisms.

a. Liquid-Phase Oxidation of SO_2 by O_2

Although liquid-phase (uncatalyzed) oxidation of SO_2 by O_2 has been studied for many years, there is no clear understanding of the primary reaction mechanism. The rate of sulfate formation is usually expressed as first order in the concentration of sulfite ion:

$$\frac{d[SO_4^=]}{dt} = k_s[SO_3^=] \quad .$$

Table C-3 summarizes several values of k_s determined experimentally. Within the pH range 5 to 6, a reasonable average of the data is represented by $k_s \cong 10^{-3}$/sec. The rate constant recommended for use is that of Larson, Horike, and Harrison (1977).

TABLE C-3. RATE CONSTANTS k_s FOR THE LIQUID-PHASE OXIDATION OF SO_2 BY O_2*

k_s (per sec)	Comments	Reference
1.7×10^{-3}	pH = 6.8, 25°C from measurements of der Heuvel and Mason (1963)	Scott and Hobbs (1967)
3×10^{-3}	25°C	Miller and de Pena (1972)
3.5×10^{-3}	pH = 7, 25°C	Winkelmann (1955)
$3.7 \times 10^{-3} - 0.6 \times 10^{-3}$	pH = 4-6, 25°C with 0.6×10^{-3} at pH = 6†	Brimblecomb and Spedding (1974)
$6 \times 10^{-3} - 0.6 \times 10^{-3}$	pH = 7-8, 25°C†	Schroeter (1963)
$1.2 \times 10^{-4}[H^+]^{-0.16}$ ($[H^+]$ in mole/ℓ)	pH = 3-6, 25°C	Beilke, Lamb, and Mueller (1975)
$0.013 + 59[H^+]^{0.5}$ ($[H^+]$ in mole/ℓ)	pH = 6, 25°C from measurements of Fuller and Crist (1941)	McKay (1971)§
$k_1 + k_2[H^+]^{1/2} + k_3 p_{O_2} [H^+]^{-1}$ $k_1 = (4.8 \pm 0.6) \times 10^{-3}$/sec (298°K) $k_2 = (4.9 \pm 1.0)$/sec/$M^{1/2}$ $k_3 = (3.9 \pm 0.6) \times 10^{-12}$/sec/M atm	pH = 4-12, 5-25°C, p_{O_2} = 0.11-1.0 atm	Larson, Horike, and Harrison (1977)

---

* $d[SO_4^{=}]/dt = k_5 [SO_3^{=}]$.

† The value given in the table has been computed for the pH range stated by Beilke and Gravenhorst (1977).

§ Beilke and Gravenhorst (1977) concluded that the value obtained by McKay (1971), deduced from the measurements of Fuller and Crist (1941), is unrealistically high because Fuller and Crist did not account for the variation in pH during the course of the reaction.

b. Liquid-Phase Oxidation of SO_2 by O_3

Sulfur dioxide is oxidized in aqueous solution by ozone. In Table C-4 we summarize three studies that have led to rate expressions for this process. Larson, Horike, and Harrison (1977) evaluated the significance of the O_2 and O_3 reactions to the atmospheric oxidation of SO_2. They concluded that the O_3 oxidation is more important than the O_2 oxidation for O_3 concentrations equal to or greater than 0.05 ppm and for a solution pH less than about 5.5. Since rainwater pH in the eastern United States rarely exceeds 5.5, the uncatalyzed O_3 oxidation appears to dominate the O_2 oxidation.

Larson and his colleagues concluded that, owing to the relatively small amount of liquid water involved, neither the O_2 nor the O_3 oxidation is fast enough to produce significant quantities of sulfate in the liquid phase at humidities less than saturation. These reactions could occur only at a significant rate under saturated conditions, i.e., in fogs or clouds, where the liquid water content may exceed 0.1 g/m^3. For cloud conditions of $[O_3] = 0.05$ ppm, $[H_2O] = 0.6$ g/m^3, $[SO_2] = [NH_3] = 0.01$ ppm, the rate for SO_2 oxidation by O_3 is in the range of 1 to 4 percent per hour.

c. Metal-Ion-Catalyzed Liquid-Phase Oxidation of SO_2

The metal-ion-catalyzed liquid-phase oxidation of SO_2 has received considerable attention as a mechanism for SO_2 conversion in plumes and contaminated droplets. In general, the mechanisms proposed are lengthy, and the derived rate expressions are largely empirical. Table C-5 summarizes a variety of studies of this process. Observed rates vary substantially depending on the particular catalyst, relative humidity, and other conditions.

d. Catalytic Oxidation of SO_2 on Particle Surfaces

Novakov, Chang, and Harker (1974) have suggested that the surface of a soot particle serves as a catalyst for the oxidation of SO_2. Such a process might be of importance in a plume containing significant quantities of carbonaceous particles or in an atmosphere where motor vehicle soot aerosol is present. Very little is now known about the rates or mechanisms of this process.

TABLE C-4. LIQUID-PHASE OXIDATION OF SO_2 BY O_3

Author	Type of Mechanism	Rate Coefficient or Expression	Comments
Penkett (1972)	$HSO_3^- + O_3 \rightarrow HSO_4^- + O_2$	$\frac{d[O_3]}{dt} = k_o[O_3][HSO_3^-]$	9.6^oC; SO_2 oxidation rate extrapolated from data
		$k_o = 3.32 \times 10^5$ mole/ℓ/sec	
		SO_2 conversion ∿ 0.21 %/min	
Penkett and Garland (1974)	$HSO_3^- + O_3 \rightarrow HSO_4^- + O_2$	$-\frac{d[SO_2]}{dt} = k_s\ [SO_3^=]$	pH = 4-7; 10^oC; 0.1 ppm SO_2; 0.05 ppm O_3 in fog
		$k_s = 4.18 \times 10^{-4} + 1.77[H^+]^{1/2}$/sec	
Larson, Horike, and Harrison (1977)		$\frac{d[SO_4^=]}{dt} = +k_4K_{HO3}P_{O_3}[HSO_3]^{-0.1+0.02}$	pH = 4-12; T = 5-25°C; P_{O_3} = 0.2 - 1.0 ppm
		$k_4 = (4.4 \pm 2.0) \times 10^4/M^{0.9}$/sec ($298^oK$)	
		K_{HO_3} = 0.0123 atm	

TABLE C-5. METAL-ION-CATALYZED LIQUID-PHASE OXIDATION OF SO_2

Author	Type of Mechanism	Rate Coefficient or Expression	Comments
Fuller and Crist (1941)	Cu^{2+} catalyst; mannitol inhibitor	$k_s = 0.013 + 2.5[Cu^{2+}]$	25°C
Basset and Parker (1951)	Metal salts		Formation of complexes such as $[O_2\ Mn(SO_3)_2]^{2-}$ and rapid oxidation
Junge and Ryan (1958)	Fe^{2+} catalyst with and without NH_3		Conversion rate = 1.8×10^{-4} %/min
Foster (1969)	Metal salts; $2SO_2 + 2H_2O + O_2 \rightarrow 2H_2SO_4$	SO_2 conversion rate = 0.09 %/min for Mn, 0.15-1.5 %/min for Fe	Theoretical study; rates for Mn and Fe depend on many factors; rate for Fe catalyzed oxidation is pH dependent
Matteson, Stober, and Luther (1969)	SO_2 oxidation catalyzed by metal salts; $Mn^{2+} + SO_2 \rightleftarrows Mn \cdot SO_2^{2+}$ $2Mn \cdot SO_2^{2+} + O_2 \rightleftarrows [(Mn \cdot SO_2^{2+})_2 \cdot O_2]$ $\rightleftarrows 2Mn \cdot SO_3^{2+}$ $Mn \cdot SO_3^{2+} + H_2O \rightleftarrows Mn^{2+} + HSO_4^- + H^+$ $HSO_4^- + H^+ \rightleftarrows H_2SO_4$	$-\frac{d[SO_2]_g}{dt} = k_1[Mn^{2+}]_0^2$ $k_1 = 2.4 \times 10^5$/M/sec	Negligible $SO_4^=$ formation for RH < 95%; similar mechanism may be responsible for catalysis by other metal salts
Cheng, Corn, and Frohliger (1971)	SO_2 oxidation catalyzed by metal salts; $2SO_2 + 2H_2O + O_2 \xrightarrow{catalyst} 2H_2SO_4$	SO_2 conversion rate ~ 0.03 %/min with Mn^{2+} levels typical of urban industrial atmosphere; ~ 0.33 %/min with levels typical of plume from coal-powered plant	Oxidation rate estimated by extrapolation to atmospheric conditions
Chen and Barron (1972)	Sulfite oxidation catalyzed by cobalt ions; free radical mechanism; Co(III) reduced	$-\frac{d[SO_2]g}{dt} = k[Co(H_2O)^{3+}]^{1/2} \cdot [SO_{3=}]^{3/2}$	Could not determine specific value for k

TABLE C-5 (Concluded)

Author	Type of Mechanism	Rate Coefficient or Expression	Comments
Brimblecomb and Spedding (1974)	SO_2 oxidation by O_2 with trace Fe catalyst	$-\frac{d[S(IV)]}{dt} = k[Fe(III)][S(IV)]$ $k = 100/M/sec$; SO_2 conversion rate ~ 3.2 %/day in fog assuming 28 $\mu g/m^3$ SO_2 and 10^{-6} M Fe(III)	Possibility of Fe(III) contamination discussed
Freiberg (1974)	SO_2 oxidation catalyzed by Fe	$-\frac{d[SO_4^=]}{dt} = K_0 K_s^2 [H_2SO_3]^2 \cdot [Fe^{3+}]/[H^+]^2$ K_s = 1st dissociation constant of H_2SO_3	Rate increases rapidly with RH and decreases by about one order of magnitude with 5°C increase in temperature
Freiberg (1975)	SO_2 oxidation catalyzed by Fe	Same as above, except K_0 is a complex function of $[Fe^{3+}]$	Rate dependence changes from $[SO_2]^2/[H^+]^3$ to $[SO_2]/[H^+]$ as pH or $[SO_2]$ increases
Barrie and Georgii (1976)	Mn and Fe catalysts	$\frac{d[SO_4^=]}{dt} = k[SO_2]_g$	8°C and 25°C; 2.1 mm diameter droplets; 10^{-6} to 10^{-4} M for Mn and Fe; SO_2 concentrations 0.01-1.0 ppm. In pH range 2-4.5 the catalytic effectiveness was $Mn^{++} > Fe^{++} > Fe^{3+}$. Increase in T from 8° to 25°C caused an increase in Mn^{++} catalyzed oxidation rate of 5-10 in pH range 2-4.5
Betz reported in Beilke and Bravenhorst (1977)	Oxidation in homogeneous aqueous phase of rainwater; metal concentrations between 10^{-7}-10^{-6} M for Mn and 10^{-6}-10^{-5} M for Fe	$\frac{d[SO_4^=]}{dt} = k_0[SO_2]_g$ $k_0 = 1.95 \times 10^{16} \exp -\left(\frac{23,000}{RT}\right)$	Rainwater pH = 3.2-5.2

3. SULFATE FORMATION IN REMOTE AREAS

Modeling the atmospheric oxidation of sulfur dioxide (SO_2) into sulfate ($SO_4^=$) in remote areas is now a difficult task because of the following combination of circumstances:

- Detailed data showing SO_2 removal rates and sulfate formation rates are lacking, making model verification difficult.
- Theoretical and observational evidence indicates that removal rates are slow, and therefore, the choice of oxidation mechanisms is large. In polluted urban areas such as Los Angeles, the sulfate formation rate has been shown to be rather fast; so the choice of mechanisms is limited to those capable of fast SO_2 oxidation rates.
- The range of uncertainty in most currently considered oxidation mechanisms is large, which further compounds the difficulty.

The data requirements necessary to elucidate a proper modeling scheme for the oxidation of SO_2 go far beyond the normal requirements necessary to exercise a proven model. The areas where detailed data are now required begin in the near-stack region of plumes containing high SO_x emissions. For the purpose of modeling on a large scale, the emissions measured at the end of this region would conceivably be much more useful than measurements at the stack itself.

a. The Near-Stack Region of Plumes

From a modeling standpoint, very complex chemistry can conceivably occur in this near-stack region, which is characterized by the following qualities:

- Water droplet formation and evaporation.
- A steep concentration and temperature gradient along the centerline of the plume.

> The presence of fresh ash and possibly soot particulates.

The length of this region can typically be on the order of 1 km or less, so that in a regional-scale grid model the source could be at the end of this near-stack region and still be considered a point source within the same grid square as the stack. However, obtaining total SO_2 emissions and the initial sulfate concentration from the end of the near-stack region is also difficult. The difficulty stems primarily from the nonuniform concentrations within the plume itself at this point and the steep gradients that define the edges of the plume. Sulfate measurements in particular require large sample volumes averaged over time and space. Hence, the determination of sulfate emissions from the end of the near-stack region requires detailed information on the concentration gradients for the duration of the sampling period over the entire plume cross section in addition to the detailed path within that cross section from which the sample was taken.

Water droplet formation and evaporation are important considerations for two reasons: First, many sulfate formation mechanisms are known to take place within water droplets, and second, it has recently been demonstrated that SO_2 concentrations far beyond bulk equilibrium levels can occur in the surface layer of growing water droplets (Matteson, 1978). The steep concentration and thermal gradient further complicate any modeling efforts of this region. However, the most difficult phenomenon to model may be the deactivation of highly reactive sites often reported to exist on certain types of fly ash and soot particles. The overall effect of the near-stack region appears to be a rapid but limited conversion of SO_2. For this reason, trade-offs between the difficulties of obtaining appropriate data from the end of the near-stack region and the difficulties associated with properly modeling this complex region need to be carefully studied. At a minimum, some reliable and detailed data are necessary to validate any modeling effort or to confirm the necessity of even being concerned about this region of plumes.

b. The Downwind Region of Plumes

The near-stack problems just discussed can occur in a plume affecting any area. Once the plume has reasonably stabilized in temperature and in centerline concentration gradient and the water droplets have either stabilized or evaporated, then the problems of modeling sulfate formation begin on the time and spatial scale appropriate to the model being discussed: a regional model in a remote area during the several hours that a plume can contribute to visibility impairment. As outlined above, the basic problems are limited detailed data and a slow overall oxidation rate that is the sum of several simultaneous rates, each slow and uncertain. A brief discussion of some representative mechanisms follows.

1) Photolysis of SO_2

This mechanism has recently been reviewed by Calvert et al. (1978). Their study shows that the mechanism is complicated by electronic excited states undergoing systems crossing and quenching competition. In their review, an upper limit of 0.04 percent per hour was estimated for this mechanism to produce sulfate from SO_2 in bright sunlight.

2) Photochemical Oxidation

This mechanism was also reviewed by Calvert et al. (1978), who reported that the most important species involved were the radicals $OH\cdot$, $HO_2^\cdot$, and $RO_2^\cdot$, where R represents a hydrocarbon fragment. These radicals are involved in photochemical oxidation of methane in the troposphere (Crutzen and Fishman, 1977), and therefore, they would be present in remote atmospheres. The hydroxyl radical ($OH\cdot$) has been measured in remote areas (Davis, Heaps, and McGee, 1976). The concentrations of these radicals were found to be lower in remote areas than in highly polluted urban areas. In remote areas, $OH\cdot$ can be generated from short wavelength photolysis of ozone followed by the resulting excited oxygen atom reaction with water:

$$O_3 + h\nu(\lambda < 315\ nm) \rightarrow O_2 + O^{(ID)} \quad ,$$

$$O^{(ID)} + H_2O \rightarrow OH\cdot + OH\cdot \quad .$$

Hydroxl radicals might also be generated indirectly from other radicals by means of transfer reactions such as

$$HO_2^{\cdot} + NO \rightarrow OH\cdot + NO_2 \quad .$$

Some OH· might also come from olefinic natural hydrocarbons reacting with ozone. Calvert et al. estimated the upper limit for this photochemical mechanism to be 4 percent per hour in highly polluted urban areas. Because OH· radicals are present in remote areas, there appears to be a strong possibility that this mechanism explains a large part of the remote area rates in the range of 0.5 percent per hour. In fact, Calvert et al. estimated a midday rate of 0.4 percent per hour in remote areas due solely to the reaction with OH· radicals.

3) Water Droplet Mechanisms

Many paths of oxidation have been explored involving SO_2 dissolved in the aqueous phase. In most cases, the ability of SO_2 to dissolve is apparently a major factor because it is a function of acidity. Some of the important oxidizing factors that have been studied are the presence of ozone, hydrogen peroxide, catalytic ions, and soot particles. Two recent reviews on this subject were made by Levy, Drewes, and Hales (1976), and Orel and Seinfeld (1977). Virtually all of the above factors might play important roles in the sulfate formation in remote areas.

4) Particulate Mechanisms

This type of mechanism depends on relative humidity and the presence of reactive particles. Because the formation of sulfuric acid by one mechanism would lead to generation of water droplets in even a moderately humid atmosphere, this mechanism readily transforms into the other mechanisms. However, many reviews of sulfate formation discuss this type of mechanism because the growth of small particulates or droplets and SO_2 into larger particulates may also affect the rate of sulfate formation.

Because all of the four mechanisms discussed above are complicated to model quantitatively in remote areas, it appears that the assumption of a simple first-order decay of SO_2 to form sulfate is currently justified. A recent study by SAI has shown, however, that such an assumption is definitely not justified in the polluted Los Angeles atmosphere. In the study of Los Angeles, a highly detailed grid-type airshed model was used. Spatial and temporal resolution of the emissions, wind field, and photochemistry produced spatial and temporal agreement near 30 percent for nitrogen oxides and oxidant levels. However, when the photochemical production of sulfate (at rates up to 2 percent per hour in highly polluted midday grid cells) was combined with a first-order decay of approximately 3 percent per hour, very poor spatial agreement was observed (80 percent average disagreement). The observed data consisted of 24-hour-average sulfate measurements at 14 monitoring stations. The poor agreement occurred even though the overall basin average sulfate level between the model and the observations was empirically fit at about 19 $\mu g/m^3$. Sulfate predictions near the western SO_2 source region were low, and eastern downwind predictions were all too high. A basin-wide spatially consistent 30 percent agreement (with the oxidant predictions) with observations was obtained by combining the photochemical sulfate mechanism with a first-order rate linearly dependent on fog intensity. The water droplet mechanism that gave this result used 12 percent per hour in total fog and 0.5 percent in clear grid cells. If spatially dependent observational data in remote areas indicate that a uniform first-order conversion of SO_2 to sulfate is inappropriate, perhaps some important clues will be provided to improve the modeling of sulfate formation in remote areas.

APPENDIX D

DESCRIPTION OF THE PLUME VISIBILITY MODEL

APPENDIX D

DESCRIPTION OF THE PLUME VISIBILITY MODEL

The plume visibility model (PLUVUE) combines a plume dispersion and chemistry model with atmospheric optics and visual effects formulations. The relevant equations, assumptions, and limitations are presented in Chapter III and Appendix B. This appendix outlines the computational procedure (logic flow), program structure, and data requirements of the code.

1. COMPUTATIONAL PROCEDURE (LOGIC FLOW)

The data required by the computer code include:

- Wind speed.
- Stability category.
- Specification of diffusion type (Pasquill-Gifford-Turner, TVA).
- Atmospheric lapse rate.
- Mixing depth.
- Sun zenith angle.
- Ambient NO_x, NO_2, SO_2, O_3, and coarse mode aerosol concentrations.
- Background visual range.
- Properties of background and emitted aerosol modes: density, mass mean radius, geometric standard deviation.
- Reaction rates (pseudo-first-order) for sulfate and nitrate formation.
- Surface deposition velocities for SO_2, NO_x, sulfates, nitrates, and coarse particulate.

- Ambient temperature.
- Ambient relative humidity.
- Elevation of terrain.
- Number of stacks.
- Height of stacks.
- Emission rates from all stacks of SO_2, NO_x, and particulates.
- Flue gas flow rate per stack.
- Flue gas temperature.

Figure D-1 illustrates the basic calculations and program structure for the computer code.

The aerosol radiative properties, b_{scat} and b_{ext}, and $p(\Theta)$, are comuted by integrating over a lognormal size distribution with the specified mass median radius and geometric standard deviation. The scattering and absorption efficiency factors and the intensity for the two polarization components at a prescribed number of scattering angles are evaluated in the IBM subroutine DAMIE. The properties are evaluated at a selected number of wavelengths (currently 9), and a spline routine is used to interpolate the results to the final number of wavelengths (currently 39).

Either the background visual range or the accumuation mode concentration must be specified. When one is specified, the other can be computed from the Koschmieder relationship. The background atmospheric radiative properties, optical depths, mean albedo and mean phase functions are then computed. The background sky intensity as a function of angle of observation is predicted for both a Rayleigh atmosphere (only molecular scattering) and the atmosphere with the specified ambient aerosol and NO_2 concentration. The intensity of a "perfect" diffuse reflector normal to the direct solar beam is calculated for later use in color quantification. With this information, the chromaticity and intensity of the background sky are computed for different scattering and zenith angles. The chromaticity differences and the ΔE ($L^*u^*v^*$), ΔE ($L^*a^*b^*$) differences between the background and the Rayleigh atmosphere are then evaluated.

The spectral intensity of an object of a particular reflectivity and distance to the observer is computed next, and its chromaticity and light

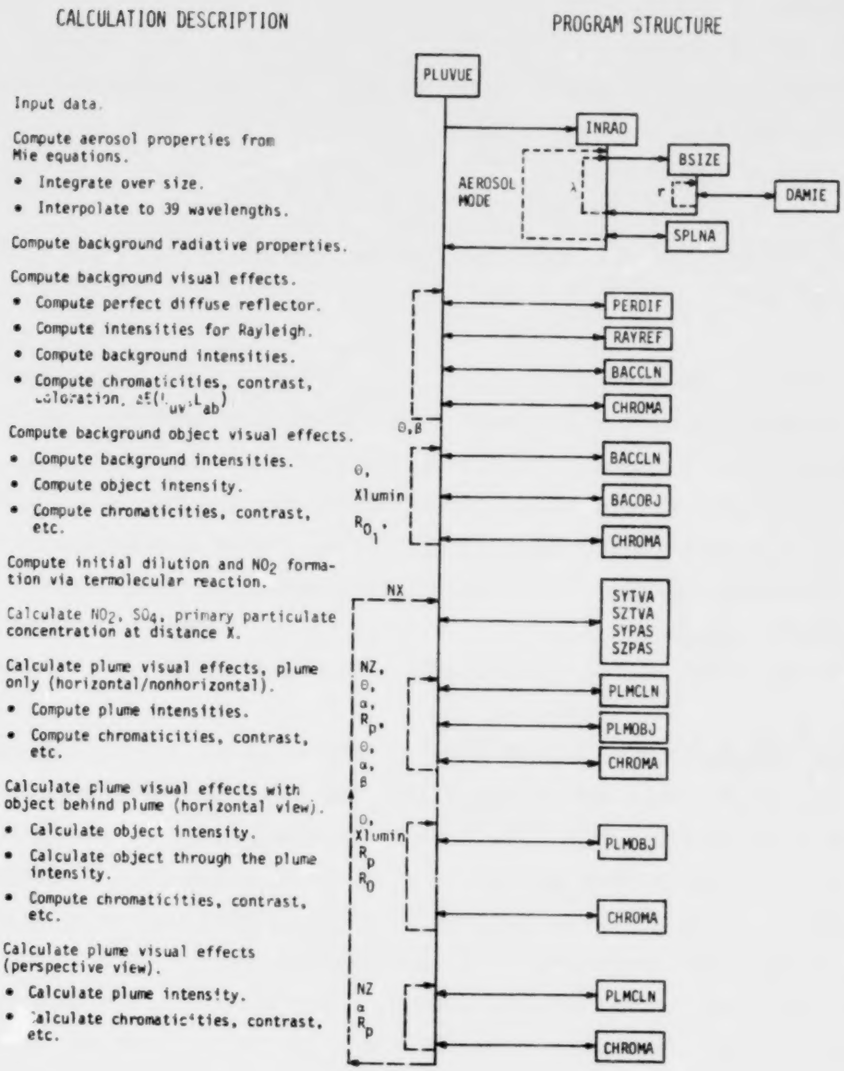

CALCULATION DESCRIPTION

Input data.

Compute aerosol properties from Mie equations.

- Integrate over size.
- Interpolate to 39 wavelengths.

Compute background radiative properties.

Compute background visual effects.

- Compute perfect diffuse reflector.
- Compute intensities for Rayleigh.
- Compute background intensities.
- Compute chromaticities, contrast, coloration, $\Delta E(L_{uv}, L_{ab})$

Compute background object visual effects.

- Compute background intensities.
- Compute object intensity.
- Compute chromaticities, contrast, etc.

Compute initial dilution and NO_2 formation via termolecular reaction.

Calculate NO_2, SO_4, primary particulate concentration at distance X.

Calculate plume visual effects, plume only (horizontal/nonhorizontal).

- Compute plume intensities.
- Compute chromaticities, contrast, etc.

Calculate plume visual effects with object behind plume (horizontal view).

- Calculate object intensity.
- Calculate object through the plume intensity.
- Compute chromaticities, contrast, etc.

Calculate plume visual effects (perspective view).

- Calculate plume intensity.
- Calculate chromaticities, contrast, etc.

PROGRAM STRUCTURE
PLUVUE
INRAD
BSIZE
AEROSOL MODE
λ
r
DAMIE
SPLNA
PERDIF
RAYREF
BACCLN
CHROMA
θ, β
θ,
Xlumin
R_{O_1},
BACCLN
BACOBJ
CHROMA
NX
SYTVA
SZTVA
SYPAS
SZPAS
NZ,
θ,
α,
R_p,
θ,
α,
β
PLMCLN
PLMOBJ
CHROMA
θ,
Xlumin
R_p
R_O
PLMOBJ
CHROMA
NZ
α
R_p
PLMCLN
CHROMA

FIGURE D-1. FLOWCHART OF THE COMPUTER CODE CALCULATIONS AND PROGRAM STRUCTURE FOR THE PLUME VISIBILITY MODEL intensity are predicted for different scattering angles, reflectivities, and distances from the observer. The object's coloration is then compared with that of the background sky in terms of chromaticity changes and ΔE values.

The program then begins the calculation of the concentrations of the plume by computing the initial dilution near the stack. The calculation of initial dilution is required to calculate accurately the initial conversion of NO to NO_2 via the termolecular reaction because of the rapid decrease in reaction rate with decreasing NO concentration. In this part of the code, the properties of the plume at 10-second intervals after emission from the top of the stack are calculated. These properties include plume rise, plume velocity, temperature, NO_2/NO ratio, and concentrations of O_2, NO_x, NO_2, particulates, and sulfur dioxide. The final NO_2/NO ratio calculated in this section of the code is used as a starting point for the calculations in the next part of the code for NO_2 at 16 downwind distances.

The code calculates the concentrations in the plume at 16 downwind distances starting at 1.2 km and ending at 350 km. Calculations are made for six altitudes at a given distance: plume centerline H, $H + 2\sigma_z$, $H + \sigma_z$, $H - \sigma_z$, $H - 2\sigma_z$, and at ground level. Pasquill or TVA diffusion coefficients (σ_y, σ_y) are computed from subroutines internal to the code or from values specified by the user. Conversion of NO to NO_2 is calculated taking into account the reaction with ozone, the thermal oxidation reaction, and the photodissociation of NO_2. The formation of sulfates and nitrates is calculated via a first-order rate constant for sulfur dioxide and nitrogen oxide reactions, respectively. Surface deposition is also calculated.

The visual effects are calculated taking into account the spatial distribution of primary and secondary particulate and NO_2 concentration at each of the 16 downwind distances for a variety of sight paths. Horizontal sight paths at 30°, 45°, 60° and 90° with respect to the plume axis are taken through the plume center and at ground level at different plume/observer distances. The plume optical depth, mean albedo, and phase function are first computed, and then the effect of the plume on the background intensity and the intensity of an object is evaluated for the given sight path. Finally, the chromaticity change and ΔE values at that particular downwind distance are computed.

2. PROGRAM STRUCTURE

The program consists of a main program, PLUVUE, and 19 subroutines. The main program reads the input cards, computes the plume concentrations, and prints the output. The various subroutines compute the radiative properties, spectral intensities and chromaticities, and coloration.

Specifically, the subroutine INRAD computes the aerosol radiative properties and the atmospheric radiative properties. The integration of the aerosol properties over the specific size distribution is done by subroutine BSIZE, which in turn calls the Mie equation subroutine DAMIE. The interpolation to the final number of wavelengths is done in a standard cubic spline package, SPLNA. The reason for the interpolation is that the Mie equations evaluation can be costly, and the dependence of the radiative properties for these assumed size distributions and refractive indices is rather smooth. A provision has been made to read in the radiative property data if desired, so that the Mie equation evaluation could be bypassed. The basic equations that INRAD and BSIZE use are described in Appendix B.

The subroutine PERDIF computes the values of spectral intensity of a perfect diffuse reflector that is normal to the direct solar beam. These values are used in the evaluation of color.

The subroutines RAYREF, BACCLN, BACOBJ, PLMCLN, and PLMOBJ compute the spectral intensity seen by an observer in differing situations. RAYREF and BACCLN compute the background atmospheric intensity [Eq. (21) in Section III.B.2]; RAYREF for an atmosphere with Rayleigh scattering only; and BACCLN for the background atmosphere. BACOBJ computes the intensity of an object [Eq. (22) in Section III.B.2] at a given distance and reflectivity. PLMCLN calculates the intensity that results from a plume at a specific distance from the observer against the background sky [Eqs. (21) and (25) through (28) in Section III. B.2]. PLMOBJ computes the effect of the plume in front of an object at a certain distance and reflectivity [Eqs. (22) and (26) through (29)].

The subroutine CHROMA computes the chromaticities and $\Delta E(L^*u^*v^*, L^*a^*b^*)$ values for two spectral intensities supplied as input. CHROMA then computes the chromaticity differences and ΔE values. It also calculates the contrast and intensity ratios at specific wavelengths.

3. PROGRAM USE

The program requires the input cards listed in Table D-1.

TABLE D-1. DATA REQUIREMENTS FOR THE PLUME VISIBILITY COMPUTER PROGRAM

Card No.	Format	Variables	Description
1	6A4	PLANT	Name of source or other label
2	F5.1	U	Wind speed (mph)
	I5	I	Stability under (1, 2, 3, ...,)
	F5.2	ALAPSE	Lapse rate (°F/1000ft)
	F5.1	ZENITH	Solar zenith angle (degrees)
3	F10.1	HPBLM	Mixing depth height (m)
4	F10.3	RH	Relative humidity (percent)
5	I5	ITVA	Index indicating diffusion parameters to be used for stability index I ("1" for TVA, "0" for Pasquill-Gifford-Turner values, "9" for user input values)
6	I5	IPERS	Index "I" if perspective view with user-input r_p and (see Cards 21-35)
7	I2	IFLG1	Index for output tables 1, 2, 3 at each downwind distance: "1" means output desired; "0" means output table is not desired
	I2	IFLG2	
	I2	IFLG3	
	I2	NX1	Indices (1-16) for downwind distances desired (it is preferable to start with NX1=1)
	I2	NX2	
	I2	NT1	Limits for scattering angles desired: θ = 22°, 45°, 90°, 135°, 158° and 180°
		NT2	
	I2	NZF	Index for the number of altitudes for visual impact calculations: "1" for plume centers only, "2" for ground-level also

TABLE D-1 (Continued)

Card No.	Format	Variable	Description
8	F10.2	QSO_2	Total SO_2, NO_x, and primary particle emissions rates (from all stacks), in tons/day
	F10.2	QNO_x	
	F10.2	QPART	
9	F10.1	FLOW	Flue gas flow rate (acfm) per stack
	F10.1	FGTEMP	Flue gas temperature (°F)
	F10.1	FGO2	Flue gas oxygen concentration mole percent
10	F5.1	UNITS	Number of stacks
	F5.1	HSTACK	Stack height (ft)
11	F10.0	ELEV	Elevation of plant site (ft MSL)
12	F10.1	TAMB	Ambient temperature (°F)
13	F10.3	AMBNOX	Ambient $[NO_x]$ in ppm
	F10.3	AMBNO2	Ambient $[NO_2]$ in ppm
	F10.3	O3AMB	Ambient $[O_3]$ in ppm
	F10.3	$AMBSO_2$	Ambient $[SO_2]$ in ppm
14	F10.3	RSO_2C	$SO_2 \rightarrow SO_4^{=}$ conversion rate (%/hr)
	F10.3	RNO_xC	$NO_x \rightarrow NO_3^{-}$ conversion rate (%/hr)
15	F10.3	ROVA	Mass median radius (μm) background accumulation mode
	F10.3	ROVC	Mass median radius (μm) background coarse mode
	F10.3	ROVS	Mass median radius (μm) plume secondary particulate
	F10.3	ROVP	Mass median radius (μm) emitted emitted primary particulate
16	F10.3	SIGA	Geometric standard deviation, accumulation mode
	F10.3	SIGC	Geometric standard deviation, coarse mode
	F10.3	SIGS	Geometric standard deviation, secondary particulate
	F10.3	SIGP	Geometric standard deviation, emitted primary particulate

TABLE D-1 (Concluded)

Card No.	Format	Variable	Description
17	F10.3	DENA	Particle density (g/cm^3), background accumulation mode
	F10.3	DENC	Particle density (g/cm^3), background coarse mode
	F10.3	DENS	Particle density (g/cm^3), plume secondary particulate
	F10.3	DENP	Particle density (g/cm^3), emitted primary particulate
18	F10.3	CORAMB	Ambient coarse mode mass concentration ($\mu g/m^3$)
19	I5	INTYP	Switch for next card (INTYP=1, AMBSO$_4$ INTYP≠1, RVAMB)
20(INTYP≠1)	F10.3	RVAMB	Background visual range (km)
20(INTYP=1)	F10.3	AMBSO$_4$	Background sulfate mass concentration ($\mu g/m^3$)
	F10.3	AMBNO$_3$	Background nitrate mass concentration ($\mu g/m^3$)
21	F5.2	VDSO$_2$	Deposition velocity (cm/sec) for SO_2
	F5.2	VDNO$_x$	Deposition velocity (cm/sec) for NO_x
	F5.2	VDCOR	Deposition velocity (cm/sec) for coarse particles
	F5.2	VDSUB	Deposition velocity (cm/sec) for submicron particles
22	I5	INCON	Switch for time-dependent sulfate and nitrate formation rates: "1" if desired; "0" if not
23	16F5.2	RSO$_2$(NX)	Sulfate formation rate (percent/hr) at each downwind distance NX
24	16F5.2	RNO$_x$(NX)	Nitrate formation rate (percent/hr) at each downwind distance NX
25-40	F10.1	RP	Distance (km) between observer and plume (for perspective runs only)
	F10.1	ALPHA	Azimuthal angle between sight path and plume centerline (for perspective views only)

APPENDIX E
PLUME MODEL SAMPLE OUTPUT

APPENDIX E

PLUME MODEL SAMPLE OUTPUT

This appendix displays two examples of the plume visibility output. The first shows output for a plume from a hypothetical 2250 Mwe coal-fired power plant during stable (Pasquill E) conditions. This sample output shows the near-source plume impact from 1.2 to 10 km downwind. At each downwind distance, the following tables are displayed:

> Pollutant concentrations.
> Visual effects for horizontal sight paths.
> Visual effects for nonhorizontal sight paths.
> Visual effects for horizontal views of various colored objects.

The second illustration is for the plume from a copper smelter during neutral conditions (TVA Category 1) with a capping layer at 2000 m. For this example, we show the output of pollutant concentrations and horizontal visual effects at large downwind distances (15, 100, 200, and 300 km.)

EXAMPLE 1: OUTPUT FOR A PLUME FROM A HYPOTHETICAL 2250 MWE COAL-FIRED POWER PLANT

```
VISUAL IMPACT ASSESSMENT FOR 2230 MW COAL POWER PLANT

   POWER PLANT DATA

       ELEVATION OF SITE =          0.  FEET MSL
                                    0.  METERS MSL

       NO. OF UNITS =     3.

       STACK HEIGHT =  700.  FEET
                       213.  METERS

       FLUE GAS FLOW RATE =   1724000.  CU FT/MIN
                                813.32  CU M/SEC

       FLUE GAS TEMPERATURE =        230.  F
                                     394.  K

       FLUE GAS OXYGEN CONTENT =         1.7  MOL PERCENT

       SO2 EMISSION RATE (TOTAL) =      276.43  TONS/DAY
                                     2.903E+03  G/SEC

       NOX EMISSION RATE (TOTAL,AS NO2) =      161.23  TONS/DAY
                                            1.693E+03  G/SEC

       PARTICULATE EMISSION RATE (TOTAL) =        3.43  TONS/DAY
                                             3.623E+01  G/SEC
```

```
METEOROLOGICAL AND AMBIENT AIR QUALITY DATA

     WINDSPEED =  11.2  MILES/HR
                   3.0  M/SEC

     PASQUILL-GIFFORD-TURNER STABILITY CATEGORY E

     LAPSE RATE =  0.00  F/1000 FT
                     0.          K/M

     POTENTIAL TEMPERATURE LAPSE RATE =    9.800E-03  K/M

     SOLAR ZENITH ANGLE =  43.0  DEGREES

     AMBIENT TEMPERATURE =  77.0  F
                           298.2  K

     RELATIVE HUMIDITY =  40.0  %

     MIXING DEPTH = 2000.  M

     AMBIENT PRESSURE =  1.00  ATM

     SO2 TO SO4 CONVERSION RATE =       .300 PERCENT/HR

     NOX TO NO3 CONVERSION RATE =      0.000 PERCENT/HR

     BACKGROUND NOX CONCENTRATION =      0.000  PPM

     BACKGROUND NO2 CONCENTRATION =      0.000  PPM

     BACKGROUND OZONE CONCENTRATION =       .040  PPM

     BACKGROUND SO2 CONCENTRATION =      0.000  PPM

     BACKGROUND COARSE MODE CONCENTRATION =       30.0  UG/M3

     BACKGROUND SULFATE CONCENTRATION =        1.7  UG/M3

     BACKGROUND NITRATE CONCENTRATION =        0.0  UG/M3

     BACKGROUND VISUAL RANGE =      130.0  KILOMETERS

     SO2 DEPOSITION VELOCITY =       1.00  CM/SEC

     NOX DEPOSITION VELOCITY =       1.00  CM/SEC

     COARSE PARTICULATE DEPOSITION VELOCITY =        .10  CM/SEC

     SUBMICRON PARTICULATE DEPOSITION VELOCITY =        .10  CM/SEC
```

```
                         BACKGROUND CONDITIONS

ACCUMULATION MODE                              COARSE PARTICLE MODE                                PRIMARY PARTICLE MODE
MASS RADIUS     SIGMA    BETA.55/MASS            MASS RADIUS      SIGMA    BETA.55/MASS              MASS RADIUS     SIGMA     BETA.55/MASS
 .1700E+00    .2100E+01    .5811E-02                .3000E+01    .2200E+01    .3343E-03                 .5000E+00    .2000E+01    .2003E-02

                           COEFFICIENTS AT 0.55 MICROMETERS , 1./KM
  BETARAY = .1000E-01   BETAAER = .2017E-01   ABSNO2 =0.                BETABAC = .3009E-01

NO.  WAVELN     TAUT02Z      TAUT0DI     PAER

 1  .3700E+00  .5882E+00  .2071E+02  .4672E+03  .4934E+01  .1510E+01  .2216E+00  .1300E+00  .3067E+00  .5936E+00
 2  .3800E+00  .5334E+00  .1891E+02  .4478E+03  .4890E+01  .1515E+01  .2189E+00  .1328E+00  .3001E+00  .5721E+00
 3  .3900E+00  .4837E+00  .1735E+02  .4301E+03  .4841E+01  .1517E+01  .2173E+00  .1343E+00  .2966E+00  .5579E+00
 4  .4000E+00  .4443E+00  .1599E+02  .4147E+03  .4786E+01  .1513E+01  .2177E+00  .1346E+00  .2972E+00  .5565E+00
 5  .4100E+00  .4082E+00  .1482E+02  .4020E+03  .4723E+01  .1509E+01  .2200E+00  .1329E+00  .3029E+00  .5698E+00
 6  .4200E+00  .3767E+00  .1380E+02  .3911E+03  .4655E+01  .1502E+01  .2236E+00  .1300E+00  .3125E+00  .5919E+00
 7  .4300E+00  .3490E+00  .1290E+02  .3814E+03  .4590E+01  .1497E+01  .2278E+00  .1266E+00  .3244E+00  .6142E+00
 8  .4400E+00  .3242E+00  .1210E+02  .3719E+03  .4536E+01  .1493E+01  .2313E+00  .1233E+00  .3371E+00  .6273E+00
 9  .4500E+00  .3017E+00  .1136E+02  .3623E+03  .4501E+01  .1500E+01  .2337E+00  .1215E+00  .3489E+00  .6214E+00
10  .4600E+00  .2810E+00  .1066E+02  .3521E+03  .4491E+01  .1512E+01  .2340E+00  .1214E+00  .3581E+00  .5900E+00
11  .4700E+00  .2620E+00  .1002E+02  .3420E+03  .4501E+01  .1527E+01  .2327E+00  .1226E+00  .3643E+00  .5415E+00
12  .4800E+00  .2447E+00  .9423E+01  .3323E+03  .4518E+01  .1544E+01  .2308E+00  .1246E+00  .3673E+00  .4887E+00
13  .4900E+00  .2292E+00  .8887E+01  .3237E+03  .4531E+01  .1539E+01  .2293E+00  .1267E+00  .3669E+00  .4445E+00
14  .5000E+00  .2154E+00  .8420E+01  .3164E+03  .4528E+01  .1568E+01  .2292E+00  .1282E+00  .3627E+00  .4222E+00
15  .5100E+00  .2035E+00  .8024E+01  .3106E+03  .4499E+01  .1571E+01  .2311E+00  .1286E+00  .3548E+00  .4326E+00
16  .5200E+00  .1932E+00  .7688E+01  .3056E+03  .4453E+01  .1568E+01  .2345E+00  .1285E+00  .3449E+00  .4730E+00
17  .5300E+00  .1840E+00  .7395E+01  .3010E+03  .4406E+01  .1563E+01  .2385E+00  .1281E+00  .3353E+00  .5365E+00
18  .5400E+00  .1757E+00  .7129E+01  .2964E+03  .4373E+01  .1553E+01  .2422E+00  .1280E+00  .3288E+00  .6134E+00
19  .5500E+00  .1679E+00  .6875E+01  .2915E+03  .4374E+01  .1543E+01  .2445E+00  .1287E+00  .3283E+00  .7009E+00
20  .5600E+00  .1603E+00  .6620E+01  .2861E+03  .4422E+01  .1533E+01  .2447E+00  .1303E+00  .3362E+00  .7830E+00
21  .5700E+00  .1530E+00  .6365E+01  .2805E+03  .4503E+01  .1522E+01  .2431E+00  .1328E+00  .3502E+00  .8515E+00
22  .5800E+00  .1460E+00  .6116E+01  .2747E+03  .4595E+01  .1507E+01  .2404E+00  .1332E+00  .3670E+00  .8959E+00
23  .5900E+00  .1394E+00  .5876E+01  .2687E+03  .4673E+01  .1490E+01  .2370E+00  .1370E+00  .3832E+00  .9055E+00
24  .6000E+00  .1333E+00  .5651E+01  .2626E+03  .4717E+01  .1471E+01  .2337E+00  .1377E+00  .3952E+00  .8696E+00
25  .6100E+00  .1276E+00  .5444E+01  .2564E+03  .4704E+01  .1451E+01  .2311E+00  .1370E+00  .4003E+00  .7834E+00
26  .6200E+00  .1225E+00  .5237E+01  .2504E+03  .4643E+01  .1431E+01  .2293E+00  .1352E+00  .3997E+00  .6671E+00
27  .6300E+00  .1178E+00  .5090E+01  .2447E+03  .4551E+01  .1413E+01  .2285E+00  .1330E+00  .3957E+00  .5475E+00
28  .6400E+00  .1137E+00  .4942E+01  .2396E+03  .4442E+01  .1404E+01  .2291E+00  .1310E+00  .3904E+00  .4519E+00
29  .6500E+00  .1100E+00  .4815E+01  .2353E+03  .4335E+01  .1401E+01  .2311E+00  .1299E+00  .3863E+00  .4089E+00
30  .6600E+00  .1068E+00  .4708E+01  .2319E+03  .4243E+01  .1407E+01  .2347E+00  .1304E+00  .3830E+00  .4389E+00
31  .6700E+00  .1040E+00  .4615E+01  .2290E+03  .4172E+01  .1421E+01  .2393E+00  .1322E+00  .3865E+00  .5274E+00
32  .6800E+00  .1014E+00  .4532E+01  .2264E+03  .4124E+01  .1439E+01  .2441E+00  .1349E+00  .3902E+00  .6420E+00
33  .6900E+00  .9895E-01  .4453E+01  .2237E+03  .4103E+01  .1458E+01  .2483E+00  .1382E+00  .3954E+00  .7592E+00
34  .7000E+00  .9655E-01  .4372E+01  .2206E+03  .4110E+01  .1473E+01  .2508E+00  .1415E+00  .4019E+00  .8463E+00
35  .7100E+00  .9409E-01  .4284E+01  .2168E+03  .4148E+01  .1481E+01  .2511E+00  .1444E+00  .4090E+00  .8782E+00
36  .7200E+00  .9160E-01  .4192E+01  .2125E+03  .4213E+01  .1481E+01  .2492E+00  .1469E+00  .4166E+00  .8586E+00
37  .7300E+00  .8909E-01  .4096E+01  .2078E+03  .4299E+01  .1476E+01  .2457E+00  .1490E+00  .4248E+00  .7991E+00
38  .7400E+00  .8661E-01  .3999E+01  .2027E+03  .4399E+01  .1467E+01  .2410E+00  .1509E+00  .4333E+00  .7121E+00
39  .7500E+00  .8420E-01  .3903E+01  .1976E+03  .4508E+01  .1455E+01  .2336E+00  .1526E+00  .4420E+00  .6101E+00
```

VISUAL EFFECTS CAUSED BY BACKGROUND ATMOSPHERE (WITHOUT PLUME)
*** CLEAR SKY VIEWS ***

THETA	BETA	TAU	YCAP	L	X	Y	DELYCAP	DELL	C(400)	C(550)	C(700)	BRATIO	DELX	DELY	E(LUV)	E(LAB)
22.	0.	6.87	208.61	132.18	.3409	.3462	103.06	30.08	.3906	.8897	1.8769	.4834	.0357	.0221	44.6680	35.3720
	15.	.65	86.43	94.30	.2930	.3041	52.59	29.64	.2697	1.5363	3.6875	.2709	.0537	.0377	42.7131	35.4569
	30.	.34	51.34	77.02	.2830	.2914	31.29	24.87	.2698	1.5446	3.6901	.2707	.0513	.0384	33.4713	29.3383
	45.	.24	38.17	68.18	.2796	.2868	22.87	22.09	.2596	1.4988	3.5837	.2747	.0500	.0377	28.9426	26.0450
	60.	.19	31.83	63.23	.2781	.2847	18.83	20.43	.2483	1.4546	3.4898	.2780	.0492	.0371	26.4661	24.1520
	75.	.17	28.81	60.65	.2774	.2837	16.90	19.53	.2403	1.4253	3.4274	.2801	.0488	.0367	25.1872	23.1479
	90.	.17	27.91	59.84	.2771	.2834	16.32	19.24	.2374	1.4152	3.4059	.2809	.0487	.0366	24.7891	22.8315
45.	0.	6.87	110.53	103.93	.3184	.3313	18.44	7.07	.0384	.1844	.6563	.6390	.0152	.0097	13.9237	9.9126
	15.	.65	49.55	73.81	.2731	.2895	19.92	14.45	-.0146	.6959	1.8252	.3488	.0369	.0450	26.7599	20.7632
	30.	.34	29.77	61.49	.2655	.2760	12.11	12.36	.0011	.7177	1.8439	.3520	.0347	.0447	20.6836	17.3462
	45.	.24	22.10	54.17	.2623	.2712	8.79	10.90	-.0011	.6942	1.7900	.3580	.0336	.0437	17.6649	15.3729
	60.	.19	18.45	50.07	.2608	.2690	7.16	9.97	-.0071	.6686	1.7376	.3627	.0329	.0430	16.0248	14.2198
	75.	.17	16.71	47.93	.2601	.2680	6.38	9.46	-.0118	.6510	1.7029	.3656	.0325	.0426	15.1837	13.6050
	90.	.17	16.19	47.26	.2599	.2677	6.14	9.29	-.0136	.6449	1.6909	.3666	.0324	.0425	14.9229	13.4110
90.	0.	6.87	64.12	84.04	.3000	.3111	-9.26	-4.60	-.0536	-.1380	.0762	.8794	.0008	-.0059	6.4645	5.7798
	15.	.65	29.82	61.53	.2633	.2744	6.04	5.63	-.1374	.2684	.8950	.4446	.0272	.0334	18.1834	12.6828
	30.	.34	18.02	49.56	.2541	.2608	3.95	5.19	-.1325	.3008	.9265	.4503	.0252	.0327	13.7199	10.6172
	45.	.24	13.40	43.40	.2511	.2560	2.86	4.56	-.1292	.2917	.9017	.4579	.0242	.0318	11.5752	9.4079
	60.	.19	11.20	39.95	.2497	.2538	2.29	4.10	-.1311	.2778	.8737	.4637	.0236	.0311	10.4403	8.7075
	75.	.17	10.14	38.14	.2490	.2528	2.01	3.83	-.1335	.2676	.8545	.4673	.0232	.0307	9.8713	8.3374
	90.	.17	9.83	37.58	.2488	.2525	1.92	3.75	-.1344	.2639	.8478	.4684	.0231	.0305	9.6968	8.2212
135.	0.	6.87	67.25	85.64	.2962	.3078	-24.84	-11.22	-.1169	-.2824	-.1689	1.0626	-.0070	-.0139	13.7082	12.6947
	15.	.65	34.22	65.17	.2594	.2704	4.60	3.81	-.1506	.1614	.5979	.5316	.0212	.0239	15.7605	10.4351
	30.	.34	20.76	52.72	.2503	.2566	3.10	3.60	-.1295	.1860	.6168	.5384	.0195	.0232	11.9561	8.7032
	45.	.24	15.46	46.30	.2472	.2517	2.15	3.03	-.1291	.1726	.5887	.5482	.0185	.0242	10.1441	7.6645
	60.	.19	12.92	42.69	.2459	.2495	1.63	2.58	-.1334	.1562	.5600	.5555	.0179	.0235	9.2144	7.0697
	75.	.17	11.71	40.79	.2452	.2484	1.38	2.32	-.1371	.1446	.5407	.5601	.0176	.0231	8.7599	6.7606
	90.	.17	11.35	40.20	.2451	.2481	1.30	2.23	-.1385	.1405	.5340	.5616	.0175	.0229	8.6228	6.6647
158.	0.	6.87	78.98	91.23	.3021	.3120	-26.57	-10.87	-.1267	-.2733	-.1061	.9770	-.0031	-.0121	13.4426	12.4765
	15.	.65	40.73	70.01	.2623	.2728	6.89	5.15	-.1272	.2008	.7229	.5066	.0230	.0264	16.9212	11.2614
	30.	.34	24.69	56.81	.2529	.2589	4.44	4.65	-.1090	.2213	.7363	.5131	.0212	.0259	12.8980	9.3774
	45.	.24	18.38	50.00	.2498	.2540	3.08	3.91	-.1108	.2043	.7014	.5226	.0202	.0249	10.9650	8.2295
	60.	.19	15.36	46.17	.2484	.2517	2.36	3.36	-.1165	.1852	.6675	.5299	.0195	.0241	9.9673	7.5665
	75.	.17	13.92	44.16	.2477	.2507	2.01	3.04	-.1211	.1720	.6450	.5343	.0192	.0237	9.4779	7.2204
	90.	.17	13.49	43.53	.2476	.2504	1.90	2.94	-.1228	.1674	.6373	.5358	.0191	.0236	9.3301	7.1127
180.	0.	6.87	91.22	96.50	.3122	.3200	-19.58	-7.53	-.1083	-.1897	.0879	.8196	.0063	-.0049	11.7559	9.6383
	15.	.65	45.89	73.50	.2688	.2781	10.41	7.35	-.1027	.3064	1.0237	.4434	.0291	.0312	20.7951	13.9390
	30.	.34	27.75	59.70	.2590	.2640	6.49	6.43	-.0864	.3245	1.0339	.4492	.0270	.0305	15.8738	11.5107
	45.	.24	20.65	52.60	.2558	.2591	4.37	5.48	-.0892	.3042	.9904	.4576	.0259	.0295	13.5176	10.0998
	60.	.19	17.25	48.61	.2544	.2569	3.58	4.82	-.0956	.2824	.9492	.4640	.0252	.0287	12.2872	9.2880
	75.	.17	15.63	46.53	.2537	.2558	3.10	4.44	-.1007	.2676	.9221	.4679	.0248	.0283	11.6758	8.8623
	90.	.17	15.15	45.87	.2535	.2555	2.96	4.32	-.1026	.2624	.9127	.4692	.0247	.0281	11.4896	8.7294

```
VISUAL EFFECTS CAUSED BY BACKGROUND ATMOSPHERE (WITHOUT PLUME)
*** WHITE, GRAY, AND BLACK OBJECTS AT INDICATED DISTANCES ***

THETA  RO/RV REFLECT   YCAP      L       X       Y DELYCAP    DELL   C(400)   C(550)   C(700)  BRATIO    DELX    DELY  E(LUV)  E(LAB)

 22.     .02   1.00   107.99  103.01  .3300  .3402 -100.61  -29.17  -.4431  -.4716  -.4894  1.0908  -.0109  -.0060 31.2890 29.8706
         .05   1.00   118.88  106.88  .3277  .3374  -89.72  -25.30  -.3495  -.4192  -.4300  1.1826  -.0132  -.0088 28.7123 26.4961
         .10   1.00   134.45  112.02  .3262  .3354  -74.16  -20.16  -.2335  -.3445  -.3910  1.2554  -.0147  -.0107 25.3648 22.0917
         .20   1.00   157.89  119.06  .3270  .3357  -50.71  -13.13  -.1068  -.2324  -.2945  1.2660  -.0139  -.0104 20.0222 15.8535
         .50   1.00   192.37  128.24  .3337  .3415  -16.24   -3.95  -.0100  -.0708  -.1222  1.1278  -.0072  -.0047  8.8827  6.0664
         .80   1.00   203.57  130.98  .3381  .3446   -5.04   -1.20  -.0010  -.0208  -.0458  1.0470  -.0028  -.0016  3.3506  2.1502
        1.00   1.00   206.46  131.67  .3396  .3455   -2.15    -.51  -.0002  -.0087  -.0204  1.0206  -.0013  -.0007  1.5240   .9611
         .02    .50    61.68   82.76  .3250  .3349 -146.92  -49.42  -.6484  -.6981  -.7179  1.2463  -.0159  -.0113 51.4969 50.1478
         .05    .50    77.59   90.60  .3200  .3293 -131.01  -41.58  -.5116  -.6206  -.6606  1.4394  -.0209  -.0168 45.8549 43.1629
         .10    .50   100.33  100.13  .3178  .3269 -108.28  -32.06  -.3446  -.5101  -.5749  1.5418  -.0231  -.0192 39.2661 34.8201
         .20    .50   134.55  112.05  .3198  .3291  -74.06  -20.13  -.1564  -.3444  -.4347  1.4924  -.0211  -.0171 29.9706 24.0728
         .50    .50   184.77  126.31  .3304  .3390  -23.84   -5.87  -.0146  -.1054  -.1843  1.2080  -.0105  -.0072 12.9889  8.9293
         .80    .50   201.04  130.37  .3366  .3437   -7.56   -1.81  -.0014  -.0315  -.0733  1.0776  -.0043  -.0024  5.0500  3.2405
        1.00    .50   205.24  131.38  .3388  .3431   -3.37    -.80  -.0003  -.0136  -.0364  1.0374  -.0021  -.0011  2.4597  1.5399
         .02   0.00    15.37   46.18  .2944  .3020 -193.24  -86.00  -.8538  -.9246  -.9464  2.7268  -.0465  -.0441 89.8687 87.6880
         .05   0.00    36.30   66.78  .2973  .3056 -172.31  -65.40  -.6736  -.8221  -.8712  2.5348  -.0436  -.0406 72.7406 68.3776
         .10   0.00    66.21   85.12  .3019  .3110 -142.40  -47.07  -.4537  -.6737  -.7588  2.2647  -.0390  -.0352 58.0835 51.4397
         .20   0.00   111.20  104.17  .3100  .3200  -97.41  -28.01  -.2059  -.4365  -.5749  1.8681  -.0309  -.0261 41.7144 33.5441
         .50   0.00   177.18  124.34  .3268  .3364  -31.43   -7.84  -.0193  -.1401  -.2464  1.3014  -.0141  -.0098 17.2681 11.8941
         .80   0.00   198.52  129.76  .3331  .3429  -10.09   -2.43  -.0018  -.0422  -.1009  1.1101  -.0058  -.0033  6.7707  4.3427
        1.00   0.00   204.01  131.09  .3380  .3447   -4.59   -1.09  -.0004  -.0185  -.0524  1.0548  -.0029  -.0015  3.4015  2.1222

 45.     .02   1.00   100.82  100.32  .3306  .3412   -9.71   -3.62  -.2592  -.0962  -.0268   .7612   .0122   .0099 11.9128  7.7332
         .05   1.00   101.94  100.74  .3283  .3388   -8.60   -3.19  -.2045  -.0855  -.0239   .8150   .0099   .0074  9.6825  6.2836
         .10   1.00   103.52  101.34  .3234  .3358   -7.02   -2.59  -.1378  -.0704  -.0195   .8794   .0070   .0045  6.9130  4.5202
         .20   1.00   105.85  102.22  .3219  .3327   -4.68   -1.72  -.0625  -.0476  -.0123   .9491   .0035   .0013  3.6805  2.5129
         .50   1.00   109.15  103.43  .3189  .3308   -1.39    -.50  -.0059  -.0148   .0006   .9935   .0005  -.0005   .9513   .7312
         .80   1.00   110.15  103.79  .3186  .3310    -.39    -.14  -.0006  -.0047   .0063   .9931   .0002  -.0003   .4156   .3130
        1.00   1.00   110.39  103.88  .3186  .3312    -.14    -.05  -.0002  -.0022   .0082   .9917   .0002  -.0002   .3046   .2104
         .02    .50    54.51   78.78  .3256  .3361  -56.02  -25.16  -.5565  -.5105  -.4867   .8640   .0072   .0048 26.4006 25.5727
         .05    .50    60.65   82.20  .3189  .3294  -49.89  -21.73  -.4391  -.4539  -.4478  1.0159   .0005  -.0020 21.9210 21.7823
         .10    .50    69.39   86.71  .3129  .3238  -41.14  -17.22  -.2957  -.3733  -.3896  1.1538  -.0035  -.0075 17.5968 17.4367
         .20    .50    82.50   92.80  .3093  .3213  -28.03  -11.13  -.1342  -.2525  -.2944  1.2271  -.0091  -.0100 13.3500 12.1276
         .50    .50   101.55  100.60  .3122  .3259   -8.98   -3.34  -.0126  -.0782  -.1244  1.1277  -.0062  -.0054  6.3540  4.6746
         .80    .50   107.62  102.87  .3157  .3293   -2.91   -1.06  -.0012  -.0243  -.0490  1.0503  -.0027  -.0020  2.5962  1.7316
        1.00    .50   109.17  103.44  .3170  .3303   -1.37    -.50  -.0003  -.0112  -.0240  1.0242  -.0014  -.0010  1.3215   .8699
         .02   0.00     8.20   34.44  .2740  .2838 -102.33  -69.49  -.8538  -.9248  -.9466  2.7376  -.0444  -.0476 69.9634 69.9490
         .05   0.00    19.36   51.14  .2767  .2873  -91.18  -52.79  -.6736  -.8224  -.8717  2.5448  -.0417  -.0439 55.2341 54.1162
         .10   0.00    35.27   65.99  .2810  .2932  -75.26  -37.95  -.4537  -.6763  -.7597  2.2737  -.0374  -.0382 43.3731 40.4082
         .20   0.00    59.15   81.39  .2887  .3028  -51.38  -22.54  -.2059  -.4574  -.5766  1.8755  -.0298  -.0286 31.6589 26.1765
         .50   0.00    93.96   97.62  .3046  .3204  -16.58   -6.32  -.0193  -.1415  -.2494  1.3066  -.0138  -.0110 13.1136  9.2865
         .80   0.00   105.10  101.94  .3126  .3273   -5.43   -2.00  -.0018  -.0438  -.1044  1.1146  -.0058  -.0038  5.2903  3.4691
        1.00   0.00   107.94  102.99  .3133  .3295   -2.59    -.94  -.0004  -.0201  -.0561  1.0590  -.0031  -.0018  2.7806  1.7758
```

```
VISUAL EFFECTS CAUSED BY BACKGROUND ATMOSPHERE (WITHOUT PLUME)
*** WHITE, GRAY, AND BLACK OBJECTS AT INDICATED DISTANCES ***

TA  RO/RV REFLECT   YCAP      L       X        Y DELYCAP    DELL  C(400)  C(550)  C(700)  BRATIO    DELX     DELY  E(LUV)  E(LAB)
 .     .02   1.00   97.40   98.99  .3317   .3419   33.29   14.95  -.0792   .5046   .8695   .4925   .0316    .0308 29.7804 22.0316
       .05   1.00   93.86   97.58  .3304   .3399   29.74   13.34  -.0625   .4485   .8020   .5202   .0303    .0288 27.8320 20.3235
       .10   1.00   88.78   95.49  .3280   .3365   24.67   11.45  -.0421   .3686   .7010   .5631   .0280    .0255 24.7446 17.7090
       .20   1.00   81.10   92.19  .3232   .3305   16.99    8.14  -.0191   .2487   .5339   .6386   .0231    .0194 19.2530 13.2961
       .50   1.00   69.71   86.87  .3111   .3184    5.39    2.83  -.0018   .0738   .2408   .8045   .0111    .0073  8.3341  5.3464
       .80   1.00   65.96   84.99  .3048   .3135    1.84     .95  -.0002   .0223   .1101   .9007   .0047    .0024  3.4041  2.1047
      1.00   1.00   64.98   84.49  .3026   .3121     .86     .45  -.0001   .0093   .0665   .9376   .0026    .0011  1.8614  1.1387
       .02    .50   51.09   76.76  .3272   .3370  -13.03   -7.29  -.4665  -.2101  -.0387   .5349   .0271    .0259 23.7340 15.8128
       .05    .50   52.57   77.64  .3210   .3298  -11.53   -6.40  -.3681  -.1871  -.0352   .6530   .0209    .0188 18.7747 12.4677
       .10    .50   54.66   78.87  .3138   .3218   -9.46   -5.18  -.2479  -.1541  -.0299   .7733   .0137    .0108 12.8125  8.5961
       .20    .50   57.76   80.62  .3039   .3139   -6.36   -3.42  -.1125  -.1047  -.0214   .9069   .0059    .0028  6.2007  4.4767
       .50    .50   62.11   82.99  .3000   .3096   -2.00   -1.05  -.0105  -.0335  -.0061   .9955  -.0001   -.0014  1.3921  1.2773
       .80    .50   63.44   83.69  .2997   .3102    -.68    -.36  -.0010  -.0115   .0007   .9983  -.0004   -.0009   .6273   .5244
      1.00    .50   63.76   83.85  .2998   .3105    -.36    -.19  -.0002  -.0061   .0029   .9968  -.0003   -.0005   .3772   .3032
       .02   0.00    4.78   26.14  .2376   .2611  -59.34  -57.90  -.8538  -.9249  -.9468  2.7307  -.0425   -.0300 58.1236 57.9362
       .05   0.00   11.28   40.09  .2601   .2649  -52.84  -43.95  -.6736  -.8226  -.8723  2.5570  -.0399   -.0462 44.3208 44.4139
       .10   0.00   20.54   52.48  .2641   .2707  -43.38  -31.36  -.4537  -.6768  -.7609  2.2846  -.0359   -.0404 33.8470 32.8933
       .20   0.00   34.41   65.31  .2714   .2806  -29.71  -18.73  -.2059  -.4582  -.5786  1.8845  -.0287   -.0304 24.0274 21.1846
       .50   0.00   54.52   78.78  .2866   .2991   -9.60   -5.26  -.0193  -.1428  -.2529  1.3128  -.0135   -.0120 10.4203  7.3476
       .80   0.00   60.91   82.35  .2942   .3067   -3.21   -1.69  -.0018  -.0453  -.1087  1.1199  -.0058   -.0043  4.3264  2.8779
      1.00   0.00   62.33   83.21  .2968   .3089   -1.38    -.83  -.0004  -.0216  -.0606  1.0641  -.0032   -.0022  2.3610  1.5236

 .     .02   1.00   97.64   99.08  .3311   .3413   30.39   13.44  -.1412   .4426   .8858   .4554   .0349    .0335 31.9026 22.4391
       .05   1.00   94.41   97.80  .3291   .3385   27.16   12.16  -.1114   .3932   .8166   .4891   .0329    .0307 29.4603 20.5130
       .10   1.00   89.78   95.91  .3258   .3343   22.33   10.27  -.0751   .3228   .7131   .5399   .0296    .0265 25.7249 17.6278
       .20   1.00   82.77   92.92  .3197   .3271   15.32    7.28  -.0341   .2173   .5440   .6236   .0235    .0193 19.4305 12.9393
       .50   1.00   72.31   88.13  .3067   .3145    5.06    2.48  -.0032   .0630   .2417   .8027   .0105    .0067  7.9340  4.9809
       .80   1.00   68.84   86.44  .3004   .3098    1.39     .79  -.0004   .0179   .1078   .9024   .0042    .0020  3.0799  1.8809
      1.00   1.00   67.93   85.98  .2984   .3086     .68     .34  -.0001   .0065   .0632   .9405   .0022    .0008  1.3993   .9721
       .02    .50   51.33   76.90  .3262   .3360  -15.92   -8.75  -.4975  -.2412  -.0307   .5184   .0300    .0282 27.0182 17.9400
       .05    .50   53.12   77.97  .3190   .3277  -14.13   -7.68  -.3925  -.2148  -.0282   .6231   .0228    .0199 21.2128 14.0846
       .10    .50   55.66   79.44  .3108   .3188  -11.39   -6.20  -.2644  -.1772  -.0244   .7340   .0146    .0109 14.3478  9.6937
       .20    .50   59.42   81.54  .3021   .3101   -7.83   -4.11  -.1200  -.1209  -.0183   .8964   .0058    .0023  6.8790  5.1129
       .50    .50   64.71   84.35  .2957   .3059   -2.34   -1.29  -.0113  -.0396  -.0074   .9961  -.0005   -.0019  1.7046  1.5672
       .80    .50   66.32   85.17  .2955   .3066    -.93    -.47  -.0011  -.0144  -.0026  1.0015  -.0007   -.0012   .8689   .6923
      1.00    .50   66.71   85.37  .2936   .3071    -.34    -.27  -.0003  -.0083  -.0010  1.0007  -.0006   -.0008   .3815   .4352
       .02   0.00    5.02   26.82  .2342   .2574  -62.23  -58.82  -.8538  -.9250  -.9471  2.7638  -.0421   -.0304 59.2338 58.8619
       .05   0.00   11.83   40.99  .2367   .2612  -53.42  -44.66  -.6736  -.8229  -.8730  2.5692  -.0396   -.0466 44.9216 45.0339
       .10   0.00   21.54   53.37  .2606   .2670  -45.71  -32.07  -.4537  -.6773  -.7620  2.2935  -.0356   -.0408 34.1520 33.3243
       .20   0.00   36.07   66.60  .2677   .2770  -31.18  -19.94  -.2059  -.4590  -.5806  1.8935  -.0285   -.0308 24.2475 21.4344
       .50   0.00   57.12   80.26  .2827   .2956  -10.13   -5.38  -.0193  -.1441  -.2365  1.3191  -.0135   -.0122 10.6379  7.6983
       .80   0.00   63.79   83.87  .2903   .3033   -3.46   -1.77  -.0019  -.0468  -.1129  1.1252  -.0060   -.0045  4.5343  3.0017
      1.00   0.00   65.48   84.75  .2928   .3055   -1.77    -.90  -.0004  -.0231  -.0651  1.0692  -.0034   -.0024  2.5365  1.6441
```

```
VISUAL EFFECTS CAUSED BY BACKGROUND ATMOSPHERE (WITHOUT PLUME)
*** WHITE, GRAY, AND BLACK OBJECTS AT INDICATED DISTANCES ***

HETA  RO/RV REFLECT    YCAP       L       X       Y DELYCAP     DELL  C(40    C(550)  C(700)  BRATIO    DELX    DELY  E(LUV)  E(LAB)

58.     .02    1.00   98.50   99.42   .3307   .3408   19.52     8.18  -.1998   .2329   .5237   .5232   .0286   .0288 26.9035 17.9933
        .05    1.00   96.44   98.61   .3283   .3376   17.46     7.37  -.1576   .2243   .4829   .5680   .0262   .0233 24.2090 16.0593
        .10    1.00   93.49   97.43   .3247   .3329   14.51     6.19  -.1062   .1841   .4220   .6286   .0226   .0209 20.3361 13.3177
        .20    1.00   88.99   95.58   .3188   .3260   10.01     4.35  -.0482   .1234   .3222   .7198   .0167   .0140 14.4280  9.2358
        .50    1.00   82.22   92.68   .3088   .3161    3.24     1.44  -.0046   .0360   .1441   .8701   .0066   .0041  5.2966  3.2348
        .80    1.00   79.95   91.67   .3046   .3131     .96      .43  -.0005   .0089   .0652   .9384   .0025   .0011  1.9635  1.1735
       1.00    1.00   79.34   91.40   .3034   .3124     .36      .16  -.0002   .0023   .0389   .9624   .0013   .0003  1.0072   .6047
        .02     .50   52.19   77.41   .3236   .3352  -26.80   -13.82  -.5268  -.3360  -.2117   .6003   .0234   .0232 26.0700 19.3961
        .05     .50   55.15   79.13   .3180   .3263  -23.83   -12.09  -.4156  -.2992  -.1949   .7259   .0139   .0143 19.9196 15.3384
        .10     .50   59.37   81.31   .3100   .3177  -19.62    -9.72  -.2800  -.2466  -.1699   .8674   .0079   .0057 13.1026 10.9203
        .20     .50   65.64   84.83   .3026   .3103  -13.34    -6.41  -.1271  -.1678  -.1290  1.0022   .0004  -.0015  6.7134  6.5072
        .50     .50   74.62   89.23   .2993   .3087   -4.36    -2.01  -.0119  -.0541  -.0558  1.0465  -.0028  -.0033  3.0140  2.4821
        .80     .50   77.42   90.32   .3003   .3104   -1.36     -.71  -.0012  -.0190  -.0234  1.0228  -.0017  -.0016  1.5107  1.0765
       1.00     .50   78.12   90.84   .3011   .3111    -.86     -.39  -.0003  -.0104  -.0126  1.0125  -.0011  -.0010   .9317   .6392
        .02    0.00    3.88   29.14   .2590   .2623  -73.11   -62.10  -.8538  -.9250  -.9470  2.7608  -.0431  -.0498 62.2124 62.1342
        .05    0.00   13.86   44.08   .2616   .2660  -65.12   -47.16  -.6736  -.8229  -.8728  2.5663  -.0405  -.0460 47.6997 47.6795
        .10    0.00   25.25   57.35   .2657   .2718  -53.74   -33.89  -.4537  -.6773  -.7618  2.2929  -.0364  -.0402 36.6832 35.3574
        .20    0.00   42.29   71.10   .2730   .2817  -36.69   -20.14  -.2059  -.4590  -.5801  1.8914  -.0291  -.0303 26.2504 22.8262
        .50    0.00   67.03   85.33   .2883   .3000  -11.95    -5.70  -.0193  -.1442  -.2557  1.3176  -.0138  -.0120 11.5344  8.2215
        .80    0.00   74.90   89.36   .2961   .3076   -4.08    -1.88  -.0019  -.0468  -.1120  1.1240  -.0061  -.0045  4.8970  3.2096
       1.00    0.00   76.90   90.28   .2987   .3097   -2.09     -.95  -.0004  -.0231  -.0641  1.0680  -.0034  -.0023  2.7496  1.7533

80.     .02    1.00   99.38   99.76   .3309   .3408    8.16     3.25  -.2356   .0813   .2002   .6369   .0187   .0209 18.7187 12.2891
        .05    1.00   98.52   99.43   .3288   .3377    7.30     2.92  -.1859   .0720   .1850   .6871   .0166   .0178 16.2785 10.5693
        .10    1.00   97.29   98.94   .3259   .3336    6.07     2.44  -.1252   .0588   .1622   .7527   .0137   .0136 12.9883  8.2860
        .20    1.00   95.41   98.20   .3216   .3280    4.19     1.69  -.0568   .0389   .1250   .8384   .0095   .0080  8.4828  5.2439
        .50    1.00   92.54   97.05   .3156   .3217    1.32      .54  -.0054   .0104   .0585   .9397   .0034   .0017  2.8014  1.6424
        .80    1.00   91.57   96.65   .3134   .3202     .34      .14  -.0006   .0015   .0290   .9713   .0013   .0003  1.0793   .6372
       1.00    1.00   91.30   96.54   .3128   .3200     .08      .03  -.0002  -.0006   .0192   .9810   .0007  -.0000   .6040   .3700
        .02     .50   53.07   77.93   .3259   .3353  -38.16   -18.57  -.3447  -.4218  -.3734   .7266   .0138   .0133 23.8563 20.8449
        .05     .50   57.23   80.33   .3192   .3272  -33.99   -16.18  -.4297  -.3734  -.3437   .8689   .0070   .0072 18.5321 17.0814
        .10     .50   63.17   83.53   .3126   .3193  -28.05   -12.96  -.2895  -.3091  -.2994  1.0142   .0004  -.0005 13.2417 13.0360
        .20     .50   72.06   88.01   .3074   .3141  -19.16    -8.50  -.1314  -.2098  -.2269  1.1236  -.0048  -.0059  9.0101  8.7485
        .50     .50   84.95   93.87   .3075   .3154   -6.27    -2.64  -.0123  -.0666  -.0974  1.0943  -.0046  -.0046  4.6433  3.5338
        .80     .50   89.04   95.60   .3099   .3180   -2.18     -.90  -.0012  -.0223  -.0401  1.0405  -.0023  -.0020  2.0897  1.4402
       1.00     .50   90.08   96.03   .3109   .3189   -1.14     -.47  -.0003  -.0115  -.0210  1.0211  -.0013  -.0011  1.1876   .7980
        .02    0.00    6.76   31.29   .2683   .2704  -84.47   -65.22  -.8538  -.9249  -.9469  2.7526  -.0439  -.0496 65.2578 65.3851
        .05    0.00   15.94   46.94   .2709   .2742  -75.28   -49.57  -.6736  -.8228  -.8724  2.5582  -.0412  -.0458 50.9262 50.4304
        .10    0.00   29.05   60.86   .2752   .2800  -62.17   -35.65  -.4537  -.6770  -.7610  2.2857  -.0370  -.0400 39.7590 37.5950
        .20    0.00   48.71   75.29   .2827   .2899  -42.51   -21.21  -.2059  -.4586  -.5788  1.8854  -.0295  -.0301 28.6074 24.3928
        .50    0.00   77.35   90.49   .2984   .3082  -13.87    -6.01  -.0193  -.1435  -.2533  1.3135  -.0138  -.0118 12.3597  8.7698
        .80    0.00   86.52   94.34   .3062   .3137   -4.70    -1.97  -.0019  -.0461  -.1091  1.1204  -.0060  -.0043  5.1424  3.3732
       1.00    0.00   88.86   95.32   .3088   .3178   -2.37     -.98  -.0004  -.0224  -.0611  1.0646  -.0033  -.0022  2.8301  1.8072
```

INITIAL PLUME RISE AND DILUTION AND NITROGEN DIOXIDE FORMATION

2250 MW COAL POWER PLANT

TIME (SEC)	X (M)	DELTA H (M)	U (M/S)	W (M/S)	V (M/S)	SIGMA (M)	TEMP (K)	O2 MOL P	NO2-NO RATIO EQUIL	ACTUAL	NOX (PPM)	NO (PPM)	NO2T (PPM)	SO2 (PPM)	PARTICULATE UG/M3
0.	0.0	0.0	5.00	27.43	27.43	0.0	394.3	1.7	2.6E+03	2.0E-03	487.833	486.875	.958	601.260	1.96E+04
10.	50.0	27.1	5.00	1.80	5.32	6.3	350.6	10.4	4.7E+04	3.2E-03	266.255	265.397	.858	328.162	1.07E+04
20.	100.0	43.0	5.00	1.43	5.20	10.0	317.4	17.1	2.7E+05	8.2E-03	97.865	97.067	.798	120.620	3.94E+03
30.	150.1	56.3	5.00	1.25	5.16	13.1	309.2	18.7	4.1E+05	1.2E-02	56.052	55.403	.649	69.085	2.26E+03
40.	200.1	68.2	5.00	1.14	5.13	15.8	305.6	19.4	4.9E+05	1.4E-02	37.965	37.441	.524	46.792	1.53E+03
50.	250.1	79.1	5.00	1.05	5.11	18.4	303.7	19.8	5.4E+05	1.6E-02	28.120	27.687	.433	34.658	1.13E+03
60.	300.1	89.3	5.00	.99	5.10	20.8	302.5	20.1	5.8E+05	1.7E-02	22.024	21.658	.366	27.144	8.87E+02
70.	350.1	98.9	5.00	.94	5.09	23.0	302.1	20.1	5.9E+05	1.8E-02	20.287	19.931	.357	25.004	8.17E+02
80.	400.2	108.1	5.00	.90	5.08	25.1	302.1	20.1	5.9E+05	1.9E-02	20.287	19.913	.375	25.004	8.17E+02
90.	450.2	117.0	5.00	.87	5.08	27.2	302.1	20.1	5.9E+05	2.0E-02	20.287	19.895	.392	25.004	8.17E+02
100.	500.2	125.5	5.00	.84	5.07	29.2	302.1	20.1	5.9E+05	2.1E-02	20.287	19.877	.410	25.004	8.17E+02
110.	550.2	133.7	5.00	.81	5.07	31.1	302.1	20.1	5.9E+05	2.2E-02	20.287	19.859	.428	25.004	8.17E+02
120.	600.2	141.7	5.00	.79	5.06	32.9	302.1	20.1	5.9E+05	2.2E-02	20.287	19.841	.446	25.004	8.17E+02
130.	650.3	149.4	5.00	.77	5.06	34.7	302.1	20.1	5.9E+05	2.3E-02	20.287	19.823	.464	25.004	8.17E+02
140.	700.3	157.0	5.00	.75	5.06	36.5	302.1	20.1	5.9E+05	2.4E-02	20.287	19.806	.482	25.004	8.17E+02
150.	750.3	164.4	5.00	.73	5.05	37.8	302.1	20.1	5.9E+05	2.5E-02	20.287	19.788	.499	25.004	8.17E+02
160.	800.3	171.6	5.00	.71	5.05	37.8	302.1	20.1	5.9E+05	2.6E-02	20.287	19.770	.517	25.004	8.17E+02
170.	850.3	178.6	5.00	.70	5.05	37.8	302.1	20.1	5.9E+05	2.7E-02	20.287	19.753	.534	25.004	8.17E+02
180.	900.3	185.6	5.00	.69	5.05	37.8	302.1	20.1	5.9E+05	2.8E-02	20.287	19.735	.552	25.004	8.17E+02
190.	950.4	192.4	5.00	.68	5.05	37.8	302.1	20.1	5.9E+05	2.9E-02	20.287	19.718	.569	25.004	8.17E+02
200.	1000.4	199.1	5.00	.66	5.05	37.8	302.1	20.1	5.9E+05	3.0E-02	20.287	19.700	.587	25.004	8.17E+02
210.	1050.4	205.6	5.00	.65	5.04	37.8	302.1	20.1	5.9E+05	3.1E-02	20.287	19.683	.604	25.004	8.17E+02
220.	1100.4	212.1	5.00	.64	5.04	37.8	302.1	20.1	5.9E+05	3.2E-02	20.287	19.666	.622	25.004	8.17E+02
230.	1150.4	218.5	5.00	.63	5.04	37.8	302.1	20.1	5.9E+05	3.3E-02	20.287	19.648	.639	25.004	8.17E+02

```
                  CONCENTRATIONS OF AEROSOL AND GASES CONTRIBUTED BY

                              2230 MW COAL POWER PLANT

DOWNWIND DISTANCE (KM) =    1.2
PLUME ALTITUDE (M)     =  439.
SIGMA Y (M)            =   39.
SIGMA Z (M)            =   24.
SO2-SO4 CONVERSION RATE=       .3000 PERCENT/HR
NOX-NO3 CONVERSION RATE=      0.0000 PERCENT/HR

ALTITUDE          NOX      NO2      NO3-   NO2/NTOT  NO3-/NTOT     SO2      SO4=  SO4=/STOT    O3    PRIMARY BSP-TOTAL  BSPSN/BSP
                 (PPM)    (PPM)   (UG/M3)  (MOLE %)  (MOLE %)    (PPM)   (UG/M3)  (MOLE %)  (PPM)   (UG/M3) (10-4 M-1)   (%)

 H+2S
INCREMENT:       2.709     .127    0.000     4.687     0.000     3.339     .180      .001    -.039   109.060    2.193      .478
TOTAL AMB:       2.709     .127    0.000     4.687     0.000     3.339    1.923      .013     .001   140.803    2.396     4.668

 H+1S
INCREMENT:      12.142     .432    0.000     3.360     0.000    14.963     .808      .001    -.040   488.773    9.833      .478
TOTAL AMB:      12.142     .432    0.000     3.360     0.000    14.963    2.333      .004     .000   320.317   10.037     1.478

 H
INCREMENT:      20.019     .687    0.000     3.432     0.000    24.673    1.333      .001    -.040   803.830   16.216      .478
TOTAL AMB:      20.019     .687    0.000     3.432     0.000    24.673    3.077      .003     .000   837.394   16.418     1.089

 H-1S
INCREMENT:      12.142     .432    0.000     3.360     0.000    14.963     .808      .001    -.040   488.773    9.833      .478
TOTAL AMB:      12.142     .432    0.000     3.360     0.000    14.963    2.333      .004     .000   320.317   10.037     1.478

 H-2S
INCREMENT:       2.709     .127    0.000     4.687     0.000     3.339     .180      .001    -.039   109.060    2.193      .478
TOTAL AMB:       2.709     .127    0.000     4.687     0.000     3.339    1.923      .013     .001   140.803    2.396     4.668

 0
INCREMENT:        .000    0.000    0.000     0.000     0.000      .000     .000      .001    0.000      .000     .000      .478
TOTAL AMB:        .000    0.000    0.000     0.000     0.000      .000    1.743   100.000     .040    31.743     .202    30.270


CUMULATIVE SURFACE DEPOSITION (MOLE FRACTION OF INITIAL FLUX)

                 SO2:     0.0000
                 NOX:     0.0000
PRIMARY PARTICULATE:      0.0000
                 SO4:     0.0000
                 NO3:     0.0000
```

```
                VISUAL EFFECTS FOR HORIZONTAL SIGHT PATHS
                2230 MW COAL POWER PLANT

DOWNWIND DISTANCE (KM) =    1.2
PLUME ALTITUDE (M)     =   439.
SIGHT PATH IS THROUGH PLUME CENTER

THETA ALPHA  RP/RV0    RV  %REDUCED    YCAP      L       X        Y DELYCAP    DELL  C(550)  BRATIO     DELX     DELY  E(LUV)  E(LAB)
  90.
       30.      .02   113.0   11.33   57.34   80.30   .3146   .3277   -6.38   -3.34  -.0959   .7737    .0146    .0166 14.1896  9.3744
       30.      .05   114.6   11.82   58.29   80.92   .3116   .3238   -5.83   -3.12  -.0845   .8268    .0116    .0127 11.3829  7.4985
       30.      .10   114.1   12.23   59.35   81.50   .3080   .3192   -4.76   -2.54  -.0696   .8904    .0079    .0081  7.8982  5.2121
       30.      .20   113.3   12.84   60.92   82.33   .3037   .3141   -3.20   -1.69  -.0473   .9592    .0037    .0030  3.8192  2.6087
       30.      .50   112.2   13.69   63.12   83.52   .3001   .3107   -1.00    -.52  -.0151  1.0025    .0001   -.0004   .6099   .5702
       30.      .80   111.9   13.93   63.78   83.87   .2999   .3107    -.33    -.17  -.0051  1.0019   -.0002   -.0004   .2701   .2316
       45.      .02   119.6    8.04   59.09   81.36   .3112   .3239   -5.03   -2.68  -.0723   .8211    .0111    .0129 11.0503  7.2674
       45.      .05   119.3    8.25   59.67   81.67   .3090   .3210   -4.45   -2.37  -.0644   .8628    .0089    .0099  8.8984  5.8391
       45.      .10   118.9    8.56   60.48   82.11   .3062   .3175   -3.64   -1.93  -.0530   .9127    .0062    .0064  6.2064  4.0794
       45.      .20   118.3    9.02   61.68   82.76   .3029   .3136   -2.44   -1.28  -.0360   .9670    .0029    .0025  3.0215  2.0471
       45.      .50   117.4    9.66   63.36   83.63   .3001   .3108    -.76    -.40  -.0115  1.0017    .0001   -.0003   .4668   .4350
       45.      .80   117.2    9.85   63.86   83.91   .2999   .3108    -.26    -.13  -.0039  1.0014   -.0001   -.0003   .2026   .1749
       60.      .02   121.5    6.52   59.87   81.78   .3094   .3220   -4.25   -2.26  -.0611   .8463    .0094    .0109  9.4214  6.1823
       60.      .05   121.3    6.70   60.35   82.05   .3076   .3196   -3.76   -2.00  -.0544   .8820    .0076    .0085  7.6008  4.9782
       60.      .10   121.0    6.96   61.04   82.42   .3053   .3166   -3.08   -1.62  -.0448   .9246    .0052    .0055  5.3148  3.4869
       60.      .20   120.5    7.34   62.06   82.96   .3025   .3132   -2.06   -1.08  -.0304   .9714    .0025    .0022  2.5962  1.7528
       60.      .50   119.8    7.88   63.48   83.71   .3001   .3109    -.64    -.33  -.0097  1.0013    .0001   -.0002   .2955   .3653
       60.      .80   119.5    8.04   63.90   83.93   .2999   .3108    -.22    -.11  -.0033  1.0012   -.0001   -.0002   .1698   .1471
       90.      .02   122.7    5.62   60.36   82.05   .3083   .3207   -3.76   -1.99  -.0540   .8628    .0083    .0097  8.3733  5.4869
       90.      .05   122.5    5.78   60.79   82.28   .3067   .3186   -3.33   -1.76  -.0480   .8945    .0067    .0075  6.7630  4.4242
       90.      .10   122.2    6.01   61.40   82.61   .3047   .3160   -2.72   -1.43  -.0396   .9327    .0047    .0049  4.7365  3.1040
       90.      .20   121.8    6.34   62.29   83.09   .3023   .3130   -1.82    -.96  -.0269   .9743    .0022    .0020  2.3186  1.5621
       90.      .50   121.1    6.82   63.55   83.75   .3001   .3109    -.57    -.30  -.0086  1.0011    .0001   -.0002   .3503   .3226
       90.      .80   120.9    6.96   63.93   83.94   .3000   .3109    -.19    -.10  -.0029  1.0010   -.0001   -.0002   .1494   .1297
```

```
          VISUAL EFFECTS FOR NON-HORIZONTAL CLEAR SKY VIEWS THROUGH PLUME CENTER

          2230 MW COAL POWER PLANT

OWNWIND DISTANCE (KM) =     1.2
LUME ALTITUDE (M)     =   439.

HETA  ALPHA   BETA     RP   YCAP      L      X        Y DELYCAP   DELL  C(550)  BRATIO   DELX    DELY  E(LUV)   E(LAB)

 90.
       30.    15.    3.31  40.48  69.84  .2875  .3017   5.90    4.38   .1852   .4950  .0311   .0370 24.0219 15.5337
       30.    30.    1.58  32.28  63.61  .2879  .3008  11.39   10.74   .3736   .3830  .0403   .0495 25.6559 19.1337
       30.    45.     .98  29.10  60.90  .2898  .3023  13.36   14.50   .9122   .3361  .0450   .0538 26.1408 21.3101
       30.    60.     .67  27.37  59.53  .2912  .3037  14.59   16.76  1.1725   .3122  .0477   .0593 26.5220 22.7167
       30.    75.     .50  26.84  58.86  .2920  .3046  15.08   17.99  1.3358   .3003  .0492   .0612 26.7924 23.5181
       30.    90.     .44  26.62  58.65  .2923  .3049  15.23   18.38  1.3915   .2965  .0497   .0618 26.8915 23.7798
       45.    15.    2.36  38.91  68.71  .2809  .2944   4.32    3.26   .1373   .5691  .0245   .0297 19.2164 12.3882
       45.    30.    1.16  29.49  61.24  .2801  .2916   8.60    8.37   .4340   .4552  .0324   .0403 20.4453 15.2363
       45.    45.     .76  25.82  57.90  .2817  .2928  10.28   11.50   .6928   .4021  .0369   .0462 20.9023 17.0917
       45.    60.     .57  24.07  56.19  .2831  .2941  11.09   13.42   .8919   .3740  .0396   .0497 21.2680 18.3186
       45.    75.     .47  23.24  55.35  .2839  .2949  11.47   14.48  1.0171   .3398  .0411   .0515 21.5172 19.0214
       45.    90.     .44  22.98  55.09  .2842  .2952  11.59   14.81  1.0599   .3354  .0415   .0521 21.6055 19.2505
       60.    15.    1.94  38.17  68.17  .2774  .2904   3.59    2.72   .1145   .6142  .0210   .0237 16.5918 10.6812
       60.    30.     .98  28.12  60.03  .2738  .2863   7.23    7.16   .3654   .5012  .0281   .0352 17.6537 13.1589
       60.    45.     .67  24.21  56.33  .2772  .2874   8.67    9.92   .5843   .4452  .0325   .0408 18.1061 14.8373
       60.    60.     .53  22.34  54.42  .2785  .2886   9.36   11.64   .7528   .4147  .0351   .0442 18.4699 15.9624
       60.    75.     .46  21.45  53.47  .2794  .2894   9.69   12.60   .8388   .3991  .0365   .0460 18.7144 16.6103
       60.    90.     .44  21.18  53.18  .2796  .2897   9.78   12.90   .8950   .3942  .0370   .0466 18.8003 16.8219
       90.    15.    1.70  37.72  67.84  .2731  .2877   3.14    2.39   .1005   .6459  .0187   .0230 14.8596  9.5583
       90.    30.     .88  27.26  59.25  .2730  .2831   6.37    6.38   .3224   .5347  .0253   .0318 15.8208 11.7971
       90.    45.     .62  23.19  55.30  .2742  .2837   7.65    8.90   .5160   .4772  .0294   .0371 16.2682 13.3334
       90.    60.     .51  21.24  53.25  .2753  .2848   8.26   10.48   .6651   .4452  .0320   .0404 16.6293 14.4066
       90.    75.     .45  20.32  52.23  .2763  .2836   8.56   11.36   .7589   .4286  .0334   .0422 16.8705 15.0137
       90.    90.     .44  20.04  51.92  .2763  .2838   8.65   11.64   .7909   .4235  .0339   .0428 16.9549 15.2130
```

PLUME VISUAL EFFECTS FOR HORIZONTAL VIEWS
PERPENDICULAR TO THE PLUME OF WHITE, GRAY, AND BLACK OBJECTS
FOR VARIOUS OBSERVER-PLUME AND OBSERVER-OBJECT DISTANCES

2250 MW COAL POWER PLANT

DOWNWIND DISTANCE (KM) = 1.2
THETA = 90.

REFLECT	RP/RV0	RO/RV0	YCAP	L	X	Y	DELYCAP	DELL	C(550)	BRATIO	DELX	DELY	E(LUV)	E(LAB)
1.0	.02	.02	83.33	93.23	.3374	.3473	-13.88	-3.74	-.1406	.9390	.0037	.0034	7.3361	6.3331
1.0	.02	.03	77.71	90.66	.8394	.3489	-16.13	-6.92	-.1706	.8333	.0091	.0090	10.4381	8.6282
1.0	.02	.10	69.40	86.71	.3419	.3506	-19.39	-8.78	-.2173	.7562	.0139	.0140	14.6367	11.7238
1.0	.02	.20	36.87	80.13	.3433	.3504	-24.23	-12.06	-.2992	.6640	.0203	.0200	20.3804	16.2093
1.0	.02	.30	38.47	68.40	.3320	.3372	-31.24	-18.47	-.4492	.6797	.0209	.0188	23.4236	21.4603
1.0	.02	.80	32.30	63.79	.3181	.3238	-33.46	-21.20	-.3038	.7718	.0134	.0123	23.3314	22.8383
1.0	.03	.03	81.31	92.36	.3342	.3431	-12.33	-3.21	-.1299	.9777	.0038	.0033	6.1396	3.6000
1.0	.03	.10	73.19	88.33	.3339	.3440	-13.39	-6.94	-.1743	.8827	.0078	.0074	9.6748	8.1933
1.0	.03	.20	60.67	82.22	.3361	.3423	-20.43	-9.97	-.2320	.7961	.0129	.0121	14.7289	12.1333
1.0	.03	.30	42.27	71.08	.3231	.3279	-27.44	-13.78	-.3944	.8276	.0120	.0095	19.3737	17.1339
1.0	.03	.80	36.30	66.78	.3100	.3168	-29.66	-18.21	-.4482	.9293	.0032	.0033	19.9323	18.7637
1.0	.10	.10	78.60	91.06	.3294	.3372	-10.18	-4.43	-.1130	1.0197	.0014	.0007	4.6023	4.4898
1.0	.10	.20	66.08	83.03	.3283	.3347	-13.02	-7.13	-.1847	.9370	.0033	.0043	8.3667	7.6989
1.0	.10	.30	47.68	74.63	.3148	.3193	-22.03	-12.22	-.3162	.9760	.0037	.0012	13.1232	12.4981
1.0	.10	.80	41.71	70.70	.3028	.3093	-24.23	-14.29	-.3639	1.0781	-.0020	-.0042	14.4413	14.3234
1.0	.20	.20	74.17	89.02	.3218	.3286	-6.93	-3.17	-.0838	1.0336	-.0013	-.0019	3.3519	3.2646
1.0	.20	.30	33.77	79.30	.3086	.3141	-13.94	-7.36	-.1991	1.0841	-.0026	-.0043	7.4830	7.4318
1.0	.20	.80	49.80	73.97	.2980	.3031	-16.16	-9.02	-.2426	1.1698	-.0067	-.0083	9.6369	9.3393
1.0	.30	.30	67.49	83.76	.3088	.3163	-2.22	-1.10	-.0301	1.0481	-.0023	-.0021	2.0276	1.3132
1.0	.30	.80	61.32	82.67	.3002	.3091	-4.44	-2.32	-.0648	1.0949	-.0046	-.0044	3.9439	3.0424
1.0	.80	.80	63.23	84.62	.30[illegible]	.3126	-.73	-.37	-.0098	1.0247	-.0012	-.0009	.9460	.6297
.3	.02	.02	49.43	73.74	.3283	.3384	-1.67	-1.02	-.0272	1.0194	.0013	.0014	1.4433	1.2272
.3	.02	.03	47.29	74.40	.3288	.3384	-3.28	-3.24	-.0960	.8612	.0078	.0086	7.0019	3.2680
.3	.02	.10	44.23	72.41	.3286	.3379	-10.43	-6.46	-.1876	.7334	.0148	.0161	13.7070	10.2363
.3	.02	.20	39.63	69.23	.3266	.3333	-18.13	-11.39	-.3124	.6366	.0207	.0216	20.9321	13.9833
.3	.02	.30	32.84	64.06	.3169	.3263	-29.28	-18.93	-.4699	.7192	.0170	.0166	23.4743	21.3637
.3	.02	.80	30.62	62.22	.3102	.3211	-32.81	-21.47	-.3140	.8092	.0103	.0109	23.4962	22.9376
.3	.03	.03	31.09	76.73	.3217	.3303	-1.48	-.89	-.0233	1.0207	.0007	.0007	1.0866	.9733
.3	.03	.10	48.03	74.87	.3211	.3296	-6.63	-4.00	-.1180	.8761	.0073	.0078	7.4813	3.6960
.3	.03	.20	43.42	71.87	.3186	.3266	-14.33	-8.73	-.2463	.7907	.0127	.0128	14.5010	11.3230
.3	.03	.30	36.63	67.03	.3090	.3173	-23.48	-13.96	-.4089	.8638	.0090	.0076	19.3643	17.1687
.3	.03	.80	34.42	63.32	.3028	.3124	-29.01	-18.36	-.4344	.9644	.0031	.0022	19.9423	18.8466
.3	.10	.10	33.44	78.13	.3139	.3219	-1.22	-.71	-.0183	1.0202	.0001	.0001	.7413	.7209
.3	.10	.20	48.83	73.37	.3111	.3187	-8.92	-3.23	-.1326	.9236	.0032	.0048	7.4334	6.1314
.3	.10	.30	42.04	70.93	.3020	.3097	-20.07	-12.06	-.3219	.9994	.0020	.0061	2.9973	12.3238
.3	.10	.80	39.83	69.38	.2964	.3033	-23.60	-14.31	-.3693	1.1044	-.0032	-.0049	14.4444	14.3362
.3	.20	.20	36.93	80.16	.3036	.3133	-.83	-.46	-.0118	1.0168	-.0003	-.0003	.4873	.4732
.3	.20	.30	30.14	76.17	.2974	.3055	-11.98	-6.82	-.1913	1.0808	-.0026	-.0041	6.8800	6.8701
.3	.20	.80	47.92	74.80	.2927	.3018	-13.31	-8.89	-.2418	1.1783	-.0069	-.0084	9.4390	9.2013
.3	.30	.30	61.83	82.83	.2997	.3094	-.26	-.14	-.0034	1.0078	-.0003	-.0003	.2333	.1893
.3	.30	.80	39.64	81.66	.2939	.3064	-3.80	-2.03	-.0379	1.0798	-.0038	-.0038	3.2746	2.3892
.3	.80	.80	63.33	83.64	.2993	.3101	-.09	-.03	-.0010	1.0035	-.0002	-.0001	.1138	.0766
0.0	.02	.02	13.33	46.12	.2872	.2971	10.34	19.97	2.2443	.4833	.0296	.0360	20.0212	20.2378
0.0	.02	.03	16.87	48.13	.2868	.2973	3.39	8.04	.3132	.3244	.0267	.0325	12.8418	11.15[illegible]
0.0	.02	.10	19.07	30.81	.2872	.2938	-1.47	-1.67	-.0610	.3777	.0230	.0281	16.0943	10.3913
0.0	.02	.20	22.38	34.46	.2896	.3027	-12.03	-10.83	-.3426	.6381	.0182	.0221	21.9431	13.8663
0.0	.02	.30	27.20	39.19	.2972	.3119	-27.32	-19.39	-.4939	.7986	.0106	.0128	23.4016	21.7432
0.0	.02	.80	28.74	60.39	.3013	.3160	-32.17	-21.76	-.3228	.8614	.0072	.0092	23.4373	23.0827
0.0	.03	.03	20.67	32.62	.2802	.2888	9.39	12.33	.8433	.6131	.0201	.0240	13.0331	13.0614
0.0	.03	.10	22.87	34.97	.2811	.2907	2.33	2.49	.1214	.6709	.0170	.0201	10.1822	7.0363
0.0	.03	.20	26.18	38.24	.2838	.2949	-8.23	-7.08	-.2339	.7611	.0124	.0143	13.0038	10.3919

```
0.0     .03     .30   31.00   62.34   .2911   .3038  -23.32  -16.23  -.4271   .9320   .0043   .0047 19.3101 17.2364
0.0     .03     .80   32.34   63.82   .2930   .3076  -28.37  -18.33  -.4611  1.0122   .0007   .0008 19.9372 18.9453
0.0     .10     .10   28.28   60.17   .2772   .2838    7.74    7.69   .3813   .7320   .0131   .0131  8.7462  8.3302
0.0     .10     .20   31.39   63.03   .2798   .2897   -2.82   -2.28  -.0787   .8346   .0084   .0090  7.9818  3.1003
0.0     .10     .30   36.41   66.86   .2863   .2977  -18.11  -11.93  -.3290  1.0398  -.0003  -.0014 12.8742 12.1623
0.0     .10     .80   37.93   68.01   .2897   .3010  -22.96  -14.34  -.3730  1.1390  -.0046  -.0037 14.4328 14.3342
0.0     .20     .20   39.68   69.27   .2789   .2888    3.27    3.93   .1339   .8403   .0073   .0082  3.3623  4.6338
0.0     .20     .30   44.30   72.38   .2843   .2934  -10.02   -6.20  -.1820  1.0736  -.0023  -.0037  6.2773  6.2339
0.0     .20     .80   46.04   73.60   .2871   .2982  -14.87   -8.73  -.2410  1.1890  -.0071  -.0086  9.2363  9.0389
0.0     .30     .30   36.21   79.73   .2892   .3013    1.69     .97   .0301   .9438   .0026   .0023  1.9328  1.4070
0.0     .30     .80   37.76   80.62   .2914   .3036   -3.16   -1.73  -.0303  1.0613  -.0029  -.0031  2.3774  2.1220
0.0     .80     .80   61.47   82.63   .2933   .3073     .36     .30   .0084   .9782   .0011   .0008   .7730   .3114
```

```
                    CONCENTRATIONS OF AEROSOL AND GASES CONTRIBUTED BY

                              2230 MW COAL POWER PLANT

DOWNWIND DISTANCE (KM) =    2.0
PLUME ALTITUDE (M)     =  439.
SIGMA Y (M)            =   93.
SIGMA Z (M)            =   33.
SO2-SO4 CONVERSION RATE=      .5000 PERCENT/HR
NOX-NO3 CONVERSION RATE=     0.0000 PERCENT/HR

ALTITUDE        NOX      NO2      NO3-    NO2/NTOT  NO3-/NTOT     SO2      SO4=   SO4=/STOT     O3     PRIMARY BSP-TOTAL  BSPSN/BSP
               (PPM)    (PPM)   (UG/M3)  (MOLE %)  (MOLE %)     (PPM)   (UG/M3)  (MOLE %)    (PPM)   (UG/M3) (10-4 M-1)   (%)
 H+2S
INCREMENT:     1.217     .081    0.000     6.634     0.000      1.499     1.389      .024     -.039    48.985     1.062     7.602
TOTAL AMB:     1.217     .081    0.000     6.634     0.000      1.499     3.134      .033      .001    80.730     1.263    14.412
 H+1S
INCREMENT:     3.434     .262    0.000     4.810     0.000      6.720     6.223      .024     -.039   219.337     4.738     7.602
TOTAL AMB:     3.434     .262    0.000     4.810     0.000      6.720     7.969      .030      .001   251.282     4.960     9.336
 H
INCREMENT:     8.992     .436    0.000     3.074     0.000     11.080    10.263      .024     -.039   361.936     7.843     7.602
TOTAL AMB:     8.992     .436    0.000     3.074     0.000     11.080    12.007      .028      .001   393.700     8.047     8.671
 H-1S
INCREMENT:     3.434     .262    0.000     4.810     0.000      6.720     6.223      .024     -.039   219.337     4.738     7.602
TOTAL AMB:     3.434     .262    0.000     4.810     0.000      6.720     7.969      .030      .001   251.282     4.960     9.336
 H-2S
INCREMENT:     1.217     .081    0.000     6.634     0.000      1.499     1.389      .024     -.039    48.985     1.062     7.602
TOTAL AMB:     1.217     .081    0.000     6.634     0.000      1.499     3.134      .033      .001    80.730     1.263    14.412
  0
INCREMENT:      .000    0.000    0.000     0.000     0.000       .000      .000      .024     0.000      .000      .000     7.602
TOTAL AMB:      .000    0.000    0.000     0.000     0.000       .000     1.743   100.000      .040    31.743      .202    30.270


CUMULATIVE SURFACE DEPOSITION (MOLE FRACTION OF INITIAL FLUX)

                  SO2:     .0000
                  NOX:     .0000
  PRIMARY PARTICULATE:     .0000
                  SO4:     .0000
                  NO3:    0.0000
```

```
                 VISUAL EFFECTS FOR HORIZONTAL SIGHT PATHS
                 2250 MW COAL POWER PLANT

DOWNWIND DISTANCE (KM) =     2.0
PLUME ALTITUDE (M)     =    439.
SIGHT PATH IS THROUGH PLUME CENTER

THETA ALPHA  RP/RV0     RV  %REDUCED    YCAP       L        X         Y DELYCAP     DELL  C(550)  BRATIO     DELX      DELY  E(LUV)   E(LAB)

  90.
         30.       .02   118.3     8.97    57.98    80.75    .3135     .3288   -6.14    -3.30  -.0886    .7628    .0155     .0177 14.8693  9.7393
         30.       .05   118.0     9.25    58.69    81.14    .3125     .3247   -5.43    -2.90  -.0788    .8170    .0124     .0137 11.9738  7.8168
         30.       .10   117.5     9.63    59.69    81.68    .3087     .3199   -4.43    -2.36  -.0649    .8823    .0086     .0089  8.3636  5.4407
         30.       .20   116.8    10.19    61.13    82.48    .3042     .3146   -2.96    -1.56  -.0441    .9535    .0041     .0035  4.1034  2.7135
         30.       .50   113.7    10.98    63.20    83.56    .3003     .3108    -.92     -.48  -.0140   1.0006    .0003    -.0003   .6120   .5400
         30.       .80   113.4    11.22    63.81    83.88    .2999     .3108    -.30     -.16  -.0047   1.0013   -.0001    -.0003   .2380   .2093
         45.       .02   121.9     6.26    59.49    81.58    .3117     .3246   -4.63    -2.47  -.0666    .8145    .0117     .0135 11.4281  7.4676
         45.       .05   121.6     6.46    60.02    81.87    .3095     .3216   -4.10    -2.18  -.0592    .8566    .0094     .0105  9.2371  6.0091
         45.       .10   121.2     6.74    60.78    82.27    .3066     .3180   -3.34    -1.77  -.0488    .9074    .0066     .0069  6.4861  4.2057
         45.       .20   120.7     7.16    61.88    82.87    .3033     .3139   -2.23    -1.17  -.0331    .9631    .0032     .0028  3.2044  2.1063
         45.       .50   119.9     7.75    63.43    83.68    .3003     .3109    -.69     -.36  -.0105   1.0002    .0002    -.0002   .4673   .4066
         45.       .80   119.7     7.93    63.89    83.92    .3000     .3108    -.23     -.12  -.0036   1.0010   -.0001    -.0002   .1763   .1360
         60.       .02   123.4     5.08    60.23    81.98    .3098     .3225   -3.89    -2.06  -.0559    .8414    .0098     .0114  9.6848  6.3147
         60.       .05   123.2     5.25    60.68    82.22    .3080     .3200   -3.44    -1.82  -.0497    .8774    .0079     .0089  7.8420  5.0929
         60.       .10   122.9     5.48    61.31    82.56    .3056     .3170   -2.81    -1.48  -.0409    .9207    .0056     .0059  5.5198  3.5741
         60.       .20   122.4     5.83    62.24    83.06    .3028     .3135   -1.88     -.99  -.0278    .9682    .0027     .0024  2.7339  1.7941
         60.       .50   121.8     6.32    63.54    83.74    .3003     .3109    -.38     -.30  -.0089   1.0001    .0002    -.0001   .3934   .3417
         60.       .80   121.6     6.47    63.93    83.94    .3000     .3109    -.19     -.10  -.0030   1.0008   -.0001    -.0002   .1470   .1304
         90.       .02   124.3     4.38    60.69    82.23    .3086     .3211   -3.43    -1.82  -.0492    .8583    .0086     .0101  8.3760  5.3843
         90.       .05   124.1     4.53    61.08    82.44    .3070     .3190   -3.03    -1.60  -.0438    .8908    .0070     .0079  6.9518  4.5100
         90.       .10   123.8     4.73    61.64    82.74    .3050     .3163   -2.48    -1.30  -.0360    .9293    .0049     .0052  4.9006  3.1764
         90.       .20   123.4     5.04    62.46    83.17    .3025     .3133   -1.65     -.87  -.0245    .9716    .0024     .0022  2.4340  1.5938
         90.       .50   122.9     5.47    63.61    83.78    .3002     .3110    -.31     -.27  -.0078   1.0000    .0002    -.0001   .3500   .3011
         90.       .80   122.7     5.61    63.95    83.95    .3000     .3109    -.17     -.09  -.0026   1.0007   -.0001    -.0002   .1290   .1146
```

```
VISUAL EFFECTS FOR NON-HORIZONTAL CLEAR SKY VIEWS THROUGH PLUME CENTER

2250 MW COAL POWER PLANT

DOWNWIND DISTANCE (KM) =    2.0
PLUME ALTITUDE (M)     =  439.

THETA  ALPHA   BETA    RP   YCAP     L      X       Y  DELYCAP  DELL  C(550)  BRATIO   DELX    DELY  E(LUV)   E(LAB)

 90.
        30.    15.   3.31  39.00  68.78  .2849  .2994   4.41    3.32   .1419  .5275   .0285   .0347 22.5455 14.4899
        30.    30.   1.38  29.95  61.64  .2844  .2973   9.06    8.78   .4596  .4171   .0367   .0460 23.5745 17.2808
        30.    45.    .98  26.44  58.48  .2861  .2986  10.90   12.08   .7366  .3679   .0413   .0521 23.7606 19.0296
        30.    60.    .67  24.75  56.87  .2875  .3000  11.77   14.09   .9494  .3419   .0440   .0556 23.9660 20.2018
        30.    75.    .50  23.94  56.06  .2883  .3009  12.18   15.19  1.0830  .3287   .0455   .0575 24.1431 20.8850
        30.    90.    .44  23.70  55.82  .2886  .3012  12.30   15.54  1.1284  .3245   .0460   .0581 24.2133 21.1107
        45.    15.   2.36  37.75  67.86  .2785  .2922   3.16    2.41   .1032  .6032   .0221   .0275 17.8639 11.4543
        45.    30.   1.16  27.63  59.58  .2767  .2881   6.73    6.71   .3427  .4951   .0290   .0368 18.5282 13.5724
        45.    45.    .76  23.69  55.81  .2779  .2888   8.15    9.40   .5516  .4413   .0332   .0423 18.6914 15.0178
        45.    60.    .57  21.80  55.85  .2792  .2899   8.82   11.08   .7124  .4117   .0357   .0455 18.8802 16.0127
        45.    75.    .47  20.91  52.88  .2800  .2907   9.15   12.01   .8135  .3965   .0371   .0473 19.0330 16.5934
        45.    90.    .44  20.64  52.59  .2802  .2910   9.24   12.31   .8480  .3917   .0376   .0479 19.0905 16.7871
        60.    15.   1.94  37.18  67.44  .2752  .2883   2.59    1.99   .0853  .6480   .0188   .0236 15.3305  9.8328
        60.    30.    .98  26.51  58.56  .2726  .2831   5.62    5.69   .2867  .5431   .0249   .0318 15.8822 11.6368
        60.    45.    .67  22.36  54.44  .2735  .2834   6.82    8.04   .4623  .4877   .0288   .0369 16.0487 12.9241
        60.    60.    .53  20.38  52.30  .2747  .2844   7.40    9.52   .5975  .4564   .0312   .0400 16.2384 13.8237
        60.    75.    .46  19.43  51.23  .2754  .2851   7.67   10.35   .6826  .4400   .0326   .0417 16.3874 14.3534
        60.    90.    .44  19.15  50.90  .2757  .2853   7.75   10.62   .7117  .4349   .0330   .0422 16.4428 14.5282
        90.    15.   1.70  36.84  67.18  .2731  .2858   2.25    1.73   .0744  .6790   .0167   .0211 13.7064  8.7747
        90.    30.    .88  25.83  57.91  .2699  .2798   4.94    5.04   .2519  .5774   .0222   .0286 14.1657 10.3830
        90.    45.    .62  21.54  53.37  .2706  .2798   6.00    7.17   .4067  .5215   .0259   .0333 14.3355 11.5645
        90.    60.    .51  19.49  51.29  .2717  .2806   6.31    8.52   .5239  .4892   .0282   .0362 14.5260 12.3987
        90.    75.    .45  18.51  50.15  .2724  .2813   6.75    9.28   .6010  .4722   .0295   .0379 14.6732 12.8924
        90.    90.    .44  18.22  49.80  .2726  .2815   6.83    9.52   .6266  .4668   .0300   .0384 14.7277 13.0555
```

```
PLUME VISUAL EFFECTS FOR HORIZONTAL VIEWS
PERPENDICULAR TO THE PLUME OF WHITE, GRAY, AND BLACK OBJECTS
FOR VARIOUS OBSERVER-PLUME AND OBSERVER-OBJECT DISTANCES

2230 MW COAL POWER PLANT

DOWNWIND DISTANCE (KM) =    2.0
THETA =   90.

REFLECT  RP/RV0  RO/RV0   YCAP     L       X       Y DELYCAP   DELL  C(550)  BRATIO    DELX    DELY  E(LUV)  E(LAB)
  1.0      .02     .02   85.11   93.94  .3387  .3486  -12.29  -5.05  -.1247   .9118   .0071   .0067  7.9038  6.4175
  1.0      .02     .05   78.98   91.23  .3410  .3504  -14.88  -6.34  -.1576   .8236   .0106   .0105 11.1121  8.7464
  1.0      .02     .10   70.22   87.11  .3438  .3323  -18.37  -8.38  -.2090   .7272   .0157   .0138 13.6126 12.1138
  1.0      .02     .20   57.02   80.21  .3458  .3325  -24.09 -11.98  -.2985   .6340   .0226   .0221 21.6839 16.9133
  1.0      .02     .50   37.62   67.77  .3344  .3391  -32.09 -19.10  -.4627   .6328   .0233   .0207 26.8739 22.4810
  1.0      .02     .80   31.33   62.81  .3196  .3269  -34.63 -22.18  -.3248   .7333   .0148   .0134 26.8638 23.9799
  1.0      .05     .05   82.93   92.99  .3353  .3444  -10.93  -4.39  -.1132   .9319   .0051   .0045  6.3466  3.3683
  1.0      .05     .10   74.16   89.01  .3374  .3454  -14.62  -6.49  -.1642   .8564   .0094   .0089 10.2979  8.2933
  1.0      .05     .20   60.96   82.37  .3380  .3442  -20.14  -9.81  -.2494   .7697   .0148   .0137 13.6681 12.3631
  1.0      .05     .50   41.56   70.60  .3248  .3290  -28.15 -16.27  -.4057   .8077   .0136   .0106 20.3332 17.8385
  1.0      .05     .80   35.27   65.99  .3107  .3171  -30.69 -19.00  -.4648   .9207   .0059   .0036 20.8824 19.6090
  1.0      .10     .10   79.78   91.39  .3307  .3384   -9.00  -3.90  -.1003   .9961   .0027   .0019  4.3131  4.1329
  1.0      .10     .20   66.38   85.31  .3299  .3359  -14.32  -6.88  -.1793   .9144   .0067   .0035  9.0160  7.7373
  1.0      .10     .50   47.18   74.33  .3158  .3201  -22.33 -12.34  -.3244   .9627   .0047   .0017 13.6840 12.8979
  1.0      .10     .80   40.89   70.12  .3030  .3091  -25.07 -14.87  -.3792  1.0773  -.0018  -.0043 13.0477 14.9077
  1.0      .20     .20   74.99   89.40  .3229  .3295   -6.12  -2.79  -.0743  1.0363  -.0003  -.0010  2.8265  2.8142
  1.0      .20     .50   55.59   79.40  .3092  .3144  -14.12  -7.47  -.2025  1.0730  -.0020  -.0040  7.3661  7.3443
  1.0      .20     .80   49.30   75.66  .2980  .3049  -16.66  -9.33  -.2510  1.1722  -.0067  -.0086  9.9663  9.6764
  1.0      .50     .50   67.76   85.90  .3093  .3166   -1.95   -.97  -.0267  1.0384  -.0018  -.0017  1.6443  1.2729
  1.0      .50     .80   61.46   82.64  .3003  .3091   -4.49  -2.35  -.0639  1.0929  -.0045  -.0044  3.9219  3.0326
  1.0      .80     .80   65.32   84.66  .3037  .3127    -.64   -.33  -.0087  1.0201  -.0010  -.0008   .7830   .3314
   .5      .02     .02   49.16   75.57  .3302  .3400   -1.93  -1.18  -.0334   .9875   .0030   .0030  2.4870  1.8714
   .5      .02     .05   46.91   74.16  .3305  .3401   -3.66  -3.48  -.1043   .8331   .0095   .0102  8.1804  6.0433
   .5      .02     .10   43.69   72.03  .3304  .3396  -10.97  -6.82  -.1988   .7085   .0167   .0178 14.9636 11.0973
   .5      .02     .20   38.83   68.66  .3285  .3372  -18.92 -11.96  -.3273   .6348   .0226   .0233 22.2632 16.9323
   .5      .02     .50   31.68   63.10  .3183  .3273  -30.44 -19.89  -.4896   .7037   .0183   .0177 26.7893 22.6746
   .5      .02     .80   29.34   61.11  .3109  .3217  -34.09 -22.37  -.3330   .8002   .0113   .0115 26.7769 24.1299
   .5      .05     .05   50.86   76.61  .3229  .3317   -1.71  -1.03  -.0289   .9989   .0020   .0018  1.8312  1.4189
   .5      .05     .10   47.64   74.62  .3224  .3307   -7.03  -4.25  -.1263   .8375   .0086   .0089  8.3936  6.2865
   .5      .05     .20   42.78   71.43  .3199  .3276  -14.98  -9.19  -.2588   .7736   .0140   .0138 13.4345 12.0009
   .5      .05     .50   35.62   66.26  .3096  .3176  -26.49 -16.73  -.4261   .8375   .0096   .0080 20.2996 17.9972
   .5      .05     .80   33.29   64.42  .3029  .3123  -30.15 -19.26  -.4730   .9664   .0032   .0021 20.8840 19.7373
   .5      .10     .10   53.26   78.03  .3147  .3226   -1.41   -.82  -.0228  1.0073   .0009   .0008  1.1719   .9604
   .5      .10     .20   48.40   75.10  .3119  .3192   -9.36  -5.32  -.1610   .9144   .0039   .0033  8.0339  6.3303
   .5      .10     .50   41.24   70.37  .3021  .3096  -20.87 -12.62  -.3336  1.0003   .0021  -.0000 13.3960 12.8937
   .5      .10     .80   38.91   68.71  .2962  .3048  -24.33 -14.98  -.3845  1.1141  -.0035  -.0034 13.1065 13.0013
   .5      .20     .20   56.80   80.09  .3060  .3138    -.93   -.33  -.0146  1.0112   .0001  -.0001   .3614   .3411
   .5      .20     .50   49.63   75.87  .2974  .3033  -12.47  -7.12  -.1999  1.0844  -.0026  -.0043  7.1905  7.1780
   .5      .20     .80   47.31   74.41  .2923  .3013  -16.12  -9.27  -.2518  1.1893  -.0073  -.0089  9.8899  9.6123
   .5      .50     .50   61.82   82.83  .2997  .3094    -.30   -.16  -.0042  1.0069  -.0003  -.0003   .2336   .1926
   .5      .50     .80   59.48   81.37  .2937  .3062   -3.93  -2.11  -.0604  1.0830  -.0039  -.0040  3.4072  2.6970
   .5      .80     .80   63.34   83.64  .2995  .3101    -.10   -.03  -.0013  1.0032  -.0001  -.0001   .1107   .0772
  0.0      .02     .02   13.22   43.13  .2838  .2932    8.43  16.98  1.7931   .3271   .0263   .0321 17.0207 17.2314
  0.0      .02     .05   14.84   45.46  .2837  .2940    3.36   3.37   .3305   .3630   .0236   .0291 11.0233  9.0472
  0.0      .02     .10   17.17   48.31  .2846  .2961   -3.38  -3.97  -.1333   .6130   .0204   .0234 16.1439 10.8334
  0.0      .02     .20   20.63   52.60  .2877  .3010  -13.76 -12.71  -.3936   .6881   .0163   .0204 22.7317 17.0363
  0.0      .02     .50   25.73   57.82  .2966  .3116  -28.79 -20.97  -.3232   .8126   .0100   .0125 26.3626 23.0172
  0.0      .02     .80   27.36   59.34  .3013  .3161  -33.33 -23.01  -.3460   .8676   .0071   .0093 26.6938 24.3240
  0.0      .05     .05   18.79   50.48  .2770  .2852    7.31  10.39   .6762   .6635   .0169   .0203 10.7635 10.8179
  0.0      .05     .10   21.11   53.11  .2784  .2878     .37    .63   .0345   .7160   .0143   .0171  9.1907  6.0336
  0.0      .05     .20   24.60   56.71  .2817  .2928   -9.81  -8.60  -.2804   .7995   .0104   .0122 13.3242 11.3801
```

0.0	.03	.30	29.68	61.41	.2901	.3029	-24.84	-17.38	-.4317	.9368	.0033	.0038	20.1744	18.2363
0.0	.03	.80	31.30	62.79	.2943	.3071	-29.61	-19.33	-.4817	1.0302	.0001	.0003	20.9049	19.9386
0.0	.10	.10	26.73	38.76	.2748	.2831	6.19	6.28	.3032	.7730	.0107	.0124	7.0808	6.7940
0.0	.10	.20	30.22	61.87	.2778	.2876	-4.19	-3.44	-.1189	.8733	.0063	.0070	7.7182	3.3069
0.0	.10	.30	33.30	66.01	.2831	.2966	-19.22	-12.78	-.3496	1.0692	-.0013	-.0026	13.3231	12.9473
0.0	.10	.80	36.92	67.23	.2888	.3002	-23.99	-13.10	-.3901	1.1633	-.0034	-.0063	13.1831	13.1123
0.0	.20	.20	38.62	68.30	.2774	.2872	4.21	3.19	.1231	.8702	.0060	.0066	4.2808	3.7231
0.0	.20	.30	43.70	72.03	.2833	.2944	-10.82	-6.73	-.1966	1.0987	-.0033	-.0047	6.7831	6.7734
0.0	.20	.80	43.33	73.13	.2863	.2974	-13.38	-9.22	-.2327	1.2111	-.0079	-.0093	9.8194	9.3488
0.0	.30	.30	33.87	79.36	.2887	.3010	1.33	.78	.0241	.9370	.0021	.0019	1.3494	1.1203
0.0	.30	.80	37.30	80.48	.2910	.3032	-3.41	-1.87	-.0346	1.0709	-.0033	-.0035	2.8649	2.3263
0.0	.80	.80	61.36	82.39	.2931	.3073	.44	.24	.0067	.9828	.0008	.0006	.6133	.4066

```
                 CONCENTRATIONS OF AEROSOL AND GASES CONTRIBUTED BY

                              2230 MW COAL POWER PLANT

WNWIND DISTANCE (KM) =    3.0
UME ALTITUDE (M)     =   439.
GMA Y (M)            =   222.
GMA Z (M)            =    37.
2-SO4 CONVERSION RATE=       .3000 PERCENT/HR
X-NO3 CONVERSION RATE=      0.0000 PERCENT/HR

TITUDE         NOX      NO2       NO3-   NO2/NTOT  NO3-/NTOT     SO2       SO4=   SO4=/STOT     O3     PRIMARY BSP-TOTAL  BSPSN/BSP
              (PPM)    (PPM)    (UG/M3)  (MOLE %)  (MOLE %)     (PPM)    (UG/M3)  (MOLE %)    (PPM)   (UG/M3) (10-4 M-1)   (%)
+2S
CREMENT:       .309     .049     0.000    13.863     0.000       .381     1.399      .107     -.037    12.447      .342    27.132
TAL AMB:       .309     .049     0.000    13.863     0.000       .381     3.343      .223      .003    44.191      .344    33.724
+1S
CREMENT:      1.386     .113     0.000     8.277     0.000      1.706     7.163      .107     -.039    33.781     1.333    27.132
TAL AMB:      1.386     .113     0.000     8.277     0.000      1.706     8.910      .133      .001    87.326     1.733    29.839

CREMENT:      2.283     .196     0.000     8.368     0.000      2.813    11.814      .107     -.039    91.968     2.328    27.132
TAL AMB:      2.283     .196     0.000     8.368     0.000      2.813    13.338      .123      .001   123.713     2.730    28.839
-1S
CREMENT:      1.386     .113     0.000     8.277     0.000      1.706     7.163      .107     -.039    33.781     1.333    27.132
TAL AMB:      1.386     .113     0.000     8.277     0.000      1.706     8.910      .133      .001    87.326     1.733    29.839
-2S
CREMENT:       .309     .049     0.000    13.863     0.000       .381     1.399      .107     -.037    12.447      .342    27.132
TAL AMB:       .309     .049     0.000    13.863     0.000       .381     3.343      .223      .003    44.191      .344    33.724
0
CREMENT:       .000     .000     0.000     0.000     0.000       .000      .000      .107     -.000      .000      .000    27.132
TAL AMB:       .000     .000     0.000    73.083     0.000       .000     1.743   100.000      .040    31.743      .202    30.270


ULATIVE SURFACE DEPOSITION (MOLE FRACTION OF INITIAL FLUX)

              SO2:      .0000
              NOX:      .0000
MARY PARTICULATE:      .0000
              SO4:      .0000
              NO3:     0.0000
```

```
                 VISUAL EFFECTS FOR HORIZONTAL SIGHT PATHS
                 2250 MW COAL POWER PLANT

OWNWIND DISTANCE (KM) =     5.0
LUME ALTITUDE (M)     =   439.
IGHT PATH IS THROUGH PLUME CENTER

HETA ALPHA  RP/RV0     RV  %REDUCED     YCAP        L        X         Y DELYCAP      DELL  C(550)  BRATIO     DELX      DELY  E(LUV)  E(LAB)

 90.
       30.       .02   121.2     6.80    58.28    80.91   .3174    .3308   -5.83     -3.13  -.0844   .7413    .0173     .0197 16.2850 10.6283
       30.       .05   120.8     7.06    58.96    81.29   .3140    .3264   -5.16     -2.75  -.0751   .7988    .0140     .0155 13.1660  8.5241
       30.       .10   120.3     7.42    59.92    81.81   .3099    .3211   -4.20     -2.23  -.0618   .8682    .0098     .0101  9.2679  5.9459
       30.       .20   119.7     7.96    61.32    82.57   .3030    .3153   -2.80     -1.48  -.0420   .9449    .0049     .0042  4.6311  2.9688
       30.       .50   118.7     8.71    63.26    83.60   .3006    .3110    -.85      -.45  -.0133   .9981    .0005    -.0001   .6808   .5438
       30.       .80   118.4     8.94    63.84    83.90   .3000    .3108    -.28      -.14  -.0045  1.0006   -.0000    -.0003   .2195   .1953
       45.       .02   123.8     4.75    59.76    81.73   .3129    .3260   -4.36     -2.32  -.0627   .7988    .0129     .0149 12.3998  8.0559
       45.       .05   123.6     4.94    60.27    82.00   .3105    .3228   -3.85     -2.04  -.0558   .8433    .0105     .0117 10.0621  6.4935
       45.       .10   123.2     5.20    60.98    82.39   .3075    .3189   -3.14     -1.66  -.0459   .8971    .0074     .0078  7.1180  4.5369
       45.       .20   122.7     5.59    62.03    82.95   .3038    .3144   -2.09     -1.10  -.0312   .9567    .0038     .0033  3.5796  2.2874
       45.       .50   122.0     6.15    63.48    83.71   .3005    .3110    -.64      -.33  -.0099   .9983    .0004    -.0000   .5195   .4076
       45.       .80   121.8     6.32    63.91  [illegible] .3000  .3109    -.21      -.11  -.0033  1.0004   -.0000    -.0002   .1615   .1440
       60.       .02   125.0     3.85    60.47    82.11   .3108    .3236   -3.65     -1.93  -.0523   .8285    .0107     .0125 10.4638  6.7832
       60.       .05   124.8     4.01    60.90    82.34   .3088    .3209   -3.22     -1.70  -.0466   .8663    .0083     .0099  8.5039  5.4805
       60.       .10   124.5     4.23    61.30    82.66   .3063    .3177   -2.62     -1.38  -.0383   .9121    .0062     .0066  6.0312  3.8572
       60.       .20   124.1     4.55    62.37    83.13   .3032    .3139   -1.75      -.92  -.0260   .9629    .0032     .0029  3.0425  1.9415
       60.       .50   123.5     5.02    63.59    83.77   .3004    .3111    -.53      -.28  -.0083   .9985    .0004    -.0000   .4393   .3419
       60.       .80   123.3     5.16    63.95    83.95   .3000    .3109    -.17      -.09  -.0028  1.0003   -.0000    -.0002   .1343   .1198
       90.       .02   125.7     3.33    60.91    82.35   .3095    .3221   -3.20     -1.69  -.0459   .8475    .0094     .0110  9.2421  5.9831
       90.       .05   125.5     3.46    61.29    82.55   .3077    .3198   -2.83     -1.49  -.0409   .8811    .0077     .0087  7.5209  4.8411
       90.       .10   125.3     3.65    61.81    82.83   .3056    .3169   -2.30     -1.21  -.0337   .9218    .0055     .0059  5.3405  3.4132
       90.       .20   124.9     3.94    62.58    83.24   .3029    .3136   -1.33      -.80  -.0223   .9669    .0028     .0026  2.6992  1.7211
       90.       .50   124.4     4.34    63.65    83.80   .3004    .3111    -.47      -.24  -.0072   .9986    .0003    -.0000   .3887   .3010
       90.       .80   124.2     4.47    63.97    83.96   .3000    .3109    -.15      -.08  -.0024  1.0003   -.0000    -.0001   .1175   .1050
```

```
                    VISUAL EFFECTS FOR NON-HORIZONTAL CLEAR SKY VIEWS THROUGH PLUME CENTER

                    2250 MW COAL POWER PLANT

DOWNWIND DISTANCE (KM) =    5.0
PLUME ALTITUDE (M)     =   439.

THETA   ALPHA    BETA      RP    YCAP      L       X        Y DELYCAP    DELL  C(550)  BRATIO    DELX     DELY  E(LUV)   E(LAB)

 90.
         30.      15.    3.31   37.31   67.69   .2828   .2980    2.93    2.23   .0989   .5388   .0264   .0333 21.6747 13.8718
         30.      30.    1.58   27.68   59.63   .2809   .2943    6.79    6.76   .3488   .4571   .0332   .0430 21.8272 15.6839
         30.      45.     .98   23.86   53.98   .2820   .2949    8.32    9.58   .5668   .4087   .0372   .0483 21.5324 16.8684
         30.      60.     .67   22.03   54.09   .2831   .2960    9.05   11.32   .7343   .3820   .0397   .0516 21.4577 17.7246
         30.      75.     .50   21.15   53.15   .2839   .2968    9.39   12.28   .8393   .3680   .0411   .0534 21.4893 18.2479
         30.      90.     .44   20.89   52.86   .2842   .2971    9.49   12.58   .8750   .3635   .0415   .0540 21.5131 18.4251
         45.      15.    2.36   36.61   67.01   .2767   .2909    2.02    1.56   .0702   .6343   .0203   .0262 17.0950 10.9283
         45.      30.    1.16   25.86   57.94   .2734   .2851    4.97    5.07   .2566   .5394   .0257   .0338 16.9810 12.1958
         45.      45.     .76   21.68   53.72   .2739   .2850    6.14    7.32   .4193   .4890   .0292   .0384 16.6959 13.1230
         45.      60.     .57   19.68   51.51   .2748   .2857    6.70    8.74   .5444   .4601   .0314   .0413 16.6146 13.8168
         45.      75.     .47   18.73   50.40   .2755   .2863    6.97    9.53   .6231   .4448   .0326   .0429 16.6220 14.2421
         45.      90.     .44   18.44   50.06   .2757   .2865    7.05    9.78   .6500   .4400   .0330   .0434 16.6338 14.3850
         60.      15.    1.94   36.22   66.71   .2736   .2871    1.63    1.26   .0374   .6781   .0172   .0224 14.6537  9.3630
         60.      30.     .98   25.01   57.12   .2695   .2803    4.12    4.26   .2133   .3885   .0219   .0290 14.4772 10.4005
         60.      45.     .67   20.65   52.60   .2698   .2797    5.11    6.20   .3494   .5381   .0250   .0331 14.2243 11.2066
         60.      60.     .53   18.57   50.21   .2705   .2802    5.39    7.44   .4541   .5084   .0271   .0358 14.1572 11.8210
         60.      75.     .46   17.57   49.01   .2710   .2806    5.81    8.14   .5201   .4924   .0282   .0373 14.1665 12.2001
         60.      90.     .44   17.28   48.64   .2712   .2808    5.88    8.36   .5426   .4874   .0286   .0377 14.1776 12.3276
         90.      15.    1.70   35.99   66.54   .2716   .2846    1.40    1.09   .0497   .7079   .0152   .0199 13.0634  8.3445
         90.      30.     .88   24.50   56.62   .2671   .2771    3.60    3.75   .1867   .6228   .0194   .0258 12.8667  9.2471
         90.      45.     .62   20.02   51.89   .2671   .2762    4.48    5.49   .3063   .5730   .0223   .0297 12.6405  9.9763
         90.      60.     .51   17.88   49.39   .2677   .2766    4.90    6.61   .3984   .5430   .0242   .0321 12.5861 10.5392
         90.      75.     .45   16.86   48.12   .2682   .2769    5.10    7.25   .4564   .5268   .0253   .0336 12.5994 10.8883
         90.      90.     .44   16.35   47.73   .2683   .2771    5.16    7.45   .4762   .5216   .0257   .0340 12.6112 11.0060
```

PLUME VISUAL EFFECTS FOR HORIZONTAL VIEWS
PERPENDICULAR TO THE PLUME OF WHITE, GRAY, AND BLACK OBJECTS
FOR VARIOUS OBSERVER-PLUME AND OBSERVER-OBJECT DISTANCES

2230 MW COAL POWER PLANT

DOWNWIND DISTANCE (KM) = 5.0
THETA = 90.

REFLECT	RP/RV0	RO/RV0	YCAP	L	X	Y	DELYCAP	DELL	C(550)	BRATIO	DELX	DELY	E(LUV)	E(LAB)
1.0	.02	.02	86.46	94.31	.3405	.3303	-10.95	-4.48	-.1114	.8802	.0089	.0084	8.8663	6.7035
1.0	.02	.05	80.05	91.72	.3429	.3322	-13.81	-5.86	-.1468	.7949	.0126	.0124	12.2412	9.2032
1.0	.02	.10	70.89	87.44	.3460	.3343	-17.89	-8.65	-.2022	.6976	.0179	.0177	16.9029	12.7440
1.0	.02	.20	57.09	80.25	.3484	.3547	-24.91	-11.94	-.2986	.6054	.0252	.0242	23.1389	17.7379
1.0	.02	.50	36.82	67.17	.3369	.3409	-32.89	-19.70	-.4756	.6284	.0258	.0225	28.3062	23.4838
1.0	.02	.80	30.23	61.89	.3211	.3279	-35.73	-23.10	-.5424	.7372	.0163	.0145	28.1309	25.0533
1.0	.05	.05	84.13	93.51	.3372	.3460	-9.73	-4.06	-.1029	.9228	.0068	.0061	7.1082	5.5096
1.0	.05	.10	74.97	89.39	.3393	.3471	-13.81	-6.10	-.1558	.8287	.0112	.0105	11.2767	8.6536
1.0	.05	.20	61.18	82.49	.3400	.3459	-19.93	-9.70	-.2478	.7440	.0168	.0134	16.7774	13.0958
1.0	.05	.50	40.90	70.13	.3264	.3301	-28.81	-16.74	-.4165	.7897	.0153	.0117	21.3894	18.5439
1.0	.05	.80	34.32	65.24	.3114	.3174	-31.64	-19.75	-.4803	.9138	.0066	.0040	21.7888	20.4086
1.0	.10	.10	80.78	92.04	.3322	.3398	-8.00	-3.45	-.0896	.9707	.0042	.0032	4.9345	4.0698
1.0	.10	.20	66.99	85.31	.3315	.3372	-14.12	-6.67	-.1752	.8918	.0083	.0068	9.6908	7.9364
1.0	.10	.50	46.71	74.03	.3169	.3207	-23.00	-12.84	-.3323	.9303	.0057	.0023	14.2538	13.2933
1.0	.10	.80	40.13	69.59	.3032	.3090	-25.83	-15.40	-.3916	1.0774	-.0016	-.0045	15.6217	15.4362
1.0	.20	.20	73.68	89.72	.3241	.3304	-5.42	-2.46	-.0664	1.0165	.0009	-.0000	2.6310	2.5188
1.0	.20	.50	55.41	79.29	.3098	.3147	-14.30	-7.37	-.2060	1.0662	-.0013	-.0037	7.6762	7.6472
1.0	.20	.80	43.82	75.36	.2980	.3046	-17.14	-9.63	-.2587	1.1747	-.0067	-.0088	10.2432	9.9740
1.0	.50	.50	67.99	86.02	.3099	.3170	-1.72	-.85	-.0238	1.0289	-.0013	-.0014	1.2881	1.0566
1.0	.50	.80	61.41	82.62	.3004	.3090	-4.33	-2.37	-.0670	1.0908	-.0044	-.0044	3.8980	3.0637
1.0	.80	.80	63.40	84.71	.3040	.3128	-.36	-.28	-.0078	1.0157	-.0008	-.0007	.6328	.4415
.5	.02	.02	48.88	75.40	.3[illegible]	.3417	-2.21	-1.36	-.0402	.9554	.0049	.0047	3.7329	2.6842
.5	.02	.05	46.33	73.91	.3325	.3419	-6.04	-3.73	-.1129	.8055	.0115	.0120	9.4788	6.9021
.5	.02	.10	43.16	71.69	.3325	.3414	-11.50	-7.18	-.2097	.6848	.0187	.0196	16.2933	12.0006
.5	.02	.20	38.08	68.11	.3305	.3389	-19.67	-12.31	-.3415	.6147	.0246	.0230	23.6124	17.9197
.5	.02	.50	30.60	62.20	.3196	.3284	-31.52	-20.79	-.5079	.6904	.0197	.0188	28.0608	23.7387
.5	.02	.80	28.16	60.06	.3116	.3224	-85.28	-23.62	-.5545	.7936	.0120	.0122	28.0033	25.2481
.5	.05	.05	50.61	76.46	.3244	.3329	-1.96	-1.18	-.0347	.9769	.0034	.0031	2.8276	2.0125
.5	.05	.10	47.24	74.37	.3238	.3320	-7.42	-4.50	-.1346	.8392	.0101	.0101	9.3323	6.9207
.5	.05	.20	42.16	71.01	.3212	.3287	-15.39	-9.61	-.2705	.7615	.0153	.0148	16.4262	12.6799
.5	.05	.50	34.68	65.33	.3103	.3180	-27.43	-17.46	-.4421	.8528	.0103	.0083	21.1965	18.7849
.5	.05	.80	32.24	63.37	.3030	.3122	-31.20	-20.12	-.4902	.9703	.0033	.0020	21.77[illegible]	20.6187
.5	.10	.10	53.05	77.93	.3157	.3234	-1.61	-.94	-.0274	.9940	.0019	.0013	1.8087	1.3199
.5	.10	.20	47.98	74.83	.3127	.3198	-9.78	-5.79	-.1693	.9055	.0068	.0039	8.6421	6.9376
.5	.10	.50	40.49	69.85	.3023	.3095	-21.62	-13.14	-.3483	1.0020	.0023	-.0001	14.1663	13.4301
.5	.10	.80	38.05	68.09	.2959	.3044	-25.38	-15.60	-.3985	1.1248	-.0037	-.0038	15.7289	15.6260
.5	.20	.20	56.67	80.01	.3065	.3141	-1.08	-.61	-.0175	1.0033	.0006	.0002	.8092	.6734
.5	.20	.50	49.19	75.59	.2973	.3051	-12.93	-7.40	-.2078	1.0881	-.0027	-.0046	7.4834	7.4678
.5	.20	.80	46.75	74.05	.2920	.3008	-16.69	-9.63	-.2611	1.2003	-.0077	-.0094	10.2914	9.9960
.5	.50	.50	61.73	82.81	.2998	.3094	-.34	-.18	-.0050	1.0058	-.0002	-.0003	.2237	.2048
.5	.50	.80	59.34	81.49	.2956	.3061	-4.10	-2.19	-.0628	1.0861	-.0040	-.0041	3.5287	2.7970
.5	.80	.80	63.33	83.63	.2995	.3101	-.11	-.06	-.0015	1.0028	-.0001	-.0001	.1069	.0797
0.0	.02	.02	11.30	40.13	.2789	.2877	6.32	13.98	1.3869	.5935	.0213	.0266	14.0232	14.1424
0.0	.02	.05	13.00	42.81	.2795	.2894	1.72	2.72	.1643	.6273	.0194	.0246	9.2827	7.1052
0.0	.02	.10	15.43	46.26	.2812	.2927	-5.11	-6.22	-.2412	.6683	.0171	.0220	16.2739	11.3820
0.0	.02	.20	19.07	50.81	.2835	.2990	-15.33	-14.50	-.4402	.7278	.0141	.0184	23.5038	18.2238
0.0	.02	.50	24.38	56.50	.2958	.3112	-30.14	-22.28	-.5484	.8311	.0092	.0121	27.6797	24.2384
0.0	.02	.80	26.08	58.15	.3011	.3162	-34.83	-24.20	-.5674	.8773	.0069	.0094	27.8812	23.3093
0.0	.05	.05	17.08	48.40	.2732	.2809	5.80	8.32	.5225	.7296	.0130	.0160	8.3092	8.3939
0.0	.05	.10	19.31	51.32	.2732	.2844	-1.03	-1.16	-.0447	.7743	.0111	.0137	8.3326	5.4463
0.0	.05	.20	23.15	55.26	.2795	.2906	-11.25	-10.05	-.3229	.8464	.0081	.0099	13.6870	12.2302

0.0	.03	.30	28.46	60.34	.2890	.3020	-26.03	-18.44	-.4743	.9836	.0024	.0029	21.0067	19.2304
0.0	.03	.80	30.17	61.83	.2937	.3065	-30.73	-20.32	-.3008	1.0314	-.0005	-.0092	21.8038	20.8799
0.0	.10	.10	23.32	37.42	.2721	.2802	4.78	4.94	.2338	.8268	.0080	.0095	3.4382	3.2891
0.0	.10	.20	28.97	60.78	.2738	.2833	-3.44	-4.33	-.1336	.9179	.0044	.0049	7.6079	3.7173
0.0	.10	.30	34.28	63.21	.2840	.2933	-20.24	-13.37	-.3683	1.1012	-.0026	-.0037	14.1361	13.6943
0.0	.10	.80	33.98	66.33	.2880	.2994	-24.93	-13.82	-.4039	1.1898	-.0062	-.0073	13.8746	13.8262
0.0	.20	.20	37.66	67.80	.2738	.2836	3.26	2.48	.0931	.9026	.0045	.0039	3.2291	2.8370
0.0	.20	.30	42.97	71.36	.2823	.2935	-11.33	-7.22	-.2100	1.1246	-.0043	-.0036	7.2920	7.2863
0.0	.20	.80	44.67	72.70	.2836	.2967	-16.24	-9.63	-.2636	1.2337	-.0087	-.0100	10.3486	10.0231
0.0	.30	.30	33.36	79.38	.2881	.3005	1.04	.60	.0186	.9680	.0015	.0014	1.1681	.8332
0.0	.30	.80	37.26	80.33	.2906	.3029	-3.63	-2.00	-.0383	1.0801	-.0036	-.0038	3.1339	2.3162
0.0	.80	.80	61.23	82.33	.2949	.3072	.34	.18	.0032	.9872	.0006	.0005	.4638	.3092

```
                 CONCENTRATIONS OF AEROSOL AND GASES CONTRIBUTED BY

                              2250 MW COAL POWER PLANT

DOWNWIND DISTANCE (KM)  =   10.0
PLUME ALTITUDE (M)      =   439.
SIGMA Y (M)             =   413.
SIGMA Z (M)             =    80.
SO2-SO4 CONVERSION RATE=        .3000 PERCENT/HR
NOX-NO3 CONVERSION RATE=       0.0000 PERCENT/HR

ALTITUDE         NOX       NO2       NO3-    NO2/NTOT  NO3-/NTOT      SO2        SO4=  SO4=/STOT      O3      PRIMARY  BSP-TOTAL   BSPSN/BSP
                (PPM)     (PPM)    (UG/M3)  (MOLE %)  (MOLE %)      (PPM)     (UG/M3)  (MOLE %)    (PPM)    (UG/M3) (10-4 M-1)   (%)
  H+2S
INCREMENT:       .116      .038     0.000    32.663     0.000        .143      1.384       .246     -.034      4.689      .174     46.132
TOTAL AMB:       .116      .038     0.000    32.663     0.000        .143      3.129       .333      .006     36.434      .376     48.331
  H+1S
INCREMENT:       .322      .069     0.000    13.303     0.000        .642      6.203       .246     -.038     21.016      .781     46.132
TOTAL AMB:       .322      .069     0.000    13.303     0.000        .642      7.947       .314      .002     32.760      .983     46.981
  H
INCREMENT:       .861      .103     0.000    12.187     0.000       1.038     10.227       .246     -.038     34.649     1.288     46.132
TOTAL AMB:       .861      .103     0.000    12.[illegible]     0.000       1.038     11.971       .287      .002     66.393     1.490     46.692
  H-1S
INCREMENT:       .322      .069     0.000    13.303     0.000        .642      6.203       .246     -.038     21.016      .781     46.132
TOTAL AMB:       .322      .069     0.000    13.303     0.000        .642      7.947       .314      .002     32.760      .983     46.981
  H-2S
INCREMENT:       .116      .038     0.000    32.663     0.000        .143      1.384       .246     -.034      4.689      .174     46.132
TOTAL AMB:       .116      .038     0.000    32.663     0.000        .143      3.129       .333      .006     36.434      .376     48.331
  0
INCREMENT:       .000      .000     0.000     0.000     0.000        .000       .000       .246     -.000       .000      .000     46.132
TOTAL AMB:       .000      .000     0.000    73.077     0.000        .000      1.743     99.833      .040     31.743      .202     50.270


CUMULATIVE SURFACE DEPOSITION (MOLE FRACTION OF INITIAL FLUX)

                   SO2:     .0000
                   NOX:     .0000
   PRIMARY PARTICULATE:     .0000
                   SO4:     .0000
                   NO3:    0.0000
```

```
              VISUAL EFFECTS FOR HORIZONTAL SIGHT PATHS
              2250 MW COAL POWER PLANT

DOWNWIND DISTANCE (KM) =    10.0
PLUME ALTITUDE (M)     =    439.
SIGHT PATH IS THROUGH PLUME CENTER

THETA ALPHA  RP/RV0    RV  %REDUCED    YCAP       L        X        Y DELYCAP    DELL  C(550)  BRATIO    DELX     DELY  E(LUV)   E(LAB)
 90.
        30.     .02   121.4    6.60   57.91   80.70   .3201   .3336   -6.21   -3.34  -.0902   .7098   .0200   .0226 18.4809 12.0517
        30.     .05   121.1    6.88   58.63   81.11   .3162   .3286   -5.49   -2.94  -.0803   .7734   .0162   .0175 14.9505  9.6552
        30.     .10   120.5    7.27   59.65   81.67   .3115   .3226   -4.47   -2.38  -.0661   .8504   .0114   .0116 10.5451  6.7300
        30.     .20   119.8    7.84   61.15   82.48   .3058   .3159   -2.97   -1.57  -.0449   .9359   .0058   .0049  5.3070  3.3624
        30.     .50   118.8    8.65   63.22   83.57   .3007   .3110    -.90    -.47  -.0142   .9965   .0007  -.0000   .7936    .6062
        30.     .80   118.4    8.90   63.83   83.89   .3001   .3108    -.29    -.15  -.0047  1.0002   .0000  -.0003   .2382    .2099
        45.     .02   124.0    4.60   59.48   81.57   .3150   .3282   -4.64   -2.47  -.0670   .7724   .0149   .0171 14.1361  9.1730
        45.     .05   123.8    4.81   60.02   81.86   .3122   .3245   -4.10   -2.18  -.0596   .8221   .0121   .0135 11.4811  7.3902
        45.     .10   123.4    5.09   60.78   82.28   .3087   .3200   -3.34   -1.76  -.0491   .8823   .0086   .0090  8.1403  5.1857
        45.     .20   122.8    5.31   61.90   82.88   .3045   .3150   -2.22   -1.16  -.0333   .9493   .0044   .0039  4.1236  2.6061
        45.     .50   122.1    6.11   63.45   83.69   .3006   .3111    -.67    -.35  -.0106   .9971   .0005   .0000   .6106    .4562
        45.     .80   121.8    6.29   63.90   83.93   .3001   .3109    -.22    -.11  -.0035  1.0001   .0000  -.0002   .1758    .1549
        60.     .02   125.1    3.74   60.23   81.98   .3125   .3235   -3.89   -2.06  -.0559   .8052   .0124   .0144 11.9534  7.7381
        60.     .05   124.9    3.90   60.69   82.23   .3102   .3224   -3.43   -1.82  -.0498   .8476   .0102   .0114  9.7267  6.2506
        60.     .10   124.6    4.14   61.33   82.57   .3073   .3187   -2.79   -1.47  -.0410   .8991   .0073   .0076  6.9136  4.4001
        60.     .20   124.2    4.49   62.26   83.07   .3038   .3144   -1.85    -.97  -.0278   .9564   .0038   .0034  3.5135  2.2182
        60.     .50   123.5    4.98   63.56   83.75   .3005   .3111    -.56    -.29  -.0088   .9974   .0005   .0000   .5178    .3835
        60.     .80   123.3    5.13   63.94   83.95   .3001   .3109    -.18    -.09  -.0029  1.0001   .0000  -.0002   .1464    .1289
        90.     .02   125.8    3.22   60.70   82.23   .3110   .3238   -3.42   -1.81  -.0491   .8264   .0109   .0127 10.5708  6.8329
        90.     .05   125.6    3.37   61.10   82.45   .3090   .3211   -3.02   -1.59  -.0437   .8642   .0089   .0101  8.6116  5.5283
        90.     .10   125.4    3.57   61.66   82.75   .3065   .3179   -2.45   -1.29  -.0360   .9100   .0064   .0068  6.1305  3.8994
        90.     .20   125.0    3.88   62.49   83.19   .3034   .3141   -1.63    -.85  -.0244   .9611   .0033   .0030  3.1217  1.9697
        90.     .50   124.4    4.31   63.63   83.79   .3005   .3111    -.49    -.26  -.0077   .9977   .0004   .0000   .4590    .3381
        90.     .80   124.2    4.44   63.96   83.96   .3001   .3109    -.16    -.08  -.0026  1.0000   .0000  -.0001   .1282    .1129
```

```
               VISUAL EFFECTS FOR NON-HORIZONTAL CLEAR SKY VIEWS THROUGH PLUME CENTER

               2250 MW COAL POWER PLANT

DOWNWIND DISTANCE (KM) =    10.0
PLUME ALTITUDE (M)     =    439.

THETA   ALPHA   BETA     RP   YCAP      L      X      Y DELYCAP   DELL  C(550) BRATIO   DELX   DELY  E(LUV)  E(LAB)
  90.
          30.    15.   3.31  37.08  67.37  .2842  .3003   2.50    1.91  .0875  .5479  .0278  .0356 23.1732 14.8306
          30.    30.   1.58  27.23  59.22  .2817  .2961   6.34    6.35  .3282  .4540  .0340  .0448 22.7596 16.2136
          30.    45.    .98  23.40  55.52  .2824  .2963   7.86    9.12  .5383  .4094  .0376  .0497 22.0940 17.1202
          30.    60.    .67  21.57  53.60  .2833  .2971   8.59   10.83  .6996  .3846  .0399  .0527 21.8037 17.8216
          30.    75.    .50  20.69  52.65  .2840  .2978   8.93   11.77  .8007  .3715  .0412  .0544 21.7299 18.2687
          30.    90.    .44  20.43  52.35  .2843  .2980   9.03   12.07  .8351  .3673  .0416  .0550 21.7237 18.4234
          45.    15.   2.36  36.27  66.76  .2779  .2928   1.69    1.30  .0615  .6235  .0215  .0281 18.3946 11.7654
          45.    30.   1.16  25.52  57.61  .2740  .2866   4.63    4.74  .2411  .5370  .0263  .0353 17.7689 12.6548
          45.    45.    .76  21.34  53.35  .2742  .2860   5.80    6.95  .3978  .4911  .0294  .0395 17.1462 13.3322
          45.    60.    .57  19.34  51.11  .2748  .2865   6.36    8.34  .5185  .4646  .0314  .0421 16.8647 13.8824
          45.    75.    .47  18.38  49.99  .2753  .2869   6.62    9.12  .5943  .4505  .0325  .0435 16.7679 14.2343
          45.    90.    .44  18.10  49.65  .2755  .2871   6.70    9.37  .6202  .4461  .0329  .0440 16.7473 14.3546
          60.    15.   1.94  35.93  66.50  .2746  .2888   1.35    1.04  .0500  .6677  .0182  .0241 15.8119 10.1106
          60.    30.    .98  24.73  56.84  .2700  .2815   3.83    3.97  .2003  .5866  .0224  .0302 15.1714 10.8090
          60.    45.    .67  20.36  52.28  .2699  .2806   4.82    5.88  .3314  .5409  .0251  .0340 14.6108 11.3885
          60.    60.    .53  18.28  49.87  .2704  .2808   5.30    7.10  .4324  .5138  .0270  .0364 14.3591 11.8708
          60.    75.    .46  17.29  48.66  .2708  .2811   5.52    7.78  .4960  .4992  .0280  .0377 14.2714 12.1816
          60.    90.    .44  16.99  48.28  .2710  .2813   5.59    8.00  .5177  .4946  .0283  .0382 14.2523 12.2880
          90.    15.   1.70  35.73  66.34  .2725  .2862   1.15     .89  .0432  .6982  .0161  .0215 14.1191  9.0267
          90.    30.    .88  24.24  56.36  .2675  .2783   3.35    3.50  .1732  .6213  .0198  .0270 13.4950  9.6188
          90.    45.    .62  19.76  51.61  .2672  .2770   4.22    5.20  .2905  .5763  .0224  .0304 12.9844 10.1392
          90.    60.    .51  17.63  49.08  .2675  .2771   4.65    6.30  .3793  .5490  .0241  .0327 12.7383 10.5794
          90.    75.    .45  16.61  47.80  .2679  .2773   4.85    6.93  .4352  .5342  .0251  .0339 12.6809 10.8646
          90.    90.    .44  16.30  47.41  .2681  .2774   4.91    7.13  .4543  .5293  .0254  .0344 12.6645 10.9626
```

```
         PLUME VISUAL EFFECTS FOR HORIZONTAL VIEWS
         PERPENDICULAR TO THE PLUME OF WHITE, GRAY, AND BLACK OBJECTS
         FOR VARIOUS OBSERVER-PLUME AND OBSERVER-OBJECT DISTANCES

         2250 MW COAL POWER PLANT

DOWNWIND DISTANCE (KM) =    10.0
THETA =    90.

REFLECT  RP/RV0  RO/RV0    YCAP      L       X        Y DELYCAP    DELL  C(550)  BRATIO    DELX     DELY  E(LUV)  E(LAB)

    1.0     .02     .02   86.29  94.44   .3423   .3519  -11.11   -4.55  -.1134   .8363   .0106    .0100 10.1826  7.4833
    1.0     .02     .05   79.88  91.64   .3447   .3537  -13.98   -5.94  -.1488   .7747   .0143    .0138 13.4696  9.9471
    1.0     .02     .10   70.72  87.36   .3476   .3536  -18.06   -8.13  -.2045   .6819   .0195    .0191 17.9871 13.4101
    1.0     .02     .20   56.92  80.13   .3498   .3538  -24.19  -12.05  -.3012   .5948   .0266    .0233 23.9911 18.2657
    1.0     .02     .50   36.62  67.02   .3379   .3416  -33.09  -19.83  -.4788   .6226   .0268    .0233 28.8033 23.8033
    1.0     .02     .80   30.02  61.70   .3217   .3285  -35.94  -23.29  -.5459   .7336   .0170    .0130 28.5294 25.3214
    1.0     .05     .05   83.99  93.45   .3387   .3473   -9.87   -4.13  -.1047   .9032   .0084    .0074  8.1832  6.1149
    1.0     .05     .10   74.83  89.32   .3407   .3482  -13.96   -6.17  -.1578   .8135   .0126    .0117 12.2235  9.1975
    1.0     .05     .20   61.02  82.41   .3412   .3467  -20.08   -9.78  -.2500   .7340   .0180    .0163 17.4916 13.3066
    1.0     .05     .50   40.72  70.01   .3271   .3305  -28.99  -16.86  -.4194   .7851   .0160    .0122 21.7471 18.7704
    1.0     .05     .80   34.13  65.09   .3118   .3177  -31.83  -19.90  -.4833   .9119   .0071    .0043 22.0397 20.5939
    1.0     .10     .10   80.68  91.99   .3334   .3407   -8.11   -3.50  -.0911   .9562   .0054    .0041  5.6802  4.4473
    1.0     .10     .20   66.87  85.45   .3325   .3379  -14.23   -6.73  -.1770   .8825   .0093    .0074 10.2390  8.2400
    1.0     .10     .50   46.57  73.94   .3173   .3209  -23.14  -12.93  -.3346   .9468   .0062    .0025 14.4675 13.4263
    1.0     .10     .80   39.98  69.48   .3034   .3091  -25.98  -15.51  -.3941  1.0770  -.0014   -.0044 15.7361 15.5712
    1.0     .20     .20   75.62  89.69   .3249   .3309   -5.49   -2.49  -.0675  1.0080   .0017    .0005  2.8911  2.6273
    1.0     .20     .50   55.32  79.24   .3101   .3148  -14.39   -7.62  -.2076  1.0634  -.0011   -.0036  7.7398  7.7010
    1.0     .20     .80   48.72  75.30   .2981   .3046  -17.24   -9.69  -.2604  1.1747  -.0067   -.0088 10.2895 10.0309
    1.0     .50     .50   67.98  86.01   .3101   .3170   -1.73    -.86  -.0242  1.0262  -.0011   -.0014  1.2184  1.0361
    1.0     .50     .80   61.39  82.60   .3004   .3090   -4.57   -2.39  -.0675  1.0901  -.0043   -.0044  3.8898  3.0707
    1.0     .80     .80   65.40  84.70   .3040   .3128    -.56    -.29  -.0079  1.0145  -.0007   -.0007   .6045   .4309
     .5     .02     .02   48.68  75.28   .3334   .3429   -2.41   -1.48  -.0444   .9398   .0062    .0059  4.6170  3.2478
     .5     .02     .05   46.33  73.78   .3337   .3429   -6.24   -3.86  -.1170   .7934   .0127    .0131 10.2743  7.4202
     .5     .02     .10   42.96  71.53   .3336   .3424  -11.70   -7.31  -.2137   .6739   .0198    .0206 17.0037 12.4621
     .5     .02     .20   37.88  67.96   .3315   .3397  -19.88  -12.66  -.3453   .6086   .0256    .0239 24.1965 18.3028
     .5     .02     .50   30.39  62.02   .3203   .3290  -31.73  -20.97  -.5115   .6872   .0203    .0194 28.4704 24.0239
     .5     .02     .80   27.94  59.87   .3122   .3229  -35.49  -23.82  -.5581   .7921   .0125    .0127 28.3558 25.3119
     .5     .05     .05   50.44  76.36   .3234   .3338   -2.14   -1.28  -.0383   .9660   .0044    .0039  3.5014  2.4314
     .5     .05     .10   47.07  74.26   .3247   .3327   -7.60   -4.61  -.1381   .8315   .0110    .0108  9.9590  7.2772
     .5     .05     .20   41.99  70.89   .3219   .3292  -15.77   -9.73  -.2739   .7567   .0160    .0134 16.8767 12.9613
     .5     .05     .50   34.49  65.38   .3107   .3183  -27.62  -17.61  -.4434   .8514   .0107    .0087 21.4792 18.9858
     .5     .05     .80   32.03  63.41   .3033   .3125  -31.39  -20.27  -.4934   .9709   .0036    .0023 22.0099 20.8041
     .5     .10     .10   52.91  77.84   .3163   .3238   -1.75   -1.02  -.0303   .9875   .0026    .0020  2.2627  1.5849
     .5     .10     .20   47.83  74.74   .3132   .3201   -9.92   -5.88  -.1720   .9018   .0073    .0062  8.9591  7.1250
     .5     .10     .50   40.34  69.74   .3025   .3096  -21.77  -13.25  -.3510  1.0019   .0025    .0000 14.3316 13.5363
     .5     .10     .80   37.89  67.97   .2960   .3045  -25.54  -15.72  -.4011  1.1267  -.0036   -.0037 15.8588 15.7430
     .5     .20     .20   56.58  79.96   .3068   .3143   -1.17    -.66  -.0194  1.0023   .0009    .0004  1.0182   .7887
     .5     .20     .50   49.09  75.53   .2974   .3031  -13.03   -7.46  -.2096  1.0883  -.0026   -.0045  7.5487  7.5309
     .5     .20     .80   46.64  73.98   .2920   .3008  -16.79   -9.70  -.2629  1.2023  -.0076   -.0094 10.3480 10.0602
     .5     .50     .50   61.75  82.80   .2999   .3094    -.36    -.19  -.0055  1.0052  -.0001   -.0003   .2340   .2190
     .5     .50     .80   59.31  81.48   .2956   .3060   -4.13   -2.21  -.0634  1.0865  -.0040   -.0042  3.5437  2.8144
     .5     .80     .80   63.32  83.63   .2995   .3101    -.11    -.06  -.0017  1.0026  -.0001   -.0001   .1068   .0831
    0.0     .02     .02   11.07  39.73   .2768   .2837    6.29   13.60  1.3372   .6287   .0192    .0246 13.6864 13.7102
    0.0     .02     .05   12.77  42.46   .2780   .2881    1.49    2.37   .1433   .6345   .0178    .0232  8.7233  6.6686
    0.0     .02     .10   15.20  45.93   .2803   .2920   -5.34   -6.53  -.2526   .6886   .0161    .0213 16.1588 11.4119
    0.0     .02     .20   18.84  50.54   .2831   .2989  -15.56  -14.77  -.4469   .7404   .0138    .0183 23.6643 18.4387
    0.0     .02     .50   24.16  56.28   .2960   .3116  -30.36  -22.50  -.5526   .8357   .0094    .0125 28.0012 24.5081
    0.0     .02     .80   25.86  57.94   .3014   .3166  -35.03  -24.41  -.5711   .8797   .0072    .0099 28.2105 25.7725
    0.0     .05     .05   16.88  48.15   .2719   .2796    5.60    8.06   .5037   .7346   .0118    .0148  8.1739  8.2707
    0.0     .05     .10   19.31  51.08   .2744   .2836   -1.23   -1.40  -.0349   .7940   .0102    .0129  8.0747  5.3031
    0.0     .05     .20   22.93  55.03   .2791   .2903  -11.46  -10.26  -.3289   .8598   .0077    .0096 13.7473 12.3694
```

0.0	.05	.50	28.26	60.16	.2890	.3021	-26.26	-18.63	-.4780	.9922	.0024	.0030	21.2235	19.4235
0.0	.05	.80	29.97	61.66	.2938	.3067	-30.95	-20.69	-.5041	1.0560	-.0004	.0000	22.0235	21.0685
0.0	.10	.10	25.15	57.26	.2714	.2795	4.61	4.78	.2273	.8431	.0073	.0088	5.1550	5.0623
0.0	.10	.20	28.80	60.63	.2754	.2852	-5.61	-4.68	-.1606	.9301	.0040	.0045	7.3658	5.7762
0.0	.10	.50	34.11	65.08	.2839	.2954	-20.41	-13.70	-.3716	1.1083	-.0027	-.0037	14.2885	13.8259
0.0	.10	.80	35.81	66.41	.2880	.2994	-25.10	-15.94	-.4086	1.1954	-.0062	-.0073	16.0042	15.9513
0.0	.20	.20	37.54	67.71	.2755	.2853	3.14	2.40	.0917	.9113	.0041	.0047	3.0339	2.7232
0.0	.20	.50	42.86	71.48	.2822	.2934	-11.66	-7.30	-.2121	1.1303	-.0044	-.0057	7.3702	7.3647
0.0	.20	.80	44.56	72.63	.2855	.2966	-16.55	-9.72	-.2655	1.2384	-.0087	-.0101	10.4197	10.0977
0.0	.50	.50	55.52	79.36	.2880	.3005	1.00	.58	.0179	.9705	.0014	.0014	1.1021	.8121
0.0	.50	.80	57.23	80.32	.2905	.3029	-3.69	-2.02	-.0589	1.0821	-.0037	-.0038	3.1721	2.5437
0.0	.80	.80	61.24	82.52	.2948	.3072	.33	.18	.0050	.9882	.0006	.0005	.4391	.2942

EXAMPLE 2: OUTPUT FOR A PLUME FROM A COPPER SMELTER

```
VISUAL IMPACT ASSESSMENT FOR COPPER SMELTER (#2)

   POWER PLANT DATA

        ELEVATION OF SITE =          0.  FEET MSL
                                     0.  METERS MSL

        NO. OF UNITS =      1.

        STACK HEIGHT =  600.  FEET
                        183.  METERS

        FLUE GAS FLOW RATE =   1162144.  CU FT/MIN
                                 548.39  CU M/SEC

        FLUE GAS TEMPERATURE =        400.  F
                                      478.  K

        FLUE GAS OXYGEN CONTENT =        2.0  MOL PERCENT

        SO2 EMISSION RATE (TOTAL) =     1180.82  TONS/DAY
                                        1.240E+04  G/SEC

        NOX EMISSION RATE (TOTAL,AS NO2) =       1.00  TONS/DAY
                                            1.030E+01  G/SEC

        PARTICULATE EMISSION RATE (TOTAL) =      1.00  TONS/DAY
                                            1.030E+01  G/SEC
```

```
METEOROLOGICAL AND AMBIENT AIR QUALITY DATA

     WINDSPEED =  11.2  MILES/HR
                   5.0  M/SEC

     PASQUILL-GIFFORD-TURNER STABILITY CATEGORY D

     LAPSE RATE =  0.00  F/1000 FT
                   0.          K/M

     POTENTIAL TEMPERATURE LAPSE RATE =    9.800E-03  K/M

     SOLAR ZENITH ANGLE =  45.0  DEGREES

     AMBIENT TEMPERATURE =  77.0  F
                           298.2  K

     RELATIVE HUMIDITY =  40.0  %

     MIXING DEPTH = 2000.  M

     AMBIENT PRESSURE =  1.00  ATM

     SO2 TO SO4 CONVERSION RATE =        .500 PERCENT/HR

     NOX TO NO3 CONVERSION RATE =       0.000 PERCENT/HR

     BACKGROUND NOX CONCENTRATION =       0.000  PPM

     BACKGROUND NO2 CONCENTRATION =       0.000  PPM

     BACKGROUND OZONE CONCENTRATION =        .040  PPM

     BACKGROUND SO2 CONCENTRATION =       0.000  PPM

     BACKGROUND COARSE MODE CONCENTRATION =        30.0  UG/M3

     BACKGROUND SULFATE CONCENTRATION =        1.7  UG/M3

     BACKGROUND NITRATE CONCENTRATION =        0.0  UG/M3

     BACKGROUND VISUAL RANGE =      130.0  KILOMETERS

     SO2 DEPOSITION VELOCITY =       1.00  CM/SEC

     NOX DEPOSITION VELOCITY =       1.00  CM/SEC

     COARSE PARTICULATE DEPOSITION VELOCITY =        .10  CM/SEC

     SUBMICRON PARTICULATE DEPOSITION VELOCITY =       .10  CM/SEC
```

```
                    CONCENTRATIONS OF AEROSOL AND GASES CONTRIBUTED BY

                                 COPPER SMELTER (*2)

DOWNWIND DISTANCE (KM)  =   20.0
PLUME ALTITUDE (M)      =   412.
SIGMA Y (M)             =  1017.
SIGMA Z (M)             =   200.
SO2-SO4 CONVERSION RATE=        .5000 PERCENT/HR
NOX-NO3 CONVERSION RATE=       0.0000 PERCENT/HR

ALTITUDE          NOX       NO2        NO3-    NO2/NTOT  NO3-/NTOT      SO2        SO4=   SO4=/STOT     O3      PRIMARY BSP-TOTAL  BSPSN/BSP
                 (PPM)     (PPM)     (UG/M3)  (MOLE %)   (MOLE %)      (PPM)     (UG/M3)  (MOLE %)     (PPM)    (UG/M3) (10-4 M-1)   (%)
 H+2S
INCREMENT:        .000      .000      0.000     0.000      0.000        .100      2.057      .522      -.000       .222      .124     96.409
TOTAL AMB:        .000      .000      0.000    75.035      0.000        .100      3.802      .963       .040     31.967      .326     67.839
 H+1S
INCREMENT:        .001      .000      0.000     0.000      0.000        .447      9.221      .522      -.000       .997      .556     96.409
TOTAL AMB:        .001      .000      0.000    74.890      0.000        .447     10.966      .622       .040     32.741      .757     84.124
 H
INCREMENT:        .001      .001      0.000    74.621      0.000        .736     15.206      .522      -.001      1.644      .917     96.409
TOTAL AMB:        .001      .001      0.000    74.768      0.000        .736     16.951      .583       .039     33.388     1.118     88.087
 H-1S
INCREMENT:        .001      .000      0.000     0.000      0.000        .452      9.338      .522      -.000      1.009      .563     96.409
TOTAL AMB:        .001      .000      0.000    74.888      0.000        .452     11.083      .620       .040     32.754      .765     84.238
 H-2S
INCREMENT:        .000      .000      0.000     0.000      0.000        .178      3.668      .522      -.000       .396      .221     96.409
TOTAL AMB:        .000      .000      0.000    75.003      0.000        .178      5.413      .770       .040     32.141      .423     74.399
 0
INCREMENT:        .000      .000      0.000     0.000      0.000        .177      3.647      .522      -.000       .394      .220     96.409
TOTAL AMB:        .000      .000      0.000    75.003      0.000        .177      5.392      .772       .040     32.139      .422     74.334


CUMULATIVE SURFACE DEPOSITION (MOLE FRACTION OF INITIAL FLUX)

                  SO2:      .0020
                  NOX:      .0020
 PRIMARY PARTICULATE:      .0002
                  SO4:      .0000
                  NO3:     0.0000
```

```
                VISUAL EFFECTS FOR HORIZONTAL SIGHT PATHS
                COPPER SMELTER (#2)

OWNWIND DISTANCE (KM) =    20.0
LUME ALTITUDE (M)     =    412.
IGHT PATH IS THROUGH PLUME CENTER

HETA ALPHA  RP/RV0    RV  %REDUCED    YCAP      L       X       Y DELYCAP     DELL  C(550)  BRATIO    DELX     DELY  E(LUV)  E(LAB)

 90.
        30.    .02  117.4     9.71   62.34   83.11   .3026   .3131   -1.78     -.93  -.0283   .9547   .0026    .0020  2.4982  1.6310
        30.    .05  113.4    11.22   62.31   83.09   .3023   .3128   -1.81     -.93  -.0291   .9586   .0024    .0018  2.3337  1.3338
        30.    .10  113.2    11.36   62.63   83.26   .3017   .3121   -1.49     -.78  -.0240   .9724   .0017    .0010  1.6749  1.1391
        30.    .20  113.0    11.33   63.11   83.32   .3008   .3112   -1.01     -.33  -.0164   .9877   .0008    .0002   .8816   .6694
        30.    .30  114.6    11.84   63.79   83.87   .3000   .3108    -.33     -.17  -.0035   .9983  -.0000   -.0003   .2316   .2231
        30.    .80  114.3    11.92   63.99   83.98   .3000   .3109    -.12     -.06  -.0021   .9987  -.0001   -.0002   .1211   .1019
        45.    .02  120.4     7.42   62.66   83.28   .3022   .3128   -1.46     -.76  -.0233   .9613   .0022    .0018  2.1083  1.3708
        45.    .05  119.7     7.90   62.73   83.33   .3019   .3123   -1.37     -.72  -.0219   .9678   .0019    .0014  1.8151  1.1927
        45.    .10  119.6     8.00   63.00   83.46   .3013   .3119   -1.12     -.39  -.0181   .9786   .0013    .0008  1.2922   .8729
        45.    .20  119.4     8.13   63.36   83.63   .3006   .3112    -.76     -.40  -.0124   .9904   .0006    .0001   .6782   .3026
        45.    .30  119.1     8.36   63.87   83.91   .3000   .3109    -.23     -.13  -.0041   .9987   .0000   -.0002   .1839   .1690
        45.    .80  119.0     8.43   64.03   83.99   .3000   .3109    -.09     -.05  -.0016   .9991  -.0000   -.0001   .0908   .0766
        60.    .02  121.7     6.38   62.82   83.36   .3020   .3127   -1.30     -.68  -.0207   .9631   .0019    .0016  1.3941  1.2293
        60.    .05  121.6     6.44   62.97   83.44   .3016   .3123   -1.15     -.60  -.0184   .9726   .0016    .0012  1.5412  1.0167
        60.    .10  121.5     6.52   63.18   83.53   .3011   .3118    -.94     -.49  -.0152   .9817   .0011    .0007  1.0973   .7292
        60.    .20  121.4     6.65   63.48   83.71   .3006   .3112    -.64     -.33  -.0104   .9918   .0005    .0001   .3753   .4243
        60.    .30  121.1     6.83   63.91   83.93   .3001   .3109    -.21     -.11  -.0035   .9989   .0000   -.0002   .1585   .1417
        60.    .80  121.1     6.88   64.04   84.00   .3000   .3110    -.08     -.04  -.0013   .9992  -.0000   -.0001   .0762   .0643
        90.    .02  122.8     5.52   62.98   83.45   .3018   .3125   -1.14     -.60  -.0182   .9690   .0017    .0014  1.6791  1.0867
        90.    .05  122.8     5.57   63.11   83.51   .3014   .3121   -1.01     -.53  -.0162   .9737   .0014    .0011  1.3666   .8951
        90.    .10  122.7     5.64   63.29   83.61   .3010   .3117    -.83     -.43  -.0134   .9838   .0010    .0006   .9733   .6344
        90.    .20  122.5     5.73   63.56   83.73   .3005   .3112    -.56     -.29  -.0092   .9927   .0005    .0001   .5099   .3739
        90.    .30  122.3     5.91   63.93   83.93   .3001   .3109    -.18     -.10  -.0031   .9990   .0000   -.0001   .1395   .1247
        90.    .80  122.3     5.96   64.05   84.01   .3000   .3110    -.07     -.04  -.0012   .9993  -.0000   -.0001   .0670   .0566
```

```
                    CONCENTRATIONS OF AEROSOL AND GASES CONTRIBUTED BY

                                      COPPER SMELTER (*2)

DOWNWIND DISTANCE (KM) =   40.0
PLUME ALTITUDE (M)     =   412.
SIGMA Y (M)            =  1837.
SIGMA Z (M)            =   288.
SO2-SO4 CONVERSION RATE=        .3000 PERCENT/HR
NOX-NO3 CONVERSION RATE=       0.0000 PERCENT/HR

ALTITUDE          NOX       NO2       NO3-    NO2/NTOT  NO3-/NTOT      SO2       SO4=   SO4=/STOT      O3     PRIMARY BSP-TOTAL   BSPSN/BSP
                 (PPM)     (PPM)    (UG/M3)   (MOLE %)  (MOLE %)      (PPM)    (UG/M3)  (MOLE %)     (PPM)   (UG/M3) (10-4 M-1)    (%)
 H+2S
INCREMENT:        .000      .000     0.000      0.000     0.000        .037      1.603     1.070      -.000      .083      .093      98.217
TOTAL AMB:        .000      .000     0.000     73.061     0.000        .037      8.330     2.247       .040    31.829      .297      63.620
 H+1S
INCREMENT:        .000      .000     0.000      0.000     0.000        .167      7.200     1.070      -.000      .379      .426      98.217
TOTAL AMB:        .000      .000     0.000     73.007     0.000        .167      8.943     1.330       .040    32.124      .628      82.812
 H
INCREMENT:        .000      .000     0.000      0.000     0.000        .279     12.037     1.070      -.000      .635      .713      98.217
TOTAL AMB:        .000      .000     0.000     74.960     0.000        .279     13.802     1.243       .040    32.380      .913      87.630
 H-1S
INCREMENT:        .000      .000     0.000      0.000     0.000        .215      9.289     1.070      -.000      .489      .330      98.217
TOTAL AMB:        .000      .000     0.000     74.987     0.000        .215     11.034     1.292       .040    32.234      .731      83.346
 H-2S
INCREMENT:        .000      .000     0.000      0.000     0.000        .197      8.321     1.070      -.000      .449      .304      98.217
TOTAL AMB:        .000      .000     0.000     74.994     0.000        .197     10.263     1.310       .040    32.193      .706      84.317
 0
INCREMENT:        .000      .000     0.000      0.000     0.000        .197      8.321     1.070      -.000      .449      .304      98.217
TOTAL AMB:        .000      .000     0.000     74.994     0.000        .197     10.263     1.310       .040    32.193      .706      84.317


CUMULATIVE SURFACE DEPOSITION (MOLE FRACTION OF INITIAL FLUX)

                    SO2:     .0179
                    NOX:     .0180
   PRIMARY PARTICULATE:     .0018
                    SO4:     .0000
                    NO3:    0.0000
                    VISUAL EFFECTS FOR HORIZONTAL SIGHT PATHS
                    COPPER SMELTER (*2)

DOWNWIND DISTANCE (KM) =   40.0
PLUME ALTITUDE (M)     =   412.
SIGHT PATH IS THROUGH PLUME CENTER

THETA ALPHA  RP/RV0    RV  %REDUCED   YCAP      L       X        Y DELYCAP    DELL  C(550)  BRATIO    DELX    DELY  E(LUV)  E(LAB)

 90.
        30.     .02   114.7   11.80   62.21   83.04   .3027   .3130   -1.91   -1.00  -.0307   .9547   .0026   .0019  2.5304  1.6630
        30.     .05   110.4   15.07   61.97   82.92   .3028   .3129   -2.14   -1.13  -.0346   .9533   .0027   .0019  2.6702  1.7756
        30.     .10   108.9   16.20   62.24   83.05   .3021   .3122   -1.88    -.99  -.0305   .9660   .0020   .0011  2.0606  1.4136
        30.     .20   108.6   16.45   62.84   83.38   .3010   .3112   -1.27    -.67  -.0209   .9847   .0009   .0001  1.0934   .8313
        30.     .50   108.1   16.81   63.70   83.82   .3000   .3107    -.42    -.22  -.0070   .9977  -.0000  -.0004   .3250   .2898
        30.     .80   108.0   16.92   63.96   83.96   .3000   .3108    -.16    -.08  -.0027   .9983  -.0001  -.0002   .1563   .1311
        45.     .02   117.9    9.29   62.48   83.18   .3024   .3129   -1.64    -.86  -.0264   .9587   .0023   .0018  2.2735  1.4842
        45.     .05   115.3   11.28   62.34   83.11   .3024   .3128   -1.77    -.93  -.0286   .9592   .0024   .0017  2.3015  1.5177
        45.     .10   115.2   11.41   62.66   83.28   .3017   .3120   -1.46    -.76  -.0236   .9727   .0016   .0009  1.6408  1.1149
        45.     .20   114.9   11.60   63.13   83.33   .3008   .3112    -.98    -.51  -.0161   .9877   .0008   .0001   .8680   .6494
        45.     .50   114.6   11.88   63.80   83.87   .3000   .3108    -.32    -.17  -.0054   .9982  -.0000  -.0003   .2496   .2226
        45.     .80   114.4   11.96   64.00   83.98   .3000   .3109    -.12    -.06  -.0021   .9987  -.0000  -.0002   .1199   .1009
        60.     .02   119.8    7.86   62.66   83.28   .3022   .3127   -1.46    -.76  -.0234   .9623   .0021   .0017  2.0602  1.3408
        60.     .05   118.1    9.18   62.61   83.25   .3021   .3125   -1.51    -.79  -.0243   .9647   .0020   .0015  1.9839  1.3044
        60.     .10   117.9    9.29   62.88   83.40   .3015   .3119   -1.24    -.65  -.0200   .9764   .0014   .0008  1.4146   .9571
        60.     .20   117.7    9.46   63.28   83.61   .3007   .3112    -.84    -.44  -.0137   .9893   .0007   .0001   .7469   .5330
        60.     .50   117.4    9.69   63.84   83.90   .3000   .3108    -.27    -.14  -.0046   .9984   .0000  -.0002   .2116   .1887
        60.     .80   117.3    9.77   64.02   83.99   .3000   .3109    -.10    -.05  -.0018   .9989  -.0000  -.0001   .1016   .0856
        90.     .02   120.9    7.01   62.78   83.34   .3020   .3126   -1.34    -.70  -.0214   .9648   .0020   .0016  1.9127  1.2425
        90.     .05   119.7    7.94   62.78   83.34   .3019   .3124   -1.34    -.70  -.0215   .9683   .0018   .0013  1.7753  1.1632
        90.     .10   119.6    8.04   63.02   83.47   .3013   .3118   -1.10    -.57  -.0178   .9788   .0013   .0008  1.2661   .8545
        90.     .20   119.4    8.18   63.38   83.65   .3006   .3112    -.74    -.39  -.0122   .9904   .0006   .0001   .6677   .4942
        90.     .50   119.1    8.39   63.88   83.92   .3001   .3109    -.24    -.13  -.0041   .9986   .0000  -.0002   .1875   .1671
        90.     .80   119.0    8.46   64.03   83.99   .3000   .3109    -.09    -.05  -.0016   .9990  -.0000  -.0001   .0900   .0759
```

```
                    CONCENTRATIONS OF AEROSOL AND GASES CONTRIBUTED BY

                                  COPPER SMELTER (#2)
DOWNWIND DISTANCE (KM) =    60.0
PLUME ALTITUDE (M)     =    412.
SIGMA Y (M)            =   2622.
SIGMA Z (M)            =    333.
SO2-SO4 CONVERSION RATE=       .3000 PERCENT/HR
NOX-NO3 CONVERSION RATE=      0.0000 PERCENT/HR
ALTITUDE         NOX      NO2      NO3-    NO2/NTOT  NO3-/NTOT    SO2      SO4=   SO4=/STOT    O3      PRIMARY  BSP-TOTAL   BSPSN/BSP
                (PPM)    (PPM)   (UG/M3)  (MOLE %)   (MOLE %)    (PPM)   (UG/M3)  (MOLE %)   (PPM)    (UG/M3) (10-4 M-1)     (%)
 H+2S
INCREMENT:       .000     .000    0.000     0.000      0.000      .021    1.391     1.607    -.000       .049     .082      98.809
TOTAL AMB:       .000     .000    0.000    73.068      0.000      .021    3.136     3.703     .040     31.793     .283      64.279
 H+1S
INCREMENT:       .000     .000    0.000     0.000      0.000      .094    6.271     1.607    -.000       .219     .369      98.809
TOTAL AMB:       .000     .000    0.000    73.037      0.000      .094    8.016     2.134     .040     31.964     .370      81.630
 H
INCREMENT:       .000     .000    0.000     0.000      0.000      .164   10.932     1.607    -.000       .383     .644      98.809
TOTAL AMB:       .000     .000    0.000    73.008      0.000      .164   12.697     1.939     .040     32.128     .846      87.233
 H-1S
INCREMENT:       .000     .000    0.000     0.000      0.000      .136   10.466     1.607    -.000       .366     .613      98.809
TOTAL AMB:       .000     .000    0.000    73.011      0.000      .136   12.210     1.932     .040     32.111     .817      86.829
 H-2S
INCREMENT:       .000     .000    0.000     0.000      0.000      .136   10.413     1.607    -.000       .364     .613      98.809
TOTAL AMB:       .000     .000    0.000    73.011      0.000      .136   12.160     1.933     .040     32.109     .814      86.786
 0
INCREMENT:       .000     .000    0.000     0.000      0.000      .136   10.413     1.607    -.000       .364     .613      98.809
TOTAL AMB:       .000     .000    0.000    73.011      0.000      .136   12.160     1.933     .040     32.109     .814      86.786


CUMULATIVE SURFACE DEPOSITION (MOLE FRACTION OF INITIAL FLUX)

                    SO2:     .0420
                    NOX:     .0424
   PRIMARY PARTICULATE:     .0043
                    SO4:     .0000
                    NO3:    0.0000
                    VISUAL EFFECTS FOR HORIZONTAL SIGHT PATHS
                    COPPER SMELTER (#2)

DOWNWIND DISTANCE (KM) =   60.0
PLUME ALTITUDE (M)     =   412.
SIGHT PATH IS THROUGH PLUME CENTER

THETA ALPHA  RP/RV0    RV  %REDUCED   YCAP      L      X        Y DELYCAP   DELL  C(550)  BRATIO   DELX    DELY  E(LUV)  E(LAB)
 90.
        30.     .02  112.0   13.85   62.10   82.98  .3027   .3129  -2.02  -1.06  -.0326   .9551   .0026   .0018  2.5502  1.6903
        30.     .05  106.8   17.82   61.86   82.85  .3028   .3128  -2.26  -1.19  -.0366   .9541   .0027   .0017  2.6744  1.7988
        30.     .10  103.1   20.73   61.92   82.89  .3024   .3122  -2.20  -1.15  -.0357   .9615   .0023   .0012  2.3434  1.6214
        30.     .20  102.7   21.03   62.63   83.26  .3011   .3111  -1.49   -.78  -.0244   .9826   .0010   .0001  1.2542   .9635
        30.     .50  102.1   21.45   63.63   83.79  .3000   .3106   -.49   -.25  -.0082   .9972  -.0000  -.0004   .3829   .3410
        80.     .80  104.0   20.00   63.93   83.95  .3000   .3108   -.18   -.10  -.0032   .9979  -.0001  -.0003   .1841   .1542
        45.     .02  116.2   10.63   62.37   83.13  .3025   .3128  -1.74   -.91  -.0281   .9581   .0024   .0018  2.3321  1.5297
        45.     .05  112.4   13.57   62.15   83.01  .3026   .3128  -1.97  -1.03  -.0318   .9565   .0025   .0017  2.4789  1.6442
        45.     .10  111.0   14.58   62.38   83.13  .3020   .3121  -1.73   -.91  -.0282   .9682   .0019   .0010  1.9170  1.3104
        45.     .20  110.7   14.82   62.94   83.43  .3009   .3112  -1.17   -.61  -.0193   .9856   .0009   .0001  1.0191   .7695
        45.     .50  110.3   15.15   63.73   83.84  .3000   .3107   -.38   -.20  -.0065   .9978  -.0000  -.0003   .3000   .2673
        45.     .80  110.2   15.25   63.97   83.97  .3000   .3109   -.14   -.08  -.0025   .9984  -.0001  -.0002   .1441   .1211
        60.     .02  118.0    9.21   62.52   83.21  .3023   .3128  -1.59   -.84  -.0256   .9604   .0023   .0017  2.1866  1.4285
        60.     .05  114.8   11.70   62.31   83.09  .3025   .3128  -1.81   -.95  -.0291   .9586   .0024   .0017  2.3359  1.3409
        60.     .10  114.6   11.88   62.63   83.26  .3017   .3120  -1.49   -.78  -.0242   .9721   .0017   .0010  1.6743  1.1384
        60.     .20  114.3   12.08   63.11   83.52  .3008   .3112  -1.01   -.53  -.0166   .9874   .0008   .0001   .8577   .6648
        60.     .50  113.9   12.36   63.79   83.87  .3000   .3108   -.33   -.17  -.0056   .9981  -.0000  -.0003   .2567   .2287
        60.     .80  113.8   12.45   63.99   83.98  .3000   .3109   -.12   -.06  -.0021   .9986  -.0001  -.0002   .1203   .1057
        90.     .02  119.1    8.37   62.62   83.26  .3022   .3127  -1.50   -.78  -.0240   .9620   .0022   .0017  2.0830  1.3577
        90.     .05  116.8   10.15   62.50   83.19  .3022   .3126  -1.62   -.85  -.0261   .9623   .0022   .0016  2.1176  1.3936
        90.     .10  116.6   10.27   62.79   83.35  .3016   .3119  -1.33   -.70  -.0216   .9748   .0015   .0009  1.5107  1.0239
        90.     .20  116.4   10.45   63.22   83.57  .3008   .3112   -.90   -.47  -.0148   .9886   .0007   .0001   .7997   .5959
        90.     .50  116.1   10.70   63.82   83.89  .3000   .3108   -.29   -.15  -.0050   .9983   .0000  -.0003   .2288   .2038
        90.     .80  116.0   10.78   64.01   83.98  .3000   .3109   -.11   -.06  -.0019   .9988  -.0000  -.0002   .1098   .0925
```

```
                    CONCENTRATIONS OF AEROSOL AND GASES CONTRIBUTED BY

                                   COPPER SMELTER (*2)

DOWNWIND DISTANCE (KM) =  100.0
PLUME ALTITUDE (M)     =   412.
SIGMA Y (M)            =  4019.
SIGMA Z (M)            =   434.
SO2-SO4 CONVERSION RATE=       .3000 PERCENT/HR
NOX-NO3 CONVERSION RATE=      0.0000 PERCENT/HR

ALTITUDE       NOX       NO2       NO3-    NO2/NTOT  NO3-/NTOT     SO2       SO4=   SO4=/STOT     O3      PRIMARY BSP-TOTAL  BSPSN/BSP
              (PPM)     (PPM)    (UG/M3)  (MOLE %)  (MOLE %)     (PPM)    (UG/M3)  (MOLE %)    (PPM)    (UG/M3) (10-4 M-1)   (%)
 H+2S
INCREMENT:     .000      .000     0.000     0.000     0.000       .010     1.138     2.625     -.000       .023      .068     99.271
TOTAL AMB:     .000      .000     0.000    73.073     0.000       .010     2.903     6.938      .040     31.769      .269     62.600
 H+1S
INCREMENT:     .000      .000     0.000     0.000     0.000       .043     3.328     2.623     -.000       .113      .312     99.271
TOTAL AMB:     .000      .000     0.000    73.037     0.000       .043     7.072     3.810      .040     31.838      .314     80.028
 H
INCREMENT:     .000      .000     0.000     0.000     0.000       .087    10.162     2.623     -.000       .216      .393     99.271
TOTAL AMB:     .000      .000     0.000    73.040     0.000       .087    11.906     3.378      .040     31.961      .796     86.864
 H-1S
INCREMENT:     .000      .000     0.000     0.000     0.000       .087    10.162     2.623     -.000       .216      .393     99.271
TOTAL AMB:     .000      .000     0.000    73.040     0.000       .087    11.906     3.378      .040     31.961      .796     86.864
 H-2S
INCREMENT:     .000      .000     0.000     0.000     0.000       .087    10.162     2.623     -.000       .216      .393     99.271
TOTAL AMB:     .000      .000     0.000    73.040     0.000       .087    11.906     3.378      .040     31.961      .796     86.864
 0
INCREMENT:     .000      .000     0.000     0.000     0.000       .087    10.162     2.623     -.000       .216      .393     99.271
TOTAL AMB:     .000      .000     0.000    73.040     0.000       .087    11.906     3.378      .040     31.961      .796     86.864


CUMULATIVE SURFACE DEPOSITION (MOLE FRACTION OF INITIAL FLUX)

                 SO2:      .0941
                 NOX:      .0933
PRIMARY PARTICULATE:      .0099
                 SO4:      .0001
                 NO3:     0.0000
```

```
                    VISUAL EFFECTS FOR HORIZONTAL SIGHT PATHS
                    COPPER SMELTER (#2)

DOWNWIND DISTANCE (KM) =  100.0
PLUME ALTITUDE (M)     =    412.
SIGHT PATH IS THROUGH PLUME CENTER

THETA ALPHA  RP/RV0    RV  %REDUCED    YCAP      L      X       Y DELYCAP   DELL  C(350)  BRATIO   DELX    DELY  E(LUV)  E(LAB)

 90.
        30.     .02  106.6    17.97   61.93  82.89  .3026  .3126   -2.18  -1.15  -.0354   .9571   .0026   .0015  2.5206  1.7048
        30.     .05  100.5    22.72   61.74  82.79  .3026  .3124   -2.38  -1.25  -.0387   .9573   .0026   .0013  2.5698  1.7726
        30.     .10   94.6    27.20   61.73  82.79  .3023  .3120   -2.39  -1.26  -.0389   .9624   .0023   .0009  2.3567  1.6770
        30.     .20   91.2    29.87   62.31  83.09  .3012  .3110   -1.81   -.95  -.0297   .9798   .0012  -.0001  1.4736  1.1564
        30.     .50   90.5    30.39   63.53  83.73  .3000  .3105    -.59   -.31  -.0100   .9966  -.0001  -.0006   .4708   .4185
        30.     .80  104.0    20.00   63.89  83.93  .2999  .3107    -.22   -.12  -.0039   .9973  -.0001  -.0003   .2264   .1888
        45.     .02  112.3    13.58   62.17  83.02  .3026  .3128   -1.95  -1.02  -.0315   .9572   .0025   .0017  2.4387  1.6184
        45.     .05  107.2    17.57   61.92  82.89  .3027  .3127   -2.19  -1.15  -.0356   .9560   .0026   .0016  2.5694  1.7312
        45.     .10  103.0    20.74   61.93  82.89  .3024  .3122   -2.18  -1.15  -.0355   .9616   .0023   .0012  2.3297  1.6116
        45.     .20  102.6    21.04   62.64  83.27  .3011  .3111   -1.48   -.77  -.0243   .9826   .0010   .0001  1.2488   .9599
        45.     .50  102.1    21.46   63.63  83.79  .3000  .3106    -.48   -.25  -.0082   .9972  -.0000  -.0004   .3819   .3399
        45.     .80  104.0    20.00   63.94  83.95  .3000  .3108    -.18   -.10  -.0032   .9978  -.0001  -.0003   .1836   .1537
        60.     .02  114.9    11.61   62.32  83.10  .3025  .3128   -1.80   -.94  -.0290   .9585   .0024   .0017  2.3324  1.5368
        60.     .05  110.6    14.89   62.09  82.98  .3026  .3127   -2.03  -1.07  -.0328   .9570   .0025   .0016  2.4741  1.6509
        60.     .10  108.0    16.89   62.21  83.04  .3021  .3122   -1.91  -1.00  -.0310   .9655   .0021   .0011  2.0818  1.4293
        60.     .20  107.7    17.14   62.83  83.37  .3010  .3112   -1.29   -.68  -.0213   .9843   .0009   .0001  1.1111   .8442
        60.     .50  107.2    17.31   63.69  83.82  .3000  .3107    -.42   -.22  -.0071   .9975  -.0000  -.0004   .3323   .2958
        60.     .80  107.1    17.62   63.96  83.96  .3000  .3108    -.16   -.08  -.0028   .9981  -.0001  -.0002   .1597   .1340
        90.     .02  116.5    10.40   62.43  83.16  .3024  .3127   -1.69   -.88  -.0272   .9598   .0023   .0017  2.2395  1.4697
        90.     .05  112.7    13.30   62.21  83.04  .3025  .3127   -1.91  -1.00  -.0309   .9581   .0024   .0016  2.3874  1.5847
        90.     .10  111.0    14.60   62.39  83.14  .3020  .3121   -1.72   -.90  -.0280   .9683   .0019   .0010  1.9057  1.3925
        90.     .20  110.7    14.83   62.95  83.43  .3009  .3112   -1.17   -.61  -.0192   .9856   .0009   .0001  1.0146   .7658
        90.     .50  110.3    15.16   63.74  83.84  .3000  .3107    -.38   -.20  -.0064   .9977  -.0000  -.0003   .2992   .2664
        90.     .80  110.2    15.26   63.97  83.97  .3000  .3109    -.14   -.07  -.0025   .9983  -.0001  -.0002   .1437   .1207
```

```
            CONCENTRATIONS OF AEROSOL AND GASES CONTRIBUTED BY

                          COPPER SMELTER (#2)

DOWNWIND DISTANCE (KM) :  130.0
PLUME ALTITUDE (M)     =   412.
SIGMA Y (M)            =  3600.
SIGMA Z (M)            =   332.
SO2-SO4 CONVERSION RATE=       .3000 PERCENT/HR
NOX-NO3 CONVERSION RATE=      0.0000 PERCENT/HR

ALTITUDE         NOX      NO2      NO3-   NO2/NTOT  NO3-/NTOT    SO2     SO4=  SO4=/STOT    O3    PRIMARY BSP-TOTAL  BSPSN/BSP
                (PPM)    (PPM)   (UG/M3) (MOLE %)  (MOLE %)    (PPM)  (UG/M3) (MOLE %)   (PPM)  (UG/M3) (10-4 M-1)   (%)
 H+2S
INCREMENT:      .000     .000    0.000     0.000     0.000     .003    1.013    3.829   -.000      .013     .039    99.303
TOTAL AMB:      .000     .000    0.000    73.074     0.000     .003    2.760   11.389    .040    31.739     .261    61.433

 H+1S
INCREMENT:      .000     .000    0.000     0.000     0.000     .026    4.776    3.829   -.000      .069     .279    99.303
TOTAL AMB:      .000     .000    0.000    73.066     0.000     .026    6.321    6.063    .040    31.814     .481    78.844

 H
INCREMENT:      .000     .000    0.000     0.000     0.000     .032    9.743    3.829   -.000      .141     .369    99.303
TOTAL AMB:      .000     .000    0.000    73.034     0.000     .032   11.488    3.280    .040    31.886     .771    86.619

 H-1S
INCREMENT:      .000     .000    0.000     0.000     0.000     .032    9.743    3.829   -.000      .141     .369    99.303
TOTAL AMB:      .000     .000    0.000    73.034     0.000     .032   11.488    3.280    .040    31.886     .771    86.619

 H-2S
INCREMENT:      .000     .000    0.000     0.000     0.000     .032    9.743    3.829   -.000      .141     .369    99.303
TOTAL AMB:      .000     .000    0.000    73.034     0.000     .032   11.488    3.280    .040    31.886     .771    86.619

 0
INCREMENT:      .000     .000    0.000     0.000     0.000     .032    9.743    3.829   -.000      .141     .369    99.303
TOTAL AMB:      .000     .000    0.000    73.034     0.000     .032   11.488    3.280    .040    31.886     .771    86.619


CUMULATIVE SURFACE DEPOSITION (MOLE FRACTION OF INITIAL FLUX)

                 SO2:     .131
                 NOX:     .1346
PRIMARY PARTICULATE:      .0164
                 SO4:     .0003
                 NO3:    0.0000
            VISUAL EFFECTS FOR HORIZONTAL SIGHT PATHS
            COPPER SMELTER (#2)

DOWNWIND DISTANCE (KM) =  130.0
PLUME ALTITUDE (M)     =   412.
SIGHT PATH IS THROUGH PLUME CENTER

THETA ALPHA  RP/RV0    RV  %REDUCED   YCAP      L       X       Y DELYCAP    DELL  C(550)  BRATIO    DELX    DELY  E(LUV)  E(LAB)
  90.
        30.     .02  100.3   22.87   61.84   82.84  .3024  .3122   -2.28   -1.20  -.0371   .9610   .0023   .0011  2.3808  1.6383
        30.     .05   93.9   27.76   61.73   82.78  .3023  .3119   -2.39   -1.26  -.0390   .9626   .0022   .0009  2.3479  1.6748
        30.     .10   83.9   33.94   61.73   82.78  .3020  .3115   -2.39   -1.26  -.0392   .9673   .0019   .0005  2.1346  1.3978
        30.     .20   78.0   39.97   62.06   82.96  .3013  .3109   -2.06   -1.08  -.0339   .9781   .0012  -.0002  1.6232  1.3036
        30.     .50   77.3   40.33   63.44   83.69  .2999  .3104    -.68    -.33  -.0114   .9961  -.0001  -.0007   .3417   .4804
        30.     .80  104.0   20.00   63.86   83.91  .2999  .3107    -.26    -.13  -.0044   .9968  -.0001  -.0004   .2603   .2162
        45.     .02  107.9   16.97   62.01   82.94  .3025  .3126   -2.10   -1.11  -.0341   .9382   .0025   .0013  2.4482  1.6317
        45.     .05  102.1   21.50   61.81   82.83  .3025  .3124   -2.31   -1.21  -.0373   .9382   .0025   .0013  2.5104  1.7262
        45.     .10   96.6   25.71   61.80   82.82  .3023  .3120   -2.32   -1.22  -.0378   .9630   .0022   .0009  2.3093  1.6368
        45.     .20   93.4   28.14   62.37   83.13  .3012  .3110   -1.75    -.92  -.0287   .9803   .0011  -.0000  1.4340  1.1206
        45.     .50   92.8   28.64   63.55   83.74  .3000  .3105    -.57    -.30  -.0096   .9967  -.0001  -.0005   .4549   .4043
        45.     .80  104.0   20.00   63.90   83.93  .2999  .3108    -.22    -.11  -.0037   .9974  -.0001  -.0003   .2187   .1825
        60.     .02  111.3   14.38   62.15   83.01  .3025  .3127   -1.97   -1.03  -.0319   .9381   .0025   .0016  2.4081  1.6056
        60.     .05  105.7   18.72   61.90   82.88  .3026  .3126   -2.22   -1.17  -.0360   .9369   .0026   .0015  2.5370  1.7291
        60.     .10  101.3   22.08   61.89   82.87  .3023  .3122   -2.23   -1.17  -.0363   .9618   .0023   .0011  2.3333  1.6238
        60.     .20  100.2   22.92   62.36   83.23  .3011  .3111   -1.55    -.81  -.0256   .9819   .0011   .0000  1.3027  1.0052
        60.     .50   99.6   23.36   63.61   83.78  .3000  .3106    -.51    -.27  -.0086   .9970  -.0000  -.0005   .4028   .3582
        60.     .80  104.0   20.00   63.93   83.94  .3000  .3108    -.19    -.10  -.0033   .9977  -.0001  -.0003   .1936   .1620
        90.     .02  113.3   12.84   62.25   83.06  .3025  .3127   -1.87    -.98  -.0302   .9586   .0024   .0016  2.3537  1.5595
        90.     .05  108.4   16.59   62.01   82.93  .3026  .3126   -2.11   -1.11  -.0342   .9572   .0025   .0016  2.4898  1.6739
        90.     .10  104.6   19.54   62.02   82.94  .3023  .3122   -2.09   -1.10  -.0341   .9628   .0022   .0011  2.2512  1.5534
        90.     .20  104.2   19.82   62.70   83.30  .3011  .3111   -1.42    -.74  -.0234   .9831   .0010   .0001  1.2059   .9229
        90.     .50  103.7   20.22   63.65   83.80  .3000  .3106    -.46    -.24  -.0078   .9972  -.0000  -.0004   .3666   .3262
        90.     .80  104.0   20.00   63.94   83.95  .3000  .3108    -.18    -.09  -.0030   .9979  -.0001  -.0002   .1762   .1476
```

```
                    CONCENTRATIONS OF AEROSOL AND GASES CONTRIBUTED BY

                                   COPPER SMELTER (#2)

DOWNWIND DISTANCE (KM) =  200.0
PLUME ALTITUDE (M)     =   412.
SIGMA Y (M)            =  7039.
SIGMA Z (M)            =   633.
SO2-SO4 CONVERSION RATE=       .5000 PERCENT/HR
NOX-NO3 CONVERSION RATE=      0.0000 PERCENT/HR

ALTITUDE        NOX      NO2      NO3-    NO2/NTOT  NO3-/NTOT    SO2      SO4=   SO4=/STOT    O3     PRIMARY  BSP-TOTAL  BSPSN/BSP
               (PPM)    (PPM)   (UG/M3)  (MOLE %)  (MOLE %)    (PPM)   (UG/M3)  (MOLE %)   (PPM)   (UG/M3)  (10-4 M-1)    (%)
 H+2S
INCREMENT:      .000     .000    0.000     0.000     0.000      .004      .981    4.930    -.000      .011      .037      99.616
TOTAL AMB:      .000     .000    0.000    73.073     0.000      .004     2.723   13.443     .040    31.736      .239      61.173
 H+1S
INCREMENT:      .000     .000    0.000     0.000     0.000      .017     4.427    4.930    -.000      .030      .258      99.616
TOTAL AMB:      .000     .000    0.000    73.069     0.000      .017     6.172    8.394     .040    31.794      .460      77.979
 H
INCREMENT:      .000     .000    0.000     0.000     0.000      .036     9.336    4.930    -.000      .103      .343      99.616
TOTAL AMB:      .000     .000    0.000    73.061     0.000      .036    11.081    7.237     .040    31.849      .746      86.281
 H-1S
INCREMENT:      .000     .000    0.000     0.000     0.000      .036     9.336    4.930    -.000      .103      .343      99.616
TOTAL AMB:      .000     .000    0.000    73.061     0.000      .036    11.081    7.237     .040    31.849      .746      86.281
 H-2S
INCREMENT:      .000     .000    0.000     0.000     0.000      .036     9.336    4.930    -.000      .103      .343      99.616
TOTAL AMB:      .000     .000    0.000    73.061     0.000      .036    11.081    7.237     .040    31.849      .746      86.281
 0
INCREMENT:      .000     .000    0.000     0.000     0.000      .036     9.336    4.930    -.000      .103      .343      99.616
TOTAL AMB:      .000     .000    0.000    73.061     0.000      .036    11.081    7.237     .040    31.849      .746      86.281


CUMULATIVE SURFACE DEPOSITION (MOLE FRACTION OF INITIAL FLUX)

                 SO2:     .2001
                 NOX:     .2033
PRIMARY PARTICULATE:     .0222
                 SO4:     .0005
                 NO3:    0.0000
```

```
                VISUAL EFFECTS FOR HORIZONTAL SIGHT PATHS
                COPPER SMELTER (#2)

DOWNWIND DISTANCE (KM) =  200.0
PLUME ALTITUDE (M)     =    412.
SIGHT PATH IS THROUGH PLUME CENTER

THETA ALPHA  RP/RV0    RV  %REDUCED   YCAP      L       X        Y DELYCAP    DELL  C(550)  BRATIO    DELX    DELY  E(LUV)  E(LAB)

 90.
        30.     .02   95.0   26.94   61.83   82.83   .3021   .3118   -2.26   -1.19  -.0370   .9637   .0021   .0007  2.1801  1.5672
        30.     .03   88.6   31.81   61.80   82.82   .3020   .3116   -2.32   -1.22  -.0380   .9678   .0019   .0003  2.1135  1.5595
        30.     .10   79.3   38.87   61.82   82.83   .3017   .3112   -2.30   -1.21  -.0378   .9720   .0016   .0001  1.9362  1.4906
        30.     .20   70.1   46.07   62.10   82.98   .3011   .3107   -2.02   -1.06  -.0333   .9803   .0010  -.0004  1.5388  1.2685
        30.     .50   66.3   48.97   63.39   83.66   .2999   .3103    -.72    -.38  -.0122   .9938  -.0001  -.0007   .5834   .5165
        30.     .80  104.0   20.00   63.84   83.90   .2999   .3107    -.27    -.14  -.0047   .9964  -.0001  -.0004   .2803   .2322
        45.     .02  104.3   19.77   61.93   82.90   .3024   .3123   -2.17   -1.14  -.0352   .9606   .0024   .0012  2.3660  1.6245
        45.     .05   98.4   24.32   61.81   82.83   .3024   .3121   -2.31   -1.22  -.0377   .9615   .0023   .0010  2.3683  1.6619
        45.     .10   91.6   29.53   61.79   82.82   .3021   .3117   -2.32   -1.22  -.0380   .9661   .0020   .0006  2.1833  1.5370
        45.     .20   83.8   34.03   62.20   83.04   .3012   .3110   -1.92   -1.01  -.0315   .9790   .0012  -.0001  1.5437  1.2217
        45.     .50   85.1   34.37   63.49   83.71   .3000   .3105    -.63    -.33  -.0106   .9963  -.0001  -.0006   .5024   .4460
        45.     .80  104.0   20.00   63.88   83.92   .2999   .3107    -.24    -.12  -.0041   .9970  -.0001  -.0003   .2415   .2011
        60.     .02  108.4   16.62   62.06   82.96   .3025   .3125   -2.05   -1.08  -.0334   .9593   .0024   .0014  2.3838  1.6093
        60.     .05  102.7   20.98   61.87   82.86   .3025   .3123   -2.25   -1.18  -.0366   .9593   .0024   .0013  2.4443  1.6817
        60.     .10   97.3   25.14   61.83   82.83   .3022   .3120   -2.27   -1.19  -.0370   .9639   .0022   .0009  2.2553  1.5995
        60.     .20   94.0   27.71   62.39   83.14   .3012   .3110   -1.73    -.91  -.0283   .9804   .0011  -.0000  1.4231  1.1108
        60.     .50   93.3   28.21   63.53   83.73   .3000   .3105    -.57    -.30  -.0096   .9967  -.0001  -.0005   .4507   .4005
        60.     .80  104.0   20.00   63.90   83.93   .2999   .3108    -.21    -.11  -.0037   .9974  -.0001  -.0003   .2166   .1808
        90.     .02  110.8   14.76   62.16   83.01   .3025   .3126   -1.96   -1.03  -.0318   .9591   .0024   .0015  2.3620  1.5803
        90.     .05  105.3   19.00   61.93   82.89   .3025   .3125   -2.19   -1.15  -.0356   .9583   .0025   .0014  2.4686  1.6804
        90.     .10  100.7   22.53   61.91   82.88   .3023   .3121   -2.20   -1.16  -.0360   .9630   .0022   .0010  2.2769  1.5927
        90.     .20   98.9   23.96   62.53   83.21   .3011   .3111   -1.59    -.83  -.0262   .9815   .0011   .0000  1.3364  1.0291
        90.     .50   98.3   24.41   63.60   83.77   .3000   .3106    -.52    -.27  -.0088   .9969  -.0000  -.0005   .4137   .3678
        90.     .80  104.0   20.00   63.92   83.94   .3000   .3108    -.20    -.10  -.0034   .9976  -.0001  -.0003   .1938   .1663
```

```
                         CONCENTRATIONS OF AEROSOL AND GASES CONTRIBUTED BY

                                     COPPER SMELTER (#2)
DOWNWIND DISTANCE (KM) =  230.0
PLUME ALTITUDE (M)     =   412.
SIGMA Y (M)            =  8428.
SIGMA Z (M)            =   703.
SO2-SO4 CONVERSION RATE=      .5000 PERCENT/HR
NOX-NO3 CONVERSION RATE=     0.0000 PERCENT/HR
ALTITUDE
                 NOX      NO2        NO3-   NO2/NTOT  NO3-/NTOT     SO2      SO4=  SO4=/STOT     O3     PRIMARY BSP-TOTAL  BSPSN/BSP
                (PPM)    (PPM)    (UG/M3)  (MOLE %)   (MOLE %)    (PPM)   (UG/M3)  (MOLE %)    (PPM)   (UG/M3) (10-4 M-1)   (%)
  H+2S
INCREMENT:      .000     .000      0.000     0.000      0.000      .003     1.092     5.944     -.000      .010      .064     99.683
TOTAL AMB:      .000     .000      0.000    75.075      0.000      .003     2.836    18.126      .040    31.755      .265     62.124
  H+1S
INCREMENT:      .000     .000      0.000     0.000      0.000      .012     4.177     5.944     -.000      .039      .243     99.683
TOTAL AMB:      .000     .000      0.000    75.071      0.000      .012     5.921    10.779      .040    31.783      .445     77.297
  H
INCREMENT:      .000     .000      0.000     0.000      0.000      .027     8.931     5.944     -.000      .082      .521     99.683
TOTAL AMB:      .000     .000      0.000    75.065      0.000      .027    10.675     9.245      .040    31.827      .722     85.886
  H-1S
INCREMENT:      .000     .000      0.000     0.000      0.000      .027     8.931     5.944     -.000      .082      .521     99.683
TOTAL AMB:      .000     .000      0.000    75.065      0.000      .027    10.675     9.245      .040    31.827      .722     85.886
  H-2S
INCREMENT:      .000     .000      0.000     0.000      0.000      .027     8.931     5.944     -.000      .082      .521     99.683
TOTAL AMB:      .000     .000      0.000    75.065      0.000      .027    10.675     9.245      .040    31.827      .722     85.886
  0
INCREMENT:      .000     .000      0.000     0.000      0.000      .027     8.931     5.944     -.000      .082      .521     99.683
TOTAL AMB:      .000     .000      0.000    75.065      0.000      .027    10.675     9.245      .040    31.827      .722     85.836


CUMULATIVE SURFACE DEPOSITION (MOLE FRACTION OF INITIAL FLUX)

                SO2:     .2423
                NOX:     .2500
PRIMARY PARTICULATE:     .0277
                SO4:     .0008
                NO3:    0.0000
```

```
                    VISUAL EFFECTS FOR HORIZONTAL SIGHT PATHS
                    COPPER SMELTER (#2)

DOWNWIND DISTANCE (KM) =  230.0
PLUME ALTITUDE (M)     =    412.
SIGHT PATH IS THROUGH PLUME CENTER

THETA ALPHA  RP/RV0    RV  %REDUCED    YCAP      L       X       Y DELYCAP    DELL  C(550)  BRATIO    DELX     DELY  E(LUV)  E(LAB)

  90.
        30.     .02    90.6   30.30   61.92   82.89   .3018   .3115   -2.20   -1.15  -.0360   .9702   .0018    .0004  1.9760  1.4662
        30.     .03    84.5   34.98   61.90   82.88   .3017   .3113   -2.22   -1.17  -.0364   .9723   .0016    .0002  1.8974  1.4461
        30.     .10    73.4   41.98   61.93   82.90   .3014   .3109   -2.17   -1.14  -.0337   .9762   .0013   -.0001  1.7348  1.3790
        30.     .20    64.3   30.36   62.21   83.04   .3008   .3103   -1.90   -1.00  -.0313   .9832   .0008   -.0006  1.4030  1.1907
        30.     .30    63.0   30.00   63.36   83.63   .2999   .3103    -.73    -.39  -.0126   .9936  -.0002   -.0008   .6094   .3388
        30.     .80   104.0   20.00   63.83   83.89   .2999   .3107    -.29    -.13  -.0049   .9962  -.0002   -.0004   .2927   .2419
        45.     .02   101.3   22.08   61.93   82.90   .3022   .3121   -2.17   -1.14  -.0334   .9633   .0022    .0010  2.2445  1.5694
        45.     .03    93.4   26.62   61.84   82.84   .3021   .3118   -2.28   -1.20  -.0372   .9630   .0021    .0008  2.2150  1.5558
        45.     .10    87.3   32.66   61.83   82.84   .3019   .3115   -2.29   -1.20  -.0375   .9692   .0018    .0004  2.0434  1.5239
        45.     .20    79.4   38.89   62.09   82.98   .3012   .3109   -2.03   -1.07  -.0334   .9782   .0012   -.0002  1.6124  1.2882
        45.     .30    78.7   39.48   63.43   83.69   .3000   .3104    -.67    -.33  -.0112   .9961  -.0001   -.0007   .3346   .4742
        45.     .80   104.0   20.00   63.87   83.91   .2999   .3107    -.25    -.13  -.0044   .9968  -.0001   -.0004   .2369   .2135
        60.     .02   106.0   18.47   62.03   82.93   .3024   .3123   -2.09   -1.10  -.0340   .9613   .0023    .0013  2.3115  1.5806
        60.     .03   100.4   22.79   61.88   82.86   .3023   .3121   -2.24   -1.18  -.0366   .9620   .0023    .0011  2.3288  1.6238
        60.     .10    94.1   27.63   61.86   82.85   .3021   .3117   -2.26   -1.19  -.0370   .9663   .0020    .0007  2.1539  1.5540
        60.     .20    88.8   31.68   62.27   83.07   .3012   .3110   -1.85    -.97  -.0395   .9794   .0012   -.0001  1.5024  1.1831
        60.     .30    88.1   32.20   63.31   83.73   .3000   .3105    -.61    -.32  -.0102   .9964  -.0001   -.0006   .4343   .4391
        60.     .80   104.0   20.00   63.89   83.92   .2999   .3107    -.23    -.12  -.0040   .9972  -.0001   -.0003   .2328   .1940
        90.     .02   108.8   16.33   62.11   82.99   .3024   .3125   -2.01   -1.06  -.0326   .9603   .0023    .0014  2.3201  1.5679
        90.     .03   103.3   20.32   61.92   82.89   .3024   .3123   -2.20   -1.15  -.0358   .9605   .0024    .0012  2.3776  1.6374
        90.     .10    98.0   24.64   61.90   82.88   .3022   .3119   -2.22   -1.17  -.0362   .9649   .0021    .0003  2.2003  1.5624
        90.     .20    94.4   27.38   62.40   83.14   .3012   .3110   -1.72    -.90  -.0283   .9805   .0011   -.0000  1.4148  1.1054
        90.     .30    93.8   27.87   63.36   83.73   .3000   .3105    -.36    -.29  -.0095   .9967  -.0001   -.0005   .4474   .3976
        90.     .80   104.0   20.00   63.91   83.93   .2999   .3108    -.21    -.11  -.0037   .9974  -.0001   -.0003   .2150   .1796
```

```
                    CONCENTRATIONS OF AEROSOL AND GASES CONTRIBUTED BY

                                   COPPER SMELTER (#2)

DOWNWIND DISTANCE (KM)  =   300.0
PLUME ALTITUDE (M)      =    412.
SIGMA Y (M)             =   9723.
SIGMA Z (M)             =    766.
SO2-SO4 CONVERSION RATE=        .3000 PERCENT/HR
NOX-NO3 CONVERSION RATE=       0.0000 PERCENT/HR

ALTITUDE         NOX       NO2       NO3-    NO2/NTOT  NO3-/NTOT     SO2      SO4=    SO4=/STOT     O3      PRIMARY BSP-TOTAL  BSPSN/BSP
                (PPM)     (PPM)    (UG/M3)  (MOLE %)  (MOLE %)     (PPM)   (UG/M3)   (MOLE %)    (PPM)   (UG/M3) (10-4 M-1)    (%)
 H+2S
INCREMENT:       .000      .000     0.000     0.000     0.000       .003     1.333      6.880    -.000       .011      .078     99.727
TOTAL AMB:       .000      .000     0.000    73.073     0.000       .003     3.078     19.622     .040     31.733      .279     64.023

 H+1S
INCREMENT:       .000      .000     0.000     0.000     0.000       .010     3.991      6.880    -.000       .032      .233     99.727
TOTAL AMB:       .000      .000     0.000    73.073     0.000       .010     3.736     13.192     .040     31.776      .434     76.738

 H
INCREMENT:       .000      .000     0.000     0.000     0.000       .021     8.339      6.880    -.000       .068      .498     99.727
TOTAL AMB:       .000      .000     0.000    73.068     0.000       .021    10.284     11.297     .040     31.812      .699     83.463

 H-1S
INCREMENT:       .000      .000     0.000     0.000     0.000       .021     8.339      6.880    -.000       .068      .498     99.727
TOTAL AMB:       .000      .000     0.000    73.068     0.000       .021    10.284     11.297     .040     31.812      .699     83.463

 H-2S
INCREMENT:       .000      .000     0.000     0.000     0.000       .021     8.339      6.880    -.000       .068      .498     99.727
TOTAL AMB:       .000      .000     0.000    73.068     0.000       .021    10.284     11.297     .040     31.812      .699     83.463

 0
INCREMENT:       .000      .000     0.000     0.000     0.000       .021     8.339      6.880    -.000       .068      .498     99.727
TOTAL AMB:       .000      .000     0.000    73.068     0.000       .021    10.284     11.297     .040     31.812      .699     83.463


CUMULATIVE SURFACE DEPOSITION (MOLE FRACTION OF INITIAL FLUX)

                   SO2:      .2794
                   NOX:      .2899
PRIMARY PARTICULATE:      .0329
                   SO4:      .0011
                   NO3:     0.0000
```

```
                 VISUAL EFFECTS FOR HORIZONTAL SIGHT PATHS
                 COPPER SMELTER (*2)

WNWIND DISTANCE (KM) =  300.0
UME ALTITUDE (M)     =    412.
GHT PATH IS THROUGH PLUME CENTER

ETA ALPHA  RP/RV0    RV  %REDUCED   YCAP     L       X       Y DELYCAP   DELL  C(550)  BRATIO   DELX    DELY  E(LUV)  E(LAB)

90.
       30.     .02   87.0   33.09   62.01   82.94  .3015  .3112  -2.10  -1.11  -.0346  .9741   .0015   .0001  1.7893  1.3689
       30.     .05   81.2   37.57   62.02   82.94  .3014  .3110  -2.10  -1.10  -.0346  .9762   .0013  -.0001  1.7111  1.3440
       30.     .10   72.2   44.49   62.08   82.97  .3011  .3107  -2.04  -1.07  -.0336  .9796   .0011  -.0003  1.5676  1.2815
       30.     .20   60.0   53.86   62.33   83.10  .3007  .3104  -1.79   -.94  -.0296  .9855   .0006  -.0007  1.2931  1.1195
       30.     .50   65.0   50.00   63.35   83.64  .2999  .3103   -.77   -.40  -.0130  .9955  -.0002  -.0008   .6265   .5334
       30.     .80  104.0   20.00   63.83   83.89  .2999  .3106   -.29   -.15  -.0050  .9961  -.0002  -.0004   .3008   .2483
       45.     .02   98.8   24.00   61.97   82.92  .3021  .3118  -2.14  -1.13  -.0350  .9665   .0020   .0008  2.1108  1.5053
       45.     .05   93.0   28.44   61.90   82.88  .3019  .3116  -2.22  -1.17  -.0363  .9682   .0019   .0006  2.0627  1.5063
       45.     .10   84.7   34.84   61.90   82.88  .3017  .3113  -2.22  -1.17  -.0364  .9722   .0016   .0002  1.9043  1.4494
       45.     .20   76.4   41.23   62.16   83.01  .3011  .3108  -1.96  -1.03  -.0323  .9803   .0010  -.0003  1.5155  1.2336
       45.     .50   73.4   43.55   63.42   83.68  .2999  .3104   -.69   -.36  -.0117  .9960  -.0001  -.0007   .5574   .4939
       45.     .80  104.0   20.00   63.86   83.91  .2999  .3107   -.26   -.14  -.0045  .9966  -.0001  -.0004   .2678   .2222
       60.     .02  104.0   20.00   62.03   82.95  .3022  .3121  -2.09  -1.10  -.0340  .9636   .0022   .0011  2.2167  1.5337
       60.     .05   98.4   24.27   61.91   82.88  .3022  .3119  -2.21  -1.16  -.0361  .9647   .0021   .0009  2.2071  1.5635
       60.     .10   91.4   29.67   61.89   82.87  .3019  .3116  -2.23  -1.17  -.0366  .9687   .0019   .0005  2.0460  1.5944
       60.     .20   84.5   34.98   62.18   83.03  .3012  .3109  -1.94  -1.02  -.0319  .9788   .0012  -.0001  1.5571  1.2346
       60.     .50   83.8   35.33   63.48   83.71  .3000  .3105   -.64   -.33  -.0107  .9963  -.0001  -.0006   .5088   .4516
       60.     .80  104.0   20.00   63.88   83.92  .2999  .3107   -.24   -.13  -.0042  .9970  -.0001  -.0003   .2445   .2035
       90.     .02  107.1   17.63   62.09   82.98  .3023  .3123  -2.02  -1.06  -.0329  .9622   .0023   .0012  2.2517  1.5372
       90.     .05  101.7   21.76   61.94   82.90  .3023  .3121  -2.18  -1.15  -.0355  .9628   .0022   .0011  2.2764  1.5859
       90.     .10   95.7   26.37   61.91   82.88  .3020  .3118  -2.20  -1.16  -.0361  .9669   .0020   .0007  2.1122  1.5217
       90.     .20   90.7   30.24   62.31   83.09  .3012  .3110  -1.81   -.95  -.0298  .9797   .0012  -.0001  1.4745  1.1575
       90.     .50   90.0   30.75   63.35   83.73  .3000  .3105   -.59   -.31  -.0100  .9965  -.0001  -.0006   .4725   .4197
       90.     .80  104.0   20.00   63.89   83.93  .2999  .3107   -.22   -.12  -.0039  .9972  -.0001  -.0003   .2271   .1894
```

APPENDIX F

DESCRIPTION OF THE NORTHERN GREAT PLAINS REGIONAL MODEL

APPENDIX F

DESCRIPTION OF THE NORTHERN GREAT PLAINS REGIONAL MODEL

Visibility reduction on a regional scale can be caused by transport of sulfur dioxide and its derivative, sulfate, over large downwind distances. Thus, a regional air quality model is an indispensable component of a visibility prediction model. The objective of the regional air quality model is to simulate the distributions of air pollutants from multiple point sources at large distances (on the order of several hundred kilometers). On this scale, the transport and horizontal dispersion of the pollutants and the attendant removal processes are the major factors to be treated in a model.

For the visibility model, a regional model originally developed by Liu and Durran (1977) was adopted. This grid-based numerical model is composed of two interconnected modules, as shown in Figure F-1: a mixing layer model, which treats transport and diffusion in the mixing layer, and a surface layer model, which calculates the pollutant loss to the ground due to dry deposition. In addition, the model accounts for chemical reactions and dry and wet deposition. As reported by Liu and Durran (1977), this model was applied to the Northern Great Plains to assess the air quality impact of current and proposed coal development in that area. Subsequently, Liu, Wojcik, and Henderson (1978) modified the wind and diffusivity algorithm in the model, creating the version used for the visibility study.

In the past few years, several modeling studies have attempted to obtain a quantitative understanding of long-range pollutant transport. For example, Rodhe (1972) of Sweden used a quasi-one-dimensional diffusion model to compute the atmospheric sulfur budget for northern Europe: He concluded that about half of the sulfate in rainfall in Sweden originates

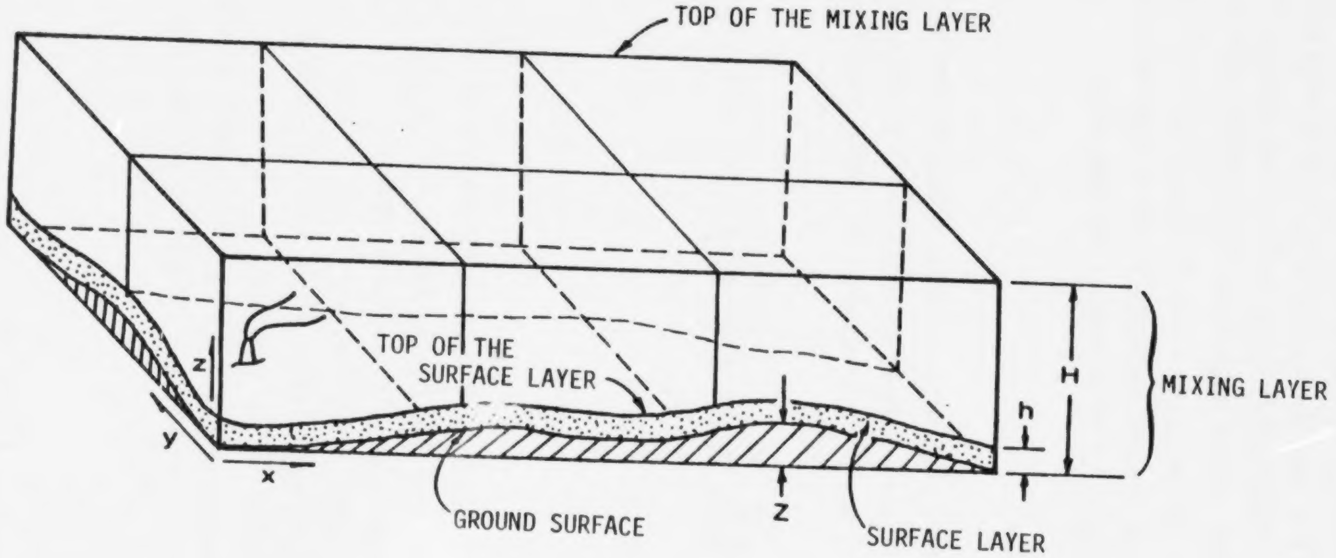
TOP OF THE MIXING LAYER
TOP OF THE SURFACE LAYER
MIXING LAYER
H
h
z
y
x
GROUND SURFACE
Z
SURFACE LAYER

FIGURE F-1. SCHEMATIC OF THE REGIONAL MODEL CONFIGURATION from foreign industrial sources. His work was followed by studies by Nordö, Eliassen, and Saltbones (1974) and Nordlund (1975) from Scandinavia and Scriven and Fisher (1975a, 1975b) from Great Britain, which have further clarified the relative roles played by different physical processes in determining the half-lives or residence times of atmospheric pollutants. Unfortunately, most of these studies employed either a time-dependent one-dimensional diffusion equation or a simple box-type model.

1. THE MIXING LAYER MODEL

The mixing layer model is designed to treat transport and diffusion within the mixing layer. The time-dependent multiple-species atmospheric diffusion equation in two dimensions is used as the model equation:

$$\frac{\partial c_i}{\partial t} + u\frac{\partial c_i}{\partial x} + v\frac{\partial c_i}{\partial y} = \frac{\partial}{\partial x}\left(K_x \frac{\partial c_i}{\partial x}\right) + \frac{\partial}{\partial y}\left(K_y \frac{\partial c_i}{\partial y}\right) + D \cdot f(D) + R_i + S_i \quad , \tag{F-1}$$

$$i = 1, 2, \ldots, N \quad ,$$

where

c_i = the vertically averaged concentration of species i in the mixing layer,

u, v = the wind velocities in the x- and y-directions, respectively,

K_x, K_y = the turbulent diffusivities in the x- and y-directions, respectively,

D = the two-dimensional divergence (= du/dx + dv/dy),

R_i, S_i = chemical reaction and volumetric source terms,

and where

$$f(D) = \begin{cases} c_i \ , & D < 0 \quad , \\ c_{iA} \ , & D > 0 \quad , \end{cases}$$

C_{iA} is the concentration of species i aloft. Although our study considered only SO_2 and sulfate via a first-order reaction, the regional model can be extended to handle multiple reactive species.

The major feature of this model equation is that the pollutant distribution is nearly uniform in the vertical direction. With this assumption, it can be shown that the model equation can be formally derived from the more general atmospheric diffusion equation. The compelling reason for this assumption is that the vertical diffusion term has been found to be one or two orders of magnitude greater than the transport term and the horizontal diffusion term (Liu and Durran, 1977).

Because of the relatively large spatial scale, pseudo-diffusion associated with the numerical solution of Eq. (F-1) can be overwhelming. Consequently, an accurate scheme must be used for the simulation of the transport term. Liu and Durran (1976) carried out a study to compare and test three finite-difference techniques for the problem at hand:

> The upstream difference scheme (Forsythe and Wasow, 1960).
> The SHASTA (sharp and smooth transport algorithm) method (Boris and Book, 1973).
> The moment method (Egan and Mahoney, 1972).

They showed that while the conventional upstream difference scheme shows intolerable spreading of the plume, both the SHASTA method and the moment method produce significant improvement, with the latter slightly better than the former. Computationally, the moment method is, however, about 10 times slower than the SHASTA method. Thus, after considering both accuracy and computing speed, they recommended the SHASTA method for solving the mesoscale atmospheric diffusion equation.

The numerical solution of Eq. (F-1) also invokes the method of fractional steps (Yanenko, 1971), which allows for the division of a two-dimensional partial differential equation into two one-dimensional equations.

Symbolically, Eq. (F-1) can be reduced to the following system of equations:

$$\frac{c^{*} - c}{\Delta t} + u\,\frac{\partial c^{*}}{\partial x} = \frac{\partial}{\partial x}\left(K_x\,\frac{\partial c^{*}}{\partial x}\right) + R \quad , \qquad \text{(F-2)}$$

$$\frac{c^{***} - c^{**}}{\Delta t} + v\,\frac{\partial c^{**}}{\partial y} = \frac{\partial}{\partial y}\left(K_y\,\frac{\partial c^{**}}{\partial y}\right) + Df(D) + S \quad . \qquad \text{(F-3)}$$

The SHASTA method can then be applied to each of these two equations.

This method consists of a transport stage followed by an antidiffusion stage. The first stage is similar to many known transport algorithms. For For example, for a uniform velocity and diffusivity field and $R_i = 0$, Eq. (F-2) can be expressed as:

$$c_j^{*} = c_j - \frac{\varepsilon}{2}\left(c_{j+1} - c_{j-1}\right) + \left(\frac{1}{8} + \frac{\varepsilon^2}{2} + K_x\right)\left(c_{j+1} - 2c_j + c_{j-1}\right) \quad , \qquad \text{(F-4)}$$

where

$$\varepsilon = \frac{u\Delta t}{\Delta x} \quad \text{and} \quad K_x = \frac{K\Delta t}{(\Delta x)^2} \quad .$$

The antidiffusion stage attempts to remove the numerical diffusion generated in the first stage by inverting

$$c_j^{*} = c_j^{**} - \frac{1}{8}\left(c_{j+1}^{**} - 2c_j^{**} + c_{j-1}^{**}\right) \quad . \qquad \text{(F-5)}$$

Further conditions must be posed to ensure that these correction fluxes will not introduce artificial peaks or negative concentrations (Boris and Book, 1973).

Exercise of the model equation also requires specification of the average winds and horizontal diffusivities in the mixing layer. In several long-range modeling studies (e.g., Nordö, Eliassen, and Saltbones, 1974; Nordlund, 1975), the average horizontal winds were computed from the geostrophic wind components given by:

$$u = -\frac{g}{f}\left(\frac{\partial z}{\partial y}\right) \quad , \qquad \text{(F-6)}$$

$$v = \frac{g}{f}\left(\frac{\partial z}{\partial x}\right) \quad , \qquad \text{(F-7)}$$

where

g = the gravitational constant,
f = the Coriolis parameter,
z = the geopotential height,
u, v = the zonal and meridional components, respectively, of the horizintal wind in the mixing layer.

This is the approach that we adopted.

Quantitative determination of the horizontal turbulent diffusivities has been a subject of many recent studies. On the scale of interest here, pollutant dispersal is strongly dependent on a length scale characteristic of the effective turbulent eddies. Pertinent field observations indicate that the regional-scale horizontal diffusivity increases with plume spread and ranges in value from 10^3 to 10^5 m^2/s (Bauer, 1973). In a study on the numerical simulation of the atmospheric circulation, Smagorinsky (1963) showed that the nonlinear lateral diffusion can be formulated on the basis of the similarity theory for turbulence in the equilibrium range (Heisenberg, 1948). If this theory is also applicable to the regional scale, the following formula for the horizontal eddy diffusivity coefficient can be derived:

$$K_H = \frac{5}{4} \cdot (\alpha\Delta)^2 \cdot |\mathrm{Def}| \quad , \qquad \text{(F-8)}$$

where Δ is the grid spacing, $\alpha \approx 0.28$, and $|\mathrm{Def}|$ is the magnitude of the velocity deformation:

$$|\mathrm{Def}| = \left[\left(\frac{\partial v}{\partial x} + \frac{\partial u}{\partial y}\right)^2 + \left(\frac{\partial u}{\partial x} - \frac{\partial v}{\partial y}\right)^2\right]^{1/2} \quad . \qquad \text{(F-9)}$$

According the the above prescription, computation of the horizontal velocities and horizontal diffusivities requires taking the first and second derivatives of the two-dimensional geopotential height field, which is usually given in either graphical or tabular form. Obtaining these derivatives apparently constitutes a stringent test for any interpolation method. In a recent study, Liu, Wojcik, and Henderson (1978) examined the following three objective analysis schemes for generating the geopotential height:

- Bilinear interpolation
- Conditional relaxation analysis method
- Bicubic spline fitting.

They demonstrated through extensive numerical experiments that both the bilinear interpolation and conditional relaxation analysis methods produce interpolated wind fields that generally have the proper magnitudes and directions but severely distort the velocity fields around the data points. As a result, the computed diffusivity fields exhibit unrealistic discontinuities. These two methods have thus been deemed to be unsuitable.

The monotonic and small amplitude characteristics of the height field that caused problems in these two methodologies render the bicubic spline fit an ideal candidate for interpolating the geopotential height data. Mathematically, the spline function is a piecewise cubic (third degree) polynomial passing through all data points and having continuous first and second derivatives. The spline can be viewed as a set of cubic equations, one equation for each interval between successive data points. The coefficients of the cubic equations are such that at any data point the equation for the left interval will yield the same values for the first and second derivatives as will the equation for the right interval.

The 850-millibar weather maps for the Northern Great Plains for 1700 MST on 30 January 1976 (Figure F-2) have been used to illustrate this technique. As shown in Figure F-3, the interpolated geopotential height field generated by the bicubic spline fit is extremely smooth. As expected, the computed meridional and zonal components of the wind field, as shown in Figures F-4 and F-5, are by far the smoothest. The horizontal diffusivities were subsequently calculated according to Eqs. (F-8) and (F-9). The results are presented in Figure F-6. The range of the computed horizontal diffusivities for the test case varies from 0.1 x 10^4 to 1.0 x 10^4 m^2/s, qualitatively in agreement with estimates made based on observational studies. The higher values of the computed horizontal diffusivities are generally located in the east and northeast parts of the modeling region, apparently because of the wind shear suggested by the weather map.

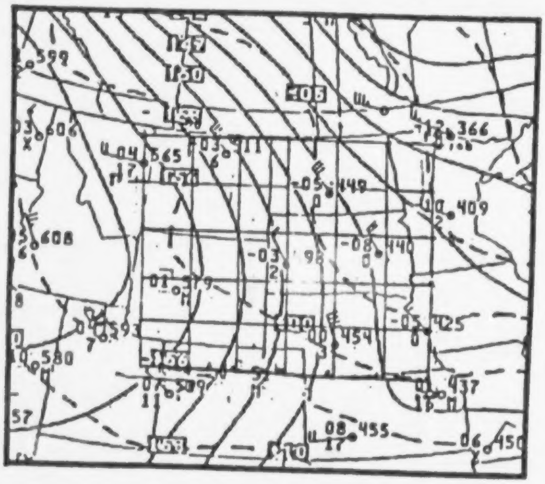

FIGURE F-2. 850-mb WEATHER MAP FOR 1700 MST 30 JANUARY 1976

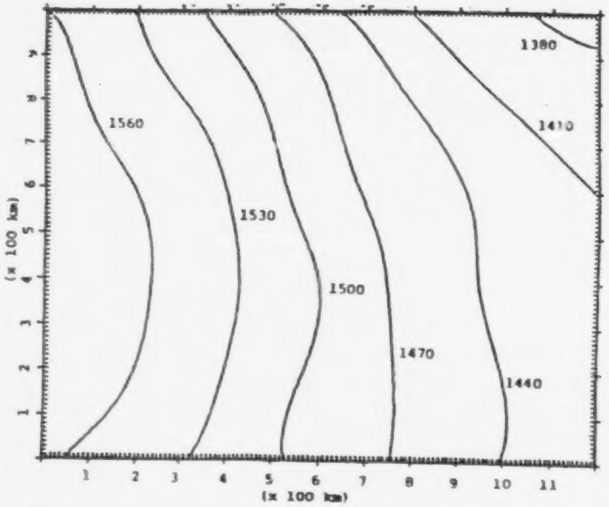

FIGURE F-3. BICUBIC SPLINE FIT OF GEOPOTENTIAL HEIGHT (IN METERS)

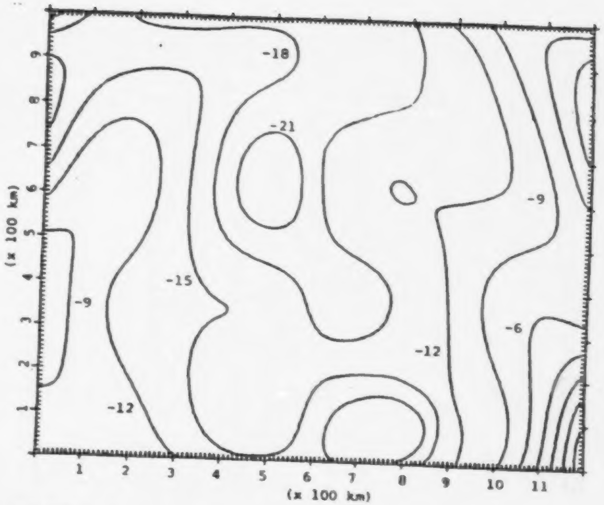

FIGURE F-4. MERIDIONAL WIND (m/s) GENERATED BY A BICUBIC SPLINE FIT OF GEOPOTENTIAL HEIGHT

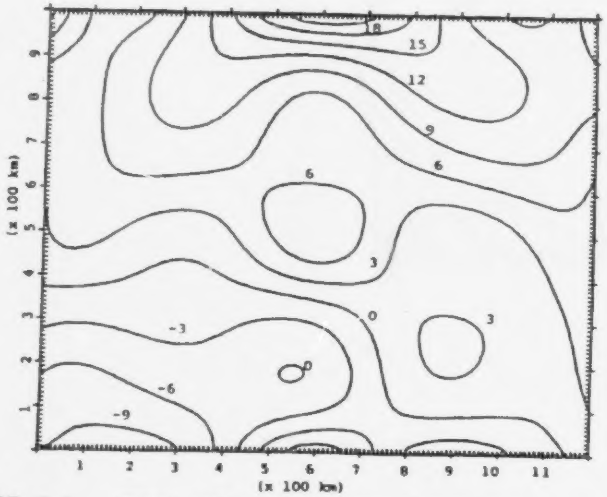

FIGURE F-5. ZONAL WIND (m/s) GENERATED BY A BICUBIC SPLINE FIT OF GEOPOTENTIAL HEIGHT

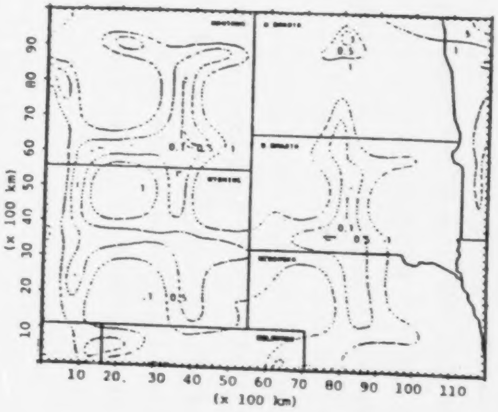
0.1
0.5
1
(x 100 km)
(x 100 km)
10
20
30
40
50
60
70
80
90
100
110

FIGURE F-6. COMPUTED HORIZONTAL EDDY DIFFUSIVITIES (10^4 m^2/s)

2. THE SURFACE LAYER MODEL

The importance of surface deposition on pollutant concentrations at large distances is well established (Nordö, 1973; Scriven and Fisher, 1975a, 1975b). Thus, an indispensable element in a long-range transport model is some treatment of pollutant depletion processes near the surface. For pollutants originating from either elevated sources or distant ground-level sources, most of the pollutant mass is contained in the mixing layer. The removal processes consist of the diffusion of the pollutants through the surface layer to the ground, followed by absorption or adsorption at the atmosphere-ground interface. A unique feature of the surface layer is its diurnal variation in temperature, which is a result of daytime heating and nighttime cooling of the surface. This variation affects the vertical pollutant distribution through atmospheric stabilities and, consequently, affects the rate of surface uptake of pollutants.

The objective of the surface layer model (see Figure F-7) is to construct an algorithm for the prescription of pollutant fluxes at the surface. The surface layer can be divided into two parts: the turbulent layer and the viscous sublayer. In the turbulent layer, after the atmosphere reaches an equilibrium state, the atmospheric diffusion equation becomes:

$$\frac{\partial}{\partial z}\left(K_V \frac{\partial c}{\partial z}\right) = 0 \quad , \qquad \text{(F-10)}$$

with the boundary conditions

$$c = \overline{c} \quad \text{at} \quad z = h \quad ,$$

$$K_V \frac{\partial c}{\partial z} = F \quad \text{at} \quad z = z_0 \quad ,$$

where $\overline{c}$ is the cell-averaged concentration in the mixing layer, F is the pollutant flux across the turbulent layer/viscous sublayer interface, and

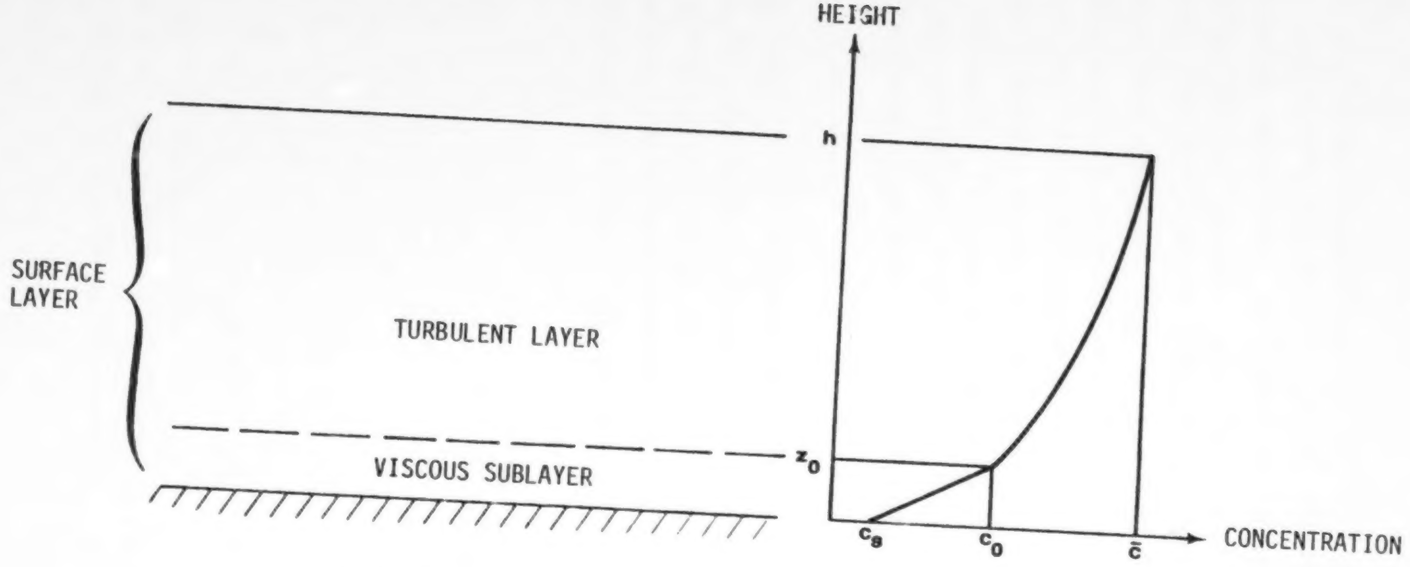
HEIGHT
h
z_0
SURFACE LAYER
TURBULENT LAYER
VISCOUS SUBLAYER
c_s
c_0
$\bar{c}$
CONCENTRATION

FIGURE F-7. SCHEMATIC ILLUSTRATION OF THE SURFACE LAYER

z_0 is the height of the surface roughness element. The vertical diffusivity K_V can be prescribed as follows (Businger et al., 1971):

$$K_V = \frac{ku_* z}{\phi\left(\frac{z}{L}\right)} \quad , \tag{F-11}$$

where k is the von Karman constant, u_* is the frictional velocity, and ϕ is a function of atmospheric stability. For either the stable or unstable case, the solution of Eq. (F-10) is simply:

$$c = \bar{c} - \int_z^h \frac{F \cdot \phi}{ku_* z} dz \quad . \tag{F-12}$$

At the turbulent layer/viscous sublayer interface, the pollutant flux can be written as:

$$F = \beta u_* (c_0 - c_s) \quad , \tag{F-13}$$

where c_0 and c_s denote the concentrations at the interface and the surface, respectively, and β, analogous to the Stanton number in heat transfer, is the inverse of a dimensionless resistance for the viscous sublayer. According to experiments carried out by Chamberlain (1966), β is dependent on the geometry of the surface roughness, a Reynolds number appropriate to the flow in the roughness layer, and the ratio of the kinematic viscosity of air to the molecular diffusion coefficient of the pollutant gas. In further investigations by Chamberlain (1966) and Thom (1972), no direct functional relationship was found between β and z_0. Thus, Thom proposed that:

$$\beta^{-1} = \alpha_1 \, u_*^{1/3} \left[\alpha_2 \left(\frac{\nu}{D}\right)^{2/3} - 1\right] \quad , \tag{F-14}$$

where α_1 and α_2 are empirical constants. This algorithm was used in this study.

Completing the description of the surface layer model requires a boundary condition at the surface. Uptake of air pollutants occurs by chemical reaction or catalytic decomposition either within soil or vegetation or at their surfaces. These processes are generally dependent on the gas concentration at the surface. A general equation for the gas loss per unit area per unit time can be written as (Benson, 1968):

$$F = \gamma c_s^a \quad , \tag{F-15}$$

where F is the pollutant flux, γ is a reaction rate constant, and c_s is the concentration of the gas at the soil or vegetation surface. The exponent a denotes the reaction order. Eliminating c_0 and c_s from Eqs. (F-13), (F-14), and (F-15), one obtains the following transcendental equation for F:

$$I \cdot F + \gamma^{-1/a} \cdot F^{1/a} - \bar{c} = 0 \quad , \tag{F-16}$$

where

$$I \equiv \frac{1}{\beta u_*} + \int_{z_0}^{h} \frac{\phi(z)}{k u_* z} \, dz \quad . \tag{F-17}$$

Although the reaction order is most likely to be 1, closed-form solutions can be found for the cases of a = 1, 2, and 3:

$$F = \begin{cases} \dfrac{\bar{c}}{I + \dfrac{1}{\gamma}} \quad , & a = 1 \\[2ex] \dfrac{-\dfrac{1}{\sqrt{\gamma}} + \left(\dfrac{1}{\gamma} + 4I\bar{c}\right)^{1/2}}{2I} \quad , & a = 2 \\[2ex] (A_+ + A_-)^3 \quad , & a = 3 \end{cases} \tag{F-18}$$

where

$$A_{\pm} = 3\left\{\frac{\bar{c}}{I} \pm \left[\left(\frac{\bar{c}}{2I}\right)^2 + \frac{1}{27\gamma I^3}\right]^{1/2}\right\}^{1/2} .$$

These formulae reduce to that of Chamberlain (1966) or Galbally (1974) for the special case of (1) a first-order surface reaction and (2) a neutrally stratified atmosphere.

To demonstrate the surface layer model outlined above, we discuss a sample calculation. Using a 2 m/s surface wind and 1 cm/s for R, we show in Table F-1 the deposition velocity for SO_2 in cm/s with the β being prescribed according to Chamberlain's algorithm. The variability of the deposition velocity as a function of the time of the day and surface roughness is clearly shown.

TABLE F-1. DEPOSITION VELOCITY ($V_g = F/\bar{c}$, IN cm/s) FOR SULFUR DIOXIDE

Exposure Class		Surface Roughness		
		0.2 cm	2 cm	20 cm
Nighttime	≤3/8	0.1196	0.1358	0.1024
Cloudiness	≥4/8	0.1379	0.1544	0.1146
Heavy overcast (day or night)		0.1176	0.1696	0.1146
Daytime insolation	Slight	0.2342	0.2149	0.1456
	Moderate	0.2399	0.2211	0.1508
	Strong	0.2461	0.2275	0.1564

APPENDIX G

APPLICATION OF THE REGIONAL MODEL TO THE PREDICTION OF VISIBILITY IMPAIRMENT IN THE NORTHERN GREAT PLAINS

APPENDIX G

APPLICATION OF THE REGIONAL MODEL TO THE PREDICTION OF VISIBILITY IMPAIRMENT IN THE NORTHERN GREAT PLAINS

In the present project, a grid-based numerical model developed by Liu and Durran (1977) was employed to calculate regional distributions of sulfate and NO_2 concentrations, which are necessary to predict visibility impairment. The description of this model is presented in Appendix F. Only the application of this model to the Northern Great Plains to assess the visibility problem and the results obtained are discussed in this appendix.

The coal field in northeastern Wyoming, eastern Montana, and western North Dakota is one of the world's largest known coal reserves. Many large coal-fired power plants using locally mined coal have been built in this area, and many more power plants and coal gasification plants are being built or planned. The air quality impacts of emissions from these plants and the associated development pose a potential future problem. For this reason and because of its simple terrain, we selected the Northern Great Plains as the target site for testing and demonstrating the regional-scale visibility model. As discussed in Chapter V, modeling the Southwest United States would require a significant additional effort to characterize the effect of complex terrain on wind distributions and pollutant dispersal.

1. APPLICATION OF THE REGIONAL-SCALE MODEL

In this section, we delineate three major tasks in the application of the regional-scale model: preparation of emissions inventories, preparation of meteorological scenarios, and specification of chemical rate data.

a. Preparation of Emission Inventories

In the Northern Great Plains, 86 percent of the total SO_x emissions are attributable to point sources (EPA, 1976b), and future energy development should increase this percentage; thus, only point source emissions were included in the emissions inventory. Durran et al. (1978) assembled emissions inventories for the base year (1976) and the year 1986 for the 1000 x 1200 km modeling region. Emissions data were obtained from permit applications provided by individual plants or from state or federal regulatory agencies. Emissions projections were drawn from data provided by the Environmental Protection Agency (EPA, 1976c), the Northern Great Plains Resource Program (NGPRP, 1974), and the Federal Power Commission (1976). Tables G-1 and G-2 list point sources in the 1976 and 1986 inventories that emit more than 10,000 tons of SO_x per year. The locations of these point sources within the grid system adopted for air quality modeling and other details of the emissions inventories are given by Liu and Durran (1977).

In addition to the above two scenarios (1976 and 1986 emissions), a hypothetical emissions scenario was prepared to illustrate the use of the model. It consists of fictitious copper smelters clustered around the center of the modeling region. The emissions data and the relative locations for these fictitious smelters are identical to those for the smelters in Arizona and New Mexico in 1972 and are shown in Table G-3 and Figure G-1.

Coal utilization in the Northern Great Plains will increase statewide emissions of sulfur oxides significantly. Emissions of the other air pollutants from coal utilization--namely, nitrogen oxides, hydrocarbons, and particulates--in the Northern Great Plains were forecast by the NGPRP for the two scenarios mentioned earlier. This report does not give detailed distributions of these emissions, but NO_x mass emission rates, Q_{NO_x} (as NO_2), have been estimated as follows:

TABLE G-1. POINT SOURCES IN THE NORTHERN GREAT PLAINS IN 1976 THAT EMITTED MORE THAN 10,000 TONS OF SO_x PER YEAR

Source	Capacity	Estimated SO_x Emissions	
		kg/s	Tons/Day
Dave Johnston, WY	750	0.892	85
Ideal Basic Industries, CO	--	0.742	71
Naughton, WY	710	0.624	59
Exxon, MT	--	0.498	47
Milton R. Young, ND	240	0.460	44
Stanton, ND	167	0.449	43
Leland Olds, ND	650	0.417	40
Hayden, CO	180	0.408	39

TABLE G-2. POINT SOURCES IN THE NORTHERN GREAT PLAINS IN 1986 THAT EMITTED MORE THAN 10,000 TONS OF SO_x PER YEAR

Source	Capacity (MW)	Estimated SO_x Emissions	
		kg/s	Tons/Day
Gerald Gentleman, NB	1300	2.83	270
Craig, CO	1520	2.53	240
Naughton, WY	1510*	1.32	126
Colstrip, MT	2060†	1.44	137
Pawnee, CO	1000	1.44	137
Coal Creek, ND	1000	1.22	116
Wyodak, WY	660	1.10	105
American Natural Gas, ND	880	1.08	103
Coyote, ND	880	1.08	103
Jim Bridger, WY	2000	1.00	95
Dave Johnston, WY	750	0.892	85
Milton R. Young, ND	688	0.892	85
Ideal Basic Industries, CO	--	0.742	71
American Natural Gas, ND	--	0.618	59
Peoples Gas, ND	--	0.618	59
Exxon, MT	--	0.498	47
Stanton, ND	167	0.449	43
Leland Olds, ND	650	0.417	40
Hayden, CO	430	0.408	39
Laramie River, WY	1500	0.316	30

---

* Units 4 and 5 may not be built; equivalent units may be built in Utah.

† Units 3 and 4 (700 megawatts each) may not be constructed.

TABLE G-3. EMISSIONS PARAMETERS FOR THE HYPOTHETICAL COPPER SMELTERS

Plant No.	Stack Height (ft)	Gas Temperature (°F)	Flow Rate (acfm)	SO_x Emissions	
				kg/s	Tons/Day
1	626 500	450 313	233,000 575,700	4.17 2.93	397 279
2	600	400	1,162,144	12.40	1181
3	605 605	530 360	490,000 928,000	2.80 7.62	267 726
4	300	241	500,437	3.74	356
5	600	400	168,670	3.37	321
6	255 290	325 330	385,000 243,000	1.64 4.46	156 425
7	544 532	365 368	389,139 438,210	10.88 4.15	1036 395
8	360	398	642,996	0.51	49
9	515 550	500 500	386,760 244,920	1.74 4.75	166 452

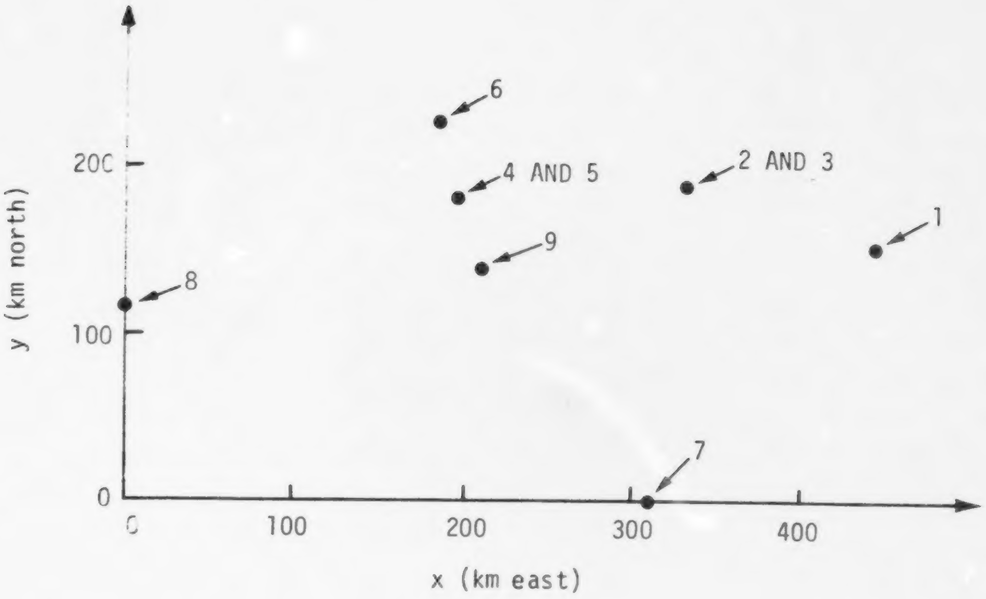

FIGURE G-1. RELATIVE LOCATIONS OF THE HYPOTHETICAL COPPER SMELTERS

Q_{NO_x}/Q_{SO_2}	Category
0.91	1976 emissions
0.71	1986 emissions
0.65	New plants only
0.00	Copper smelters (hypothetical)

Although these are only approximate estimates, they are in line with those given by the New Source Performance Standards and the total emissions estimates.

b. Preparation of Meteorological Scenarios

In addition to the emissions inventories dicussed earlier, application of the model requires meteorological and surface uptake data. The average winds in the mixing layer were computed from 850 millibar maps (available every 12 hours) based on the geostrophic relationship. Wind speeds and wind directions in the surface layer were obtained through interpolation of surface measurements according to the rule of inverse distance. Averaged afternoon mixing height data were derived from vertical temperature soundings to define the top of the modeling region.

Both atmospheric turbulence and surface deposition rates are affected by vegetation and ground cover. Vegetation in the Northern Great Plains was divided into six categories, and the surface roughness associated with each vegetation type was estimated from experimental data compiled by Sellers (1965). These data were used with the algorithm described earlier to calculate surface deposition velocities for three-hour intervals during the periods to be modeled. The calculated deposition velocities showed considerable spatial variation and temporal variation: In general, these velocities were lowest in the early morning and highest in the late afternoon (Liu and Durran, 1977).

For the assessment of the impact of emissions in the Northern Great Plains on long-range air quality and visibility, three meteorological patterns were selected. The selection was based on considerations of meteorological and air quality conditions of interest and data availability. Three cases probably represent typical situations for winter, spring, and summer in that area.

Winter Case. The winter case used meteorological data for 27-31 January 1976. The 850 millibar weather map for 0500 MST 29 January 1976, typical of this period, shows northwest winds of 21 m/s in Montana and 13 to 16 m/s in the Dakotas. These winds and the low mixing depths occurring in winter produce conditions favorable for long-range transport. Predicted SO_2 concentrations for 1976 emissions for 500 to 800 and 1700 to 2000 MST on 29 January 1976 are given in Figure G-2. Long-range transport of air pollutants is quite evident in this case.

Spring Case. Unlike the winter case, the spring case (4-7 April 1976) is favorable for the retention of pollutants within the Northern Great Plains, with a stagnant high pressure system over the region. The resulting winds in the mixing layer are light and variable. This scenario is characterized by the meandering of the plumes in the area.

Summer Case. A typical 850 millibar map for the summer case, 9-11 July 1975, is given in Figure G-3, which shows slow winds from the east in Wyoming and moderate northwest winds in the Dakotas. Although the winds are slower than in the strong-wind winter case, the mixing layer is relatively thicker in the summer.

c. Specification of Chemical Rate Data

Oxidation of SO_2 to sulfate in the atmosphere can be accomplished via homogeneous and heterogeneous processes. Gas phase reactions between SO_2 and free radicals lead to the formation of sulfur trioxide (SO_3), which dissolves in water droplets and subsequently oxidizes to sulfate. The rate-controlling reaction path depends on both the nature of the emissions source (e.g., oil-fired versus coal-fired power plant) and the environment (e.g., the presence of other reactive pollutants, the humidity, and the

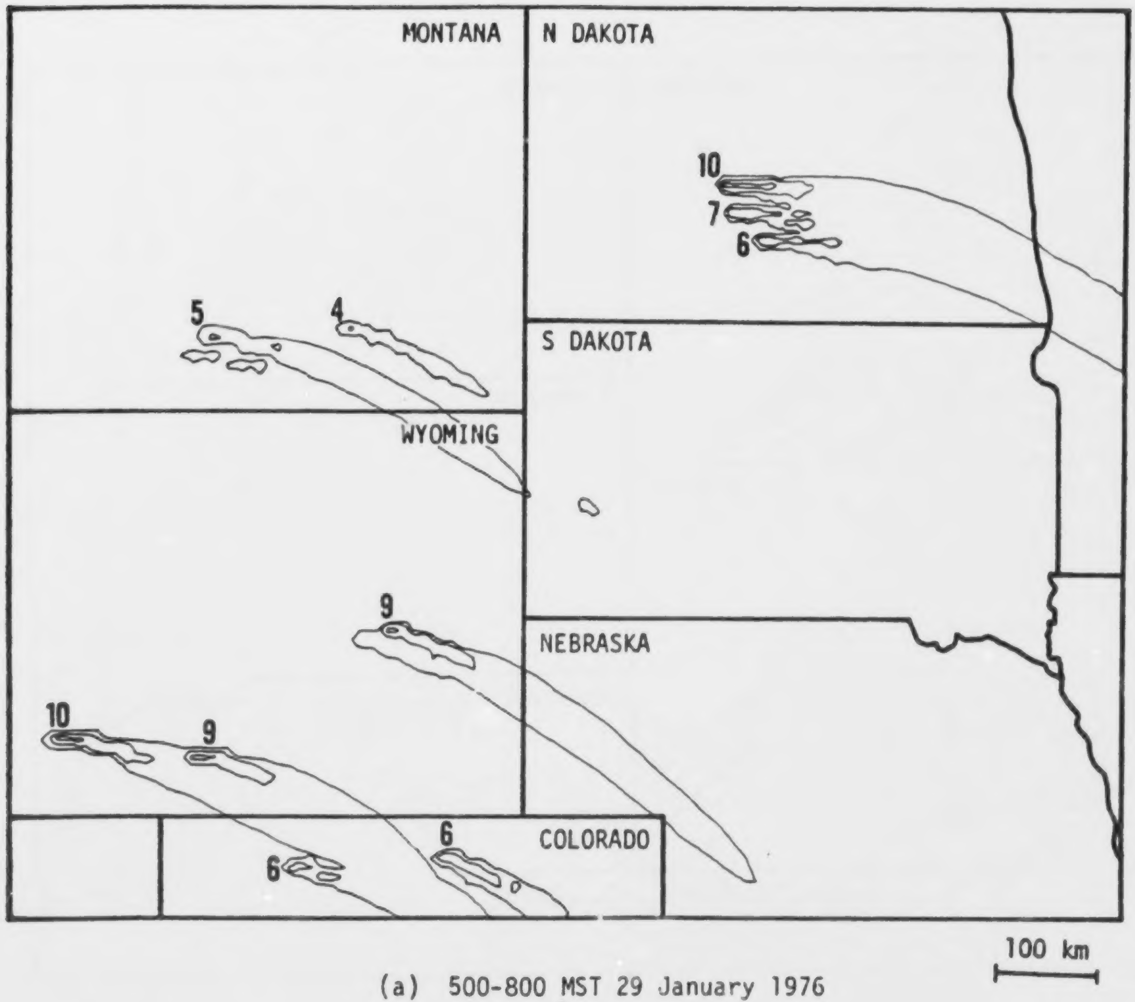
MONTANA
N DAKOTA
S DAKOTA
WYOMING
NEBRASKA
COLORADO
10
7
6
5
4
9
10
9
6
6
100 km

(a) 500-800 MST 29 January 1976

FIGURE G-2. SO_2 CONCENTRATIONS PREDICTED BY THE REGIONAL AIR POLLUTION MODEL FOR THE WINTER CASE. Isopleths at 2, 4, 8, ... μg/m^3; numbers indicate maximum concentrations in plumes.

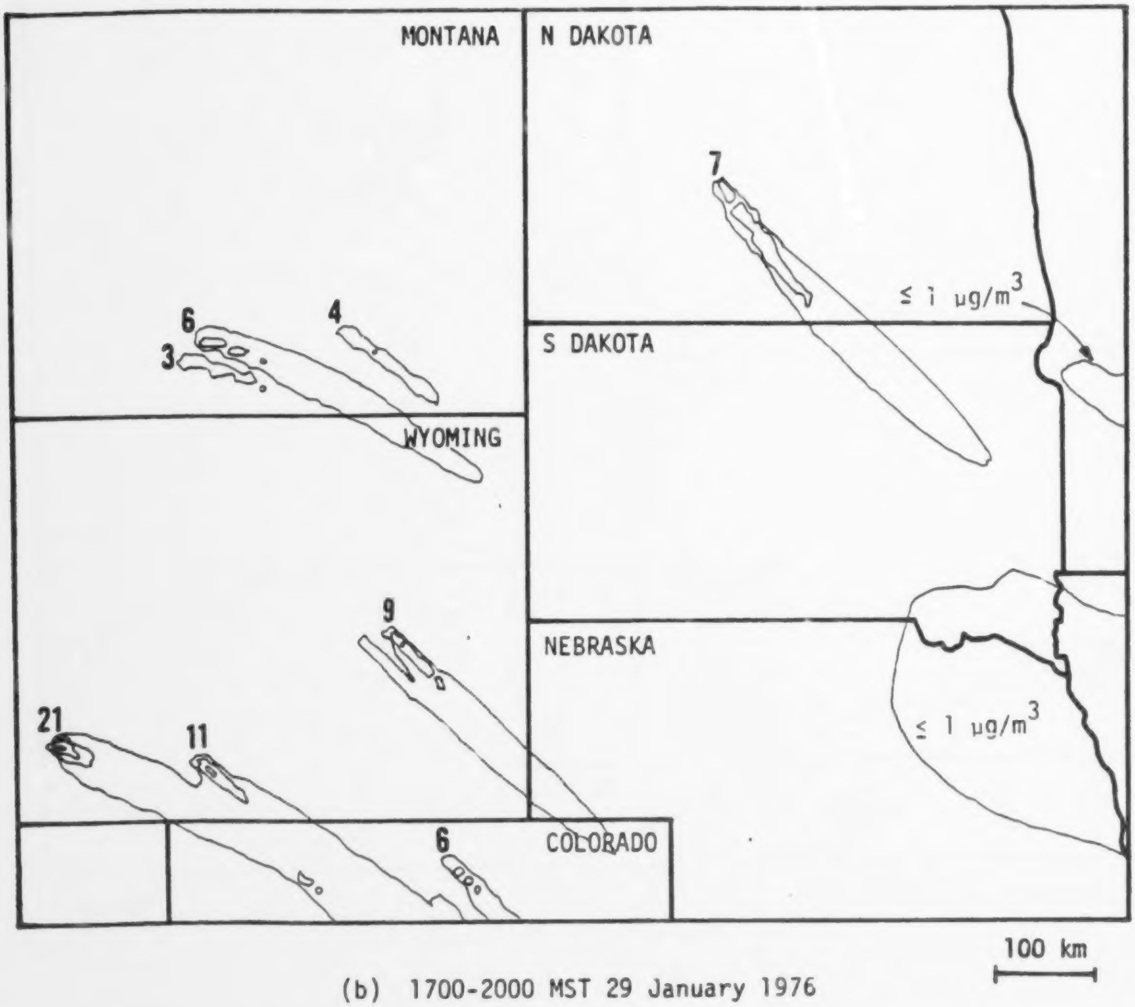
MONTANA
N DAKOTA
S DAKOTA
WYOMING
NEBRASKA
COLORADO
7
6
4
3
9
21
11
6
≤ 1 μg/m³
≤ 1 μg/m³
100 km

(b) 1700-2000 MST 29 January 1976

FIGURE G-2 (Concluded)

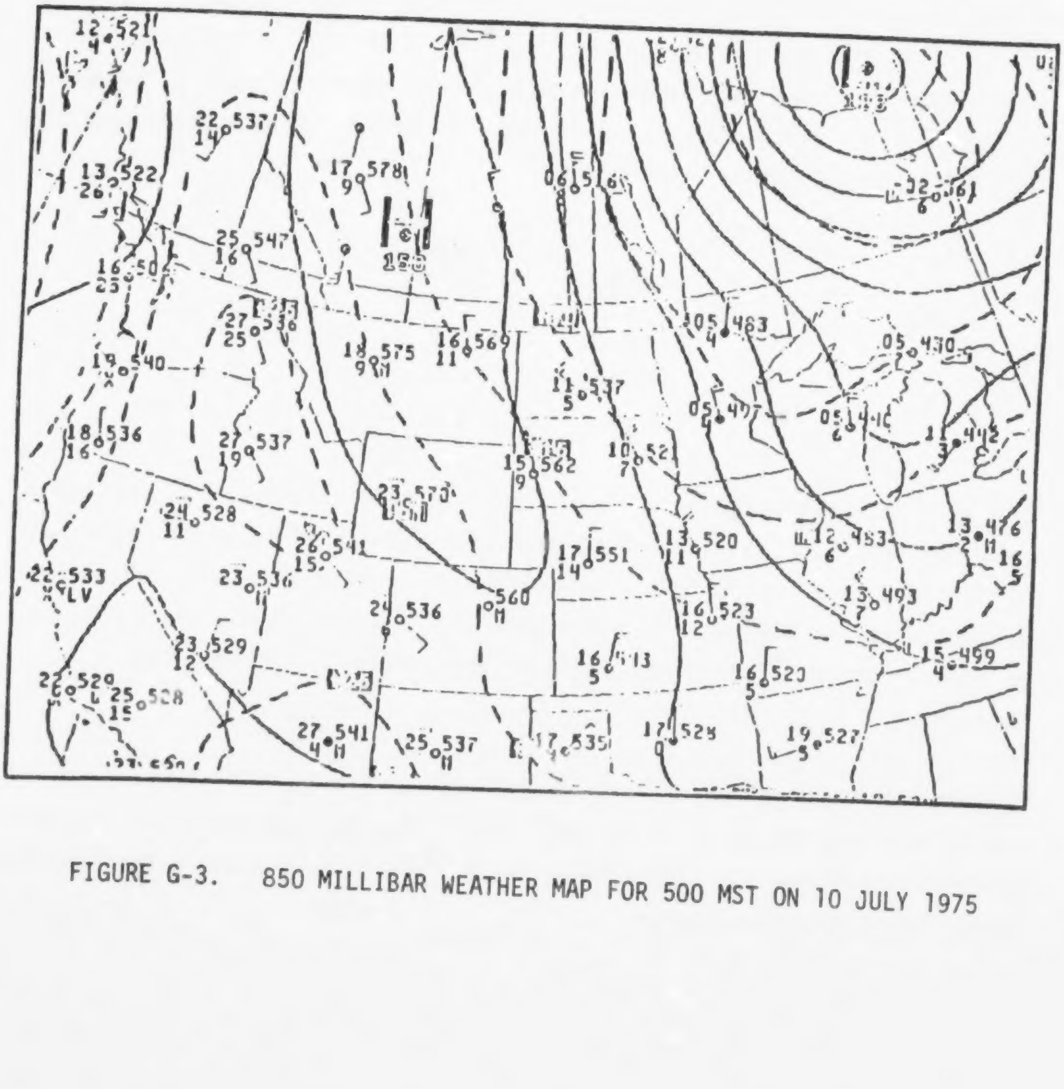
12 521 4
22 537 14
13 522 26
17 578 9
06 56
25 547 16
16 50 25
27 536 25
18 575 9 M
16 569 11
05 483 4
05 430 2
19 540
11 537 5
05 40 6
05 410 6
11 442 3
18 536 16
27 537 19
15 562 9
10 52 7
23 570
24 528 11
26 541 15
17 551 14
13 520 11
12 453 6
13 476 2 M
16 5
22 533 LV
23 536
24 536
560 M
16 523 12
13 493 7
23 529 12
16 413 5
16 520 5
15 459 4
22 520
25 528 15
27 541 4 M
25 537 M
17 535
17 528 0
19 527 5

FIGURE G-3. 850 MILLIBAR WEATHER MAP FOR 500 MST ON 10 JULY 1975 temperature). Overall conversion rates of SO_2 to sulfate in the atmosphere have been observed to vary widely, with a characteristic half-life ranging from a few minutes to a few days. A review of these estimates reveals that the overall conversion rates range between 1 and 13 percent in humid or urban environments and from 0 to 3 percent in dry, nonurban environments. The lower range of the above estimates appears to be more appropriate for the present application. We decided to use the following three SO_2-to-sulfate conversion rates:

Category	Rate (%/hr)
Low	0.3
Medium	0.5
High	1.0

As discussed earlier, calculation of visual range from air quality data requires both sulfate and NO_2 concentrations. Although the regional air quality model described in Appendix F is general in nature, extension of this model to include the photochemical formation of NO_2 would require an effort beyond the original scope of this project. We thus took a shortcut.

We first calculated the NO_x concentration using the regional-scale model, treating NO_x as an inert pollutant. The NO_2 concentration required to calculate atmospheric discoloration was then obtained using the modified steady-state approximation:

$$[NO_2] + \frac{1}{2}\left[\left([NO_x] + [O_3] + \frac{k_1}{k_3}\right) - \left\{\left([NO_x] + [O_3] + \frac{k_1}{k_3}\right)^2 - 4[NO_x][O_3]\right\}^{1/2}\right] ,$$

where $k_3 = 25\ ppm^{-1}min^{-1}$ and $[O_3] = 0.04$ ppm. The temporally varying k_1 is given in Figure G-4.

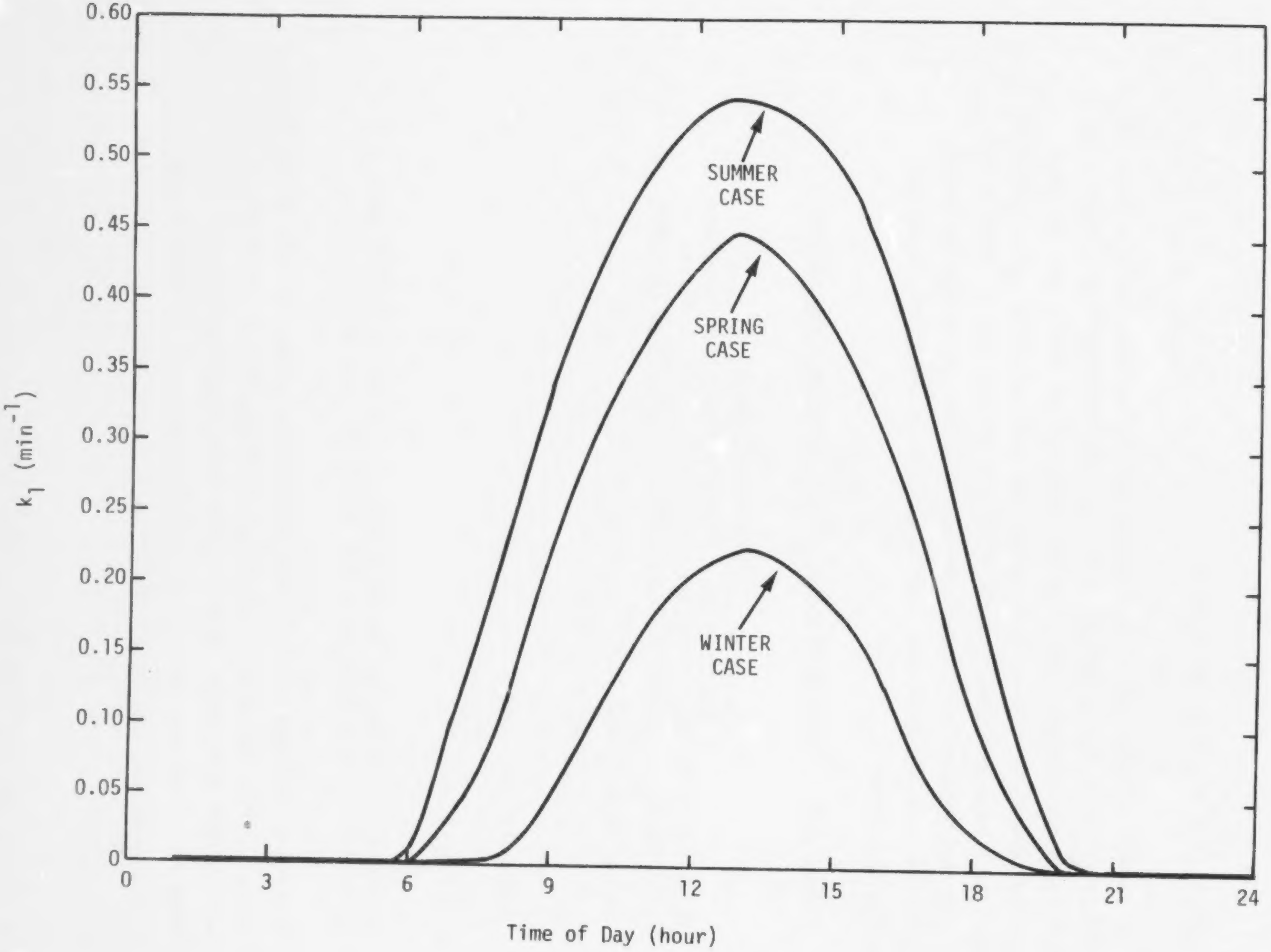

FIGURE G-4. PHOTODISSOCIATION RATE CONSTANT TEMPORAL VARIATION

2. ANALYSIS OF THE MODELING RESULTS

As shown in Table G-4, five computer simulations were made to examine the effect of different emissions scenarios and meteorological patterns on visibility in the Northern Great Plains. For all of these runs, an SO_2-to-sulfate conversion rate of 0.5 percent per hour was used. Two additional computer runs were performed for the more interesting case of April meteorology and the hypothetical case of smelter emissions using the estimated "high" (1 percent per hour) and "low" (0.3 percent per hour) conversion rates for this area.

TABLE G-4. THE FIVE REGIONAL VISIBILITY MODEL SIMULATIONS

	Emissions Scenario		
Meteorological Scenario	Hypothetical Copper Smelter Emissions	Northern Great Plains 1976 Emissions	Northern Great Plains 1986 Emissions
Spring (April)	Run 1	Run 6	Run 7
	Run 4 (1 %/hr)		
	Run 5 (0.3 %/hr)		
Summer (July)	Run 2		
Winter (January)	Run 3		

a. Hypothetical Copper Smelter Emissions, Assuming 0.5 Percent per Hour Sulfate Formation, Using the Spring (April) Scenario

Figures G-5 through G-10 present the computer output for the hypothetical copper smelter emission scenario with the assumption of 0.5 percent per hour sulfate formation. These figures show computed isopleths for the following for three-hour periods during the three-day simulation (using April 1976 meteorological conditions):

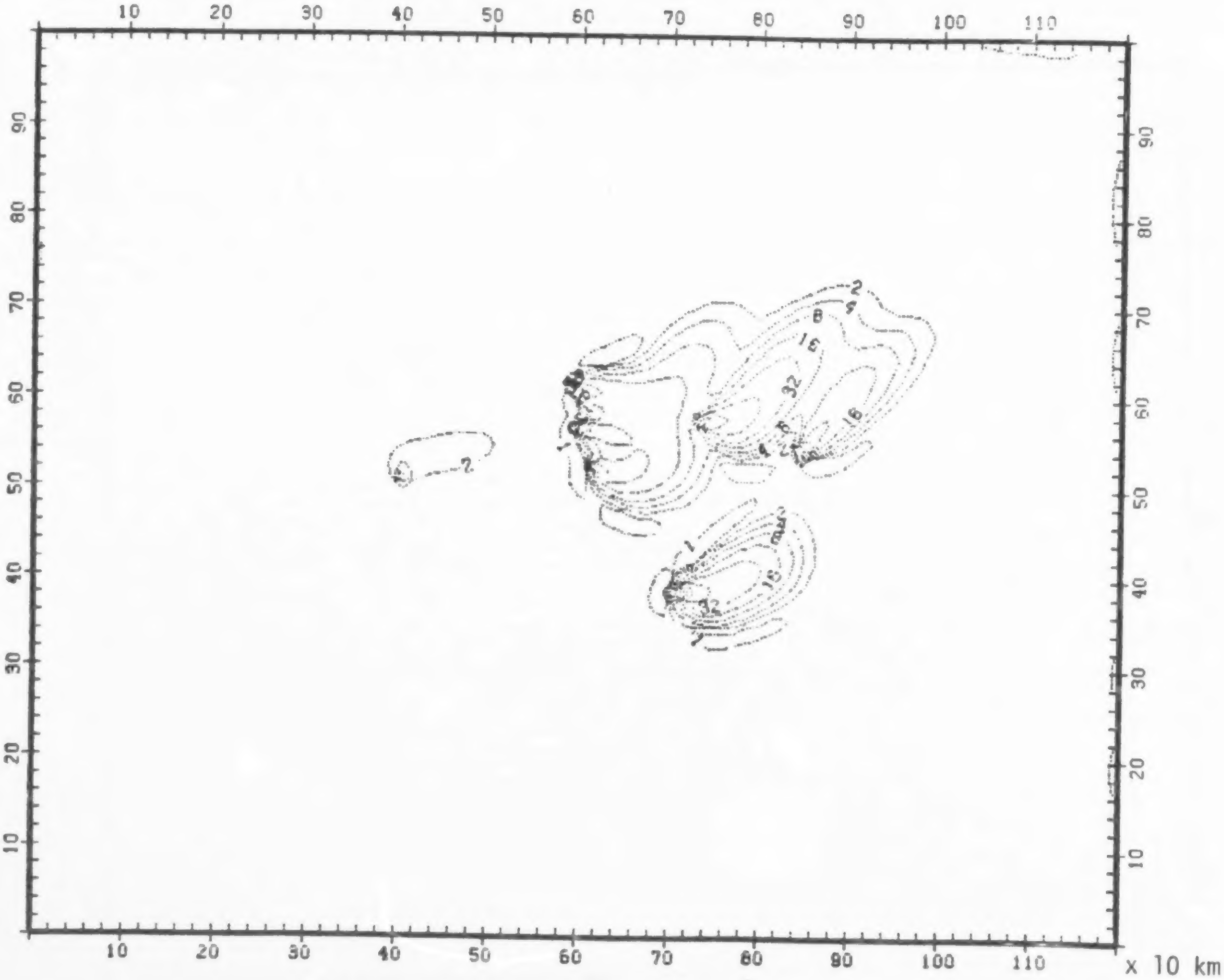
10
20
30
40
50
60
70
80
90
100
110
2
4
8
16
32
x 10 km

(a) SO_2 Concentrations ($\mu g/m^3$)

FIGURE G-5. HYPOTHETICAL COPPER SMELTER ISOPLETHS FOR 1700-2000 MST ON 4 APRIL 1976 ASSUMING 0.5 PERCENT PER HOUR SULFATE FORMATION

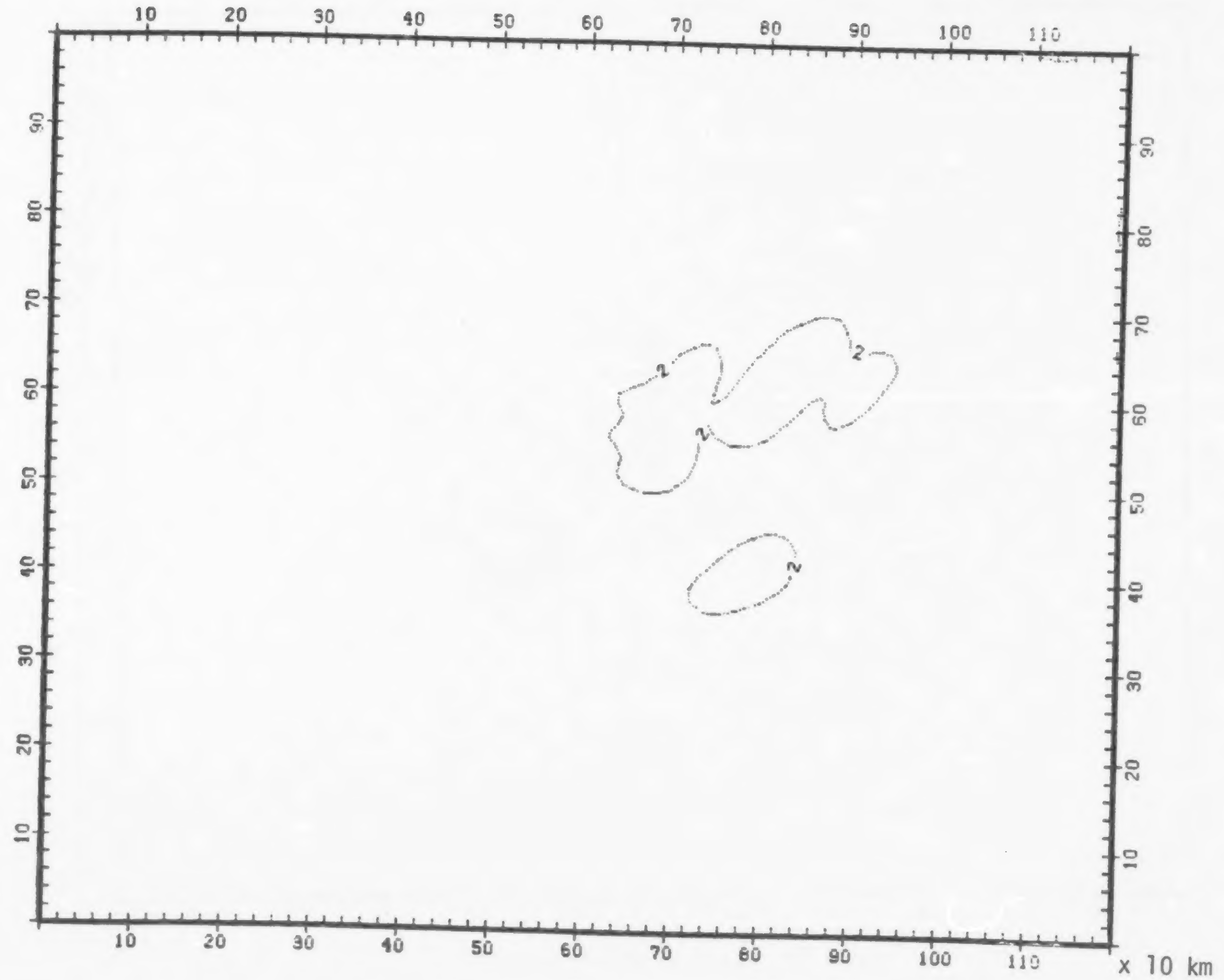
10
20
30
40
50
60
70
80
90
100
110
2
2
2
2
x 10 km

(b) $SO_4^=$ Concentrations ($\mu g/m^3$)

FIGURE G-5 (Continued)

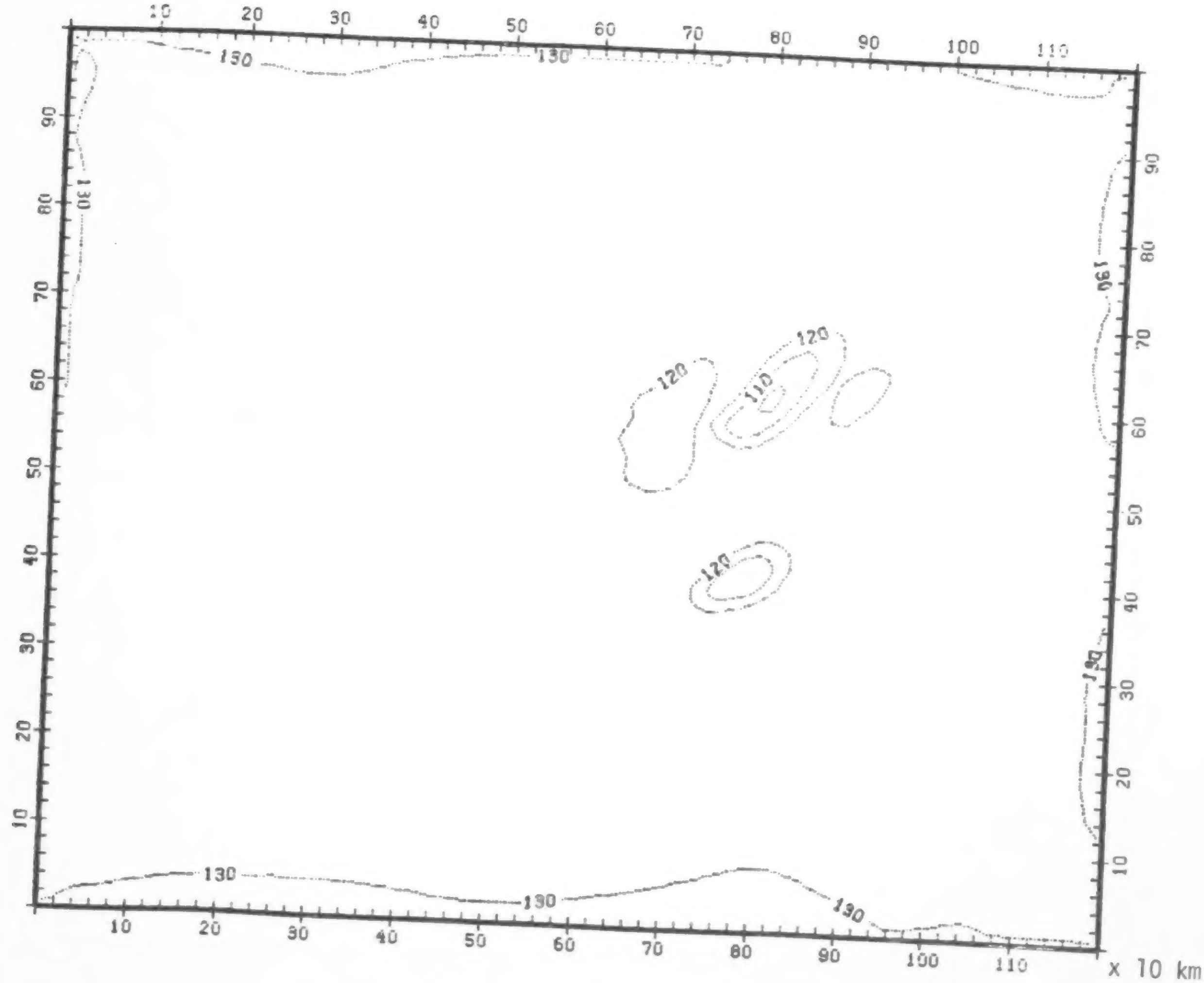
10
20
30
40
50
60
70
80
90
100
110
150
130
120
110
x 10 km

(c) Visual Range (km)

FIGURE G-5 (Concluded)

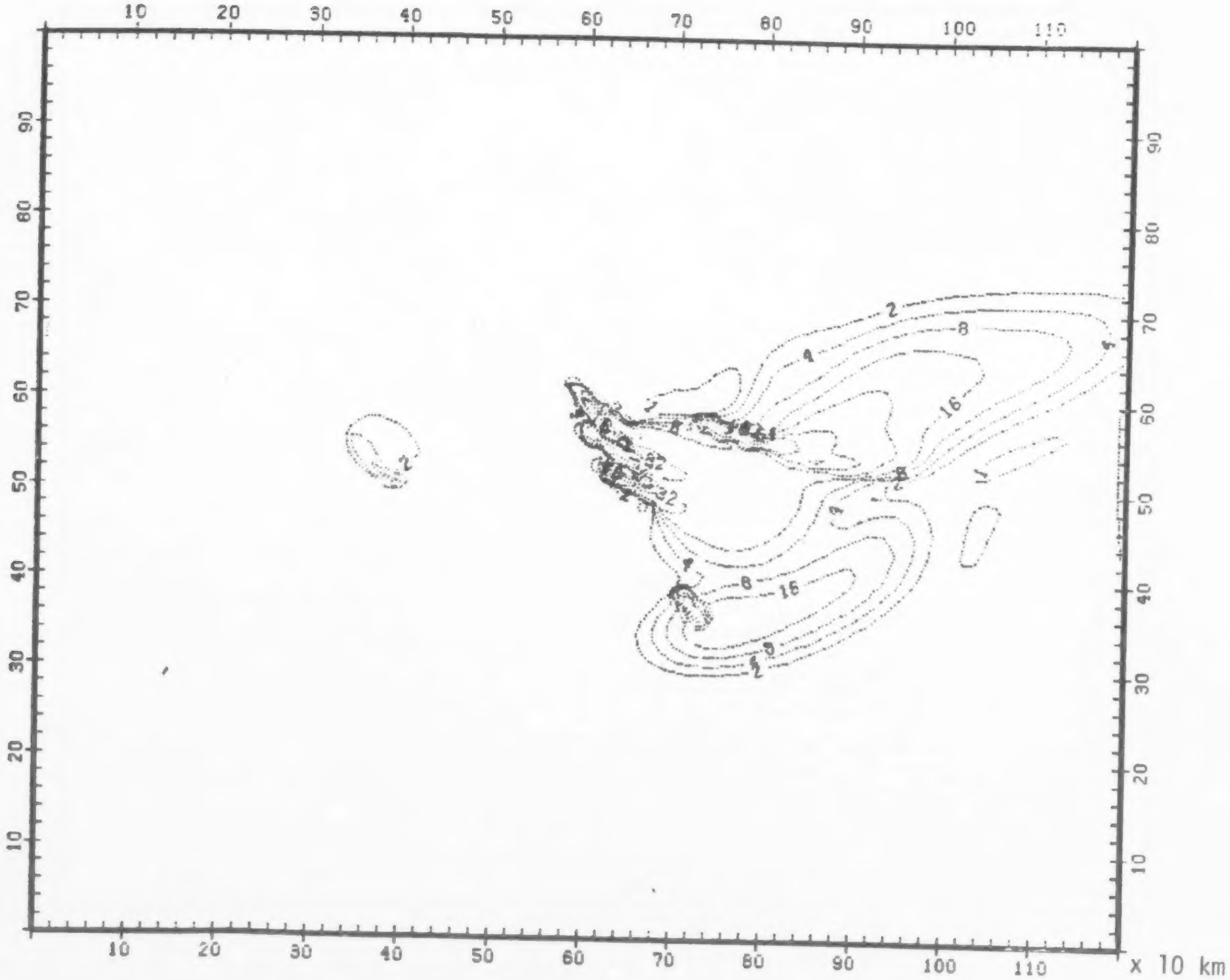
10
20
30
40
50
60
70
80
90
100
110
x 10 km
2
4
8
16
32

(a) SO_2 Concentrations ($\mu g/m^3$)

FIGURE G-6. HYPOTHETICAL COPPER SMELTER ISOPLETHS FOR 200-500 MST ON 5 APRIL 1976 ASSUMING 0.5 PERCENT PER HOUR SULFATE FORMATION

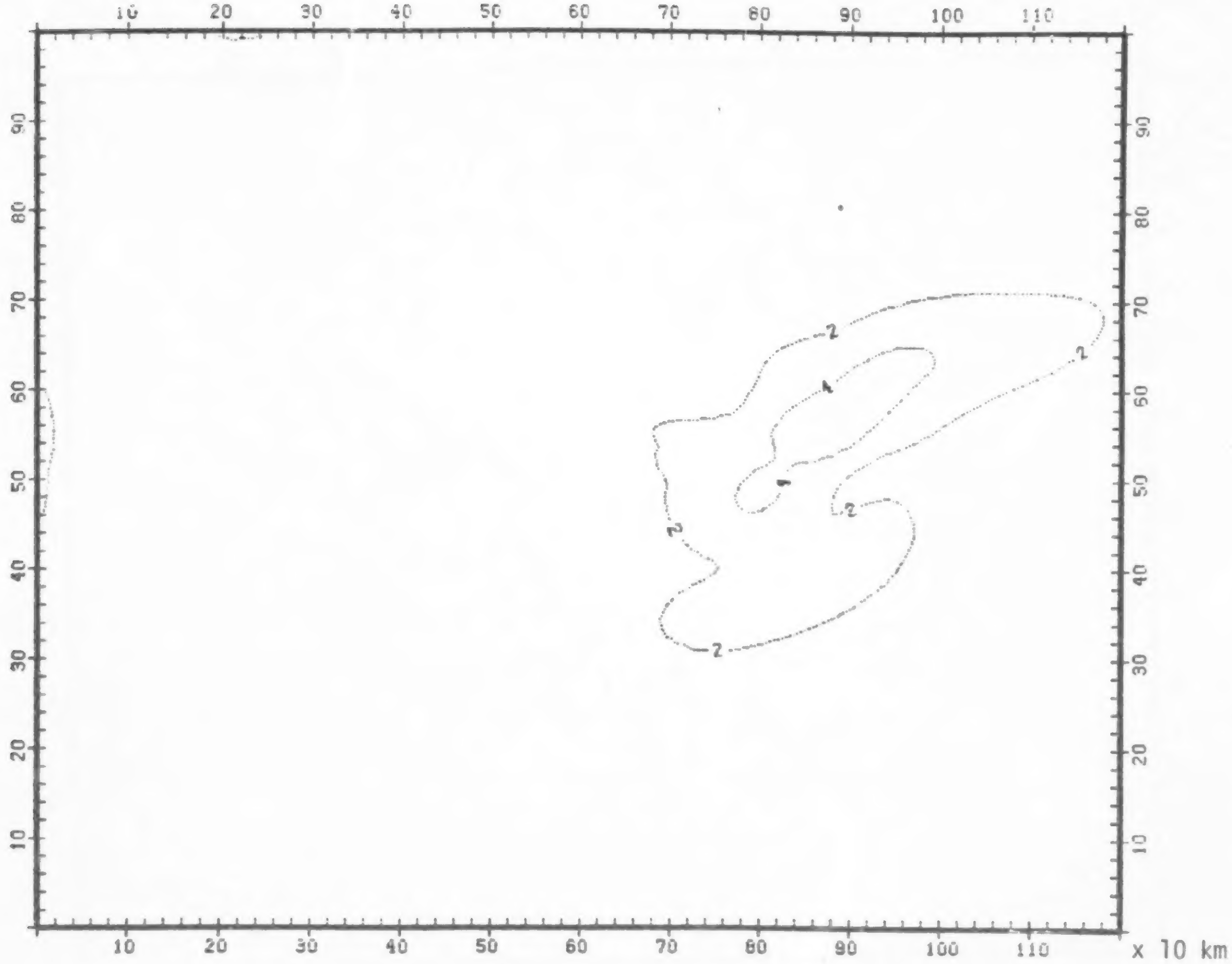
10
20
30
40
50
60
70
80
90
100
110
x 10 km
2
4

(b) $SO_4^=$ Concentrations ($\mu g/m^3$)

FIGURE G-6 (Continued)

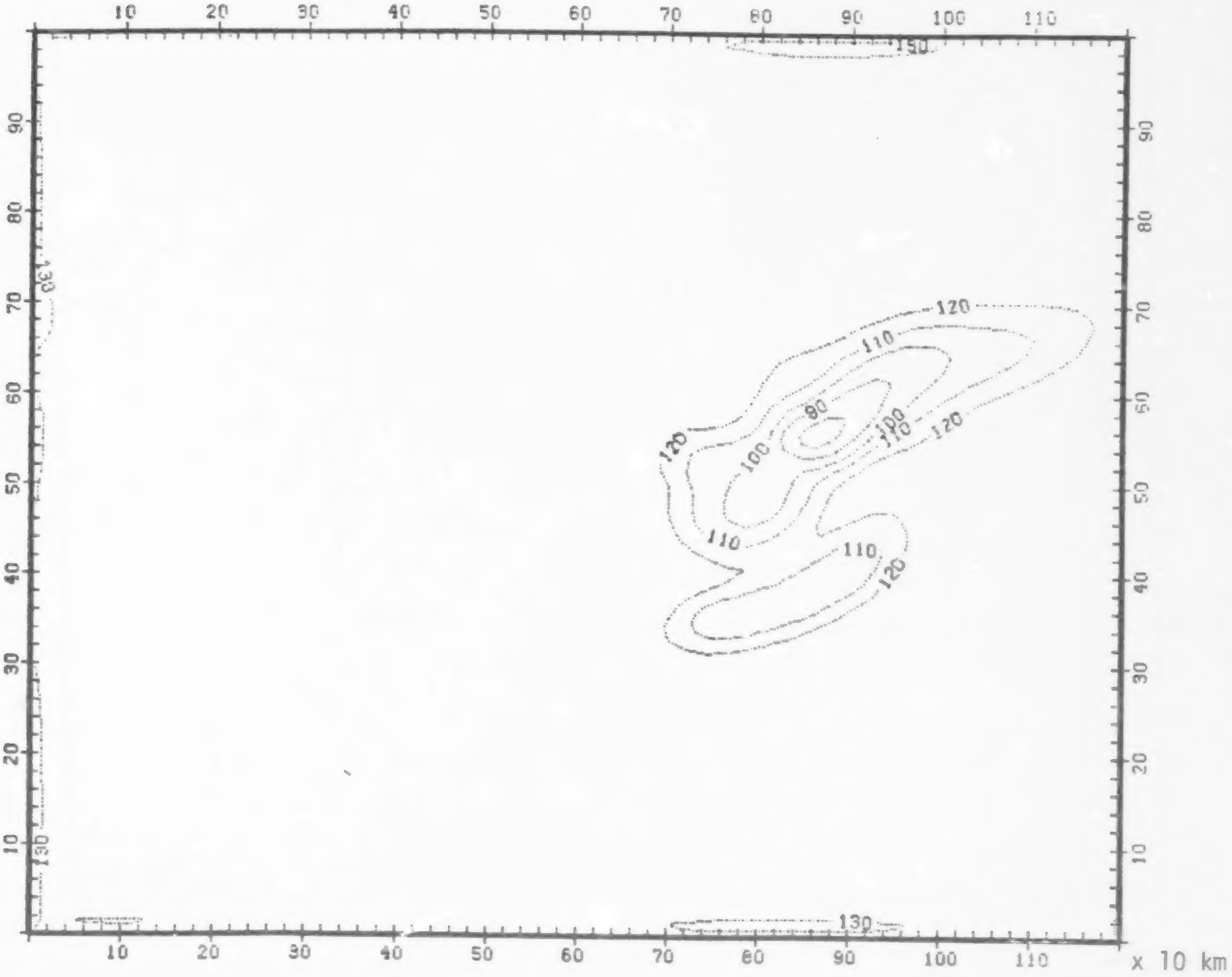
10
20
30
40
50
60
70
80
90
100
110
130
120
110
90
100
110
120
120
100
110
110
120
130
x 10 km

(c) Visual Range (km)

FIGURE G-6 (Concluded)

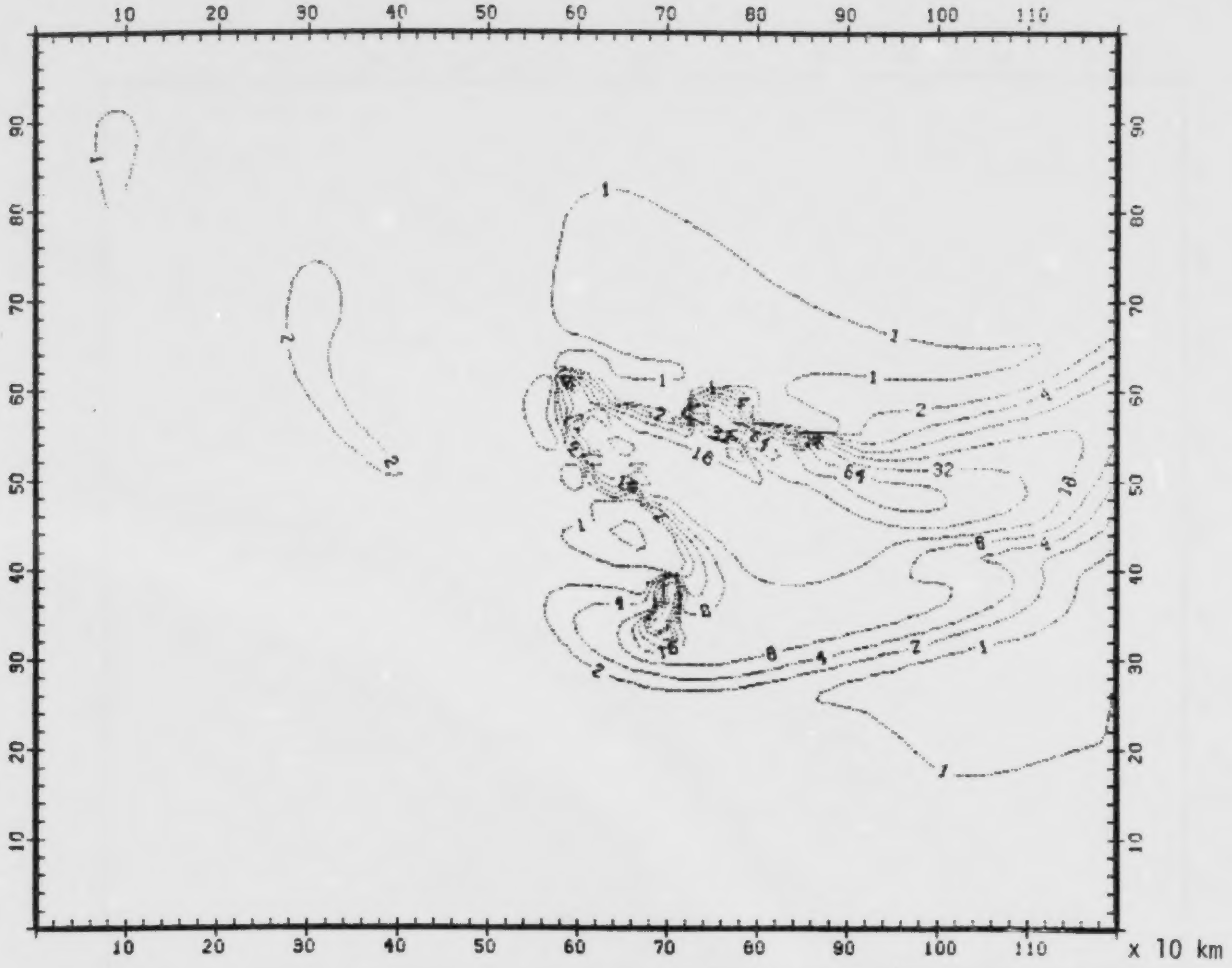
10
20
30
40
50
60
70
80
90
100
110
x 10 km
1
2
4
8
16
32
64

(a) SO_2 Concentrations ($\mu g/m^3$)

FIGURE G-7. HYPOTHETICAL COPPER SMELTER ISOPLETHS FOR 1100-1400 MST ON 5 APRIL 1976 ASSUMING 0.5 PERCENT PER HOUR SULFATE FORMATION

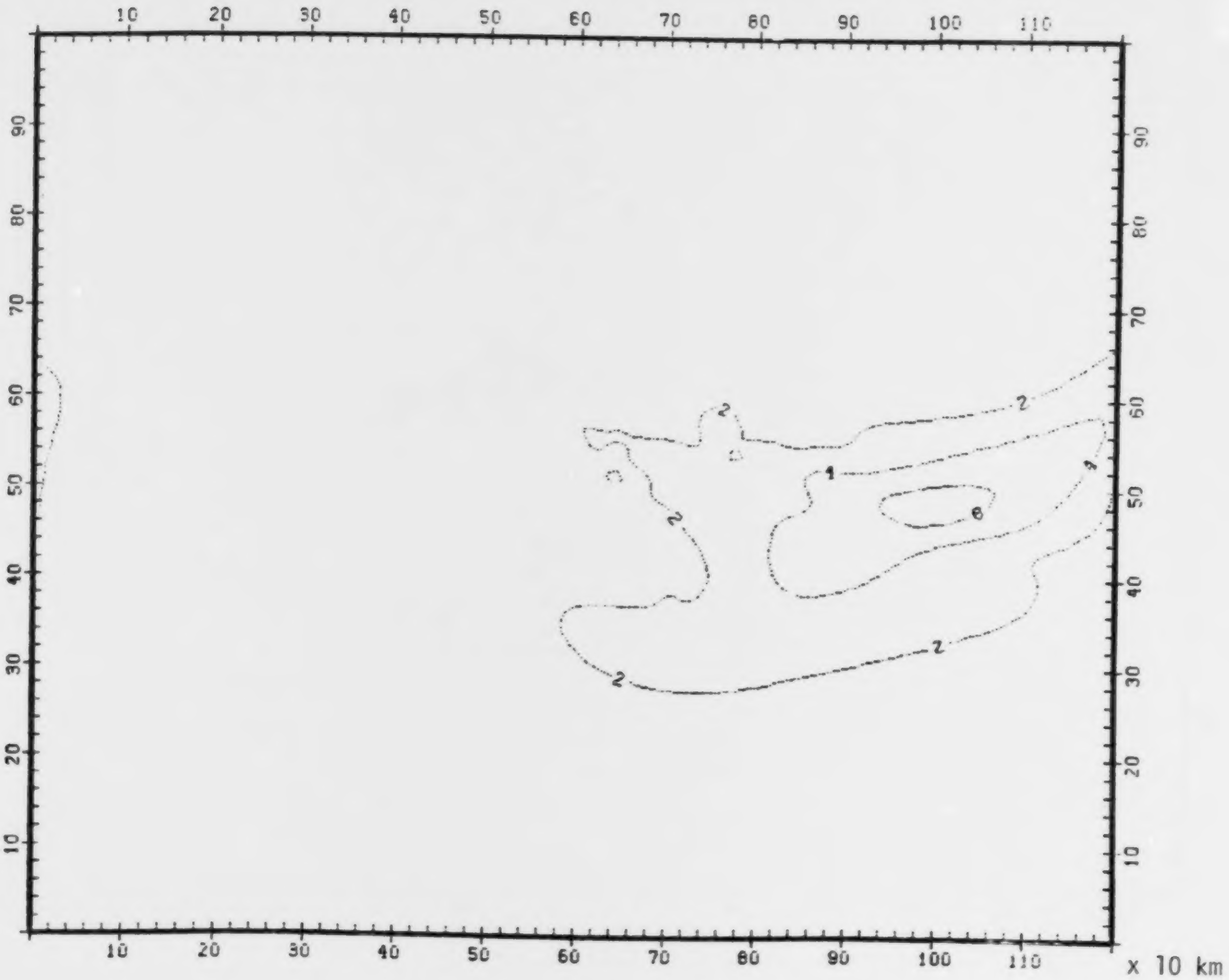
10
20
30
40
50
60
70
80
90
100
110
x 10 km
2
4
6

(b) $SO_4^=$ Concentrations (μg/m^3)

FIGURE G-7 (Continued)

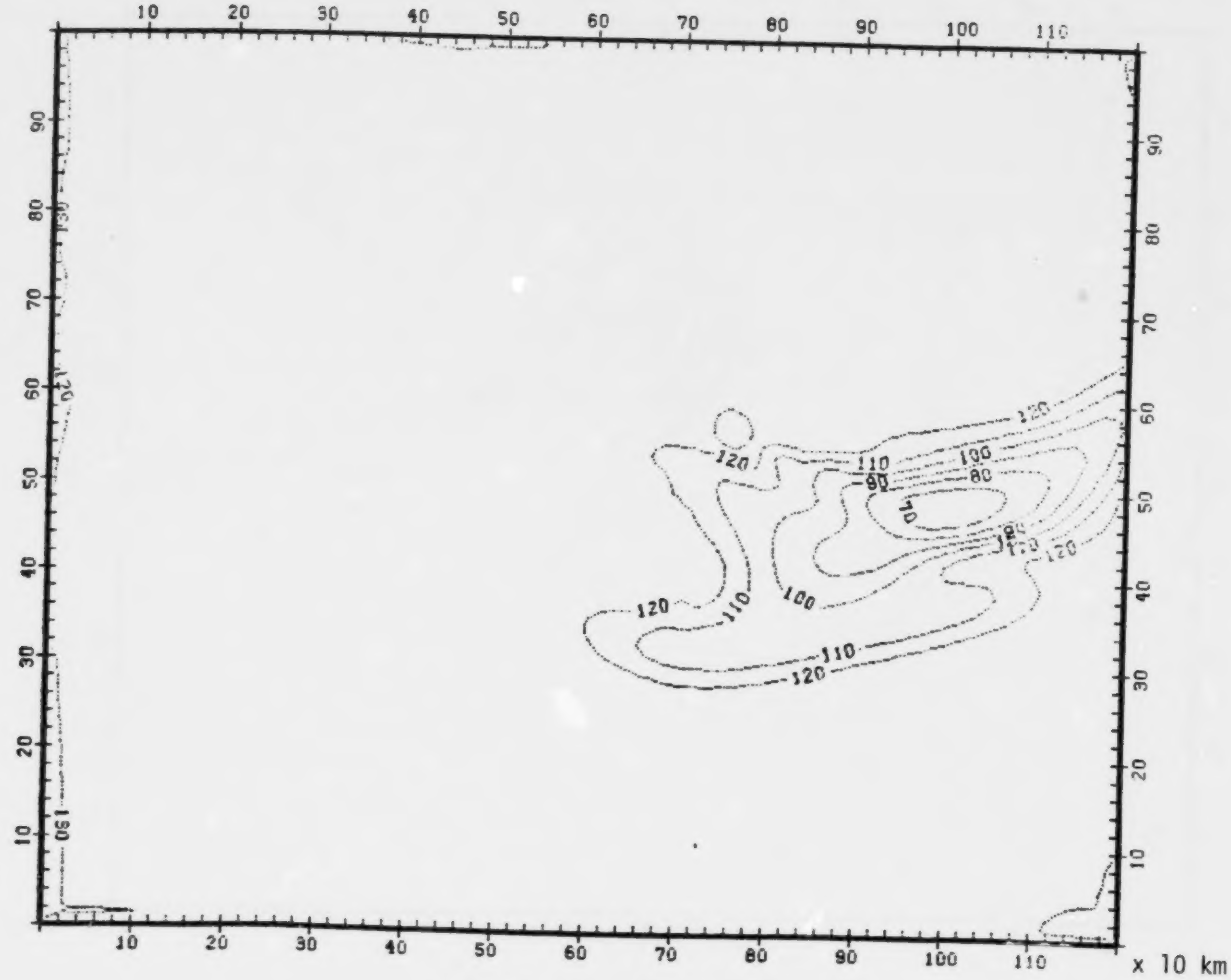
10
20
30
40
50
60
70
80
90
100
110
x 10 km
120
110
100
90
80
70
130

(c) Visual Range (km)

FIGURE G-7 (Concluded)

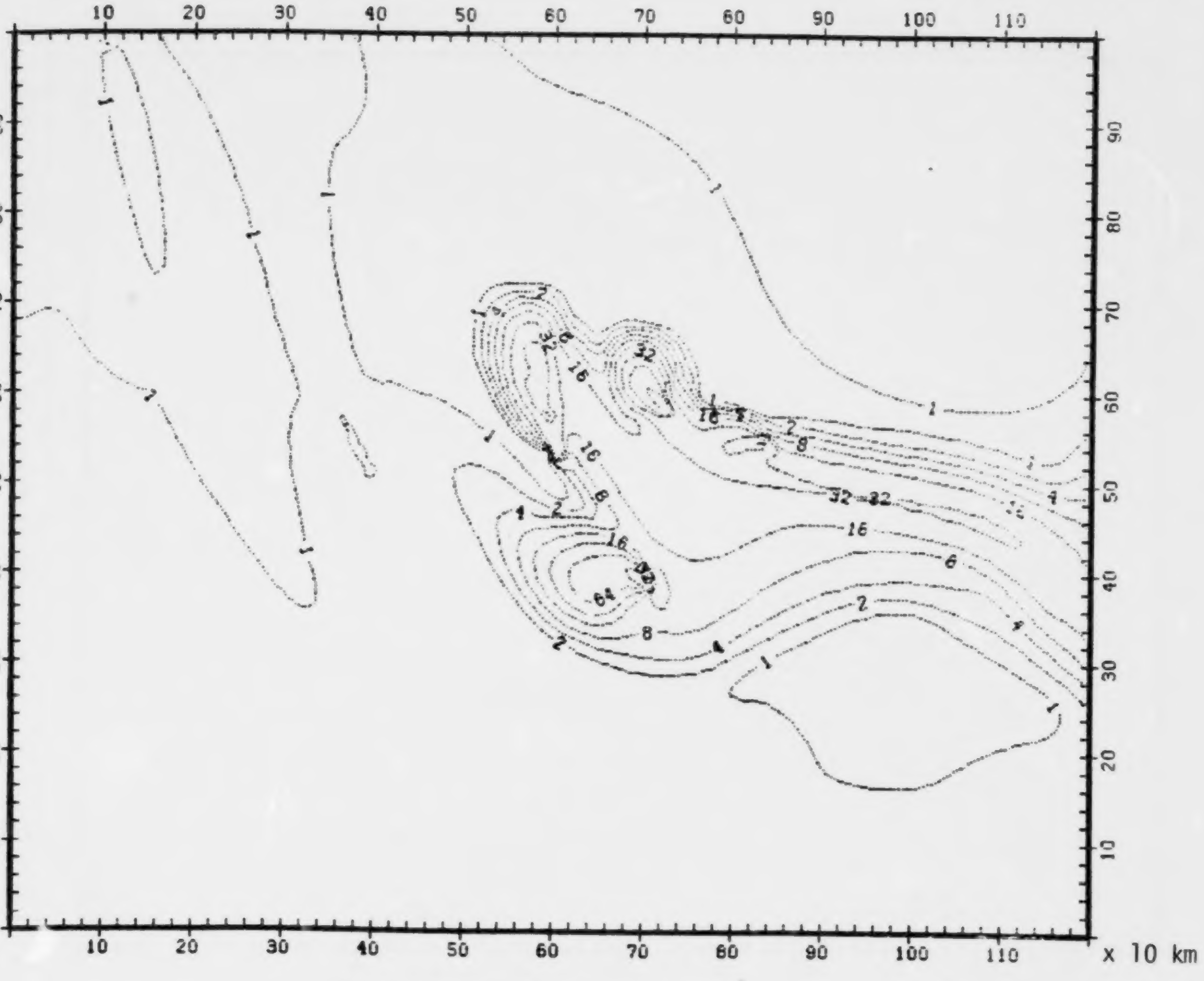

(a) SO_2 Concentrations ($\mu g/m^3$)

FIGURE G-8. HYPOTHETICAL COPPER SMELTER ISOPLETHS FOR 2000-2300 MST ON 5 APRIL 1976 ASSUMING 0.5 PERCENT PER HOUR SULFATE FORMATION

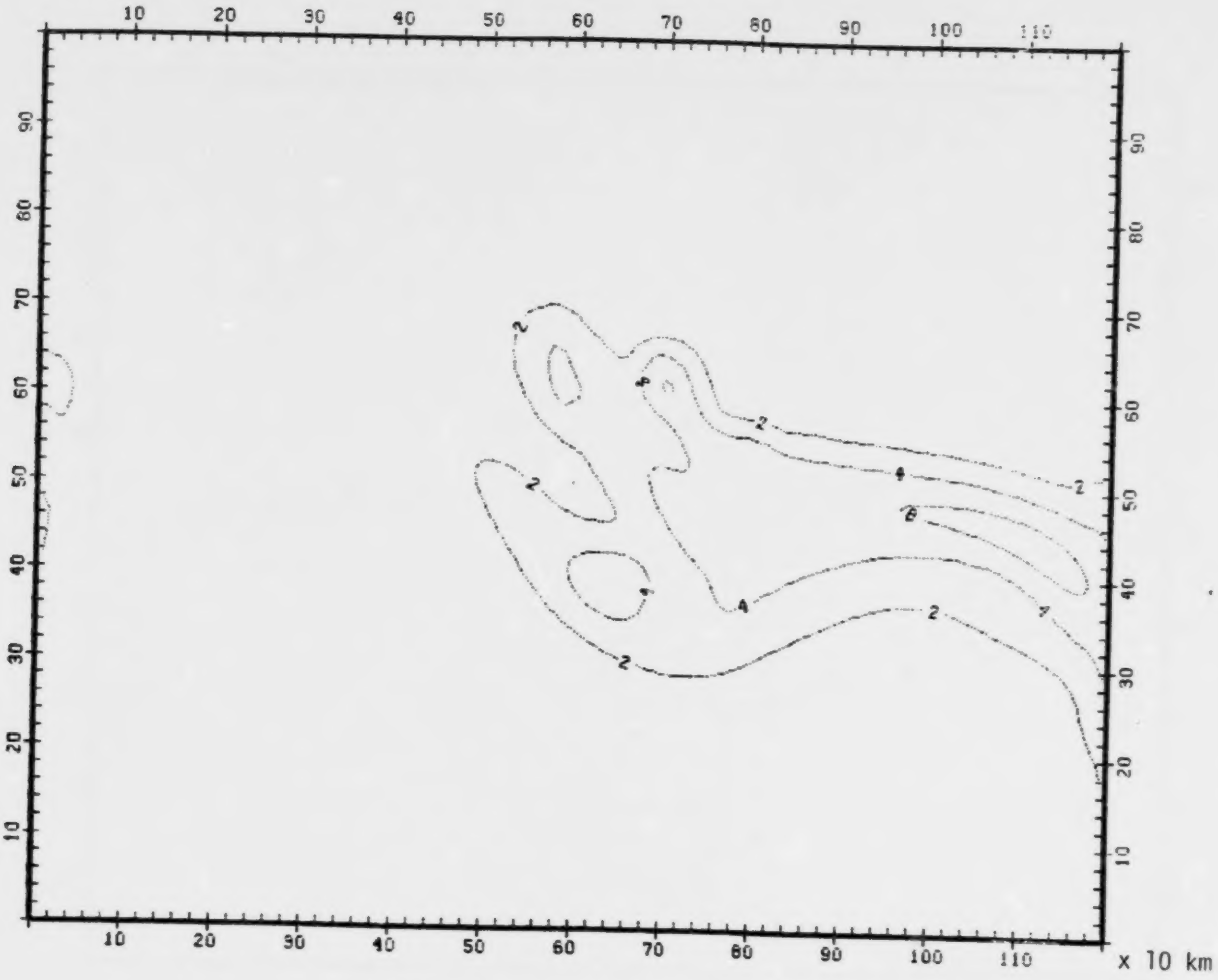
10
20
30
40
50
60
70
80
90
100
110
2
4
6
x 10 km

(b) $SO_4^=$ Concentrations ($\mu g/m^3$)

FIGURE G-8 (Continued)

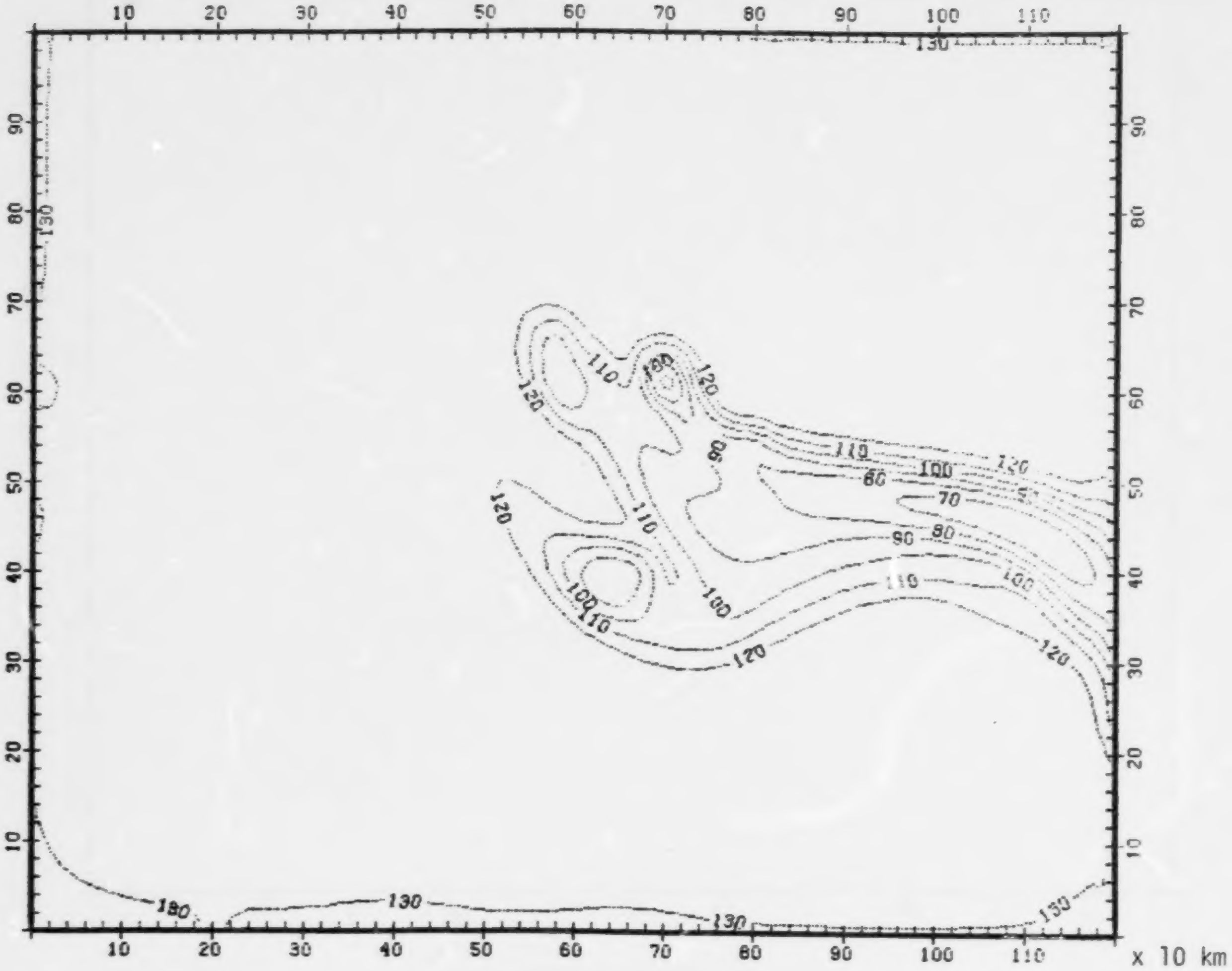
10
20
30
40
50
60
70
80
90
100
110
x 10 km
130
120
110
100
90
80
70
60

(c) Visual Range (km)

FIGURE G-8 (Concluded)

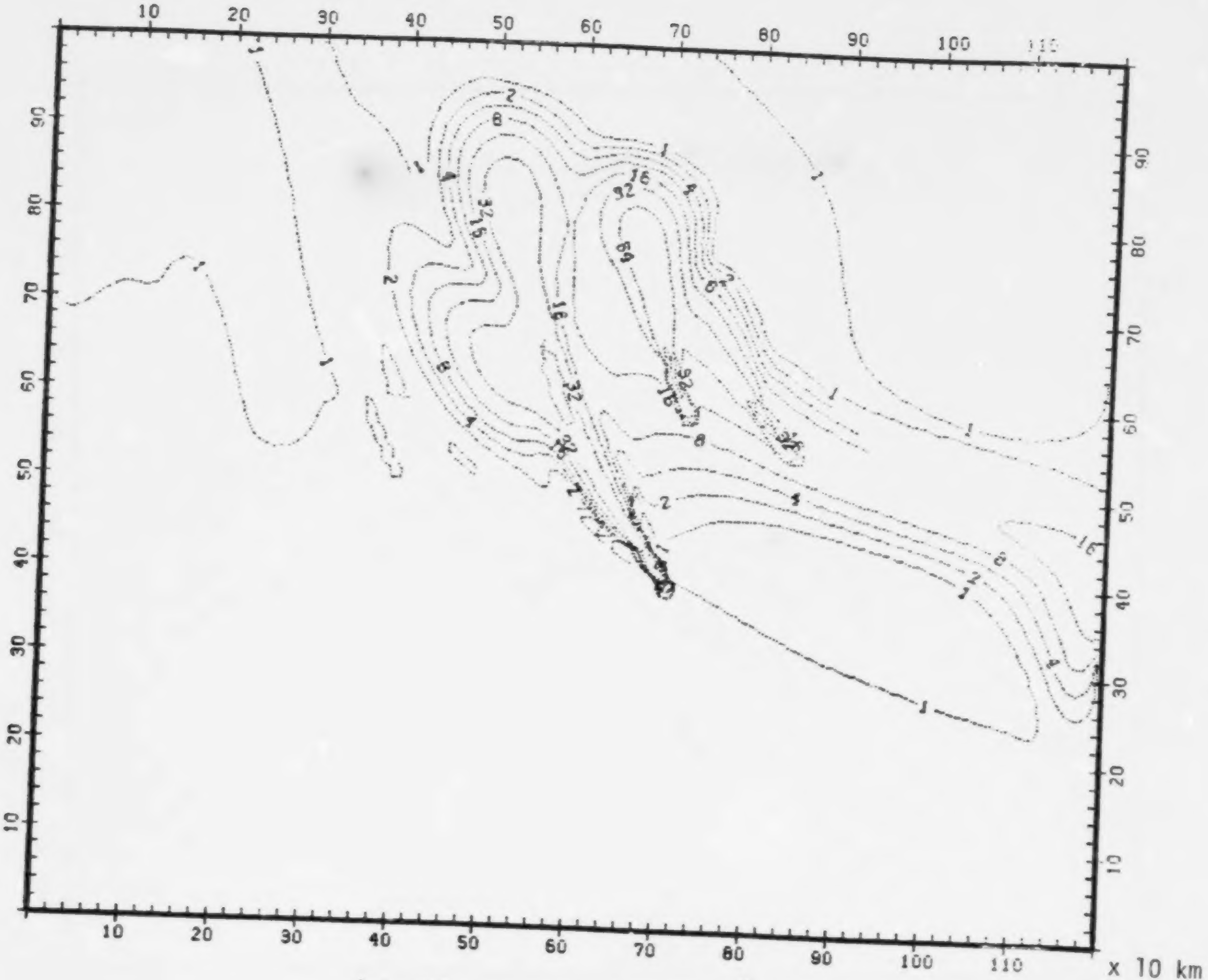
10
20
30
40
50
60
70
80
90
100
110
x 10 km
1
2
4
8
16
32
64

(a) SO_2 Concentrations ($\mu g/m^3$)

FIGURE G-9. HYPOTHETICAL COPPER SMELTER ISOPLETHS FOR 500-800 MST ON 6 APRIL 1976 ASSUMING 0.5 PERCENT PER HOUR SULFATE FORMATION

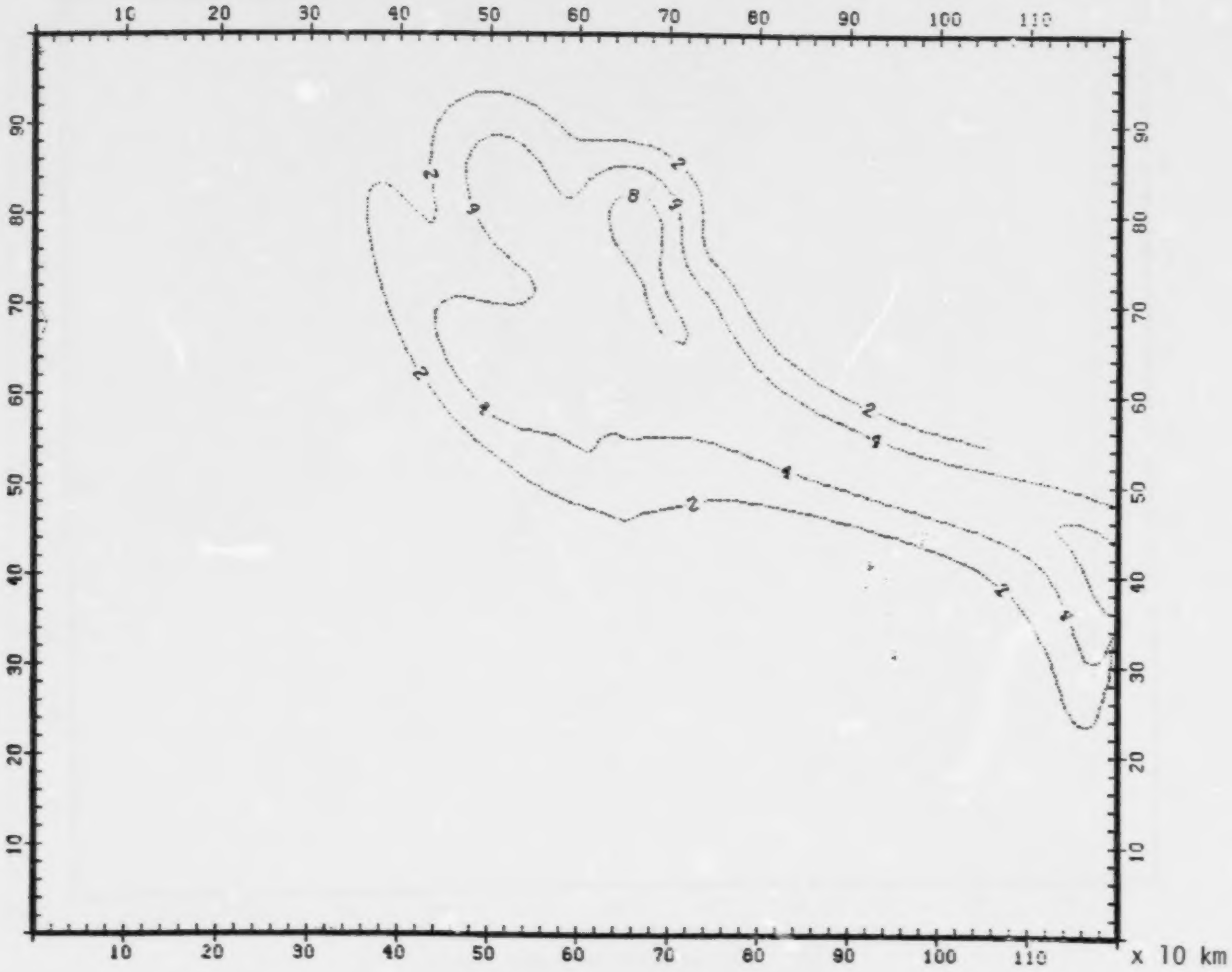
10
20
30
40
50
60
70
80
90
100
110
x 10 km
2
4
8

(b) $SO_4^=$ Concentrations ($\mu g/m^3$)

FIGURE G-9 (Continued)

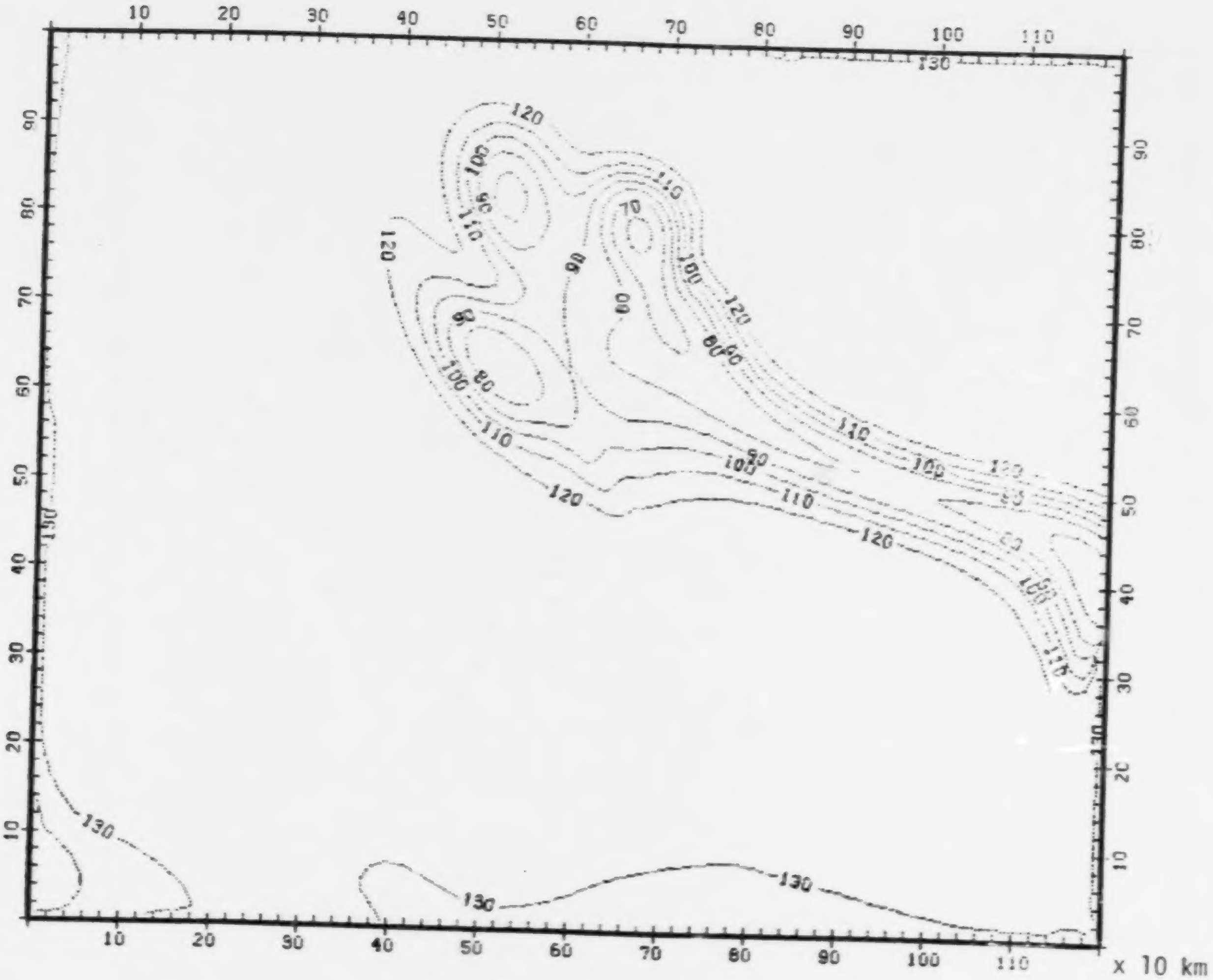
10
20
30
40
50
60
70
80
90
100
110
x 10 km
120
110
100
90
80
70
130

(c) Visual Range (km)

FIGURE G-9 (Concluded)

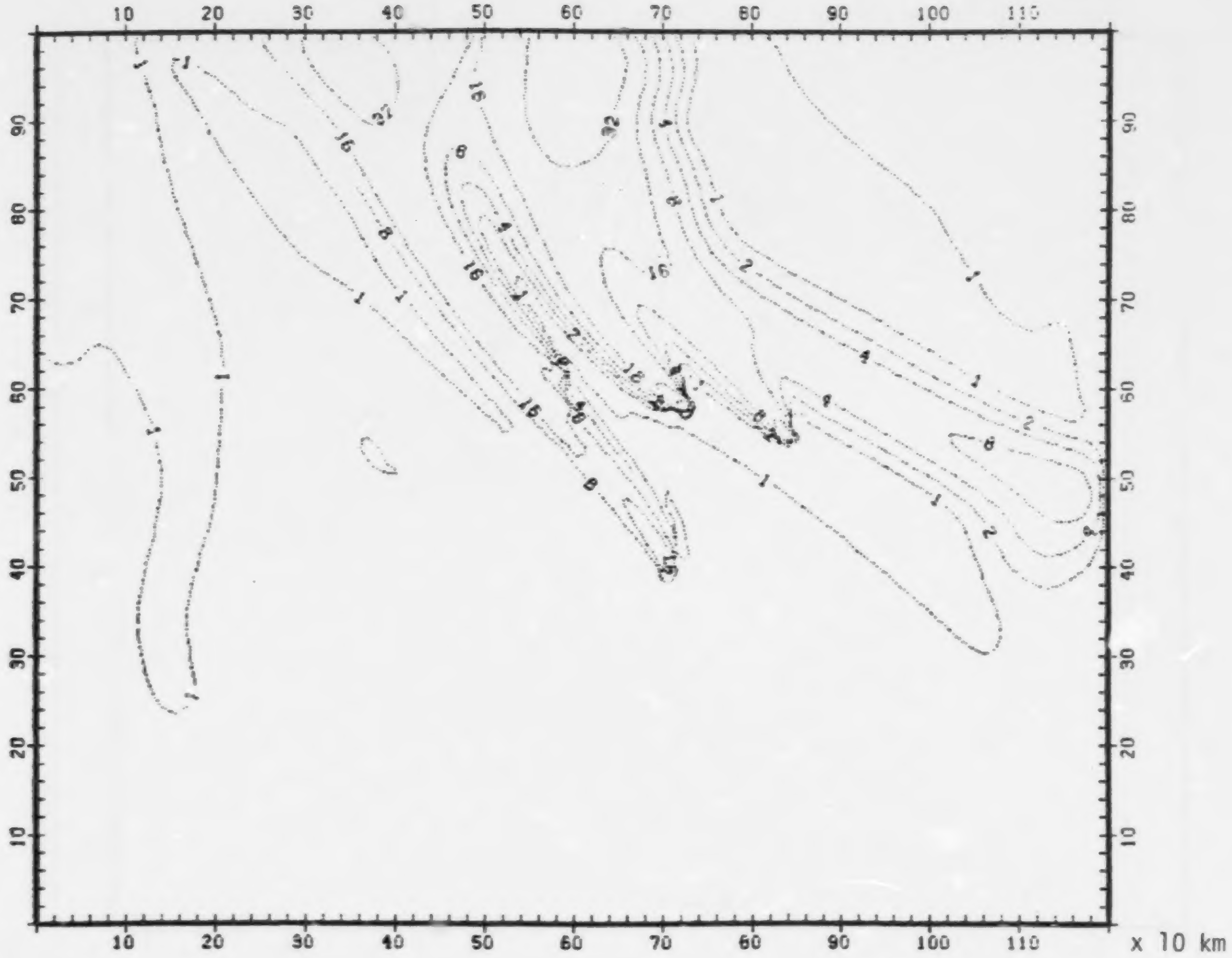
x 10 km
10
20
30
40
50
60
70
80
90
100
110
1
2
4
8
16
32

(a) SO_2 Concentrations ($\mu g/m^3$)

FIGURE G-10. HYPOTHETICAL COPPER SMELTER ISOPLETHS FOR 1400-1700 MST ON 6 APRIL 1976 ASSUMING 0.5 PERCENT PER HOUR SULFATE FORMATION

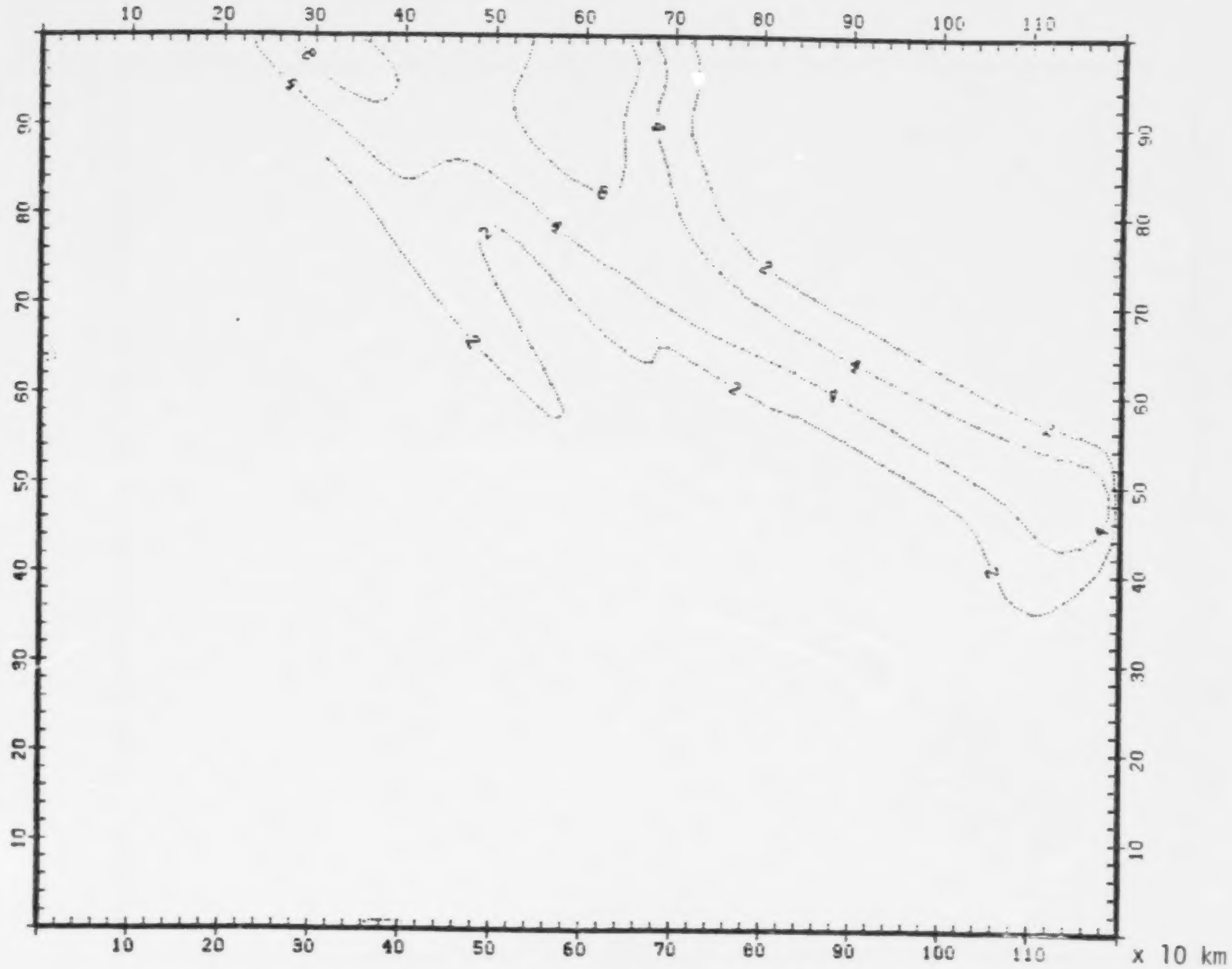
10
20
30
40
50
60
70
80
90
100
110
x 10 km
8
6
4
2
6
2
4
2
2
4
4
2
2
4
2

(b) $SO_4^=$ Concentrations ($\mu g/m^3$)

FIGURE G-10 (Continued)

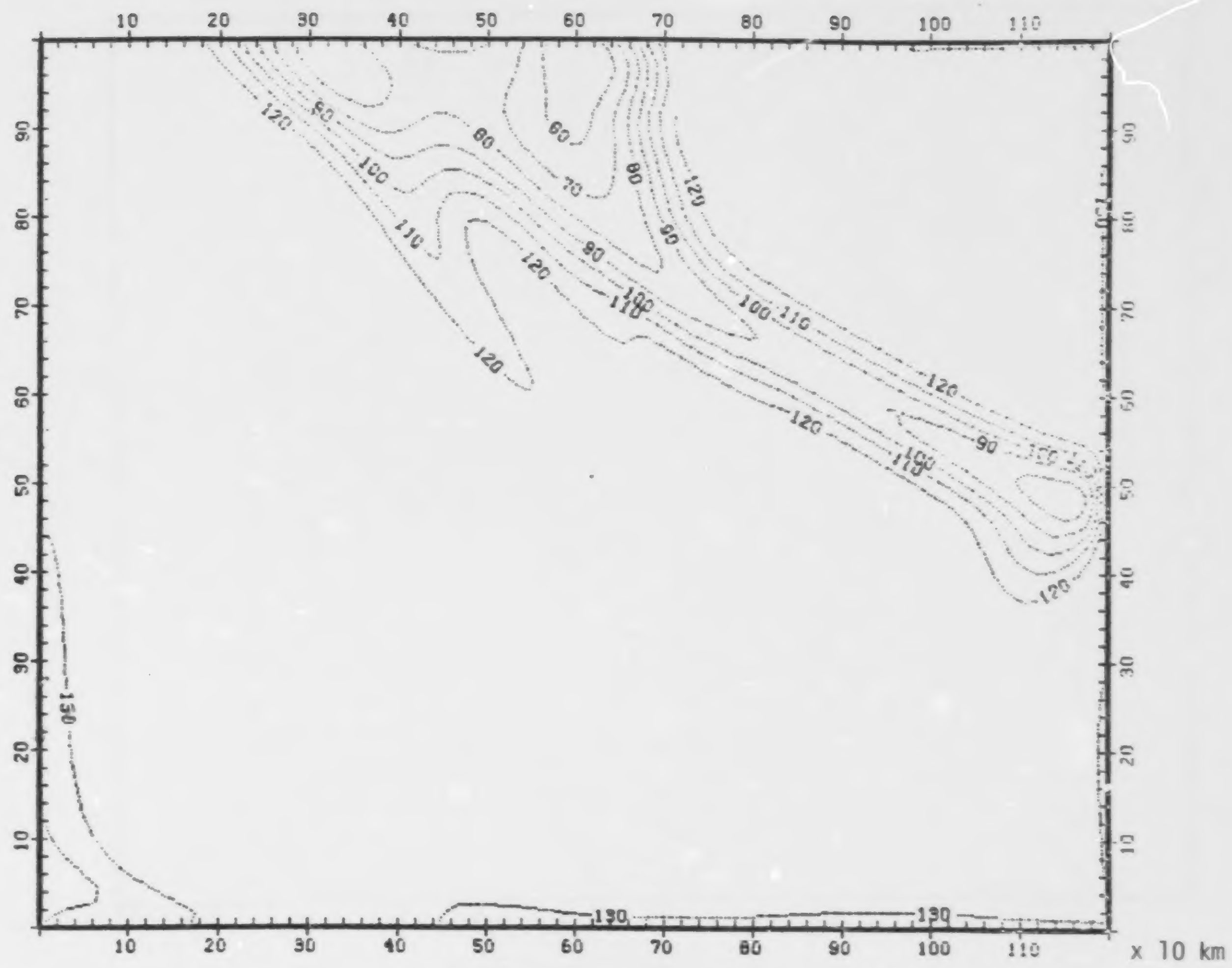

(c) Visual Range (km)

FIGURE G-10 (Concluded)

- SO_2 concentrations ($\mu g/m^3$) at isopleth intervals of 2, 4, 8, 16,....
- $SO_4^=$ concentrations ($\mu g/m^3$) at these same intervals.
- Visual range (km) at isopleth intervals of 10, 20, 30,....

(The axes are labeled in tens of kilometers.) The background concentration of $SO_4^=$ is 1.5 $\mu g/m^3$, corresponding to a background visual range of 130 km. Note the effect of the change in wind direction that occurred at the beginning of 6 April 1976. The maximum values of [SO_2] occur near the sources, whereas maximum [$SO_4^=$] values and minimum visual ranges occur several hundred kilometers from the sources.

b. Hypothetical Copper Smelter Emissions, Assuming 0.5 Percent per Hour Sulfate Formation, Using the Summer (July) Scenario

Figures G-11 through G-16 show the results of the second simulation (Run 2) for the hypothetical smelter emissions for the summer (July) meteorological conditions. Note that the strong, steady, and generally northerly winds used for this simulation result in the transport of SO_2 and $SO_4^=$ to the south. Also, the concentrations of $SO_4^=$ are much lower, resulting in less visibility impairment than occurred in the April scenario (Run 1), which had light and variable winds (stagnant conditions).

c. Hypothetical Copper Smelter Emissions, Assuming 0.5 Percent per Hour Sulfate Formation, Using the Winter (January) Scenario

The winter (January) scenario results (Run 3) are presented in Figures G-17 through G-22. Note that, as with the summer scenario, good ventilation causes rapid transport and dilution of the hypothetical copper smelter emissions; the calculated visibility impairment is much less than that which occurred with the April stagnation scenario.

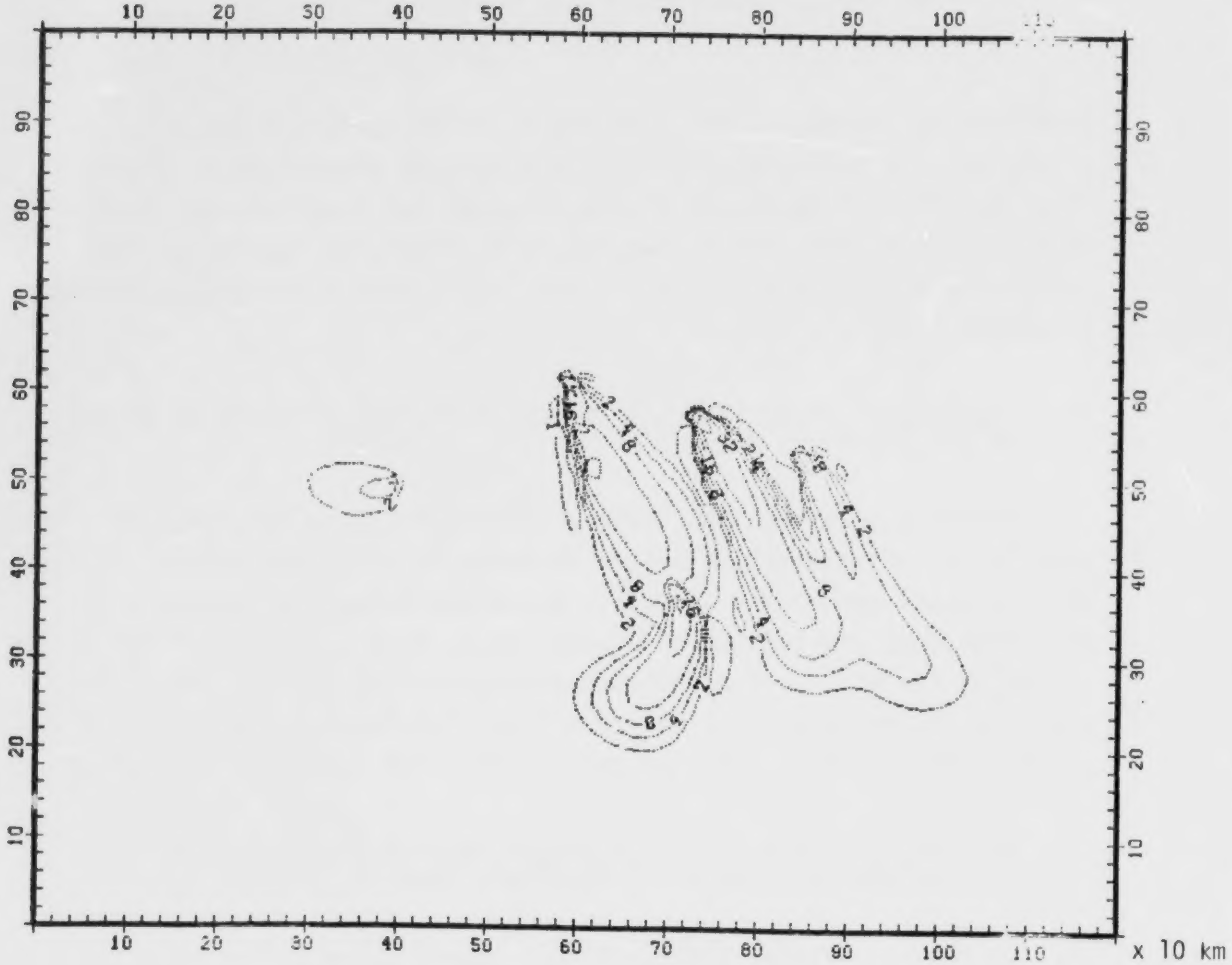
10
20
30
40
50
60
70
80
90
100
110
x 10 km
2
4
8
16
32

(a) SO$_2$ Concentrations (μg/m^3)

FIGURE G-11. HYPOTHETICAL COPPER SMELTER ISOPLETHS FOR 1700-2000 MST ON 9 JULY 1975 ASSUMING 0.5 PERCENT PER HOUR SULFATE FORMATION

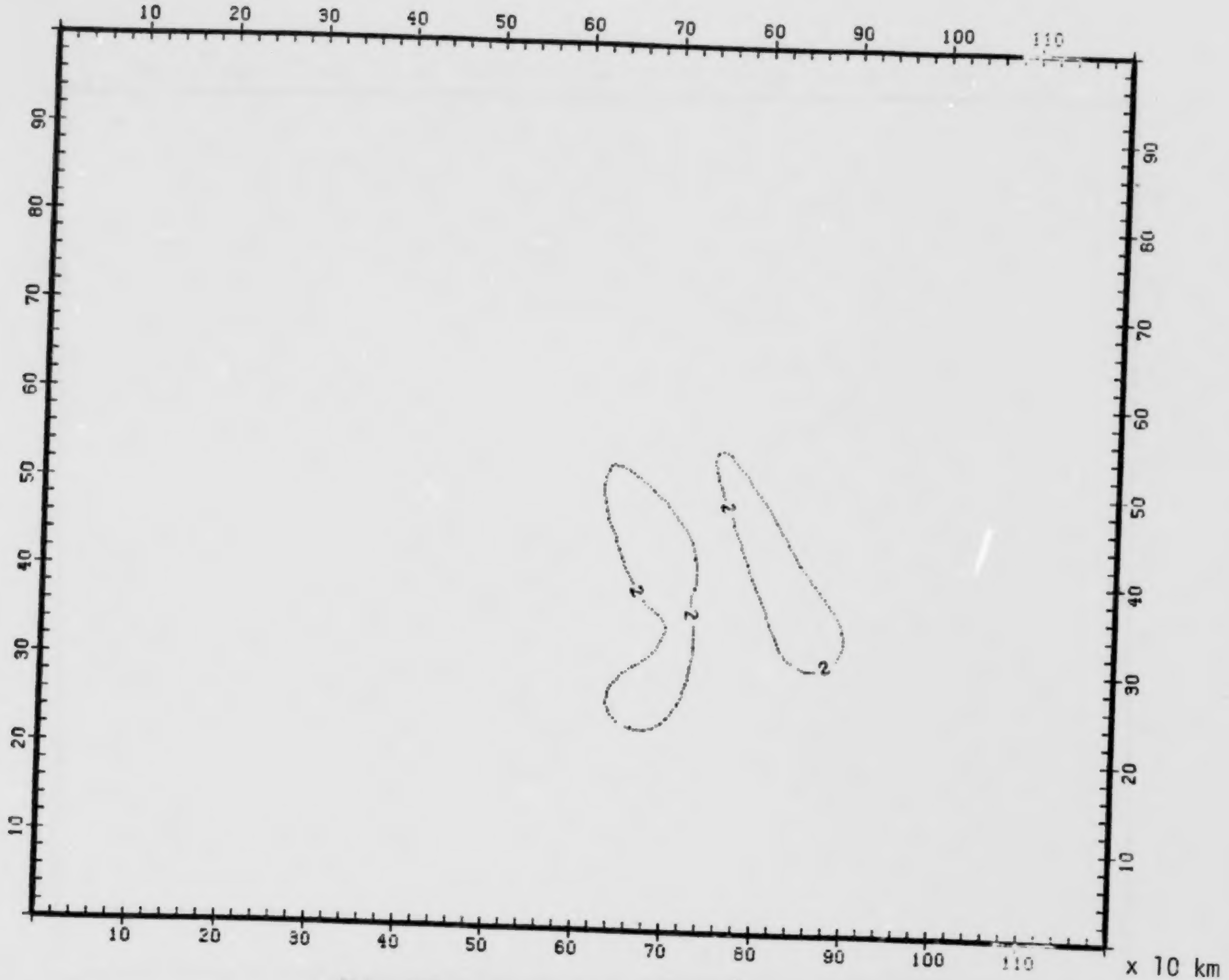
10
20
30
40
50
60
70
80
90
100
110
2
x 10 km

(b) $SO_4^=$ Concentrations ($\mu g/m^3$)

FIGURE G-11 (Continued)

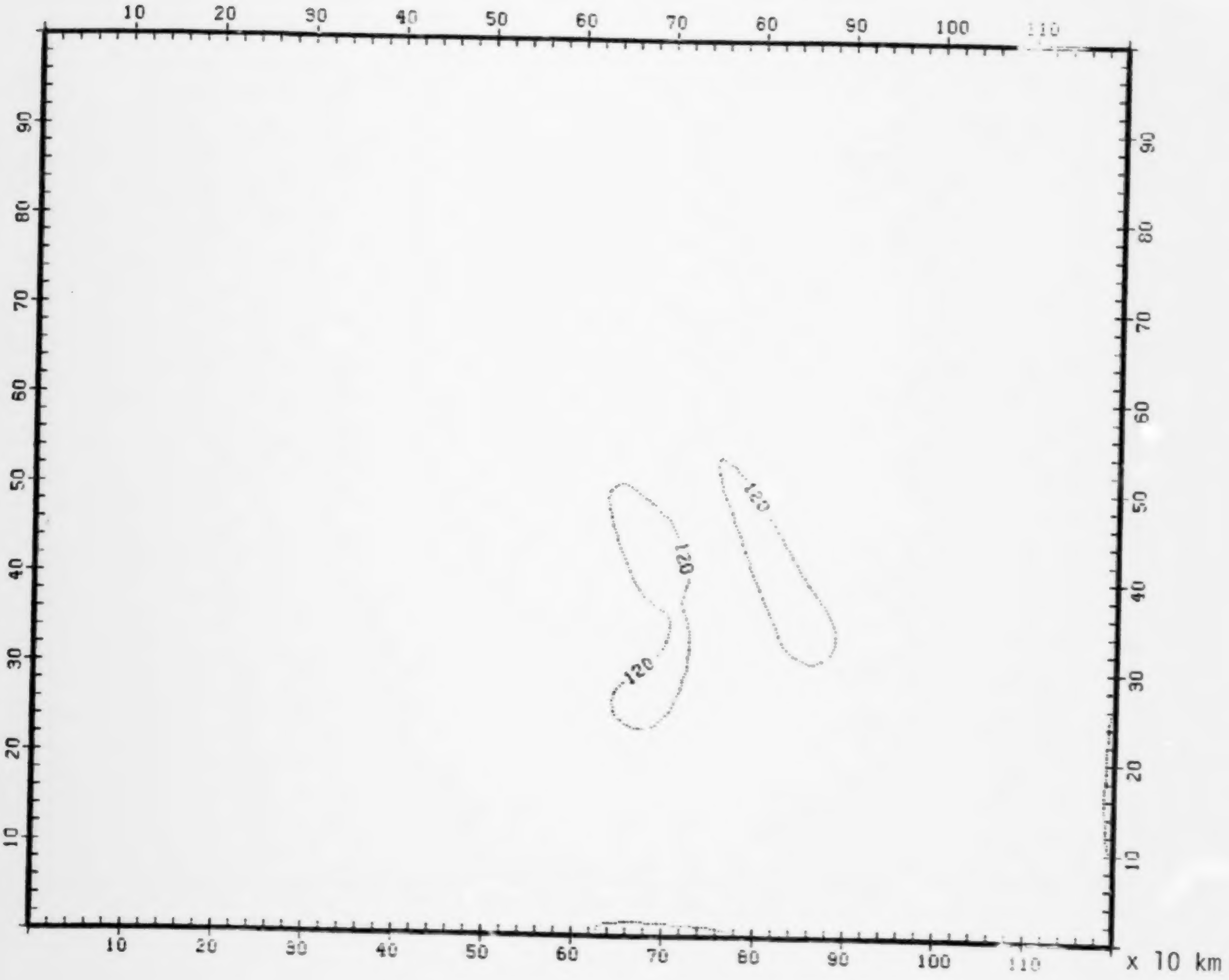
10
20
30
40
50
60
70
80
90
100
110
120
120
120
x 10 km

(c) Visual Range (km)

FIGURE G-11 (Concluded)

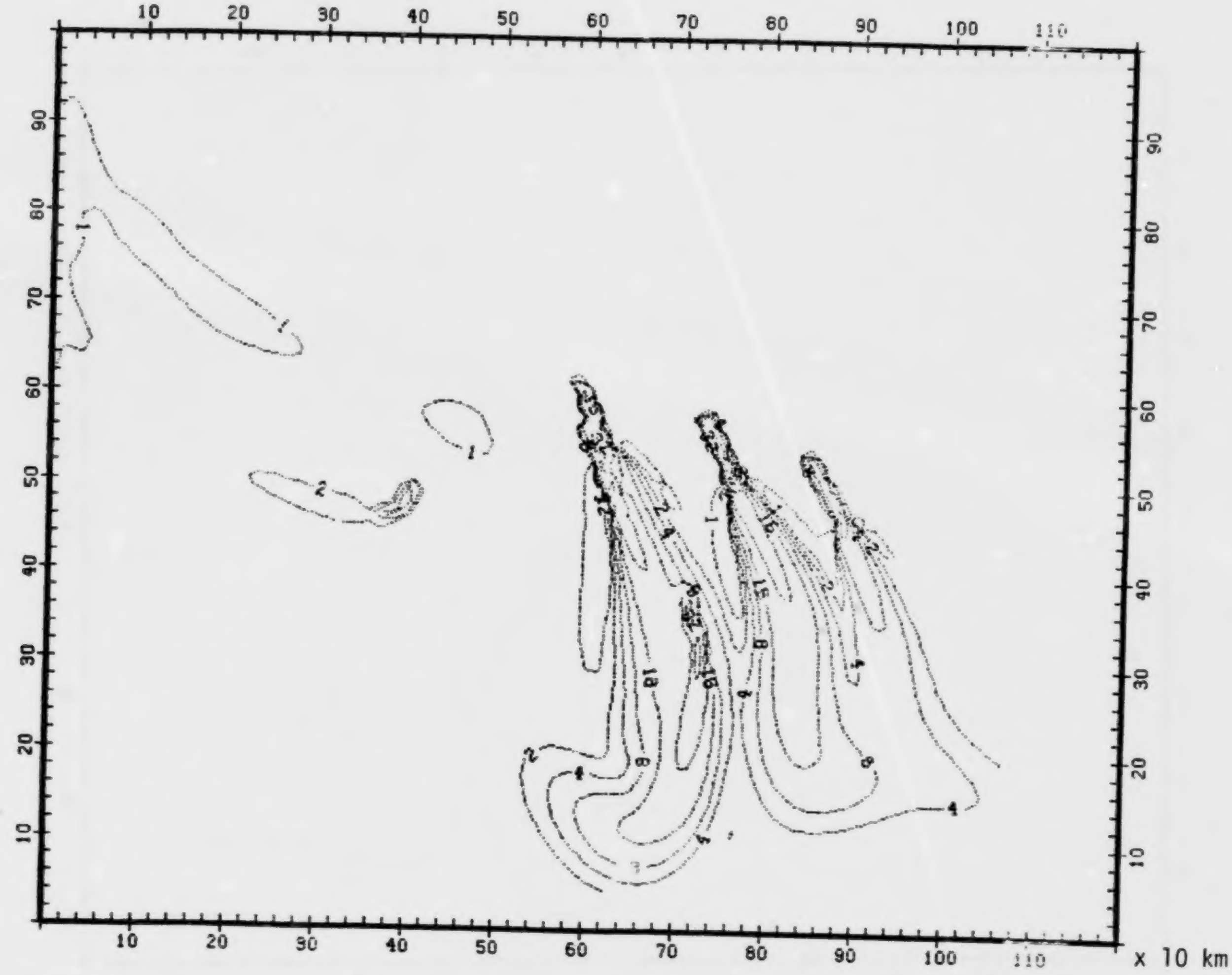
10
20
30
40
50
60
70
80
90
100
110
x 10 km
1
2
4
8
16

(a) SO_2 Concentrations ($\mu g/m^3$)

FIGURE G-12. HYPOTHETICAL COPPER SMELTER ISOPLETHS FOR 200-500 MST ON 10 JULY 1975 ASSUMING 0.5 PERCENT PER HOUR SULFATE FORMATION

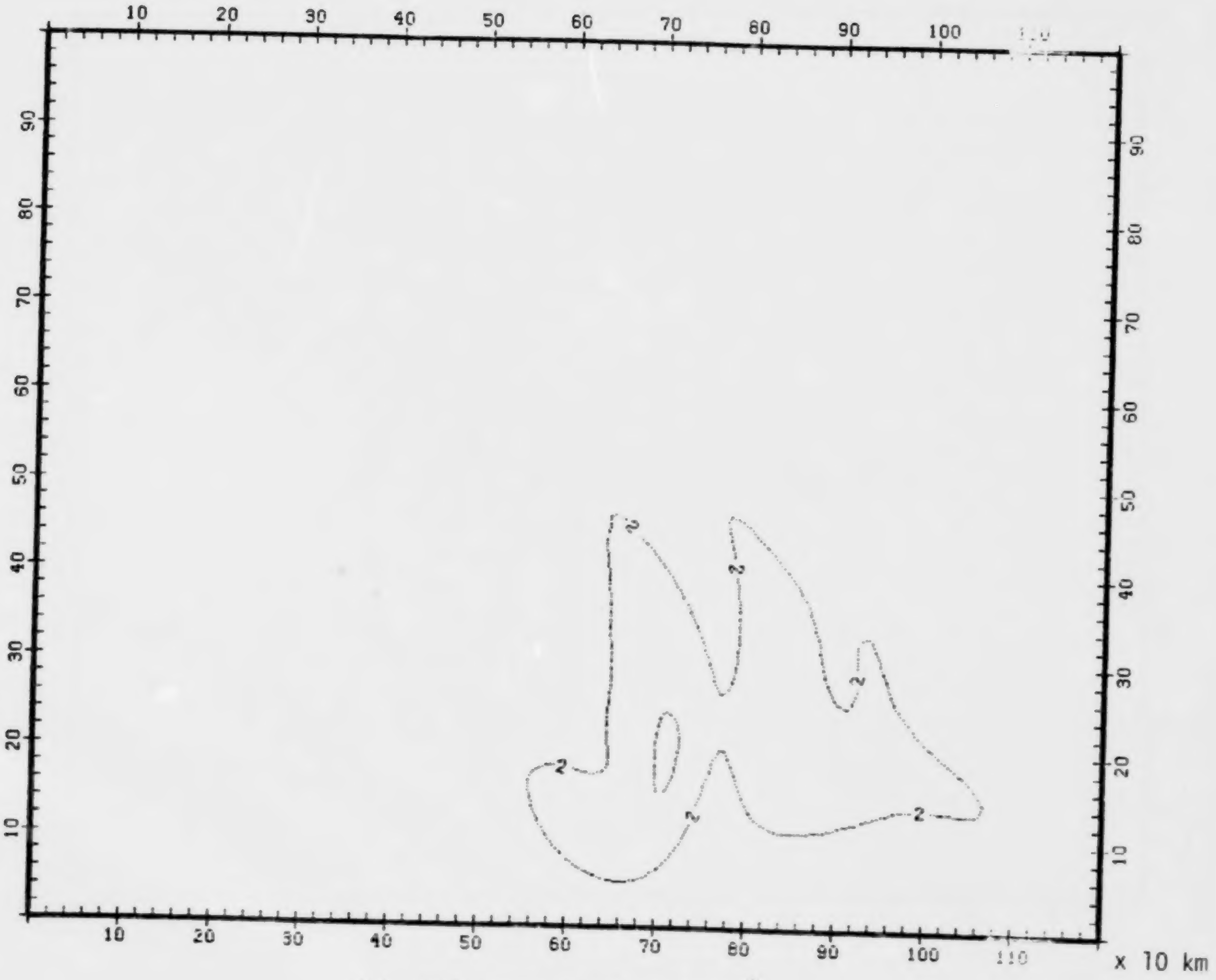
10
20
30
40
50
60
70
80
90
100
110
2
x 10 km

(b) $SO_4^=$ Concentrations ($\mu g/m^3$)

FIGURE G-12 (Continued)

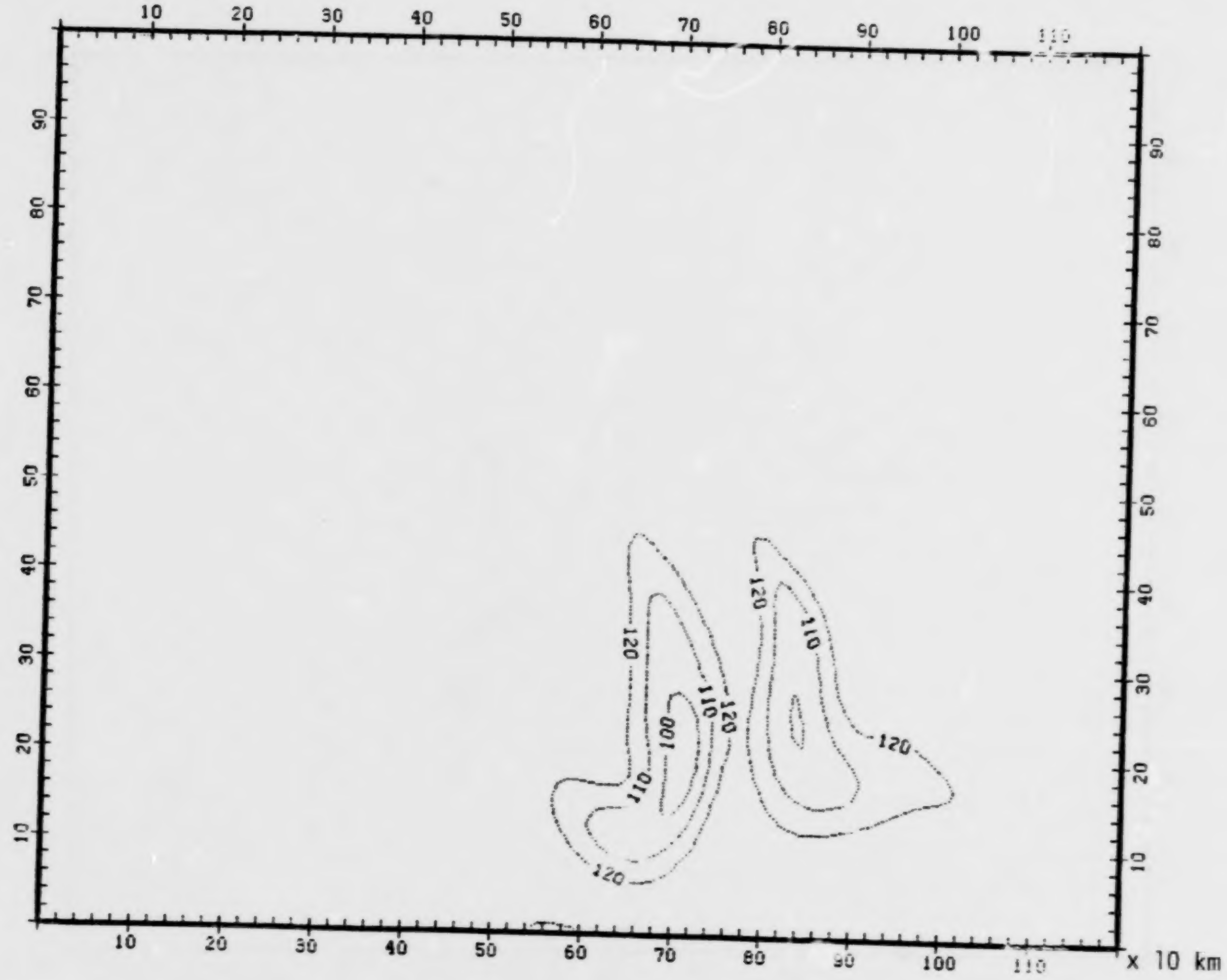

(c) Visual Range (km)

FIGURE G-12 (Concluded)

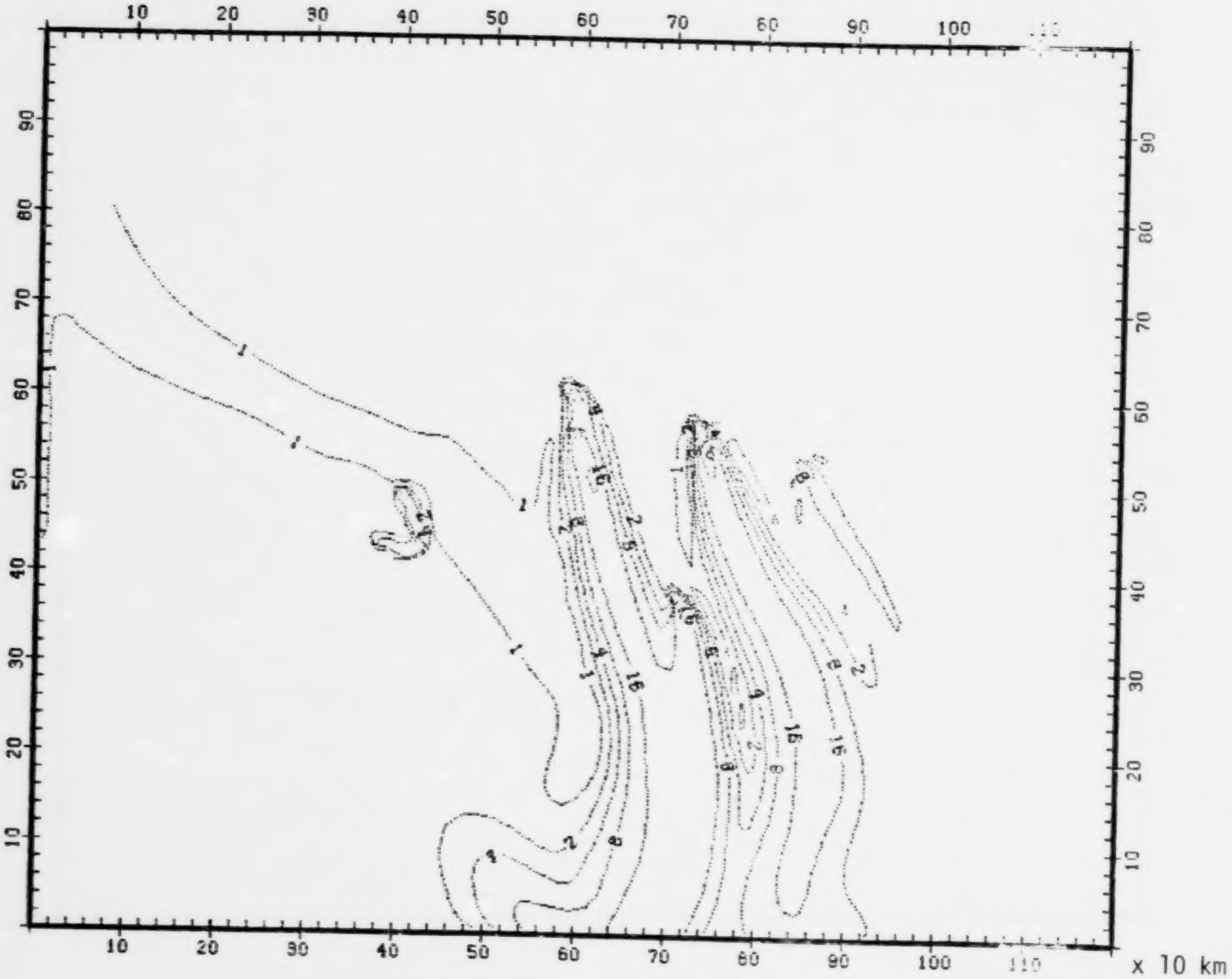

(a) SO_2 Concentrations ($\mu g/m^3$)

FIGURE G-13. HYPOTHETICAL COPPER SMELTER ISOPLETHS FOR 1100-1400 MST ON 10 JULY 1975 ASSUMING 0.5 PERCENT PER HOUR SULFATE FORMATION

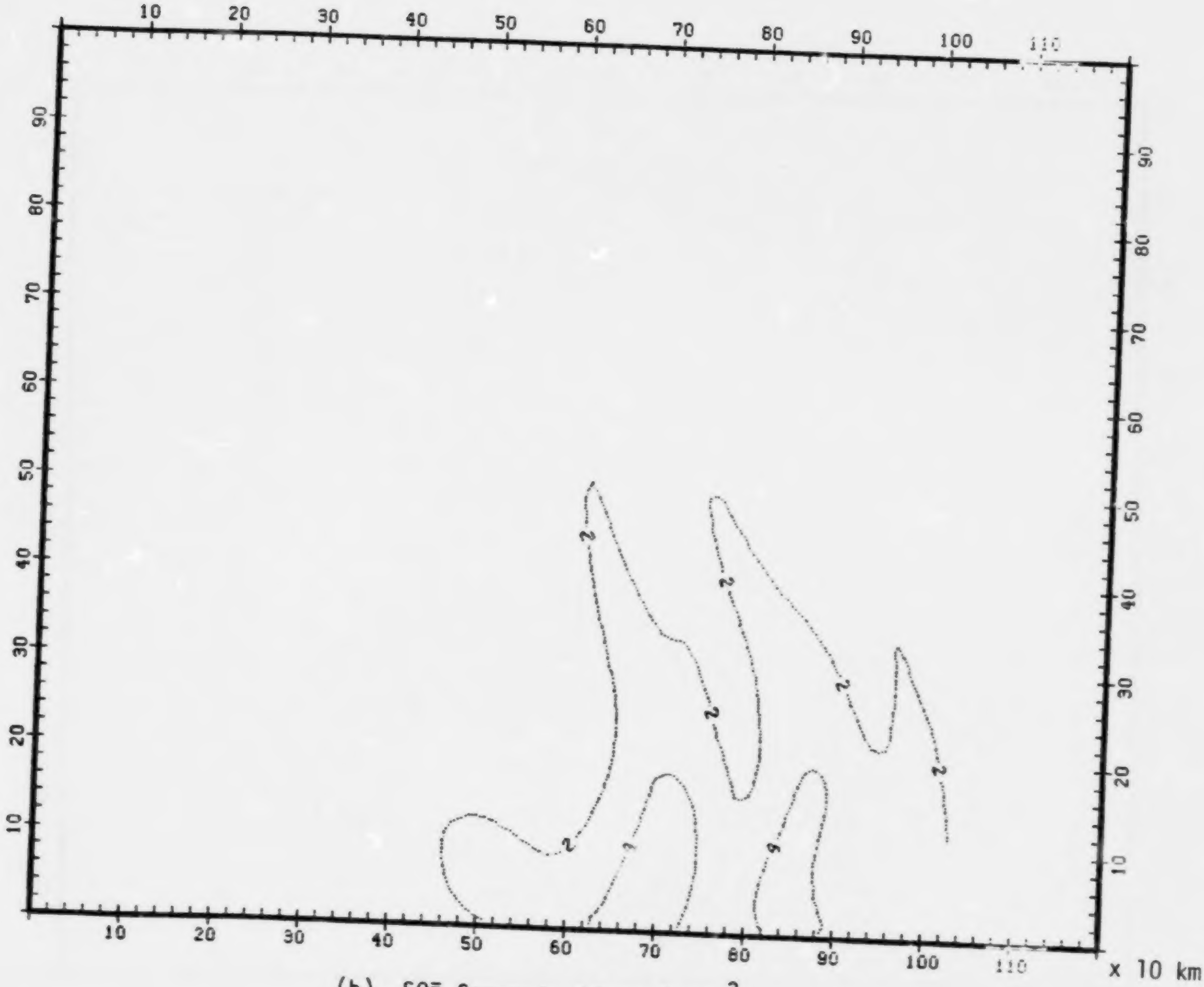
10
20
30
40
50
60
70
80
90
100
110
x 10 km
2
2
2
2
2
2
4
6

(b) $SO_4^=$ Concentrations (μg/m^3)

FIGURE G-13 (Continued)

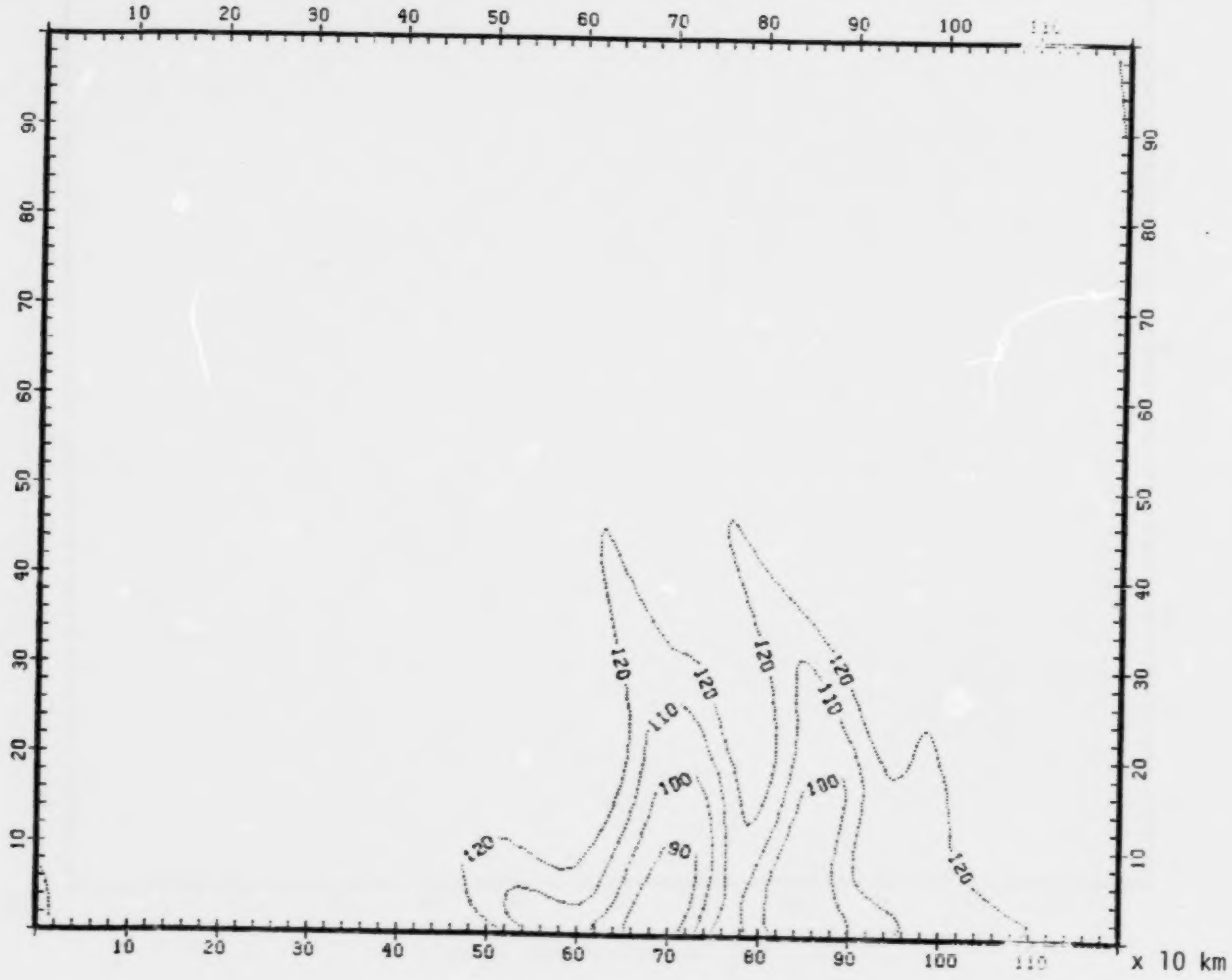

(c) Visual Range (km)

FIGURE G-13 (Concluded)

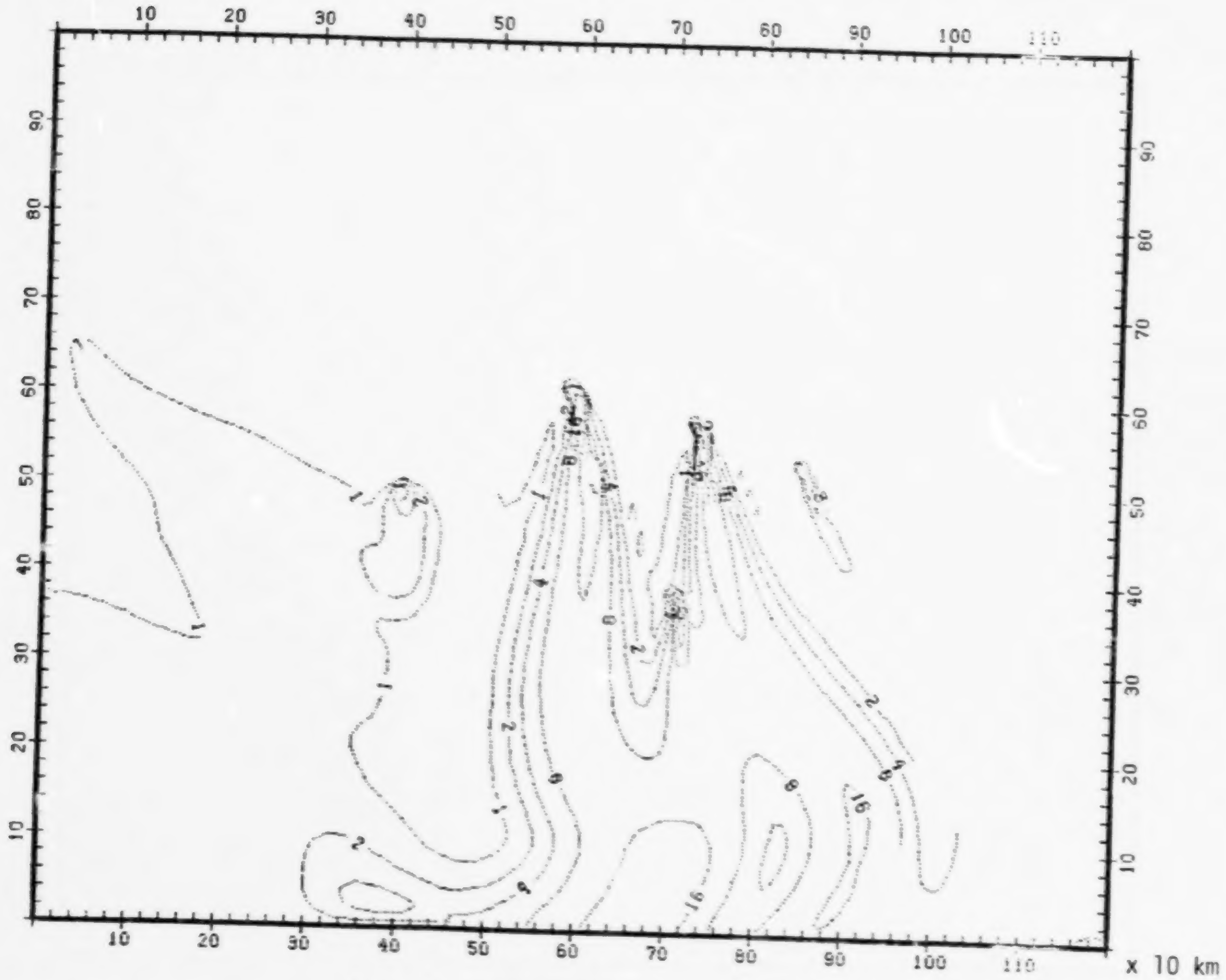
10
20
30
40
50
60
70
80
90
100
110
x 10 km
1
2
4
8
16

(a) SO_2 Concentrations ($\mu g/m^3$)

FIGURE G-14. HYPOTHETICAL COPPER SMELTER ISOPLETHS FOR 2000-2300 MST ON 10 JULY 1975 ASSUMING 0.5 PERCENT PER HOUR SULFATE FORMATION

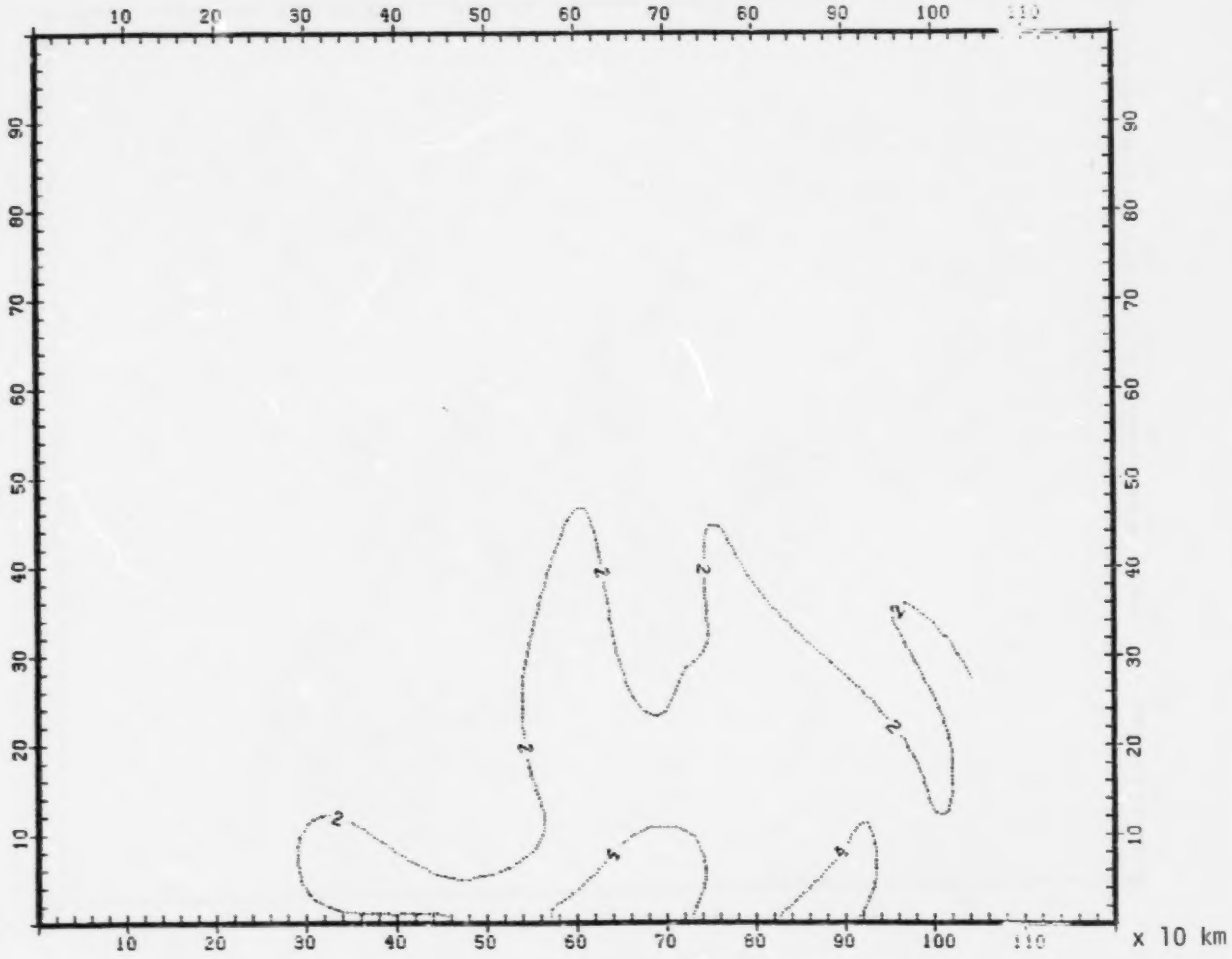
10
20
30
40
50
60
70
80
90
100
110
2
4
x 10 km

(b) $SO_4^=$ Concentrations ($\mu g/m^3$)

FIGURE G-14 (Continued)

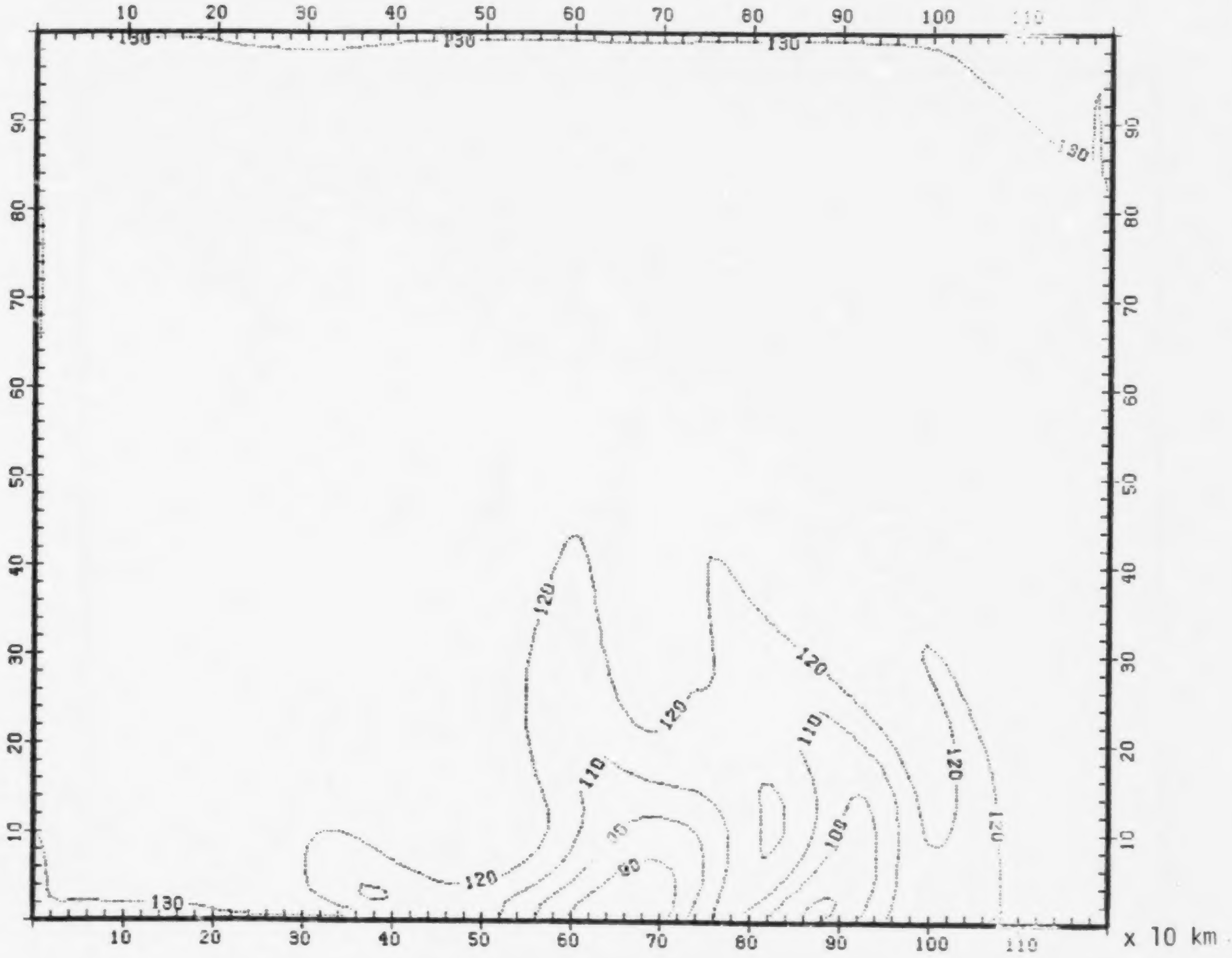

(c) Visual Range (km)

FIGURE G-14 (Concluded)

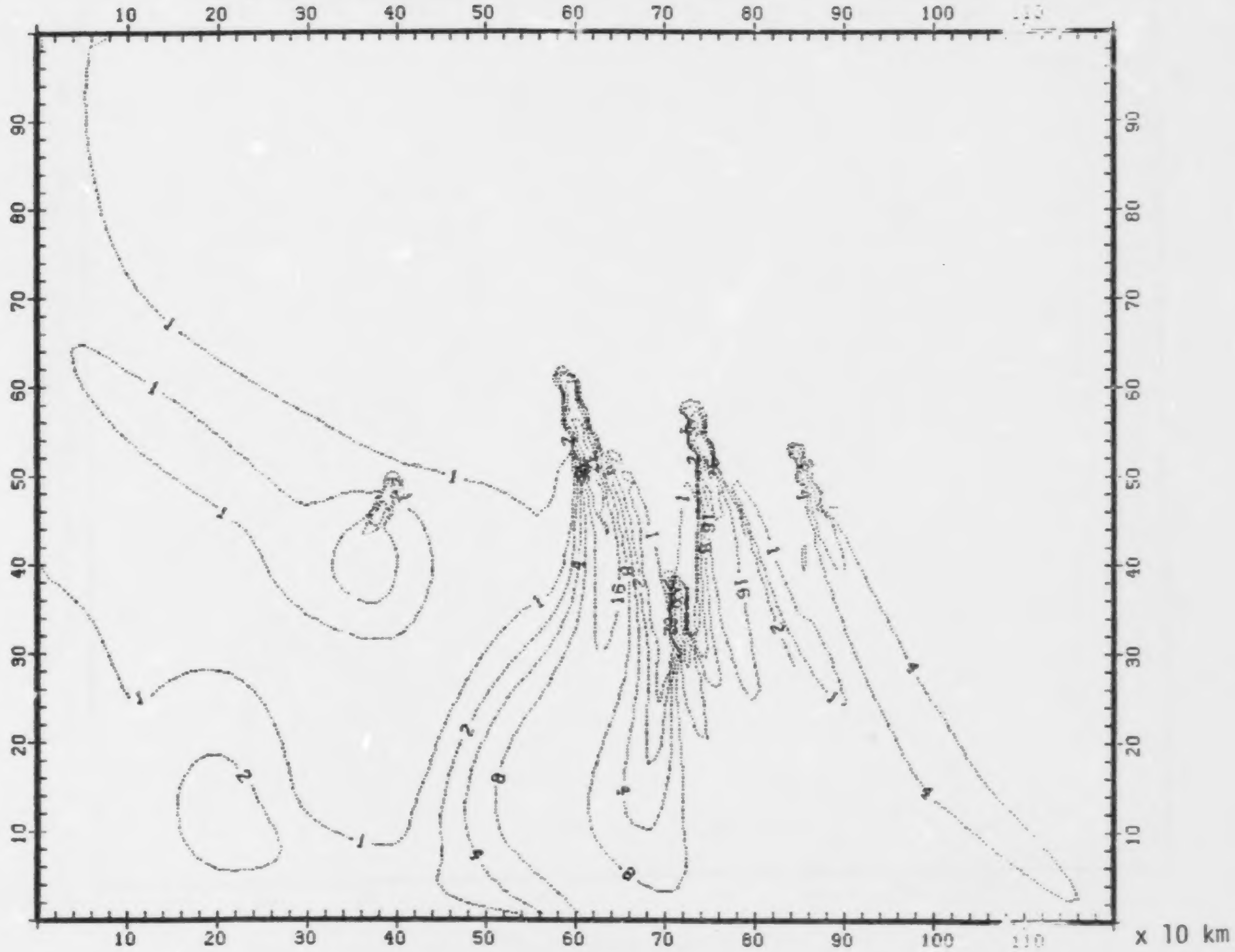
10
20
30
40
50
60
70
80
90
100
110
x 10 km
1
2
4
8
16

(a) SO_2 Concentrations ($\mu g/m^3$)

FIGURE G-15. HYPOTHETICAL COPPER SMELTER ISOPLETHS FOR 500-800 MST ON 10 JULY 1975 ASSUMING 0.5 PERCENT PER HOUR SULFATE FORMATION

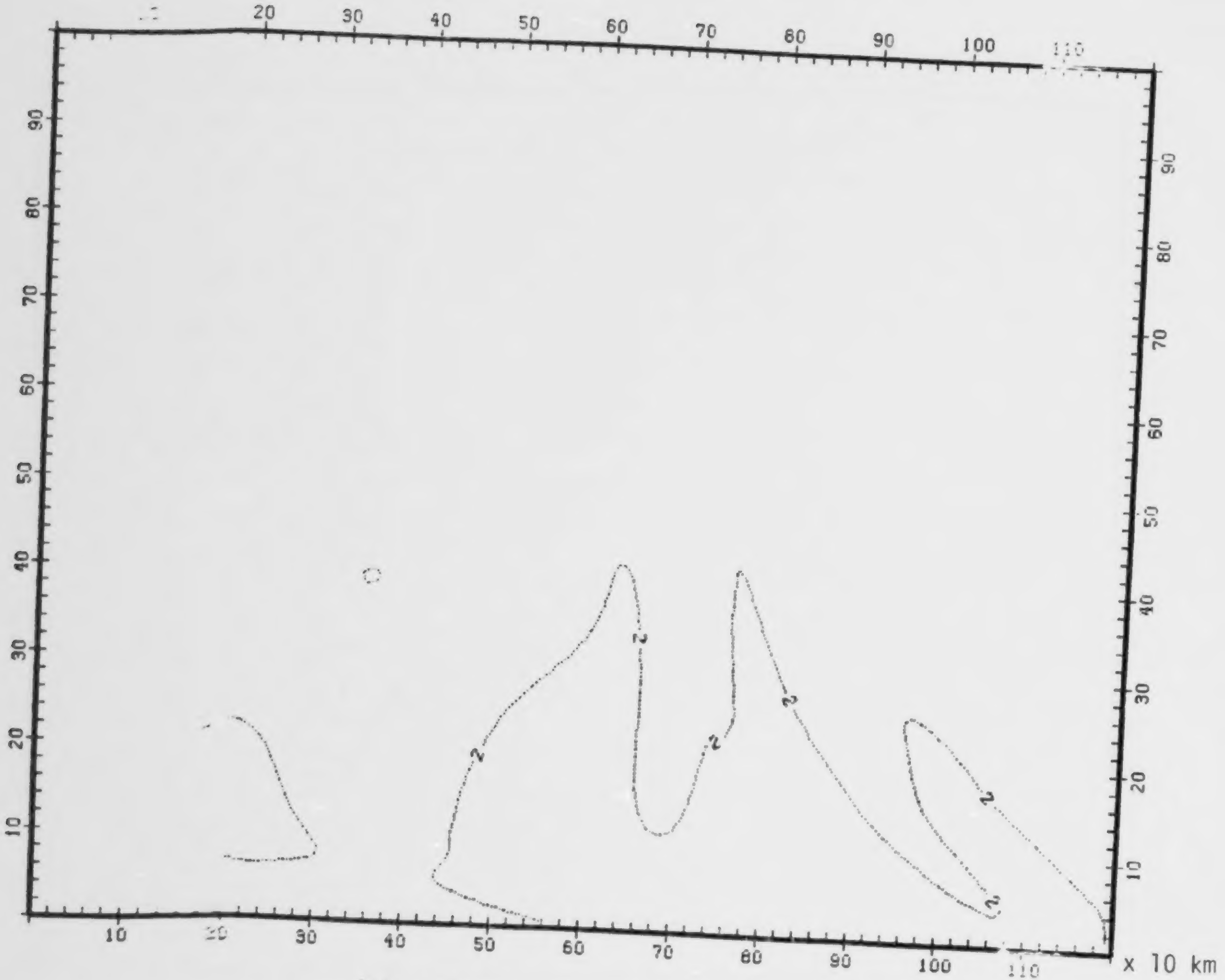
10
20
30
40
50
60
70
80
90
100
110
2
x 10 km

(b) $SO_4^=$ Concentrations ($\mu g/m^3$)

FIGURE G-15 (Continued)

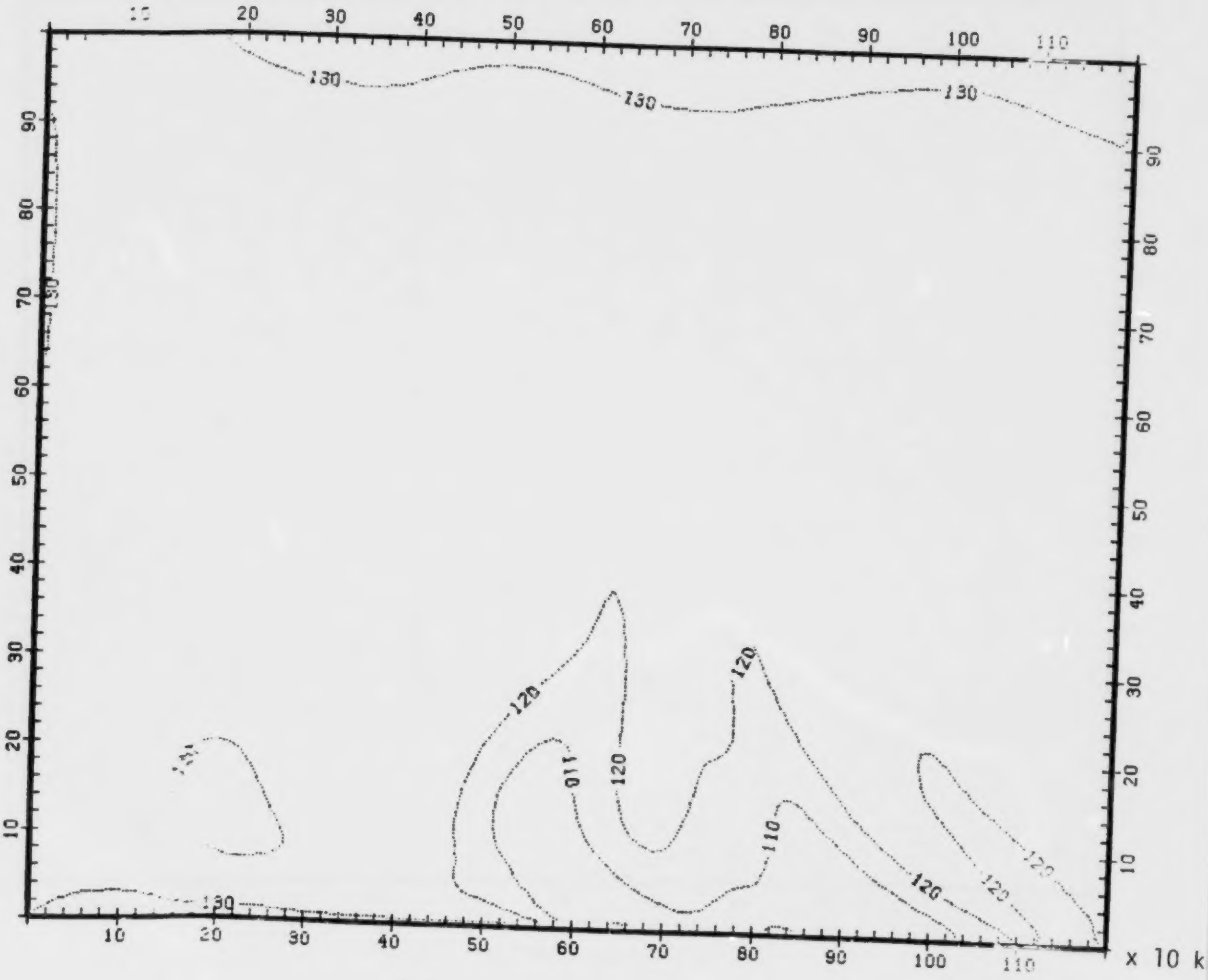

(c) Visual Range (km)

FIGURE G-15 (Concluded)

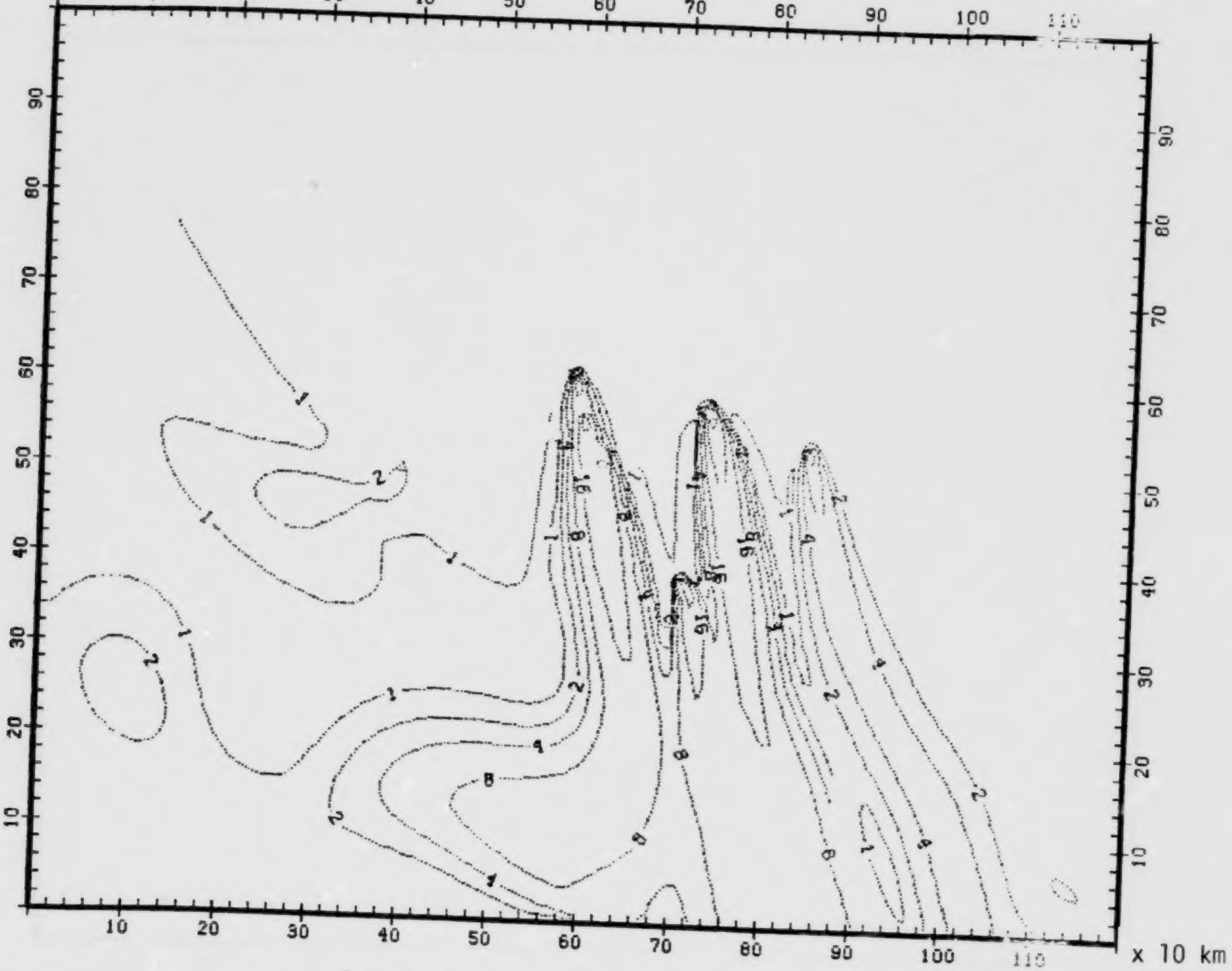
10
20
30
40
50
60
70
80
90
100
110
x 10 km
1
2
4
8
16

(a) SO_2 Concentrations ($\mu g/m^3$)

FIGURE G-16. HYPOTHETICAL COPPER SMELTER ISOPLETHS FOR 1400-1700 MST ON 10 JULY 1975 ASSUMING 0.5 PERCENT PER HOUR SULFATE FORMATION

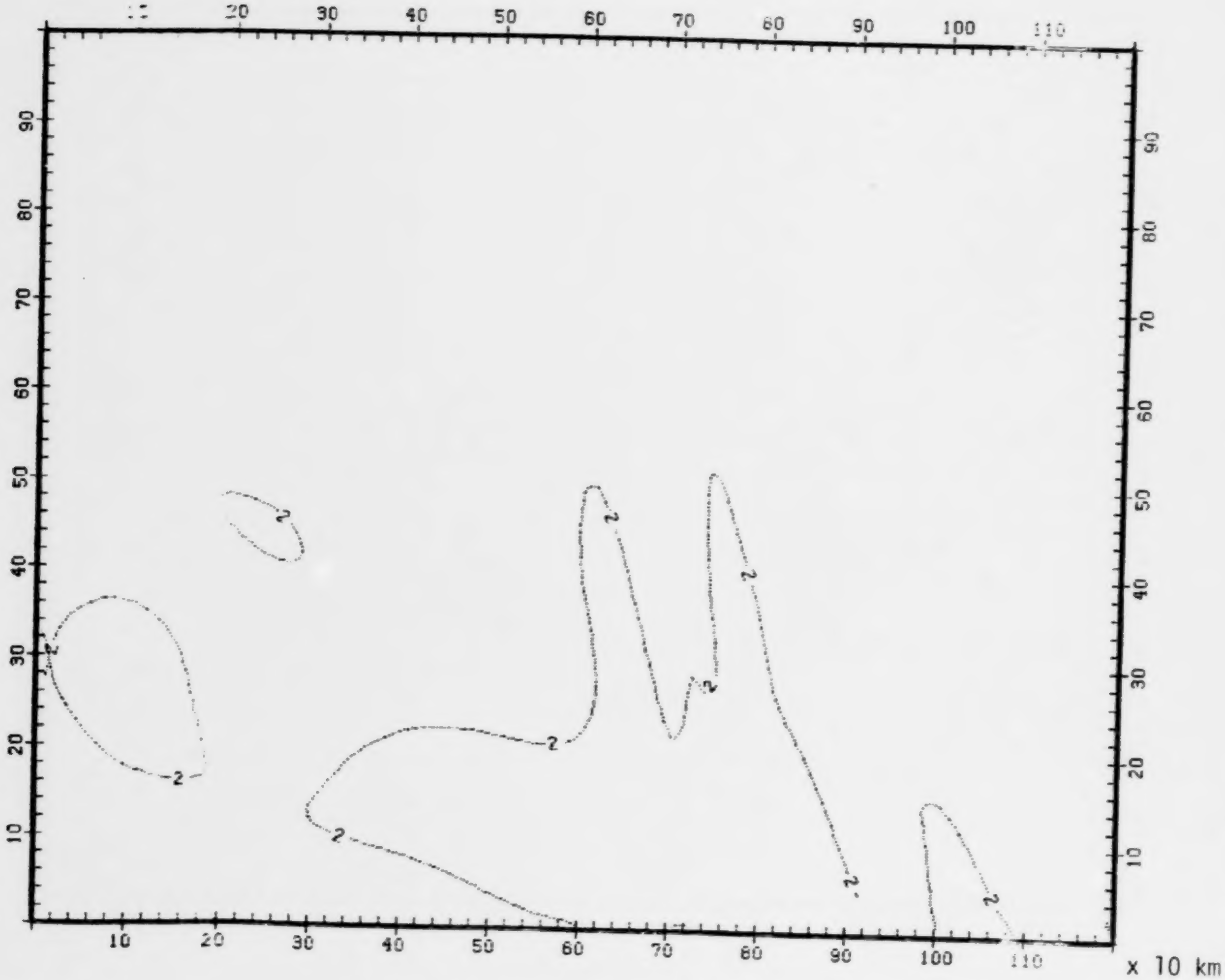
10
20
30
40
50
60
70
80
90
100
110
2
x 10 km

(b) $SO_4^=$ Concentrations ($\mu g/m^3$)

FIGURE G-16 (Continued)

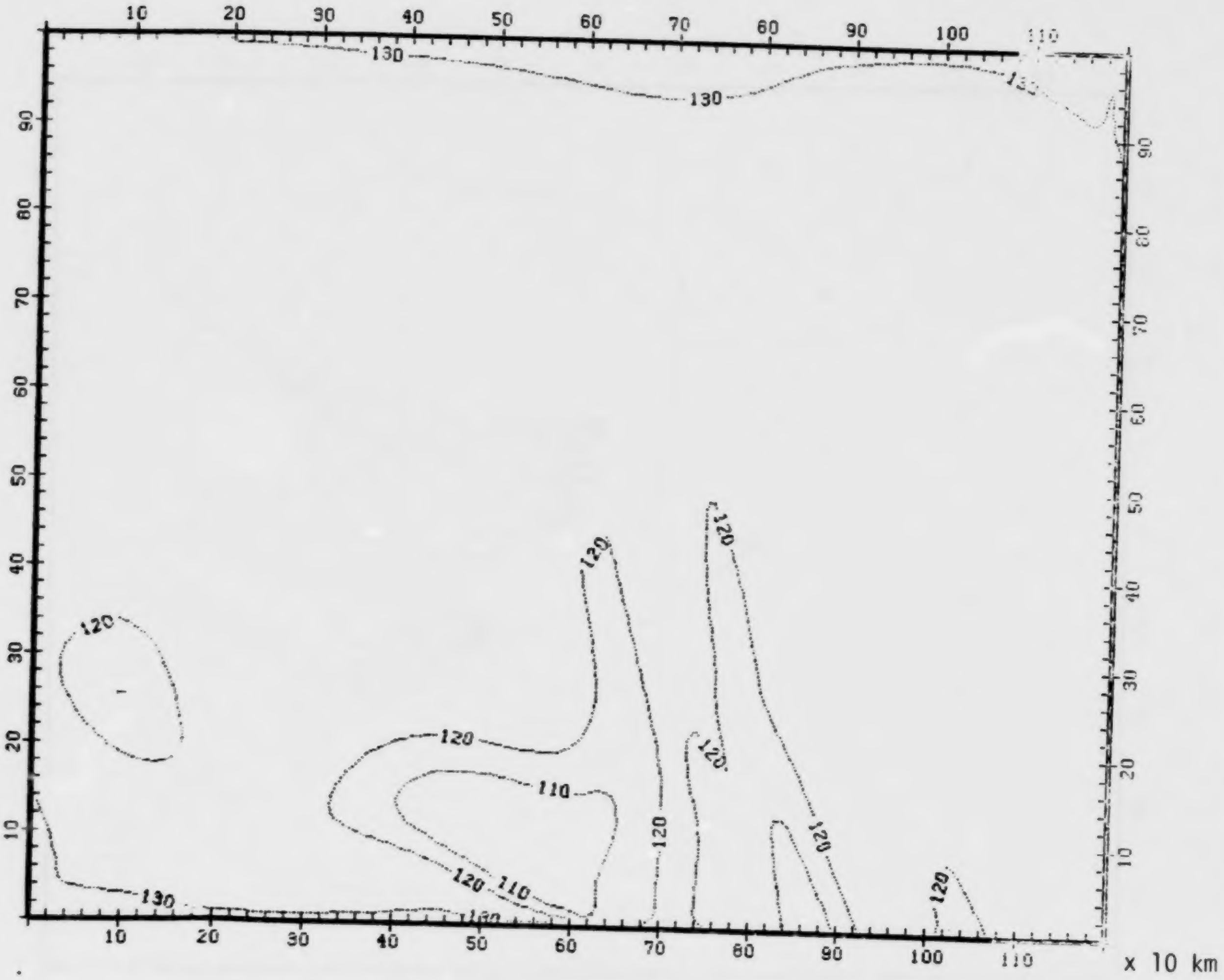

(c) Visual Range (km)

FIGURE G-16 (Concluded)

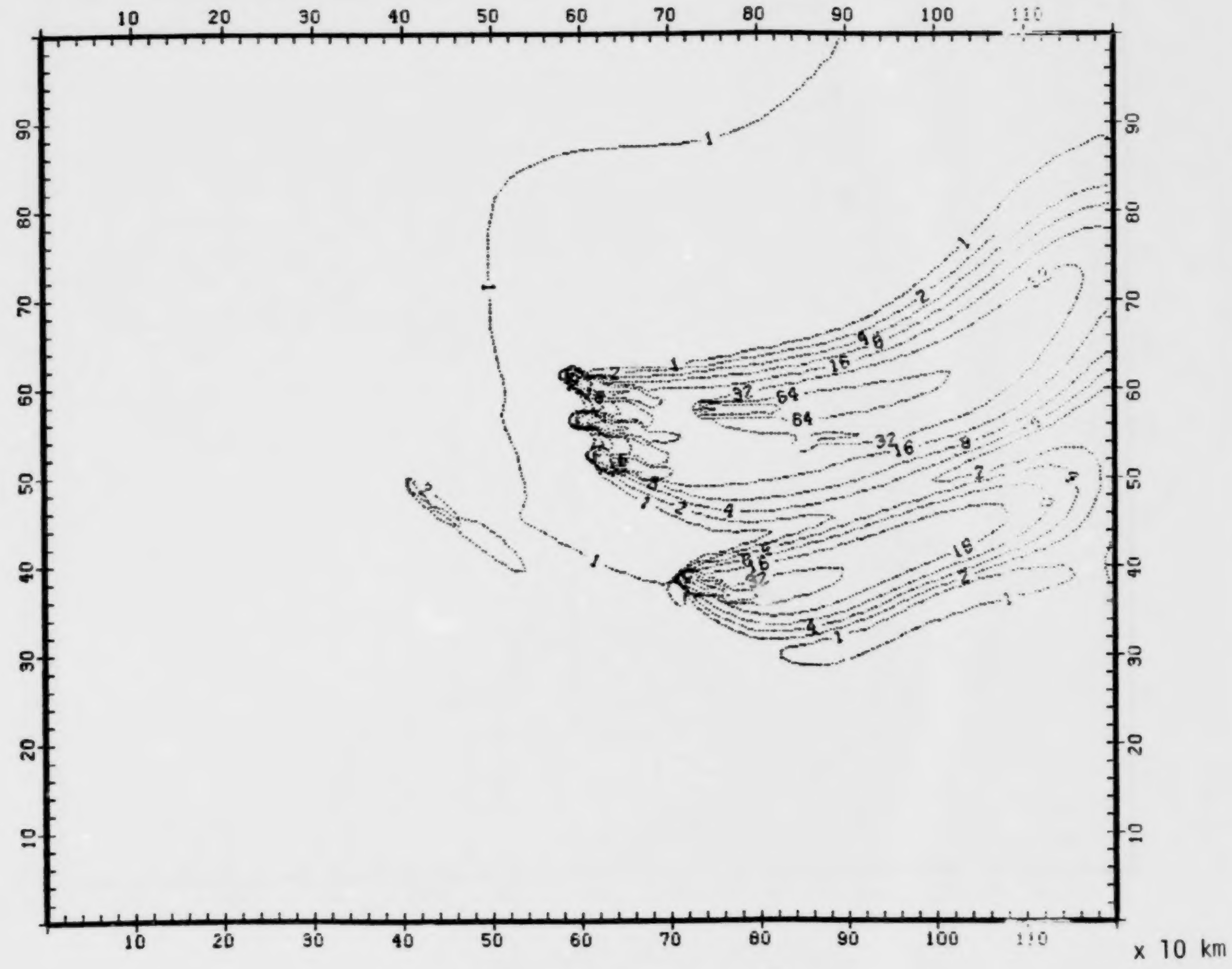

(a) SO_2 Concentrations ($\mu g/m^3$)

FIGURE G-17. HYPOTHETICAL COPPER SMELTER ISOPLETHS FOR 1700-2000 MST ON 27 JANUARY 1976 ASSUMING 0.5 PERCENT PER HOUR SULFATE FORMATION

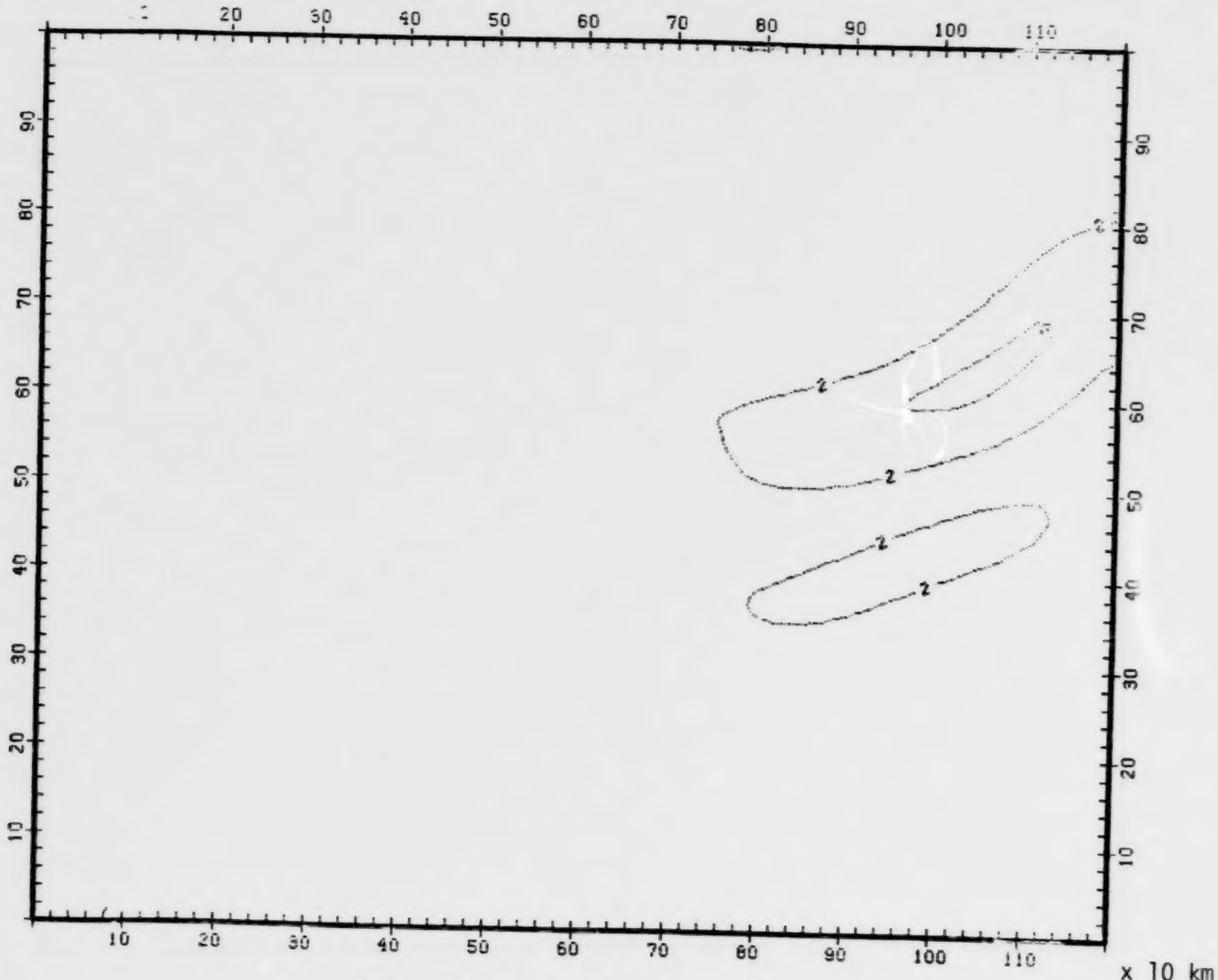

(b) $SO_4^=$ Concentrations ($\mu g/m^3$)

FIGURE G-17 (Continued)

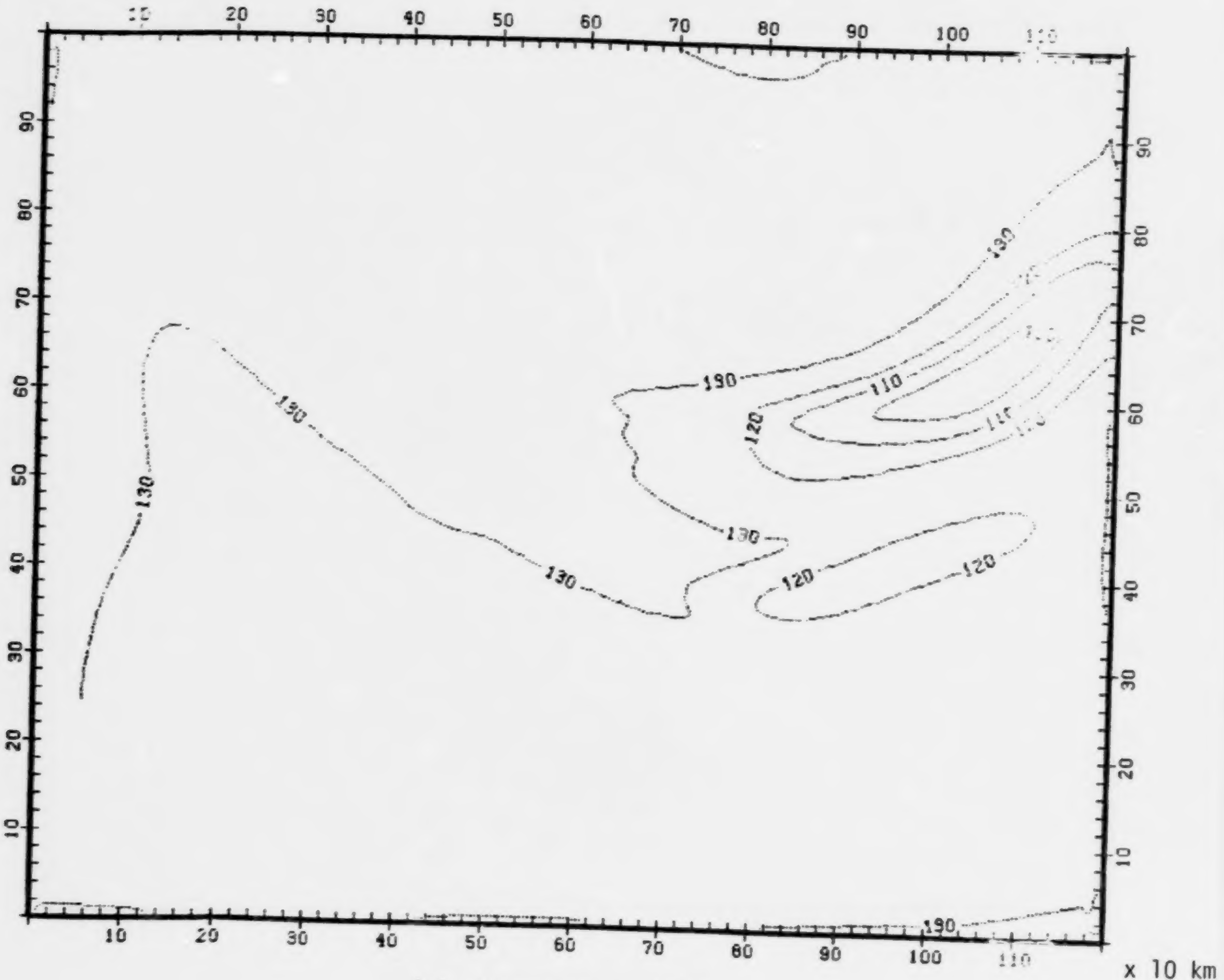

(c) Visual Range (km)

FIGURE G-17 (Concluded)

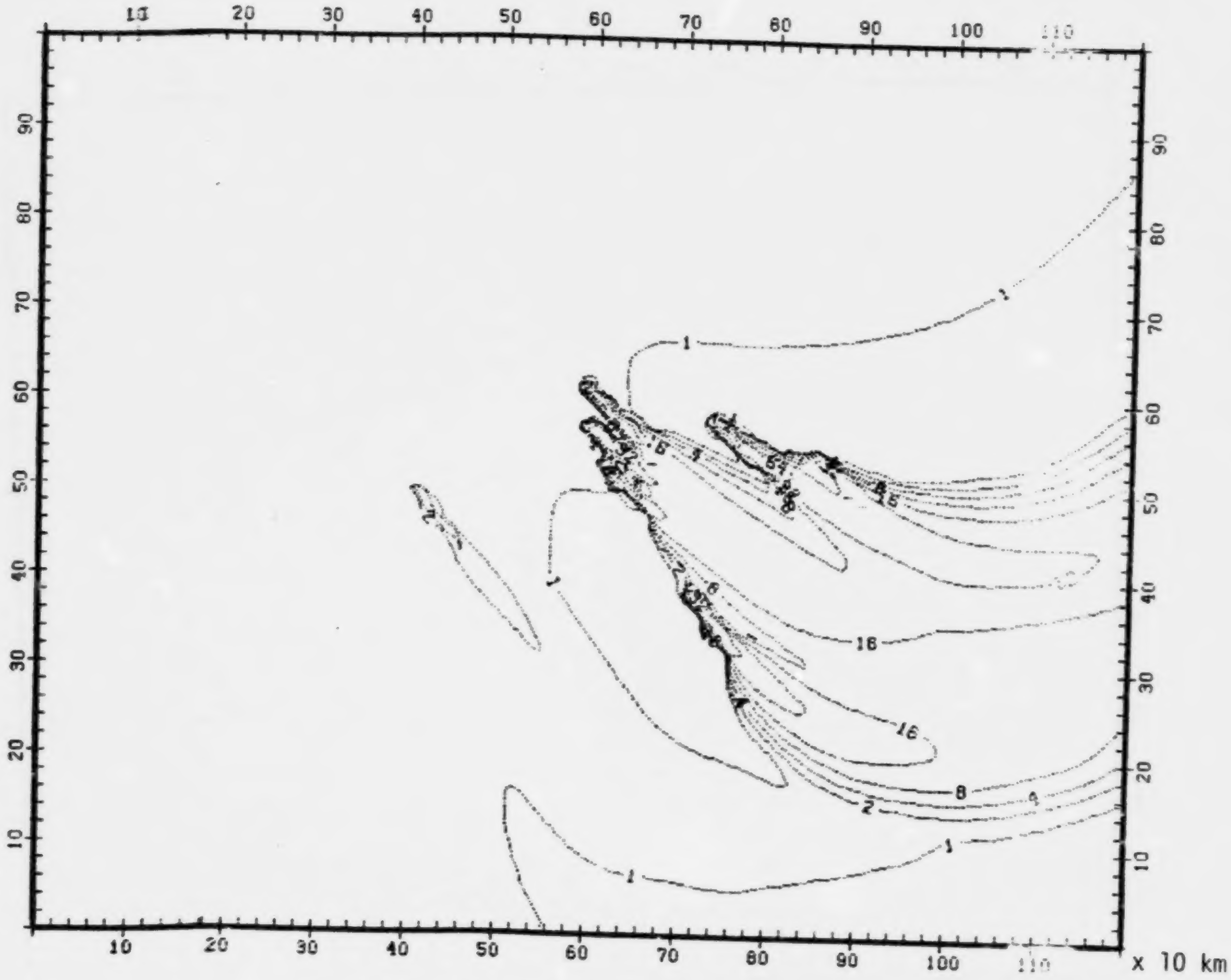
10
20
30
40
50
60
70
80
90
100
110
x 10 km
1
2
4
8
16

(a) SO_2 Concentrations ($\mu g/m^3$)

FIGURE G-18. HYPOTHETICAL COPPER SMELTER ISOPLETHS FOR 200-500 MST ON 28 JANUARY 1976 ASSUMING 0.5 PERCENT PER HOUR SULFATE FORMATION

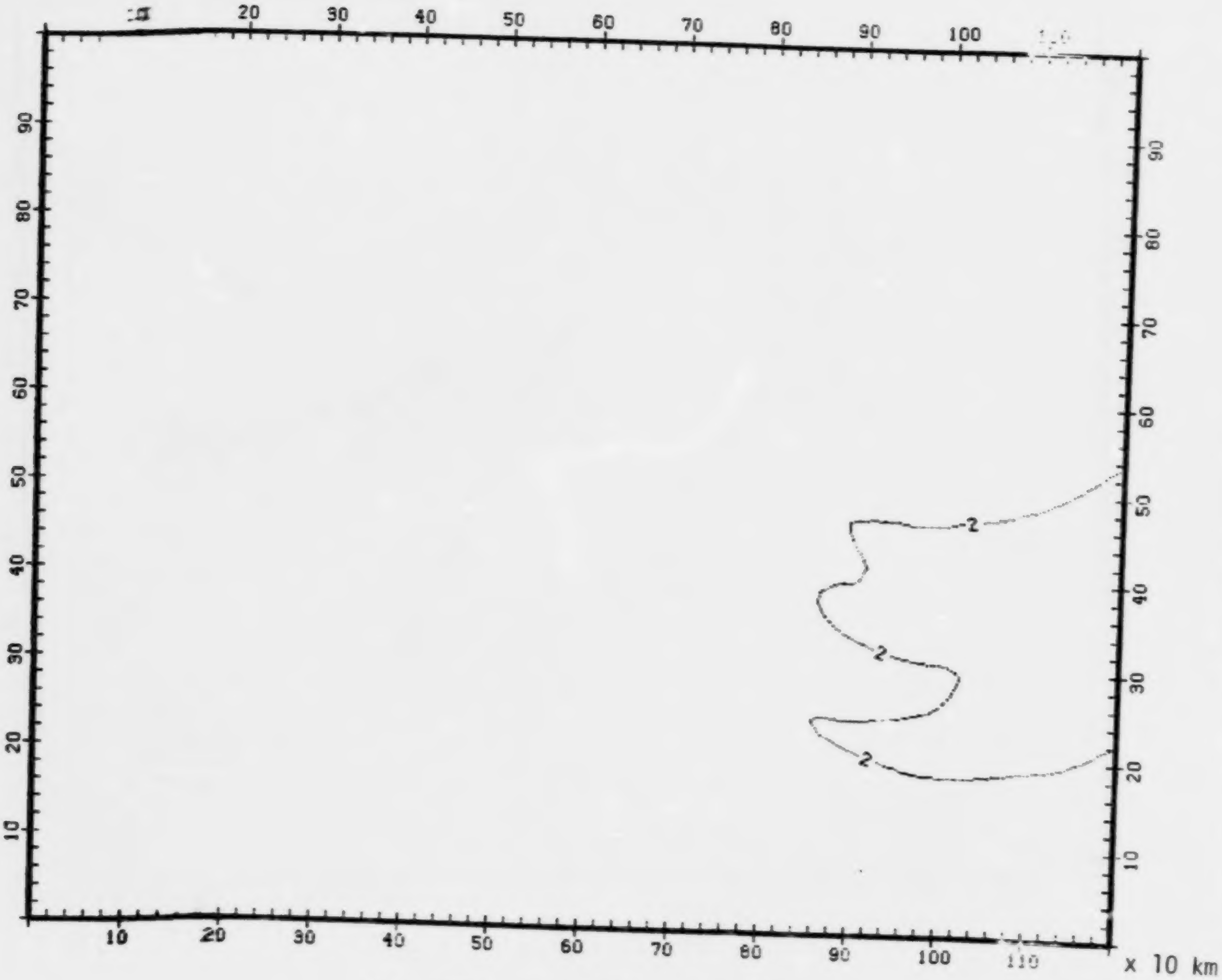
10
20
30
40
50
60
70
80
90
100
110
2
x 10 km

(b) $SO_4^=$ Concentrations ($\mu g/m^3$)

FIGURE G-18 (Continued)

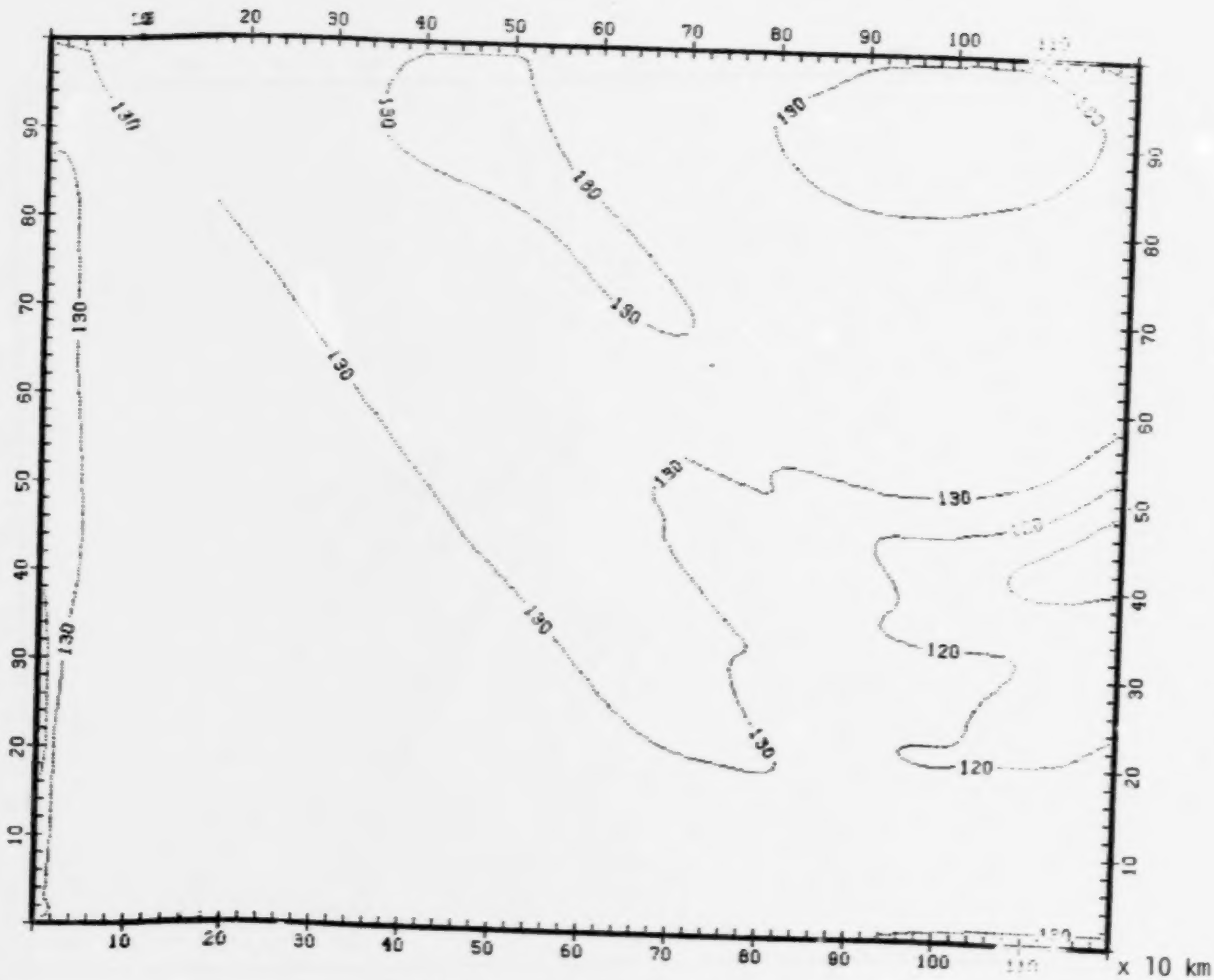

(c) Visual Range (km)

FIGURE G-18 (Concluded)

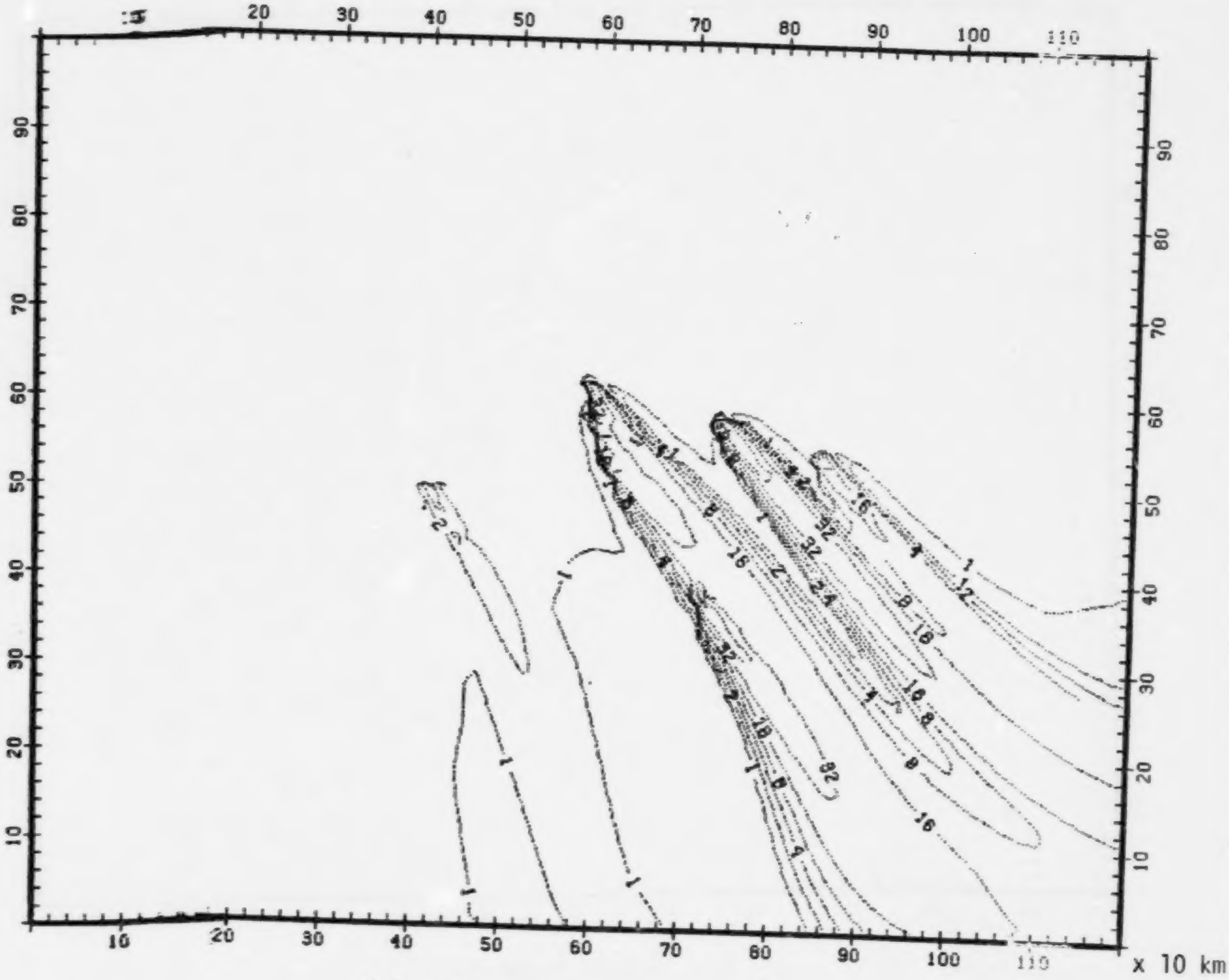
10
20
30
40
50
60
70
80
90
100
110
x 10 km
1
2
4
8
16
32

(a) SO_2 Concentrations ($\mu g/m^3$)

FIGURE 5-19. HYPOTHETICAL COPPER SMELTER ISOPLETHS FOR 1100-1400 MST ON 28 JANUARY 1976 ASSUMING 0.5 PERCENT PER HOUR SULFATE FORMATION

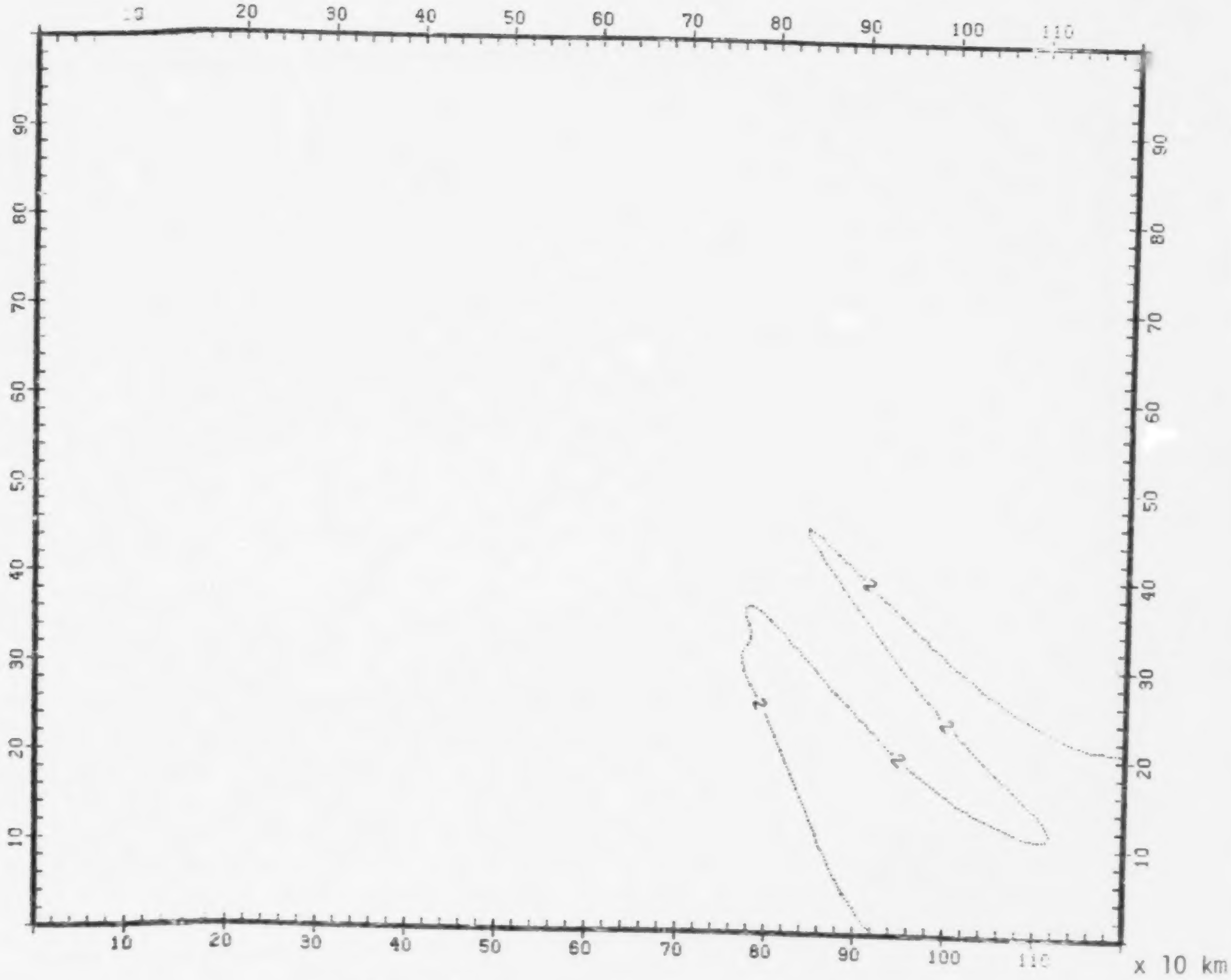
10
20
30
40
50
60
70
80
90
100
110
x 10 km
2
2
2
2

(b) $SO_4^=$ Concentrations ($\mu g/m^3$)

FIGURE G-19 (Continued)

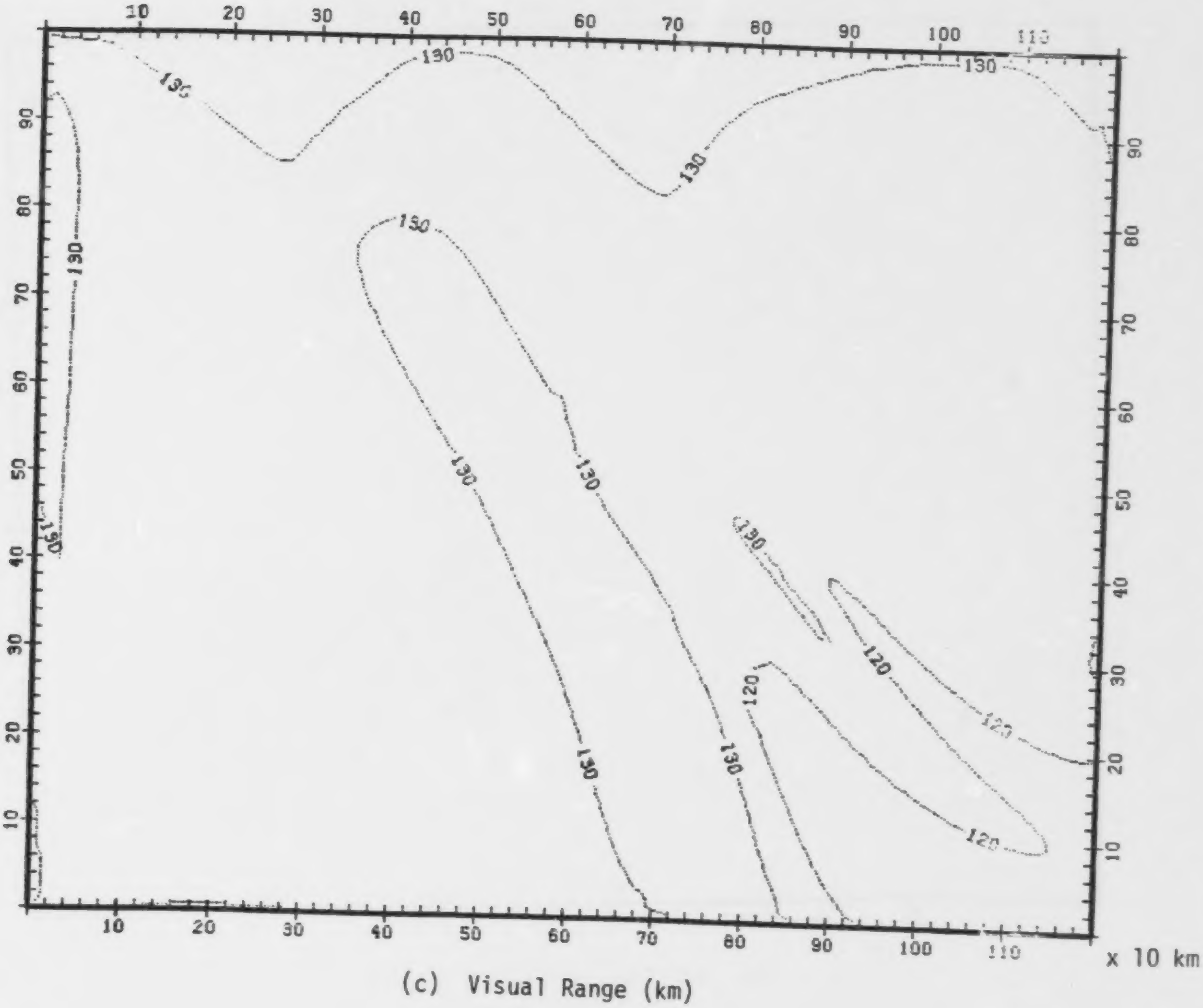

(c) Visual Range (km)

FIGURE G-19 (Concluded)

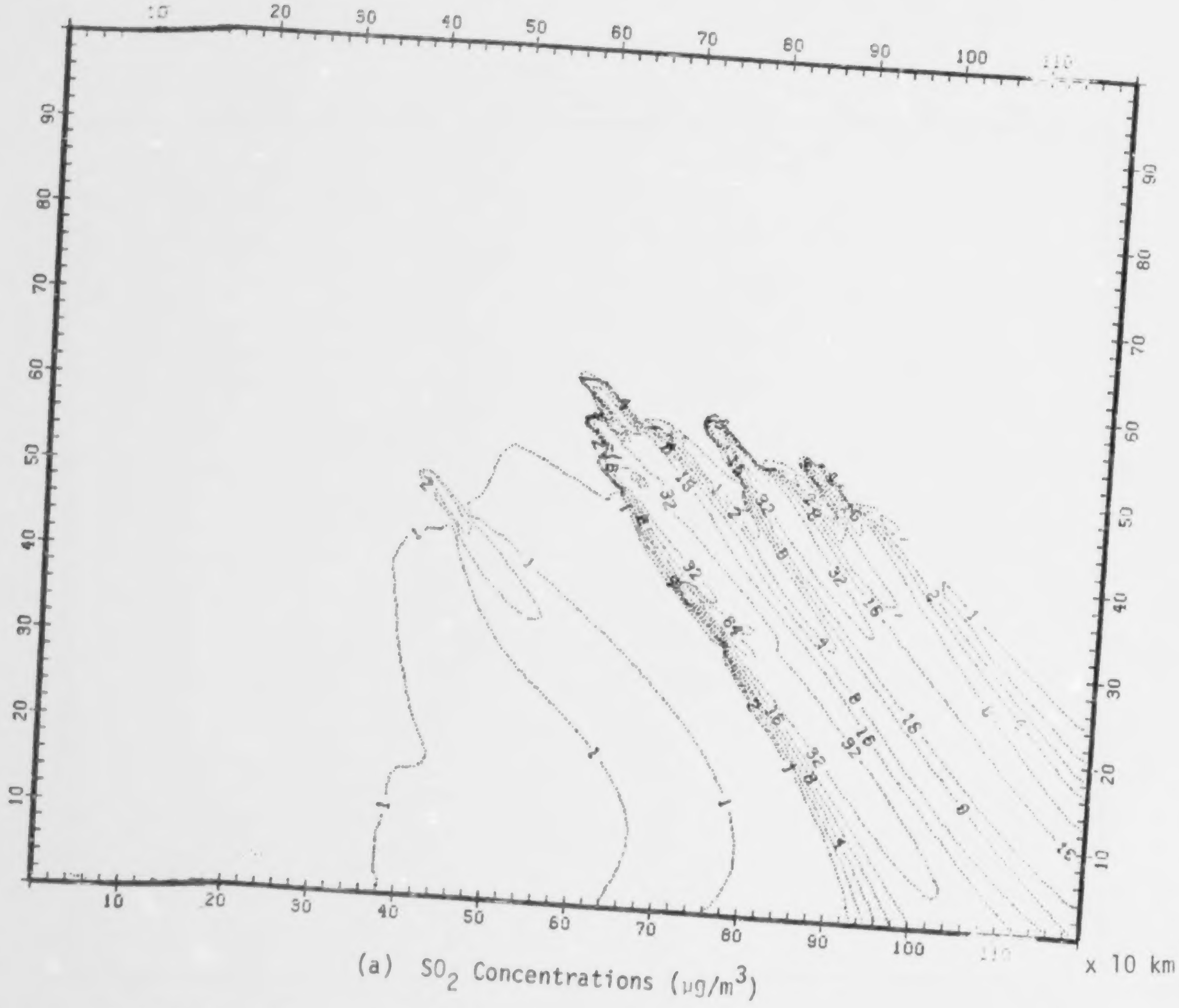
10
20
30
40
50
60
70
80
90
100
110
x 10 km
1
2
4
8
16
32
64

(a) SO$_2$ Concentrations ($\mu g/m^3$)

FIGURE B-20. HYPOTHETICAL COPPER SMELTER ISOPLETHS FOR 2000-2300 MST ON 28 JANUARY 1976 ASSUMING 0.5 PERCENT PER HOUR SULFATE FORMATION

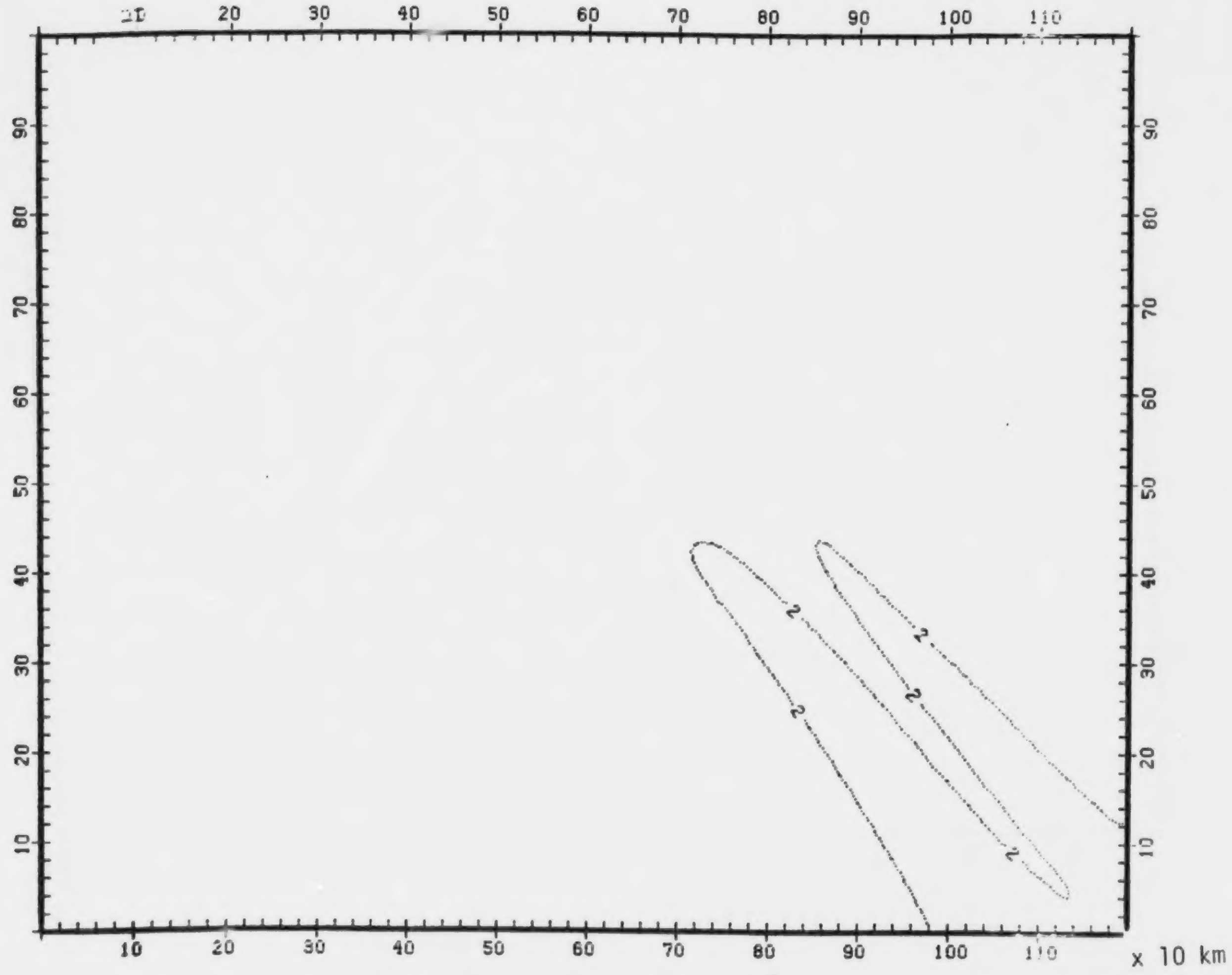
10
20
30
40
50
60
70
80
90
100
110
2
2
2
2
2
x 10 km

(b) $SO_4^=$ Concentrations ($\mu g/m^3$)

FIGURE G-20 (Continued)

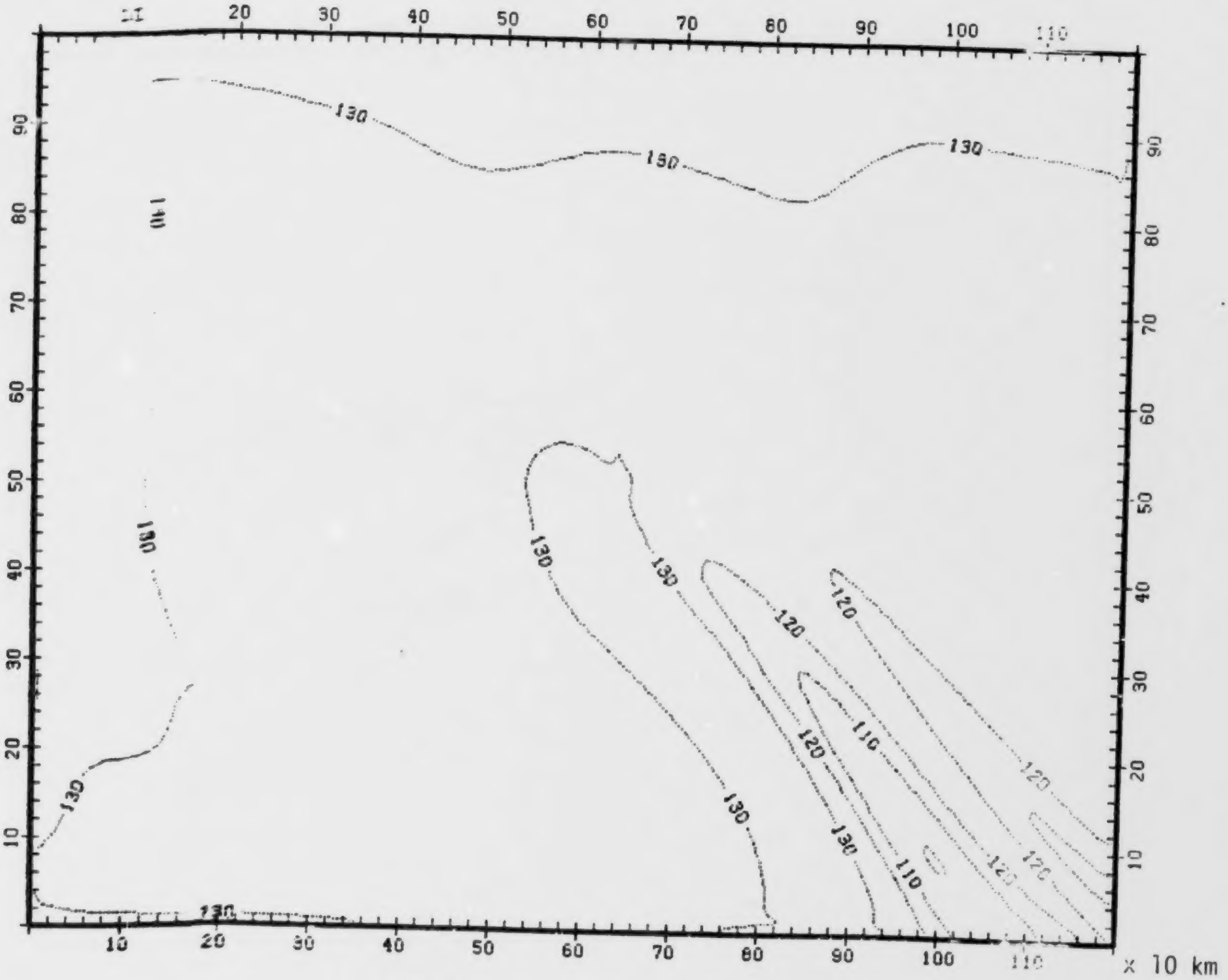

(c) Visual Range (km)

FIGURE G-20 (Concluded)

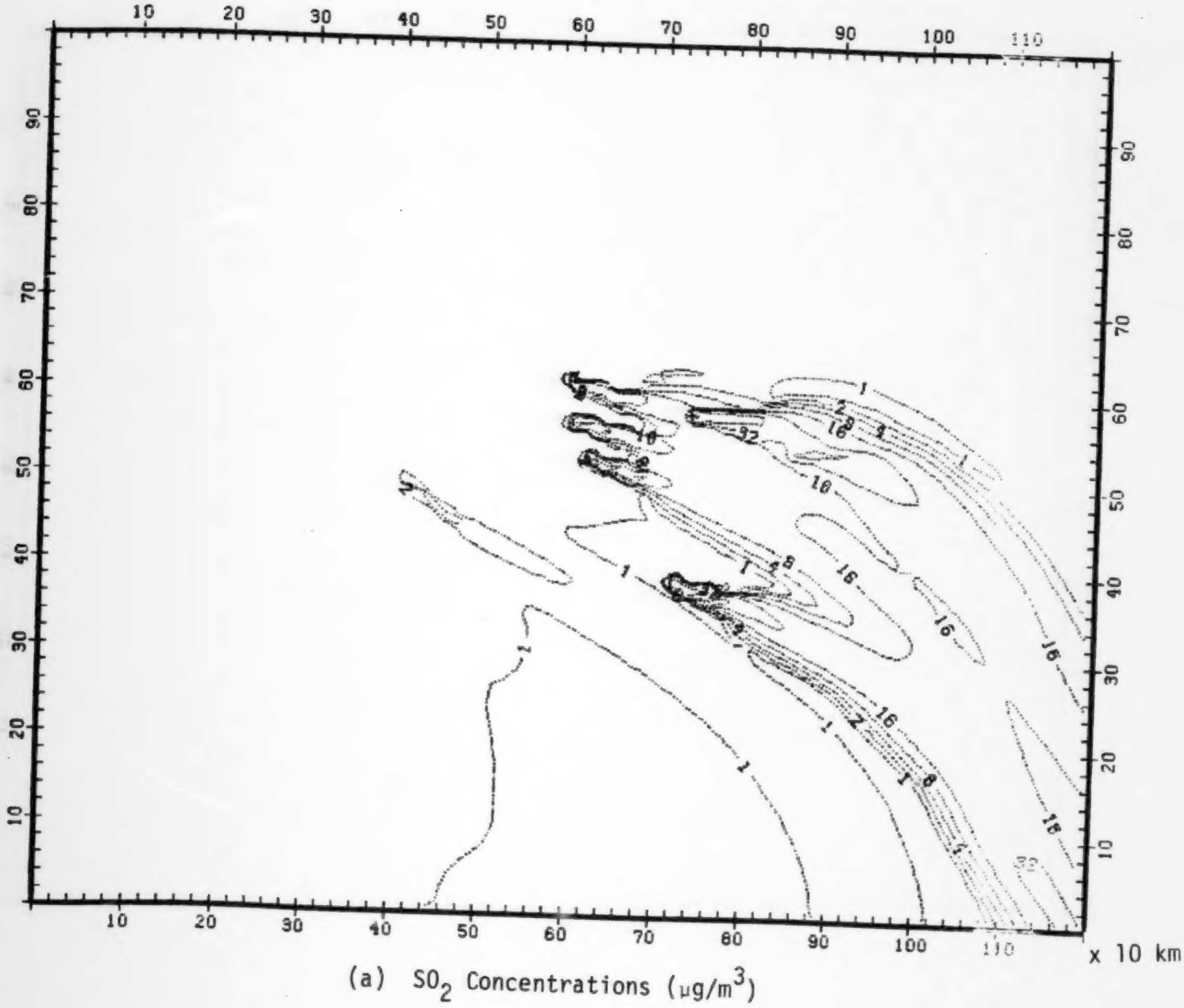
10
20
30
40
50
60
70
80
90
100
110
x 10 km
1
2
8
16
32

(a) SO_2 Concentrations ($\mu g/m^3$)

FIGURE G-21. HYPOTHETICAL COPPER SMELTER ISOPLETHS FOR 500-800 MST ON 29 JANUARY 1976 ASSUMING 0.5 PERCENT PER HOUR SULFATE FORMATION

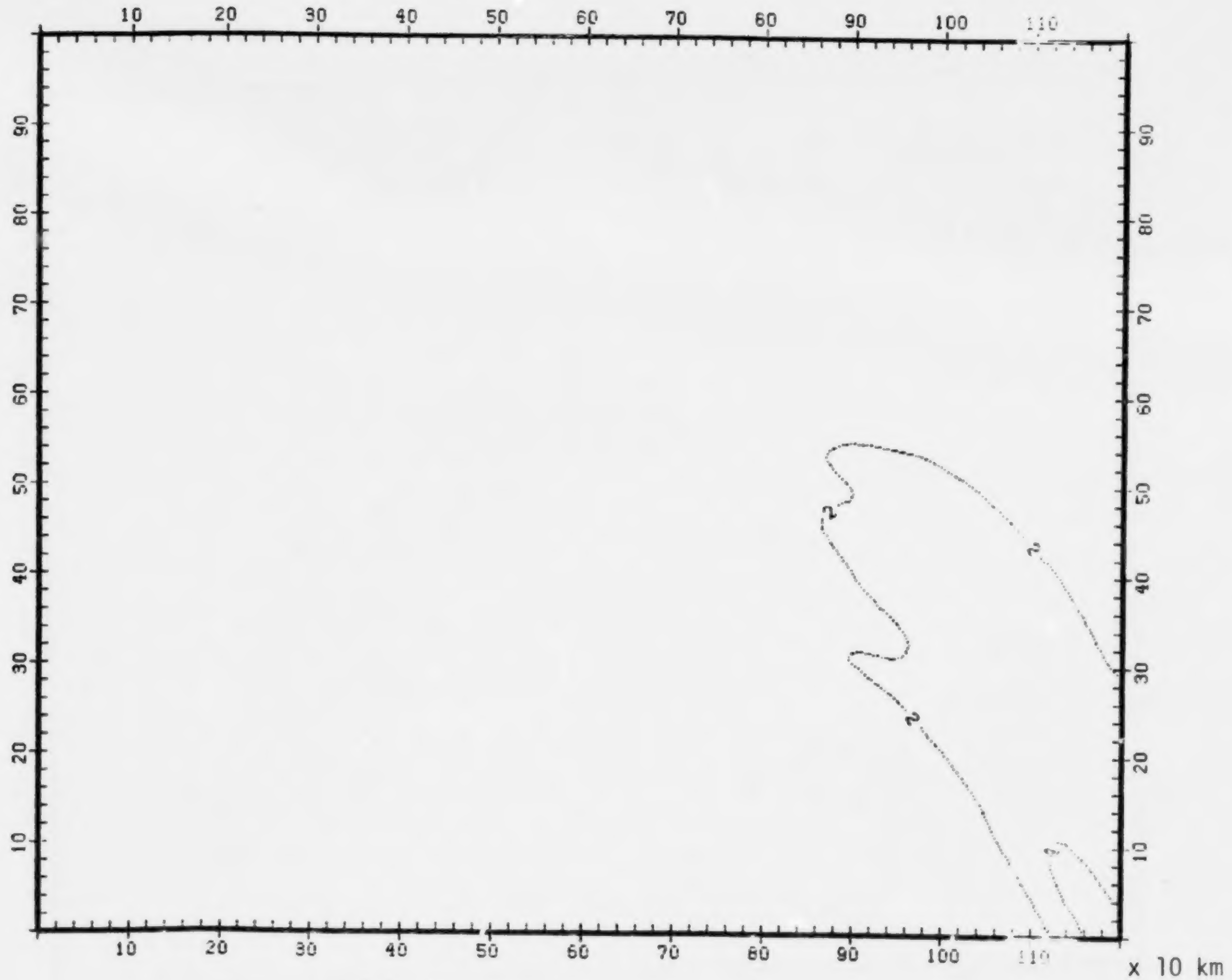
10
20
30
40
50
60
70
80
90
100
110
2
2
2
x 10 km

(b) $SO_4^=$ Concentrations (μg/m^3)

FIGURE G-21 (Continued)

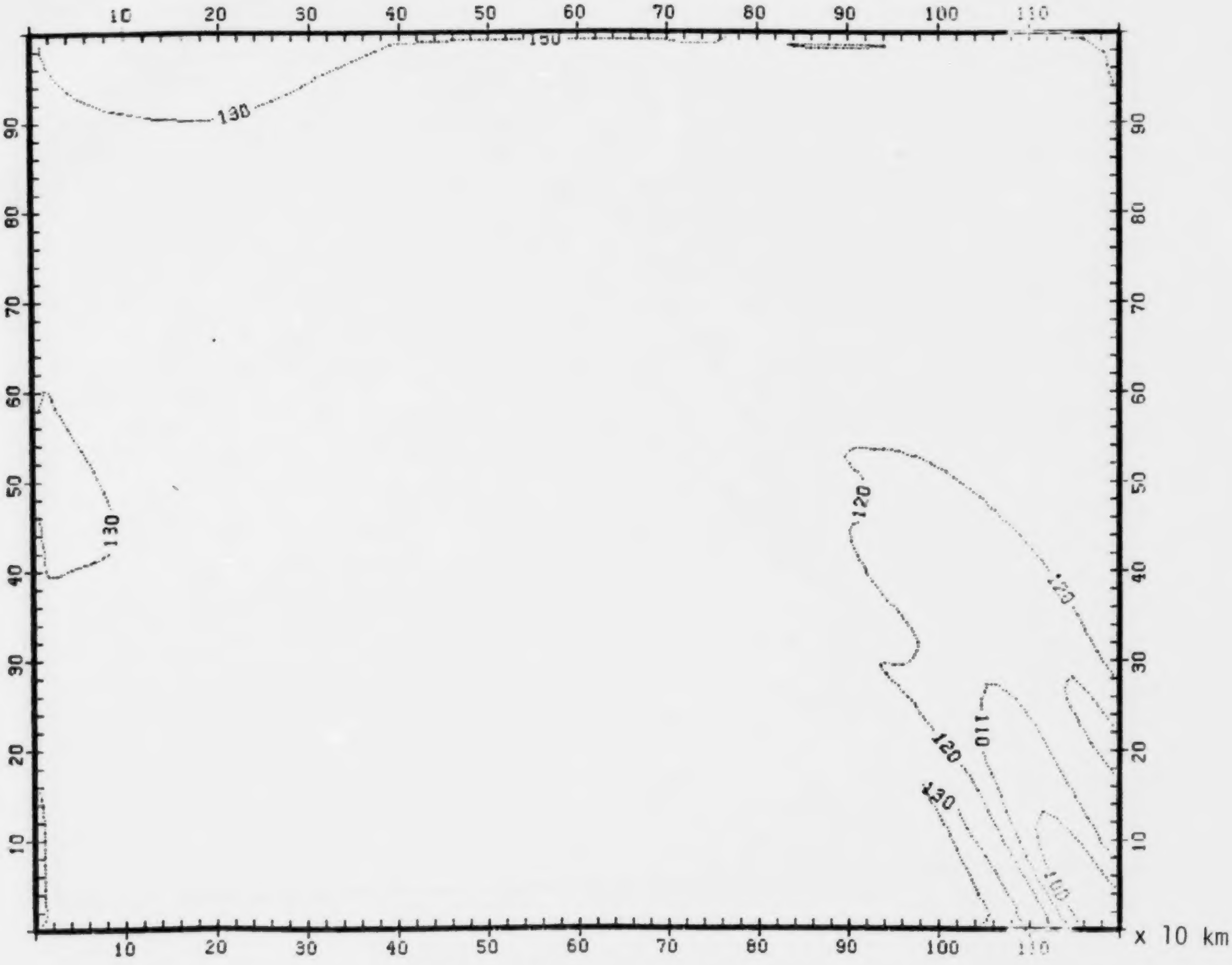

(c) Visual Range (km)

FIGURE G-21 (Concluded)

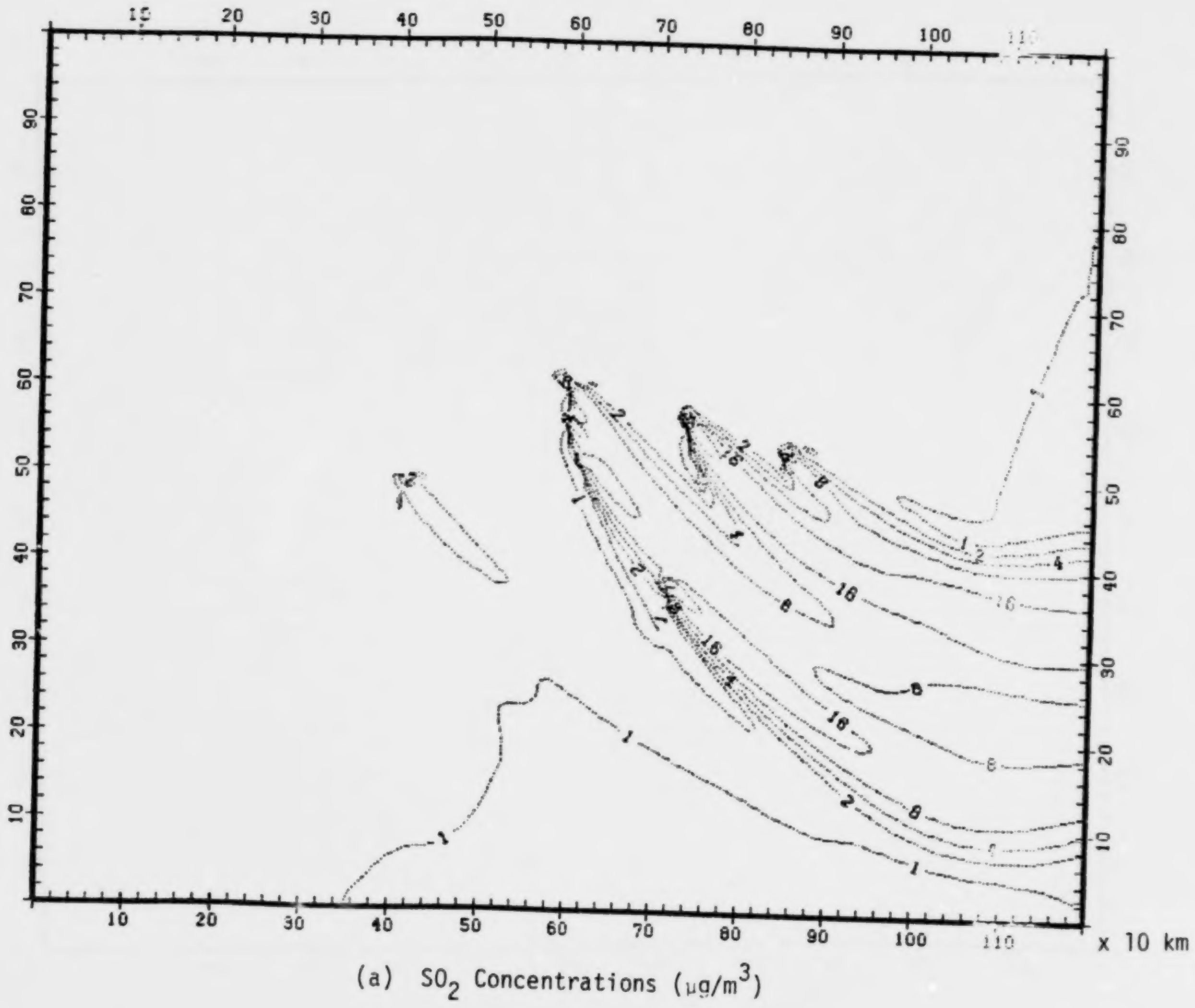
10
20
30
40
50
60
70
80
90
100
110
x 10 km
1
2
4
8
16

(a) SO_2 Concentrations ($\mu g/m^3$)

FIGURE G-22. HYPOTHETICAL COPPER SMELTER ISOPLETHS FOR 1400-1700 MST ON 29 JANUARY 1976 ASSUMING 0.5 PERCENT PER HOUR SULFATE FORMATION

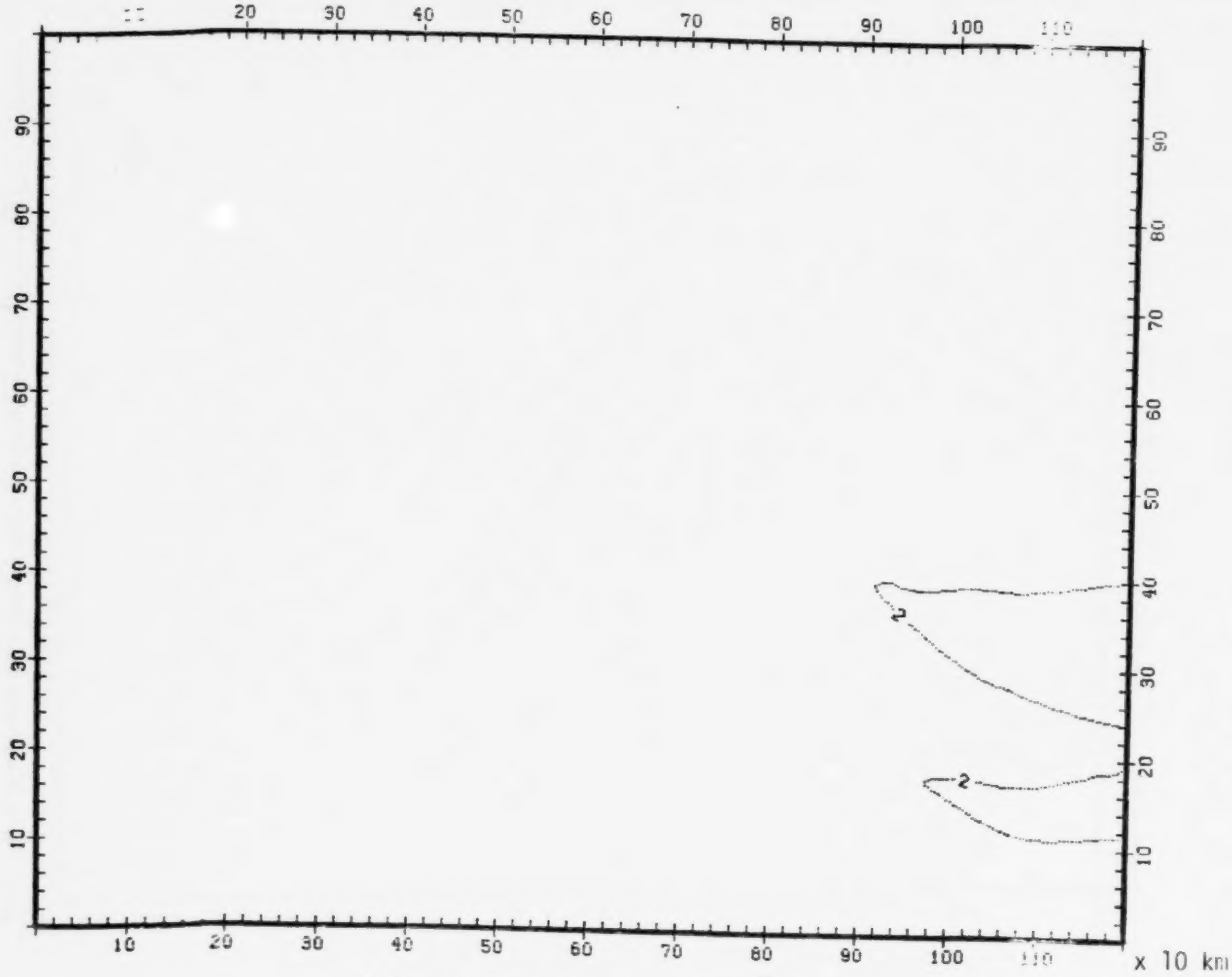
10
20
30
40
50
60
70
80
90
100
110
x 10 km
2
2

(b) $SO_4^=$ Concentrations ($\mu g/m^3$)

FIGURE G-22 (Continued)

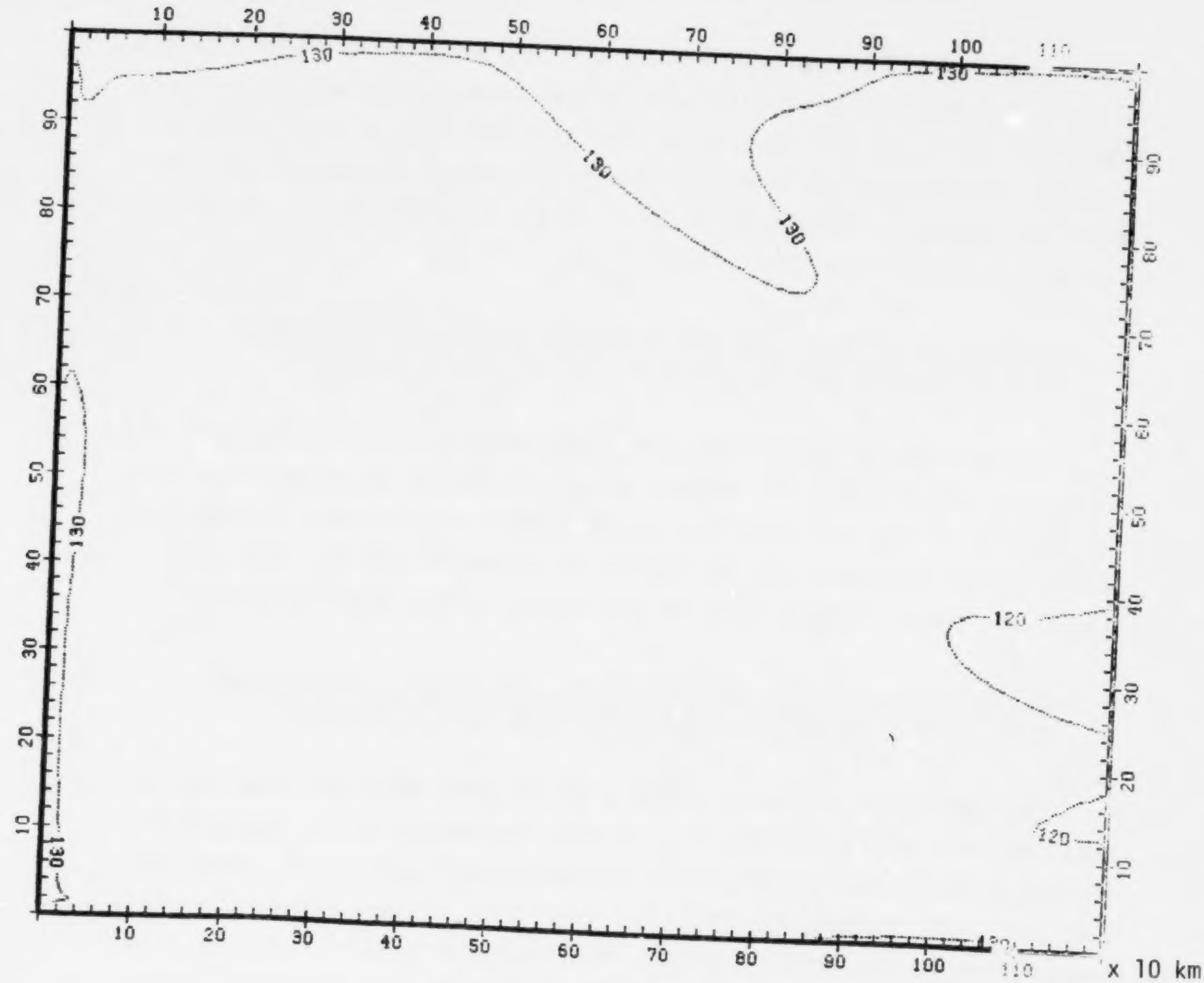

(c) Visual Range (km)

FIGURE G-22 (Concluded)

d. Hypothetical Copper Smelter Emissions, Assuming 1 Percent per Hour Sulfate Formation, Using the Spring (April) Scenario

Figures G-23 through G-28 present the results of a run (Run 4) designed to test the sensitivity of calculated visual range to the assumed sulfate formation rate. We used the spring (April) meteorological conditions and assumed a higher sulfate formation rate of 1 percent per hour. Note that the visual range is reduced to 40 km in this run, compared with the 60 km minimum in the previous simulation.

e. Hypothetical Copper Smelter Emissions, Assuming 0.3 Percent per Hour Sulfate Formation, Using the Spring (April) Scenario

To complete the set of runs using the hypothetical copper smelter SO_2 emissions, we assumed a low sulfate formation rate of 0.3 percent per hour. The results of this run (Run 5) are presented in Figures G-29 through G-34. Note that, as expected, the minimum visual range (70 km) is higher than the visual ranges calculated using the higher sulfate formation rates.

f. Northern Great Plains 1975 Emissions, Assuming 0.5 Percent per Hour Sulfate Formation, Using the Spring (April) Scenario

The results of the calculations with the 1975 emissions from the large point sources in the Northern Great Plains are presented in Figures G-35 through G-40 for the spring (April) meteorological conditions. Note that even with the stagnant meteorological conditions of this three-day period, the minimum visual range is 120 km, less than a 10 percent reduction from the assumed background visual range of 130 km. The calculated NO_2 concentrations are displayed in parts per billion (ppb).

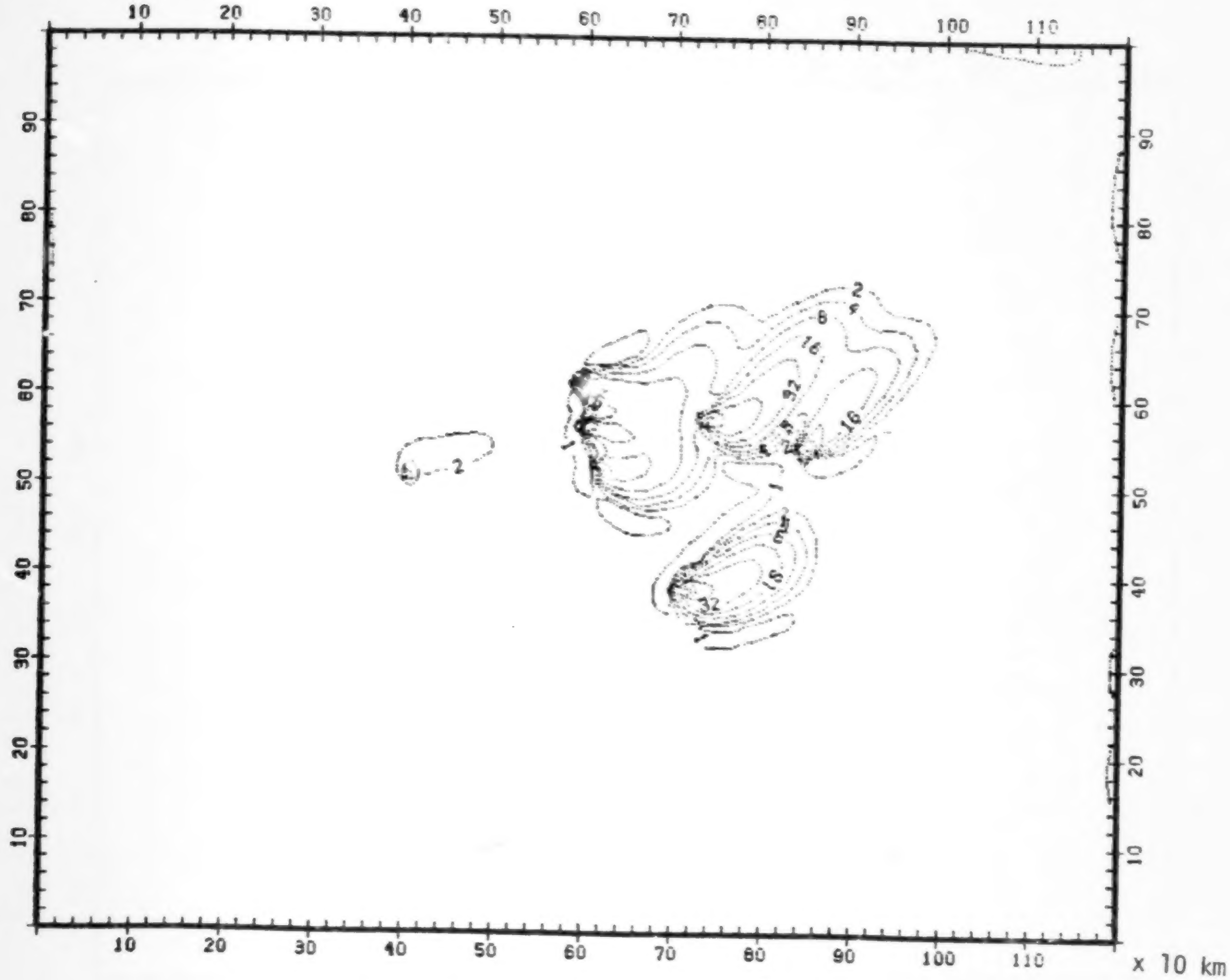
10
20
30
40
50
60
70
80
90
100
110
x 10 km
2
4
8
16
32
2
1
16
32
16

(a) SO$_2$ Concentrations (μg/m^3)

FIGURE G-23. HYPOTHETICAL COPPER SMELTER ISOPLETHS FOR 1700-2000 MST ON 4 APRIL 1976 ASSUMING 1 PERCENT PER HOUR SULFATE FORMATION

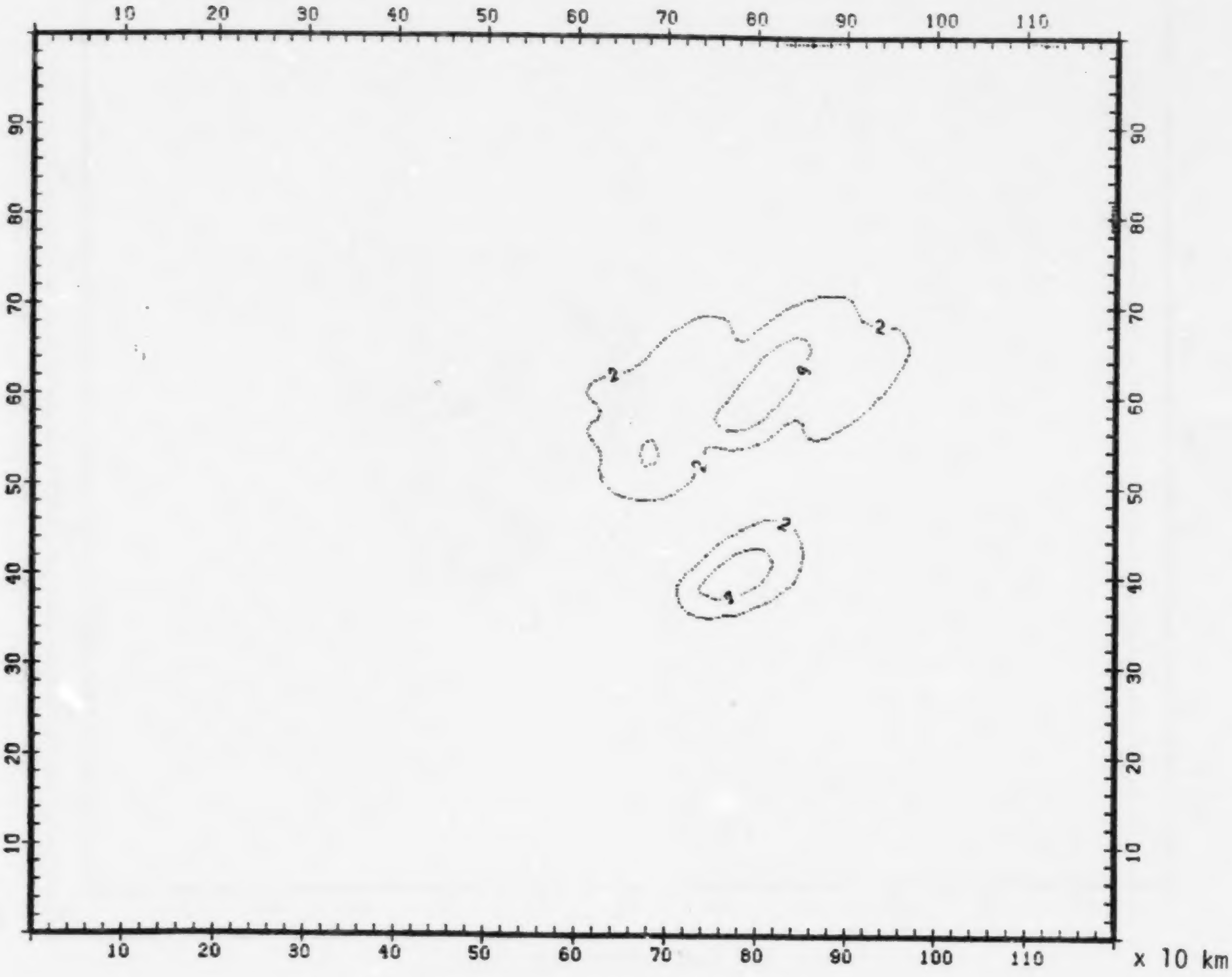
10
20
30
40
50
60
70
80
90
100
110
2
4
x 10 km

(b) $SO_4^=$ Concentrations ($\mu g/m^3$)

FIGURE G-23 (Continued)

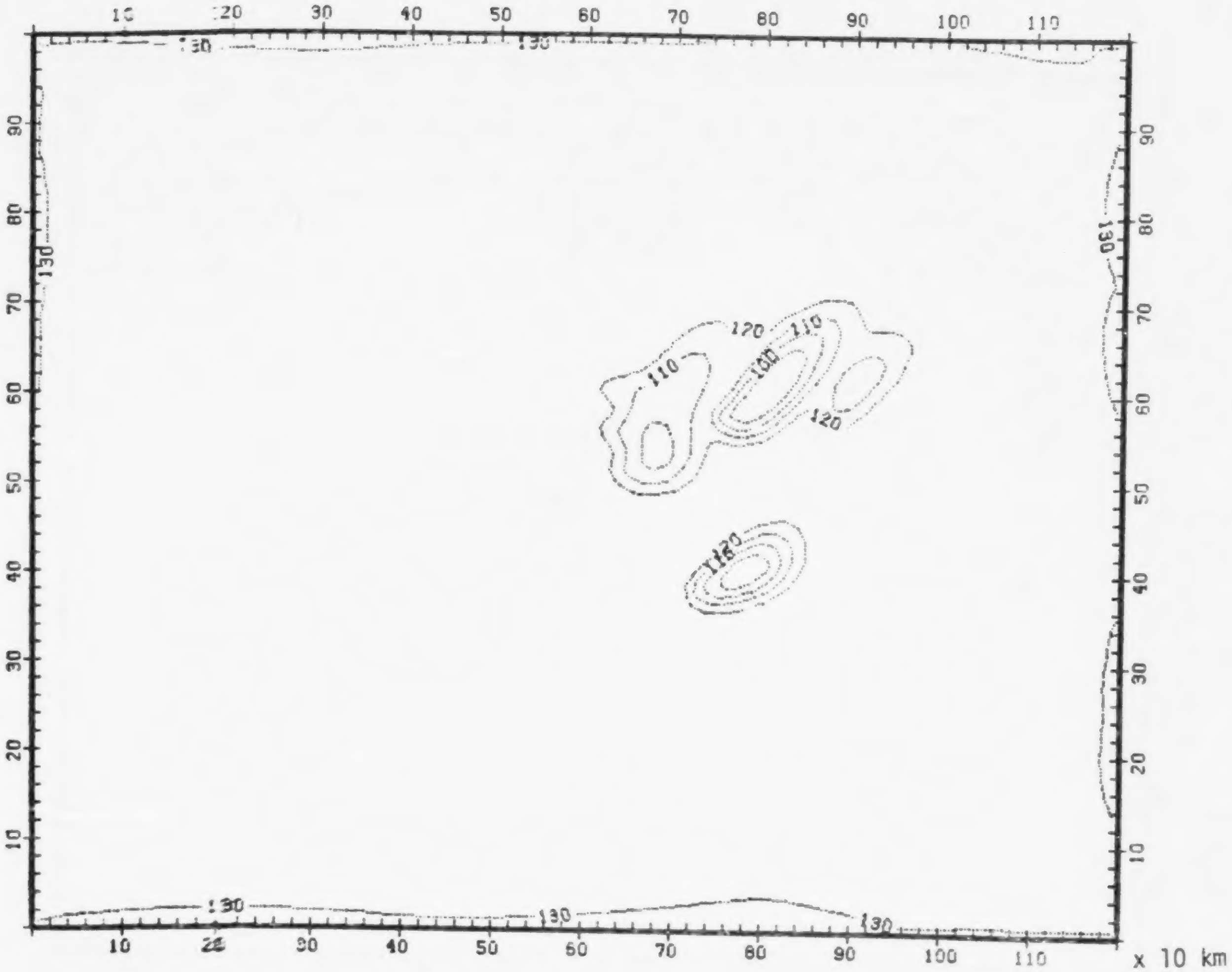

(c) Visual Range (km)

FIGURE G-23 (Concluded)

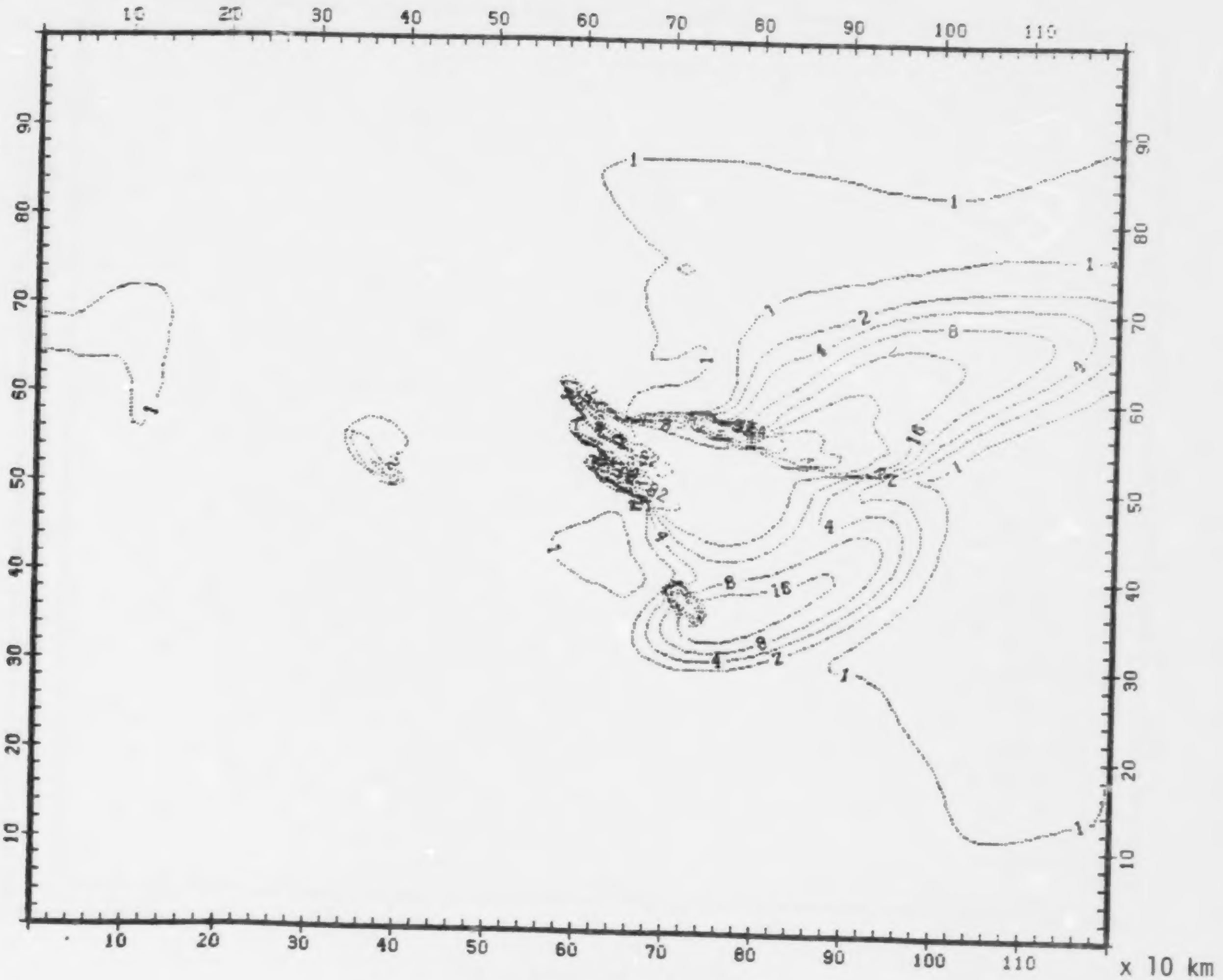

(a) SO_2 Concentrations ($\mu g/m^3$)

FIGURE G-24. HYPOTHETICAL COPPER SMELTER ISOPLETHS FOR 200-500 MST ON 5 APRIL 1976 ASSUMING 1 PERCENT PER HOUR SULFATE FORMATION

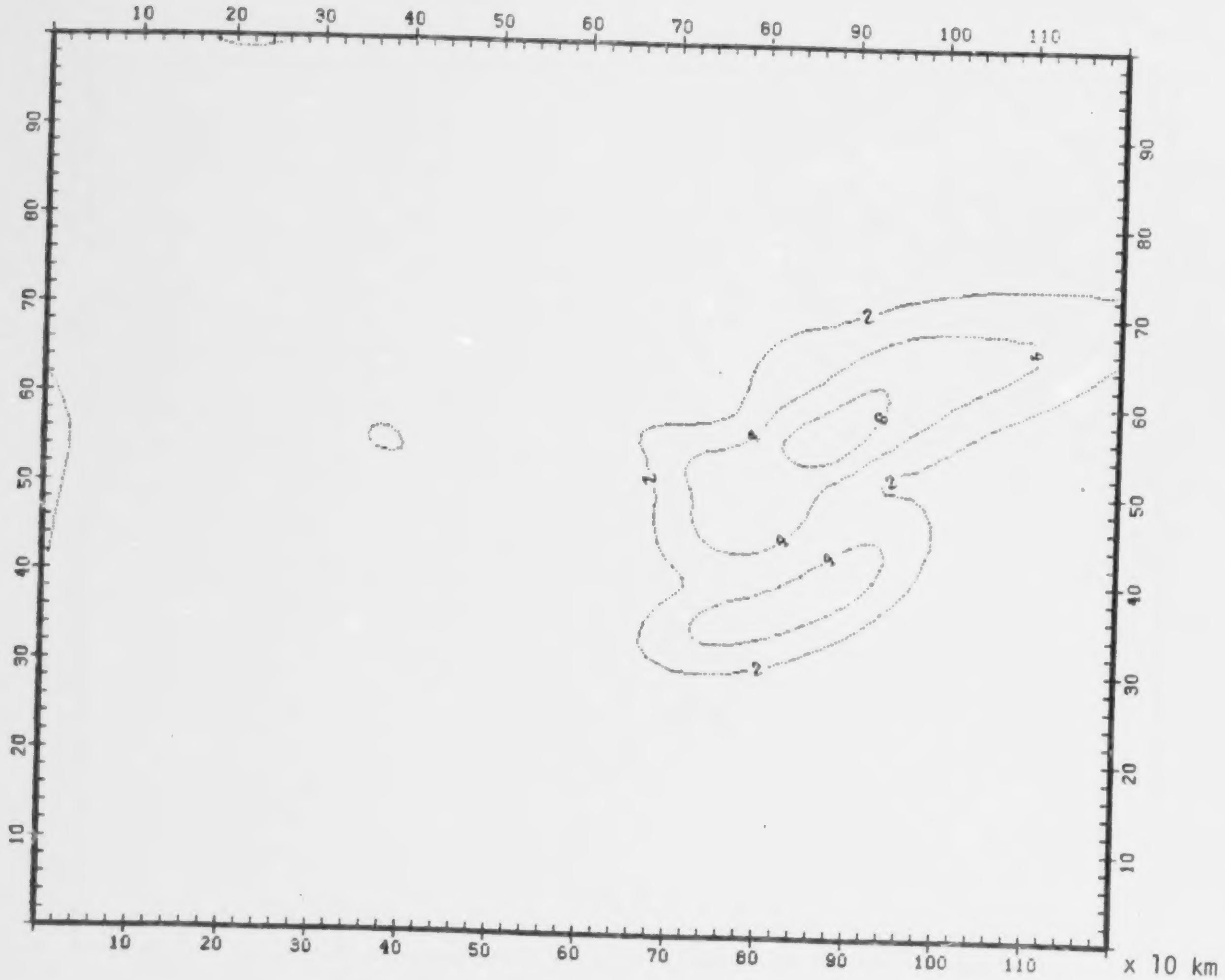
10
20
30
40
50
60
70
80
90
100
110
x 10 km
2
4
6
8

(b) $SO_4^=$ Concentrations ($\mu g/m^3$)

FIGURE G-24 (Continued)

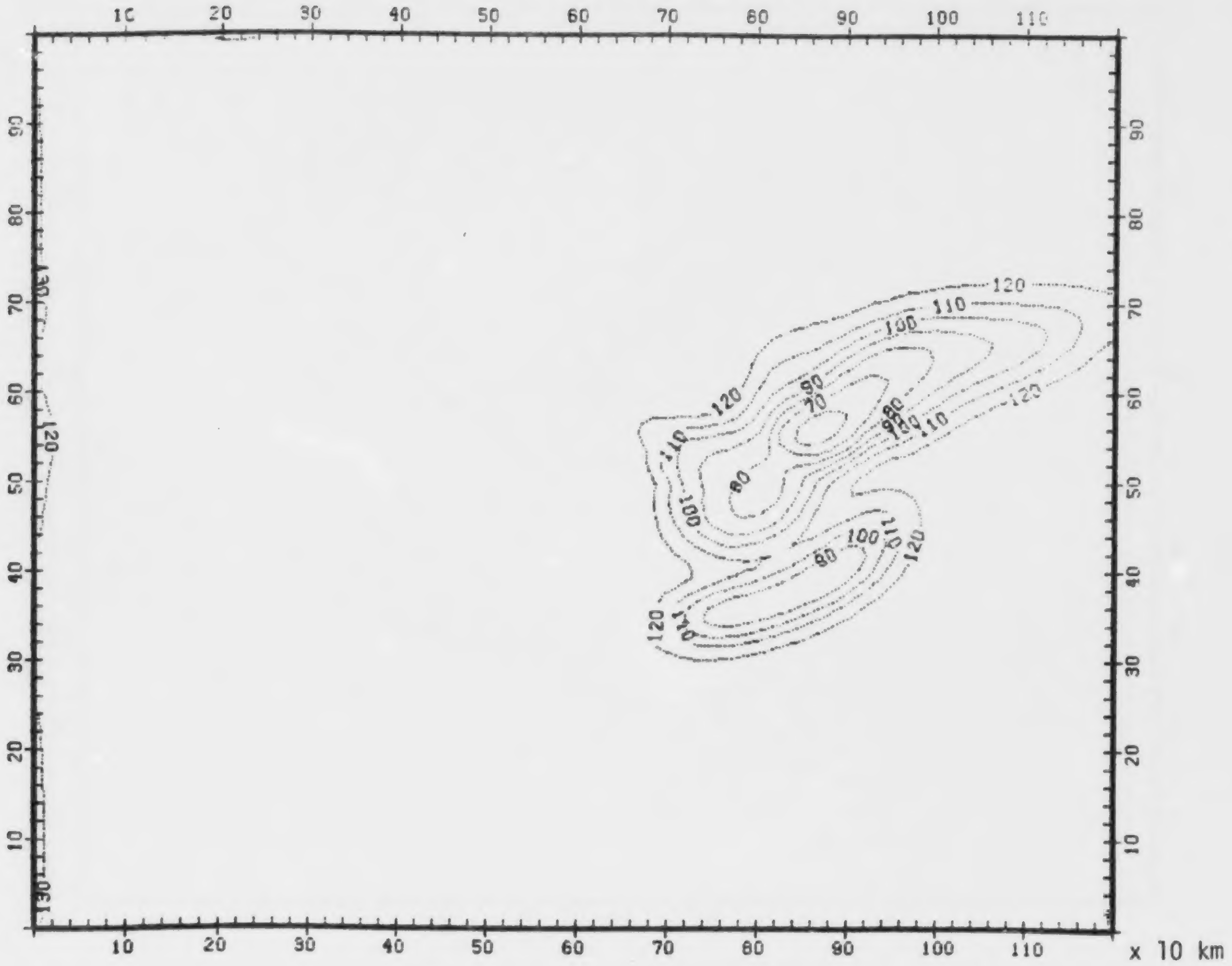

(c) Visual Range (km)

FIGURE G-24 (Concluded)

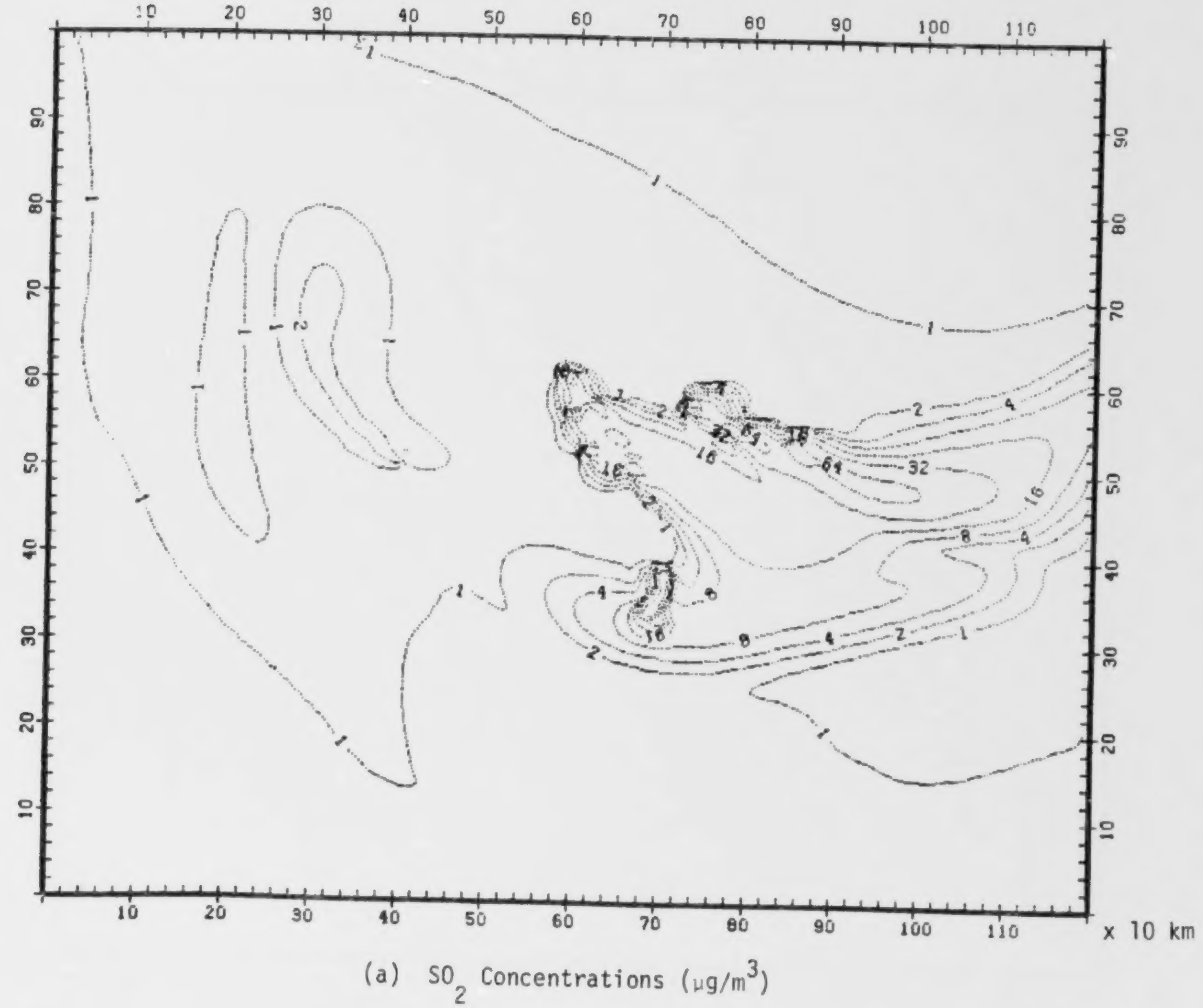
10
20
30
40
50
60
70
80
90
100
110
x 10 km
1
2
4
8
16
32
64

(a) SO_2 Concentrations ($\mu g/m^3$)

FIGURE G-25. HYPOTHETICAL COPPER SMELTER ISOPLETHS FOR 1100-1400 MST ON 5 APRIL 1976 ASSUMING 1 PERCENT PER HOUR SULFATE FORMATION

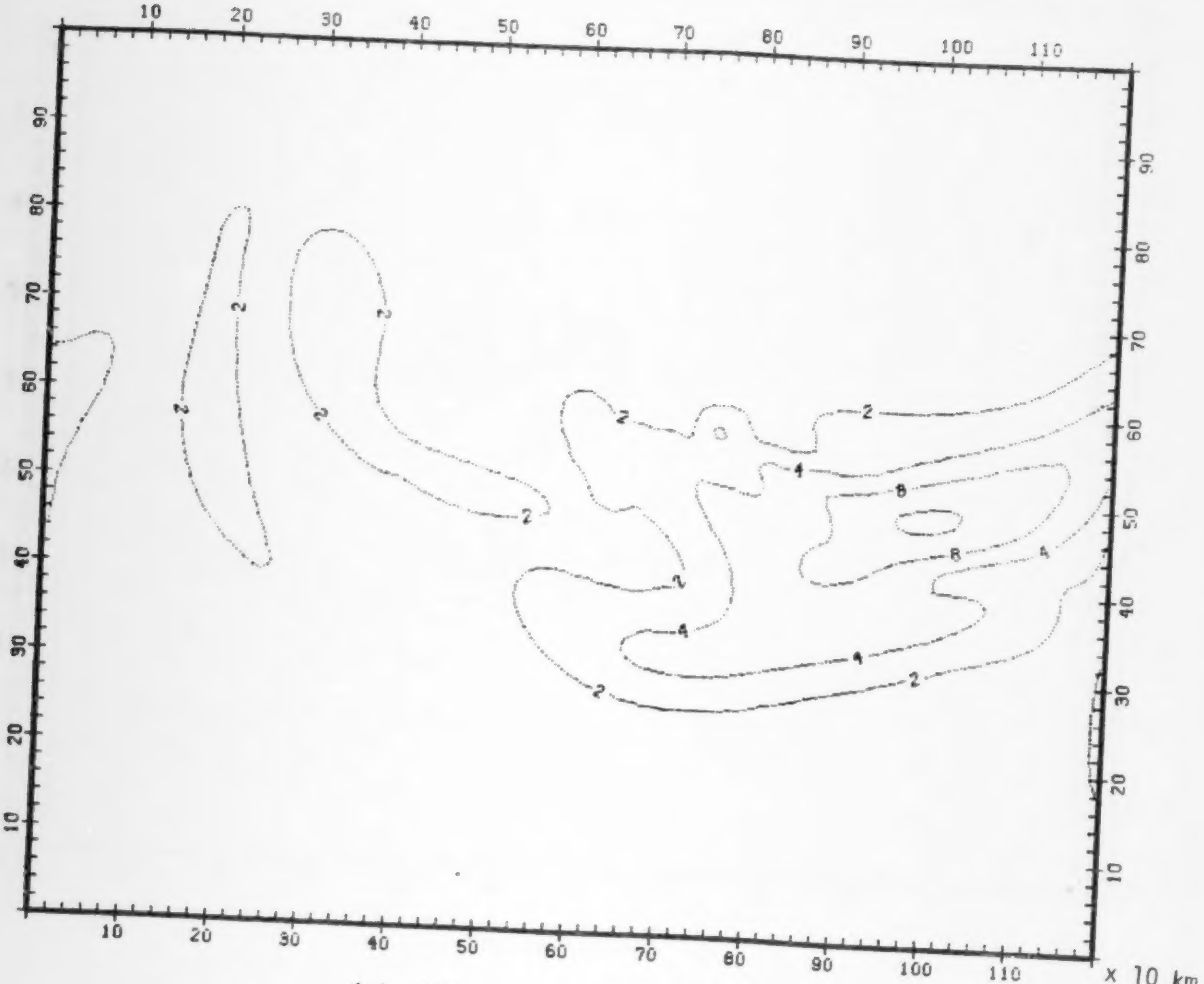
10
20
30
40
50
60
70
80
90
100
110
x 10 km
2
4
8

(b) $SO_4^=$ Concentrations ($\mu g/m^3$)

FIGURE G-25 (Continued)

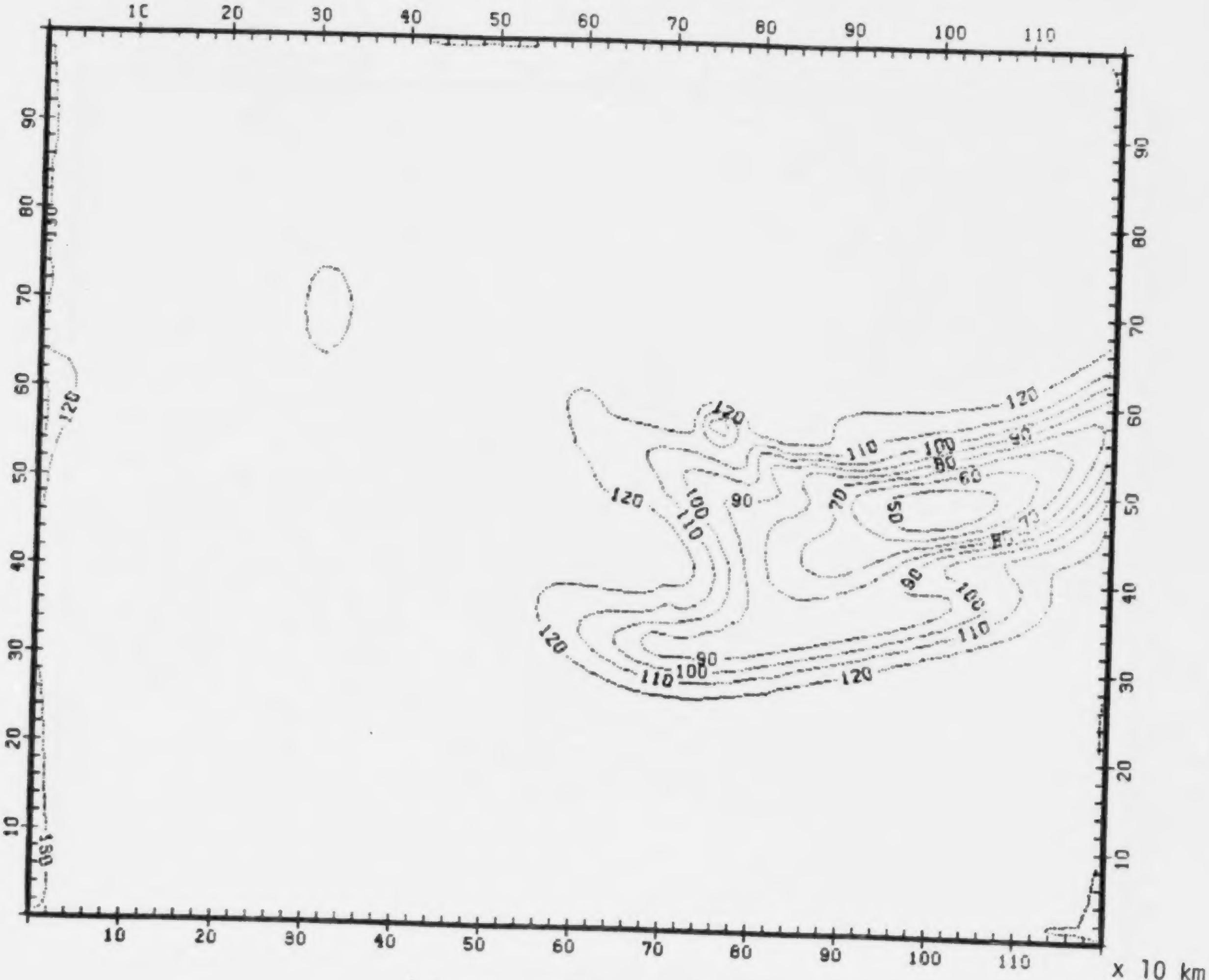
10
20
30
40
50
60
70
80
90
100
110
120
110
100
90
80
60
70
50
x 10 km

(c) Visual Range (km)

FIGURE G-25 (Concluded)

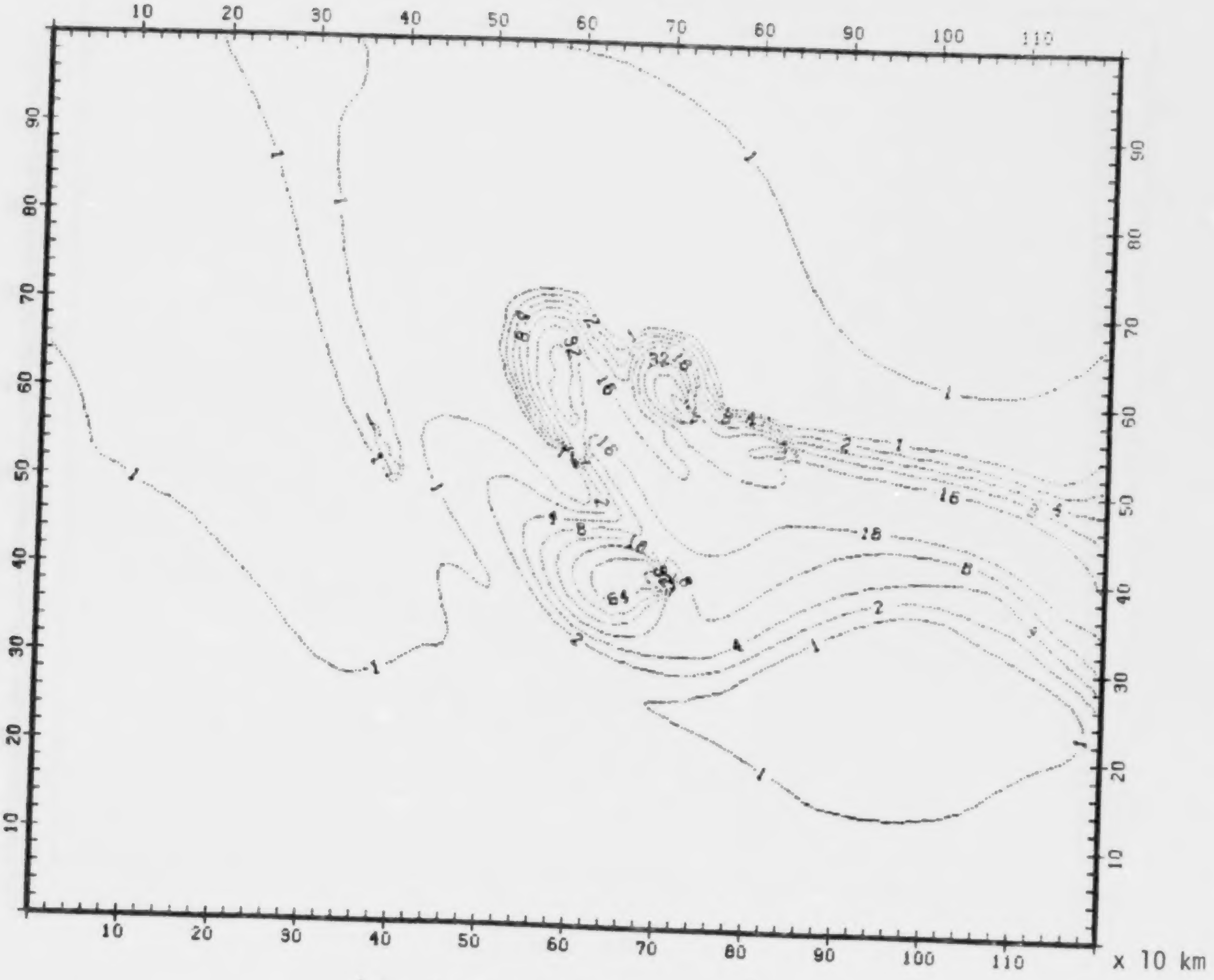

(a) SO$_2$ Concentrations ($\mu g/m^3$)

FIGURE G-26. HYPOTHETICAL COPPER SMELTER ISOPLETHS FOR 2000-2300 MST ON 5 APRIL 1976 ASSUMING 1 PERCENT PER HOUR SULFATE FORMATION

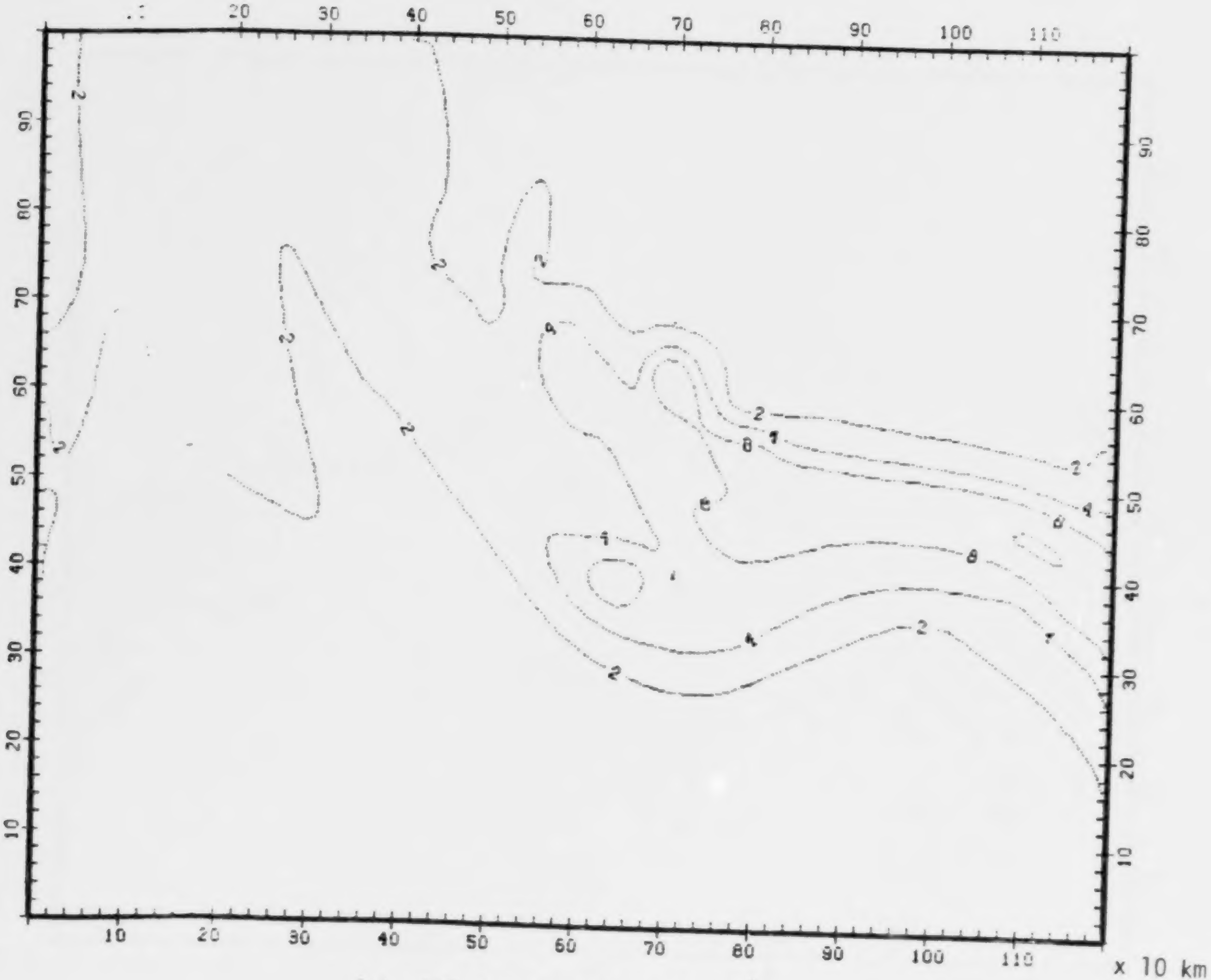
10
20
30
40
50
60
70
80
90
100
110
x 10 km
2
4
8

(b) $SO_4^=$ Concentrations ($\mu g/m^3$)

FIGURE G-26 (Continued)

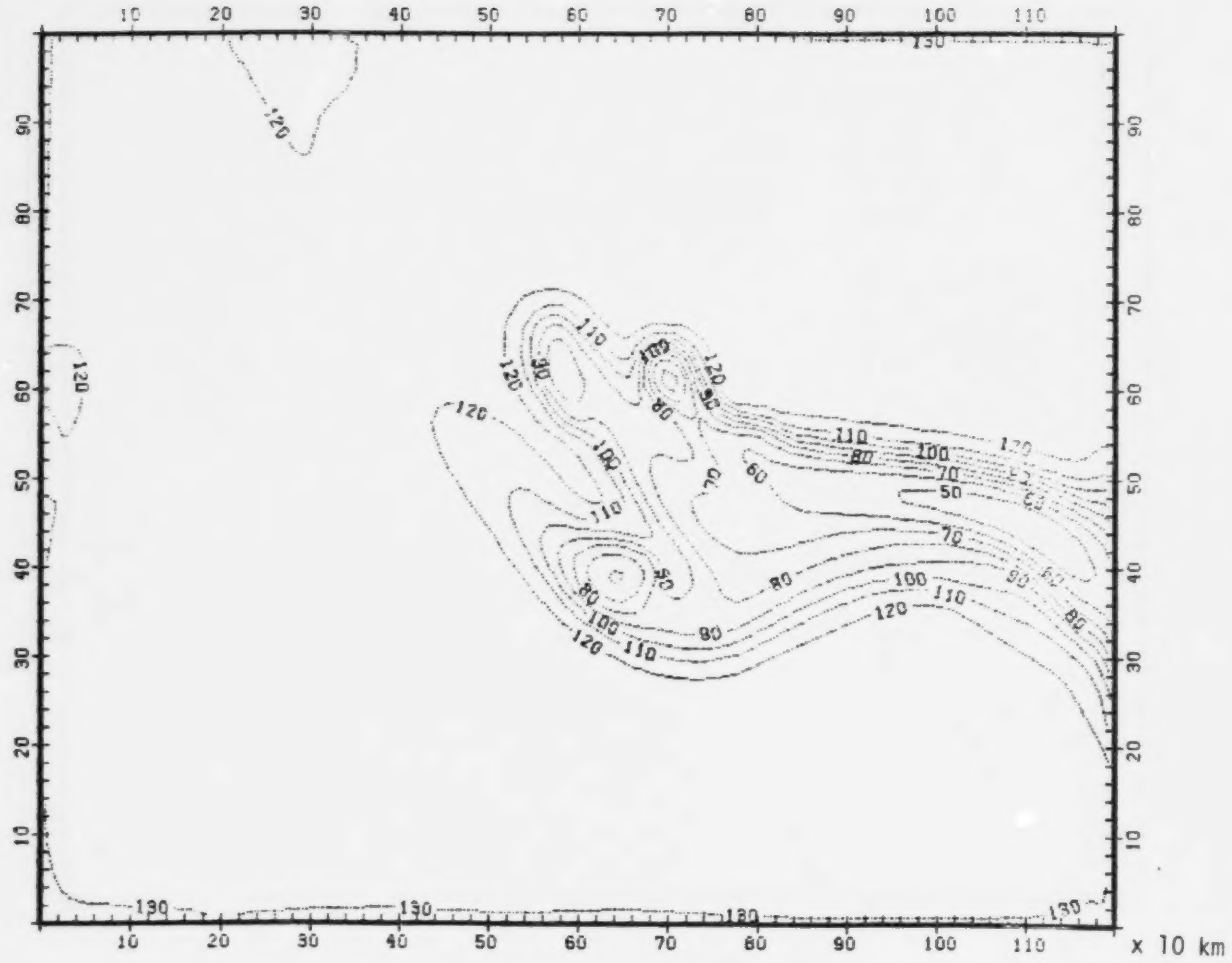
10
20
30
40
50
60
70
80
90
100
110
x 10 km
120
130
110
100
90
80
70
60
50

(c) Visual Range (km)

FIGURE G-26 (Concluded)

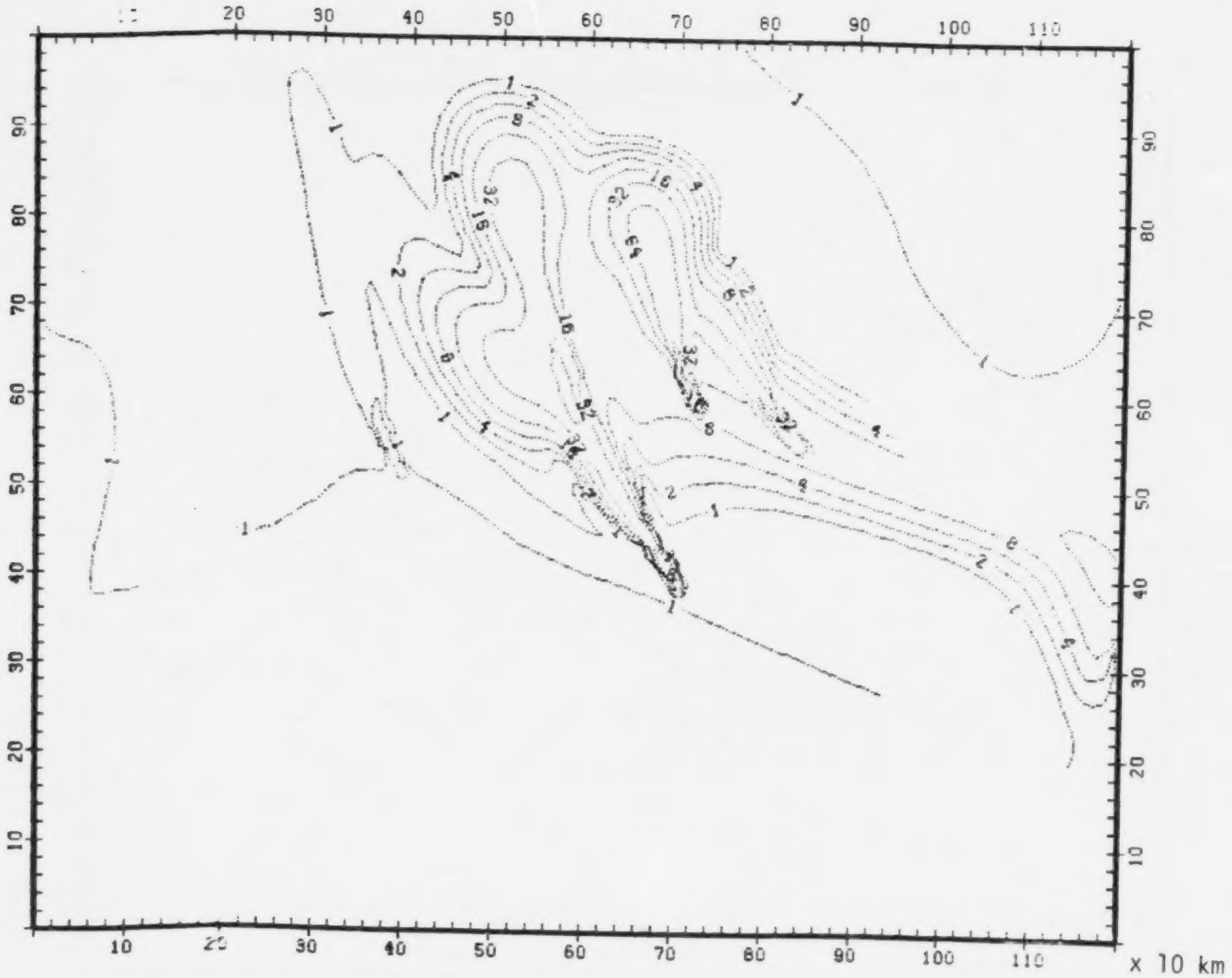
10
20
30
40
50
60
70
80
90
100
110
x 10 km
1
2
4
8
16
32
64

(a) SO_2 Concentrations ($\mu g/m^3$)

FIGURE 6-27. HYPOTHETICAL COPPER SMELTER ISOPLETHS FOR 500-800 MST ON 6 APRIL 1976 ASSUMING 1 PERCENT PER HOUR SULFATE FORMATION

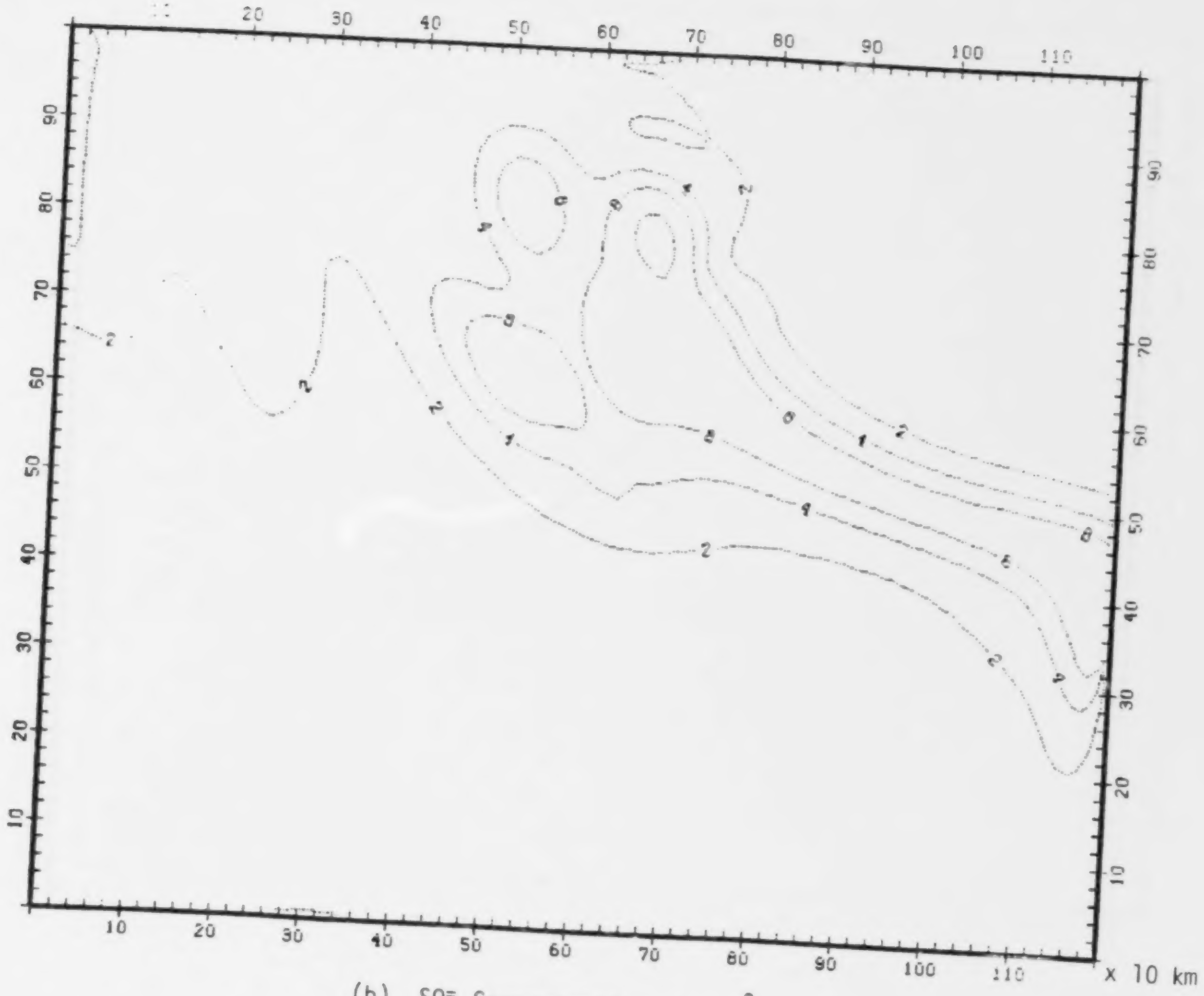
10
20
30
40
50
60
70
80
90
100
110
x 10 km
2
4
6
8

(b) $SO_4^=$ Concentrations ($\mu g/m^3$)

FIGURE G-27 (Continued)

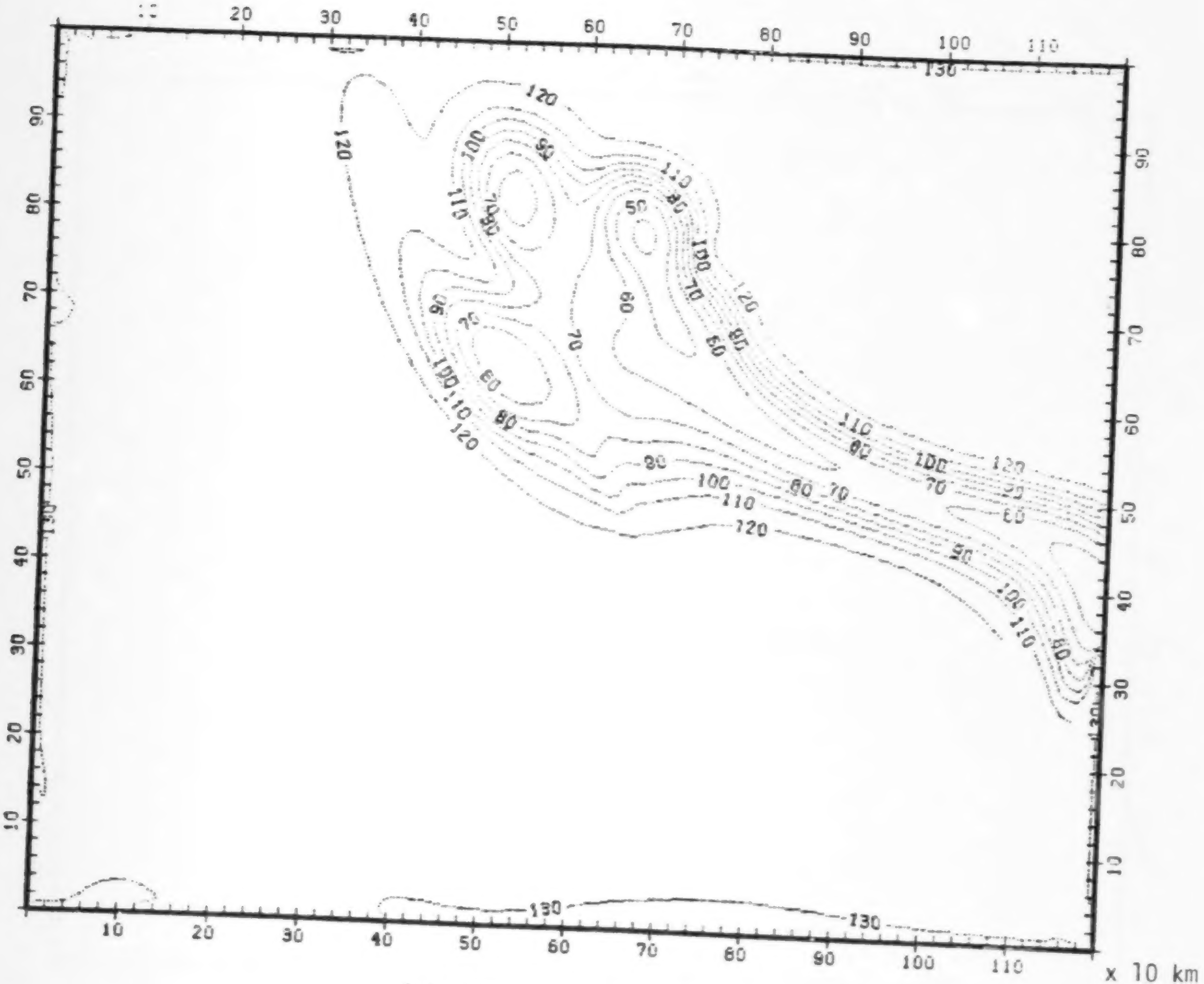

(c) Visual Range (km)

FIGURE G-27 (Concluded)

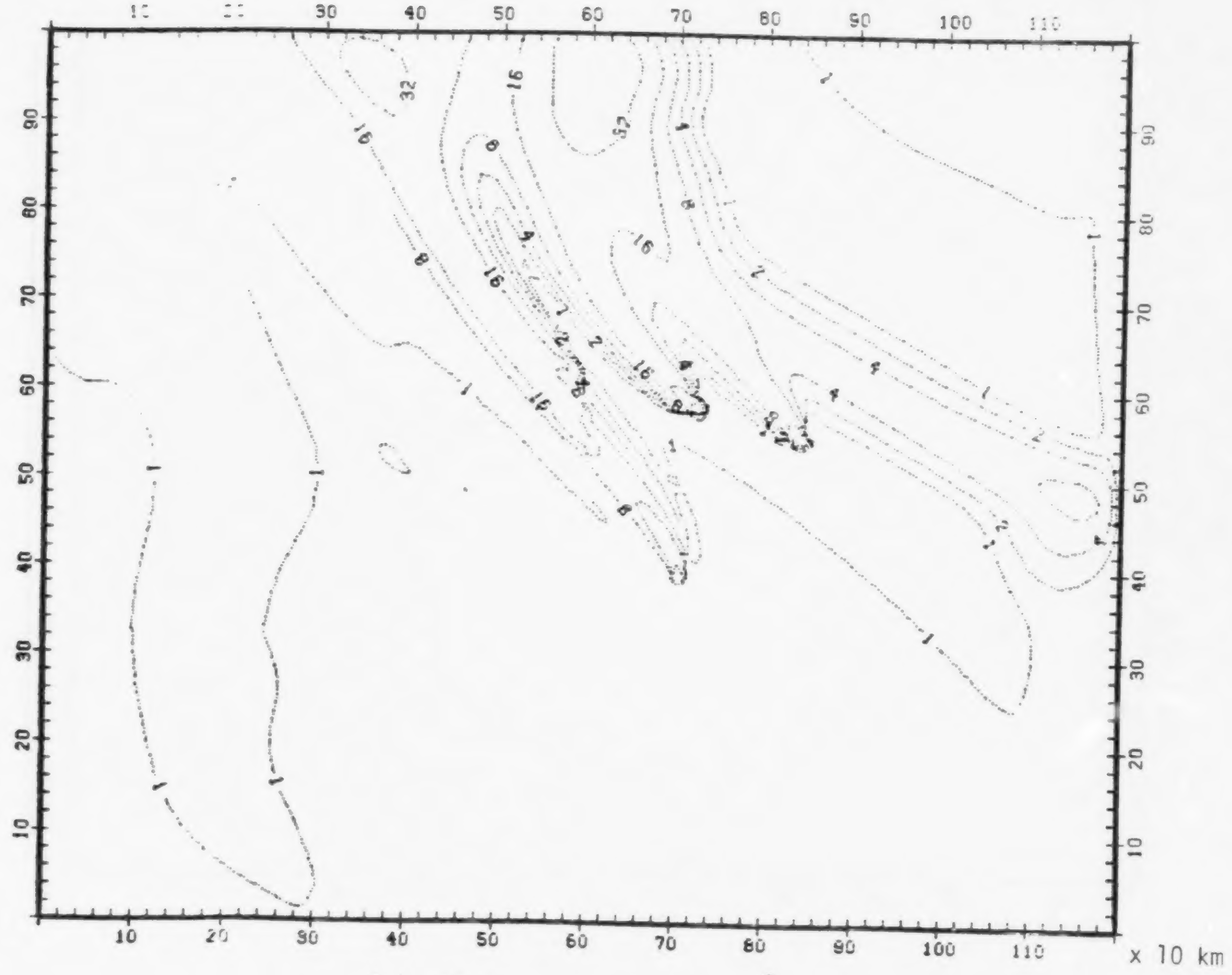
10
20
30
40
50
60
70
80
90
100
110
x 10 km
32
16
8
4
2
1

(a) SO_2 Concentrations ($\mu g/m^3$)

FIGURE G-28. HYPOTHETICAL COPPER SMELTER ISOPLETHS FOR 1400-1700 MST ON 6 APRIL 1976 ASSUMING 1 PERCENT PER HOUR SULFATE FORMATION

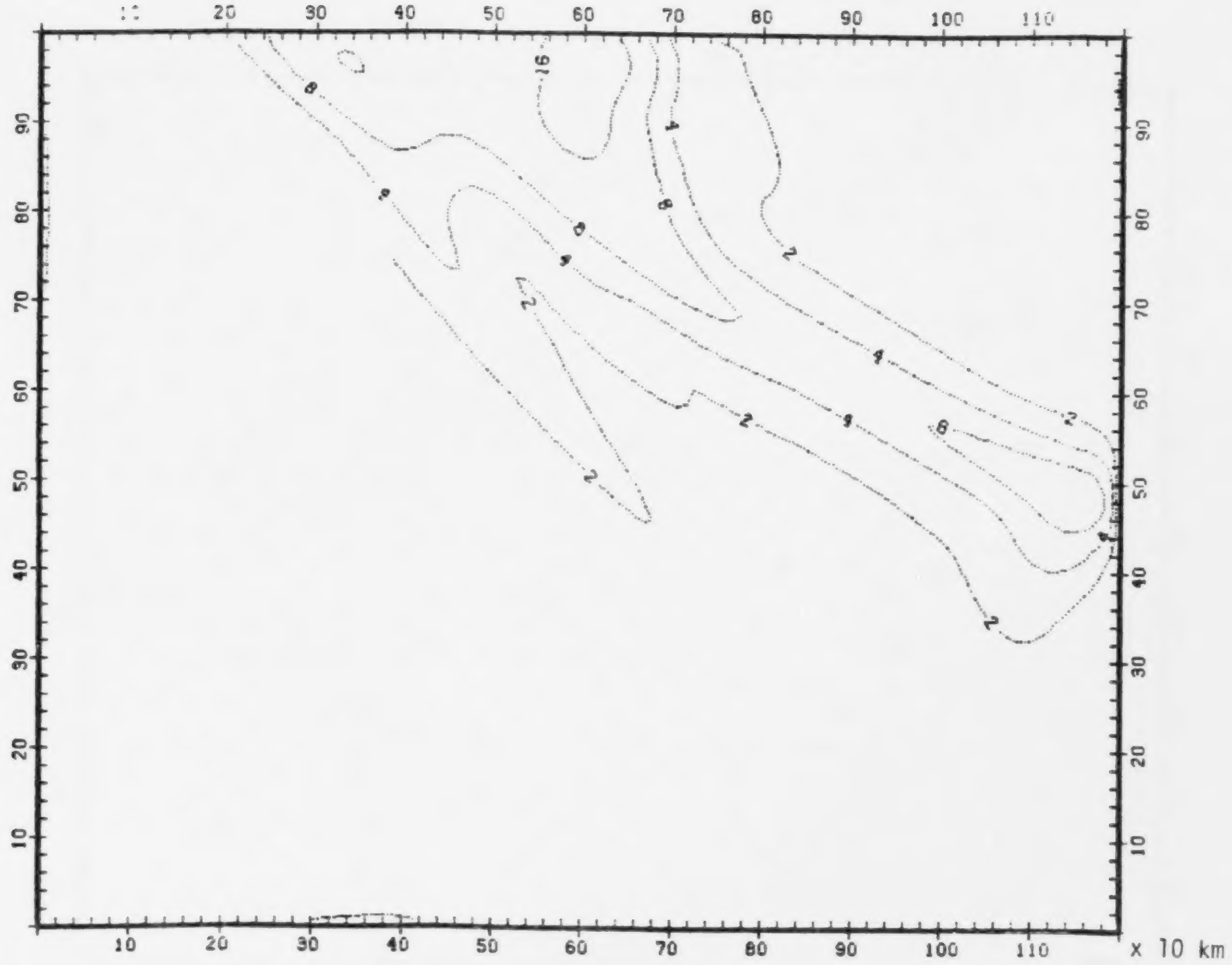
10
20
30
40
50
60
70
80
90
100
110
x 10 km
16
8
4
2

(b) $SO_4^=$ Concentrations ($\mu g/m^3$)

FIGURE G-28 (Continued)

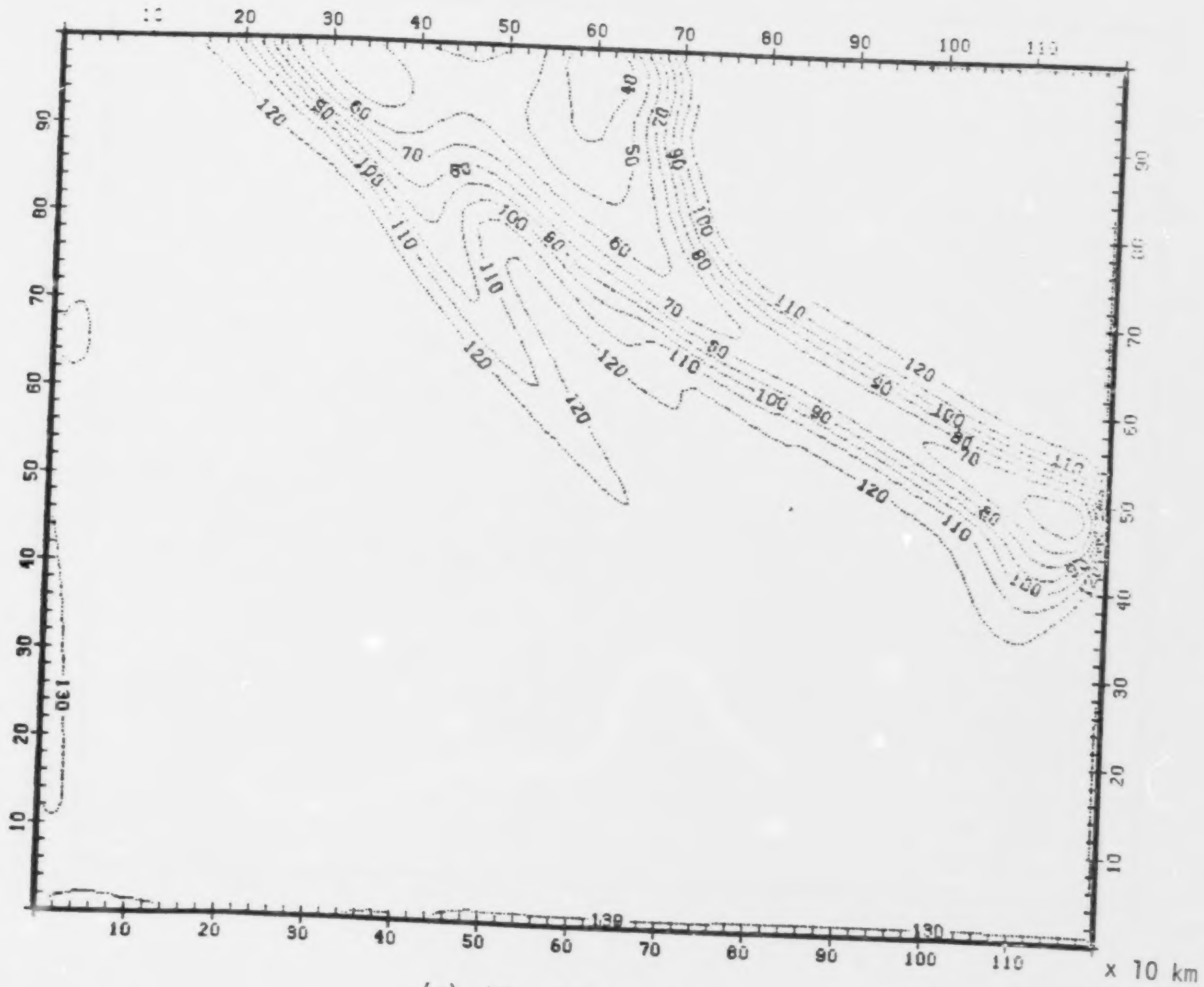

(c) Visual Range (km)

FIGURE G-28 (Concluded)

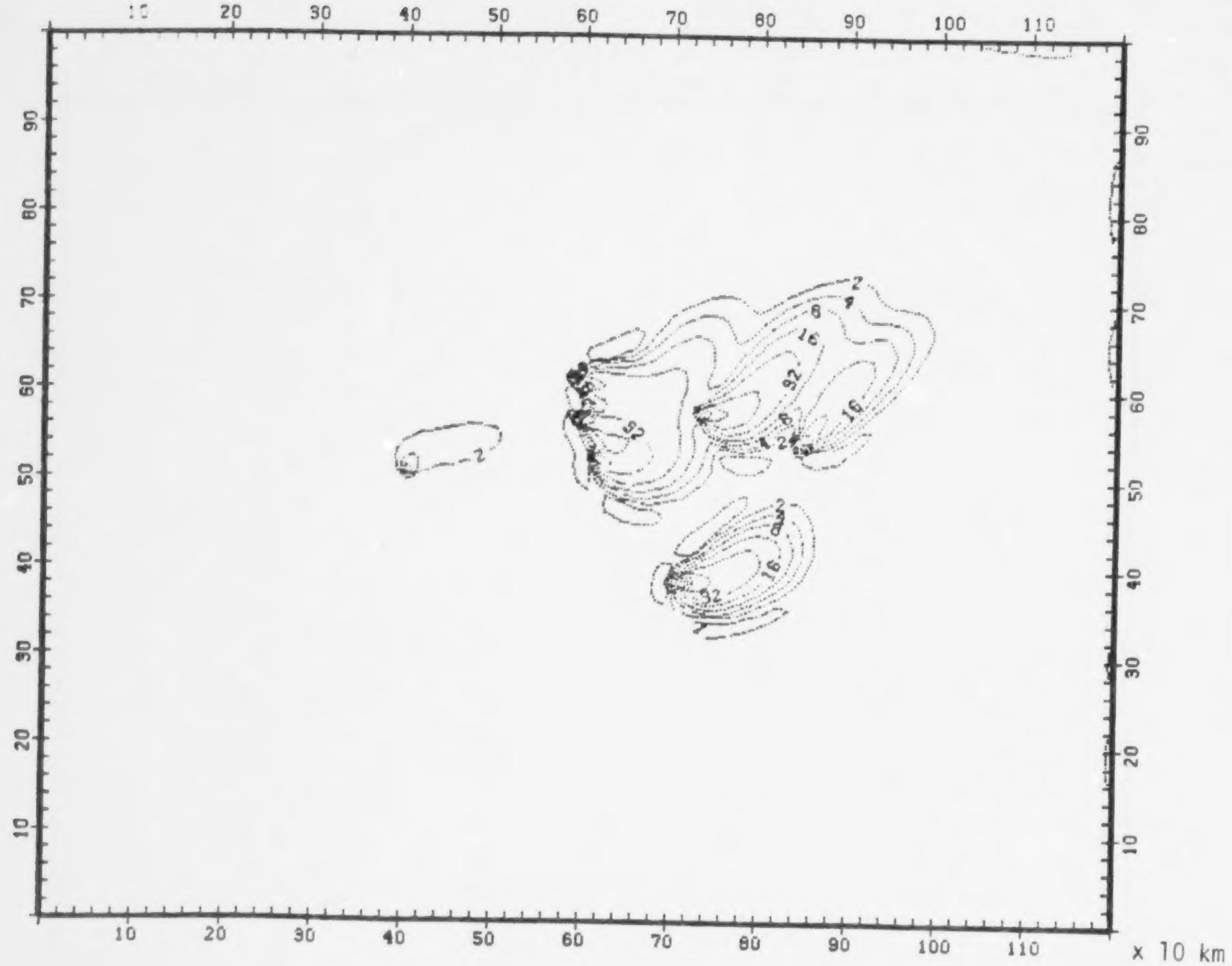
10
20
30
40
50
60
70
80
90
100
110
x 10 km
2
8
16
32

(a) SO_2 Concentrations ($\mu g/m^3$)

FIGURE G-29. HYPOTHETICAL COPPER SMELTER ISOPLETHS FOR 1700-2000 MST ON 4 APRIL 1976 ASSUMING 0.3 PERCENT PER HOUR SULFATE FORMATION

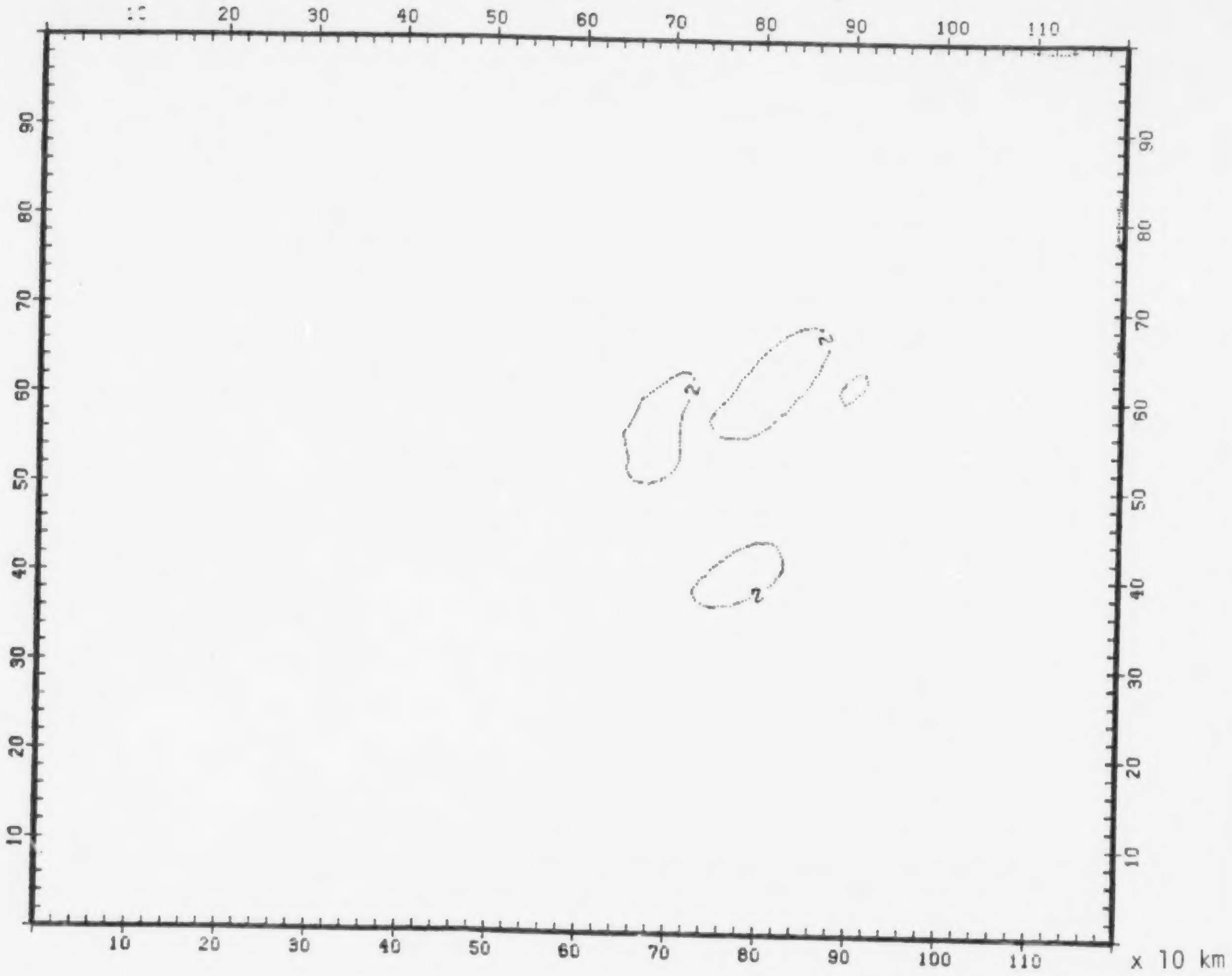
10
20
30
40
50
60
70
80
90
100
110
x 10 km
2
2
2

(b) SO$_4^=$ Concentrations (μg/m^3)

FIGURE G-29 (Continued)

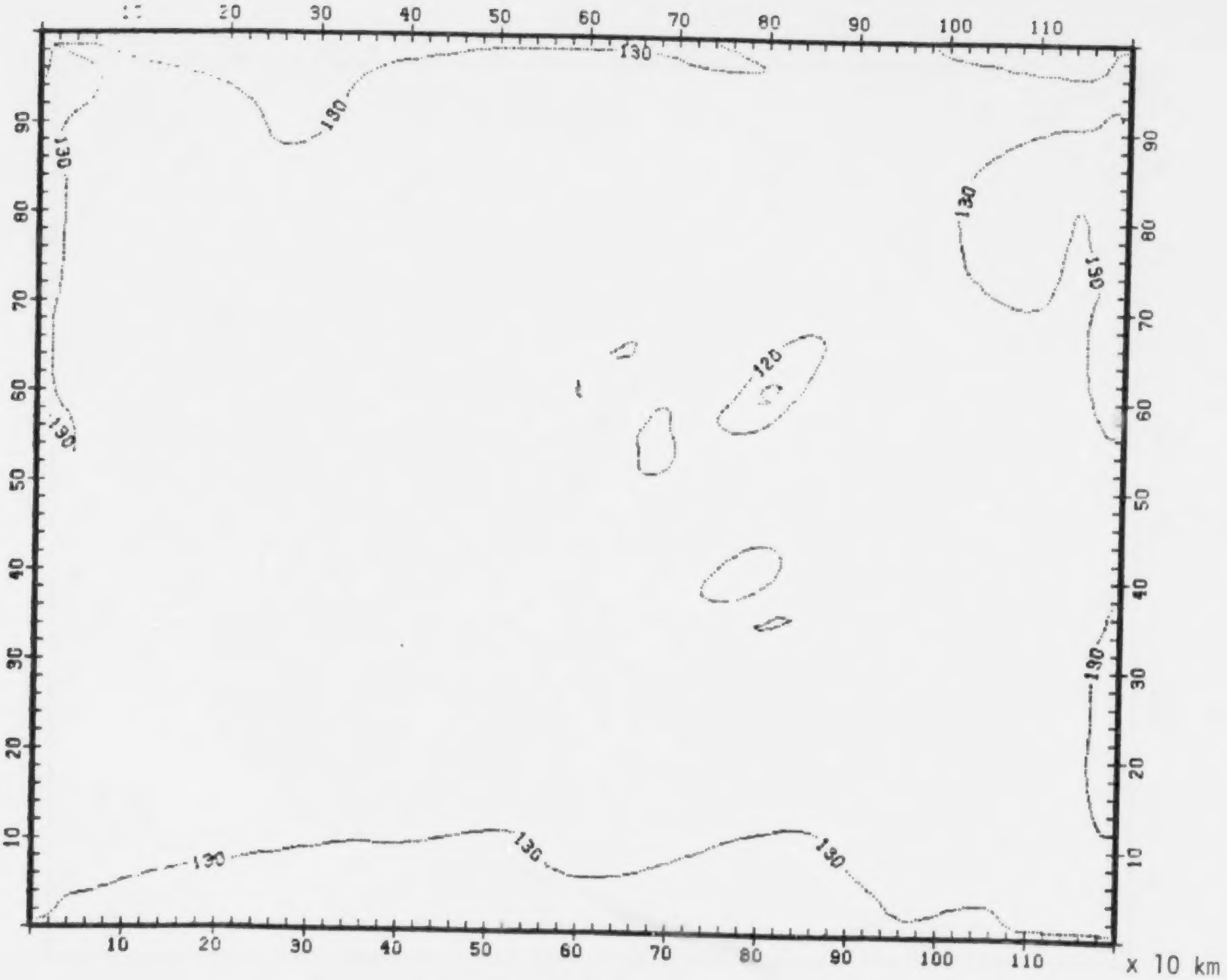
130
130
130
130
130
130
130
130
120
10
20
30
40
50
60
70
80
90
100
110
x 10 km

(c) Visual Range (km)

FIGURE G-29 (Concluded)

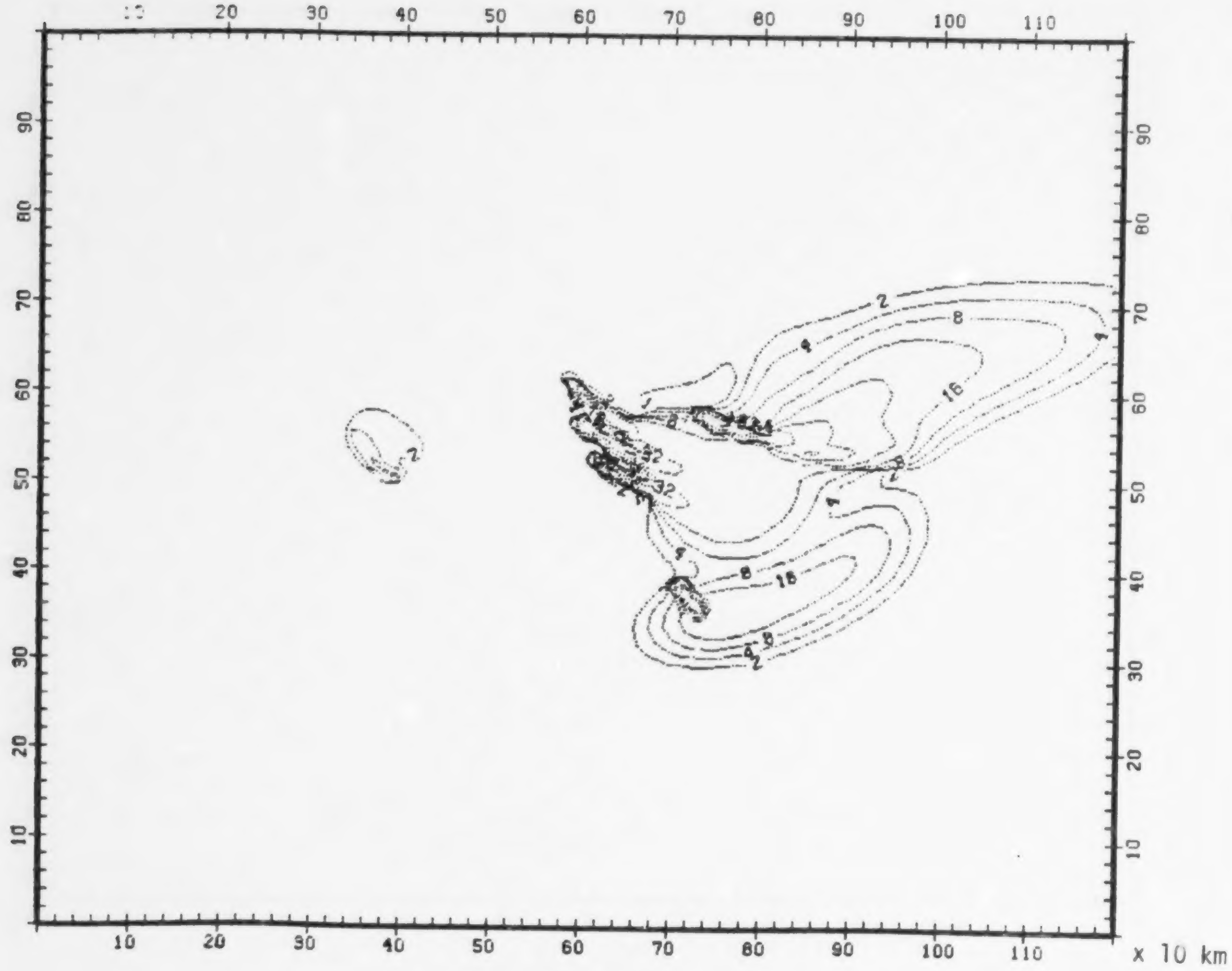
20
30
40
50
60
70
80
90
100
110
10
20
30
40
50
60
70
80
90
100
110
x 10 km
10
20
30
40
50
60
70
80
90
2
8
4
16
32
32
2
4
8
16
8
4
2

(a) SO_2 Concentrations ($\mu g/m^3$)

FIGURE G-30. HYPOTHETICAL COPPER SMELTER ISOPLETHS FOR 200-500 MST ON 5 APRIL 1976 ASSUMING 0.3 PERCENT PER HOUR SULFATE FORMATION

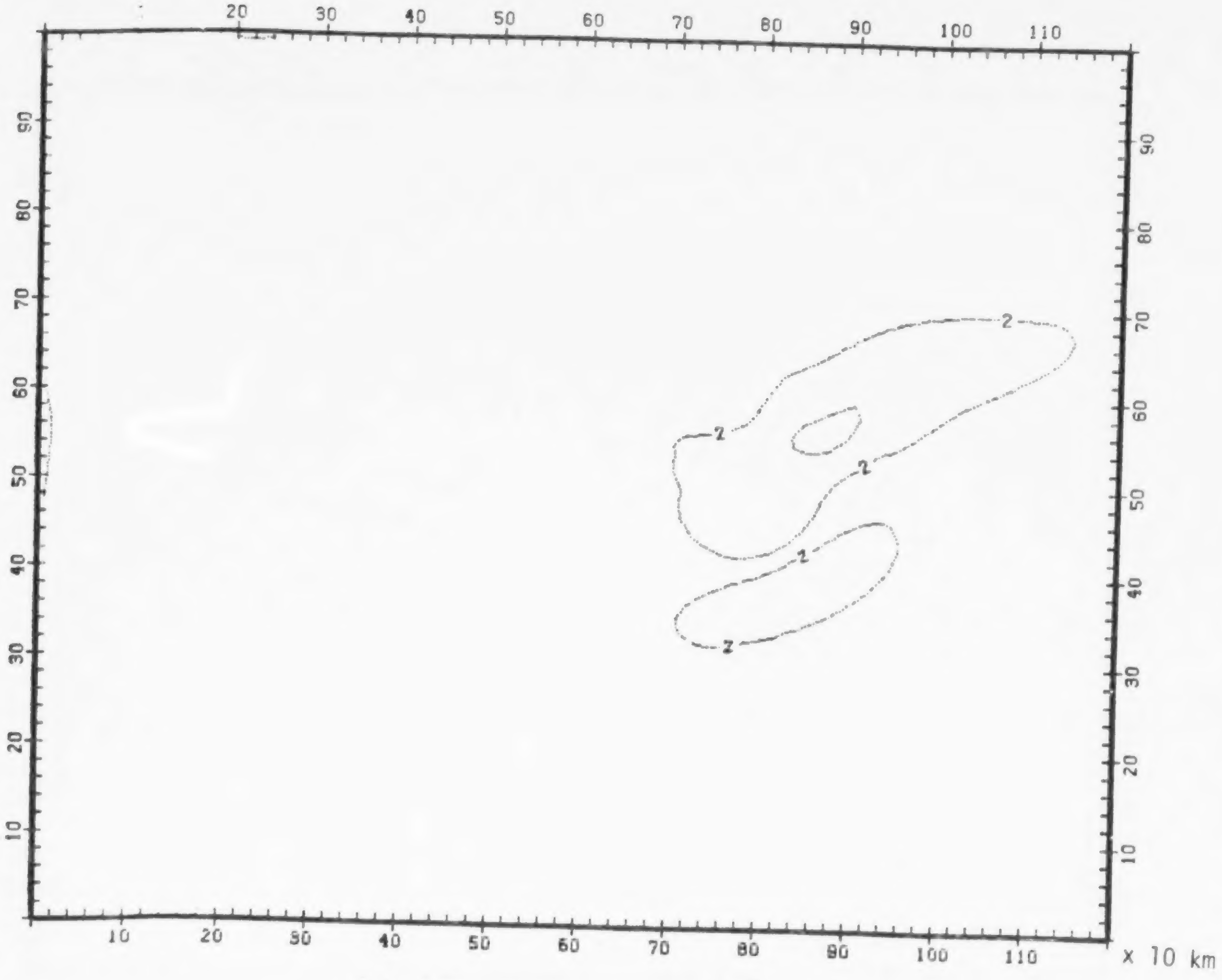
10
20
30
40
50
60
70
80
90
100
110
2
2
2
2
2
x 10 km

(b) $SO_4^=$ Concentrations ($\mu g/m^3$)

FIGURE G-30 (Continued)

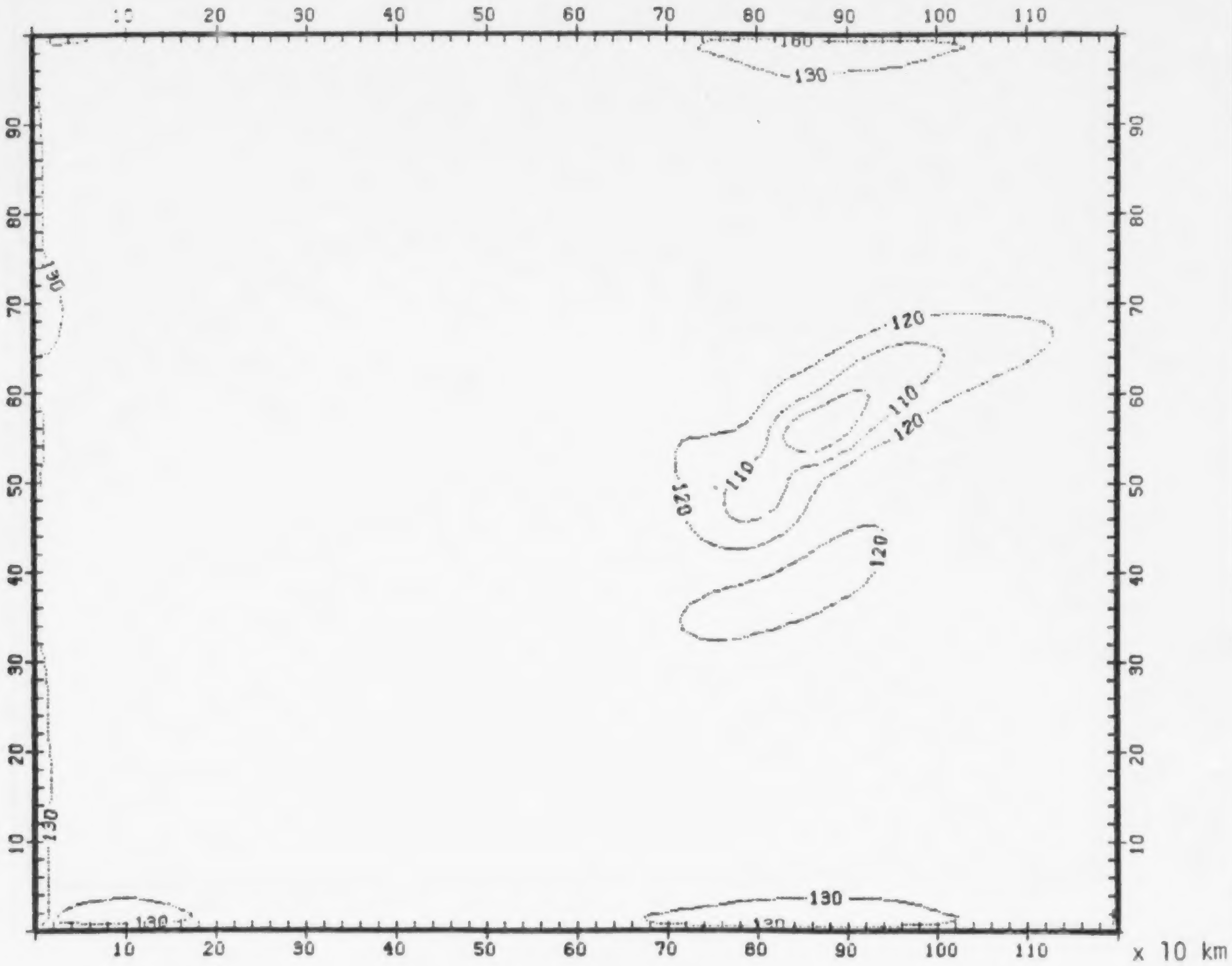

(c) Visual Range (km)

FIGURE G-30 (Concluded)

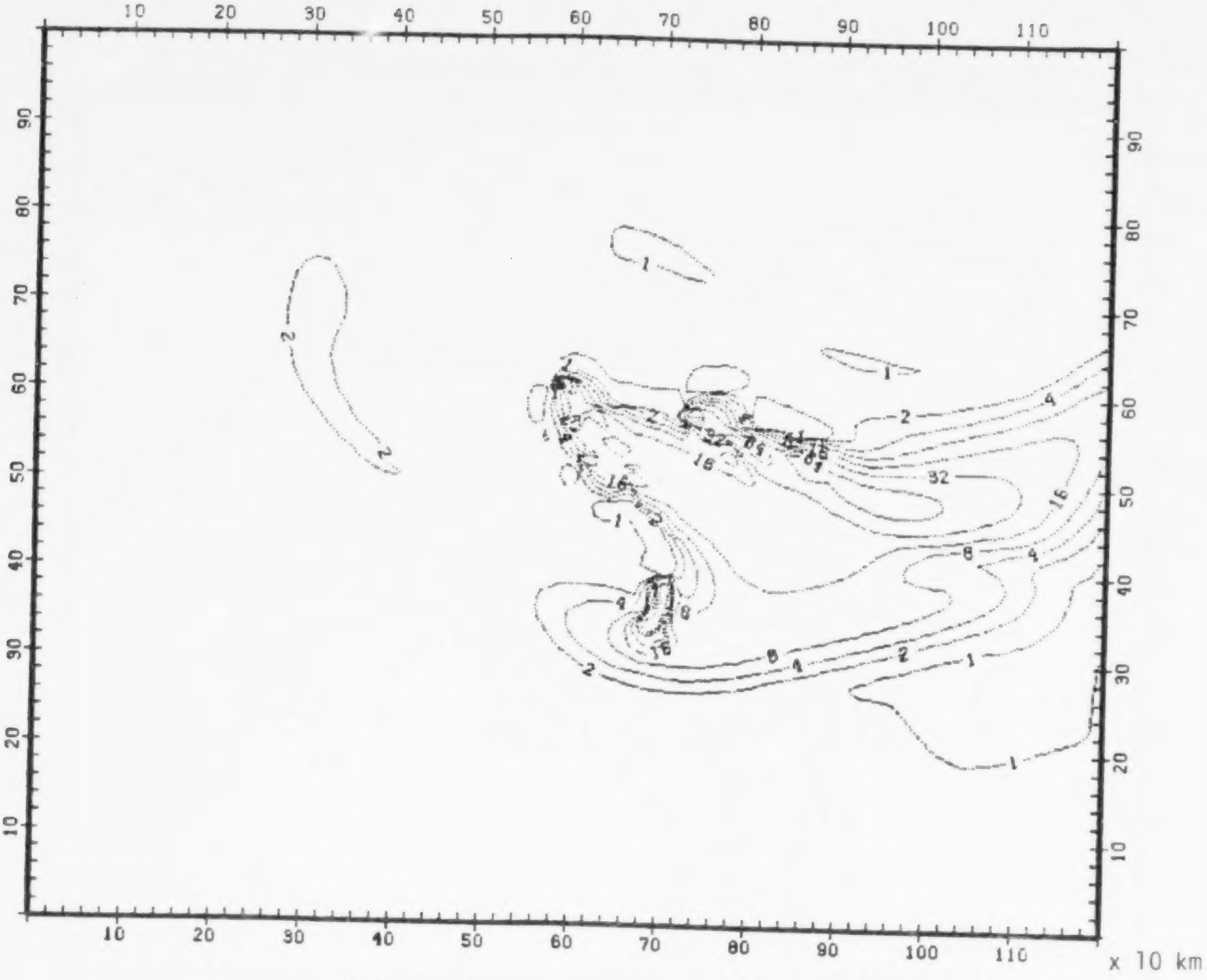
10
20
30
40
50
60
70
80
90
100
110
x 10 km
1
2
4
8
16
32
64

(a) SO_2 Concentrations ($\mu g/m^3$)

FIGURE G-31. HYPOTHETICAL COPPER SMELTER ISOPLETHS FOR 1100-1400 MST ON 5 APRIL 1976 ASSUMING 0.3 PERCENT PER HOUR SULFATE FORMATION

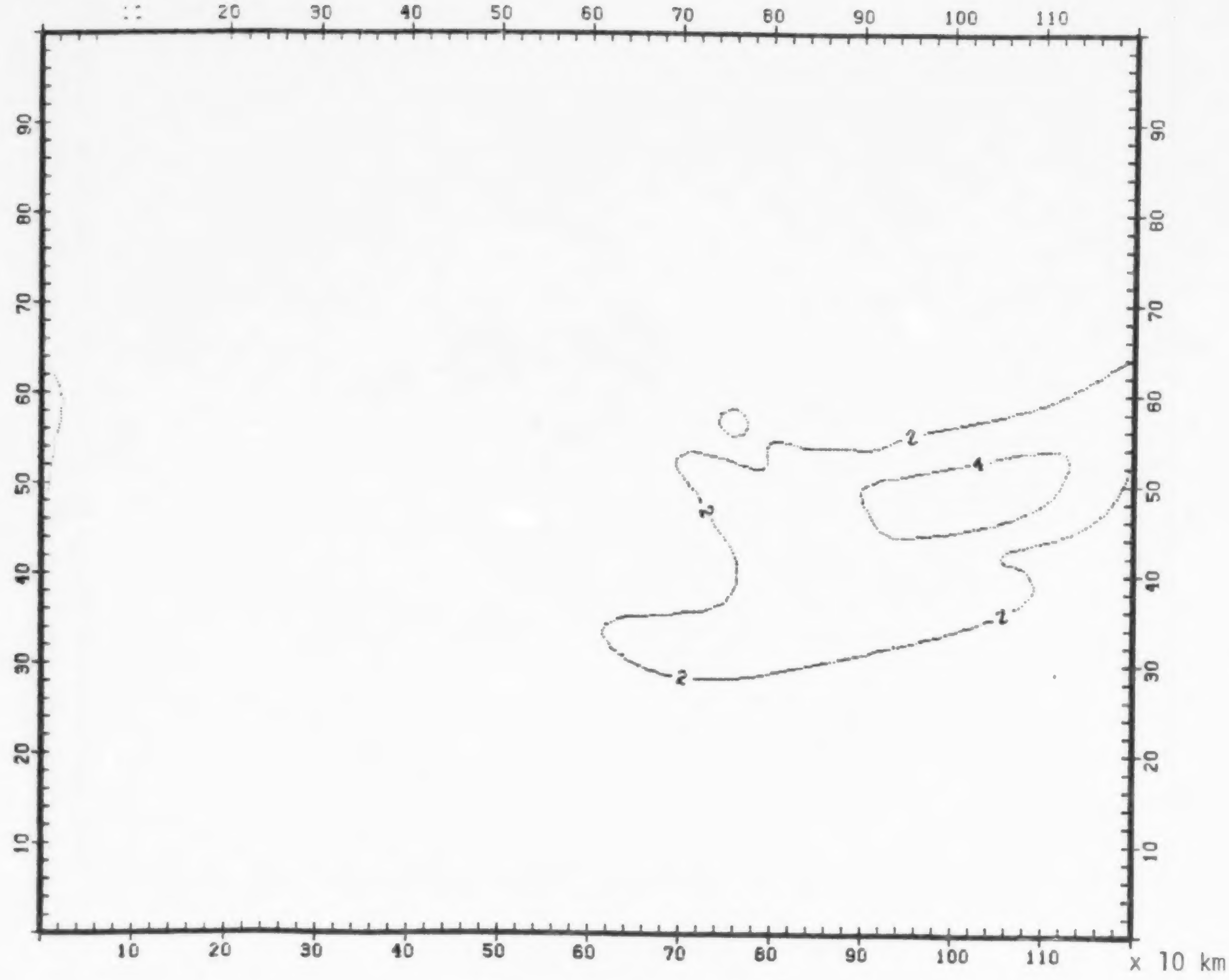
10
20
30
40
50
60
70
80
90
100
110
x 10 km
2
4
2
2
2

(b) $SO_4^=$ Concentrations ($\mu g/m^3$)

FIGURE G-31 (Continued)

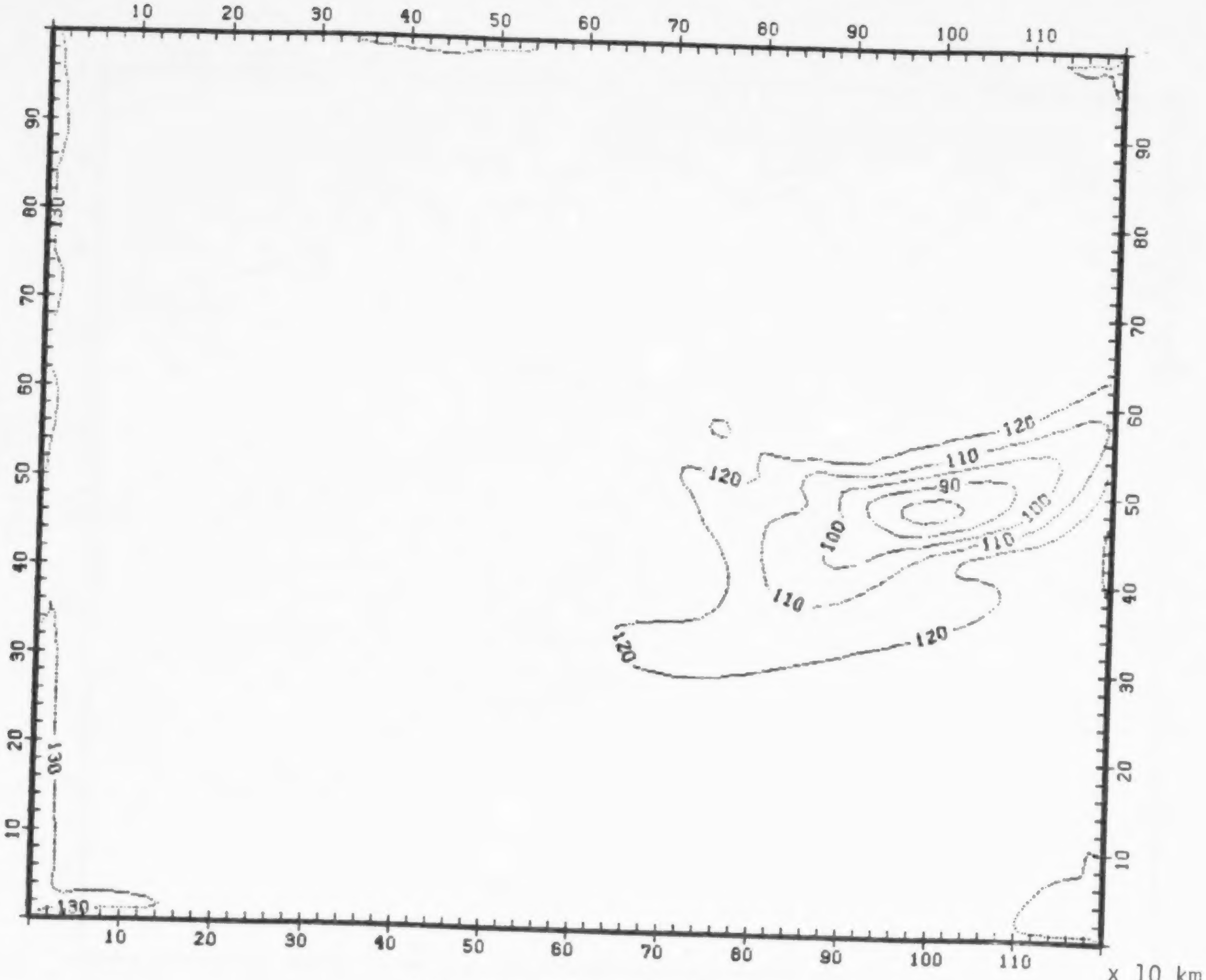

(c) Visual Range (km)

FIGURE G-31 (Concluded)

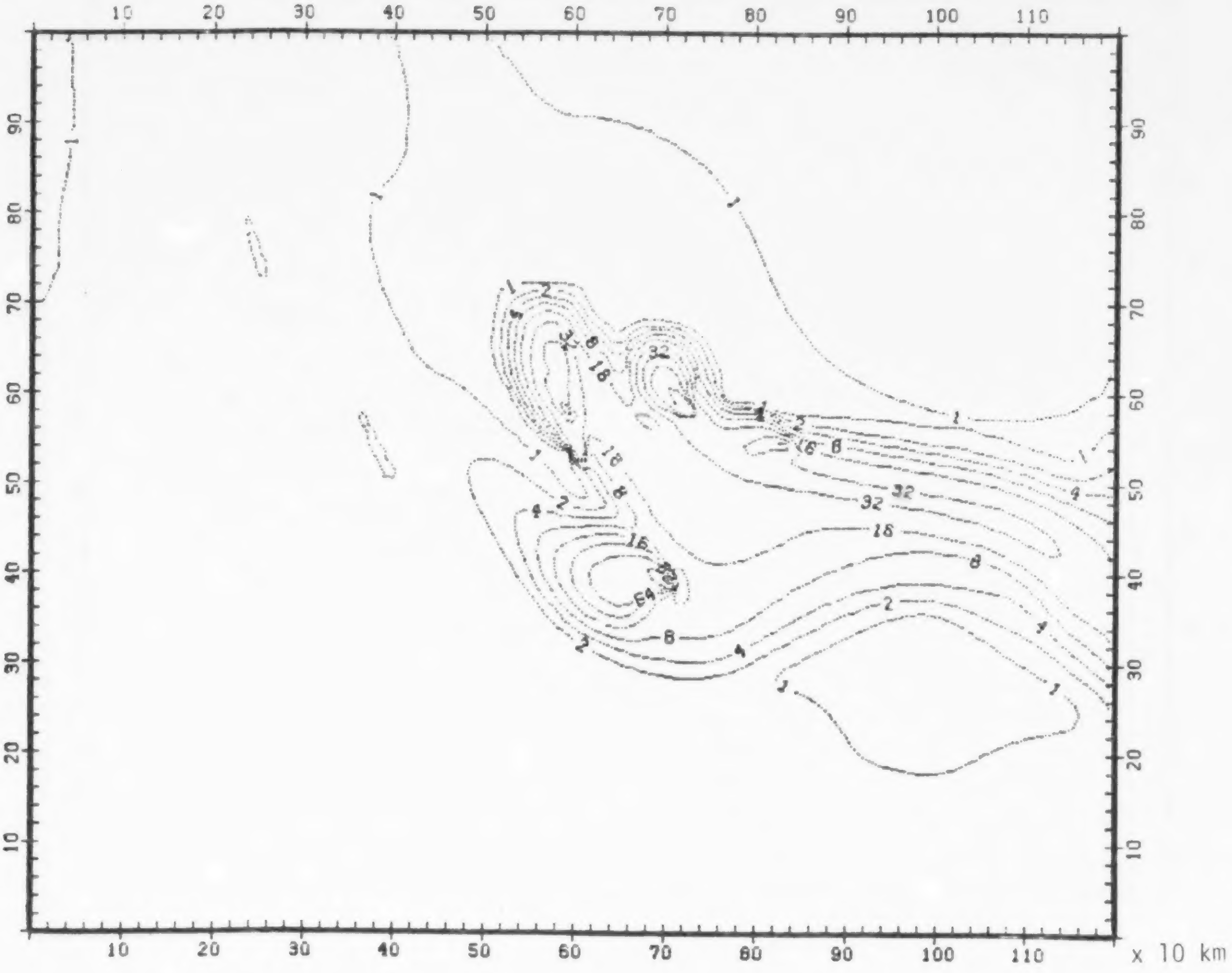
10
20
30
40
50
60
70
80
90
100
110
x 10 km
1
2
4
8
16
32
64

(a) SO_2 Concentrations ($\mu g/m^3$)

FIGURE G-32. HYPOTHETICAL COPPER SMELTER ISOPELTHS FOR 2000-2300 MST ON 5 APRIL 1976 ASSUMING 0.3 PERCENT PER HOUR SULFATE FORMATION

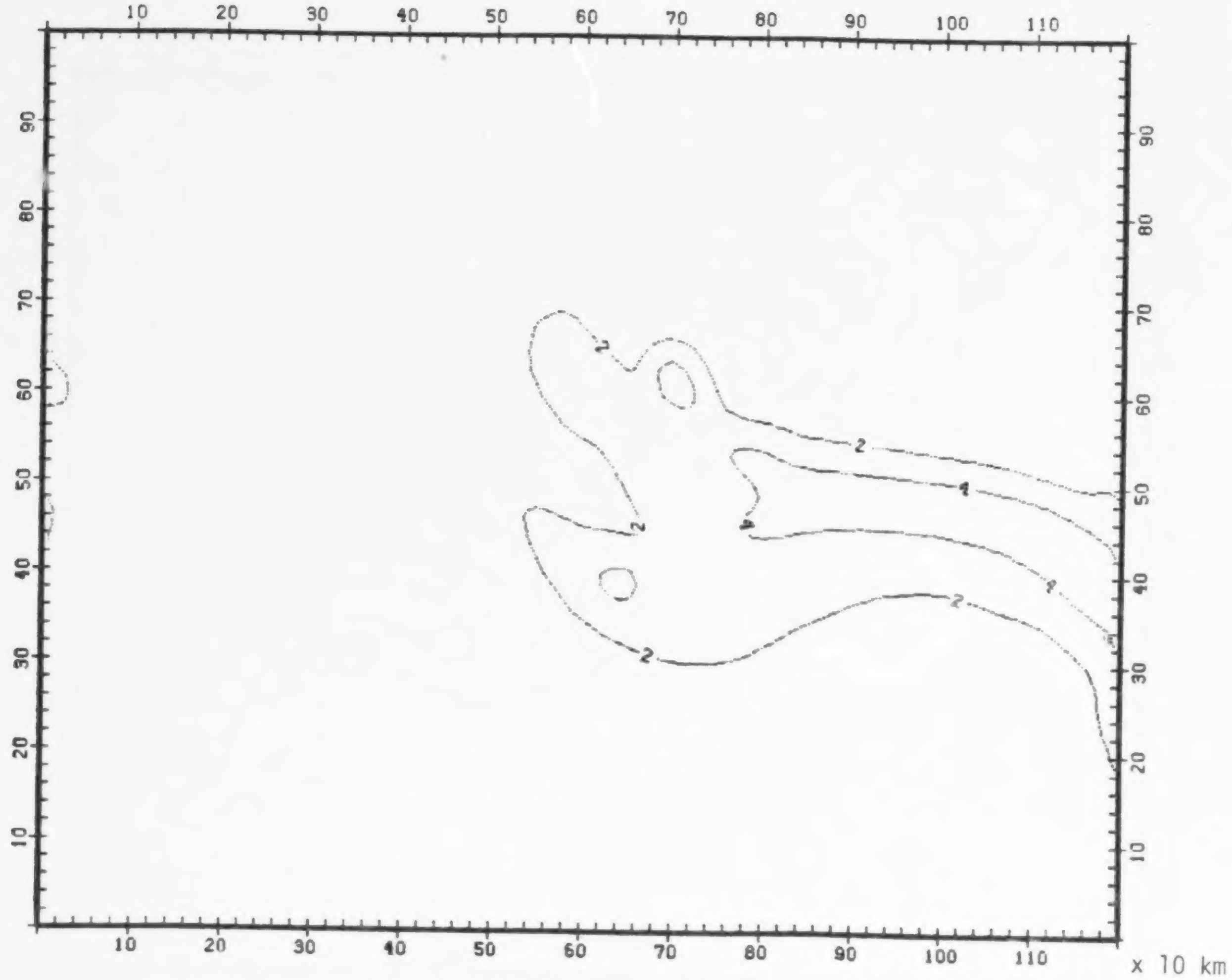
10
20
30
40
50
60
70
80
90
100
110
2
4
x 10 km

(b) $SO_4^=$ Concentrations ($\mu g/m^3$)

FIGURE G-32 (Continued)

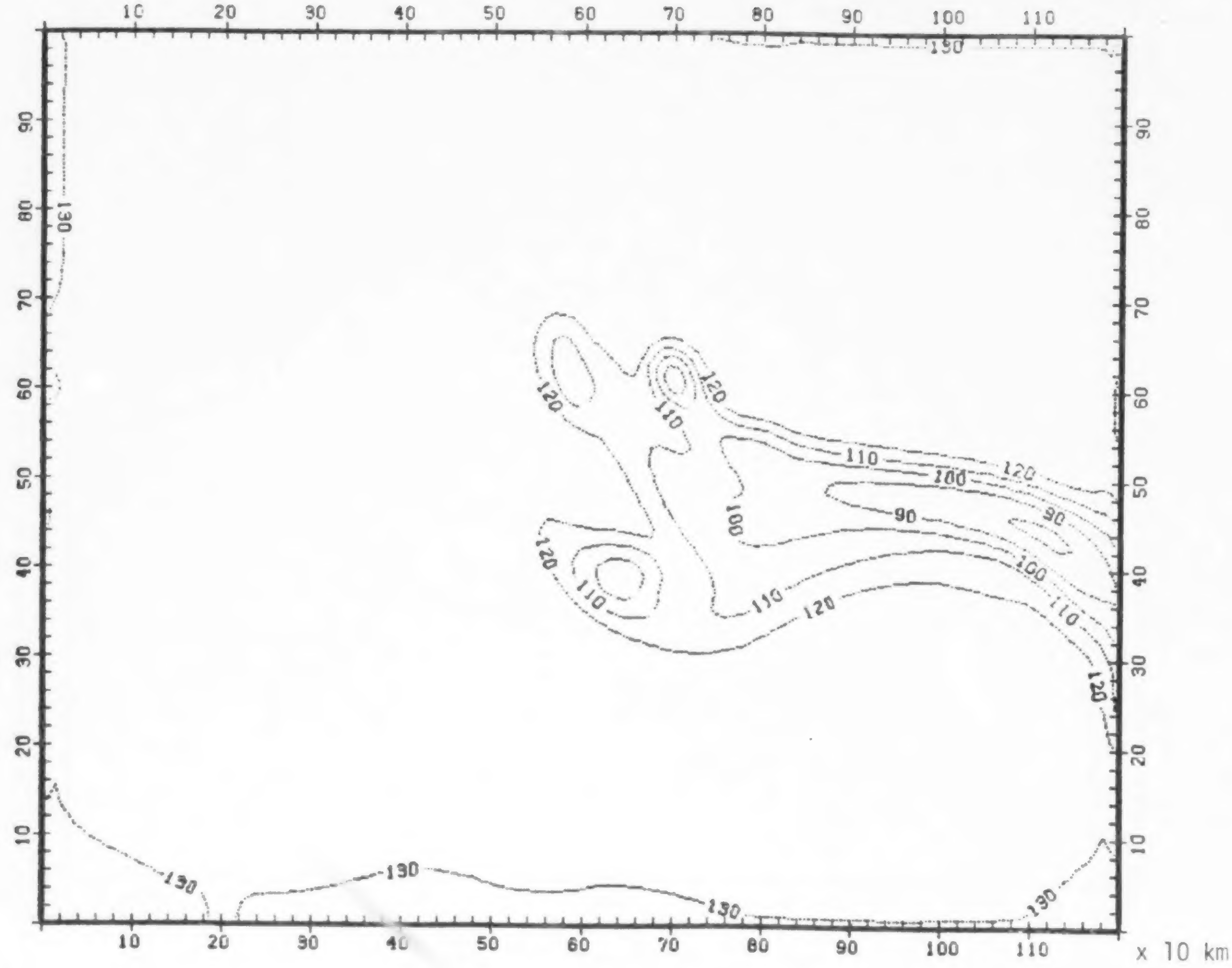
10
20
30
40
50
60
70
80
90
100
110
x 10 km
130
120
110
100
90

(c) Visual Range (km)

FIGURE G-32 (Concluded)

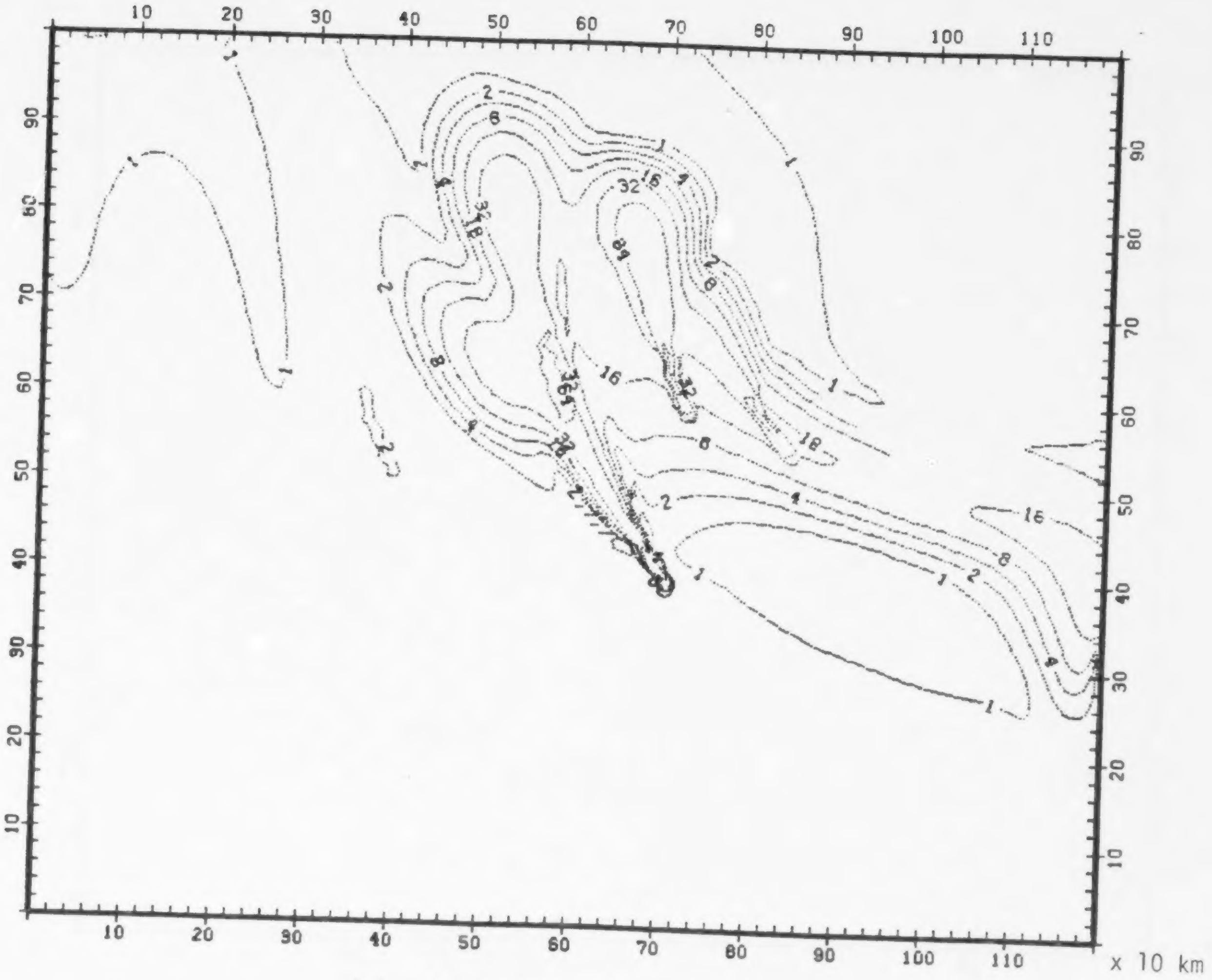
10
20
30
40
50
60
70
80
90
100
110
x 10 km
1
2
4
8
16
32
64

(a) SO_2 Concentrations ($\mu g/m^3$)

FIGURE G-33. HYPOTHETICAL COPPER SMELTER ISOPLETHS FOR 500-800 MST ON 6 APRIL 1976 ASSUMING 0.3 PERCENT PER HOUR SULFATE FORMATION

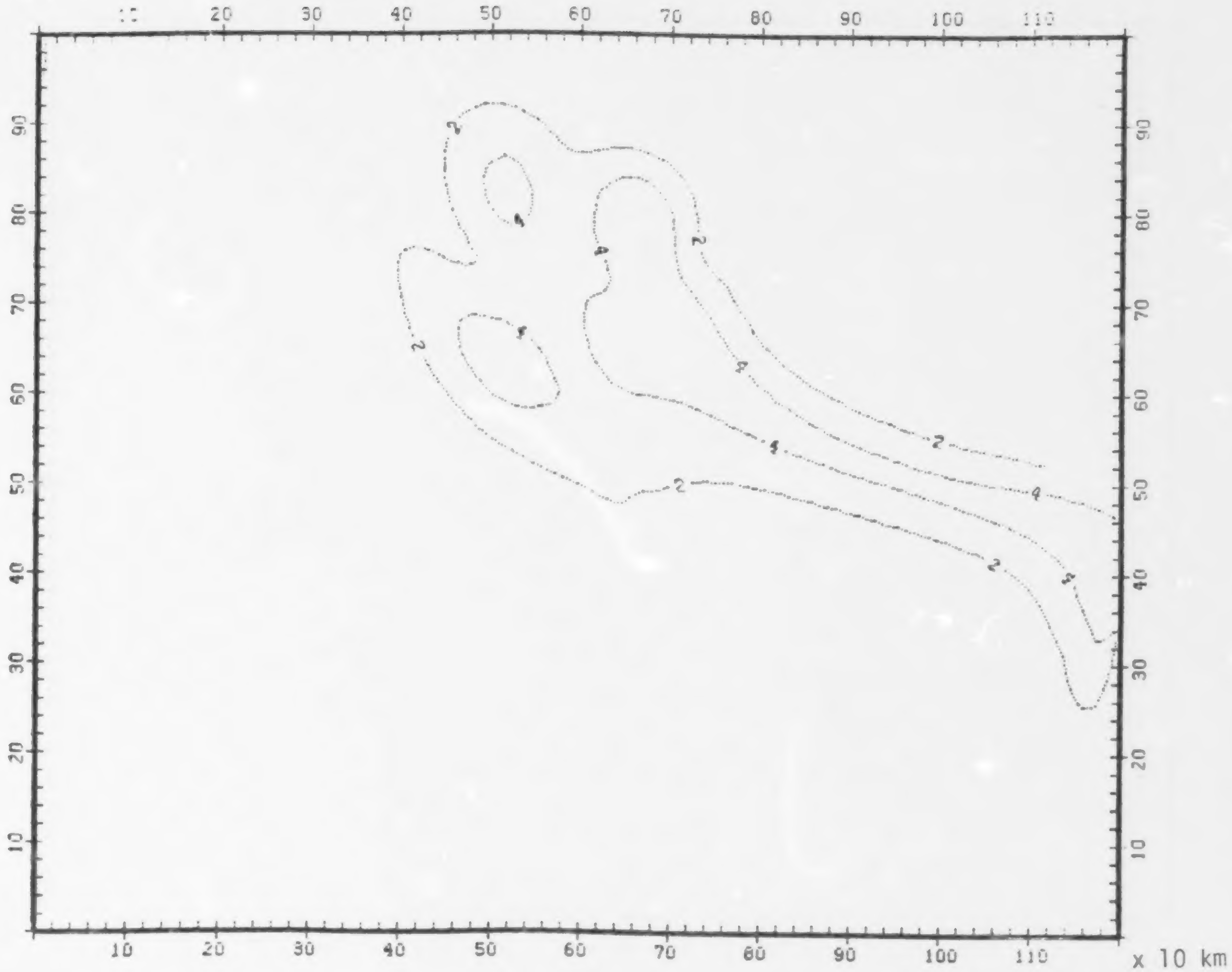

(b) $SO_4^=$ Concentrations ($\mu g/m^3$)

FIGURE G-33 (Continued)

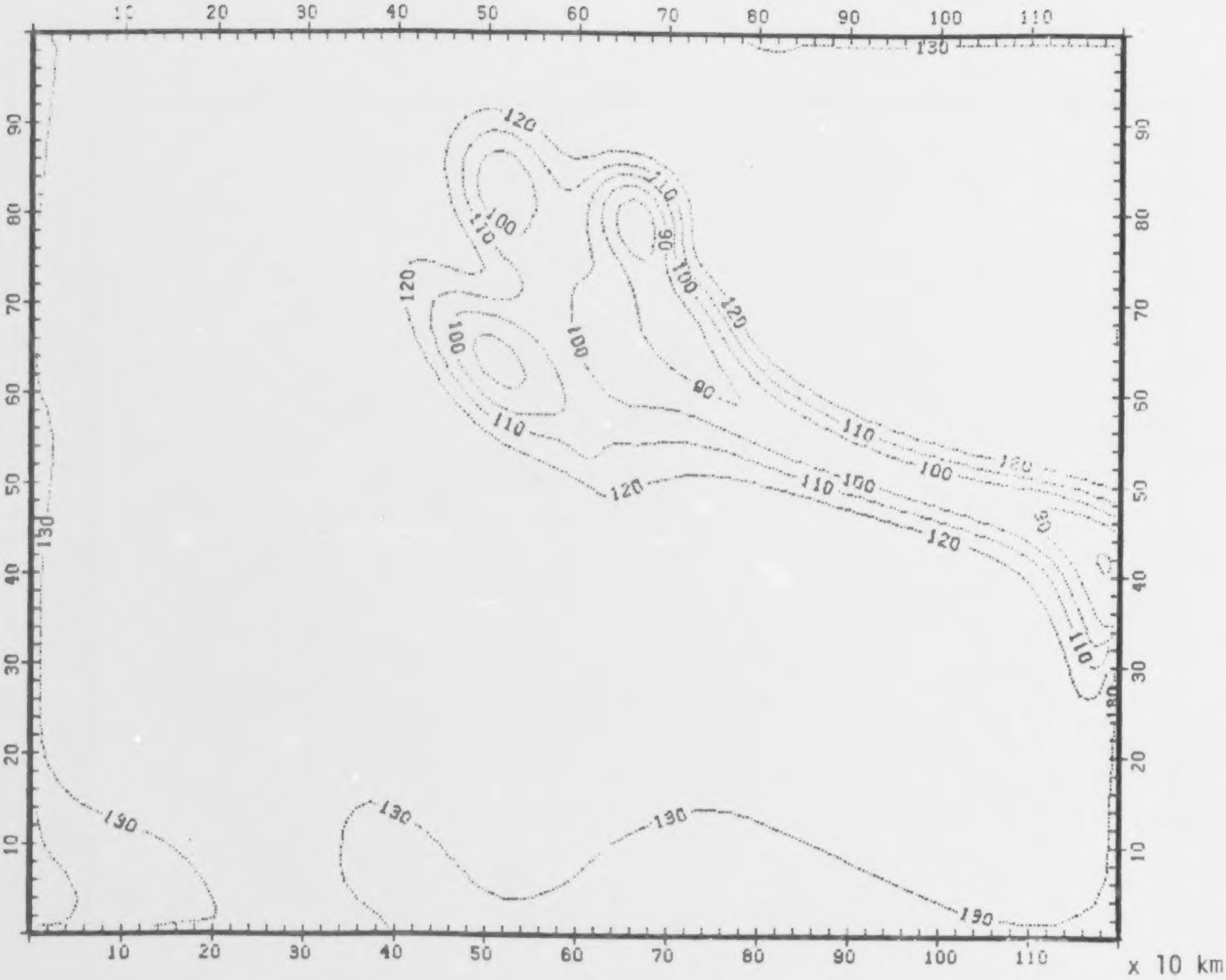
10
20
30
40
50
60
70
80
90
100
110
130
120
110
100
90
130
x 10 km

(c) Visual Range (km)

FIGURE G-33 (Concluded)

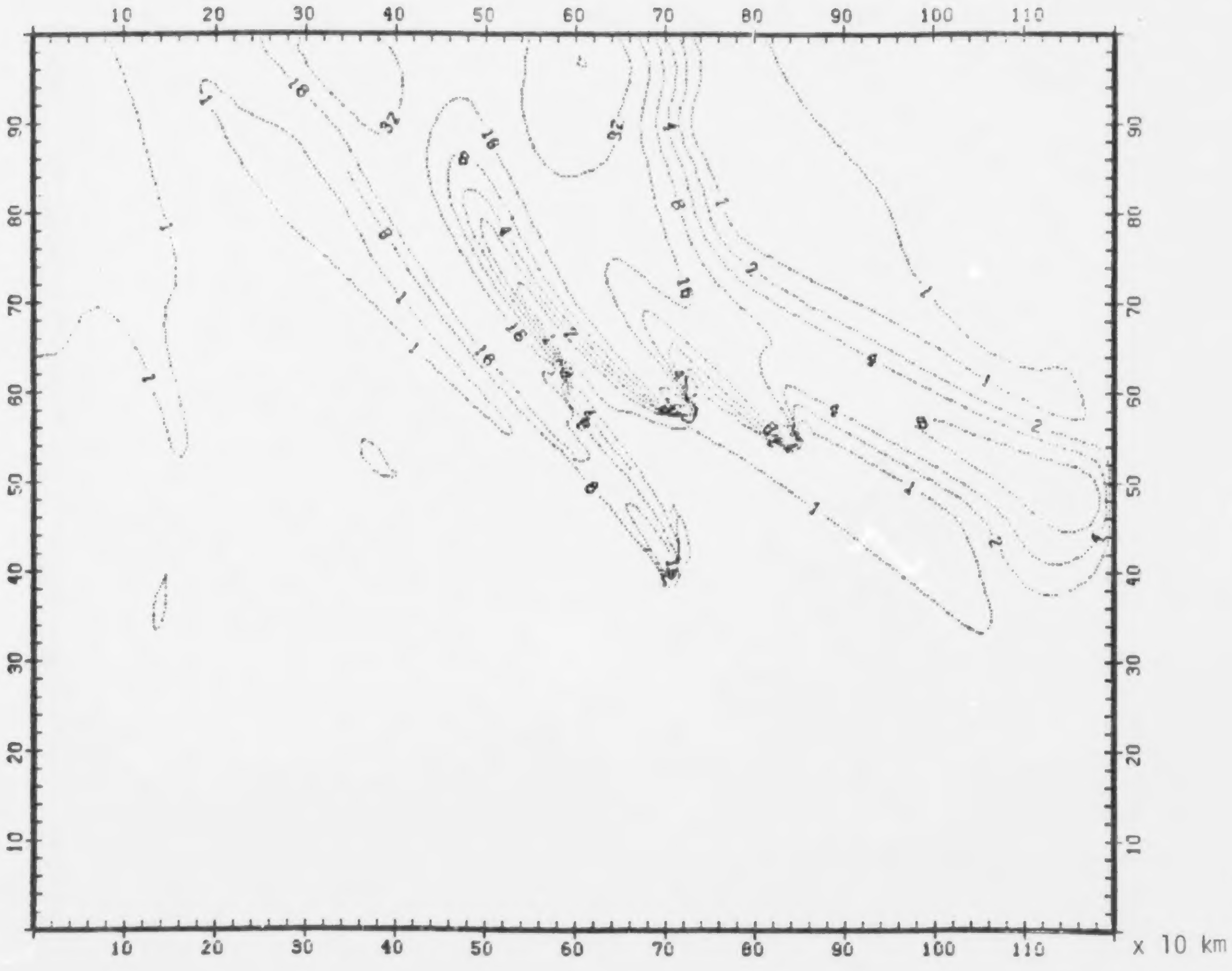

(a) SO_2 Concentrations ($\mu g/m^3$)

FIGURE G-34. HYPOTHETICAL COPPER SMELTER ISOPLETHS FOR 1400-1700 MST ON 6 APRIL 1976 ASSUMING 0.3 PERCENT PER HOUR SULFATE FORMATION

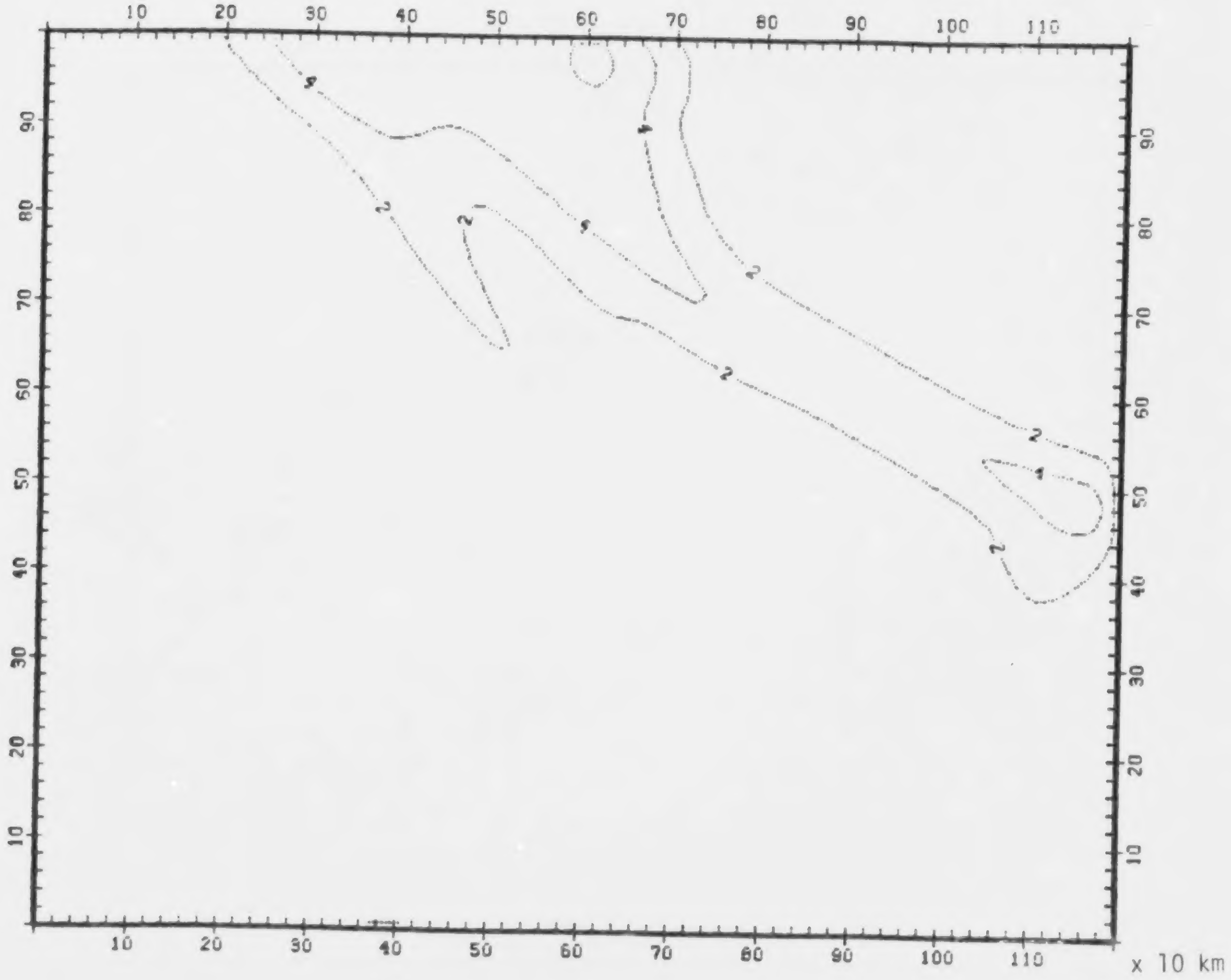
10
20
30
40
50
60
70
80
90
100
110
x 10 km
1
2

(b) $SO_4^=$ Concentrations ($\mu g/m^3$)

FIGURE G-34 (Continued)

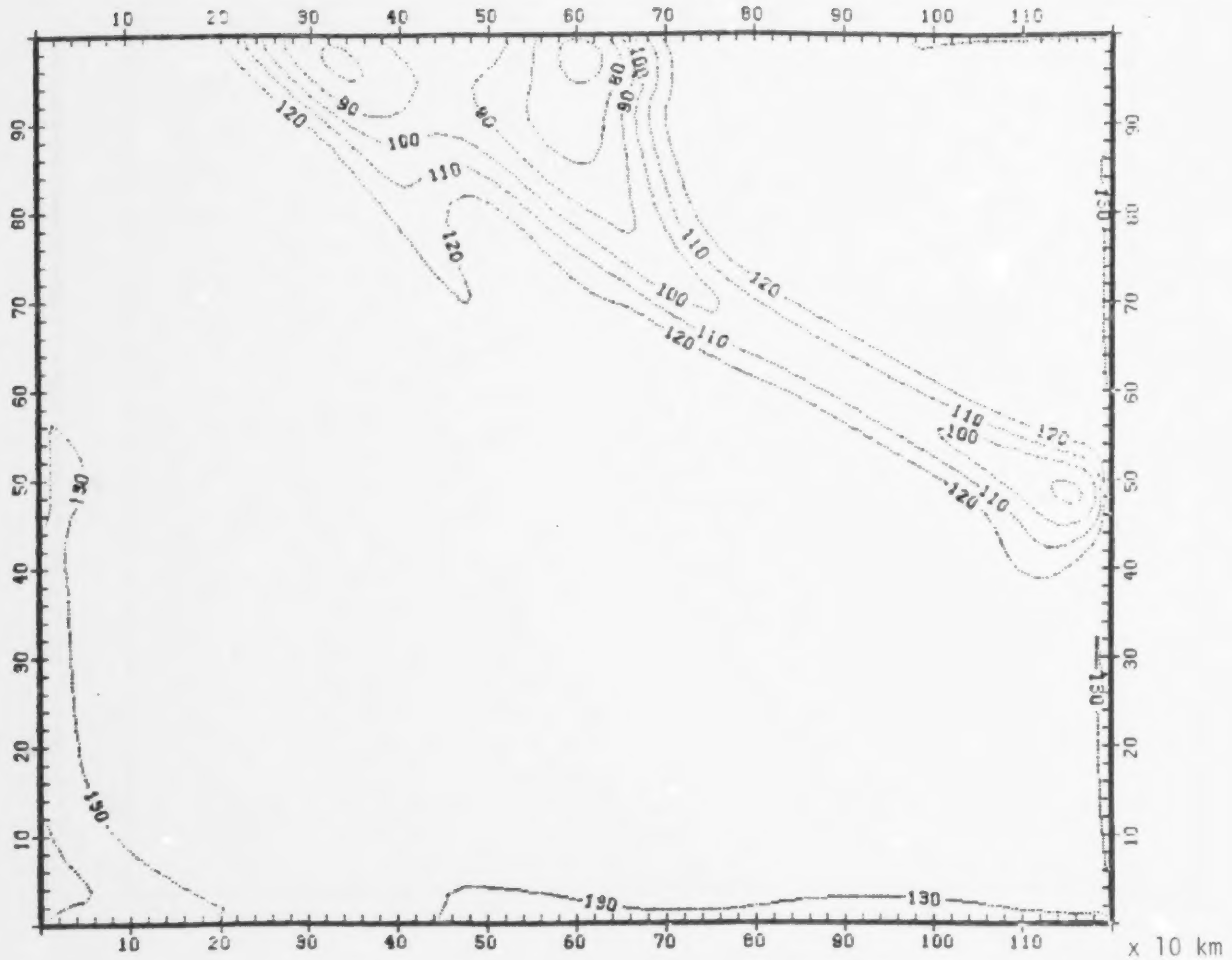
10
20
30
40
50
60
70
80
90
100
110
x 10 km
80
90
100
110
120
130

(c) Visual Range (km)

FIGURE G-34 (Concluded)

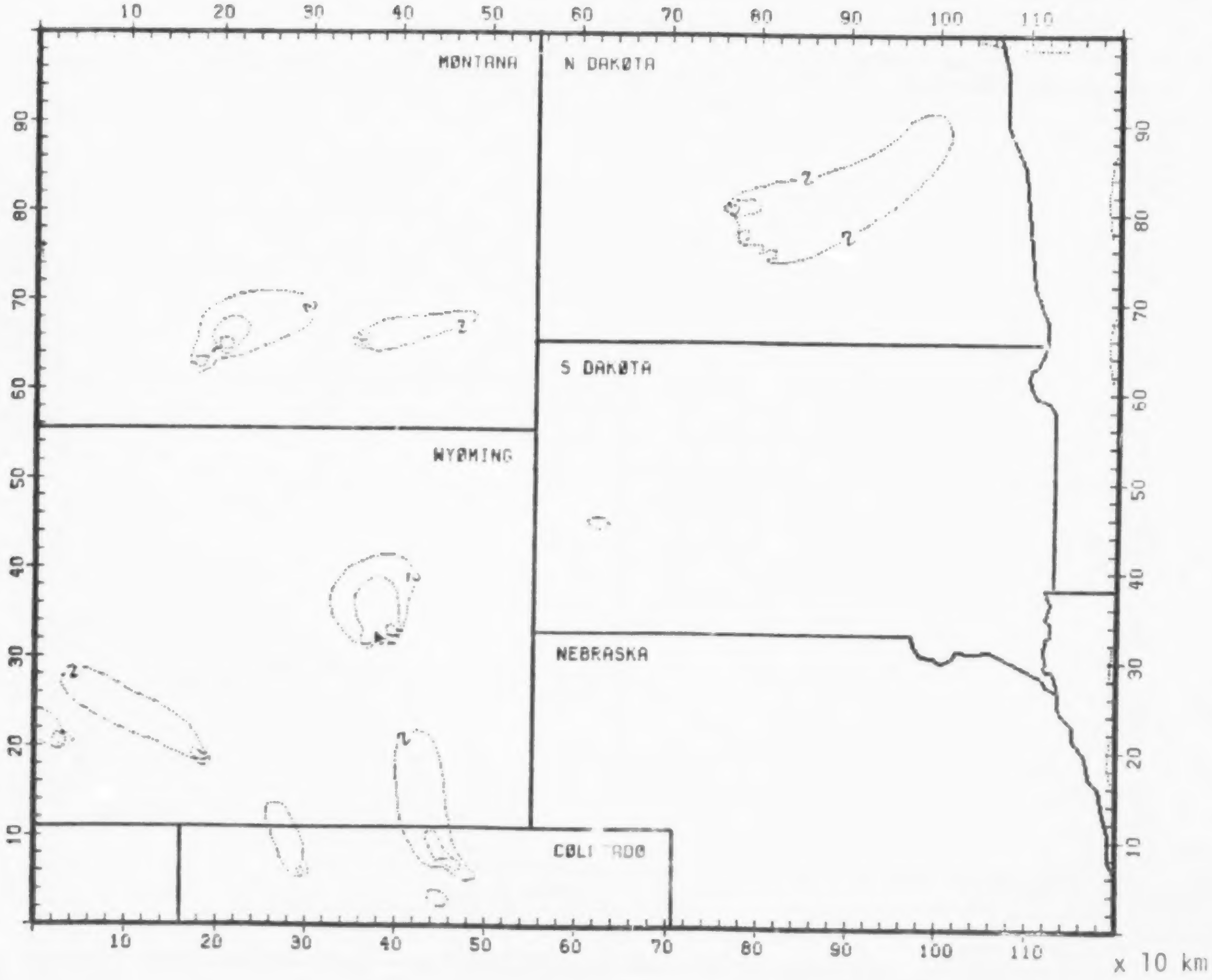
MONTANA
N DAKOTA
S DAKOTA
WYOMING
NEBRASKA
COLORADO
2
x 10 km
10
20
30
40
50
60
70
80
90
100
110

(a) SO_2 Concentrations ($\mu g/m^3$)

FIGURE G-35. 1975 NORTHERN GREAT PLAINS ISOPLETHS FOR 1700-2000 MST ON 4 APRIL 1976 ASSUMING 0.5 PERCENT PER HOUR SULFATE FORMATION

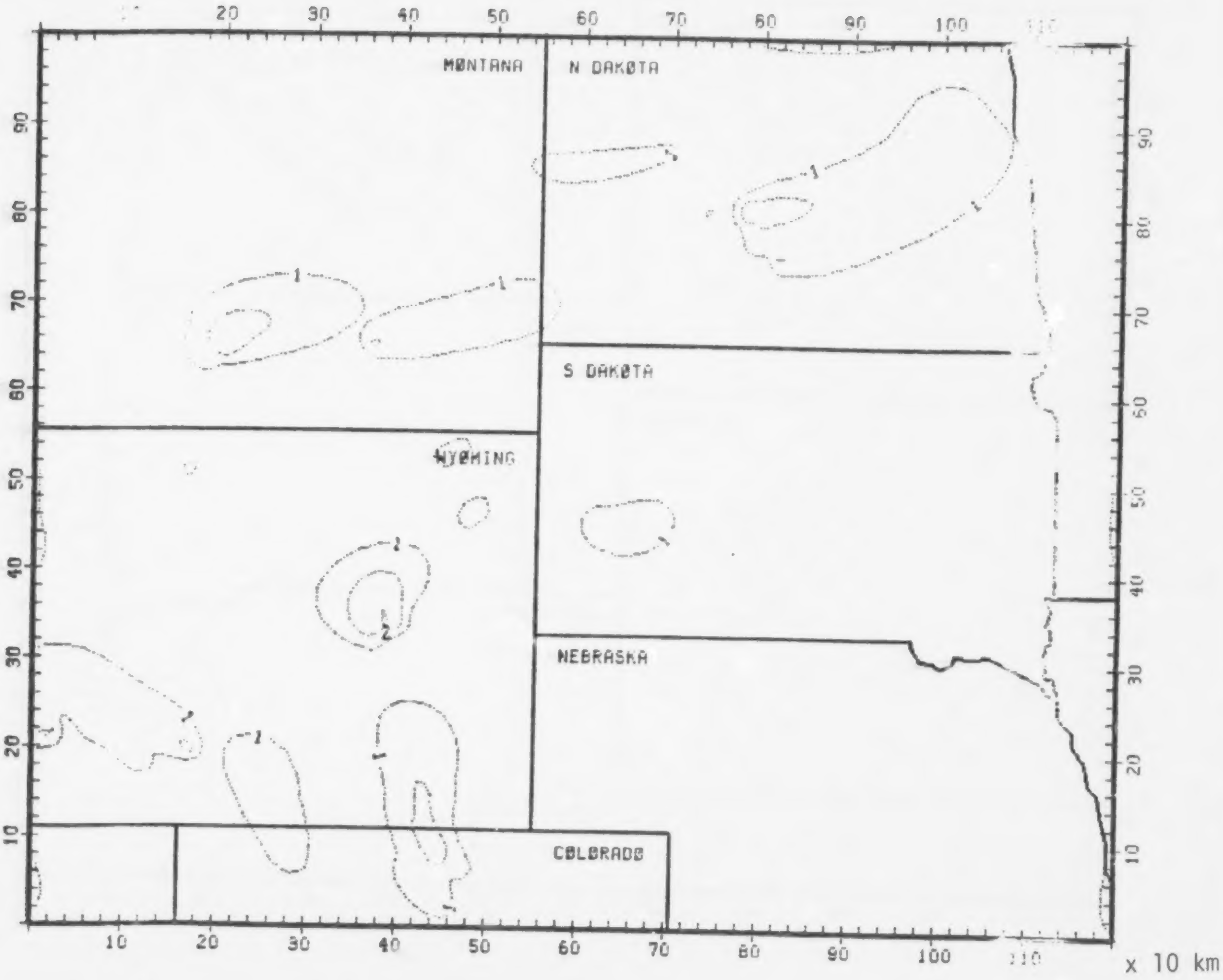
MONTANA
N DAKOTA
S DAKOTA
WYOMING
NEBRASKA
COLORADO
1
2
10
20
30
40
50
60
70
80
90
100
110
x 10 km

(b) NO_2 Concentrations (ppb)

FIGURE G-35 (Continued)

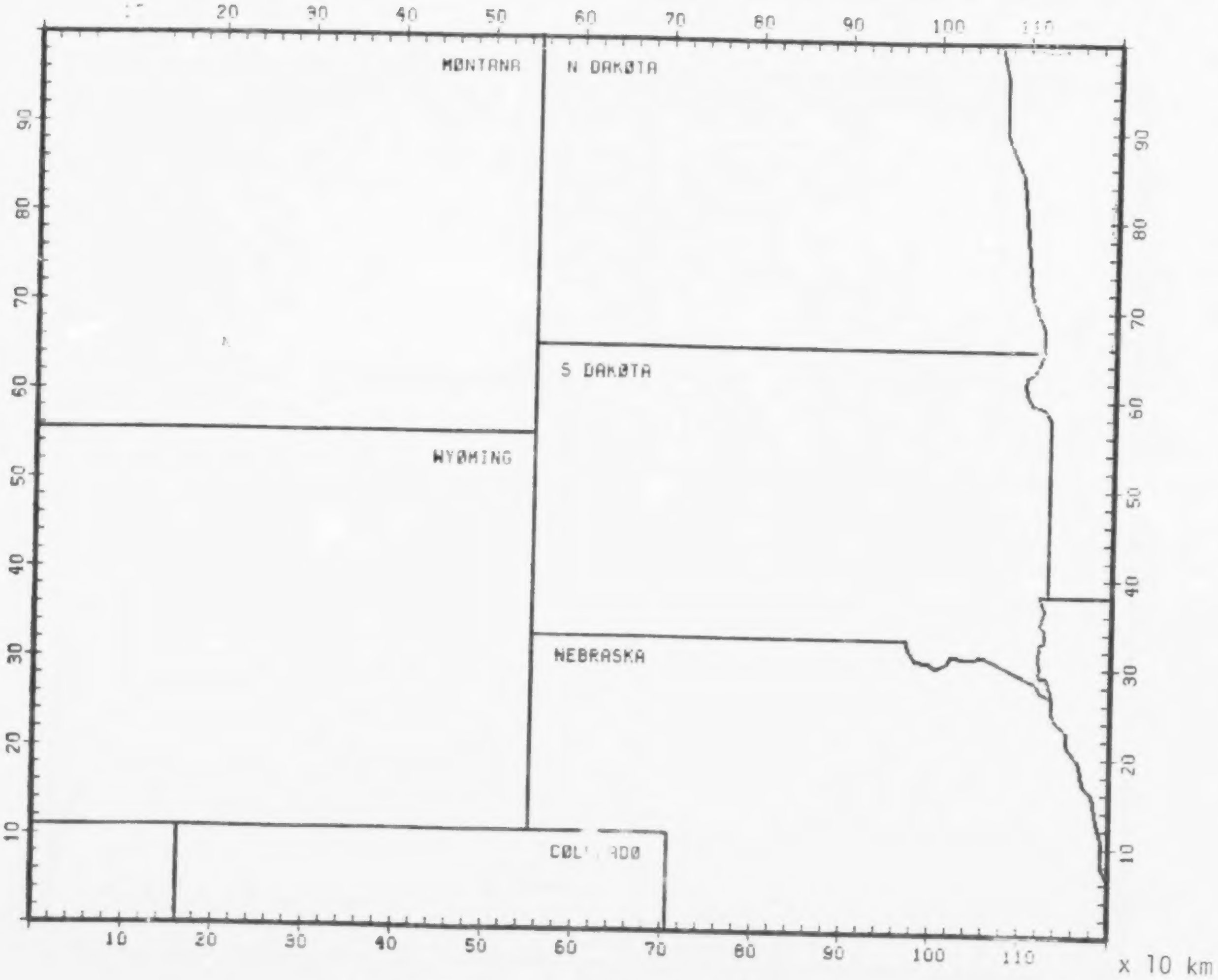
MONTANA
N DAKOTA
S DAKOTA
WYOMING
NEBRASKA
COLORADO
10
20
30
40
50
60
70
80
90
100
110
x 10 km

(c) $SO_4^=$ Concentrations ($\mu g/m^3$)

FIGURE G-35 (Continued)

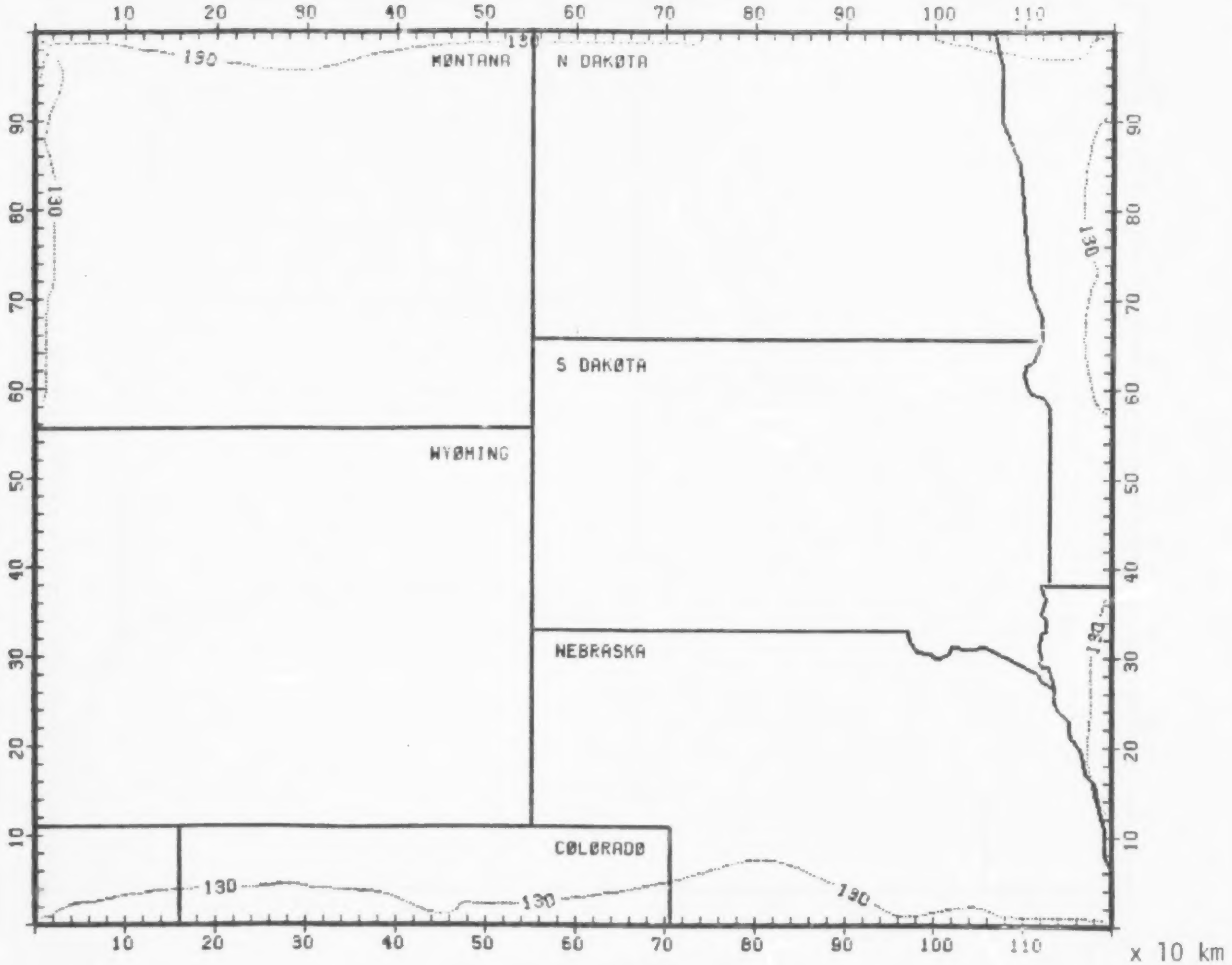
MONTANA
N DAKOTA
S DAKOTA
WYOMING
NEBRASKA
COLORADO
130
x 10 km
10
20
30
40
50
60
70
80
90
100
110

(d) Visual Range (km)

FIGURE G-35 (Concluded)

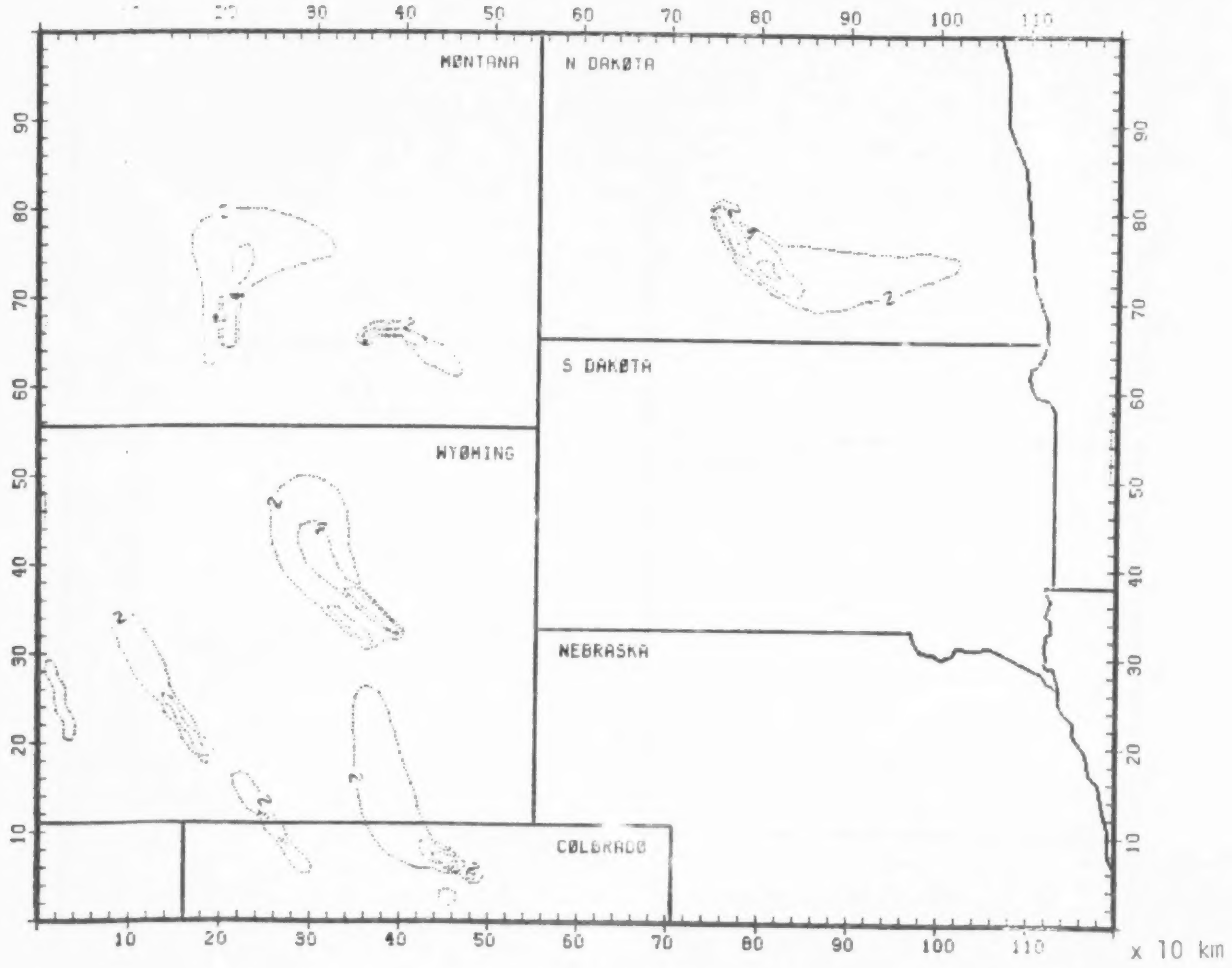
MONTANA
N DAKOTA
S DAKOTA
WYOMING
NEBRASKA
COLORADO
2
10
20
30
40
50
60
70
80
90
100
110
x 10 km

(a) SO_2 Concentrations ($\mu g/m^3$)

FIGURE G-36. 1975 NORTHERN GREAT PLAINS ISOPLETHS FOR 200-500 MST ON 5 APRIL 1976 ASSUMING 0.5 PERCENT PER HOUR SULFATE FORMATION

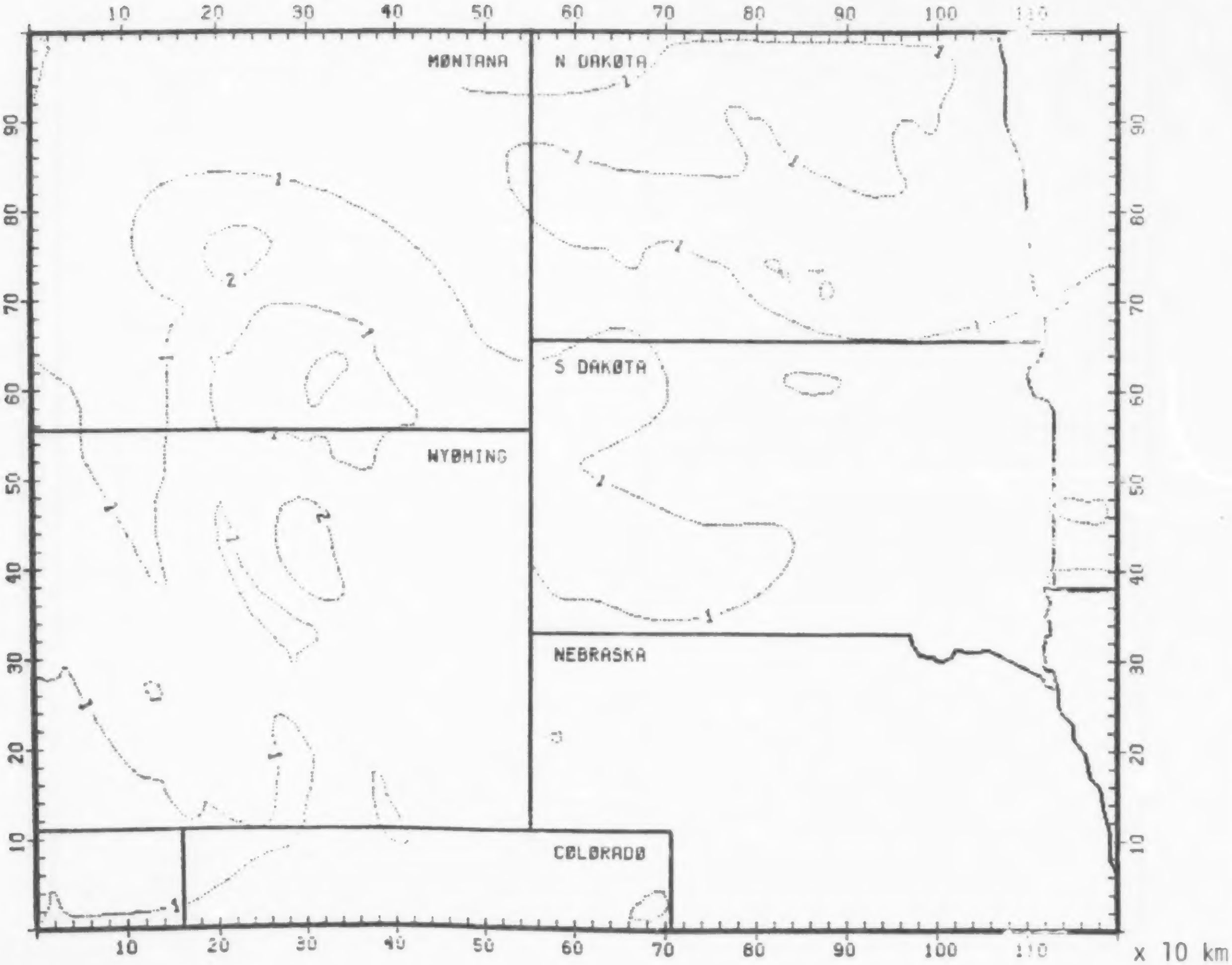
MONTANA
N DAKOTA
S DAKOTA
WYOMING
NEBRASKA
COLORADO
1
2
10
20
30
40
50
60
70
80
90
100
110
x 10 km

(b) NO$_2$ Concentrations (ppb)

FIGURE G-36 (Continued)

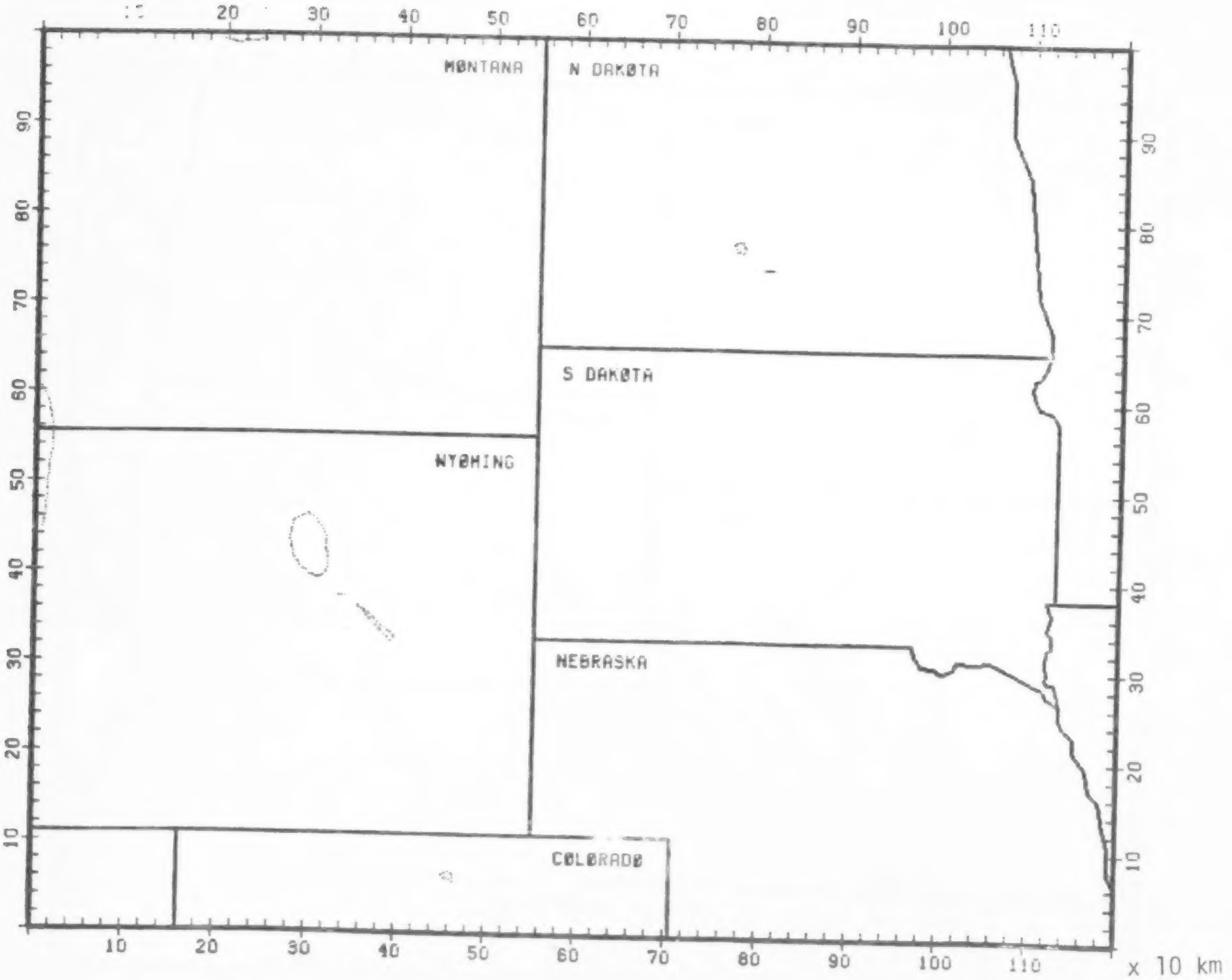
MONTANA
N DAKOTA
S DAKOTA
WYOMING
NEBRASKA
COLORADO
10
20
30
40
50
60
70
80
90
100
110
x 10 km

(c) $SO_4^=$ Concentrations ($\mu g/m^3$)

FIGURE G-36 (Continued)

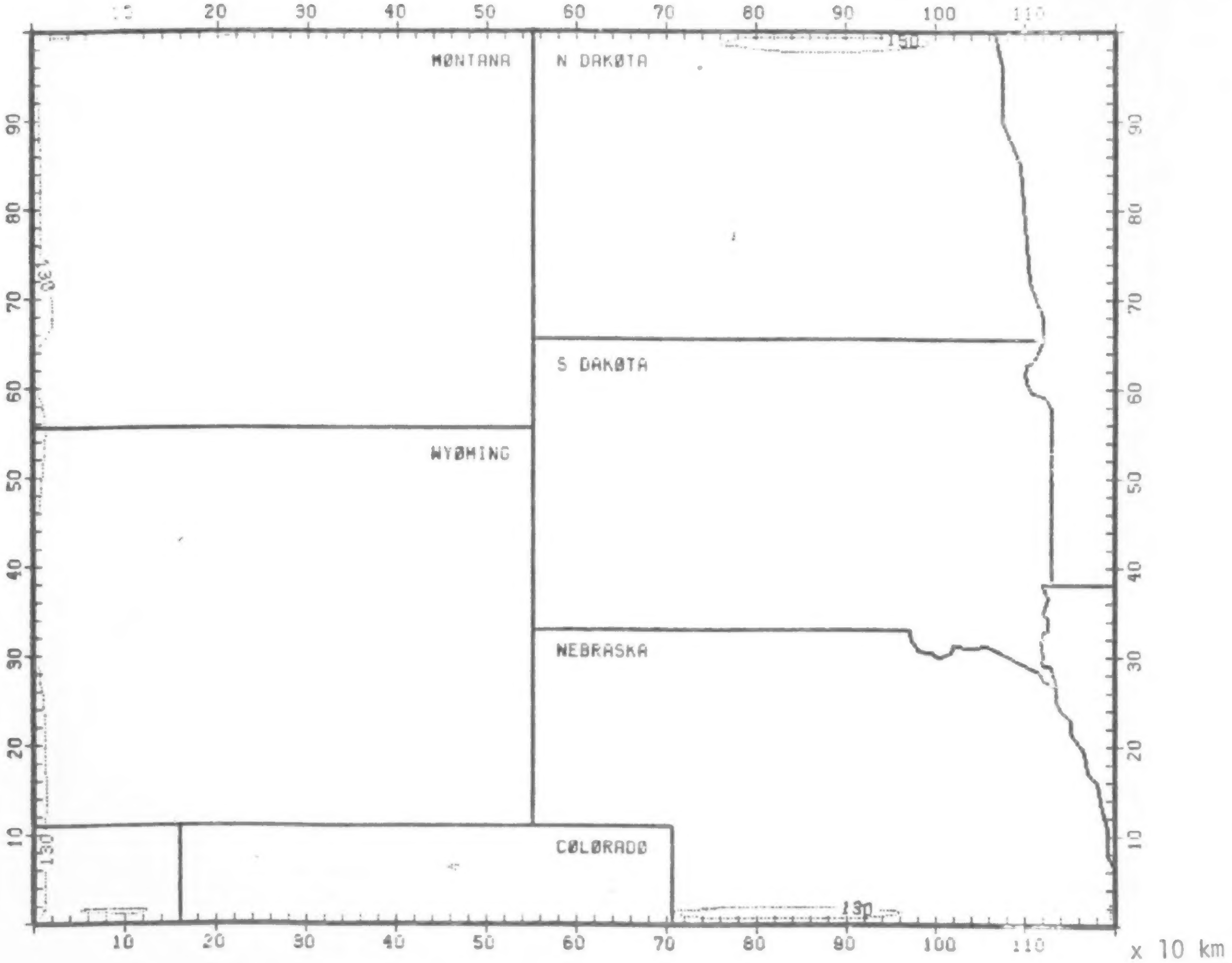
MONTANA
N DAKOTA
S DAKOTA
WYOMING
NEBRASKA
COLORADO
150
130
130
130
10
20
30
40
50
60
70
80
90
100
110
x 10 km

(d) Visual Range (km)

FIGURE G-36 (Concluded)

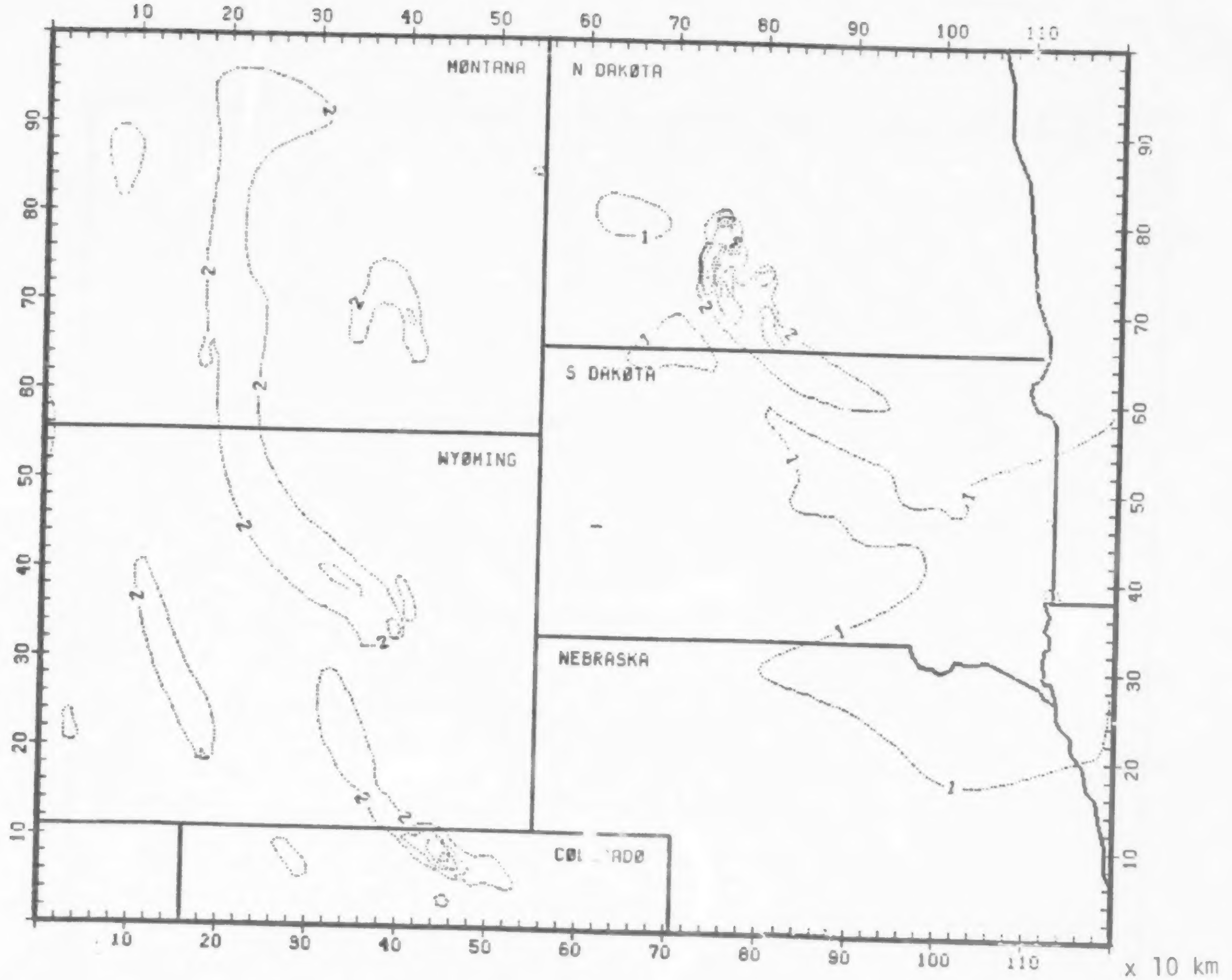
MONTANA
N DAKOTA
S DAKOTA
WYOMING
NEBRASKA
COLORADO
2
1
x 10 km
10
20
30
40
50
60
70
80
90
100
110

(a) SO_2 Concentrations ($\mu g/m^3$)

FIGURE G-37. 1975 NORTHERN GREAT PLAINS ISOPLETHS FOR 1100-1400 MST ON 5 APRIL 1976 ASSUMING 0.5 PERCENT PER HOUR SULFATE FORMATION

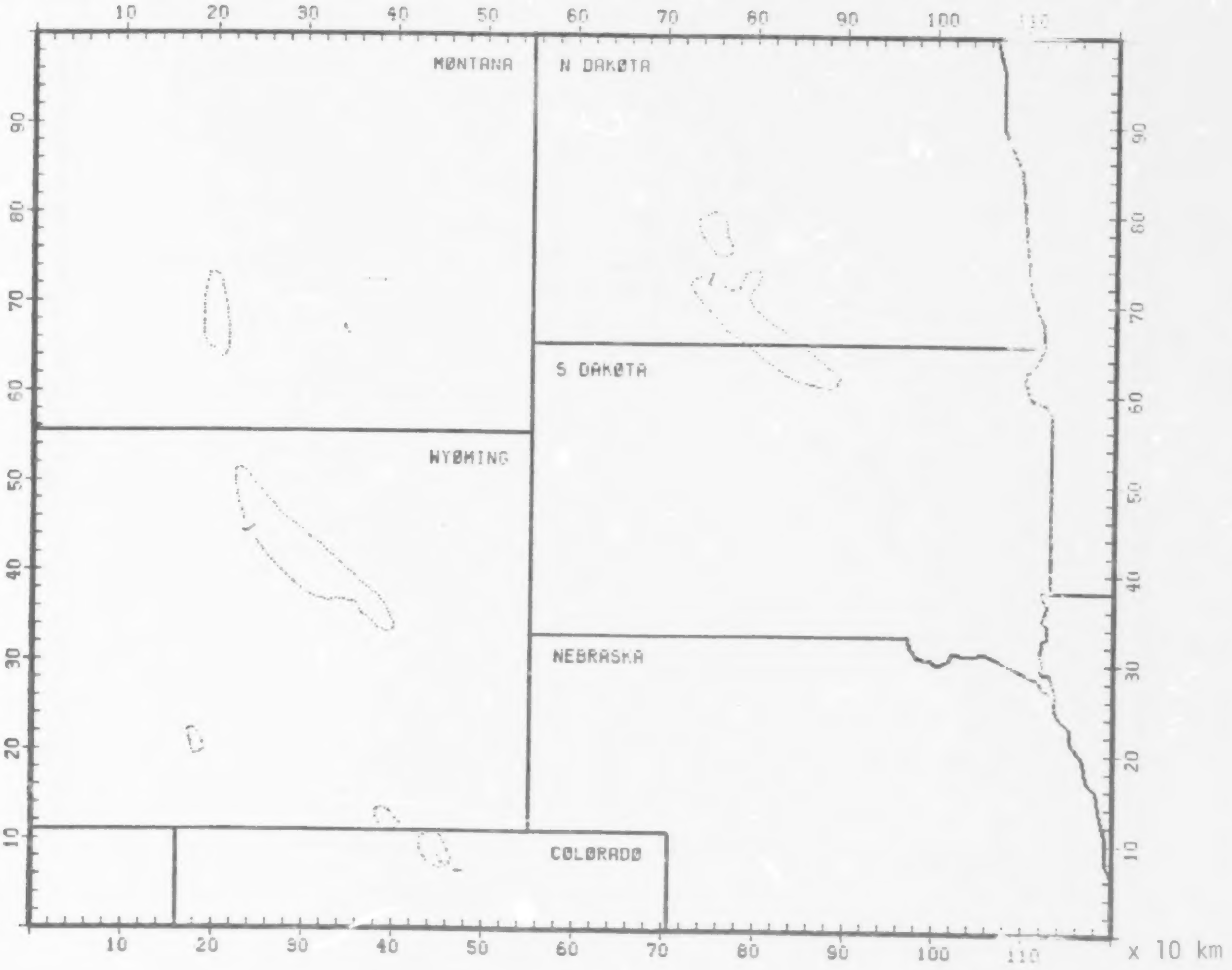
MONTANA
N DAKOTA
S DAKOTA
WYOMING
NEBRASKA
COLORADO
10
20
30
40
50
60
70
80
90
100
110
x 10 km

(b) NO$_2$ Concentrations (ppb)

FIGURE G-37 (Continued)

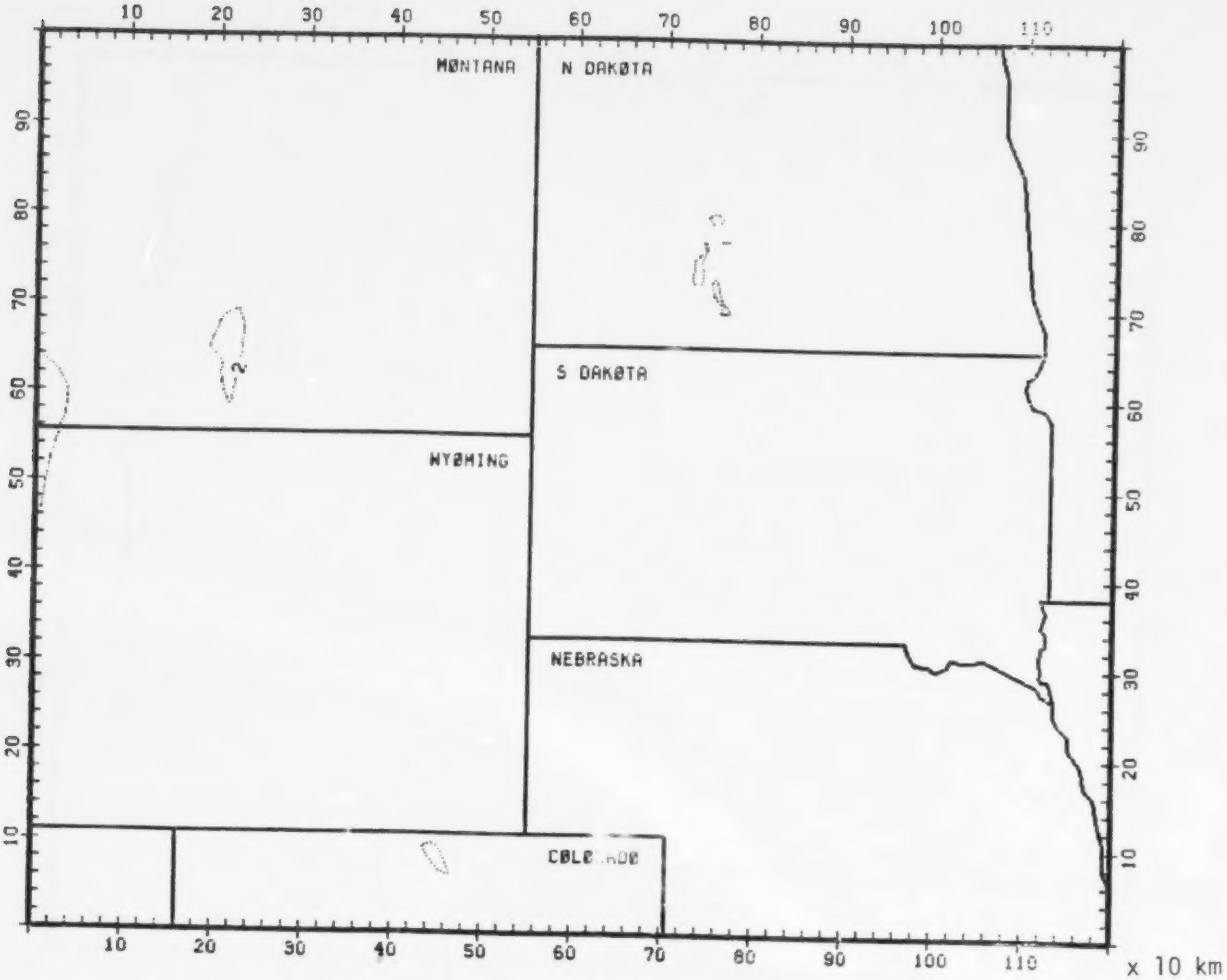
MØNTANA
N DAKØTA
S DAKØTA
WYØMING
NEBRASKA
CØLØRADØ
2
10
20
30
40
50
60
70
80
90
100
110
x 10 km

(c) $SO_4^=$ Concentrations ($\mu g/m^3$)

FIGURE G-37 (Continued)

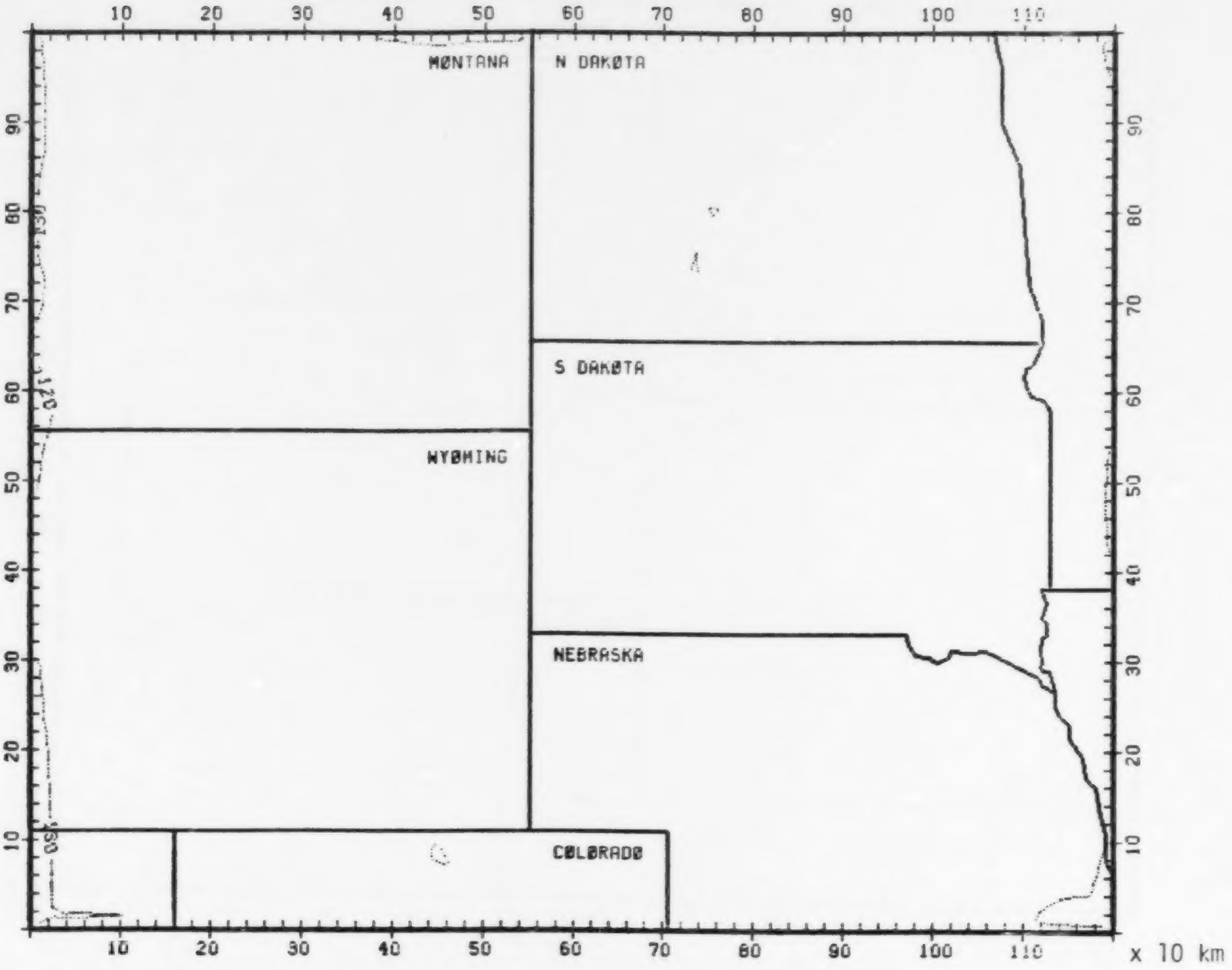
MØNTANA
N DAKØTA
S DAKØTA
WYØMING
NEBRASKA
CØLØRADØ
130
120
150
x 10 km
10
20
30
40
50
60
70
80
90
100
110

(d) Visual Range (km)

FIGURE G-37 (Concluded)

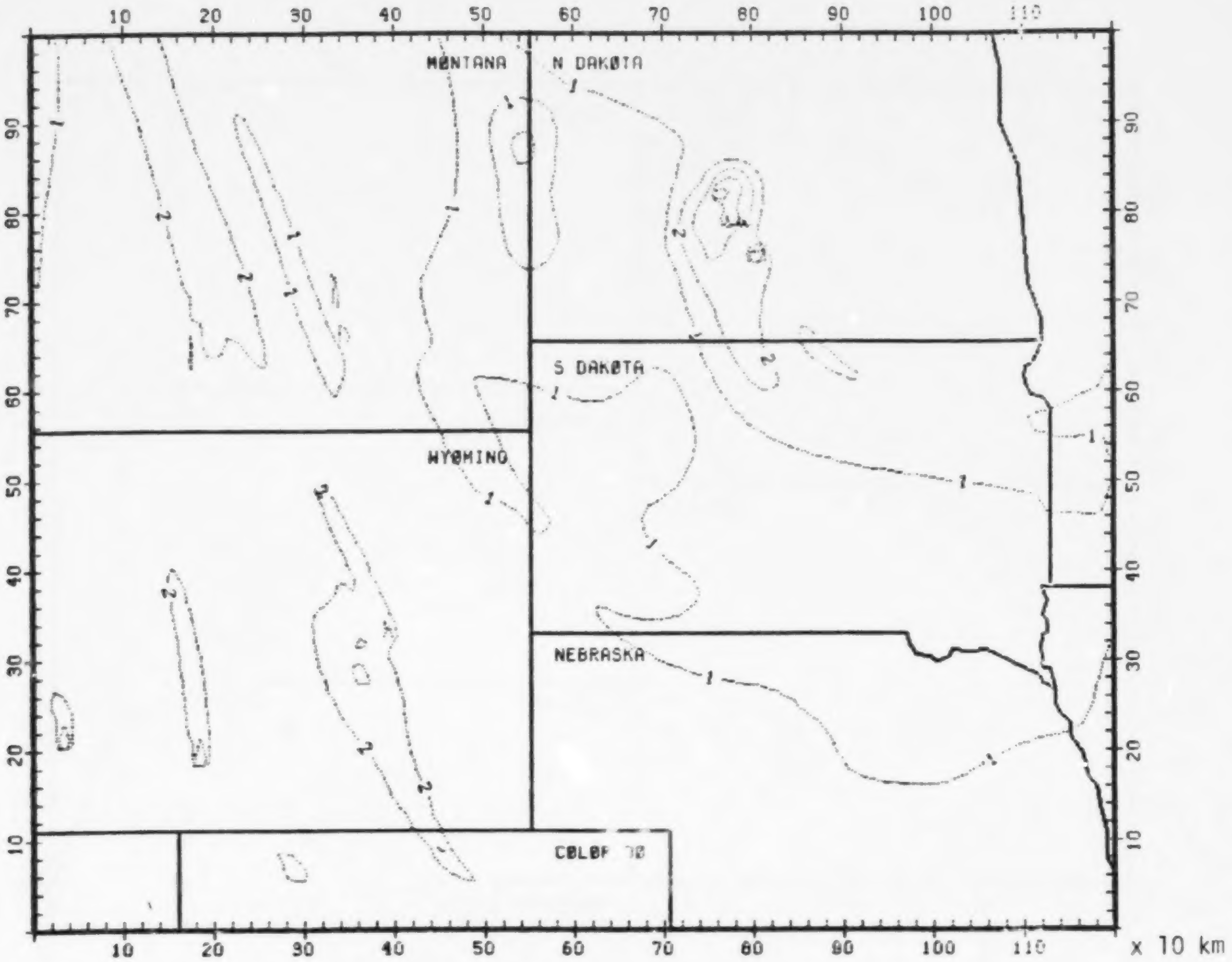
MONTANA
N DAKOTA
S DAKOTA
WYOMING
NEBRASKA
COLORADO
1
2
10
20
30
40
50
60
70
80
90
100
110
x 10 km

(a) SO_2 Concentrations ($\mu g/m^3$)

FIGURE G-38. 1975 NORTHERN GREAT PLAINS ISOPLETHS FOR 2000-2300 MST ON 5 APRIL 1976 ASSUMING 0.5 PERCENT PER HOUR SULFATE FORMATION

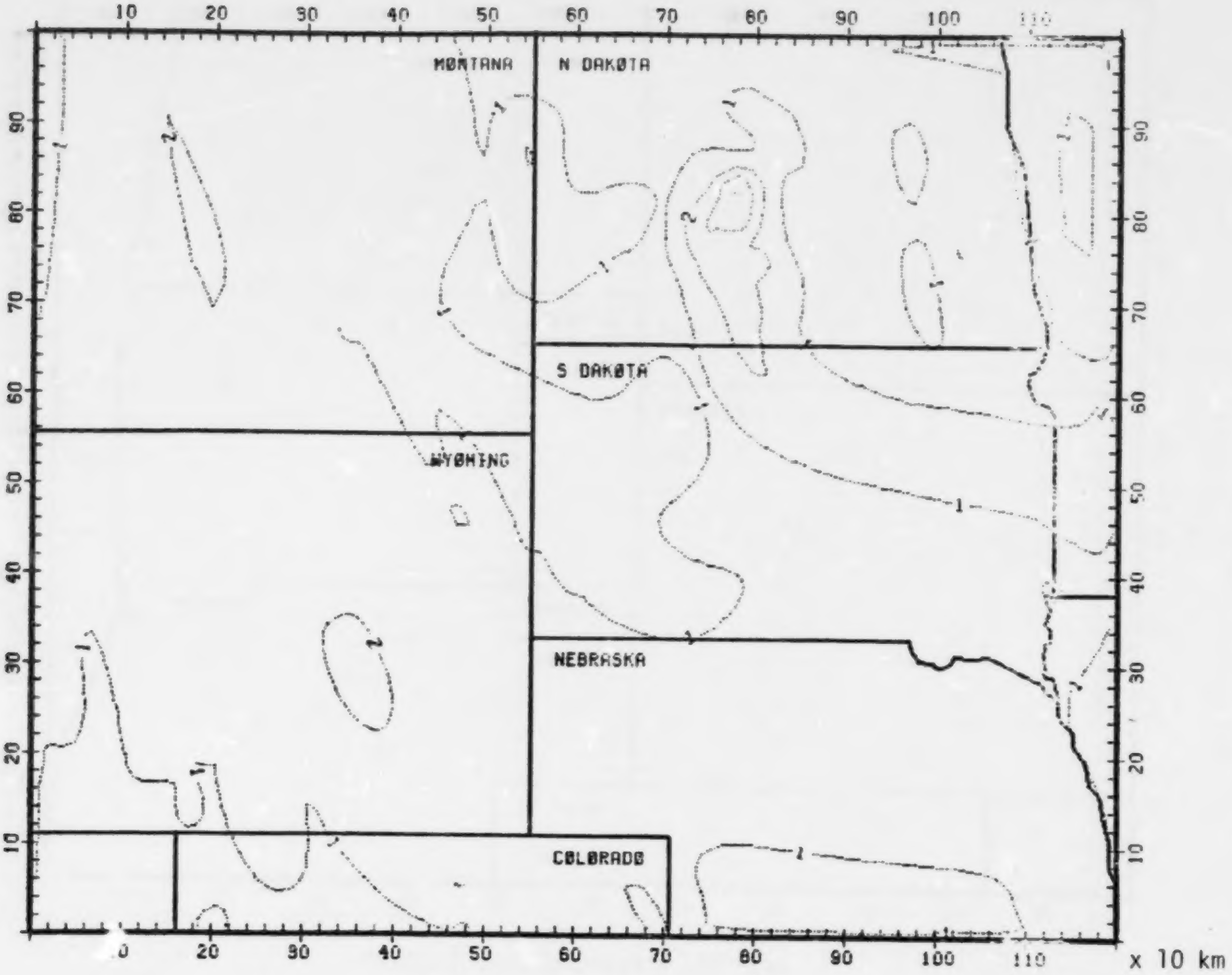
MONTANA
N DAKOTA
S DAKOTA
WYOMING
NEBRASKA
COLORADO
1
2
10
20
30
40
50
60
70
80
90
100
110
x 10 km

(b) NO_2 Concentrations (ppb)

FIGURE G-38 (Continued)

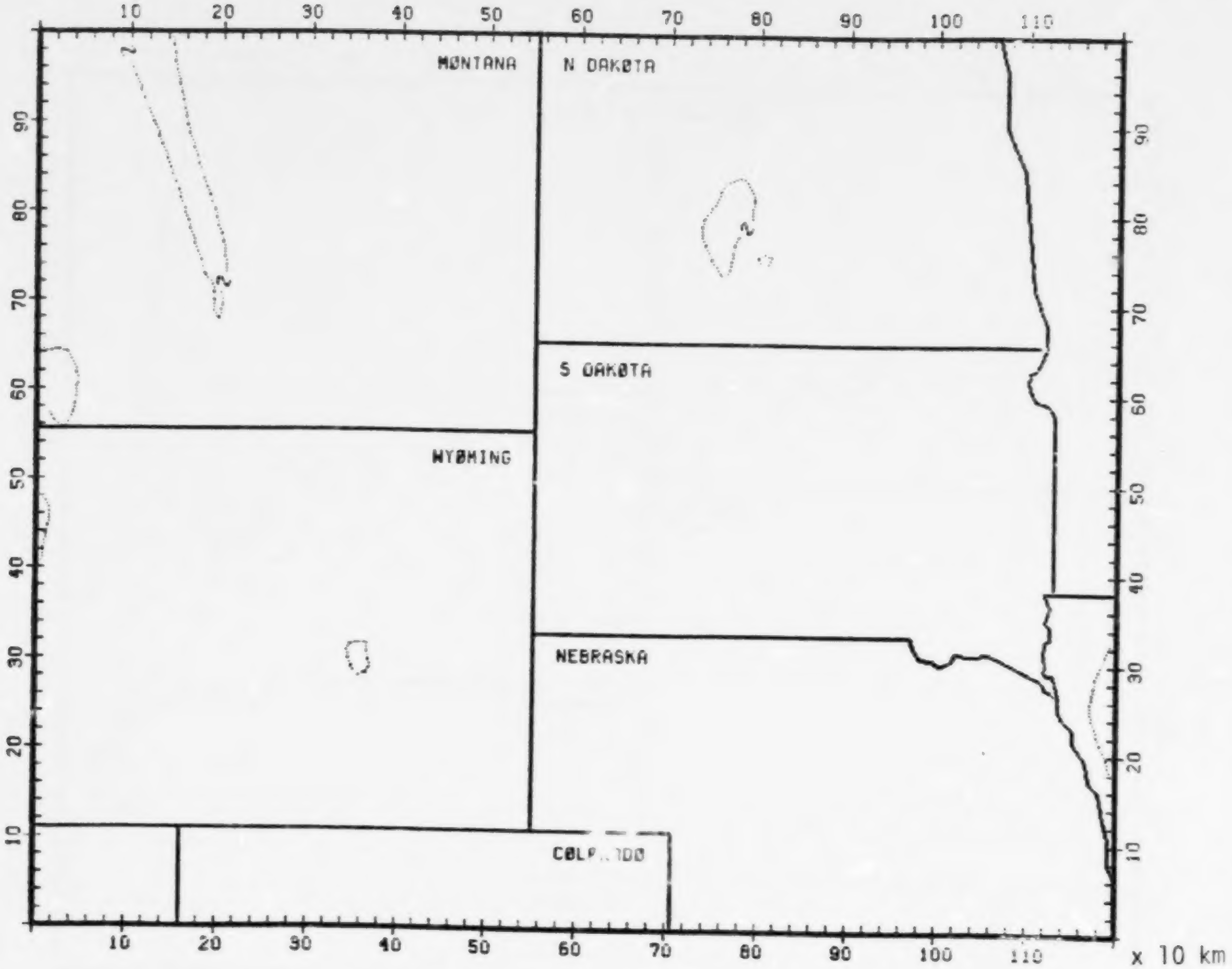
MØNTANA
N DAKØTA
S DAKØTA
WYØMING
NEBRASKA
CØLORADO
2
2
10
20
30
40
50
60
70
80
90
100
110
x 10 km

(c) $SO_4^=$ Concentrations ($\mu g/m^3$)

FIGURE G-38 (Continued)

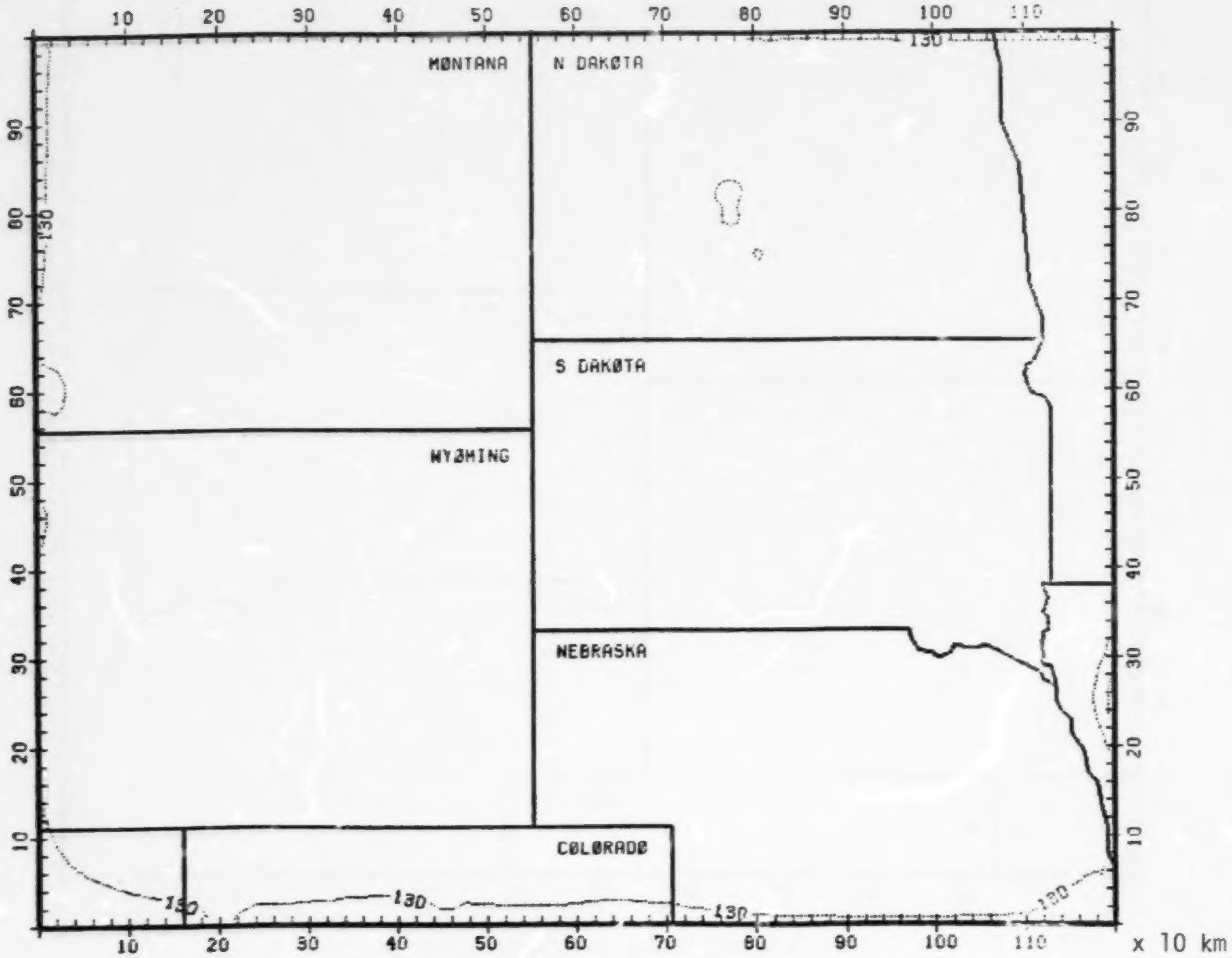
MØNTANA
N DAKØTA
S DAKØTA
WYØMING
NEBRASKA
CØLØRADØ
130
130
130
130
130
130
130
10
20
30
40
50
60
70
80
90
100
110
x 10 km

(d) Visual Range (km)

FIGURE G-38 (Concluded)

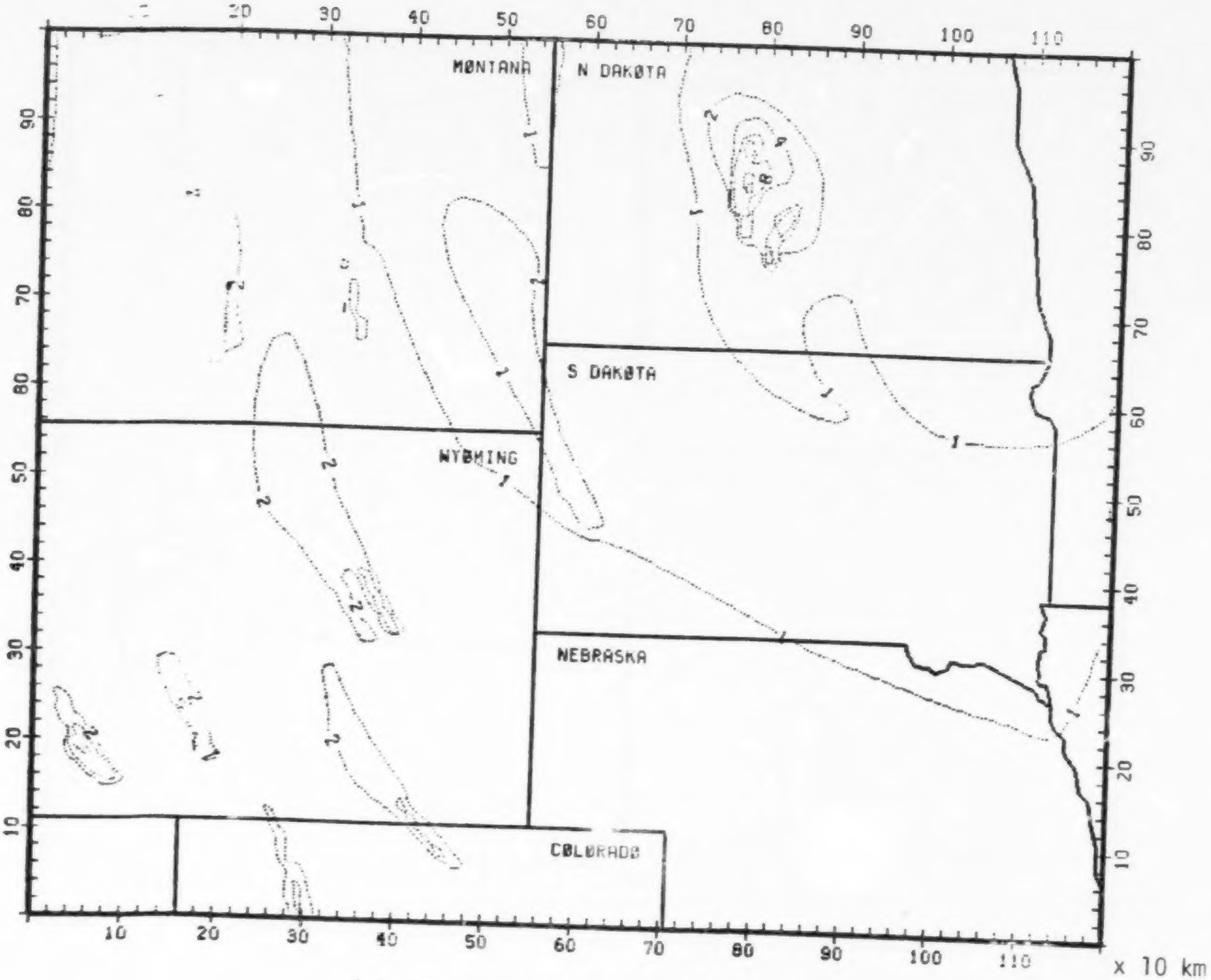
MØNTANA
N DAKØTA
S DAKØTA
WYØMING
NEBRASKA
CØLØRADØ
10
20
30
40
50
60
70
80
90
100
110
x 10 km
1
2
4
8

(a) SO_2 Concentrations ($\mu g/m^3$)

FIGURE G-39. 1975 NORTHERN GREAT PLAINS ISOPLETHS FOR 500-800 MST ON 6 APRIL 1976 ASSUMING 0.5 PERCENT PER HOUR SULFATE FORMATION

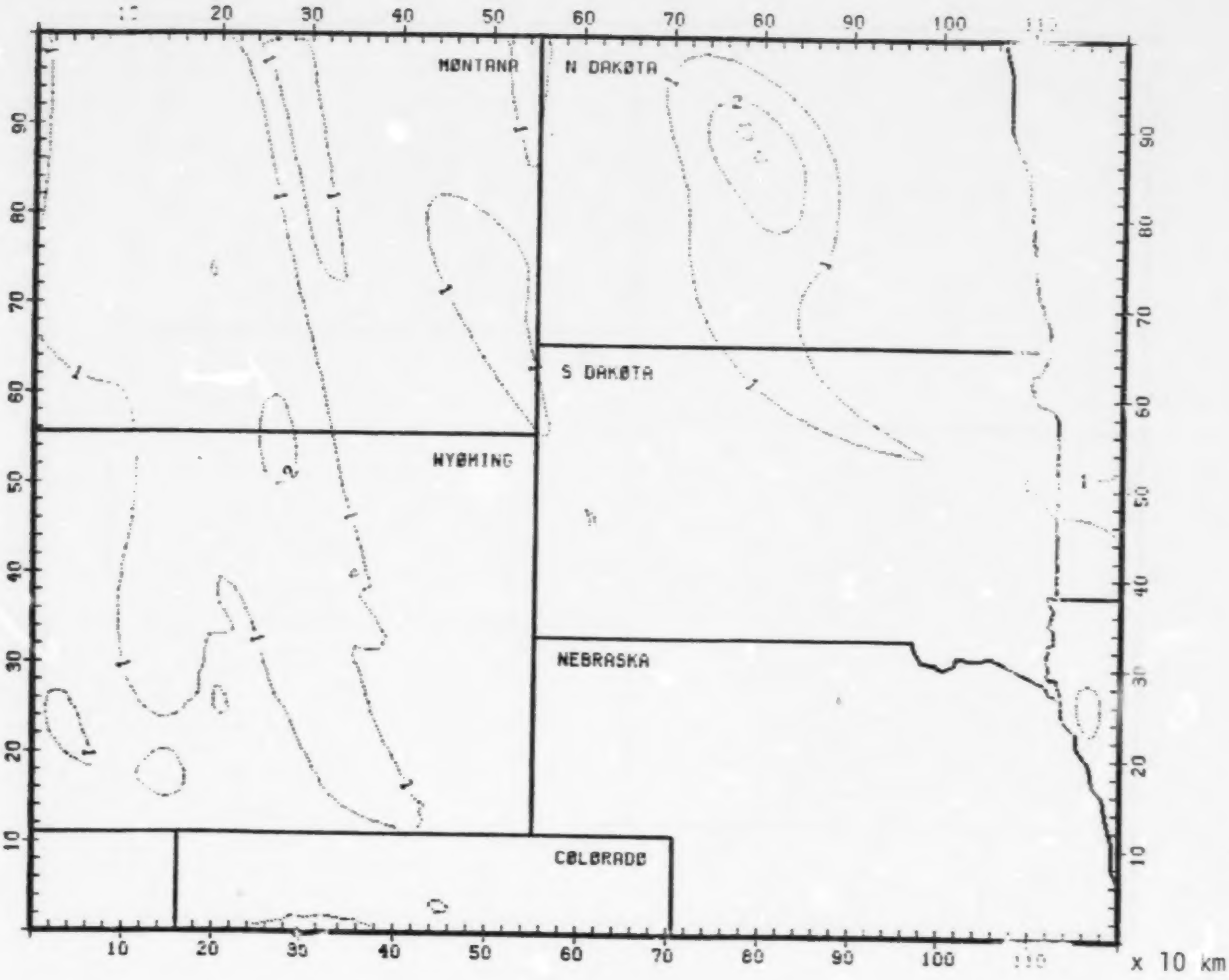
MONTANA
N DAKOTA
S DAKOTA
WYOMING
NEBRASKA
COLORADO
1
2
4
10
20
30
40
50
60
70
80
90
100
110
x 10 km

(b) NO_2 Concentrations (ppb)

FIGURE G-39 (Continued)

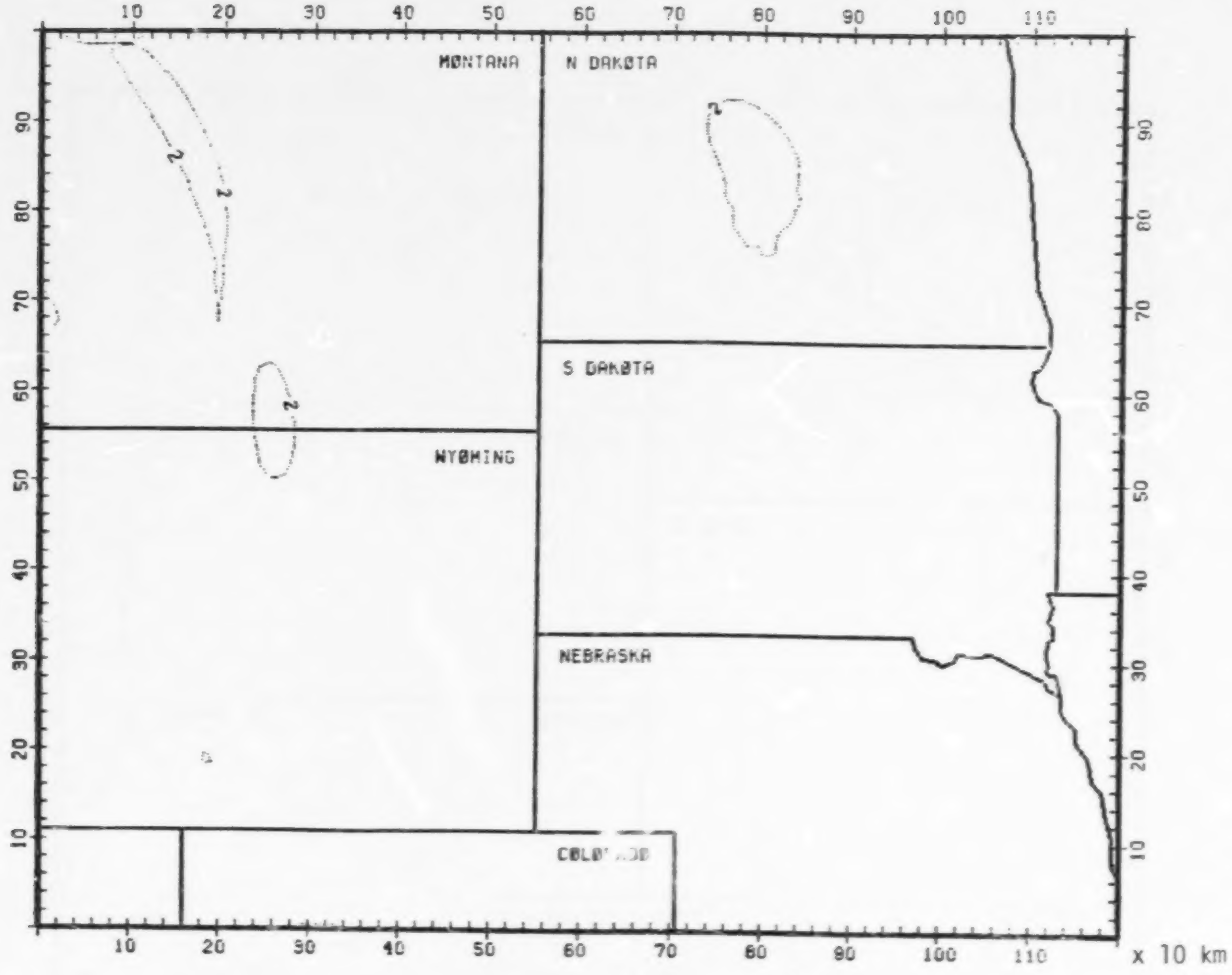
MØNTANA
N DAKØTA
S DAKØTA
WYØMING
NEBRASKA
CØLØRADO
2
2
2
2
10
20
30
40
50
60
70
80
90
100
110
x 10 km

(c) $SO_4^=$ Concentrations ($\mu g/m^3$)

FIGURE G-39 (Continued)

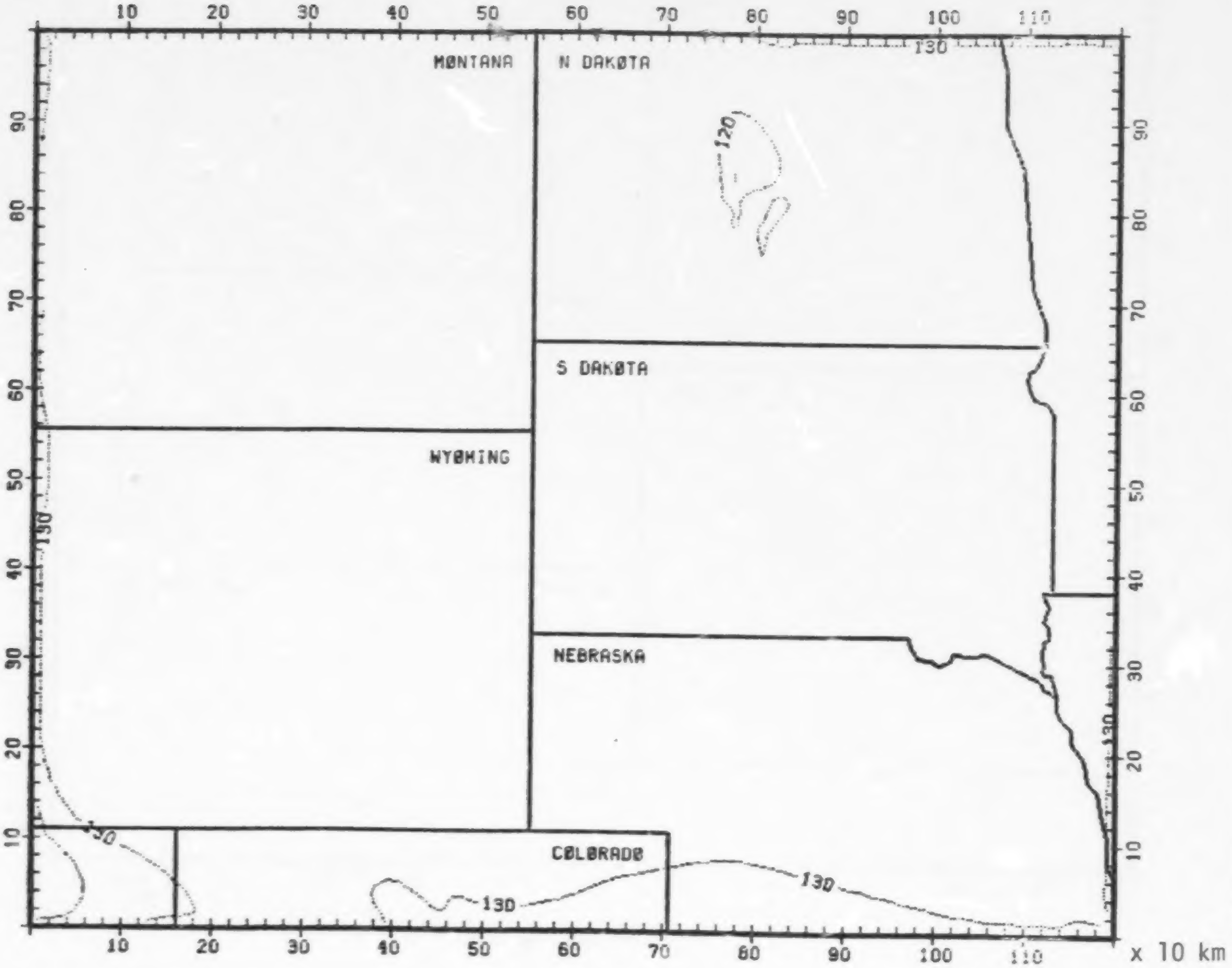
MØNTANA
N DAKØTA
S DAKØTA
WYØMING
NEBRASKA
CØLØRADØ
120
130
x 10 km
10
20
30
40
50
60
70
80
90
100
110

(d) Visual Range (km)

FIGURE G-39 (Concluded)

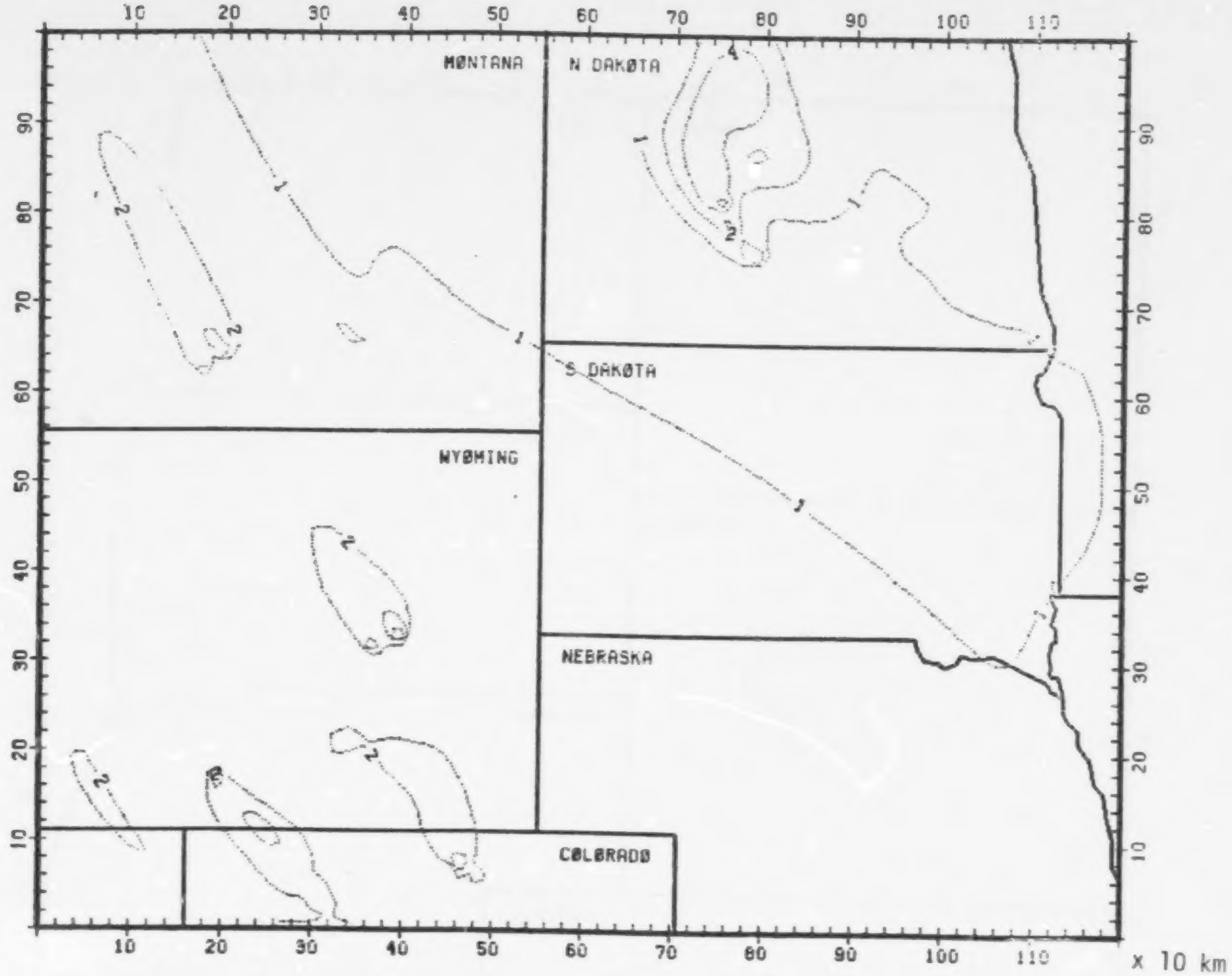
MONTANA
N DAKOTA
S DAKOTA
WYOMING
NEBRASKA
COLORADO
1
2
4
10
20
30
40
50
60
70
80
90
100
110
x 10 km

(a) SO_2 Concentrations ($\mu g/m^3$)

FIGURE G-40. 1975 NORTHERN GREAT PLAINS ISOPLETHS FOR 1400-1700 MST ON 6 APRIL 1976 ASSUMING 0.5 PERCENT PER HOUR SULFATE FORMATION

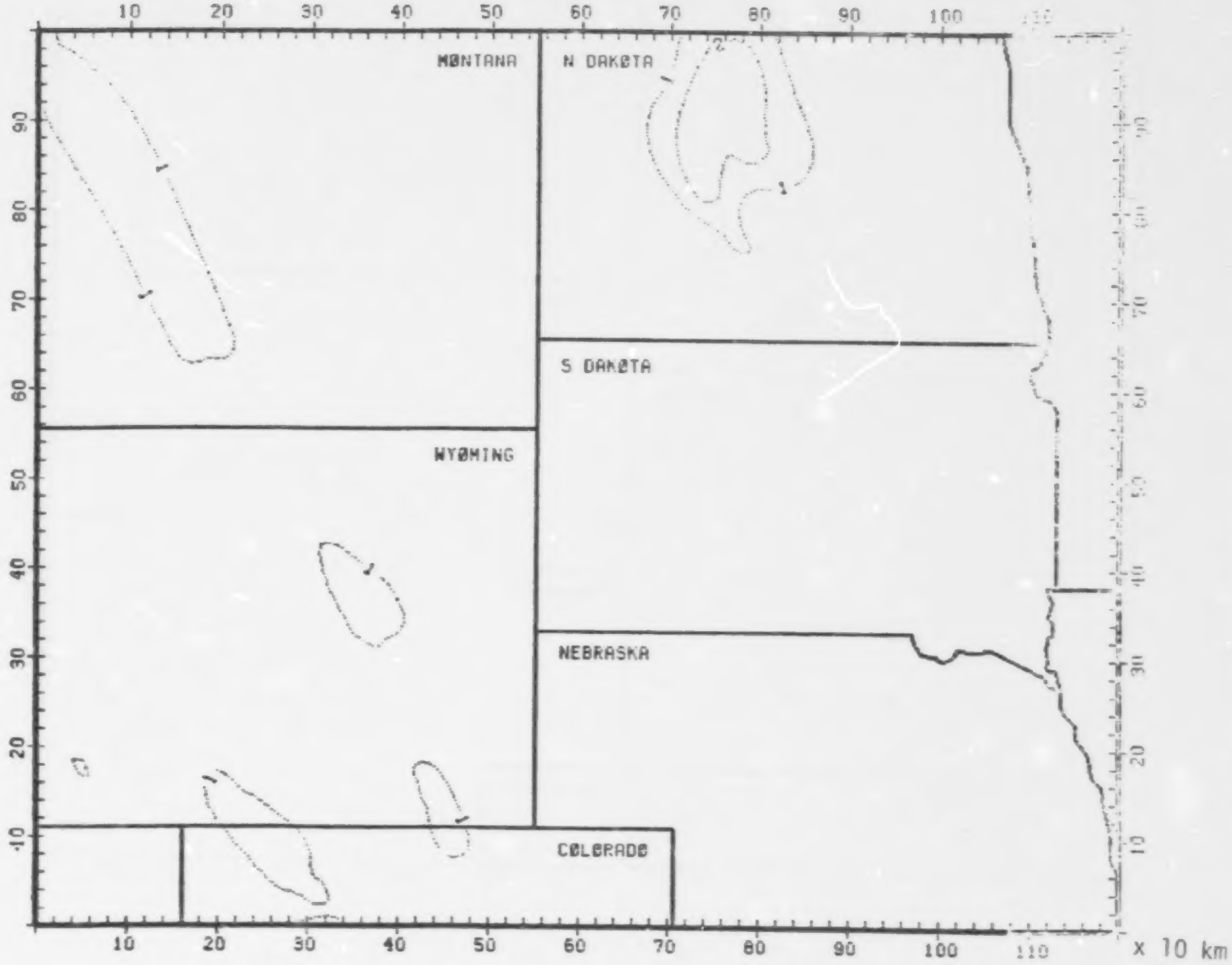
MONTANA
N DAKOTA
S DAKOTA
WYOMING
NEBRASKA
COLORADO
1
2
x 10 km
10
20
30
40
50
60
70
80
90
100
110

(b) NO$_2$ Concentrations (ppb)

FIGURE G-40 (Continued)

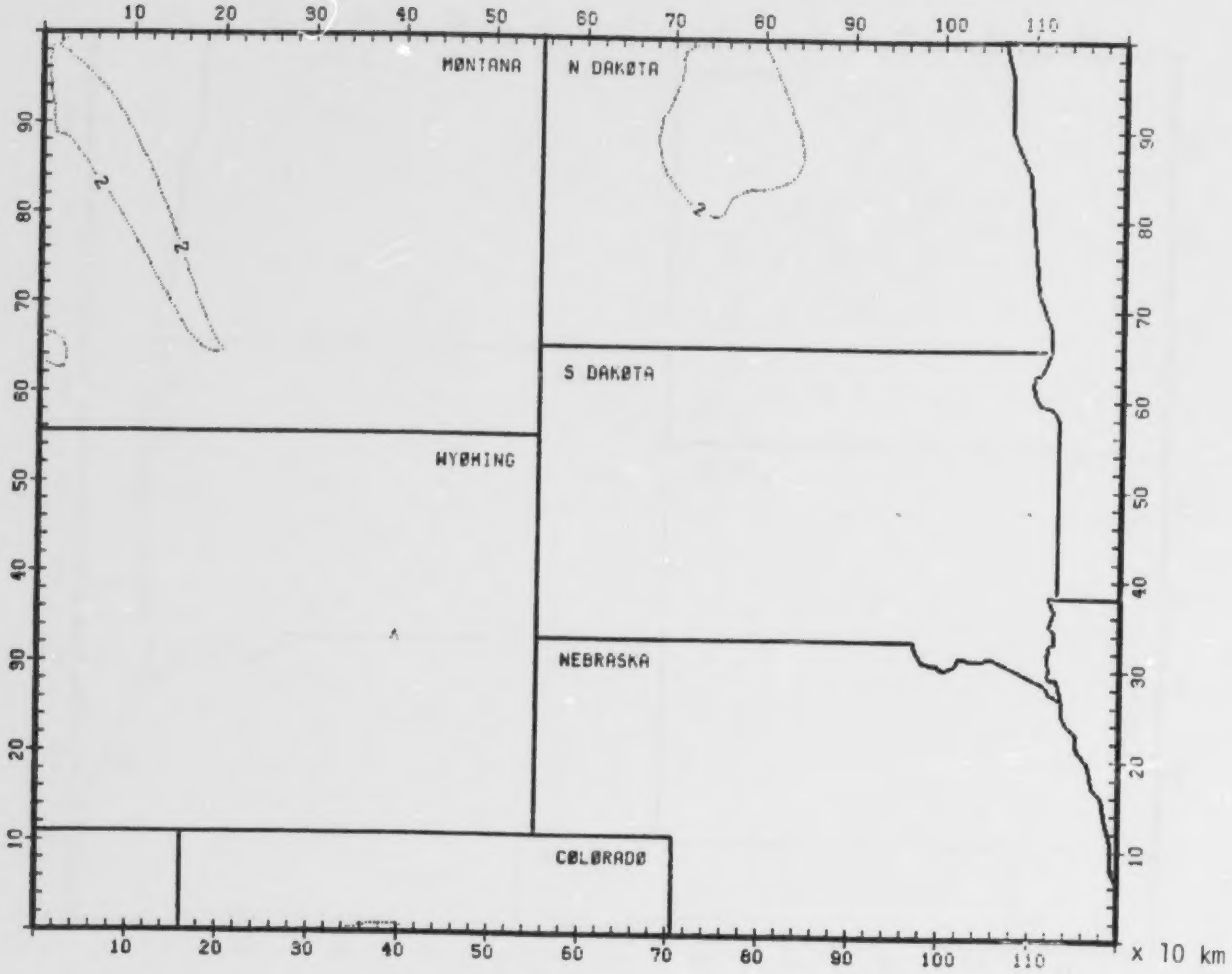
MONTANA
N DAKOTA
S DAKOTA
WYOMING
NEBRASKA
COLORADO
2
2
2
10
20
30
40
50
60
70
80
90
100
110
x 10 km

(c) $SO_4^=$ Concentrations ($\mu g/m^3$)

FIGURE G-40 (Continued)

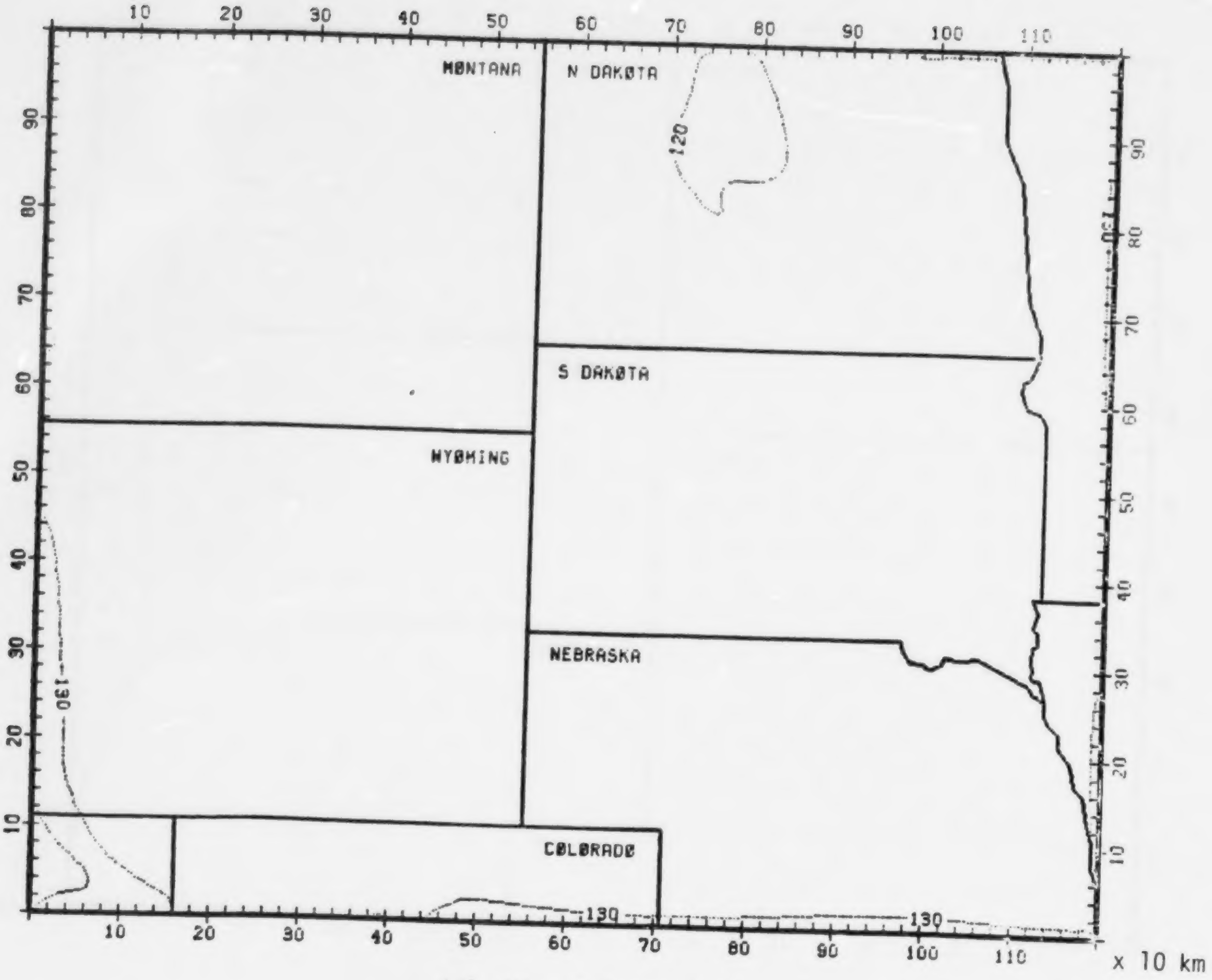
MONTANA
N DAKOTA
S DAKOTA
WYOMING
NEBRASKA
COLORADO
120
130
130
130
130
10
20
30
40
50
60
70
80
90
100
110
x 10 km

(d) Visual Range (km)

FIGURE G-40 (Concluded)

g. Northern Great Plains 1975 Emissions, Assuming 0.5 Percent per Hour Sulfate Formation, Using the Spring (April) Scenario

The final group of simulations (Run 7), as shown in Figures G-41 through G-46, shows the impact of projected 1986 point source emissions assuming the stagnant meteorological conditions of the three-day April 1976 simulation period. Note that visibility impairment is increased as a result of the projected region-wide SO_2 emissions rate of nearly 2000 tons per day. The minimum visual range is 100 km, about a 25 percent reduction from the 130 km background value.

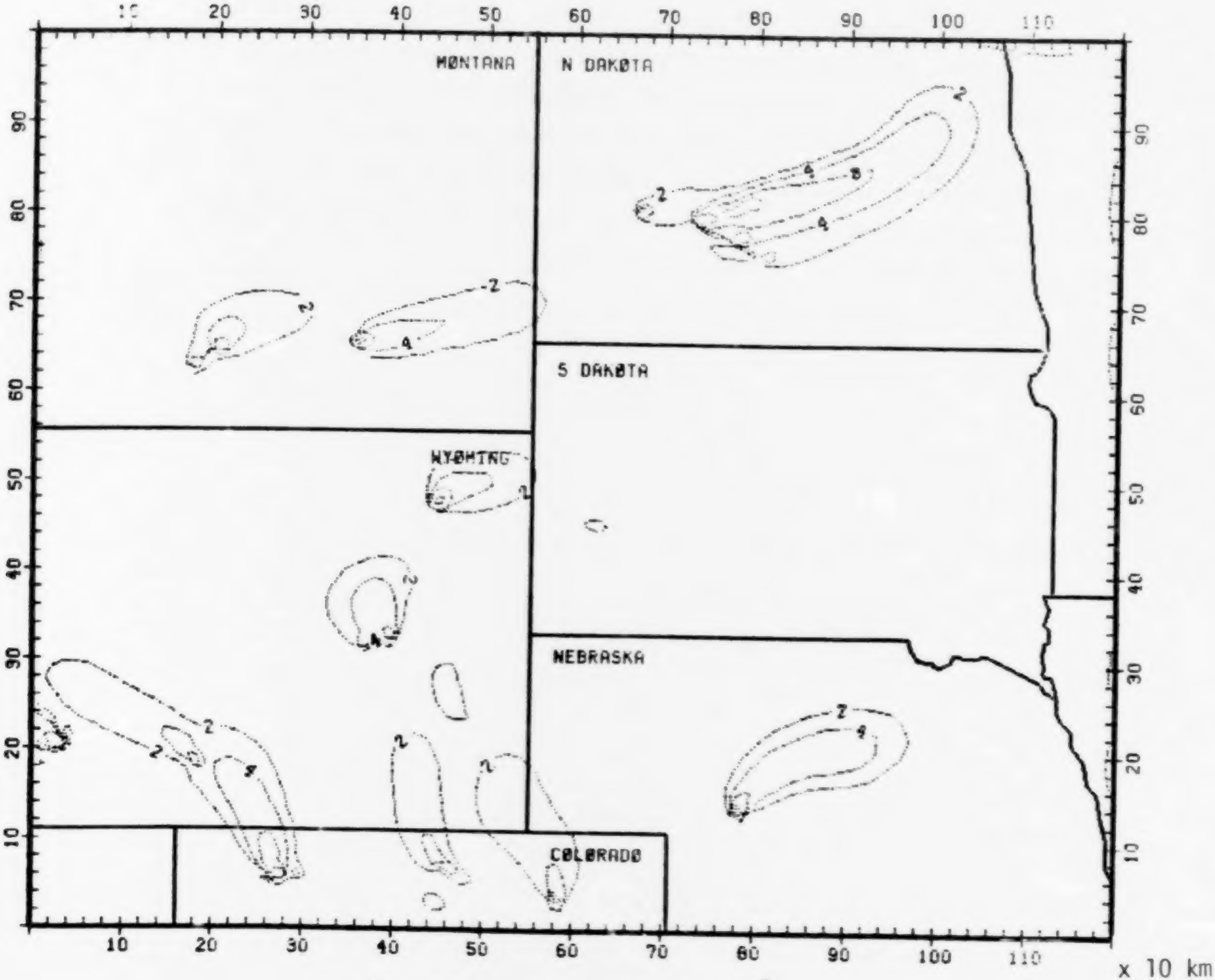
MONTANA
N DAKOTA
S DAKOTA
WYOMING
NEBRASKA
COLORADO
2
4
8
10
20
30
40
50
60
70
80
90
100
110
x 10 km

(a) SO_2 Concentrations ($\mu g/m^3$)

FIGURE G-41. 1986 NORTHERN GREAT PLAINS ISOPLETHS FOR 1700-2000 MST ON 4 APRIL 1976 ASSUMING 0.5 PERCENT PER HOUR SULFATE FORMATION

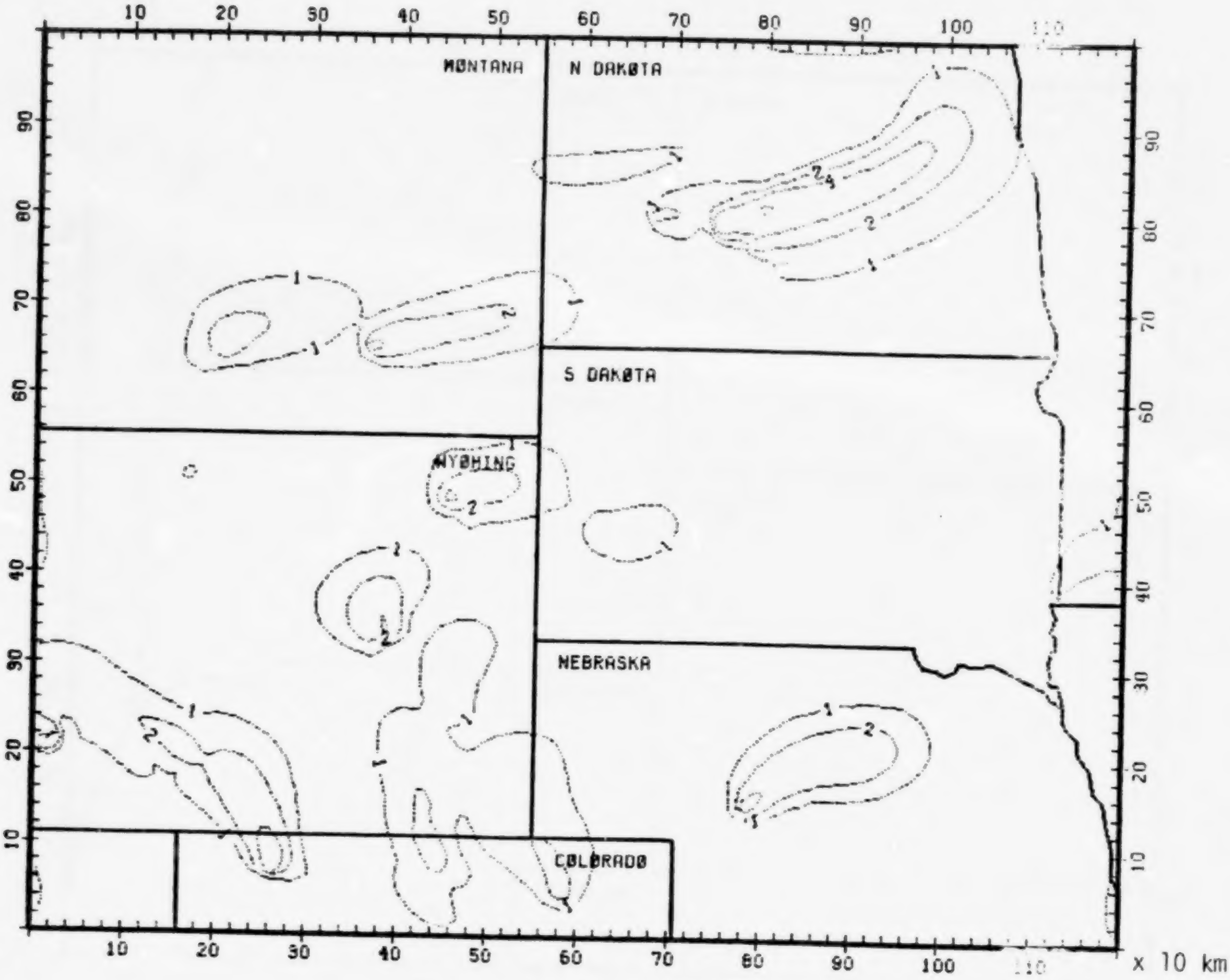
MØNTANA
N DAKØTA
S DAKØTA
WYØMING
NEBRASKA
CØLØRADØ
10
20
30
40
50
60
70
80
90
100
110
x 10 km
1
2

(b) NO_2 Concentrations (ppb)

FIGURE G-41 (Continued)

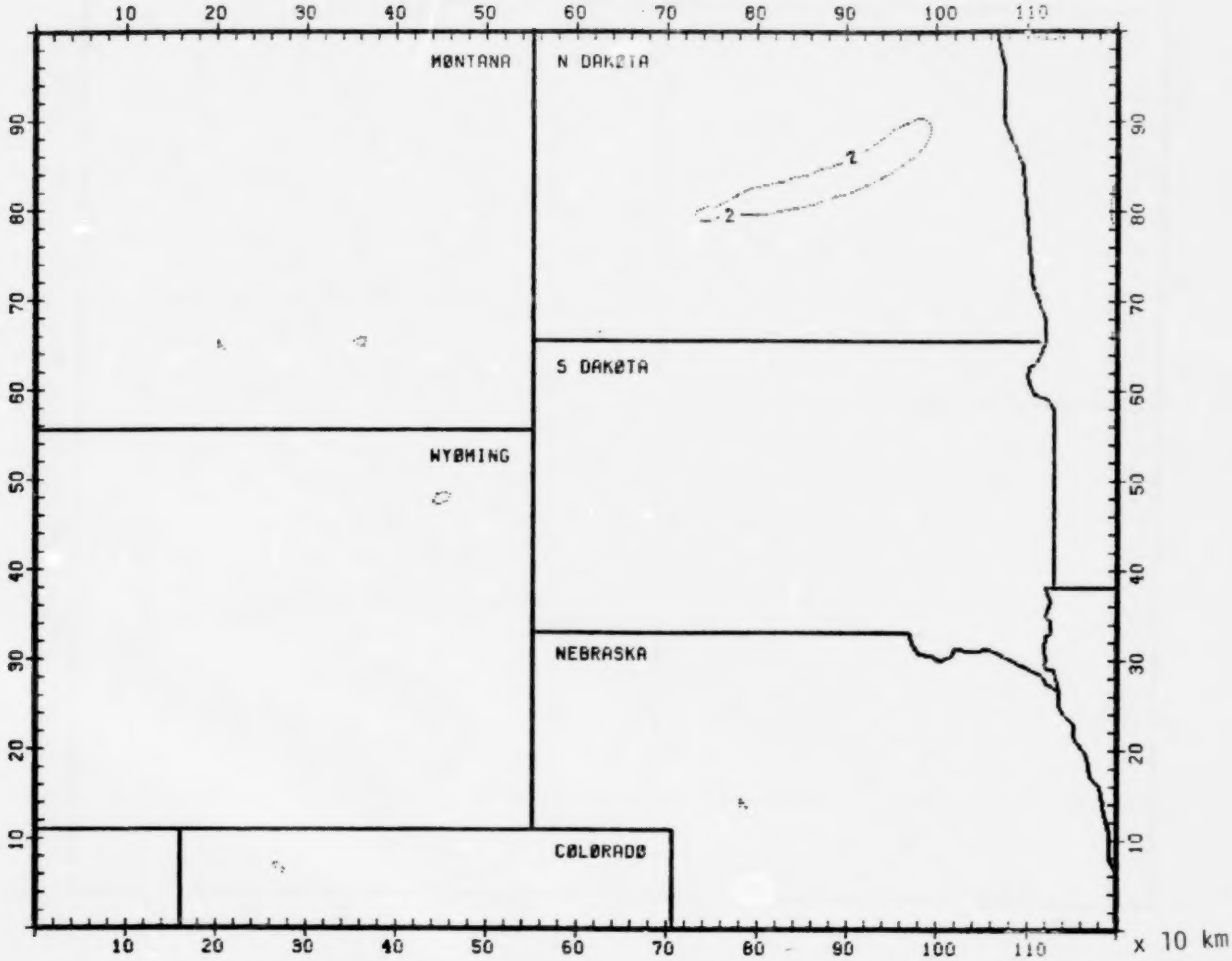
MONTANA
N DAKOTA
S DAKOTA
WYOMING
NEBRASKA
COLORADO
2
2
x 10 km
10
20
30
40
50
60
70
80
90
100
110

(c) $SO_4^=$ Concentrations ($\mu g/m^3$)

FIGURE G-41 (Continued)

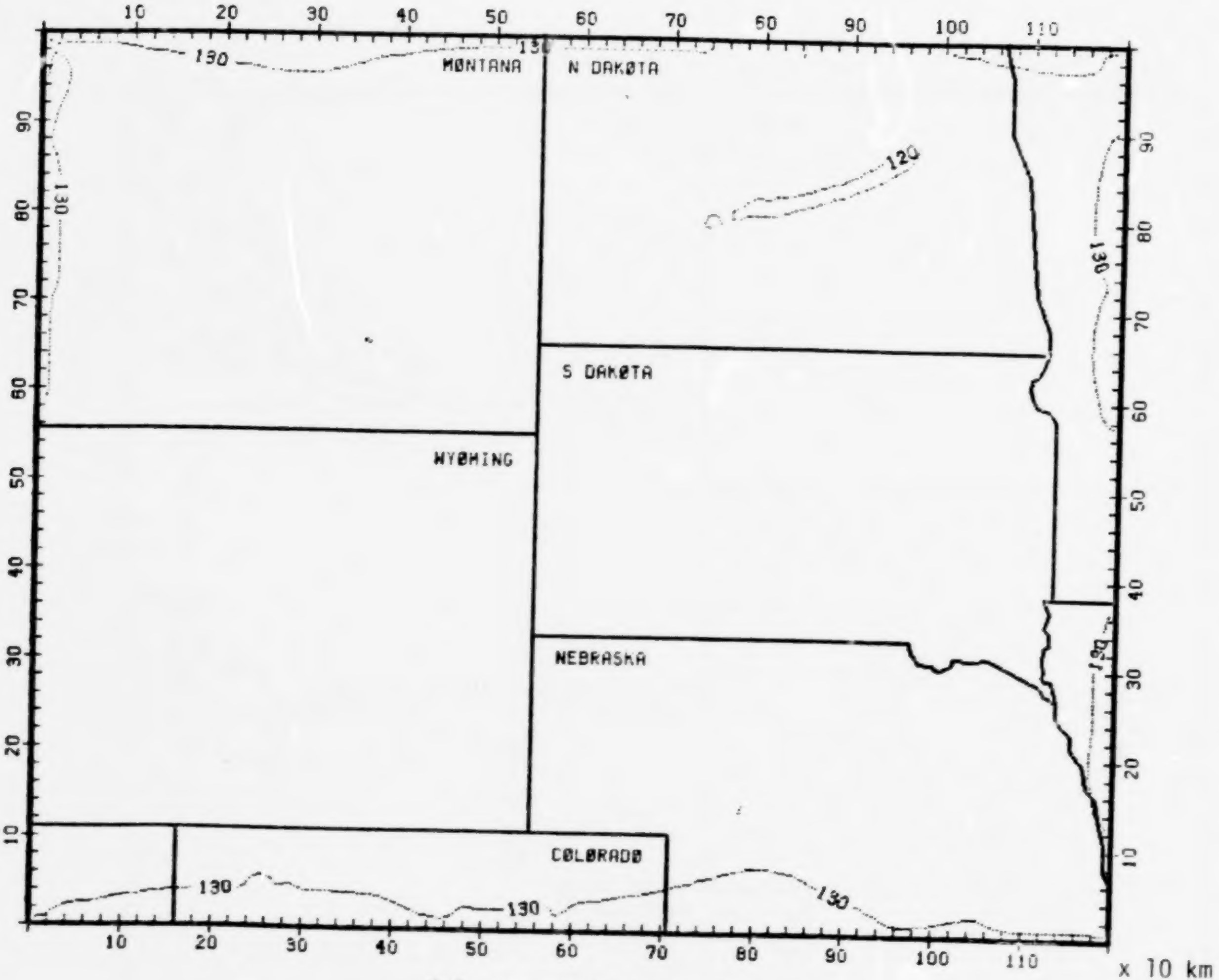
MØNTANA
N DAKØTA
S DAKØTA
WYØMING
NEBRASKA
CØLØRADØ
130
120
10
20
30
40
50
60
70
80
90
100
110
x 10 km

(d) Visual Range (km)

FIGURE G-41 (Concluded)

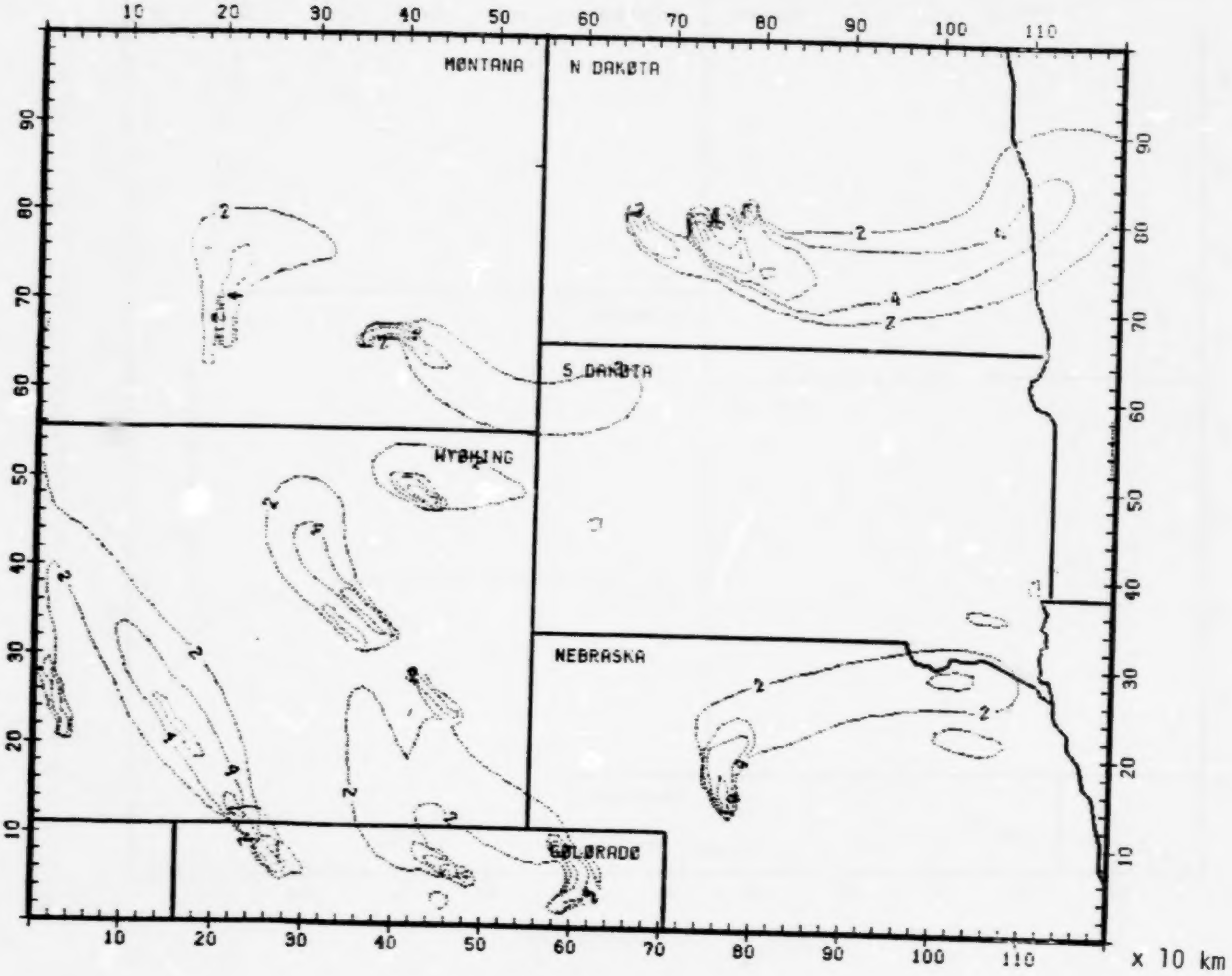
MONTANA
N DAKOTA
S DAKOTA
WYOMING
NEBRASKA
COLORADO
2
4
10
20
30
40
50
60
70
80
90
100
110
x 10 km

(a) SO_2 Concentrations ($\mu g/m^3$)

FIGURE G-42. 1986 NORTHERN GREAT PLAINS ISOPLETHS FOR 200-500 MST ON 5 APRIL 1976 ASSUMING 0.5 PERCENT PER HOUR SULFATE FORMATION

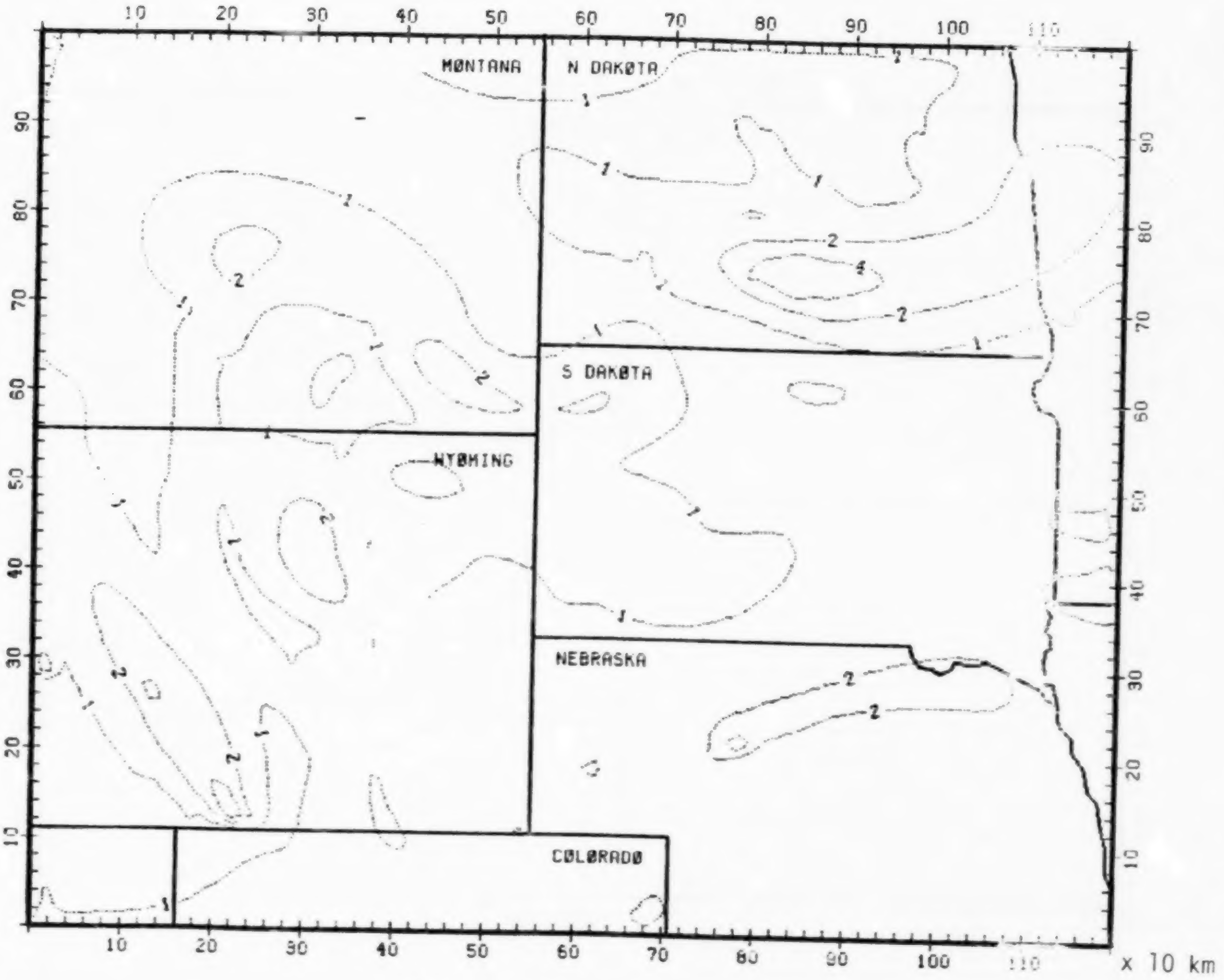
MONTANA
N DAKOTA
S DAKOTA
WYOMING
NEBRASKA
COLORADO
10
20
30
40
50
60
70
80
90
100
110
x 10 km
1
2
4

(b) NO$_2$ Concentrations (ppb)

FIGURE G-42 (Continued)

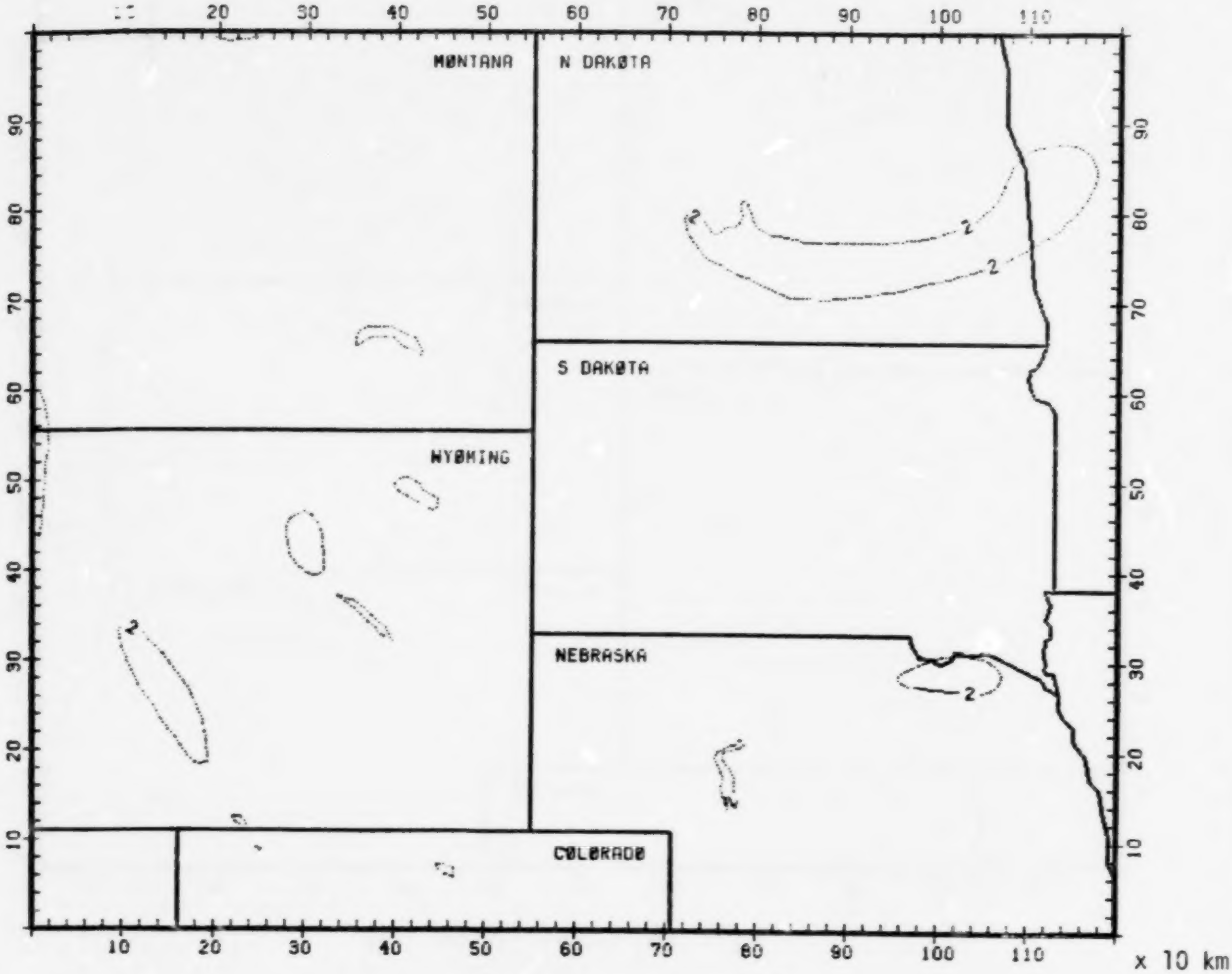
10
20
30
40
50
60
70
80
90
100
110
MØNTANA
N DAKØTA
S DAKØTA
WYØMING
NEBRASKA
CØLØRADØ
2
2
2
2
2
x 10 km

(c) $SO_4^=$ Concentrations ($\mu g/m^3$)

FIGURE G-42 (Continued)

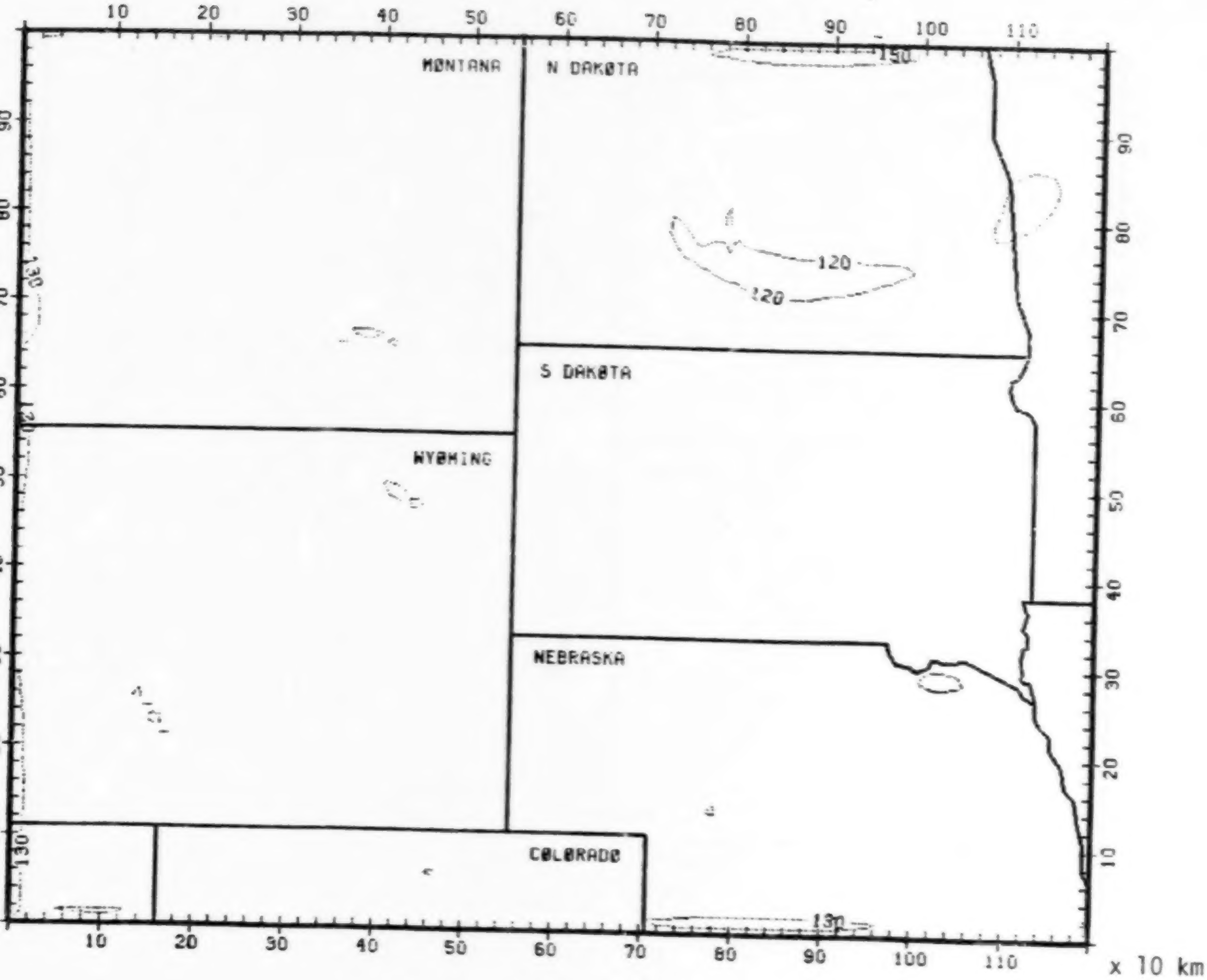
MØNTANA
N DAKØTA
S DAKØTA
WYØMING
NEBRASKA
CØLØRADØ
150
120
120
130
130
130
120
x 10 km

(d) Visual Range (km)

FIGURE G-42 (Concluded)

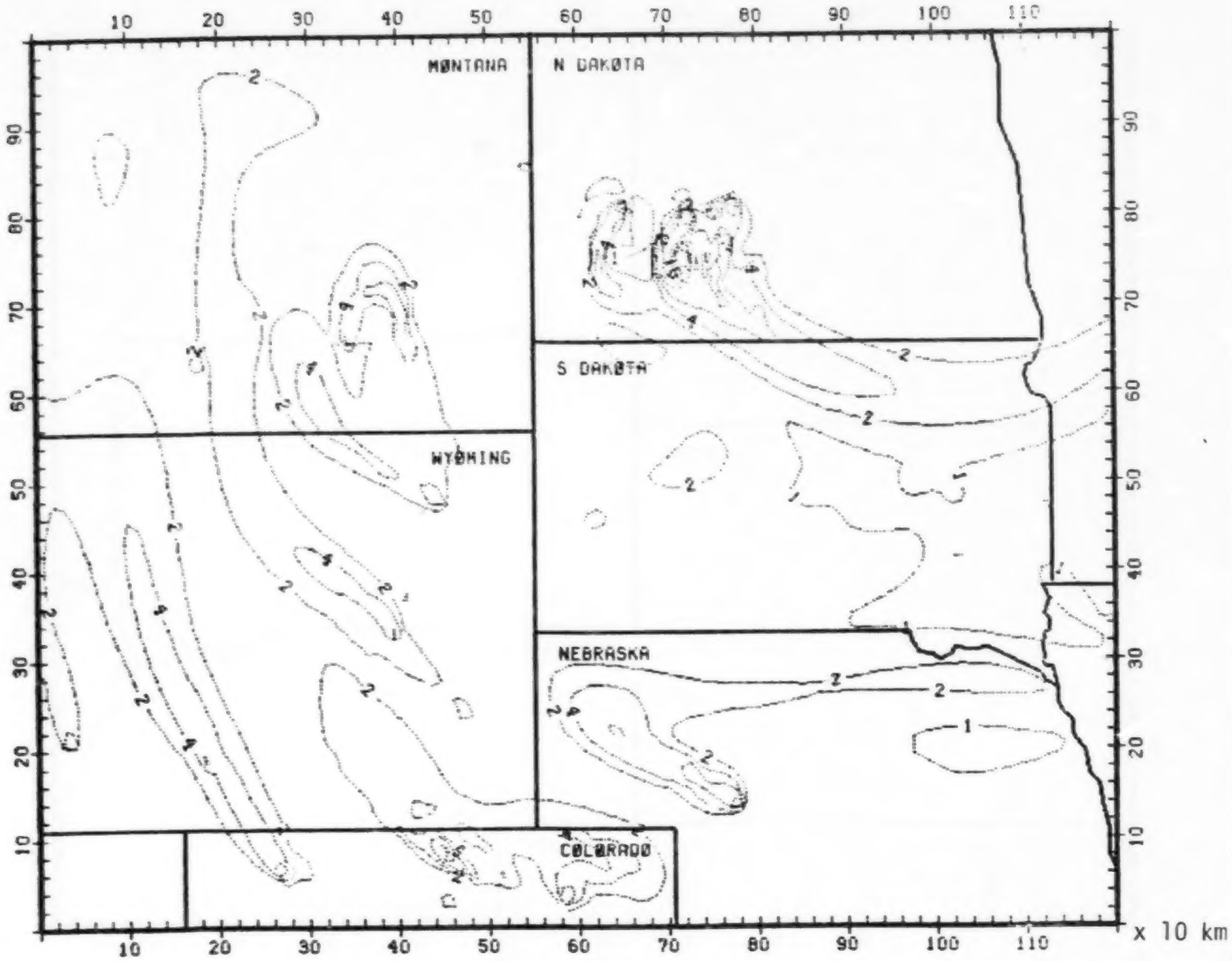
10
20
30
40
50
60
70
80
90
100
110
MØNTANA
N DAKØTA
S DAKØTA
WYØMING
NEBRASKA
CØLØRADØ
x 10 km
1
2
4

(a) SO_2 Concentrations ($\mu g/m^3$)

FIGURE G-43. 1986 NORTHERN GREAT PLAINS ISOPLETHS FOR 1100-1400 MST ON 5 APRIL 1976 ASSUMING 0.5 PERCENT PER HOUR SULFATE FORMATION

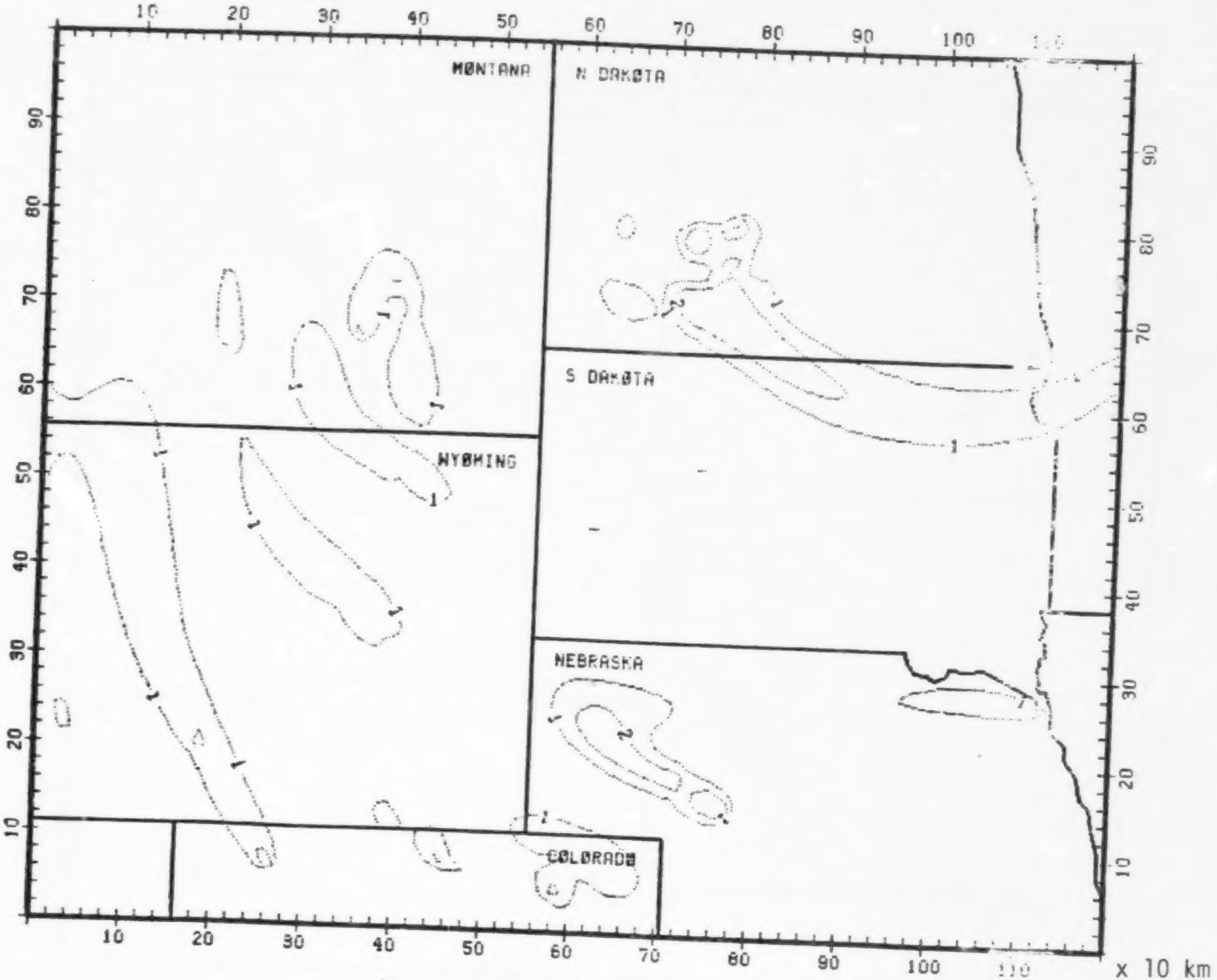
MONTANA
N DAKOTA
S DAKOTA
WYOMING
NEBRASKA
COLORADO
1
2
10
20
30
40
50
60
70
80
90
100
110
x 10 km

(b) NO$_2$ Concentrations (ppb)

FIGURE G-43 (Continued)

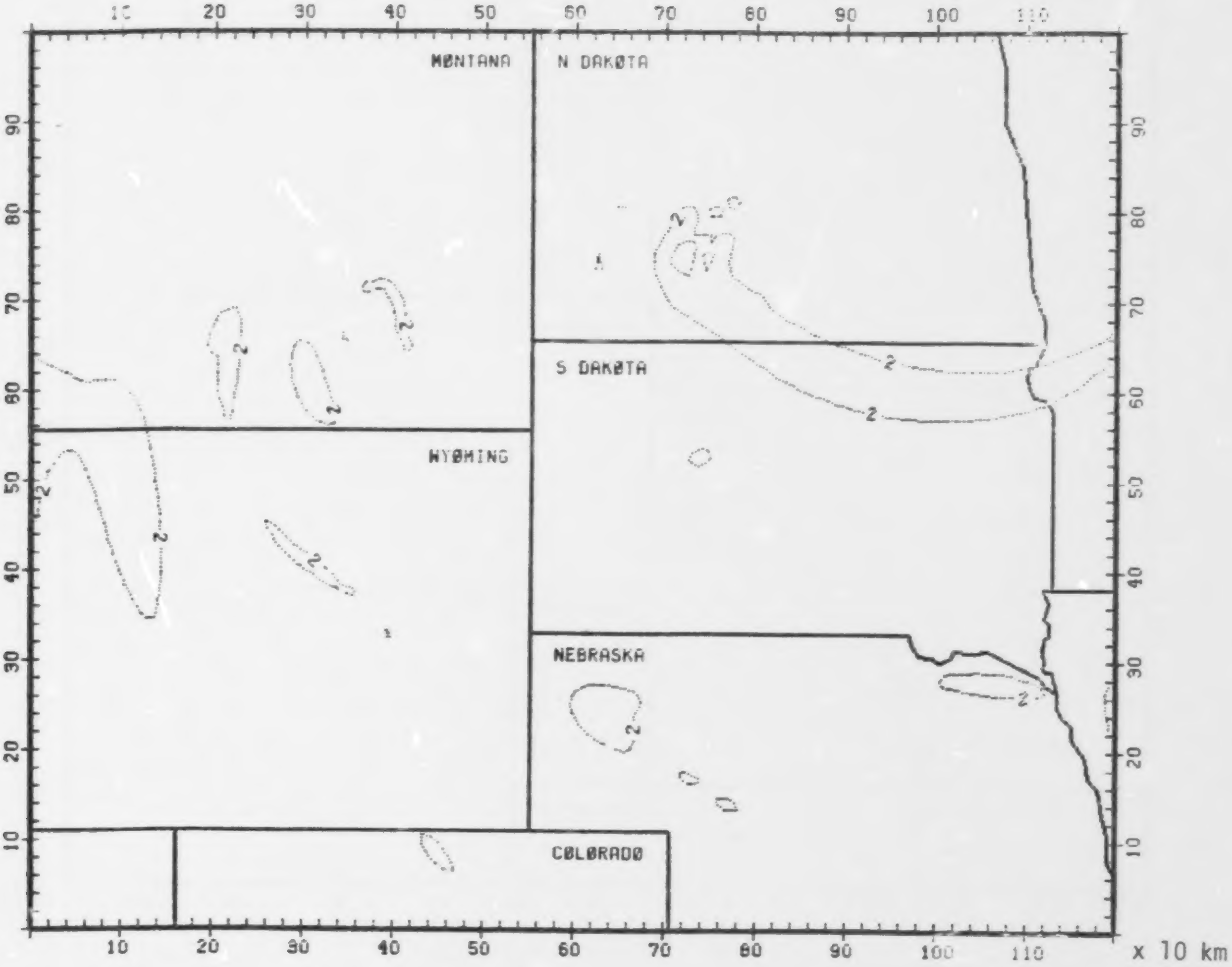
MØNTANA
N DAKØTA
S DAKØTA
WYØMING
NEBRASKA
CØLØRADØ
2
10
20
30
40
50
60
70
80
90
100
110
x 10 km

(c) $SO_4^=$ Concentrations ($\mu g/m^3$)

FIGURE G-43 (Continued)

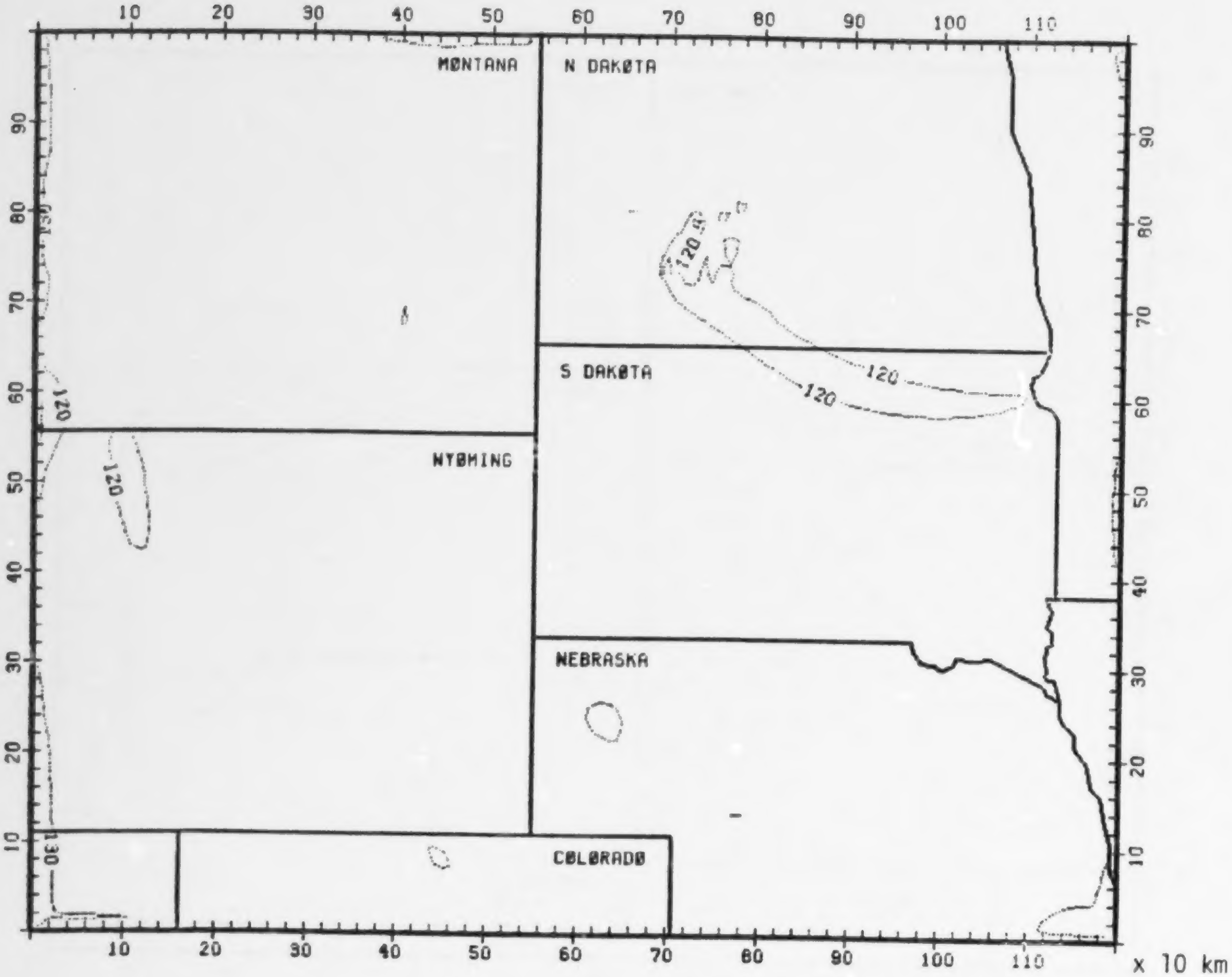
MØNTANA
N DAKØTA
S DAKØTA
WYØMING
NEBRASKA
CØLØRADØ
120
130
x 10 km
10
20
30
40
50
60
70
80
90
100
110

(d) Visual Range (km)

FIGURE G-43 (Concluded)

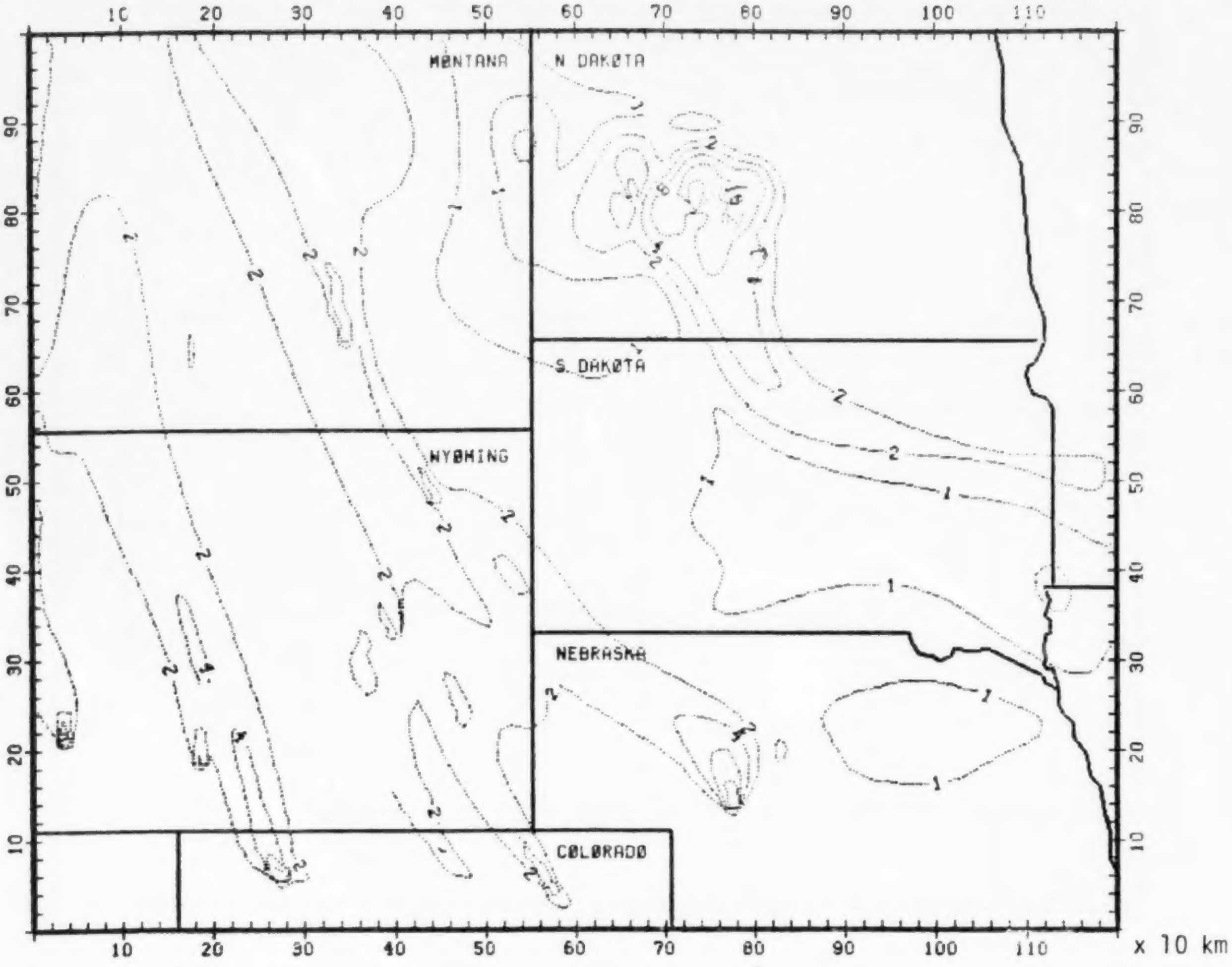
MONTANA
N DAKOTA
S. DAKOTA
WYOMING
NEBRASKA
COLORADO
10
20
30
40
50
60
70
80
90
100
110
x 10 km

(a) SO_2 Concentrations ($\mu g/m^3$)

FIGURE G-44. 1986 NORTHERN GREAT PLAINS ISOPLETHS FOR 2000-2300 MST ON 5 APRIL 1976 ASSUMING 0.5 PERCENT PER HOUR SULFATE FORMATION

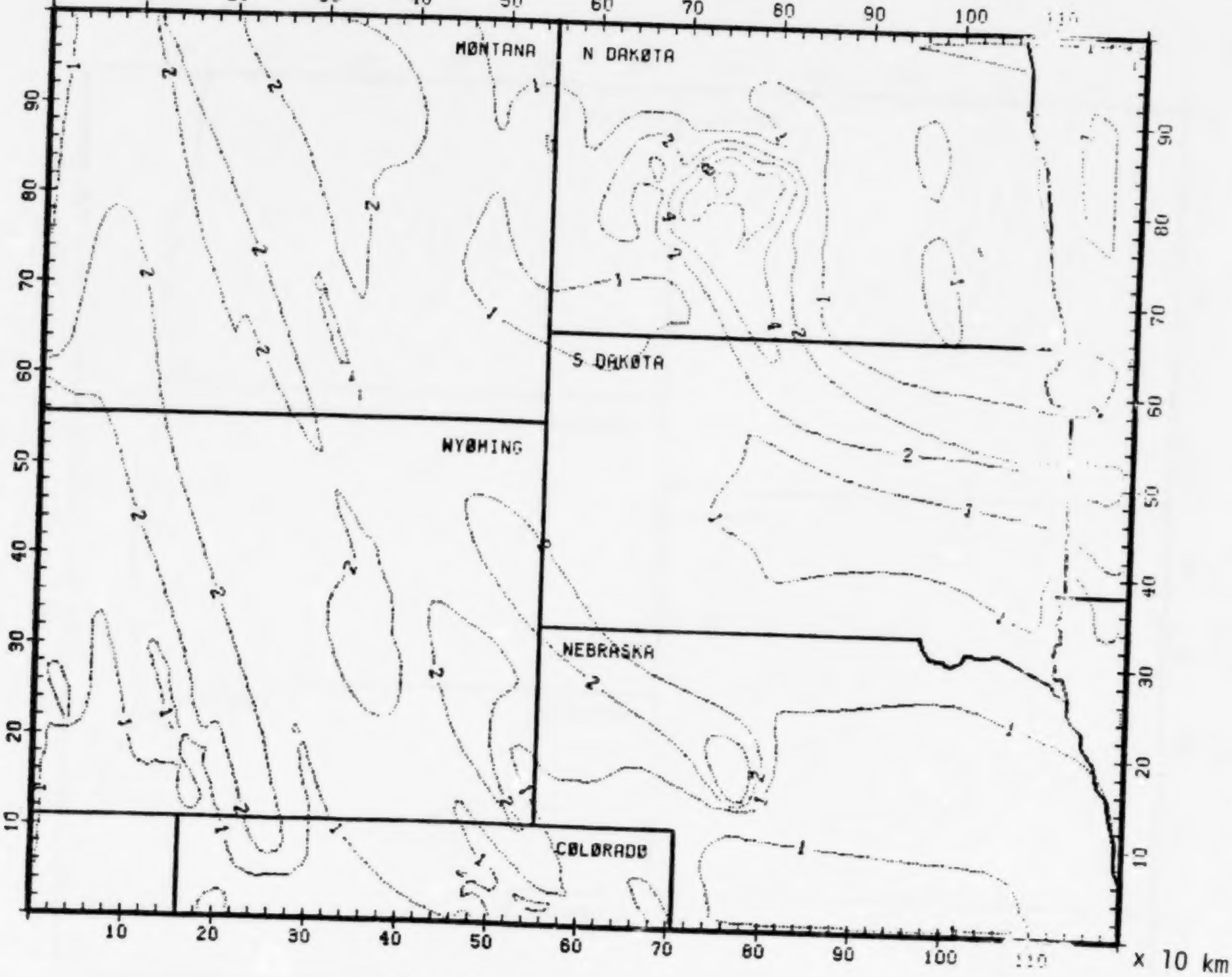
MONTANA
N DAKOTA
S DAKOTA
WYOMING
NEBRASKA
COLORADO
x 10 km
10
20
30
40
50
60
70
80
90
100
110
1
2
4
8

(b) NO_2 Concentrations (ppb)

FIGURE G-44 (Continued)

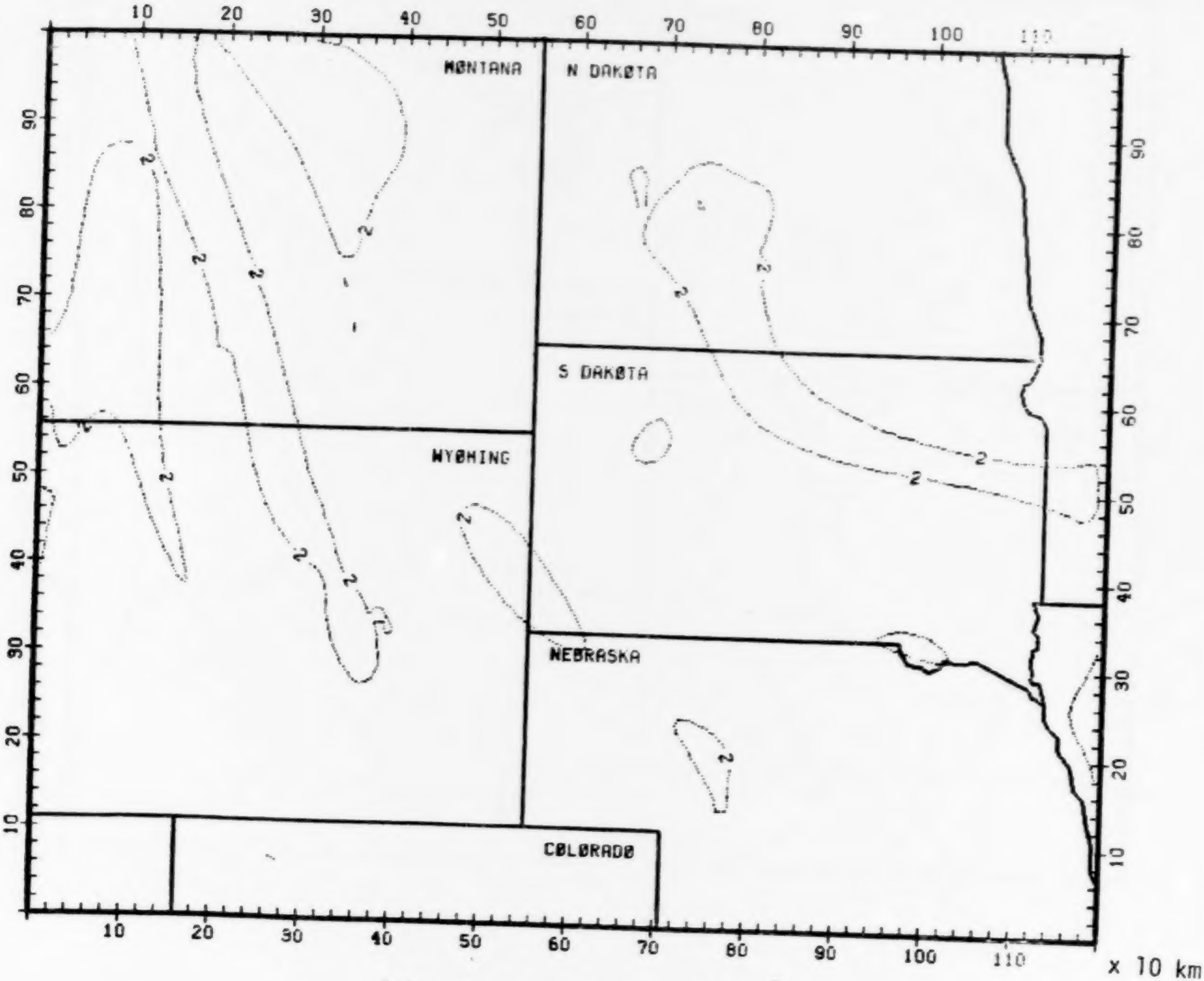
MONTANA
N DAKOTA
S DAKOTA
WYOMING
NEBRASKA
COLORADO
2
10
20
30
40
50
60
70
80
90
100
110
x 10 km

(c) $SO_4^=$ Concentrations ($\mu g/m^3$)

FIGURE G-44 (Continued)

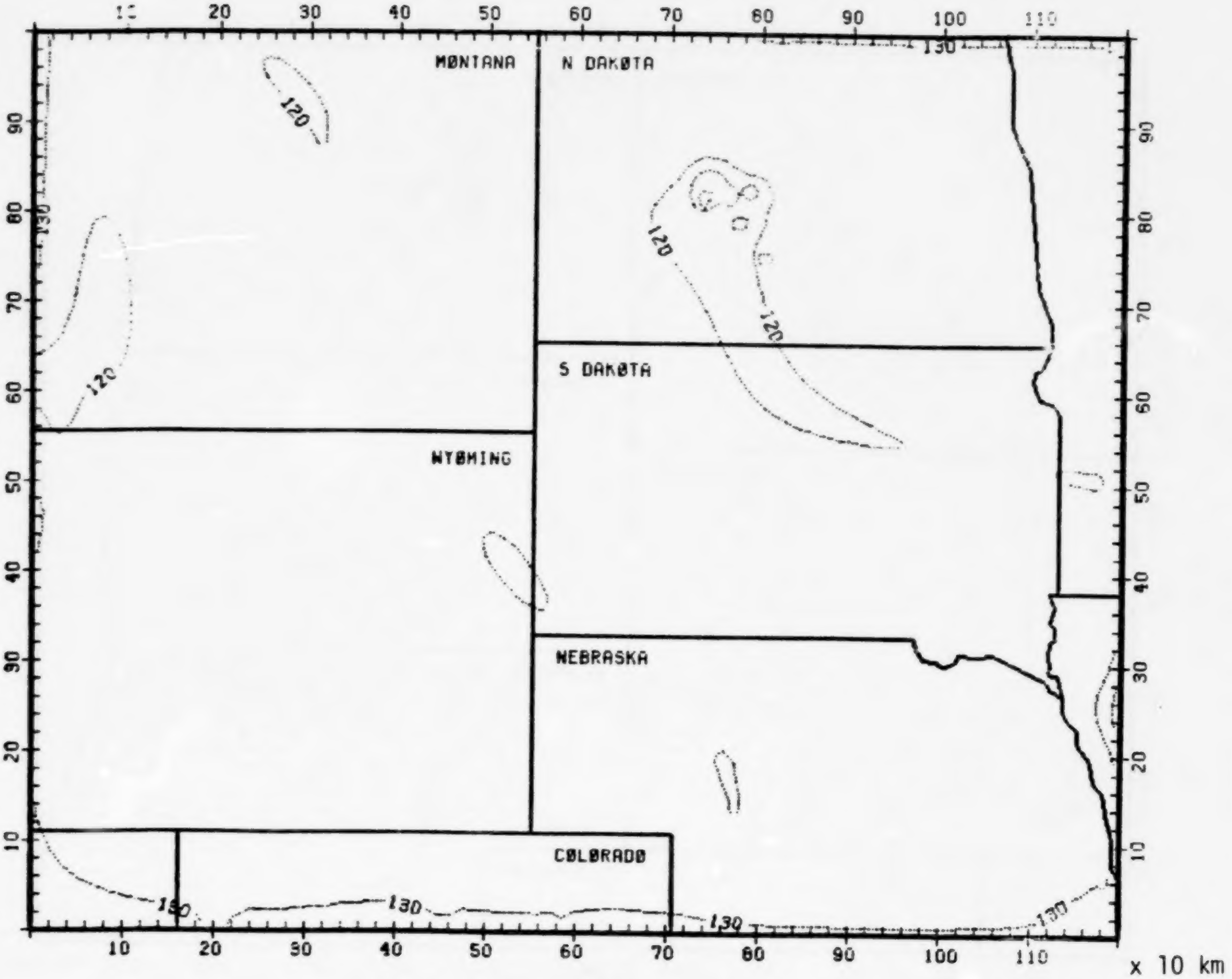
MONTANA
N DAKOTA
S DAKOTA
WYOMING
NEBRASKA
COLORADO
120
130
10
20
30
40
50
60
70
80
90
100
110
x 10 km

(d) Visual Range (km)

FIGURE G-44 (Concluded)

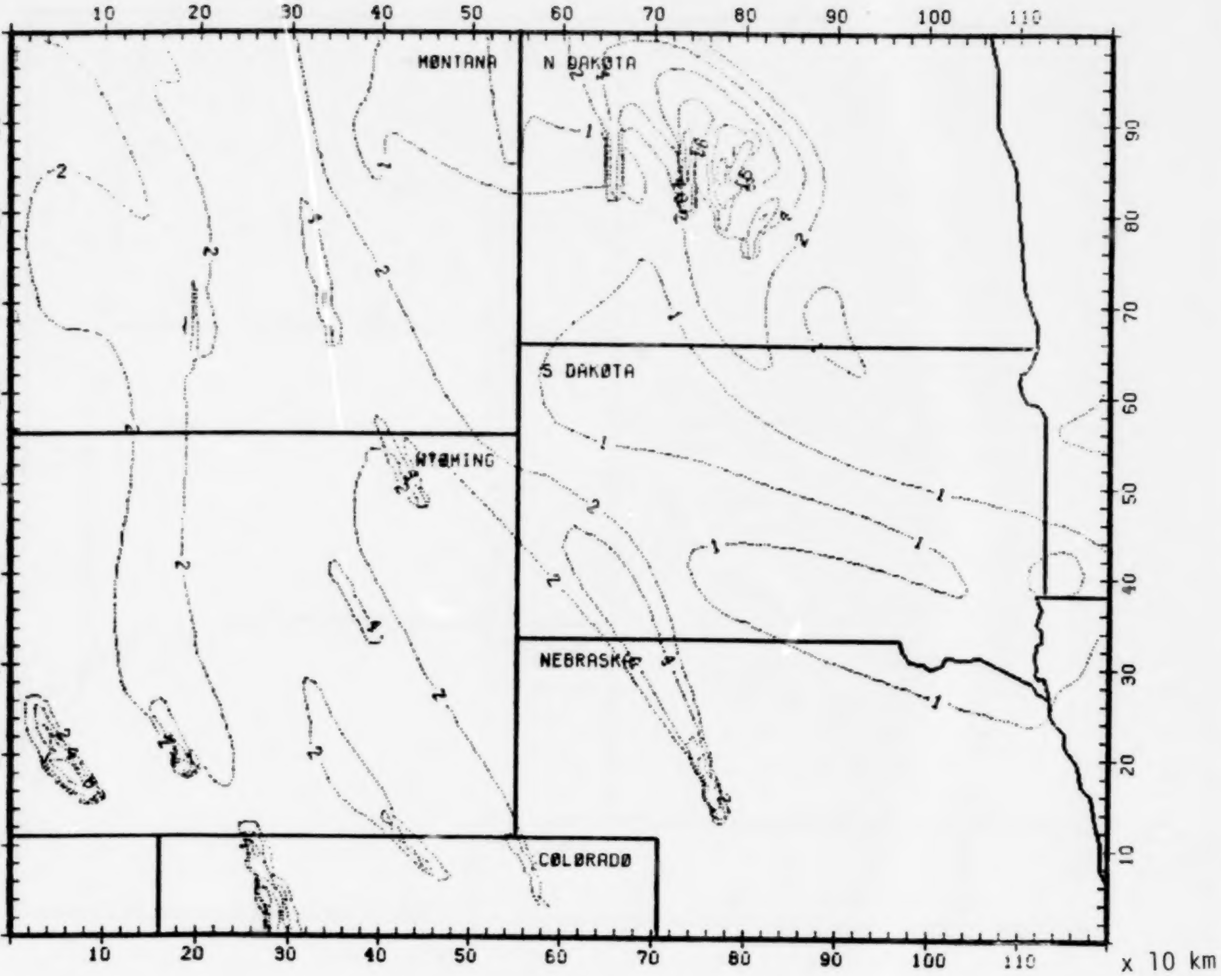
MONTANA
N DAKOTA
S DAKOTA
WYOMING
NEBRASKA
COLORADO
10
20
30
40
50
60
70
80
90
100
110
x 10 km
1
2
4
8
16

(a) SO_2 Concentrations ($\mu g/m^3$)

FIGURE G-45. 1986 NORTHERN GREAT PLAINS ISOPLETHS FOR 500-800 MST ON 6 APRIL 1976 ASSUMING 0.5 PERCENT PER HOUR SULFATE FORMATION

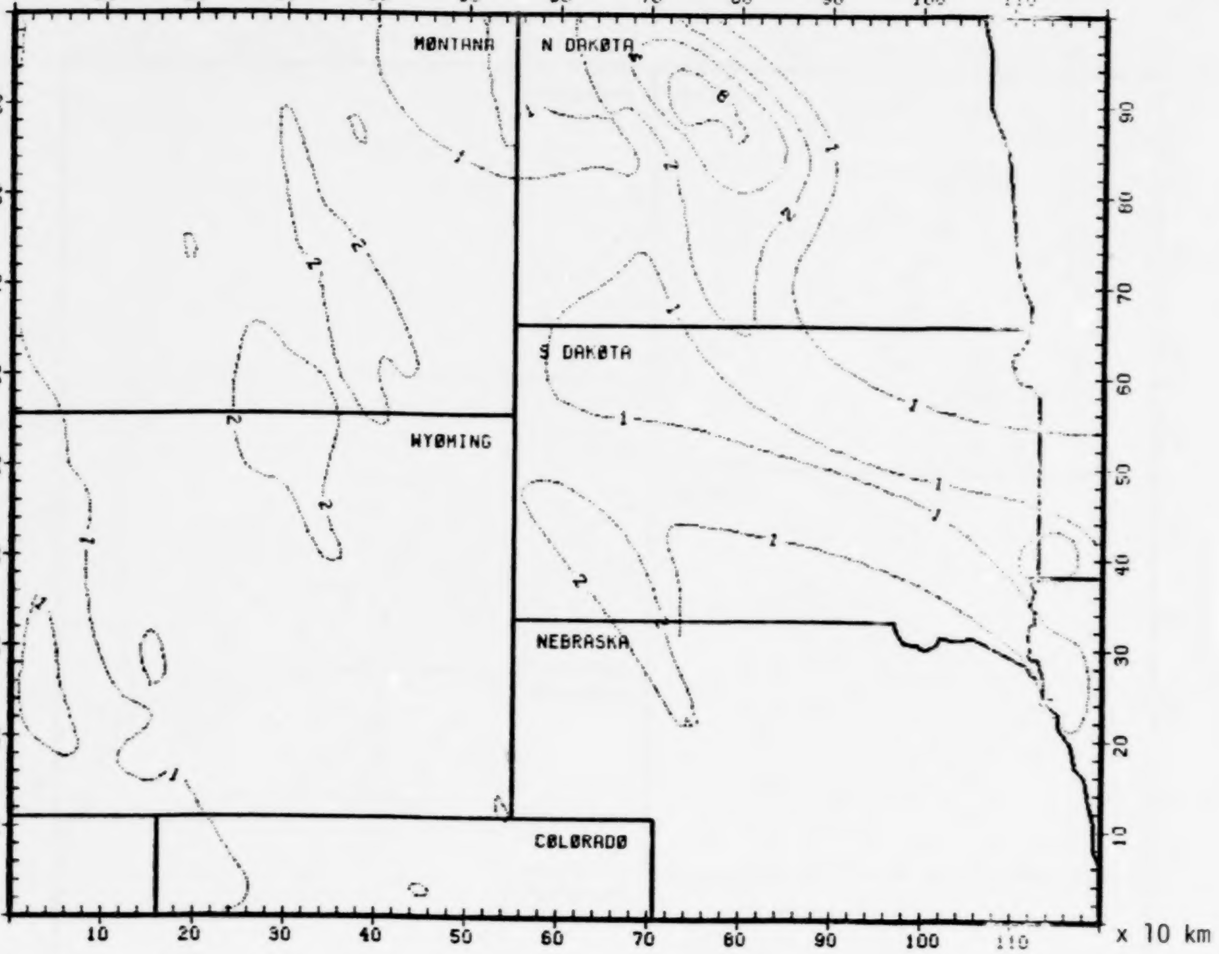
MONTANA
N DAKOTA
S DAKOTA
WYOMING
NEBRASKA
COLORADO
10
20
30
40
50
60
70
80
90
100
110
x 10 km
1
2
4
6

(b) NO$_2$ Concentrations (ppb)

FIGURE G-45 (Continued)

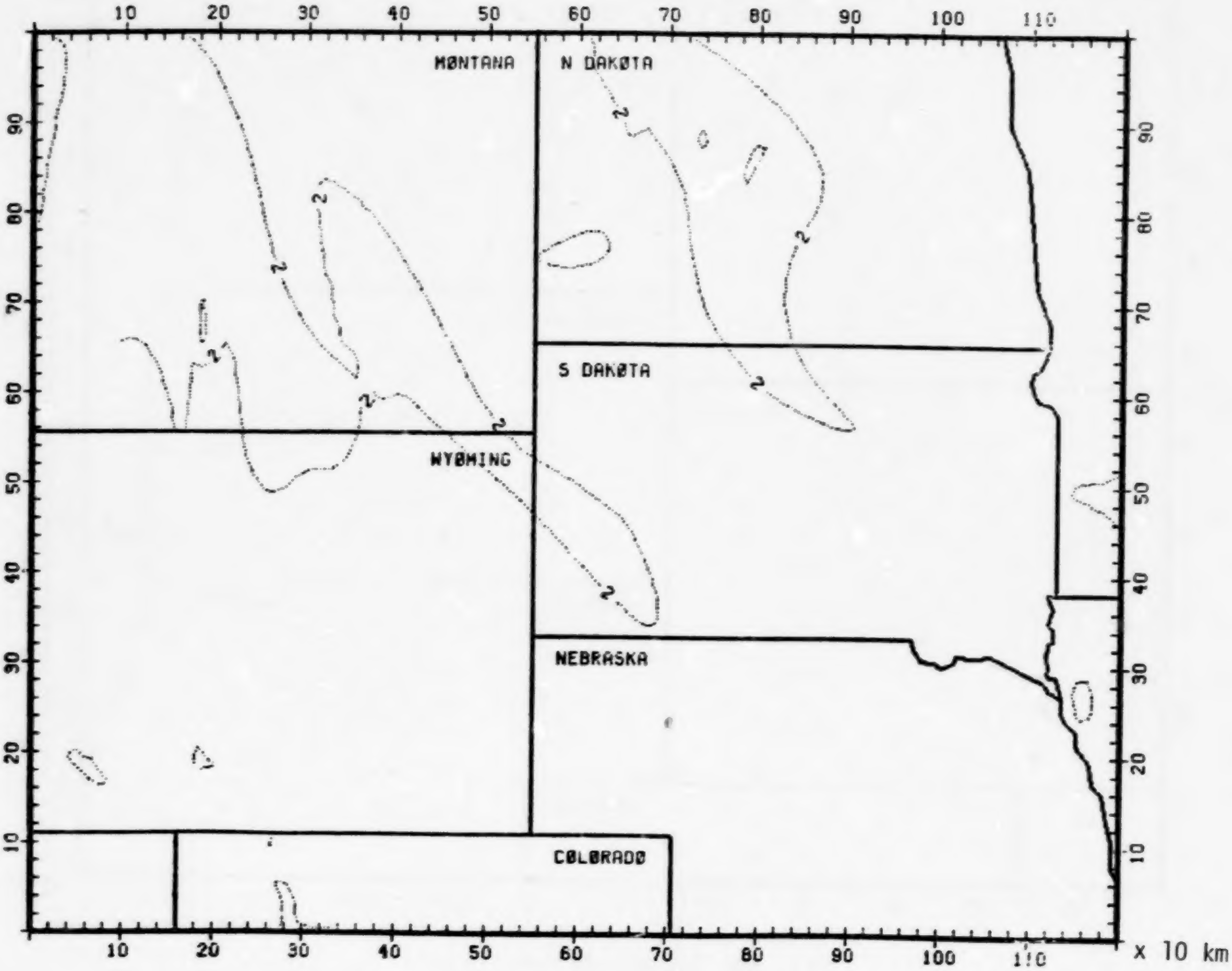

MONTANA
N DAKOTA
S DAKOTA
WYOMING
NEBRASKA
COLORADO
2
10
20
30
40
50
60
70
80
90
100
110
x 10 km

(c) $SO_4^=$ Concentrations ($\mu g/m^3$)

FIGURE G-45 (Continued)

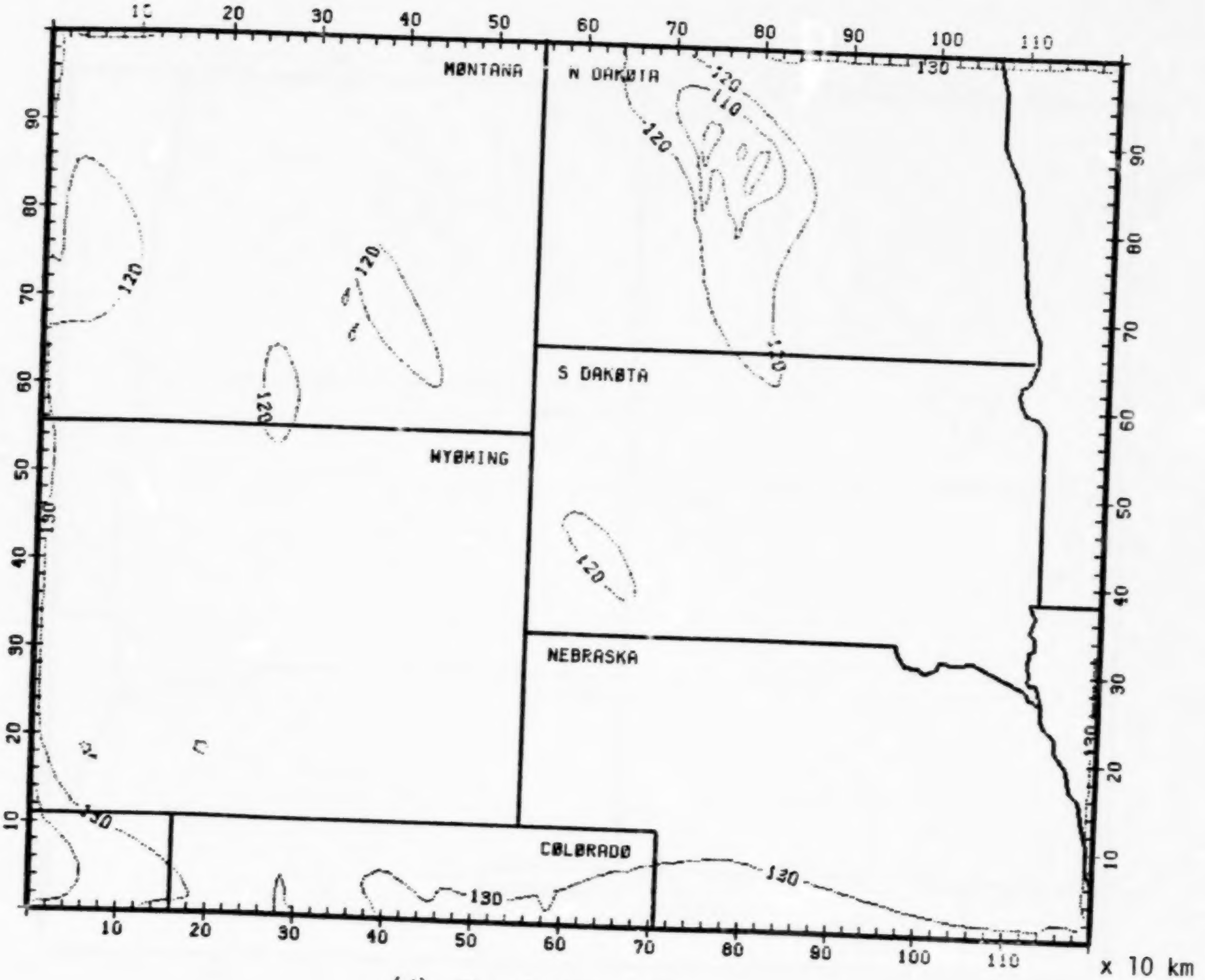
MØNTANA
N DAKØTA
S DAKØTA
WYØMING
NEBRASKA
CØLØRADØ
110
120
130
x 10 km

(d) Visual Range (km)

FIGURE G-45 (Concluded)

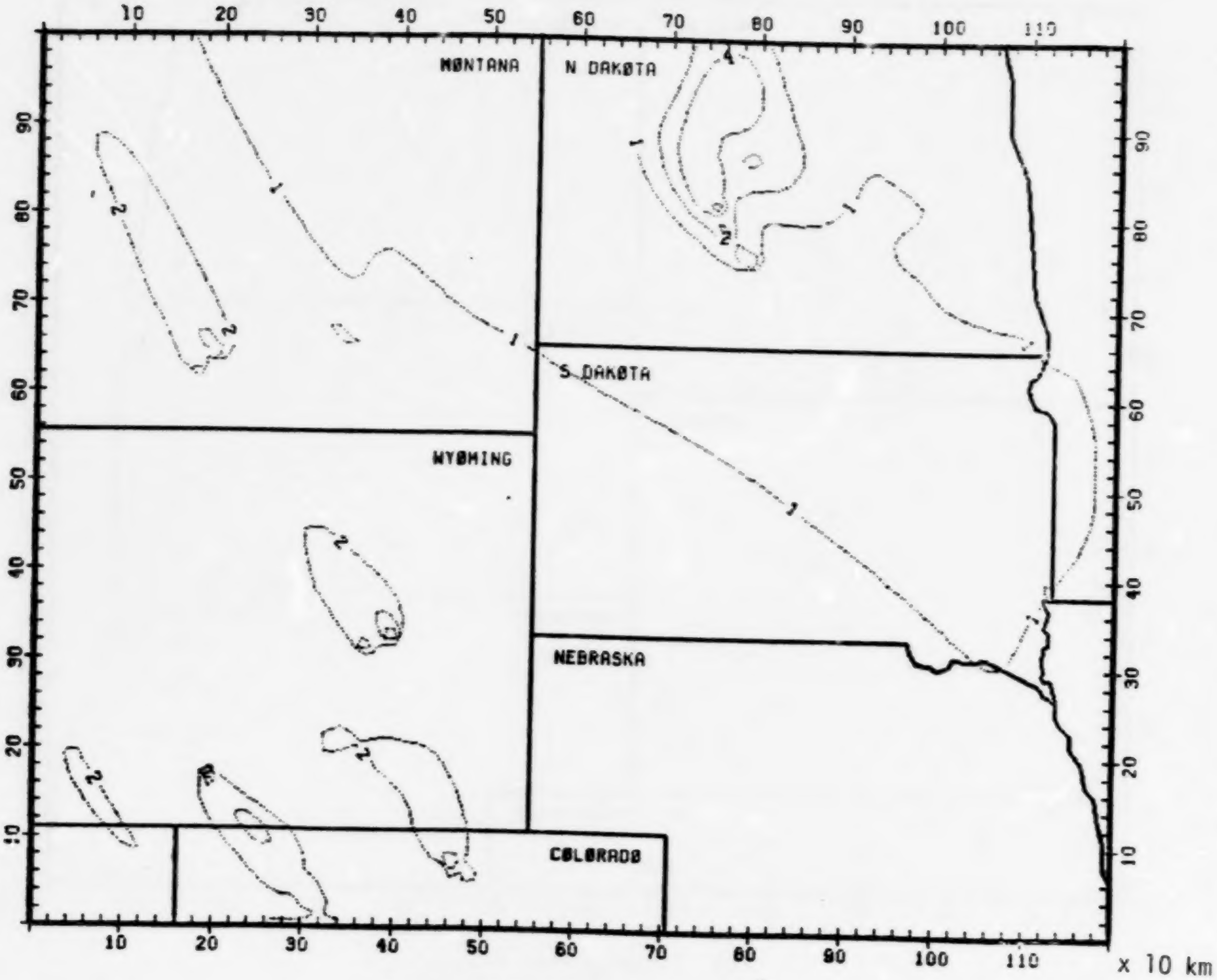
MONTANA
N DAKOTA
S DAKOTA
WYOMING
NEBRASKA
COLORADO
10
20
30
40
50
60
70
80
90
100
110
x 10 km
1
2
4

(a) SO_2 Concentrations ($\mu g/m^3$)

FIGURE G-46. 1986 NORTHERN GREAT PLAINS ISOPLETHS FOR 1400-1700 MST ON 6 APRIL 1976 ASSUMING 0.5 PERCENT PER HOUR SULFATE FORMATION

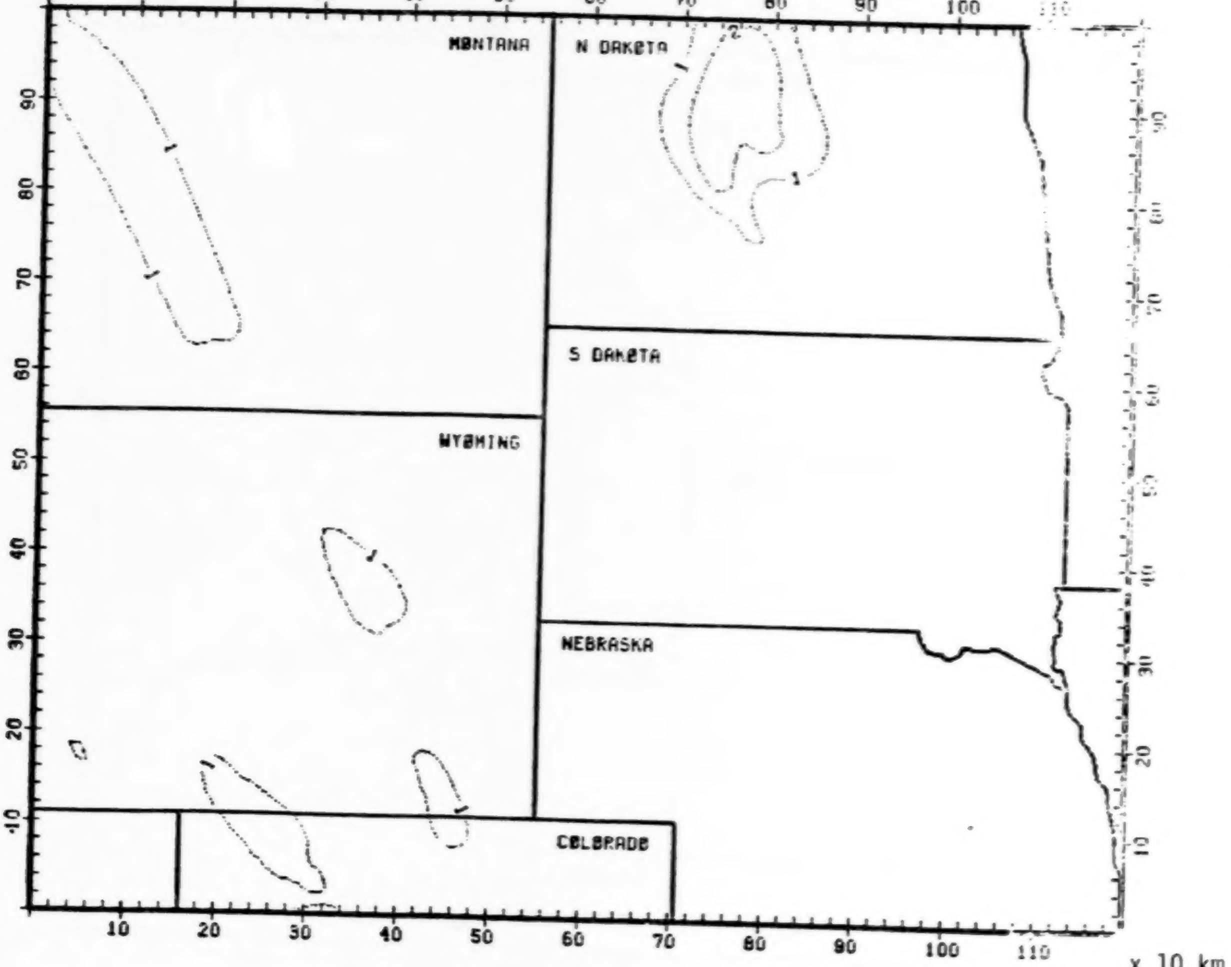
MONTANA
N DAKOTA
S DAKOTA
WYOMING
NEBRASKA
COLORADO
1
2
10
20
30
40
50
60
70
80
90
100
110
x 10 km

(b) NO$_2$ Concentrations (ppb)

FIGURE G-46 (Continued)

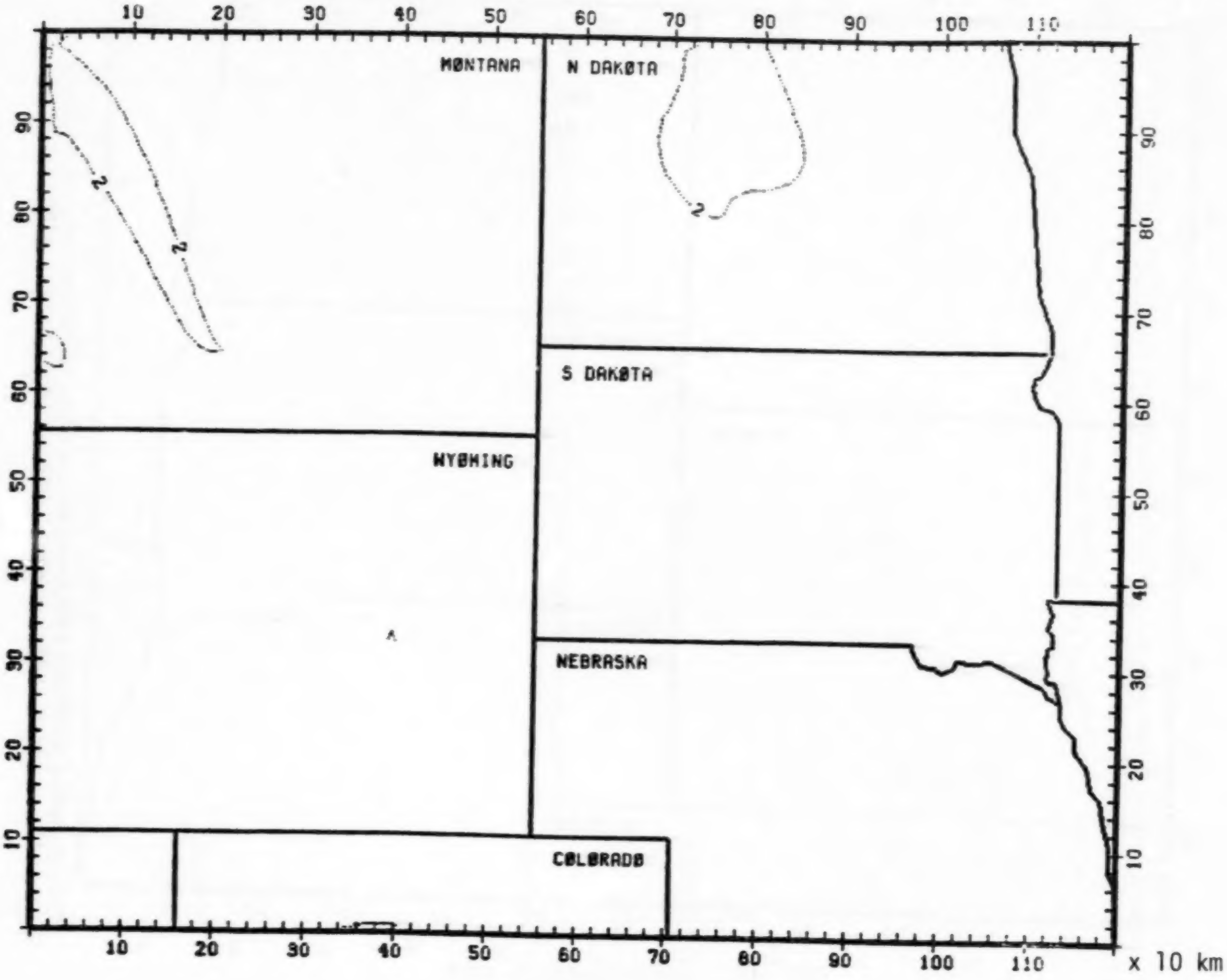
MØNTANA
N DAKØTA
S DAKØTA
WYØMING
NEBRASKA
CØLØRADØ
2
2
2
A
10
20
30
40
50
60
70
80
90
100
110
x 10 km

(c) $SO_4^=$ Concentrations ($\mu g/m^3$)

FIGURE G-46 (Continued)

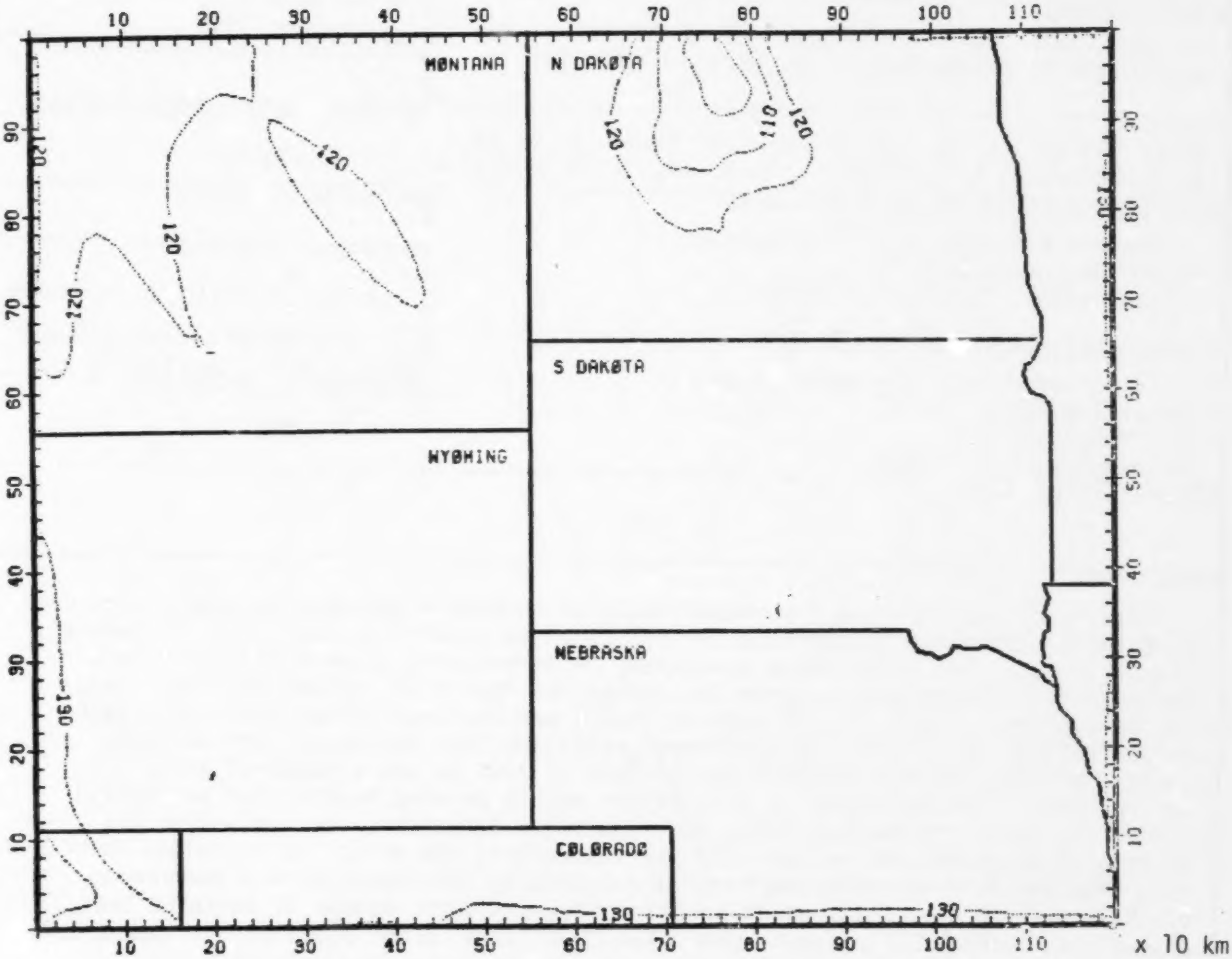
MONTANA
N DAKOTA
S DAKOTA
WYOMING
NEBRASKA
COLORADO
120
110
130
x 10 km
10
20
30
40
50
60
70
80
90
100
110

(d) Visual Range (km)

FIGURE G-46 (Concluded)